Spring 5-8-2008

Refining models of crustal growth and evolution in southwestern Laurentia with paired U-Pb and Lu-Hf analyses of igneous and detrital zircon

Mark E. Holland

Mark E. Holland

Candidate

Earth and Planetary Sciences

Department

This dissertation is approved, and it is acceptable in quality and form for publication:

Approved by the Dissertation Committee:

Dr. Karl E. Karlstrom, Chairperson

Dr. Matthew Heizler

Dr. Laura Crossey

Dr. Brandon Schmandt

REFINING MODELS OF CRUSTAL GROWTH AND EVOLUTION WITH PAIRED U-PB AND LU-HF ANALYSES OF IGNEOUS AND DETRITAL ZIRCON

by

MARK E. HOLLAND

B.S., Geology, University of Massachusetts, Amherst
M.S. Earth and Planetary Sciences, University of New Mexico

DISSERTATION

Submitted in Partial Fulfillment of the
Requirements for the Degree of

Doctor of Philosophy
Earth and Planetary Sciences

The University of New Mexico
Albuquerque, New Mexico

July, 2018

ACKNOWLEDGEMENTS

These documents exist due to the work of many people other than myself, including but not limited to the following groups of people: my instructors, my friends, and my family.

My instructors. Thanks to Dr. Karl Karlstrom for all of the obvious reasons like obtaining the funding to support my M.S. and Ph.D., his boundless enthusiasm for all aspects of geology, his prompt turnaround on proposals, letters of recommendation, and manuscripts, and always encouraging his students to bite off more than we can chew. But thanks also, Karl, for less obvious things like all of the mannerisms that I've acquired from you, the "difference of a piñon" joke – oh, and five once in a lifetime river trips.

Thanks to Dr. Matt Heizler for helping me become not just a geochronologist, but a thermochronologist as well. There is still so much we need to do to maximize the thermochronologic potential of muscovite, but in meantime, thanks for being as willing to shoot the breeze as to talk about science, and for putting up with all the bad luck I brought into your lab.

Thanks to Dr. Laura Crossey for her broad insights, quick wit, and always being the first one to notice my haircuts – although, through no fault of her own, not lately. Laurie and Karl make their students part of their family. That family environment so greatly enriched my graduate experience that I don't see how it would be possible to get through it otherwise.

Thanks to Dr. Brandon Schmandt for showing me the light at the end of the tunnel, he was one of the first young professors I met during my studies. Thanks for demonstrating that it is in fact possible for the younger generation to get to where our

advisors are now, and thanks for teaching me how many Big Macs it takes to build the Himalayas.

I've been at UNM long enough that I've been a TA, or taken classes with almost all of the faculty here, so thanks to Dr. Adrian Brearley, Dr. Dave Gutzler, Dr. Maya Elrick, Dr. Yemane Asmerom, Dr. Peter Fawcett, Dr. Les McFadden, Dr. Zach Sharp, Dr. Gary Weissmann, Mike Spilde, and Dr. Aurora Pun. And let's be honest, I'd be nowhere without the outstanding office staff that the Department of Earth and Planetary Sciences is blessed to have. Thanks to Cindy, Paula, Faith, and Mabel.

Before UNM, when I was a wee undergraduate at UMass, it was Dr. Sheila Seaman who first told me that majoring in geology was a "wonderful idea!" Not long after that, Dr. Mike Williams shipped me off to northern Saskatchewan and nudged me down the rabbit hole.

My friends. I've been lucky my whole life to make great friends wherever I go, and New Mexico has been no exception. Thanks, Chris McGibbon, for our morning coffee therapy. Thanks, Aaron Scott, Paine Settle, and Ben Ziegler for rocking out in the non-silicate way. Thanks to The Boys, Brad Jeffrey, Zoltan Vaci, Spencer Staley, and Zach Gallegos. Thanks to the ultimate group, Dunbar Carpenter, Kel Cook, Eric Kruger, Jon Lee, and Mark Gorski. Thanks to the chronically Unnamed Adventuring Group, which is now, I think, our official name. Thanks, Jack Mulder, for spicing up New Mexico with some Tasmanian flavor, long ping-pong matches, and even longer talks about Proterozoic geology. And thanks to a whole bunch of other current and former UNM grad students (read: friends) that have gotten me through this: Marisa Repasch, Ben Holt, Jordan Gibbons, Jordan Anderson, Jeff Hrncir, Jeff Williams, Kathleen Vander

Kaaden, Remy Rovelli, Magdalena Donahue, Jason Ricketts, Carmen Winn, Mike Timmons, Valerie Blomgren, and Jared Smith.

Thanks to my oldest and best friend, Rick Lamothe, for supporting me through a lifetime of struggles – my graduate studies being only the latest of these. And innumerable thanks to Sean Regan for being a constant teacher, starting in Mineralogy and Structure lab, then in Saskatchewan, and continuing till today, for lending both critical and sympathetic ears, and for embracing Boatlife.

My family. What can I say? Thanks to Mom and Dad for literally everything. Thanks to Mike and Becky for letting me perform their wedding ceremony with half grown-out hair. Thanks to Natasha for all our adventures, and thanks in advance for those yet to come.

And thanks to Gato.

REFINING MODELS OF CRUSTAL GROWTH AND EVOLUTION IN SOUTHWESTERN LAURENTIA WITH PAIRED U-Pb AND Lu-Hf ANALYSES OF IGNEOUS AND DETRITAL ZIRCON

by

Mark E. Holland

B.S., Geology, University of Massachusetts, Amherst, 2012

M.S., Earth and Planetary Sciences, University of New Mexico, 2014

Ph.D., Earth and Planetary Sciences, University of New Mexico, 2018

ABSTRACT

The origin and evolution of continental crust is a fundamental and debated topic in geoscience. For over thirty years, Proterozoic crust of the southwestern United States has been a field laboratory for studying orogenic processes in the middle crust, and the growth of continental lithosphere via accretionary orogenesis. Three distinct crustal provinces are delineated based on differences in isotopic, structural, and geochronologic characteristics. To address questions about the origin of each province, this dissertation is composed of three chapters that present new U-Pb and Lu-Hf isotope analysis of plutonic, volcanic, and detrital zircon from the oldest known rocks in each crustal province in order to better understand the processes responsible for initial lithospheric formation and subsequent modification. Collectively, these chapters present a new

synthesis of lithospheric formation during successive accretionary orogenic episodes that builds on three decades of prior field-based structural, metamorphic, and geochronologic studies. Major conclusions of each chapter are summarized below.

Chapter 1 addresses the Mojave crustal province. In the Mojave crustal province, metasedimentary rocks from central Arizona to southern California share the same detrital zircon populations, indicating that they were all deposited in the same regional basin system, that we name the Vishnu basin. Detrital zircon populations in the Vishnu basin are remarkably similar to Australian and Antarctic cratons, providing evidence that these cratons were joined with Laurentia in the Nuna supercontinent at ~1.8 Ga. 1.79-1.72 Ga plutonic rocks that intrude the Vishnu basin in the Mojave province are progressively younger from west to east, suggesting arc migration. The enigmatic isotopic signature of plutonic rocks the Mojave province is attributed to mixing between a >1.8 Ga lower crustal substrate, Vishnu basin metasedimentary material, and depleted mantle derived melts. At the time of completion of this dissertation, Chapter 1 is published in the journal Precambrian Research with the following reference:

Holland, M.E., Karlstrom, K.E., Gehrels, G., Shufeldt, O.P., Begg, G., Griffin, W.L., and Belousova, E., 2018, The Paleoproterozoic Vishnu basin in southwestern Laurentia: Implications for supercontinent reconstructions, crustal growth, and the origin of the Mojave crustal province: Precambrian Research, v. 308, p. 1-17.

The following is a description of the contributions of each author:

Mark E. Holland: field sampling for all samples collected from 2013-2014, conducted all analyses at the Arizona Laserchron Center, drafted all figures, and wrote the bulk of the manuscript; Karl E. Karlstrom: field sampling of all samples, assisted in analyses at the Arizona Laserchron Center, provided abundant suggestions and edits to the manuscript and figures; George E. Gehrels: coordinated all analytical work at the Arizona Laserchron Center, assisted in data processing, and helped draft the analytical methods for the Arizona Laserchron Center section; Mark Pecha: indispensable aid with data acquisition and processing at the Arizona Laserchron Center, assisted in drafting analytical methods section for the Arizona Laserchron Center; Owen P. Shufeldt: first suggested the Paleoproterozoic connection between southwestern Laurentia and the Gawler craton, provided edits and suggestions on manuscript; Graham Begg: collected plutonic samples 2005-2006, conducted analyses at the GEMOC Key Centre at Macquarie University in Sydney, Australia, drafted the Macquarie analytical methods section, provided abundant comments and suggestions to manuscript; William L. Griffin: conducted analyses at the GEMOC Key Centre at Macquarie University in Sydney, Australia, drafted the Macquarie analytical methods section; Elena Belousova: conducted analyses at the GEMOC Key Centre at Macquarie University in Sydney, Australia, drafted the Macquarie analytical methods section.

Chapter 2 applies U-Pb and Hf isotope analyses of zircon from the Yavapai and Mazatzal provinces in northern and central New Mexico. Oldest rocks in northern New Mexico include juvenile 1.76 Ga Maquanita granodiorite that intrudes and older volcanogenic greenstone-metasedimentary succession of the Yavapai province. This is

unconformably overlain by 1.7 Ga isotopically juvenile rhyolites interlayered and overlain by immature clastic metasedimentary rocks that become more compositionally mature up-section. Detrital zircon populations in the overlying metasedimentary rocks include almost exclusively 1.7-1.8 Ga zircon grains, indicating that they were derived from erosion of local basement complexes. In conjunction with the compositional change towards more mature sedimentary rocks up-section, detrital zircon grains yield a progressively broader range of ages from the bottom to the top of the section. A very similar but ~50 Ma younger sequence of rhyolite volcanism and sedimentation is repeated in the Mazatzal province of central New Mexico and is interpreted to represent the evolution of basin systems with progressively wider provenance through time. Across northern and central New Mexico, plutons that intrude supracrustal packages have inherited zircon and Hf-isotope compositions that suggest they were derived in part from Yavapai province crust. Together, these data suggest that the Mazatzal province formed as a continental margin arc built atop the previously accreted Yavapai province. This continental margin arc was episodically extended and inverted causing repeated cycles of volcanism, sedimentation, and deformation. Chapter 2 is thus a positive test of the slab roll back model of Jones et al. (2009) for development of Paleoproterozoic quartzite basins across southwestern Laurentia. This chapter is intended for submission to the journal Geosphere in 2018. The co-authored manuscript will have similar authors and contributions as Holland et al. (2018): Karl E. Karlstrom, Tyler Grambling, George E. Gehrels, and Mark Pecha.

Chapter 3 uses new Hf analyses to test the global tectonic setting within which Proterozoic lithosphere of southern Laurentia formed and compare the history of

lithospheric formation to the global supercontinent cycle. Changes in the Hf-isotope composition of a continental scale compilation of >3,500 igneous and detrital zircon from southern Laurentia show an overall increase in εHf(t) values from 1.8-1.3 Ga. This trend is similar in both time and space to changes in Hf-isotope composition observed in the Phanerozoic Circum-Pacific orogenic system. In southern Laurentia, continental growth took place by a combination of accretion of juvenile terranes and reworking of older crust by extensional processes along a long-lived convergent margin similar to the Circum-Pacific orogenic system. Comparison of the southern Laurentia record with global zircon compilations suggests that the plate tectonic regime of a long-lived Laurentian convergent margin was a globally important accretionary orogen. The southern Laurentia accretionary orogen initially developed during and on the margin of the assembling 1.8 Ga Paleoproterozoic supercontinent Nuna. Comparison to the Hf record of other cratons indicates that this long-lived accretionary orogen facilitated one of the largest episodes of juvenile crustal growth in Earth history. Crustal growth was terminated by the Grenville orogeny and the assembly of the Neoproterozoic supercontinent Rodinia, in which Laurentia was centrally located due to an inversion of Nuna. This chapter is intended for submittal as a co-authored publication in 2018 and will have similar author contributions as the previous papers.

TABLE OF CONTENTS

LIST OF FIGURES

CHAPTER 1

CHAPTER 2

LIST OF TABLES

CHAPTER 1

CHAPTER 2

CHAPTER 1 The Paleoproterozoic Vishnu basin in southwestern Laurentia: Implications for supercontinent reconstructions, crustal growth, and the origin of the Mojave crustal province

Mark E. Holland[1], Karl E. Karlstrom[1], George Gehrels[2], Owen P. Shufeldt[3], Graham Begg[4], William Griffin[5], and Elena Belousova[5]

[1]Department of Earth and Planetary Sciences, University of New Mexico, Northrop Hall, 221 Yale Boulevard NE, Albuquerque, New Mexico 87131, USA;

[2]Arizona LaserChron Center, Department of Geoscience, University of Arizona, Tucson, Arizona 85721, USA

[3]Rio Tinto Iron Ore, Perth, WA 6000, Australia

[4]Minerals Targeting International PL, West Perth, WA 6005, Australia

[5]Australian Research Council Centre of Excellence for Core to Crust Fluid Systems/GEMOC, Macquarie University, Sydney, NSW 2109, Australia

ABSTRACT

The formation of the Mojave crustal province has been a persistent enigma in models of the Proterozoic tectonic history of southwestern Laurentia. It is composed of similarly-aged 1.8- 1.7 Ga rocks as the adjacent Yavapai province, yet shows evidence of much older (>2.2 Ga) lithospheric components in all isotopic systems. We present >700 new U-Pb analyses and >350 new Lu-Hf analyses of zircon from the oldest metasedimentary and plutonic rocks of the Mojave province to better understand its origin and evolution. Six metasedimentary rocks have detrital zircon age populations dominated by ~1.87 and 2.4-2.7 Ga grains. This age distribution is like the Vishnu Schist in Grand Canyon and we suggest that together they comprise a regional turbidite basin

that we name the Vishnu basin. Cross cutting relationships indicate that deposition of the Vishnu basin proceeded from west to east (present coordinates) from ~1.8-1.75 Ga. The Vishnu basin extends from central Arizona to the Transverse Ranges in California and possibly beyond the present boundaries of Laurentia to previously adjacent cratonic blocks. We propose the Mawson continent as the source of Vishnu basin detritus, and hence favor Nuna accretion at ~1.8 Ga. Paleoproterozoic plutons that intrude the Vishnu basin sampled in this study range in age from 1791±15 to 1691±15 Ma. Plutons show a systematic change in Hf-isotope composition through time and space. The oldest plutons in the western Mojave province have the most isotopically evolved signatures and contain inherited zircon cores and xenocrysts with age and Hf-isotope characteristics that suggest they were derived from Vishnu basin sediments and/or 1.8-2.7 Ga lower crust. The Hf-isotope composition of plutons becomes more radiogenic (juvenile) from west-to-east and from old-to-young. The magnitude of Hf-isotope variation requires increased influence of depleted mantle sources through time. Hf-isotope compositions of the younger 1.7-1.68 Ga syn-to-post orogenic granites show more evolved compositions attributed to lower crustal melting due to crustal thickening during the Yavapai orogeny.

Key Words: *Mojave province, Hf-isotopes, detrital zircon geochronology, southwestern Laurentia, Nuna*

INTRODUCTION

Ancient orogenic belts that once extended beyond present cratonic margins provide potential piercing points for reconstructions of Precambrian supercontinents. The Paleoproterozoic Mojave province (Mojavia of Bennett and DePoalo, 1987; Mojave terrane of Wooden et al., 1988; Mojave block of Karlstrom and Bowring, 1988) lies on

the southwestern margin of Laurentia (inset to Fig. 1), and has remained enigmatic in the context of the growth and evolution of the craton (Whitmeyer and Karlstrom, 2007; Mueller et al., 2011). The location of the Mojave province makes it potentially important for understanding the configuration of the Paleoproterozoic supercontinent Nuna (Hoffman, 1998; Zhang et al., 2012) because the growth and assembly of southern Laurentia from 1.8-1.6 Ga likely coincided with the final assembly of Nuna (Perhsson et al., 2016). Moreover, Laurentia is one of the largest and more central components of Nuna in most paleogeographic reconstructions (Rogers and Santosh, 2002; Zhang et al., 2012; Pisarevsky et al., 2014; Perhsson et al., 2016). Thus, the Proterozoic tectonic history of Laurentia is fundamental to understanding the assembly of Nuna. Conversely, long-standing questions regarding the tectonic history of Laurentia, such as the tectonic significance of the Mojave province, may be better answered when considered in a global plate tectonic context.

The Paleoproterozoic crust of the southwestern United States is regarded as an example of continental growth through accretionary orogenesis (Condie, 1982; Hoffman, 1988; Karlstrom and Bowring 1988; Bowring and Karlstrom, 1990; Windley, 2003; Whitmeyer and Karlstrom, 2007). The prevailing tectonic model delineates three Paleoproterozoic crustal provinces based on isotopic composition (Wooden et al., 1988; Wooden and DeWitt, 1991; Karlstrom and Bowring, 1993; Hawkins et al., 1996; Duebendorfer et al., 2006; Holland et al., 2015), and orogenic style and timing (Karlstrom et al., 1987; Karlstrom and Bowring, 1988; Bowring and Karlstrom, 1990; Karlstrom and Bowring, 1993; Shaw and Karlstrom, 1999). From northwest to southeast, these are the Mojave, Yavapai, and Mazatzal provinces (Whitmeyer and Karlstrom,

2007) (Figure 1-1). The 1.8-1.7 Ga Yavapai and 1.7-1.6 Ga Mazatzal provinces are characterized by dominantly juvenile Nd isotopic compositions and yield model ages that are typically ≤100 Ma older than crystallization ages (Bennett and DePaolo, 1987). In contrast, the Mojave province contains ~1.8-1.7 Ga rocks characterized by an evolved isotopic signature evident in all isotope systems so far applied to the region (Bennett and DePaolo, 1987; Wooden et al., 1988; Ramo and Calzia, 1998; Lee et al., 2001; Barth et al., 2000; Wooden et al., 2012; Holland et al., 2015; Armytage et al., 2014).

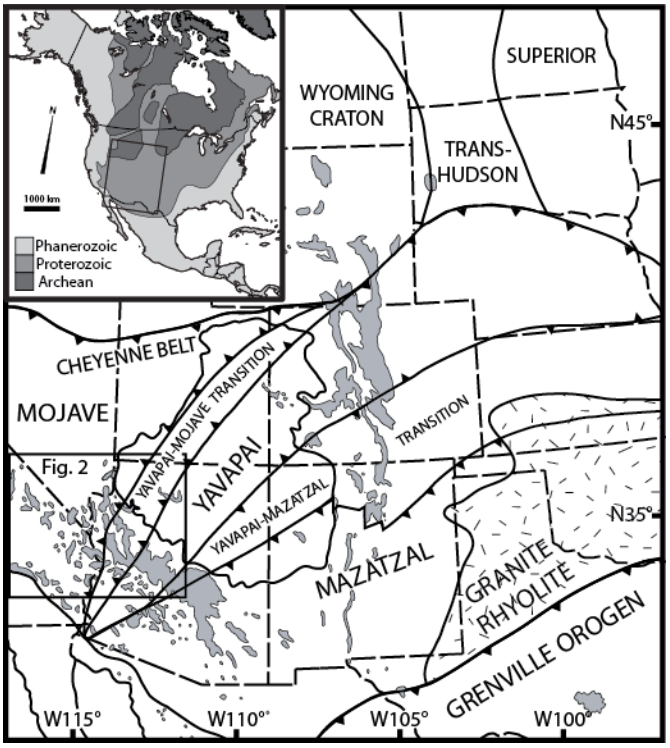

Figure 1-1. Precambrian crustal provinces of southwestern North America showing Proterozoic outcrops in gray (adapted from Whitmeyer and Karlstrom, 2007). Box shows area of Figure 2.

The evolved isotopic signature is the most enigmatic feature of the Mojave province. While most workers have attributed the isotopic signature to incorporation of Archean crust during the formation of the Mojave province, two parallel debates persist in the literature: 1) the specific cratonic source(s) of older crust, and 2) the process(es) by

which older crust became incorporated into the Mojave province. Some workers have favored the Wyoming craton as the source of older crust (Bennett and DePaolo, 1987; Wooden et al., 1988; Ramo and Calzia, 1998; Nelson et al., 2011), while others have favored Antarctic or Australian cratons (Wooden and DeWitt, 1991; Borg and DePaolo, 1994; Barth et al., 2000; Shufeldt et al., 2010; Goodge and Fanning, 2016). Debates concerning the introduction of Archean crustal material to the Mojave province largely focus on whether older crust was introduced in the form of Archean detritus (Bennett and DePaolo, 1987; Wooden et al., 1988; Ramo and Calzia, 1998; Coleman et al., 2002; Nelson et al., 2011), and/or the province was built on older Paleoproterozoic and Archean igneous/metaigneous crust and mantle (Lee et al., 2001) with tectonic fragments of Archean-influenced metasedimentary and metaigneous rocks (Wooden and Miller, 1990; Barth et al., 2000; Karlstrom et al., 2001; Shufeldt et al., 2010; Wooden et al., 2012; Holland et al., 2015).

Wooden et al. (2012) concluded that the characteristic isotopic signature of the oldest Mojave province rocks reflects the combined effects of mixing between depleted (juvenile/asthenospheric) and enriched mantle melts, along with partial melts and tectonic fragments of 2.0-1.8 Ga and 2.6-2.4 Ga crust. The sources proposed perhaps realistically include nearly every possible geologic or geochemical reservoir that could contribute to crust formation in any convergent margin setting. However, similar to work in younger orogens (DeCelles et al., 2009; Kemp et al., 2009), our goal is to examine spatial and temporal patterns across the Mojave province that may help identify times, regions, and processes in which one reservoir dominates over the others, and hence help resolve the

tectonic and magmatic evolution of the Mojave province in the context of lithospheric growth of southwestern Laurentia.

The Lu-Hf isotope system can distinguish between crust and mantle sources in magmatic systems (Ibanez-Mejia et al., 2015), and combined U-Pb and Lu-Hf-isotope data from temporally and spatially related plutonic and detrital zircon provide a unique perspective on crust formation along convergent margins (Barth et al., 2013; Holland et al., 2015). Specifically, the Hf-isotope composition of dated detrital zircon grains provide insights into the age and isotopic maturity of crust exposed at the surface at the time of deposition and at scales determined by the catchment and sedimentary setting. Detrital zircon studies also offer a means to fingerprint sedimentary contributions from previously adjacent terranes (Doe et al., 2012; 2013). In contrast, data from plutonic zircon provide insight into the nature and evolution of magmatic contributions to the crust during crust formation. The perspective offered by comparing the Hf-isotope composition of detrital and plutonic zircon allows us to address many of the standing questions regarding the tectonic significance of the isotopic signature of the Mojave province, as well as the broader significance of the Mojave province in the assembly of Laurentia and Nuna.

This study presents >700 new U-Pb analyses and >350 new Lu-Hf analyses from Paleoproterozoic rocks exposed in uplifts of the greater Death Valley and southeastern Mojave region (Figure 1-2). We build on a study of whole rock Sm-Nd isotope data from the Death Valley region (Ramo and Calzia, 1998) and provide the first U-Pb data from Proterozoic rocks of Death Valley. The paper complements a study of the boundary zone between Mojave and Yavapai basement rocks exposed in Grand Canyon (Holland et al., 2015) and finds: 1) similar detrital zircon age distributions in metasedimetnary rocks

across the Mojave province with characteristic older zircon ages of 2.0-1.8 and 2.7-2.4 Ga; 2) an eastward younging of plutonic and metasedimentary rocks indicated by cross cutting relationships, 3) heterogeneous Hf-isotope composition of plutonic rocks that suggests complex mixing of evolved and juvenile melt source regions and increased depleted mantle influence to the east and through time and from 1.79-1.73 Ga; 4) likely origin of Archean detritus and possible cryptic older lower crust from an Antarctic and/or Australian cratonic source, and 5) crustal recycling via lower crustal melting during and after the 1.71-1.68 Ga Yavapai orogeny.

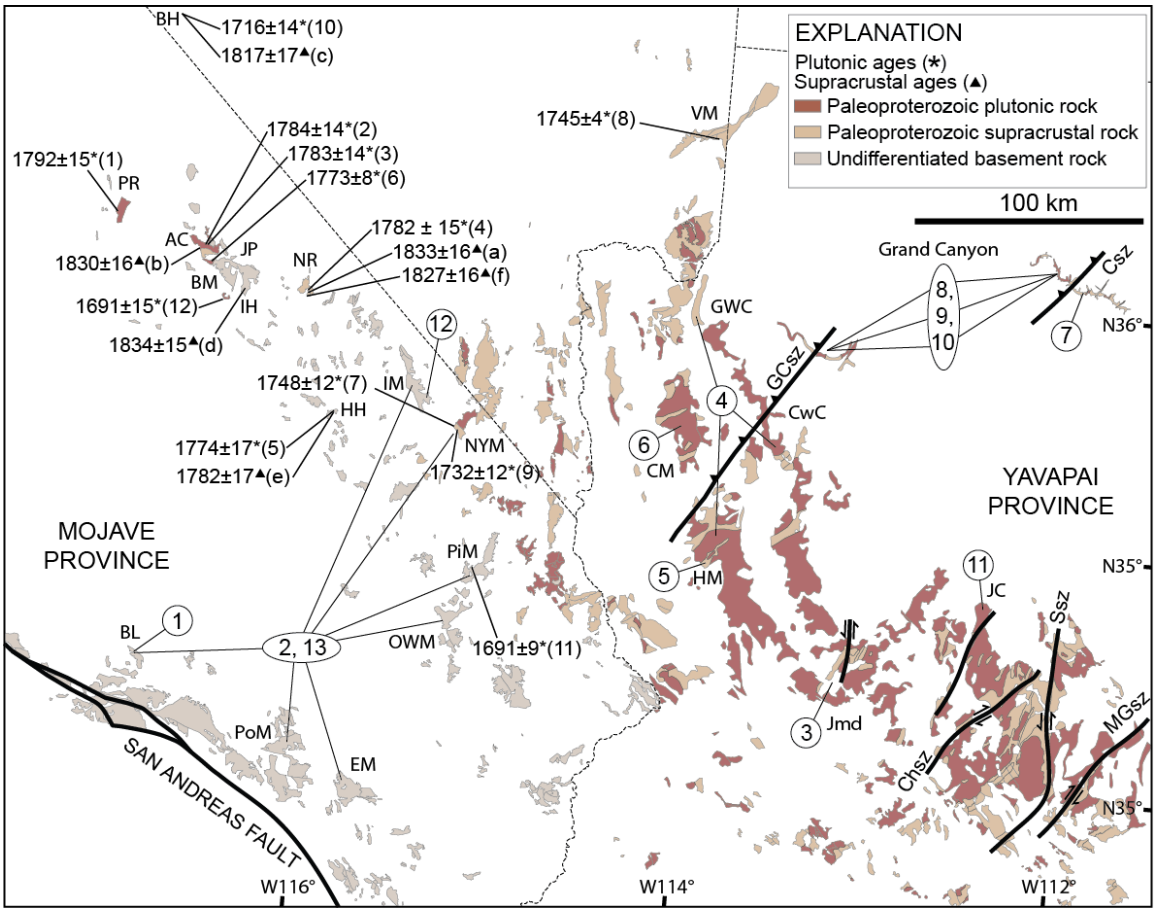

Figure 1-2. Simplified regional geologic map of the study area showing sample locations and a compilation of all existing geochronologic data discussed in this paper. Metasedimentary samples from this study (triangles) are shown with their maximum depositional ages (see text for discussion), with letters in parentheses keyed to age spectra in Figure 3. Plutonic samples (stars) are shown with numbers in parentheses keyed to

Table 2. Major structures are shown as solid black lines. Dip-slip sense shear zones are shown with teeth on the upper plate, and strike-slip sense is indicated with arrows. GCsz = Gneiss Canyon shear zone, Csz = Crystal shear zone, Chsz = Chaparral shear zone, Ssz = Shylock shear zone, MGsz = Moore Gulch shear zone. Circled numbers show the general locations of previous geochronologic studies of the region. Citations are as follows: 1) Barth et al., 2000; 2) Barth et al., 2009; 3) Bryant et al., 2001; 4) Chamberlain and Bowring, 1990; 5) Doe, 2014; 6) Duebendorfer et al., 2001; 7) Hawkins et al., 1996; 8) Holland et al., 2015; 9) Karlstrom et al., 2003; 10) Shufeldt et al., 2010; 11) Spencer et al., 2016; 12) Strickland et al., 2013; 13) Wooden et al., 2012. Locations mentioned by name in the text or references listed above, and their abbreviations on the map are: AC = Ashford Canyon, BL = Baldwin Lake, BM = Black Mountains, BH = Bullfrog Hills, CM = Cerbat Moutains, CwC = Cottonwood Cliffs, EM = Eagle Mountains, GWC = Grand Wash Cliffs, HH = Halloran Hills, HM = Hualapai Mountains, IH = Ibex Hills, IM = Ivanpah Mountains, JC = Jerome Canyon, Jmd = Jerome mining district, JP = Jubilee Pass, NYM = New York Mountains, NR = Nopah Range, OWM = Old Woman Mountains, PR = Panamint Range, PoM = Pinto Mountains, PiM = Piute Mountains, VM = Virgin Mountains.

BACKGROUND

Rocks of the Mojave crustal province include a complex assemblage of upper amphibolite to low-pressure granulite grade meta-supracrustal and granitoid rocks (Karlstrom and Bowring, 1988; Wooden and Miller., 1990). The oldest known rock unit in the Mojave province is the isotopically juvenile 1.840 Ga Elves Chasm gneiss in Grand Canyon which has been interpreted as an older arc-related substrate upon which the 1.750-1.741 Ga Vishnu Schist was deposited (Babcock, 1979; Hawkins et al., 1996; Ilg et al., 1996; Holland et al., 2015). Further west, the oldest known rocks are metasedimentary schists and gneisses whose protoliths were deposited between ~1.79-1.75 Ga. Detrital zircon age populations in these rocks range from 3.3-1.75 Ga (Barth et al., 2000; 2009; Strickland et al., 2013; this study), like those found in the Vishnu Schist in Grand Canyon (Shufeldt et al., 2010). Associated with metasedimentary rocks are amphibolites with tholeiitic bulk compositions, modestly enriched in large ion lithophile elements, and modestly depleted in high field strength elements (Miller and Wooden, 1992; Barth et al., 2009). These amphibolites may be as old as 1.81 Ga based on Nd-

isotope systematics (Coleman et al., 1999) and have been interpreted to indicate that Mojave province metasedimentary rocks were deposited in part on oceanic crust (Barth et al., 2009), or in a marginal marine arc environment (Wooden et al., 2012). Alternatively, amphibolites may be tectonic slices of submarine basalt of magmatic arc origin imbricated during orogenesis (Ilg et al., 1996). Synchronously with, and outlasting, the deposition of metasedimentary protoliths, a suite of calc-alkaline plutonic bodies intruded and became imbricated in the Mojave province from 1.79-1.73 Ga (Wooden and DeWitt, 1990; Ilg et al., 1996; Hawkins et al., 1996; Barth et al., 2009). During and after peak deformation and metamorphism from 1.71-1.68 Ga, plutonism was dominated by more evolved potassic melts enriched in high field strength elements from 1.69-1.65 Ga (Wooden and Miller, 1990; Bender et al., 1993; Barth et al., 2009). This later magmatism has been interpreted to reflect crustal melting in response to crustal thickening (Karlstrom et al., 2003; Barth et al., 2009).

Multiple episodes of deformation and magmatism have been identified throughout the Mojave province. Two-main regional deformational and metamorphic episodes are as follows. A well-developed shallowly-dipping S_1 fabric is recorded in central Arizona (Karlstrom et al., 1987), the Grand Wash Cliffs (Albin and Karlstrom, 1991), Grand Canyon (Ilg et al., 1996), and the Cerbat Mountains (Duebendorfer et al., 2001). The S_1 fabric and F_1 folds are overprinted by a penetrative subvertical northeast-striking S_2 fabric, which is the dominant fabric across much of southwestern Laurentia (Whitmeyer and Karlstrom, 2007). The timing of development of these fabrics, based on cross-cutting relationships and structural characteristics, varies with location and commonly overlap (Karlstrom et al., 1987; Albin and Karlstrom, 1991; Ilg et al., 1996; Duebendorfer et al.,

2001). Thus, deformation has been interpreted to be a progressive event beginning at or before ~1.75 Ga (Duebendorfer et al., 2001; Shufeldt et al., 2010), and culminating with peak deformation and metamorphism ranging from granulite-to-amphibolite facies across both Yavapai and Mojave provinces at 1.71-1.68 Ga (Karlstrom et al., 1987; Wooden and Miller, 1990; Ilg et al., 1996).

Metamorphic studies suggest that peak assemblages across the Mojave province reflect variable temperatures that were achieved during D_2 at near-isobaric conditions of 0.5-0.7 GPa that corresponds to middle crustal depths of 20-25 km. Peak metamorphic temperatures in the Mojave province range from 600-775 C at 0.6 GPa in Ivanpah and McCulloch Mountains (Strickland et al., 2013), 675-725 at 0.5-0.6 GPa in Cerbat Mountains (Duebendorfer et al., 2001), and 450-750 °C at 0.5-0.7 GPa in Grand Canyon (Dumond et al., 2007). Near-isothermal decompression from 0.5-0.7 to 0.3-0.4 GPa at 1.67-1.68 Ga, late during D_2, occurred in the Grand Canyon (Dumond et al., 2007), the Ivanpah Mountains (Strickland et al., 2013), and the Cerbat Mountains (Duebendorfer et al., 2001), and is attributed to orogenic exhumation via isostatic and erosional processes (Dumond et al., 2007) and/or D_2 orogenic collapse (Bonamici and Duebendorfer, 2009; Strickland et al., 2013).

METHODS

U-Pb and Lu-Hf isotope data were collected over the course of several years at two different laboratories. Five plutonic samples were analyzed at the Geochemical Evolution and Metallogeny of Continents (GEMOC) Key Centre at Macquarrie University in Sydney, Australia in 2006. All other samples were analyzed at the Arizona Laserchron Center at the University of Arizona in Tucson in 2013 and 2014. Both

laboratories employ similar techniques, which are detailed in Appendix 1. In both laboratories, zircon separates obtained via standard heavy mineral separation techniques were mounted in epoxy and hand polished. Grain mounts were then imaged via backscattered electron (BSE) imaging (at the GEMOC Key Centre) or cathodoluminescence (CL) imaging (at the ALC) to reveal internal textures of individual zircon grains.

The main difference in the analytical procedure GEMOC Key Centre and the ALC lies in the beam placement during Hf-isotope analysis. At the ALC, Hf-isotope analyses were conducted on top of the ablation pits left from U-Pb isotopic analysis, while at the GEMOC Key Centre, Hf-isotope analyses were placed elsewhere on the crystal, but in the same age domain as interpreted by BSE imaging. Placement of the Hf beam atop the U-Pb ablation pit reduces uncertainty in the age assigned to a given $^{176}Hf/^{177}Hf$ ratio, but increases the analytical uncertainty (Gehrels and Pecha, 2014). The average standard deviation reported for $^{176}Hf/^{177}Hf$ ratios from the GEMOC Key Center in this study was 0.000015, equating to ~0.5 epsilon units. Meanwhile, the average standard deviation reported for $^{176}Hf/^{177}Hf$ ratios from the ALC in this study was 0.000036, equating to ~1.3 epsilon units.

Previously, Holland et al. (2015) conducted an interlaboratory comparison and demonstrated that data from the ALC and GEMOC Key Centre reproduced the U-Pb and Lu-Hf isotopic results from the Elves Chasm Gneiss and the Tuna Creek pluton in Grand Canyon within 2-sigma uncertainty. Samples presented in this contribution were analyzed during the same laboratory sessions as those samples used for the interlaboratory

comparison discussed by Holland et al. (2015). Therefore, data reported in this paper can be presented and discussed as one dataset.

Hf-isotope data visualization and interpretation

Based on discussions in the literature of the complexities and potential pitfalls of interpreting time-integrated Hf-isotope data from zircon in terms of εHf values (Amelin et al., 2000; Ibanez-Mejia et al., 2015; Vervoort and Kemp, 2016), we prefer to visualize and interpret our data in terms of initial $^{176}Hf/^{177}Hf$ ratios. In short, there are two reasons for this approach. First, because the $^{176}Hf/^{177}Hf$ ratio of the reference for epsilon notation (BSE) evolves much faster than that of a given zircon, the εHf value assigned to a zircon grain is more sensitive to its apparent age than its Hf-isotope composition. This issue is particularly important for Hf-isotope analysis of Precambrian detrital zircon grains, in which Pb loss is nearly ubiquitous and can introduce significant uncertainties in apparent ages (Nemchin and Cawood, 2005). Second, secular changes in $^{176}Hf/^{177}Hf_{(i)}$ ratios of zircon from genetically related rocks can be attributed to distinct geologic processes depending on the magnitude of the change (see Figure 4 in Ibanez-Mejia et al., 2015). The magnitude of change in $^{176}Hf/^{177}Hf_{(i)}$ ratio through time is a function of an apparent $^{176}Lu/^{177}Hf$ ratio, which is equal to the slope of a line fit to data graphed in $^{176}Hf/^{177}Hf_{(i)}$ vs. time space. In this graphical representation, negative slopes (apparent $^{176}Lu/^{177}Hf < 0$) are caused by progressive mixing of more evolved material (e.g. older crust), horizontal slopes (apparent $^{176}Lu/^{177}Hf \approx 0$) represent Pb loss trajectories, and positive slopes (apparent $^{176}Lu/^{177}Hf > 0$) can represent either radiogenic ingrowth in a crustal reservoir (Payne et al., 2016), or progressive input from a highly radiogenic source (e.g. the depleted mantle) depending on the magnitude of the slope.

A time-integrated $^{176}Lu/^{177}Hf$ ratio, or slope, interpreted as the result of crustal reworking must reflect the isotopic composition of the crustal source. As subduction-related magmatism during orogenesis is likely to rework mafic to intermediate lower arc crust (Klepeis et al., 2003; Annen et al., 2006), an upper limit on apparent $^{176}Lu/^{177}Hf$ that could plausibly be the result of crustal reworking can be estimated from mafic rocks in modern arcs (Hawkesworth et al., 2010; Payne et al., 2016). Such a compilation shows that $^{176}Lu/^{177}Hf$ ratios in modern mafic arc rocks range from 0.017-0.039. Therefore, secular changes in $^{176}Hf/^{177}Hf_{(i)}$ ratios with apparent $^{176}Lu/^{177}Hf > \sim 0.04$ are likely the result of progressive mantle contributions to magmatism.

RESULTS

We report U-Pb-Hf isotope data for 18 samples; 12 plutonic and 6 detrital zircon samples. 5 plutonic samples were analyzed at the GEMOC Key Centre, and 7 plutonic samples were analyzed at the ALC. All six detrital zircon samples were analyzed at the ALC. Sample specific descriptions and complete analytical results and are available in Appendix 1 and 2 respectively. Sample locations are shown in Figure 1-2, and precise coordinates along with a summary of geochronologic results are given for detrital and plutonic samples in Tables 1-1 and 1-2 respectively.

Key to Fig. 2	Sample	Latitude and longitude (°N, °W)	n_{total}	MIN AGE (Ma)	MAX AGE(Ma)	# $GRAINS_R$	PEAK AGE (Ma)	# $GRAINS_P$	PEAK AGE (Ma)	# $GRAINS_P$
E	K14-HH-1	35.372979	83	1739	1932	65	1788	24	1863	20
		115.959602		2604	2652	6	1802	22	1912	3
							1819	17	2608	4
							1828	16	2617	3
							1849	18	2639	4
							1856	21		
A	K13-NOP-4	35.820257	67	1815	2042	54	1830	8	1995	8
		116.092069		2077	2105	2	1874	28	2090	3
				2457	2469	1	1908	11	2463	3
				2528	2534	2	1949	7	2533	3
							1974	9		
F	K13-NOP-1	35.808836	86	1802	1942	50	1827	9	1987	7
		116.101951		1959	1971	3	1860	23	1996	4
				1977	2014	9	1868	26	2002	4
				2066	2138	4	1910	8	2108	4
				2423	2430	2	1934	6	2427	3
							1965	4		
D	K13-IBEX-1	35.783471	86	1795	1926	64	1844	32	1979	4
		116.417697		1935	1939	1	1856	38	2395	3
				1964	1996	3	1881	17		
				2390	2403	2	1899	10		

B	K13-ASH-1	35.952497	76	1811	1897	20	1830	4	2502	3
		116.657093		1903	2013	16	1856	9	2543	3
				2313	2336	4	1878	12	2589	5
				2497	2559	4	1913	5	2658	5
				2581	2607	3	1942	6	2673	6
				2617	2622	0	1997	9	2685	5
				2637	2698	11	2317	3	2698	3
							2328	3		
C	K14-BLFG-2	36.892183	23	1797	1860	10	1827	9		
		116.886725		1868	1873	1				

NOTE: Detrital zircon geochronologic data summaries were generated with the Exel macro "AgePick" (available from www.geo.arizona.edu/alc). Data summarized above includes only 90-105% concordant ages. N_{total} gives the total number of 90-105% concordant ages for each sample. MIN and MAX AGE columns gives a range of ages that contains age probability from three or more overlapping (at 2σ) analyses, and # $GRAINS_R$ gives the number of grains that fall within that range. Similarly, PEAK AGE gives the maximum in age probability that comprises age-probability contributions (at 2σ) from 3 or more analyses, and # $GRAIN_P$ gives the number of grains that contribute to that peak.

Table 1-1. Detrital zircon geochronologic results.

Key to Fig. 2	Sample	Latitude and longitude (°N, °W)	Locality	Weighted Mean Age	MSWD	n_{wm}	Laboratory
1	K14-WB	36.031316 117.123341	World Beater Gneiss Complex - Paniment Mountains	1791 ± 15	0.8	18	ALC
2	13H-060	35.957821 116.643541	Ashford Canyon - Black Mountains	1784 ± 14	0.5	39	ALC
3	13H-080	35.968648 116.637203	Ashford Canyon - Black Mountains	1783 ± 16	0.9	52	ALC
4	K13-NOP-3	35.820257 116.092069	Southern Nopah Range	1782 ± 15	0.9	6	ALC
5	K14-HH-2	35.369155 115.962711	Halloran Hills	1774 ± 17	0.7	29	ALC
6	K06DV-37	35.911620 116.579650	Jubilee Pass	1773 ± 8	0.2	38	GEMOC
7	K06DV-31C	35.332460 115.893530	New York Mountains	1748 ± 12	0.7	33	GEMOC
8	K07-VIR-1	36.771460 113.91067	Virgin Mountains	1745 ± 4	1.2	22	GEMOC
9	K06DV-31A	35.333520 115.258750	New York Mountains	1732 ± 12	0.4	18	GEMOC
10	K14-BLFG-1	36.892273 116.887230	Bullfrog Hills	1716 ± 14	0.4	4	ALC
11	K06-DV-30	34.767510 115.124090	Piute Mountains	1691 ± 9	0.3	22	GEMOC
12	K13-BL-1	35.773491 116.526979	Southern Black Mountians	1691 ± 15	1.5	5	ALC

Table 1-2. Plutonic zircon geochronologic results

Results of detrital zircon geochronology and Hf-isotope analysis

The detrital zircon age spectra of all six metasedimentary samples analyzed in this study are dominated by peaks at ~1.83-1.88 Ga (Figure 1-3, Table 1-1). Only one sample (K14-HH-2) contained a robust population of >90% concordant zircon younger than 1.8 Ga (Figure 1-3, Table 1-1). Each sample also shows varied smaller peaks throughout the early Paleoproterozoic and late Archean; the total range of detrital zircon ages is from 3.25 to 1.75 Ga. These results are consistent with previous findings of Barth et al. (2000; 2001; 2009), Strickland (2012), and Shufeldt et al., (2010) who showed that the oldest micaceous gneisses in the Mojave province are dominated by 1.9-1.8 Ga detrital zircon ages, but yield ages as old as 3.3 Ga.

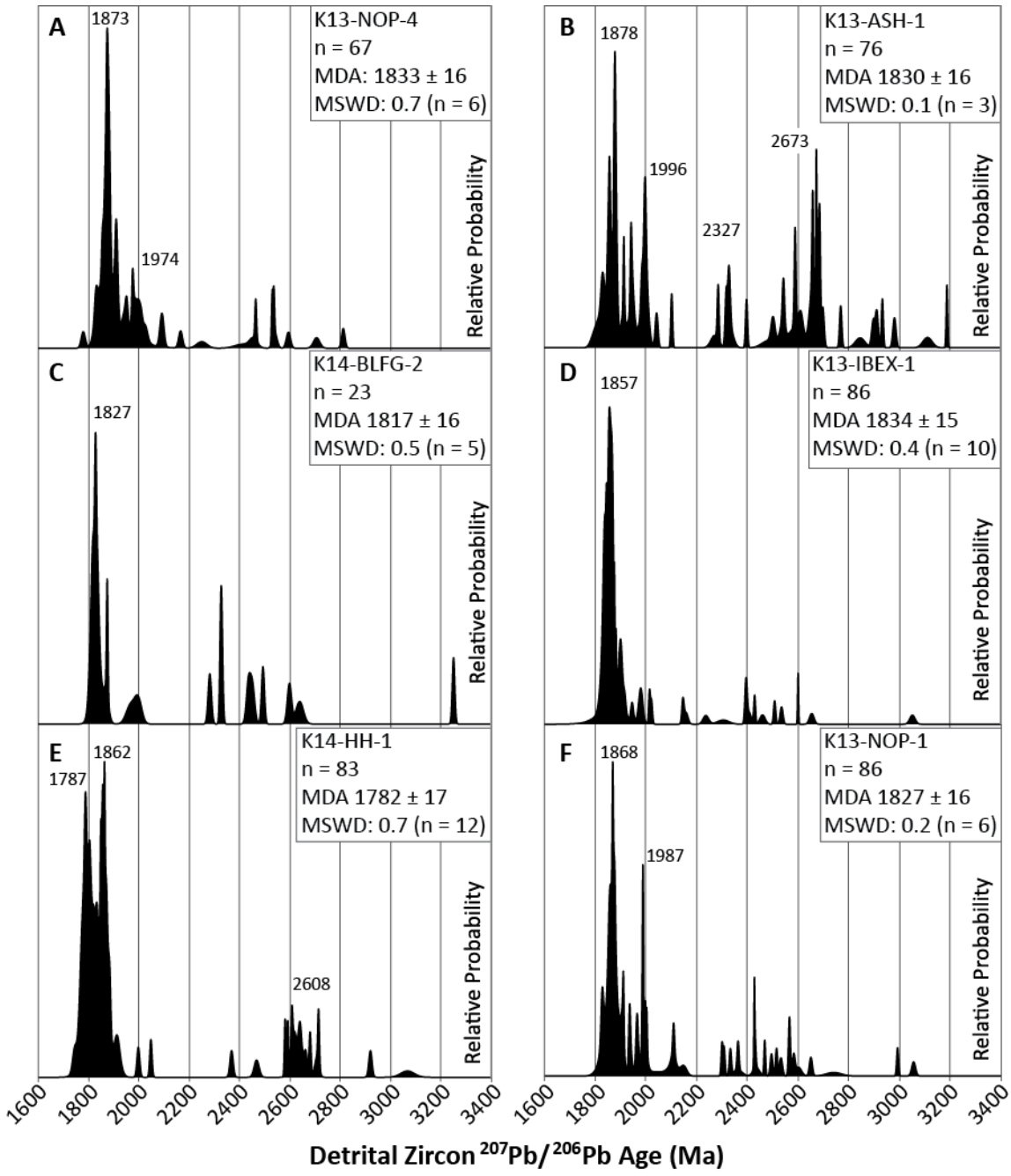

Figure 1-3. Probability density distributions (PDDs) showing>90% concordant 207Pb/206Pb detrital zircon ages (Ma) from Paleoproterozoic metasedimentary rocks in the Death Valley region sampled in this study. The number of zircon analyses displayed in the PDDs is shown below sample names. Maximum depositional ages (MDAs) are the weighted mean of >90% concordant ages from the youngest age peak with 2-sigma uncertainty, and the number of ages used in the calculation of weighted mean ages is indicated. Samples are keyed to Figure 2 with letters in the top left of each panel.

Hf-isotope data from detrital zircon grains yield a broad range of $^{176}Hf/^{177}Hf_{(t)}$ ranging from 0.281116 to 0.281904 ($\varepsilon_{Hf(t)}$ ~ -17 to +11) at 1.87 Ga (Figure 1-4), although most U-Pb-Hf analyses fall between $\varepsilon_{Hf(t)}$ of -5 to +5 at 1.87 Ga (>70%). A 2.0 Ga peak yielded a spread of $^{176}Hf/^{177}Hf_{(t)}$ ranging from 0.280980 to 0.281639 ($\varepsilon_{Hf\,(t)}$ ~ -8 to +5). The 1.79 Ga peak in sample K14-HH-2 yielded generally lower $^{176}Hf/^{177}Hf_{(t)}$ ratios than the ~1.87 Ga population, ranging from 0.281337 to 0.281673 ($\varepsilon_{Hf\,(t)}$ ~ -11 to +1). Neoarchean to earliest Paleoproterozoic 2.7-2.3 Ga detrital zircon grains yield a similar spread of $^{176}Hf/^{177}Hf_{(t)}$ ranging from 0.281418 to 0.280626 ($\varepsilon_{Hf\,(t)}$ ~ -17 to +7), with most grains yielding $\varepsilon_{Hf\,(t)}$ ranging from +5 to -5 at ~2.6 Ga. Finally, a minor component of Mesoarchean grains yield $^{176}Hf/^{177}Hf_{(t)}$ ranging from 0.280650 to 0.280983 ($\varepsilon_{Hf\,(t)}$ ~ -5 to +6). These data are similar to those presented by Wooden et al. (2012) from a garnet-bearing paragneiss in the New York Mountains, and the Vishnu Schist in Grand Canyon (Holland et al., 2015) (Figure 1-4).

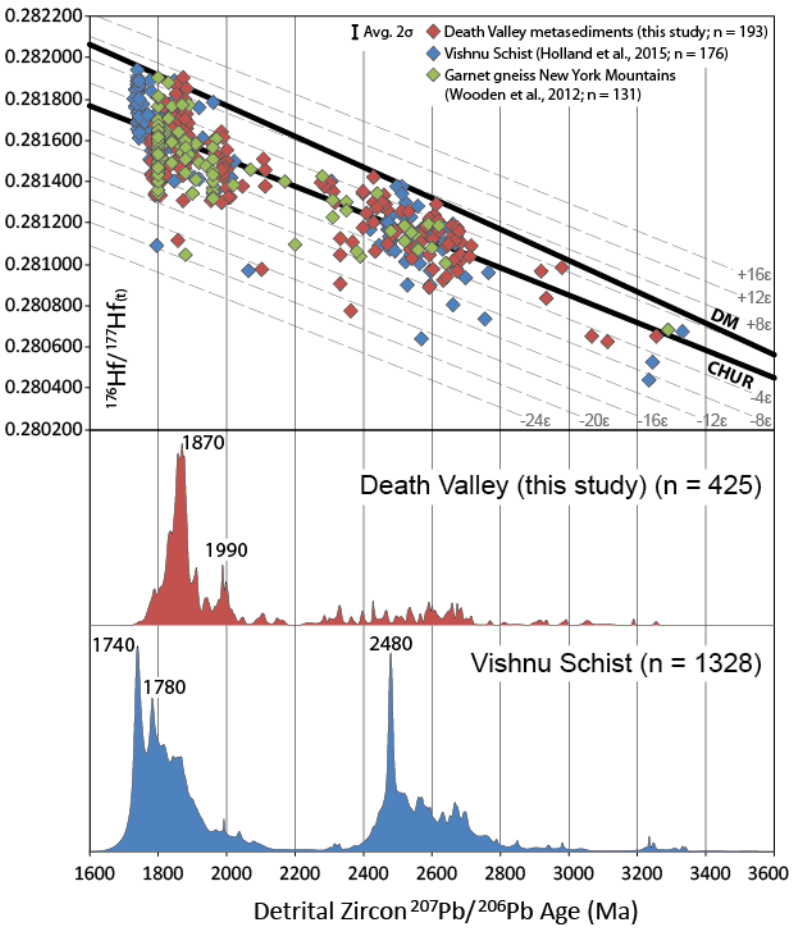

Figure 1-4. Comparison of U-Pb-Hf isotopic data from metasedimentary rocks of the Mojave province with the Vishnu Schist of Grand Canyon. A) 176Hf/177Hf(t) vs. 207Pb/206Pb age for detrital zircon grains. Only Hf isotope analyses from >90% concordant grains are plotted. Heavy black lines indicate the Chondritic Uniform Reservoir (CHUR) of Bouvier et al. (2008), and the depleted mantle (DM) evolution of Vervoort and Blichert-Toft (1999). Dashed gray lines show εHf values relative to CHUR in increments of ±4 ε units. The average 2-sigma uncertainty of Hf isotopic analyses of detrital zircon reported in this study is shown, and equates to approximately ±2 εHf units. B) PDD of >90% concordant 207Pb/206Pb detrital zircon ages from samples analyzed in this study. C) PDD of >90% concordant 207Pb/206Pb detrital zircon ages from the Vishnu Schist (Shufeldt et al., 2010; Holland et al., 2015).

Plutonic zircon U-Pb and Hf summary

Plutonic rocks in the Death Valley region sampled in this study range in age from 1.79-1.68 Ga (Table 2). Our dating results are presented in more detail in Appendix 1 and Supplementary Figure 1-1. In addition, zircon grains from several samples preserved inherited cores ranging in age from 2.6 to 1.8 Ga, similar to inherited zircon components

described elsewhere in the Mojave province (Barth et al., 2000; 2009). Inherited grains are discussed in detail in the supplementary material associated with this article.

The Hf-isotope compositions of plutonic zircon analyzed in this study display both intra- and inter-sample variations in $^{176}Hf/^{177}Hf_{(t)}$ (Figure 1-5). In some cases, the intra-sample variations equate to differences of nearly 10 epsilon units at the time of crystallization, consistent with variations reported by Wooden et al. (2012) from other Mojave province granitoids. The intra-sample spread in Hf-isotope composition is greater than can be accounted for by analytical uncertainties alone (Figure 1-5).

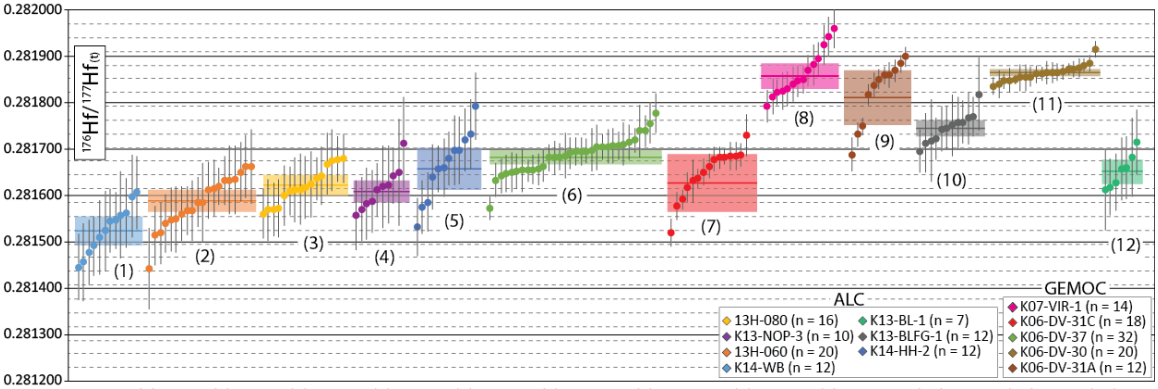

	(1)	(2)	(3)	(4)	(5)	(6)	(7)	(8)	(9)	(10)	(11)	(12)
Sample name	K14-WB	13H-060	13H-080	K13-NOP-3	K14-HH-2	K06-DV-37	K06-DV-31C	K07-VIR1	K06-DV-31A	K14-BLFG-1	K06-DV-30	K13-BL-1
Sample age (Ma)	1792	1784	1783	1782	1774	1773	1748	1745	1732	1716	1691	1691
$^{176}Hf/^{177}Hf_{(t)}$	0.281527	0.281589	0.281623	0.281609	0.281657	0.281682	0.281627	0.281858	0.281811	0.281745	0.281865	0.281676
± (95% conf.)	0.000034	0.000024	0.000023	0.000023	0.000045	0.000015	0.000023	0.0000	0.000059	0.000018	0.000008	0.000026
MSWD	1.8	2.6	2.0	1.14	4.9	6.1	87	6.7	68	1.2	3.8	1.8

Figure 1-5. Initial Hf-isotope composition of magmatic zircon from plutonic rocks of the Mojave province, with sample numbers keyed to Table 2. Gray dashed lines represent 100 ppm differences in Hf isotopic composition (equivalent to one εHf unit, or changing 176Hf/177Hf ratios in increments of 0.000028). Colored circles show 176Hf/177Hf(t) values from individual zircon, and their uncertainties expressed at the 2-sigma confidence level. Colored bars show the error-weighted mean 176Hf/177Hf(t) values and uncertainty for each sample. Below, data are summarized with sample names corresponding to colored symbols, U-Pb crystallization ages, the weighted mean of 176Hf/177Hf(t) values, weighted mean age, uncertainty, and mean squares weighted deviation (MSWD) determined by the Isoplot macro (Ludwing, 2003). A MSWD >>1 indicates that the variation about the mean is greater than can be accounted for by analytical uncertainties alone.

DISCUSSION

Regional correlations in detrital zircon provenance

Detrital zircon from the Paleoproterozoic metasedimentary rocks analyzed in this study have age populations similar to those of the Vishnu Schist (Figure 1-6) (Shufeldt et al., 2010; Holland et al., 2015). In addition, age data from detrital-zircon cores from paragneisses in the Ivanpah Mountains were noted by Strickland et al. (2013) to resemble those of the Vishnu Schist. Recently, Spencer et al. (2016) reported a detrital-zircon age population from a metasandstone in Jerome Canyon with an age distribution nearly identical to that of the Vishnu Schist, and proposed that the entire region from Jerome Canyon to Grand Canyon, and correlative units in the Hualapai block (Karlstrom and Bowring, 1993) comprise a single tectonostratigraphic terrane. This proposition is supported by a new sample of mica schist of interpreted sedimentary origin from the Hualapai Mountains that yields a detrital-zircon age and Hf-isotope signature comparable to those of the Grand Canyon and Mojave province metasedimentary rocks (Figure 1-6) (Doe, 2014).

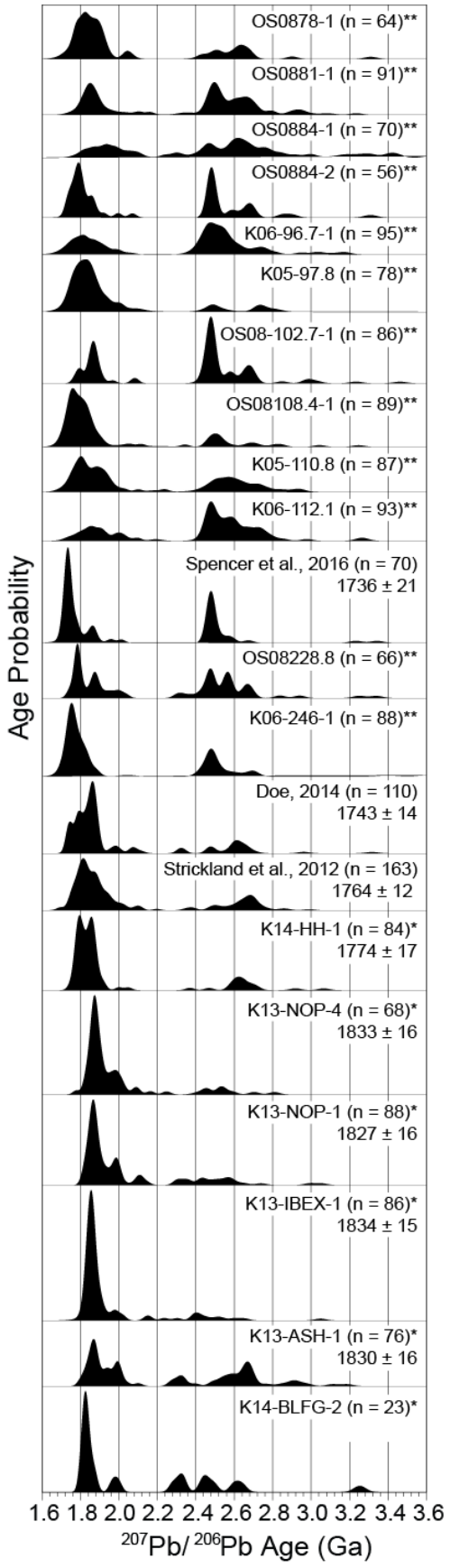
OS0878-1 (n = 64)**
OS0881-1 (n = 91)**
OS0884-1 (n = 70)**
OS0884-2 (n = 56)**
K06-96.7-1 (n = 95)**
K05-97.8 (n = 78)**
OS08-102.7-1 (n = 86)**
OS08108.4-1 (n = 89)**
K05-110.8 (n = 87)**
K06-112.1 (n = 93)**
Spencer et al., 2016 (n = 70)
1736 ± 21
OS08228.8 (n = 66)**
K06-246-1 (n = 88)**
Doe, 2014 (n = 110)
1743 ± 14
Strickland et al., 2012 (n = 163)
1764 ± 12
K14-HH-1 (n = 84)*
1774 ± 17
K13-NOP-4 (n = 68)*
1833 ± 16
K13-NOP-1 (n = 88)*
1827 ± 16
K13-IBEX-1 (n = 86)*
1834 ± 15
K13-ASH-1 (n = 76)*
1830 ± 16
K14-BLFG-2 (n = 23)*
Age Probability
1.6 1.8 2.0 2.2 2.4 2.6 2.8 3.0 3.2 3.4 3.6
207Pb/ 206Pb Age (Ga)

Figure 1-6. PDDs of >90% concordant detrital-zircon ages from the Mojave province arranged by longitude; samples furthest to the west are plotted at the bottom. * = this study, ** = Shufeldt et al., 2010. Other sources of data are indicated in the figure. Cross cutting and maximum depositional age constraints discussed in the text are indicated below sample names and citations.

We suggest that metasedimentary rocks across the southern Mojave province were deposited in the same regionally extensive basin system, which we call the Vishnu basin. The detritus supplied to the Vishnu basin was derived from predominantly 2.0-1.8 and 2.7-2.4 Ga crust. Both detrital zircon populations display a broad range of $^{176}Hf^{177}Hf_{(t)}$ values (>10 epsilon units) indicating that the crust that provided the source of the Vishnu basin detritus was a mixture of juvenile and recycled crust (Figure 1-4). The sediments of the Vishnu basin are distinct from those deposited in parts of the Yavapai and Mazatzal provinces. Younger, ~1.7-1.65 Ga sediments in the Yavapai and Mazatzal provinces are characterized by strongly unimodal detrital zircon ages that reflect the age of the basement upon which they were deposited (Jones et al., 2009; 2011; Doe, 2014; Daniel et al., 2013). Available Hf-isotope data from detrital zircon grains in Yavapai province metasedimentary rocks indicates that they are also more isotopically juvenile in nature (Doe, 2014; Bickford et al., 2008). The differences in detrital zircon age populations and Hf-isotope compositions suggest that the Vishnu basin system was separated in both time and space from the basins of the Yavapai and Mazatzal provinces.

Timing of deposition in the Vishnu basin

Determining the timing of deposition of metasedimentary rocks across the Mojave province is important for understanding the history and tectonic significance of the Vishnu basin. Previous field and geochronologic studies have shown that metasedimentary schists and gneisses are older than associated plutonic rocks (Wooden and Miller, 1991; Ilg et al., 1996; Hawkins et al., 1996; Barth et al., 2000; Duebendorfer

et al., 2001; Barth et al., 2009). Thus, the timing of deposition of Vishnu basin sediments is best constrained by the plutonic rocks that cross cut them. However, some of the metasedimentary rocks sampled in this study had contacts that were not exposed, or were ambiguous due to tectonic interleaving. Therefore, we compare maximum depositional ages from our detrital zircon geochronologic results to a compilation of crystallization ages from plutonic rocks that intrude metasedimentary schists and gneisses across the Mojave province.

It has been suggested that the most statistically robust estimate of a maximum depositional age from detrital zircon geochronologic data is determined by a weighted mean of the youngest cluster of ages that overlap within 2-sigma uncertainty (Dickinson and Gehrels, 2009). However, discordance in detrital zircon populations can easily compromise the significance of age clustering if there has been ancient Pb loss (Gehrels, 2012). Proterozoic plutonic rocks of the Mojave province yield discordia arrays with late Paleozoic to Mesozoic lower intercepts (Barth et al., 2000; 2009), which requires careful consideration of the significance of discordant detrital zircon ages. Thus, we calculated maximum depositional ages by taking the weighted mean of the youngest cluster (≥3) of >90% concordant ages that overlap at 2-sigma uncertainty after Dickinson and Gehrels (2009) (Figure 1-3). Our results yielded maximum depositional ages that range from 1834 ± 15 to 1782 ± 17 Ma (Figure 1-3).

Maximum depositional ages and cross cutting relationships show that sedimentation and magmatism in the Mojave province began prior to ~1.79 Ga, and continued until ~1.74 Ga, and proceeded from west to east (present coordinates) (Figure 1-7). Specifically, samples with detrital zircon populations characteristic of the Vishnu

basin have minimum depositional ages constrained by cross cutting plutonic rocks that young from west to east. Barth et al. (2009) state that paragneisses at Baldwin Lake, CA with detrital zircon cores ranging in age from 1860-2700 Ma are locally intruded by ~1770 Ma orthogneisses. Our sample of quartzite from the Halloran Hills, CA (K14-HH-1) is intruded by an augen gneiss (K14-HH-2) dated at 1774 ± 17 Ma (Table 2). Paragneisses in the Ivanpah Mountains are intruded by a suite of plutonic rocks as old as ~1760 Ma (Strickland et al., 2013). Deposition of the Vishnu Schist in Grand Canyon is constrained by interlayered 1750 ± 2 and 1740 ± 1 Ma metavolcanics rocks (Hawkins et al., 1996; Ilg et al., 1996). Finally, the metasandstone in Jerome Canyon with Vishnu Schist-like detrital zircon populations is intruded by the 1736 ± 21 Ma Williamson Valley granodiorite (Spencer et al., 2016).

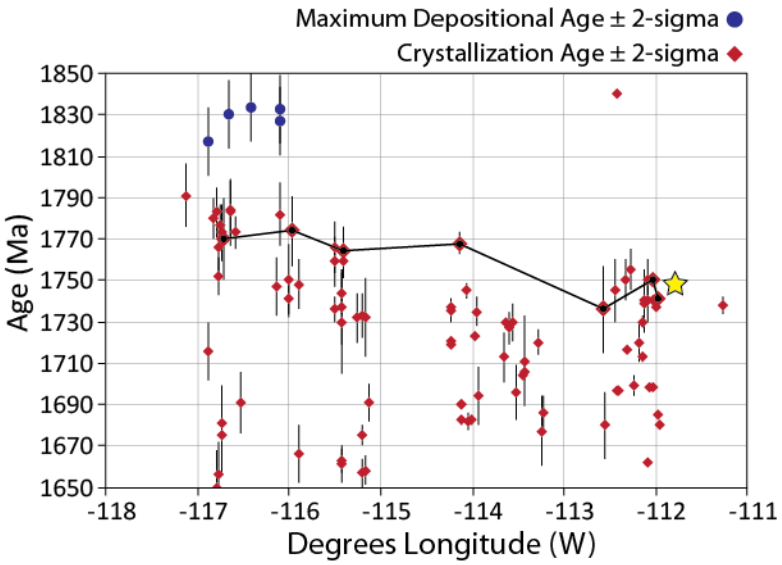

Figure 1-7. Geochronologic compilation of Paleoproterozoic igneous rocks from the Mojave province. Sources of data are from Figure 2. Plutonic rocks that constrain deposition of Vishnu basin sediments via cross cutting relationships are linked with a solid black line. Star is direct age of the Vishnu Schist of Grand Canyon (Hawkins et al., 1996).

Hf isotopic composition of Mojave province plutonic zircon

A striking feature of Mojave province plutonic rocks is the intra-sample variation in Hf- isotope composition (Figure 1-5) (Wooden et al., 2012; this study). Vertical arrays in isotopic space are typically interpreted as reflecting mixing between components with distinct Hf-isotope compositions. A variety of mechanisms have been proposed to explain these kinds of intra-sample variations in Hf-isotope composition. Mechanisms include: direct mixing of juvenile asthenospheric mantle melts with crustally-derived melts (Shaw and Flood, 2009), mixing between mantle-derived basaltic underplated material with crustal melts (Griffin et al., 2002), or mixing of fractionated melts from mantle-derived basalt with crustal melts (Kemp et al., 2007). Alternatively, chemical and isotopic heterogeneities may be inherited only from the crustal magma source (Kurhila et al., 2010; Villaros et al., 2012; Clemens and Stevens, 2012), and mantle melts provide only the heat to drive crustal melting. Here, we examine the change in Hf-isotope composition of Mojave province plutonic rocks through time in order to gain insight into the melt-source region complexities for granitic melts of the Mojave province.

Hf-isotope composition of magmatic zircon through time and space

Hf-isotopic variability of 4-8 epsilon units is characteristic of most plutonic rocks of the Mojave province, regardless of age (Fig. 5; Wooden et al., 2012), and indicates that multiple sources contributed to magmatism throughout the evolution of the Mojave province. While this precludes the possibility of linking time-integrated changes in Hf-isotope composition to specific sources, the magnitude of change can still provide insight into whether crustal or mantle sources predominate through time.

As outlined in the Methods section, secular changes in Hf-isotope composition due to in situ radioactive decay are likely to plot on a $^{176}Hf^{177}Hf_{(i)}$ versus time graph within an envelope between slopes equivalent to $^{176}Lu/^{177}Hf$ ratios ranging from 0.017-0.039 (Figure 1-8). A compilation of all available Hf-isotope data from the Mojave province show that the change in average $^{176}Hf^{177}Hf_{(t)}$ between 1.79-1.73 Ga is far more rapid than is possible from closed system radiogenic ingrowth (Figure 1-8). A least squares regression through the arithmetic mean of $^{176}Hf^{177}Hf_{(t)}$ values from 1.79-1.73 Ga plutons yields an apparent $^{176}Lu/^{177}Hf$ ratio ≈ 0.3181 – an order of magnitude greater than is likely in crustal sources. The isotopic heterogeneity of Mojave province plutonic rocks indicates that this single $^{176}Lu/^{177}Hf$ ratio has no geologic meaning, however its magnitude suggests that the change in average Hf-isotope composition from ~1.79-1.73 Ga is the result of progressive depleted mantle input to granodioritic plutons emplaced into Mojave province crust.

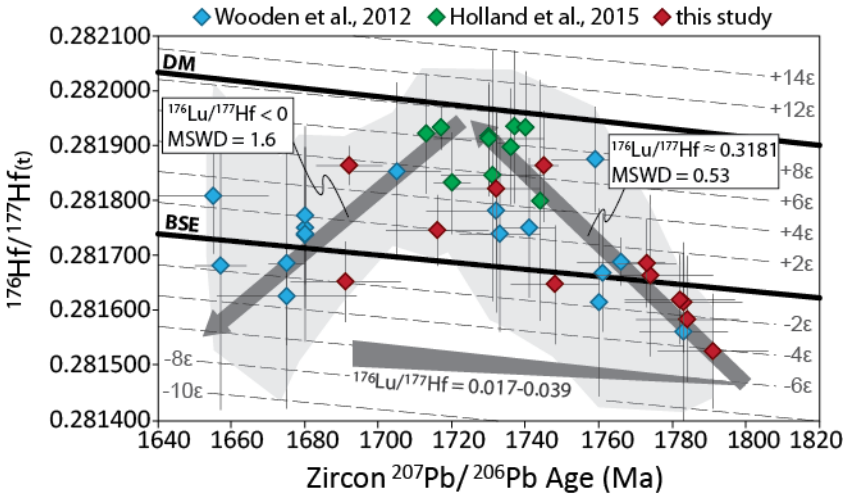

Figure 1-8. Summary of Paleoproterozoic U-Pb-Hf isotope data from the Mojave province. Diagrams and symbols as in Figure 4. The arithmetic mean and standard deviation (expressed as 2σ) of 176Hf/177Hf(i) values for individual plutons is plotted against crystallization age (± 2σ). Intrasample heterogeneity is shown by the light gray envelope around data points that encompasses the minima and maxima 176Hf/177Hf(i) from all samples. Dark gray arrows define least-squares regressions through mean values

from 1.79-1.73 Ga and 1.73-1.65 Ga. Dark gray wedge in the lower part of the plot indicates the trajectory of Hf-isotope composition expected from radiogenic ingrowth (see text).

The Hf-isotope composition of Mojave province plutonic rocks reaches the most radiogenic values about 1.74-1.72 Ga (Figure 1-8). In contrast, 1.72-1.66 Ga syn-to post-tectonic granitic plutonic rocks show a crude trend towards less radiogenic values (Figure 1-8) consistent with the likely crustal source for post 1.7 Ga plutons (Anderson et al., 1993). The timing of this change from increasing to decreasing $^{176}Hf^{177}Hf_{(t)}$ values roughly coincides with the onset of D_1 deformation during the Yavapai orogeny (Ilg et al., 1996; Duebendorfer et al., 2001), and a change to more potassic and HFSE enriched melts in the Mojave province (Barth et al., 2009) coincides with the onset of D_2 deformation. This isotopic excursion and change in melt compositions was likely the result of crustal thickening and melting during the Yavapai orogeny (Ilg et al., 1996; Barth et al., 2009).

Hf-isotope compositions become more radiogenic from west to east irrespective of age (Figure 1-9), however the significance of this trend is almost certainly different for early arc-related granodiorite plutons compared to syn-to-post orogenic granites. For example, $^{176}Hf^{177}Hf_{(t)}$ values of >1.73 plutonic rocks in the San Bernardino, Pinto, and Old Woman Mountains are nearly identical to those of 1.68-1.65 Ga plutons from the same localities (Wooden et al., 2012) (Figure 1-9). This is to be expected given the proposed crustal origin of syn-to-post orogenic granites, because their Hf-isotope compositions reflect only minor radiogenic ingrowth between ~1.73-1.68 Ga. In contrast, the spatial variation in early arc-related granodiorites may reflect variations in magmatic sources or processes during crustal formation. Lower $^{176}Hf^{177}Hf_{(t)}$ values in older and more western plutons may indicate that crustal melt components were more important

early in the Mojave province genesis, or that an older crustal component is more abundant in the western part of the province.

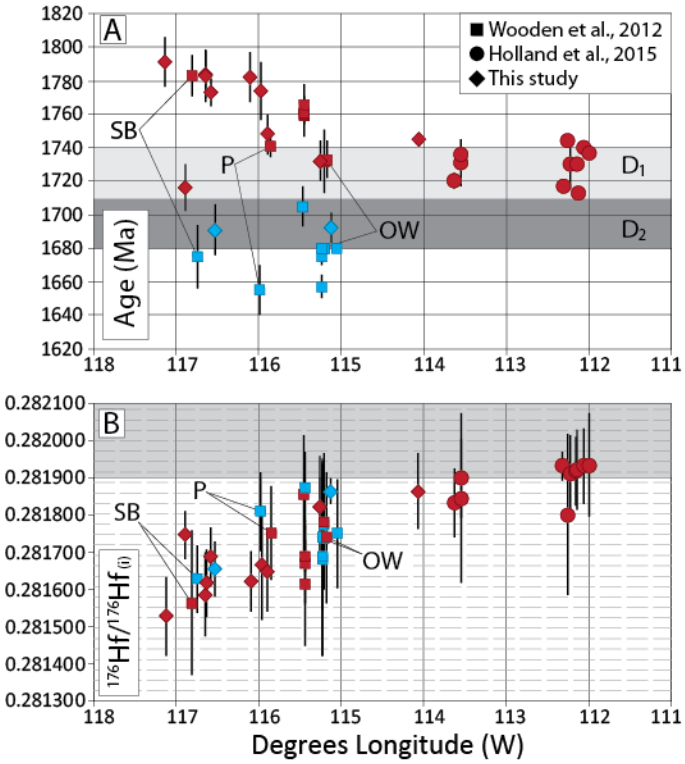

Figure 1-9. Summary of temporal and spatial variation in Hf-isotope composition of Mojave province plutons. Samples that are part of the syn-to-post orogenic (D2) suite of plutonic rocks are plotted in blue. A) Longitude is a crude approximation of the main northeast striking subvertical penetrative fabric (S2) in southwestern Laurentia. The longitude of a sample is plotted against crystallization ages (± 2σ) for plutonic samples with U-Pb-Hf isotope data. B) Arithmetic mean and standard deviation (2σ) 176Hf/177Hf(i) values for Mojave province plutons plotted against sample longitude. Gray dashed lines represent 100 ppm differences in Hf isotopic composition, as in figure 5. Gray field indicates the range of 176Hf/177Hf(i) values of the depleted mantle from 1.79-1.65 Ga. The resulting plot shows that plutonic rocks are younger and progressively more isotopically juvenile from west to east, perpendicular to the NE-strike of S2 foliation and shear zones in the orogen.

Inherited zircon

Inherited zircon cores or xenocrysts can provide a wealth of information about the melt source region of the plutons in which they are included, but interpretation of the origin of inherited components is often ambiguous (Corfu et al., 2003). We identified

inherited zircon cores or xenocrystic grains within seven of the twelve dated plutonic rocks in this study. Geochronologic results indicate that inherited cores and xenocrysts were most common in >1.73 Ga plutons. Inherited cores ranged in age from 1.8 to 2.6 Ga, but primarily fall in the 2.0-1.8 Ga age range, similar to the dominant population of detrital zircon ages obtained from the metasedimentary rocks that these plutons intruded (Figure 1-10). The Hf-isotope compositions of inherited cores and xenocrystic zircon grains are also similar to detrital zircon from the Vishnu basin (Figure 1-10).

The similarity of the detrital and inherited zircon age populations and Hf-isotope compositions suggests that the plutons sampled in this study either assimilated detrital zircon from Vishnu basin wallrocks, were derived in part from melting of Vishnu basin sediments, or were derived in part from metaigneous crust similar in age and Hf-isotope composition to that which provided detritus to the Vishnu basin.

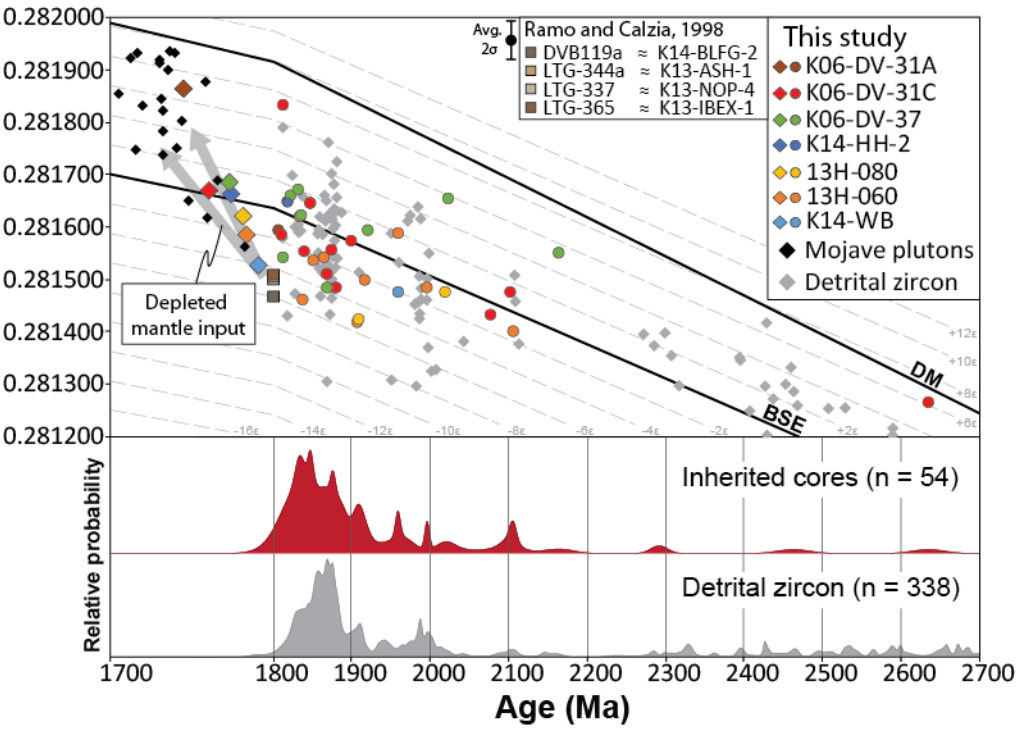

Figure 1-10. Summary of core and overgrowth U-Pb-Hf isotopic systematics compared to U-Pb-Hf data from detrital zircons. Colored diamonds represent the arithmetic mean

176Hf/177Hf(i) values from the main magmatic populations of zircon in plutonic rocks. Inherited zircon cores and xenocrysts are shown as colored circles, color coded to match the diamonds. Gray diamonds are U-Pb-Hf isotopic data from >90% concordant detrital zircons analyzed in this study. A summary of all >90% concordant ages from inherited cores or xenocrysts is shown as a PDD in red, and compared to the PDD of detrital zircon from Vishnu basin metasedimentary rocks, shown in gray. Bulk-rock Nd isotopic data from Ramo and Calzia (1998), projected onto Hf-isotope space based on the linear relationship defined by Vervoort et al. (2011) are shown as colored squares. The bulk-rock Nd-isotope data are more isotopically evolved than the average zircon Hf-isotope data from all Mojave province plutons. Gray arrows schematically show the depleted mantle contributions evident from the average change in 176Hf/177Hf(i) values through time (Figure 8). Thus, mixing of depleted mantle melts and partial melts of Vishnu basin metasedimentary rocks is a possible explanation for the evolved isotopic signature of the oldest Mojave province plutons. Black diamonds are Mojave province plutons without inherited zircon components (note change in scale to better show the increase in plutonic 176Hf/177Hf(i) values through time.

Origin of the Isotopically Evolved Mojave Province

Comparison between our new U-Pb-Hf data and bulk rock Sm-Nd isotope data from the same rocks (Ramo and Calzia, 1998) may provide additional insight into the source of inherited zircon cores and xenocrysts, and the nature of the evolved isotopic signature of the Mojave province.

Ramo and Calzia (1998) argued that the evolved isotopic signature of plutonic rocks in the Mojave province was introduced by assimilation of subducted sedimentary material based on a negative correlation between εNd values and aluminum saturation index (A/CNK). The aluminum saturation index is the molar ratio of Al_2O_3/Na_2O+K_2O+CaO, and has historically been used to distinguish granitoids with supracrustal sources (S-type) from those with infracrustal (I-type) sources (Chappell and White, 1974). However, major element geochemistry alone is not enough to conclude that a granite was derived from a supracrustal source (Chappell et al., 2012).

Further evidence for supracrustal involvement in the petrogenesis of Mojave province plutonic rocks can be found in a comparison between our new zircon Hf-isotope

data and bulk-rock Nd isotope data reported by Ramo and Calzia (1998). In our study, we sampled metasedimentary rocks from similar localities as Ramo and Calzia (1998). Samples K14-BLFG-2, K13-ASH-1, K13-NOP-4, and K13-IBEX-1 (this study) were taken from similar locations as samples DVB119a, LTG-344a, LTG-337, and LTG-365 respectively (Ramo and Calzia, 1998). Thus, we compared the bulk-rock Nd-isotope composition of metasedimentary rocks to plutonic zircon Hf-isotope data using the "initial" Terrestrial Array, a linear relationship between Nd and Hf isotopes defined by Vervoort et al. (2011). Ramo and Calzia (1998) did not present geochronologic data for their samples, and so presented all Nd-isotope data as εHf(at 1.7 Ga) values. Based on our regional geochronologic summary indicating Vishnu basin deposition prior to ~1.79 Ga (Figure 1-7), we recalculated the εNd(t) values of samples DVB119a, LTG-344a, LTG-337, and LTG-365 from εNd(at 1.7 Ga) to εNd(at 1.8 Ga). Our recalculation resulted in changes of ~1 εNd unit for each sample, from approximately -5 at 1.7 Ga to -4 at 1.8 Ga. When these values are projected onto Hf-isotope space using the "initial" Terrestrial Array, they equate to εHf(at 1.8 Ga) ≈ -5 (Figure 1-10).

The Nd-isotope data projected onto Hf-isotope space shows that the bulk-rock isotopic composition of Vishnu basin metasedimentary rocks is slightly more evolved than the average Hf-isotope composition of the oldest Mojave province plutonic rocks. Thus, partial melting of Vishnu basin metasedimentary rocks and mixing with juvenile depleted mantle melts in the lower crust could give rise to plutonic rocks with the isotopic variability, inherited zircon components, and major element geochemistry observed in the oldest Mojave province plutons. Lower crustal xenoliths in Tertiary igneous dikes from the Piute Mountains indicate that metasedimentary rocks with Pb and

Nd-isotope systematics identical to those of the Vishnu basin were present in the lower crust during the Paleoproterozoic (Hanchar et al., 1994). Thus, the origin of the characteristically evolved isotopic signature of Mojave province plutonic rocks may be rooted in the assimilation of Vishnu basin sediments

Alternatively, both metasedimentary rocks and plutonic zircons could have been derived from heterogeneous older crust involving a mix of 2.0-1.8 Ga and 2.7-2.4 Ga lithosphere. The Elves Chasm Gneiss in Grand Canyon, AZ provides direct evidence for the presence of pre-1.8 Ga igneous crust in the Mojave province (Hawkins et al., 1996). However, it differs from most of the rest of the Mojave province rocks in being isotopically juvenile at 1.84 Ga (Holland et al., 2015). Cryptic ~2.5 Ga lower crust was proposed as the source of inherited zircon cores and xenocrysts in Mojave province plutons west of the Crystal shear zone in Grand Canyon, AZ (Holland et al., 2015). Re-Os studies of mantle xenoliths from the Mojave province have yielded model ages ranging from 3.4-1.8 Ga (Lee et al., 2001; Armytage et al., 2014), which were interpreted to be related to contemporaneous juvenile crust formation. Thus, there is abundant evidence to suggest that the Mojave province includes lithospheric components with Archean origins.

Source of the Vishnu Basin and Implications for Supercontinent Reconstructions

Determining the source of detritus shed into the Vishnu basin may provide important constraints on viable models to explain the tectonic evolution of southwestern Laurentia, as well as Paleoproterozoic supercontinent reconstruction. This is particularly important for the Mojave province, as its distinct isotopic signature has made it a proposed piercing point in many supercontinent reconstructions (Borg and DePaolo,

1994; Karlstrom et al., 2001; Li et al., 2002; Goodge et al., 2008; Goodge and Fanning, 2016). Comparable Nd and Pb isotopic systematics from Proterozoic rocks and economic ore deposits in the Mojave province and the Gawler craton were proposed as evidence for continuation of the southern Laurentian accretionary margin by Karlstrom et al. (2001). Similarities between the Proterozoic tectonic histories of Laurentia and Australia (Betts et al., 2008; 2011) also include the detrital zircon age population of the Vishnu Schist (Shufeldt et al., 2010). Goodge and Fanning (2016) linked the ages of basement rocks in the Nimrod Range of East Antarctica to those recorded by detrital zircon in Mesoproterozoic to Neoproterozoic metasedimentary rocks in the Mojave province (Barth et al., 2009). They and others have interpreted the Gawler craton to have been joined with Archean/Paleoproterozoic terranes of East Antarctica in the Mawson continent during much of the Proterozoic (Oliver and Fanning, 1997; Payne et al., 2009; Aitken et al., 2016; Goodge and Fanning, 2016), with the Mawson continent adjacent to western Laurentia in the supercontinent Nuna (Borg and DePaolo, 1994; Goodge et al., 2001; Cawood and Korsch, 2008; Betts et al., 2008; 2011; Pisarevsky et al., 2014; Betts et al., 2016; Goodge and Fanning, 2016; Goodge et al., 2017).

Recent contributions have enhanced our understanding of the timing and kinematic evolution of Nuna by combining global paleomagnetic, stratigraphic, geochronological and metallogenic datasets (Eglington et al., 2009; Zhang et al., 2012; Pisarevsky et al., 2014; Perhsson et al., 2016). However, the timing of assembly of individual cratons and the paleogeography of the supercontinent are debated. Many models place Australian cratons adjacent to western Canada in a “proto-SWEAT” configuration for Nuna (Goodge et al., 2001; Betts et al., 2008; 2016) (Figure 1-11). Betts

et al. (2016) correlate the 1880-1840 Ma Wopmay and 1870-1850 Ma Barramundi orogens and interpret them to represent the "amalgamation of several arc and microcontinent terranes…between the larger continental masses of the Slave craton and proto-North Australia craton during Nuna assembly." In contrast, Pisarevsky et al. (2014) suggested that Australia and Laurentia may have been in close proximity, but that their final collision did not take place until the 1650-1600 Ma Racklan orogeny (Figure 1-11). These models the juxtaposition of Australian, Antarctic, and Laurentia cratonic blocks within a ~200 Ma time span, highlighting the need for improved Paleoproterozoic piercing points.

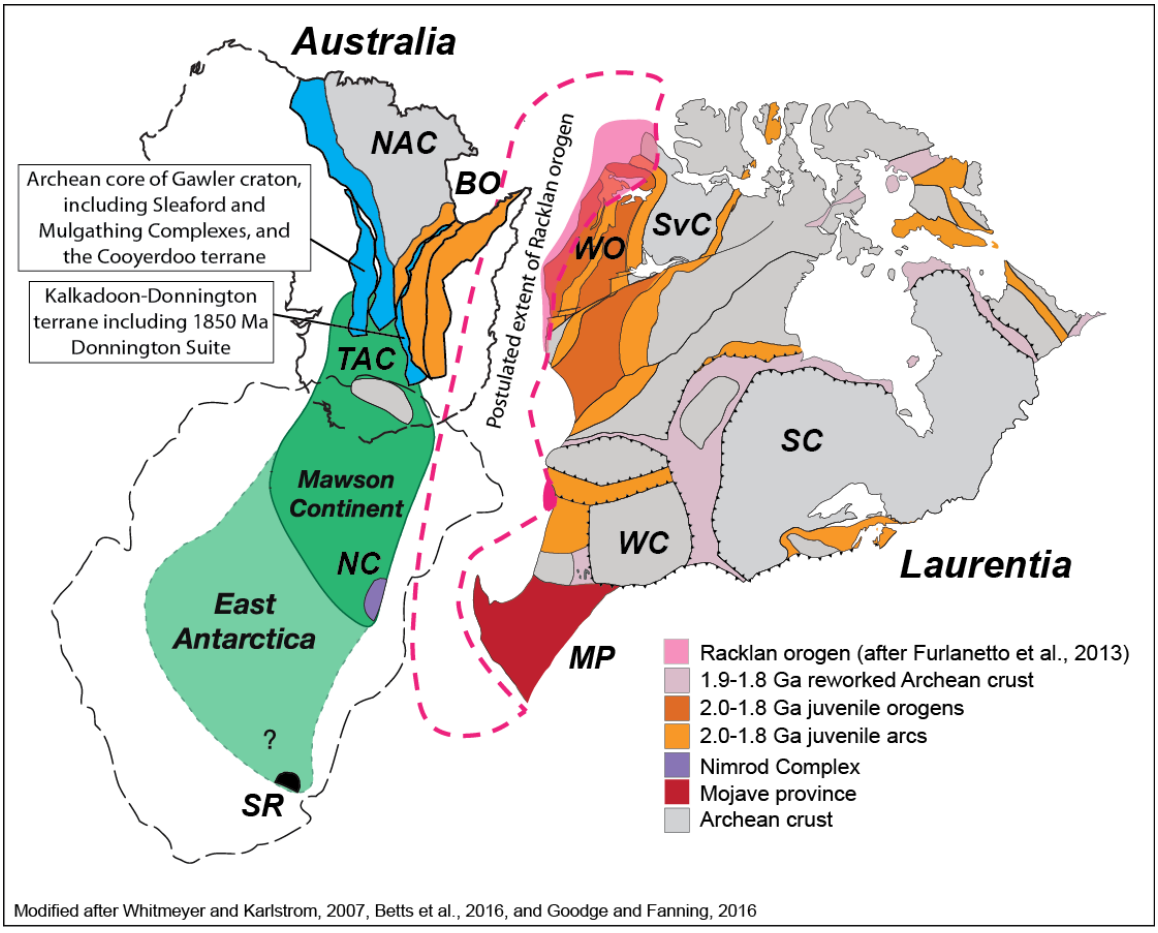

Figure 1-11. Possible plate reconstruction of Australia, Antarctica (Mawson), and Laurentia in Nuna from 1.8-1.6 Ga. Australian cratons are shown as depicted in Betts et

al., 2016. BO = Barramundi Orogen, MP = Mojave province, NC = Nimrod Complex, NAC = North Australian Craton, SR = Shackleton Range, SvC = Slave Craton, SC = Superior Craton, TA = Terre Adélie Craton, WO = Wopmay Orogen, WC = Wyoming Craton.

Our new U-Pb and LuHf isotope data from the Vishnu basin provide an additional test for Mawson-Laurentia reconstructions. A temporal and isotopic framework highlighting major crust-forming events in the Mawson continent is outlined by a compilation of >600 U-Pb and Hf-isotope analyses of detrital zircon grains from modern and ancient drainages in the Gawler craton (Belousova et al., 2009), zircon ages from crystalline basement of the Nimrod Complex (Fanning and Goodge, 1999; Goodge et al., 2001; Goodge and Fanning, 2016; Goodge et al., 2017), whole-rock Sm-Nd model ages from Phanerozoic plutonic rocks in the Transantarctic Mountains (Borg et al., 1990; Borg and DePaolo, 1994), and detrital zircon ages from Proterozoic to modern deposits in Antarctica compiled by Mulder et al. (2015). This temporal and isotopic profile of the Mawson continent shows remarkable agreement in major age populations and Hf-isotope composition when compared to a compilation of all detrital zircon U-Pb-Hf isotope data from the Vishnu basin (Figure 1-12).

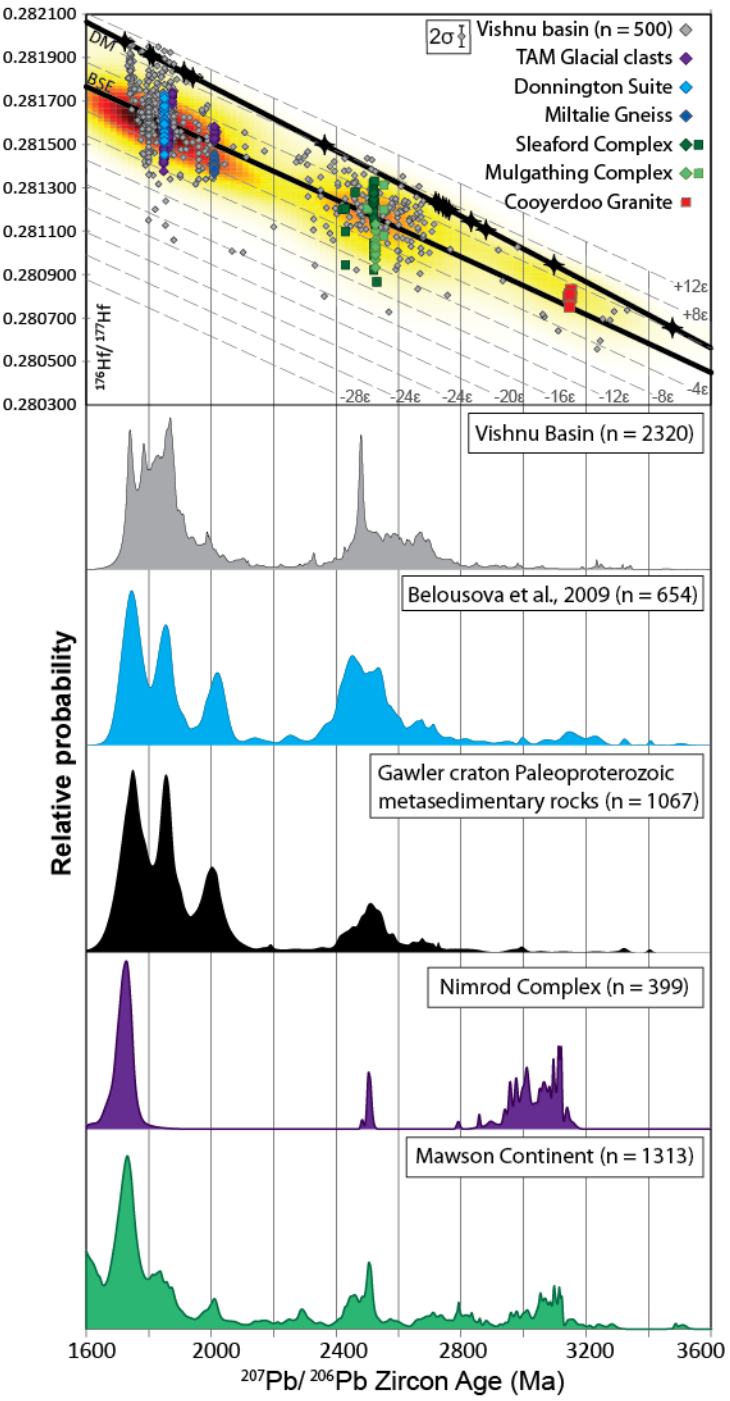

Figure 1-12. Comparison of U-Pb-Hf isotopic data from detrital grains from the Vishnu basin with the Gawler craton, and the Mawson continent. Diagram and symbols as in Figure 4. Gray diamonds are U-Pb-Hf isotope data from >90% concordant detrital zircon grains from the Vishnu basin. Black stars on the Depleted Mantle array are Nd model ages from Phanerozoic rocks in the Transantarctic Mountains (Borg et al., 1990; Borg and DePaolo, 1994). U-Pb-Hf zircon data from the Gawler craton (n = 654) (Belousoava et al., 2009) are projected onto a 2D kernel density estimate heat map of U-Pb-Hf isotope data where darker red sections represent a higher density of data points than light yellow

sections. Colored symbols correspond to bedrock units from the Gawler craton discussed in the text. Diamonds are Hf-isotope measurements from zircon, and squares are Nd-isotope data that have been projected onto Hf-isotope space using the "initial" Terrestrial Array of Vervoort et al., 2011. Below are PDD's of detrital zircon data discussed in the text. From top to bottom, they include detrital zircon from modern drainages in the Gawler craton (Belousova et al., 2009), a compilation of detrital zircon age distributions of Paleoproterozoic metasedimentary rocks from the Gawler craton (Jagodzinski, 2005; Howard et al., 2009; 2011; Szpunar et al., 2011), bedrock from the Nimrod complex (Goodge and Fanning, 1999; 2016; Goodge et al., 2001), and detrital zircon from the Mawson continent as compiled by Mulder et al. (2015).

Specific rock units from the Mawson continent can be linked to the detrital zircon age populations in the Vishnu basin. The prominent ~1.85 Ga peak in the Vishnu basin can be linked to the 1850 Ma Donnington Suite in the Gawler craton (Reid et al., 2008), and glacial clasts from the Transantarctic Mountains of the same age (Goodge et al., 2017). The 2.0 Ga zircon population can be linked to the 2020-2000 Ma Miltalie Gneiss in the Gawler craton (Howard et al., 2009), and additional glacial clasts from the Transantarctic Mountains (Goodge et al., 2017) (Figure 1-12). The 2.7-2.4 Ga detrital zircon age population in the Vishnu basin is comparable with the ~2.55-2.44 Ga Sleaford and Mulgathing complexes (Hand et al., 2007). Specific rock units from the Sleaford Complex that fall in this age range and have similar isotopic character include the 2540-2520 Ma Hall Bay Volcanics, the 2460 Ma Kiana Granite (Swain et al., 2005), the 2550-2520 Ma Coulta Granodiorite (Howard et al., 2009), the 2520-2515 Ma Carpa Granite, and 2420 Ma Minbrie Gneiss (Wade and Curtis, 2017). Rocks from the Mulgathing Complex include the 2553 Ma Devil's Playground Volcanics, the 2499 Ma Glenloth Granite (Swain et al., 2005), and a 2526 Ma orthogneiss from GOMA Drill Hole 4 (Reid et al., 2014), (Figure 1-12).

Paleo-to-Mesoarchean detrital zircon grains are present but not abundant in the Vishnu basin. Our compilation of detrital zircon grains from the Mojave province

contains only 55 (3%) Mesoarchean, and 29 (1%) Paleoarchean ages. While Mesoarchean crust of roughly the same age and isotopic composition of >90% concordant Vishnu basin detrital zircon grains is present in the Gawler craton (Fraser et al., 2010) and Nimrod Complex (Goodge and Fanning, 2016), a compilation of detrital zircon data from ~1.8-1.7 Ga metasedimentary rocks in the Gawler craton also lacks a prominent Paleo-to-Mesoarchean population (Figure 1-12). Thus, if the Mawson continent was the source of Vishnu basin detritus, it is possible that Paleo-to-Mesoarchean crust was present, but poorly exposed such that it did not provide substantial detritus to the Vishnu basin or other coeval basins in the Gawler craton.

Detrital zircon age and Hf-isotope composition strongly support a Mawson continent source for the detritus of the Vishnu basin. This interpretation has significant implications for the timing of the assembly of Australia, Antarctica, and Laurentia in the supercontinent Nuna, and favors models that posit Nuna accretion by ~1.8 Ga (Betts et al., 2016). If our interpretation is correct, then the deposition of the Vishnu basin marks the beginning of a long-term (~1.0 Ga) association between Australia, Antarctica, and Laurentia beginning in the Paleoproterozoic, continuing through the Mesoproterozoic (Goodge et al., 2008; Doe et al., 2013; Mulder et al., 2015), and persisting until the final breakup of Rodinia in the Neoproterozoic (Li et al., 2008).

Plate Tectonic Models for the Mojave Province

The evolution of the Mojave province, and differences between the Mojave and Yavapai provinces, have been explained in terms of subduction-related collision of multiple arc terranes with distinct basement characteristics (Barth et al., 2000; Duebendorfer et al., 2001; Whitmeyer and Karlstrom, 2007; Duebendorfer, 2015).

Additional interpretations of the province boundary have involved an isotopically mixed zone resulting from closure of a back arc rift basin (Duebendorfer, 2006; 2015) and/or an imbricated middle crustal suture zone (Holland et al., 2015).

Any viable tectonic model should explain the new isotopic synthesis presented in this paper as well as other geologic constraints. Figure 1-13 presents alternative plate tectonic models for the formation and evolution of continental lithosphere in the Mojave province. These are not intended as the only competing models, but rather to depict a spectrum of plate tectonic interactions involved in plate tectonic evolution and crustal growth of southwestern Laurentia. Model 1 builds on the concept of crustal provinces (Whitmeyer and Karlstrom, 2007), emphasizes the *differences* in Hf-isotope signatures between provinces, and attributes these differences to subduction related juxtaposition of terranes with distinct isotope signatures. Model 2 emphasizes the temporal and spatial *changes* in Hf-isotope composition and attributes them to processes active primarily on the upper plate of a single subduction zone. This discussion highlights the continued uncertainty in developing even first-order plate tectonic evolutionary models, such as uncertainty about the orientation and polarity of subduction zones and any sutures (Duebendorfer, 2015).

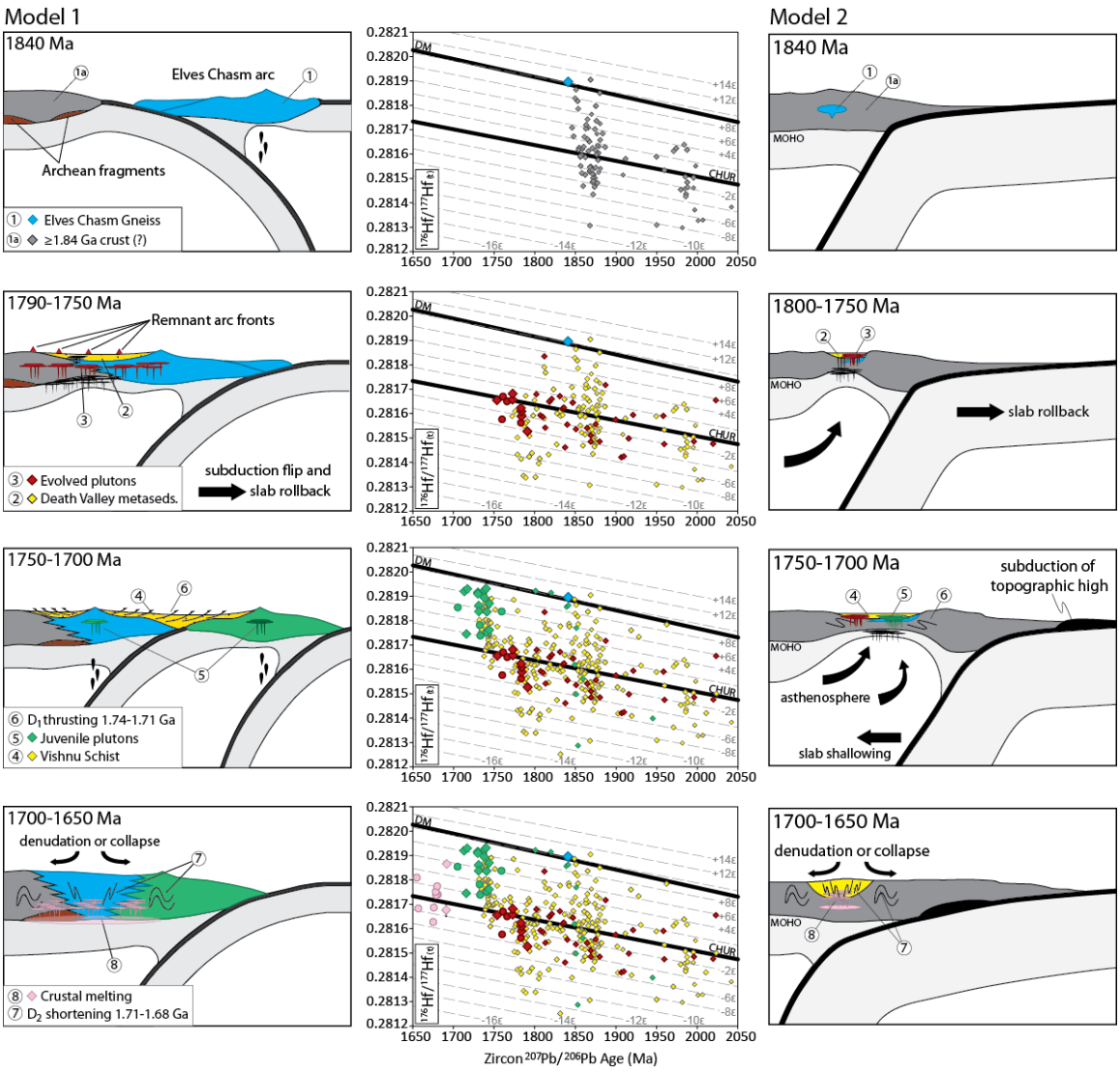

Figure 1-13. Possible tectonic models for the Mojave province. Model 1 portrays terrane accretion of a juvenile 1.84 arc (Elves Chasm pluton) to Mojave ~ 1.8 Ga followed by accretion of the juvenile Yavapai province ~ 1.75- 1.70 Ga. Model 2 portrays a single subduction system that evolves through slab roll back, back arc extension, and instigation of the Yavapai orogeny by arrival of an oceanic plateau into the subduction system. Diamonds represent data from this study and Holland et al. (2015), circles are data from Wooden et al. (2012).

Model 1: collision and accretion across subduction zones of three separate crustal blocks discriminated based on their age and Hf-isotope composition: a Mojave microcontinent, the 1840 Ma Elves Chasm arc, and the 1750-1710 Ma Yavapai arc (Figure 1-13). At 1840 Ma, eastward dipping subduction below the Elves Chasm block

would produce a juvenile arc, explain the apparent absence of >1790 Ma plutons in the western Mojave province, and result in convergence of the Mojave microcontinent and Elves Chasm arc. By 1790 Ma, the two terranes have collided, and the subduction zone has flipped, jumped east, and dips west to explain 1790-1750 Ma plutons in the Mojave province. Detritus from Mojave crust supplies western parts of the Vishnu basin in a backarc or interarc setting. The Eastward migration of magmatism from 1.79-1.74 Ga (Figure 1-7) suggests eastward rollback of the lower plate. The trend towards more radiogenic Hf-isotope compositions eastwards and through time is interpreted as a decreasing contribution from older Mojave microplate crust, and an increasing contribution from the depleted mantle due to slab rollback (Figure 1-9). Juvenile 1.74-1.71 Ga plutons in the Grand Canyon area are interpreted to have formed on a separate island arc from 1750-1710 Ma (Holland et al., 2015). Convergence between the composite Mojave-Elves Chasm terrane and the Yavapai arc was progressive event from 1750-1710 (D_1) and may have involved complex subduction geometries (e.g. Jessup et al., 2005). The Vishnu Schist in Grand Canyon was deposited from 1750-1740 Ma in interarc or forearc setting and overlapped onto stitched and thickening Mojave and Yavapai crust (Holland et al., 2015). Peak deformation and crustal thickening occurred from 1700-1680 Ma (D_2) during the Yavapai orogeny (Ilg et al., 1996). Synchronously with, and outlasting peak D_2 deformation, a suite of granites enriched in potassium and high field strength elements was emplaced across all three crustal blocks (Anderson et al., 1993; Ilg et al., 1996; Duebendorfer et al., 2001; Barth et al., 2009). This late phase of plutonism has been interpreted as the result of crustal melting after orogenic thickening

(Ilg et al., 1996; Barth et al., 2009) and shows a negative shift in Hf-isotope composition due to crustal melting in response to thickening from ~1.73-1.65 Ga (Figure 1-13).

Model 2: extensional accretionary orogeny involving slab rollback of a single subduction system with opening and closing of an upper plate back arc basin (Collins, 2002b; Collins and Richards, 2008; Kemp et al., 2009). More specifically, Model 2 is based on the similarities between the spatial, temporal, geochemical, and isotopic changes observed in the Mojave province, and those described in the Tasmanide orogenic system (Kemp et al., 2009). In the Tasmanides, successive episodes of back-arc extension and closure result in predictable geochemical and isotopic changes in plutonism: 1) mantle flux with a slab-derived component drives melting of turbidites during back-arc extension and produces isotopically evolved peraluminous (S-type) granites (Collins and Richards, 2008), 2) melts become increasingly more isotopically juvenile as slab rollback causes the arc to retreat, the metasedimentary contribution wanes, and asthenospheric contributions increase due to progressive thinning of back-arc crust (Kemp et al., 2009), and 3) a transition to high-Fe/Mg and REE-enriched (A-type) magmatism (Collins et al., 1982) emplaced after contractional deformation associated with compression and subsequent thickening of the arc (Kemp et al., 2009).

In the Mojave province, metasedimentary schists and gneisses of the Vishnu basin were deposited at least in part on an older arc terrane (Ilg et al., 1996), and possibly on ocean crust (Barth et al., 2009). Upper plate extension of older arc crust could accommodate deposition of the Vishnu basin turbidites in a back arc setting. Detrital zircon from the Vishnu basin suggest that this older crust may have been part of the Mawson continent. Early arc plutons are isotopically evolved due recycling of Vishnu

basin sediments and/or older crust (Figure 1-13). As slab rollback continues to extend the back-arc, plutonic rocks become progressively more isotopically juvenile through space and time (Figure 1-9). Juvenile arc plutons are typified by 1.74-1.71 Ga granodiorite plutons that intrude the Vishnu Schist in the Grand Canyon (Holland et al., 2015). This trend towards more juvenile melts is evident in all 1.79-1.73 Ga Mojave province plutons (Figure 1-8), and is mimicked in detrital zircon from Death Valley metasedimentary rocks, and the Vishnu Schist (Figure 1-13). Back-arc extension reached its maximum by ~1.75 Ga, and closure began by 1.74 Ga as evident in the development of the shallow S_1 fabric attributed to west-vergent thrusting in the Cerbat Mountains (Duebendorfer et al., 2001), and continued development of S_1 until as late as 1.71 Ga in the Grand Wash Cliffs (Albin and Karlstrom, 1991) and the Grand Canyon (Ilg et al., 1996). Syn-to-post tectonic granites are as in Model 1. When considered with the isotopic trends observed throughout the Mojave province, this late stage plutonism may be analogous to the third phase of an orogenic cycle that resembles the tripartite association of S-type, I-type, and A-type granites described in the Tasmanide orogenic system (Collins and Richards, 2008; Kemp et al., 2009).

CONCLUSIONS

U-Pb and Lu-Hf geochronologic analysis of zircon from Paleoproterozoic metasedimentary and plutonic rocks across the Mojave crustal province provide insights into lithospheric growth in southwestern Laurentia. We propose the existence of a regionally extensive sedimentary basin composed dominantly of turbidites and other immature clastic sedimentary rocks, which we name the Vishnu basin. The Vishnu basin received isotopically evolved detritus from a 2.0-1.8 and 2.7-2.4 Ga cratonic source,

which may have been the Mawson continent. Maximum depositional ages and cross cutting relationships suggest that the Vishnu basin was deposited between 1.79-1.74 Ga, and deposition proceeded from west to east. Arc related plutonic rocks that intrude the Vishnu basin from 1.79-1.71 Ga show a systematic change in Hf-isotope composition through time and space. The oldest plutons in the western Mojave province have the most isotopically evolved signatures, and inherited zircon cores and xenocrysts that suggest they were derived in part from Vishnu basin sediments or cryptic crust similar to the source of this detritus. The Hf-isotope composition of plutonic rocks becomes more radiogenic from west to east and from old to young. The apparent $^{176}Lu/^{177}Hf$ calculated from the change in initial Hf-isotope composition of plutons through time is an order of magnitude greater than is likely from radiogenic ingrowth in a crustal reservoir, and requires additions from the depleted mantle. Initial Hf-isotope compositions of syn-to-post orogenic crustally derived granites show a departure towards more evolved Hf-isotope compositions after 1.73-1.70 Ga, likely due to crustal thickening and melting during the Yavapai orogeny. Similarity of Mojave rocks with those of the Mawson craton favor assembly of Nuna ~1.85 Ga rather than 1.65 Ga. A spectrum of tectonic processes and models remain viable, ranging from the amalgamation of multiple arc terranes, to slab roll back and arc retreat of a single subduction system.

ACKNOWLEDGMENTS

We thank the National Science Foundation for funding through grant EAR-1145247 to Karl Karlstrom and George Gehrels, and grant EAR-1649254 for support of the Arizona LaserChron Center. This is contribution XXX from the ARC Centre of Excellence for Core to Crust Fluid Systems (http://www.ccfs.mq.edu.au) and XXX in the

GEMOC Key Centre (http://www.gemoc.mq.edu.au). This manuscript benefitted from reviews by Paul Mueller, Peter Betts, and an anonymous reviewer. Field time and sample collection was made possible by the National Park Service; special thanks to Kevin P. Wilson for helping obtain scientific research and collecting permits. We thank Sean Regan for assistance in field mapping, sample collection, and many, many insightful discussions. Thanks to Darrel Cowan for helping arrange accommodations in Shoshone, CA. Thanks also to the Arizona LaserChron Center staff, particularly Heather Alvarez, Nicky Giesler, Mark Pecha, and Chelsi White for laboratory assistance.

REFERENCES CITED

Aitken, A.R.A., Betts, P.G., Young, D.A., Blankenship, D.D., Roberts, J.L., and Siegert, M.J., 2016, The Australo-Antarctic Columbia to Gondwana transition: Gondwana Research, v. 29, p. 136–152, doi: 10.1016/j.gr.2014.10.019.

Albin. A., and Karlstrom. K.E., 1991, Orthogonal fabrics in northwestern Arizona: Multiple orogenic events or progressive deformation during continental assembly. In: Karlstrom, K.E., (Ed.), Proterozoic Geology and Ore Deposits of Arizona, Arizona Geological Society Digest, v. 19, p. 67-84

Amelin, Y., Lee, D.-C., and Halliday, A.N., 2000, Early-middle Archean crustal evolution deduced from Lu-Hf and U-Pb isotopic studies of single zircon grains, Geochemica et Cosmochemica Acta, v. 64, p. 4205-4225.

Anderson, J.L., Wooden, J.L., and Bender, E.E., 1993, Mojave province of southern California and Vicinity, Proterozoic orogenic history of Arizona in Reed, J.C., Jr., Bickford, M.E., Houston, R.S., Link, P.K., Rankin, D.W., Sims, P.Pk., and Van

Schmus, W.R., eds., Precambrian of the Conterminous U.S.: Geological Society of America Decade of North American Geology, v. C-2, p. 176-188.

Armytage, R.M.G., Brandon, A.D., Peslier, A.H., and Lapen, T.J., 2014, Osmium isotope evidence for Early to Middle Proterozoic mantle lithosphere stabilization and concomitant production of juvenile crust in Dish Hill, CA peridotite xenoliths: Geochimica et Cosmochimica Acta, v. 137, p. 113–133, doi: 10.1016/j.gca.2014.04.017.

Babcock, R.S., Brown, E.H., Clark, M.D., and Livingston, D.E., 1979, Geology of the older Precambrian rocks of the Grand Canyon Part II. The Zoroaster Plutonic Complex and related rocks: Precambrian Research, v. 8, p. 243–275.

Barth, A.P., Wooden, J.L., Coleman, D.S., and Fanning, C.M., 2000, Geochronology of the Proterozoic basement of southwesternmost North America, and the origin and evolution of the Mojave crustal province: Tectonics, v. 19, 616-629.

Barth, A.P., Wooden, J.L., Coleman, D.S., and Vogel, M.B., 2009, Assembling and disassembling California: A zircon and monazite geochronologic framework for Proterozoic crustal evolution in southern California: Journal of Geology 117, 221-239.

Barth, A.P., Wooden, J.L., Jacobsen, C.E., and Economos, R.C., 2013, Detrital zircon as a proxy for tracking the magmatic arc system: The California arc example: Geology, v. 41, p. 223-226, doi:10.1130/G33619.1.

Belousova, E.A., Reid, A.J., Griffin, W.L., O'Reilly, Y., Suzanne, Y., 2009, Rejuvenation vs. Recycling of Archean crust in the Gawler Craton, South Australia: evidence from U-Pb and Hf isotopes in detrital zircon: Lithos, v. 113, p. 570–582.

Bennett, V.C., and DePaolo, D.J., 1987, Proterozoic crustal history of the western United States as determined by neodymium isotopic mapping, Geological Society of America Bulletin, v. 99, p. 674-685.

Bergh, S.G., and Karlstrom, K.E., 1992, The Chaparral shear zone: deformation partitioning and heterogeneous bulk crustal shortening during Proterozoic orogeny in central Arizona: Geological Society of America Bulletin, v. 104, p. 329-345.

Betts, P.G., Giles, and D., Schaefer, B.F., 2008, Comparing 1800-1600 Ma accretionary and basin processes in Australia and Laurentia: Possible geographic connections in Columbia: Precambrian Research, v. 166, p. 81-92.

Betts, P.G., Giles, D., and Aitken, A., 2011; Palaeoproterozoic accretion processes of Australia and comparison with Laurentia: International Geology Review, v. 53, p. 1357-1376.

Betts, P.G., Armit, R.J., Stewart, J., Aitken, A.R.A., and Ailleres, L., 2016, Australia and Nuna: Geological Society, London, Special Publications, v. 424, p. 47–81.

Bickford, M.E., Mueller, P.A., Kamenov, G.D., Hill, B.M., Mueller, P.A., and Kamenov, G.D., 2008, Crustal evolution of southern Laurentia during the Paleoproterozoic: Insights from zircon Hf isotopic studies of ca. 1.75 Ga rocks in central Colorado: Geology, v. 36, p. 555–558, doi: 10.1130/G24700A.1.

Bonamici, C.E., and Duebendorfer, E.M., 2009, Gravitational collapse of a Paleoproterozoic orogen, southern Hualapai Mountains, Arizona: Precambrian Research, v. 175, p. 35–50, doi: 10.1016/j.precamres.2009.08.003.

Bouvier, A., Vervoort, J.D., and Patchett, P.J., 2008, The Lu–Hf and Sm–Nd isotopic composition of CHUR: Constraints from unequilibrated chondrites and implications

for the bulk composition of terrestrial planets: Earth and Planetary Science Letters, v. 273, p. 48–57, doi: 10.1016/j.epsl.2008.06.010.

Borg, S.G., and DePaolo, D.J., 1994, Laurentia, Australia, and Antarctica as a Late Proterozoic supercontinent: Constraints from isotopic mapping: Geology, v. 22, p. 307–310.

Borg, S.G., Depaolo, D.J., and Smith, B.M., 1990, Isotopic structure and tectonics of the central Transantarctic mountains: Journal of Geophysical Research, v. 95, p. 6647–6667.

Bowring, S.A., and Karlstrom, K.E., 1990, Growth, stabilization, and reactivation of Proterozoic lithosphere in the southwestern United States: Geology, v. 18, p. 1203–1206.

Cawood, P. a., and Korsch, R.J., 2008, Assembling Australia: Proterozoic building of a continent: Precambrian Research, v. 166, p. 1–35, doi: 10.1016/j.precamres.2008.08.006.

Chappell, B.W., and White, A.J.R., 1974. Two contrasting granite types. Pacific Geology. v. 8, p. 173–174.

Chappell, B.W., Bryant, C.J., and Wyborn, D., 2012, Peraluminous I-type granites: Lithos, v. 153, p. 142-153.

Clemens, J.D., and Stevens, G., 2012, What controls chemical variation in granitic magmas? Lithos, v. 134–135, p. 317–329, doi: 10.1016/j.lithos.2012.01.001.

Coleman, D. S.; Wooden, J. L.; and Barth, A. P. 1999. The origin of mixed-province isotopic signatures: an example from the Proterozoic Mojave province. Geol. Soc. Am. Abstr. Programs 31:260.

Coleman, D.S., Barth, A.P., and Wooden, J.L., 2002, Early to Middle Proterozoic Construction of the Mojave Province, Southwestern United States: Gondwana Research, v. 5, p. 75–78.

Collins, W. J., Beams, S. D., White, A. J. R., and Chappell, B. W., 1982, Nature and origin of A-type granites with particular reference to southeastern Australia. Contributions to Mineralogy and Petrology, v. 80, p. 189–200. https://doi.org/10.1007/BF00374895

Collins, W.J., 2002, Nature of extensional accretionary orogens: Tectonics, v. 21, p. 1–12.

Collins, W.J., and Richards, S.W., 2008, Geodynamic significance of S-type granites in circum-Pacific orogens: Geological Society of America Bulletin, v. 36, p. 559–562, doi: 10.1130/G24658A.1.

Condie, K.C., 1982, Geology Plate-tectonics model for Proterozoic continental accretion in the southwestern United States Plate-tectonics model for Proterozoic continental accretion in the southwestern United States: Geology, v. 10, p. 37–42, doi: 10.1130/0091-7613(1982)10<37.

Corfu, F., Hanchar, J.M., Hoskin, P.W.O., and Kinny, P.D., 2003, Atlas of Zircon Textures: Reviews in Mineralogy and Geochemistry, v. 53, p. 469–500.

Daniel, C.G., Pfeifer, L.S., Jones, J. V., and McFarlane, C.M., 2013, Detrital zircon evidence for non-Laurentian provenance, Mesoproterozoic (ca. 1490-1450 Ma) deposition and orogenesis in a reconstructed orogenic belt, northern New Mexico, USA: Defining the Picuris orogeny: Geological Society of America Bulletin, v. 125, p. 1423–1441, doi: 10.1130/B30804.1.

Dickinson, W.R., and Gehrels, G.E., 2009, Use of U-Pb ages of detrital zircons to infer maximum depositional ages of strata: A test against a Colorado Plateau Mesozoic database: Earth and Planetary Science Letters, v. 288, p. 115–125, doi: 10.1016/j.epsl.2009.09.013.

Doe, M.F., 2014, Reassessment of Paleo-and Mesoproterozoic basin sediments of Arizona: Implications for tectonic growth of southern Laurentia and global tectonic configurations [Ph.D. Thesis]: Colorado School of Mines, 649 p.

Doe, M.F., Jones, J. V., Karlstrom, K.E., Thrane, K., Frei, D., Gehrels, G., and Pecha, M., 2012, Basin formation near the end of the 1.60-1.45 Ga tectonic gap in southern Laurentia: Mesoproterozoic Hess Canyon Group of Arizona and implications for ca. 1.5 Ga supercontinent configurations: Lithosphere, v. 4, p. 77–88, doi: 10.1130/L160.1.

Doe, M.F., Jones, J.V.III., Karlstrom, K.E., Dixon, B., Gehrels, G.E., and Pecha, M., 2013, Using detrital zircon ages and Hf isotopes to identify 1.48-1.45 Ga sedimentary basins and fingerprint sources of exotic 1.6-1.5 Ga grains in southwestern Laurentia: Precambrian Research, v. 231, p. 409-421.

Duebendorfer, E.M., Chamberlain, K.R., Jones, C.S., 2001, Paleoproterozoic tectonic history of the Cerbat Mountains, northwestern Arizona: Implications for crustal assembly in the southwestern United States: Geological Society of America Bulletin, v. 113, p. 575-590.

Duebendorfer, E.M., Chamberlain, K.R., and Fry, B., 2006, Mojave – Yavapai boundary zone, southwestern United States: A rifting model for the formation of an isotopically mixed crustal boundary zone: Geology, v. 34, p. 681-684.

Duebendorfer, E.M., 2015, Refining the early history of the Mojave-Yavapai boundary zone: Rifting vs. arc accretion as mechanisms for Paleoproterozoic crustal growth in southwestern Laurentia: Journal of Geology, v. 123, p. 21-38.

Dumond, G., Mahan, K.H., Williams, M.L., and Karlstrom, K.E., 2007, Crustal segmentation, composite looping pressure-temperature paths, and magma-enhanced metamorphic field gradients: Upper Granite Gorge, Grand Canyon, USA: Geological Society of America Bulletin, v. 119, p. 202–220, doi: 10.1130/B25903.1.

Eglington, B. M., Reddy, S.M. and Evans, D. A. D. 2009. The IGCP 509 database system: design and application of a tool to capture and illustrate litho-and chrono-stratigraphic information for Palaeoproterozoic tectonic domains, large igneous provinces and ore deposits; with examples from southern Africa. in: Reddy, S. M., Mazumder, R. and Evans, D.A.D. (eds) Palaeoproterozoic Supercontinents and Global Evolution. Geological Society, London, Special Publications, v. 323, p. 27–47.

Fraser, G., Mcavaney, S., Neumann, N., Szpunar, M., and Reid, A., 2010, Discovery of early Mesoarchean crust in the eastern Gawler Craton , South Australia: Precambrian Research, v. 179, p. 1–21, doi: 10.1016/j.precamres.2010.02.008.

Gehrels, G., 2012, Detrital zircon U-Pb geochronology: current methods and new opportunities. In. Busby, C., and Azor, A., (Ed.) Tectonics of Sedimentary Basins: Recent Advances, p. 47-62.

Gehrels, G.E., Valencia, V., Pullen, A., 2006, Detrital zircon geochronology by Laser-Ablation Multicollector ICPMS at the Arizona LaserChron Center, in Loszewski,

T., and Huff, W., eds., Geochronology: Emerging Opportunities, Paleontology Society Short Course: Paleontology Society Papers, v. 11, 10 p.

Gehrels, G.E., Valencia, V. A., and Ruiz, J., 2008, Enhanced precision, accuracy, efficiency, and spatial resolution of U-Pb ages by laser ablation-multicollector-inductively coupled plasma-mass spectrometry: Geochemistry, Geophysics, Geosystems, v. 9, p. n/a–n/a, doi: 10.1029/2007GC001805.

Gehrels, G., 2010, AgePick: Arizona Laserchron Center, https://docs.google.com/document/d/1MYwm8GcdYFOsfNV62B6PULb_-g2r1AS3vmm4gHMOFxg/preview

Gehrels, G., and Pecha, M., 2014, Detrital zircon U-Pb geochronology and Hf isotope geochemistry of Paleozoic and Triassic passive margin strata of western North America: Geosphere, v. 10, p. 49–65, doi: 10.1130/GES00889.1.

Goodge, J.W., Vervoort, J.D., Fanning, C.M., Brecke, D.M., Farmer, G.L., Williams, I.S., Myrow, P.M., DePaolo, D.J., 2008, A positive test of East Antarctica-Laurentia juxtaposition within the Rodinia Supercontinent: Science, v. 321, p. 235-240.

Goodge, J.W., and Fanning, C.M., 2010, Composition and age of the East Antarctic Shield in eastern Wilkes Land determined by proxy from Oligocene-Pleistocene glaciomarine sediment and Beacon Supergroup sandstones, Antarctica: Geological Society of America Bulletin, v. 122, p. 1135–1159, doi: 10.1130/B30079.1.

Goodge, J.W., and Fanning, C.M., 2016, Mesoarchean and Paleoproterozoic history of the Nimrod Complex, central Transantarctic Mountains, Antarctica: Stratigraphic revisions and relation to the Mawson Continent in East Gondwana: Precambrian Research, v. 285, p. 242–271, doi: 10.1016/j.precamres.2016.09.001.

Goodge, J.W., Fanning, C.M., and Bennett, V.C., 2001, U–Pb evidence of 1.7 Ga crustal tectonism during the Nimrod Orogeny in the Transantarctic Mountains, Antarctica: implications for Proterozoic plate reconstructions: Precambrian Research, v. 112, p. 261–288.

Goodge, J. W., Fanning, C. M., Fisher, C. M., and Vervoort, D., 2017, Proterozoic crustal evolution of central East Antarctica : Age and isotopic evidence from glacial igneous clasts, and links with Australia and Laurentia, Precambrian Research, v. 299, p. 151–176. https://doi.org/10.1016/j.precamres.2017.07.026

Griffin, W., Wang, X., Jackson, S., Pearson, N., O'Reilly, S.Y., Xu, X., and Zhou, X., 2002, Zircon chemistry and magma mixing, SE China: In-situ analysis of Hf isotopes, Tonglu and Pingtan igneous complexes: Lithos, v. 61, p. 237–269, doi: 10.1016/S0024-4937(02)00082-8.

Hand, M., Reid, A., and Jagodzinski, E., 2007, Tectonic Framework and Evolution of the Gawler Craton, Southern Australia: Economic Geology, v. 102, p. 1377–1395.

Hawkins, D.P., Bowring, S.A., Ilg, B.R., Karlstrom, K.E., and Williams, M.L., 1996, U-Pb geochronologic constraints on the Paleoproterozoic crustal evolution of the Upper Granite Gorge, Grand Canyon, Arizona: Geological Society of America Bulletin, v. 108, p. 1167–1181.

Hoffman, P.F., 1988, United Plates of America, and Growth of Laurentia: American Journal of Science, v. 16, p. 543 – 603.

Holland, M.E., Karlstrom, K.E., Doe, M.F., Gehrels, G.E., Pecha, M., Shufeldt, O.P., Begg, G., Griffin, W.L., and Belousova, E., 2015, An imbricate midcrustal suture

zone: the Mojave-Yavapai province boundary in Grand Canyon, AZ, Geological Society of American Bulletin, v. 127, p. 1391-1410.

Howard, K.E., Hand, M., Barovich, K.M., Reid, A., Wade, B.P., and Belousova, E. A., 2009, Detrital zircon ages: Improving interpretation via Nd and Hf isotopic data: Chemical Geology, v. 262, p. 277–292, doi: 10.1016/j.chemgeo.2009.01.029.

Howard, K.E., Hand, M., Barovich, K.M., Payne, J.L., and Belousova, E. A., 2011, U–Pb, Lu–Hf and Sm–Nd isotopic constraints on provenance and depositional timing of metasedimentary rocks in the western Gawler Craton: Implications for Proterozoic reconstruction models: Precambrian Research, v. 184, p. 43–62, doi: 10.1016/j.precamres.2010.10.002.

Ibanez-Mejia, M., Pullen, A., Arenstein, J., Gehrels, G.E., Valley, J., Ducea, M.N., Mora, A.R., Pecha, M., and Ruiz, J., 2015, Unraveling crustal growth and reworking processes in complex zircons from orogenic lower-crust: The Proterozoic Putumayo Orogen of Amazonia: Precambrian Research, v. 267, p. 285–310, doi: 10.1016/j.precamres.2015.06.014.

Ilg, B.R., Karlstrom, K.E., Hawkins, D.P., and Williams, M.L., 1996, Tectonic evolution of Paleoproterozoic rocks in the Grand Canyon: Insights into middle-crustal processes: Geological Society of America Bulletin, v. 108, p. 1149–1166, doi: 10.1130/0016-7606(1996)108<1149.

Jagodzinski, E.A., 2005. Compilation of SHRIMP U-Pb geochronological data, Olympic Domain, Gawler Craton, South Australia, 2001-2003. Geoscience Australia Record 2005/20, 211pp.

Jessup, M.J., Karlstrom, K.E., Connelly, J., Williams, M.L., Livaccari, R., Tyson, A., and Rogers, S.A., 2005, Complex Proterozoic crustal assembly of southwestern North America in an arcuate subduction system: The Black Canyon of the Gunnison, southwestern Colorado, in Karlstrom, K.E., and Keller, G.R., eds., Lithospheric structure and evolution of the Rocky Mountains: American Geophysical Union Geophysical Monograph 154, p. 21–38.

Jones III, J. V., Connelly, J.N., Karlstrom, K.E., Williams, M.L., and Doe, M.F., 2009, Age, provenance, and tectonic setting of Paleoproterozoic quartzite successions in the southwestern United States: Geological Society of America Bulletin, v. 121, p. 247–264, doi: 10.1130/B26351.1.

Jones, J.V., III, Daniel, C.G., Frei, D., and Thrain, K., 2011, Revised regional correlations and tectonic implications of Paleoproterozoic and Mesoproterozoic metasedimentary rocks in northern New Mexico, USA: New findings from detrital zircon studies of the Hondo Group, Vadito Group, and Marqueñas Formation: Geosphere, v. 7, no. 4, p. 974–991, doi:10.1130/GES00614.1.

Karlstrom, K.E., and Houston, R.S., 1984, The Cheyenne Belt: Analysis of a Proterozoic suture in southern Wyoming: Precambrian Research, v. 25, p. 415–446.

Karlstrom, K.E., Bowring, S.A., Conway, C.M., 1987, Tectonic significance of an Early Proterozoic two-province boundary in central Arizona: Geological Society of America Bulletin, v. 99, p. 529-538.

Karlstrom, K.E., and Bowring, S.A., 1988, Early Proterozoic Assembly of Tectonostratigraphic Terranes in Southwestern North America: Journal of Geology, v. 96, p. 561–576.

Karlstrom, K.E., and Bowring, S.A., 1993, Proterozoic orogenic history of Arizona in Reed, J.C., Jr., Bickford, M.E., Houston, R.S., Link, P.K., Rankin, D.W., Sims, P.Pk., and Van Schmus, W.R., eds., Precambrian of the Conterminous U.S.: Geological Society of America Decade of North American Geology, v. C-2, p. 171-334.

Karlstrom, K.E., Ahall, K.-I., Harlan, S.S., Williams, M.L., Mclelland, J., and Geissman, J.W., 2001, Long-lived (1.8-1.0 Ga) convergent orogen in southern Laurentia, its extensions to Australia and Baltica, and implications for refining Rodinia: Precambrian Research, v. 111, p. 5–30.

Karlstrom, K.E., Ilg, B.R., Williams, M.L., Hawkins, D.P., Bowring, S.A., and Seaman, S.J., 2003, Paleoproterozoic rocks of the Granite Gorges, in Bues, S.S., and Morales, M., eds., Grand Canyon Geology: New York, Oxford University Press, p. 9-38.

Kemp, A.I.S., Hawkesworth, C.J., Foster, G.L., Paterson, B.A., Woodhead, J.D., Hergt, J.M., Gray, C.M., and Whitehouse, M.J., 2007, Magmatic and crustal differentiation history of granitic rocks from Hf-O isotopes in zircon: Science, v. 2519, p. 980–983.

Kemp, A.I.S., Hawkesworth, C.J., Collins, W.J., Gray, C.M., and Blevin, P.L., 2009, Isotopic evidence for rapid continental growth in an extensional accretionary orogen: The Tasmanides, eastern Australia: Earth and Planetary Science Letters, v. 284, p. 455–466, doi: 10.1016/j.epsl.2009.05.011.

Kurhila, M., Andersen, T., and Rämö, O.T., 2010, Lithos Diverse sources of crustal granitic magma: Lu – Hf isotope data on zircon in three Paleoproterozoic

leucogranites of southern Finland: Lithos, v. 115, p. 263–271, doi: 10.1016/j.lithos.2009.12.009.

Lee, C.T., Yin, Q., Rudnick, R.L., and Jacobsen, S.B., 2001, Preservation of ancient and fertile lithospheric mantle beneath the southwestern United States: Nature, v. 411, p. 69–73, doi: 10.1038/35075048.

Li, Z.X., Li, X.H., Zhou, H.W. and Kinny, P.D., 2002. Grenvillian continental collision in south China: new SHRIMP U-Pb zircon results and implications for the configuration of Rodinia. Geology, v. 30, p. 163–166.

Li, Z.X., Bogdanova, S.V., Collins, A.S., Davidson, A., De Waele, B., Ernst, R.E., Fitzsimons, I.C.W., Fuck, R.A., Gladkochub, D.P., Jacobs, J., Karlstrom, K.E., Lu, S., Natapov, L.M., Pease, V., Pisarevsky, S.A., Thrane, K. and Vernikovsky, V., 2008. Assembly, configuration, and break-up history of Rodinia: a synthesis. Precambrian Research, v. 160, p. 179–210, doi: 10.1016/j.precamres. 2007.04.021.

Miller, D.M., and Wooden, J.L., 1992, Proterozoic Geology of the New York, Ivanpah, and

Providence Mountains, California: Field Guide: U.S. Geological Survey Open-File Report

92-000, 21 p.

Mueller, P.A., Wooden, J.L., Mogk, D.W., and Foster, D.A., 2011, Paleoproterozoic evolution of the Farmington zone: Implications for terrane accretion in southwestern Laurentia: Lithosphere, v. 3, p. 401–408, doi: 10.1130/L161.1.

Mulder, J.A., Halpin, J.A., Daczko, N.R., 2015, Mesoproterozoic Tasmania: Witness to the East Antarctica-Laurentia connection within Nuna: Geology, v. 43, p. 759-762.

Nelson, S.T., Hart, G.L., Frost, C.D., 2011, A reassessment of Mojavia and a new Cheyenne Belt alignment in the eastern Great Basin: Geosphere, v. 7, p. 513-527, doi:10.1130/GES00595.1

Nemchin, A.A., and Cawood, P.A., 2005, Discordance of the U–Pb system in detrital zircons: Implication for provenance studies of sedimentary rocks: Sedimentary Geology, v. 182, p. 143–162, doi: 10.1016/j.sedgeo.2005.07.011.

Oliver, R.L., and Fanning, C.M., 1997, Australia and Antarctica: Precise correlation of Palaeoproterozoic terrains. In: Ricci, C.A. (Ed.), The Antarctic Region: Geological Evolution and Processes. Terra Antarctica Publication, Siena, pp. 163-172.

Payne, J.L., Hand, M., Barovich, K.M., Reid, A., Evans, D.A.D., and Evans, D.A.D., 2009, Correlations and reconstruction models for the 2500-1500 Ma evolution of the Mawson Continent: Geological Society, London, Special Publications, v. 323, p. 319–355, doi: 10.1144/SP323.16.

Payne, J.L., Mcinerney, D.J., Barovich, K.M., Kirkland, C.L., Pearson, N.J., and Hand, M., 2016, Strengths and limitations of zircon Lu-Hf and O isotopes in modelling crustal growth: Lithos, v. 248–251, p. 175–192, doi: 10.1016/j.lithos.2015.12.015.

Pehrsson, S.J., Eglington, B.M., Evans, D.A.D., Huston, D., Reddy, S.M., 2016, Metallogeny and its link to orogenic style during the Nuna supercontinent cycle: Geological Society, London, Special Publications, v. 424, p. 83–94.

Pisarevsky, S.A., Elming, S-A., Pesonen, L.J., and Li, Z-X., 2014, Mesoproterozoic paleogeography: supercontinent and beyond: Precambrian Research, v. 244, p. 207-225.

Ramo, O.T., and Calzia, J.P., 1998, Nd isotopic composition of cratonic rocks in the southern Death Valley region; evidence for a substantial Archean source component in Mojavia: Geology, v. 26, p. 891-894.

Reid, A., Hand, M., Jagodzinski, E., Kelsey, D., and Pearson, N., 2008, Paleoproterozoic orogenesis in the southeastern Gawler Craton, South Australia: Australian Journal of Earth Sciences, v. 55, p. 449–471, doi: 10.1080/08120090801888594.

Reid, A.J., Jagodzinski, E.A., Armit, R.J., Dutch, R.A., Kirkland, C.L., Betts, P.G., and Schaefer, B.F., 2014, U-Pb and Hf isotopic evidence for Neoarchean and Paleoproterozoic basement in the buried northern Gawler Craton , South Australia: Precambrian Research, v. 250, p. 127–142, doi: 10.1016/j.precamres.2014.05.019.

Rogers, J.J.W., and Santosh, M., 2002, Configureation of Columbia, a Mesoproterozoic supercontinent: Gondwana Research, v. 5, p. 5-22, doi:10.1016/S1342-937X(05)70883-2.

Shaw, C.A., and Karlstrom, K.E., 1999, The Yavapai-Mazatzal crustal boundary in the southern Rocky Mountains: Rocky Mountain Geology, v. 34, n. 2, p. 37-52.

Shaw, S.E., and Flood, R.H., 2009, Zircon Hf Isotopic Evidence for Mixing of Crustal and Silicic Mantle-derived Magmas in a Zoned Granite Pluton, Eastern Australia: Journal of Petrology, v. 0S0, p. 1–22, doi: 10.1093/petrology/egn078.

Shufeldt, O.P., Karlstrom, K.E., Gehrels, G.E., and Howard, K.E., 2010, Archean detrital zircons in the Proterozoic Vishnu Schist of the Grand Canyon, Arizona: Implications for crustal architecture and Nuna supercontinent reconstructions: Geology, v. 38, p. 1099–1102, doi: 10.1130/G31335.1.

Spencer, J.E., Pecha, M.E., Gehrels, G.E., Dickinson, W.R., Domanik, K.J., and Quade, J., 2016, Paleoproterozoic orogenesis and quartz-arenite deposition in the Little Chino Valley area, Yavapai tectonic province, central: Geosphere, v. 12, p. 1–21, doi: 10.1130/GES01339.1.

Strickland, A., Wooden, J.L., Mattinson, C.G., Ushikubo, T., Miller, D.M., and Valley, J.W., 2013, Proterozoic evolution of the Mojave crustal province as preserved in the Ivanpah Mountains, southeastern California: Precambrian Research, v. 224, p. 222–241, doi: 10.1016/j.precamres.2012.09.006.

Swain, G.,Woodhouse, A.,Hand, M., Barovich, K., Schwarz, M. and Fanning, C. M., 2005, Provenance and tectonic development of the late Archaean Gawler Craton, Australia: U–Pb zircon, geochemical and Sm-Nd isotopic implications: Precambrian Research, v. 141, p. 106–136.

Szpunar, M., Hand, M., Barovich, K., Jagodzinksi, E., and Belousova, E., 2011, Isotopic and geochemical constraints on the Paleoproterozoic Hutchinson Group, southeastern Australia: implications for Paleoproterozoic continental reconstructions: Precambrian Research, v. 187, p. 99-126.

Vervoort, J.D., and Blichert-Toft, J., 1999, Evolution of the depleted mantle: Hf isotope evidence from juvenile rocks through time: Geochimica et Cosmochimica Acta, v. 63, p. 533–556, doi: 10.1016 /S0016 -7037(98)00274-9.

Vervoort, J.D., Plank, T., and Prytulak, J., 2011, The Hf–Nd isotopic composition of marine sediments: Geochimica et Cosmochimica Acta, v. 75, p. 5903–5926, doi: 10.1016/j.gca.2011.07.046.

Vervoort, J.D., and Kemp, A.I.S., 2016, Clarifying the zircon Hf isotope record of crust-mantle evolution: Chemical Geology, v. 425, p. 65-75.

Villaros, A., Buick, I.S., and Stevens, G., 2012, Isotopic variations in S-type granites: an inheritance from a heterogeneous source? Contributions to Mineralogy and Petrology, v. 163, p. 243–257, doi: 10.1007/s00410-011-0673-9.

Wade, C. E., and McAvaney, S.O., 2017, Neoarchaean to earliest Palaeoproterozoic magmatism in the southern Gawler Craton: petrogenesis of the Minbrie Gneiss and Carpa Granite, Report Book 2016/00019. Department for State Development, South Australia, Adelaide.

Whitmeyer, S.J., and Karlstrom, K.E., 2007, Tectonic model for the Proterozoic growth of North America: Geosphere, v.3, p. 220–259, doi: 10.1130/GES00055.1.

Windley, B.F., 2003, Continental growth in the Proterozoic: a global perspective, Geological Society of London, Special Publications, v. 206, p. 23-33.

Wooden, J.L., Stacey, J.S., Doe, B., Howard, K.A., and Miller, D.M., 1988, Pb isotopic evidence for the formation of Proterozoic crust in the southwestern United States, in Ernst, W.G., ed., Metamorphism and crustal evolution of the western United States: Rubey Volume VII: Englewood Cliffs, New Jersey, Prentice Hall, p. 68–86.

Wooden, J.L., and Miller, D.M., 1990, Chronologic and isotopic framework for early Proterozoic crustal evolution in the eastern Mojave Desert region, SE California: Journal of Geophysical Research, v. 95, p. 20133-20146.

Wooden, J.L., and DeWitt, E., 1991, Pb isotopic evidence for the boundary between the Early Proterozoic Mojave and central Arizona crustal provinces in western Arizona: Arizona Geological Society Digest, v. 19, p. 27-50.

Wooden, J.L., Barth, A. P., and Mueller, P. A., 2012, Crustal growth and tectonic evolution of the Mojave crustal province: Insights from hafnium isotope systematics in zircons: Lithosphere, v. 5, p. 17–28, doi: 10.1130/L218.1.

Zhang, S., Li, Z., Evans, D.A.D., Wu, H., Li, H., and Dong, J., 2012, Pre-Rodinia supercontinent Nuna shaping up: A global synthesis with new paleomagnetic results from North China: Earth and Planetary Science Letters, v. 353–354, p. 145–155, doi: 10.1016/j.epsl.2012.07.034.

APPENDIX 1: Detailed analytical methods from both the ALC and GEMOC Key Centre, along with sample descriptions and geochronogic plots

Geochemical Evolution and Metallogeny of Continents (GEMOC) Methods

U-Pb geochronology

U-Pb geochronology at the GEMOC Key Centre was conducted *in-situ* using an HP 4500 inductively coupled plasma quadrupole mass spectrometer (ICP-MS) paired with a custom-made UV laser ablation microprobe (LAM) that incorporates a petrographic microscope for detailed sample scrutiny (Norman et al., 1996). Samples and standards were ablated also in a custom-made chamber and transported to the ICP-MS with He carrier gas in order to minimize U/Pb fractionation. In addition, the laser was focused above the sample in order to further minimize fractionation effects; laser conditions were rigorously maintained throughout the duration of sample analysis.

Samples were compared to the zircon standard 02123, with four standard analyses completed before and after every 12 unknowns. The 02123 standard is a gem quality zircon from a Norwegian syenite that yields a perfectly concordant ID-TIMS age of 295 ± 1 Ma (Ketchum et al., 2001). Isotope ratios for both standards and unknowns are determined from background-subtracted signals; the uncertainties in both the background and signal are added in quadrature.

Masses 206, 207, 208, 232, and 238 were measured, and all isotopic ratios were calculated using the in-house on-line data reduction software GLITTER. Mass 204 was not measured due to large isobaric interference from Hg. Common Pb correction was therefore conducted after Andersen (2002), using $^{206}Pb/^{238}U$, $^{207}Pb/^{235}U$, and $^{208}Pb/^{232}Th$

ratios to solve mass-balance equations and correct the data in three-dimensional concordia space.

For additional details regarding analytical methods see Belousova et al. (2001), Griffin et al. (2004), and Jackson et al. (2004).

Hf isotopes

Hf-isotope analyses at GEMOC were carried out in-situ using a New Wave/Merchantek UP-213 laser-ablation microprobe, attached to a Nu Plasma multi-collector ICPMS. The analyses were carried out with a beam diameter of ca 55 μm and a 5 Hz repetition rate. This resulted in total Hf signals of 1-6 × 10^{-11} A, depending on conditions and the Hf contents. Typical ablation times were 100-120 seconds, resulting in pits 40-60 μm deep. He carrier gas transported the ablated sample from the laser-ablation cell via a mixing chamber to the ICPMS torch.

Interference of ^{176}Lu on ^{176}Hf is corrected by measuring the intensity of the interference-free ^{175}Lu isotope and using ^{176}Lu/^{175}Lu = 0.02669 (DeBievre & Taylor 1993) to calculate ^{176}Lu/^{177}Hf. Similarly, the interference of ^{176}Yb on ^{176}Hf has been corrected by measuring the interference-free ^{172}Yb isotope and using ^{176}Yb/^{172}Yb to calculate ^{176}Yb/^{177}Hf. The appropriate value of ^{176}Yb/^{172}Yb was determined by spiking the JMC475 Hf standard with Yb, and finding the value of ^{176}Yb/^{172}Yb (0.58669) required to yield the value of 176Hf/177Hf obtained on the pure Hf solution. Detailed discussions regarding the overlap corrections for ^{176}Lu and ^{176}Yb are provided in Pearson et al. (2008). Analyses of standard zircons (Griffin et al., 2000; Pearson et al., 2008) illustrate the precision and accuracy obtainable on the ^{176}Hf/^{177}Hf ratio, despite the severe

corrections on ^{176}Hf. The typical 2 SE precision on the $^{176}Hf/^{177}Hf$ ratios presented here is ± 0.00002, equivalent to ± 0.7 εHf unit.

The Mud Tank and 91500 zircon standards, analyzed together with the samples, were used as independent control on reproducibility and instrument stability. Average $^{176}Hf/^{177}Hf$ obtained for the Mud Tank (0.282523 ± 0.000066) and 91500 (0.282299 ± 0.000042) during this study are similar to the long-term averages, which in turn are similar to those measured by thermal ionization mass spectrometry (TIMS) (Griffin et al., 2006, 2007).

For the calculation of εHf values, we have adopted the chondritic values of Bouvier et al. (2008): $^{176}Lu/^{177}Hf$ (CHUR, today) = 0.0336 and $^{176}Hf/^{177}Hf$ (CHUR, today) = 0.282785. For the calculation of εHf values, we have adopted the decay constant (1.867 × 10-11 yr^{-1}) for ^{176}Lu proposed by Scherer et al. (2001) because it gives the best fit for terrestrial rocks (Amelin and Davis, 2005; Albarède et al., 2006).
For additional details regarding analytical methods see Griffin et al. (2000, 2002, 2004).

Arizona Laserchron Center (ALC) Methods

U-Pb geochronology

U-Pb geochronology of zircons is conducted *in-situ* by laser ablation multicollector inductively coupled plasma mass spectrometry (LA-MC-ICPMS). The analyses involve ablation of zircon with a New Wave UP193HE Excimer laser prior to May 2011, and afterwards a Photon Machines Analyte G2 excimer laser using a spot diameter of 30 microns. The ablated material is carried in helium into the plasma source of a Nu HR ICPMS, which is equipped with a flight tube of sufficient width that U, Th, and Pb isotopes are measured simultaneously. All measurements are made in static mode,

using Faraday detectors with 3×10^{11} ohm resistors for ^{238}U, ^{232}Th, ^{208}Pb-^{206}Pb, and discrete dynode ion counters for ^{204}Pb and ^{202}Hg. Ion yields are ~0.8 mv per ppm. Each analysis consists of one 15-second integration on peaks with the laser off (for backgrounds), 15 one-second integrations with the laser firing, and a 30 second delay to purge the previous sample and prepare for the next analysis. The resulting ablation pit is ~15 microns in depth.

For each analysis, the errors in determining $^{206}Pb/238U$ and $^{206}Pb/^{204}Pb$ result in a measurement error of ~1-2% (at 2-sigma level) in the $^{206}Pb/^{238}U$ age. The errors in measurement of $^{206}Pb/^{207}Pb$ and $^{206}Pb/^{204}Pb$ also result in ~1-2% (at 2-sigma level) uncertainty in age for grains that are >1.0 Ga, but are substantially larger for younger grains due to low intensity of the ^{207}Pb signal. For most analyses, the cross-over in precision of $^{206}Pb/^{238}U$ and $^{206}Pb/^{207}Pb$ ages occurs at ~1.0 Ga.

^{204}Hg interference with ^{204}Pb is accounted for measurement of ^{202}Hg during laser ablation and subtraction of ^{204}Hg according to the natural $^{202}Hg/^{204}Hg$ of 4.35. This Hg is correction is not significant for most analyses because our Hg backgrounds are low (generally ~150 cps at mass 204).

Common Pb correction is accomplished by using the Hg-corrected ^{204}Pb and assuming an initial Pb composition from Stacey and Kramers (1975). Uncertainties of 1.5 for $^{206}Pb/^{204}Pb$ and 0.3 for $^{207}Pb/^{204}Pb$ are applied to these compositional values based on the variation in Pb isotopic composition in modern crystal rocks.

Inter-element fractionation of Pb/U is generally ~5%, whereas apparent fractionation of Pb isotopes is generally <0.2%. In-run analysis of fragments of a large zircon crystal (generally every fifth measurement) with known age of 563.5 ± 3.2 Ma (2-sigma error) is

used to correct for this fractionation. The uncertainty resulting from the calibration correction is generally 1-2% (2-sigma) for both $^{206}Pb/^{207}Pb$ and $^{206}Pb/^{238}U$ ages.

For additional details regarding analytical methods see Gehrels et al. (2006, 2008), and Gehrels and Pecha (2014).

Hf isotopes

Hf isotope analyses are conducted with a Nu HR ICPMS connected to a New Wave UP193HE laser (2009-2010) or a Photon Machines Analyte G2 excimer laser (2011). Instrument settings are established first by analysis of 10 ppb solutions of JMC475 and a Spex Hf solution, and then by analysis of 10 ppb solutions containing Spex Hf, Yb, and Lu. The mixtures range in concentration of Yb and Lu, with $^{176}(Yb+Lu)$ up to 70% of the ^{176}Hf. When all solutions yield $^{176}Hf/^{177}Hf$ of ~0.28216, instrument settings are optimized for laser ablation analyses and seven different standard zircons (Mud Tank, 91500, Temora, R33, FC52, Plesovice, and Sri Lanka) are analyzed. These standards are included with unknowns on the same epoxy mounts. When precision and accuracy are acceptable, unknowns are analyzed using exactly the same acquisition parameters.

Laser ablation analyses are conducted with a laser beam diameter of 40 microns, with the ablation pits located on top of the U-Pb analysis pits. CL images are used to ensure that the ablation pits do not overlap multiple age domains or inclusions. Each acquisition consists of one 40-second integration on backgrounds (on peaks with no laser firing) followed by 60 one-second integrations with the laser firing. Using a typical laser fluence of ~5 J/cm2 and pulse rate of 7 hz, the ablation rate is ~0.8 microns per second. Each standard is analyzed once for every ~20 unknowns.

Isotope fractionation is accounted for using the method of Woodhead et al. (2004): βHf is determined from the measured $^{179}Hf/^{177}Hf$; βYb is determined from the measured $^{173}Yb/^{171}Yb$ (except for very low Yb signals); βLu is assumed to be the same as βYb; and an exponential formula is used for fractionation correction. Yb and Lu interferences are corrected by measurement of $^{176}Yb/^{171}Yb$ and $^{176}Lu/^{175}Lu$ (respectively), as advocated by Woodhead et al. (2004). Critical isotope ratios are $^{179}Hf/^{177}Hf$ =0.73250 (Patchett & Tatsumoto, 1980); $^{173}Yb/^{171}Yb$ = 1.132338 (Vervoort et al. 2004); $^{176}Yb/^{171}Yb$ =0.901691 (Vervoort et al., 2004; Amelin and Davis, 2005); $^{176}Lu/^{175}Lu$ = 0.02653 (Patchett, 1983). All corrections are done line-by-line. For very low Yb signals, βHf is used for fractionation of Yb isotopes. The corrected $^{176}Hf/^{177}Hf$ values are filtered for outliers (2-sigma filter), and the average and standard error are calculated from the resulting ~58 integrations. There is no capability to use only a portion of the acquired data.

All solutions, standards, and unknowns analyzed during a session are reduced together such that unknown values are calibrated based on the standards analyzed during the same session. The most weight is put on the following standards: Temore2, 91500, Mud Tank, FC1, and Plesovice, with less reliance placed on R33. The cutoff for using βHf versus βYb is determined by monitoring the average offset of the standards from their known values, and the cutoff is set at the minimum offset. For most data sets, this is achieved at ~6 mv of ^{171}Yb. For sessions in which the standards yield $^{176}Hf/^{177}Hf$ values that are shifted consistently from the know values, a correction factor is applied to the $^{176}Hf/^{177}Hf$ of all standards and unknowns. This correction factor is generally less than 1 epsilon unit. For example: all values were increased by 1.0 epsilon units for samples

analyzed in August 2012, all values increased by 0.3 epsilon units for samples analyzed in May 2013, all values were decreased by 0.2 epsilon units for samples analyzed in May 2014.

The $^{176}Hf/^{177}Hf$ at time of crystallization is calculated from measurement of present-day $^{176}Hf/^{177}Hf$ and $^{176}Lu/^{177}Hf$, using the decay constant of ^{176}Lu ($\lambda = 1.867 \times 10^{-11}$) from Scherer et al. (2001) and Söderlund et al. (2004). No capability is provided for calculating Hf Depleted Mantle model ages because the $^{176}Hf/^{177}Hf$ and $^{176}Lu/^{177}Hf$ of the source material(s) from which the zircon crystallized is not known.

Detrital zircon samples

K14-HH-1

Sample K14-HH-1 is a quartzite from the Halloran Hills, CA, intimately interleaved with and intruded by an augen gneiss (sample K14-HH-2; see below). The quartzite has cm-scale crossed bedding defined by black oxide-rich layers.
Zircon grains from this sample show varied morphologies, with most grains being elongate and rounded, and few grains showing subhedral to euhedral aspects. Cathodoluminescent imaging of internal textures reveals igneous growth zoning in most grains.

U-Pb geochronology. We obtained 91 ages from 91 grains. One grain was interpreted as metamorphic based on high U/Th, and was excluded from further consideration here. Detrital zircon ages ranged from 1744 ± 16 Ma to 3068 ± 53 Ma. The probability density distribution shows prominent peaks at 1788, 1803, and 1849 Ma, and scattered smaller peaks from 1912 Ma to 2639 Ma (Figure 3a).

Hf isotopes. We obtained 70 Hf isotopic analyses from dated zircons in this sample. Hf targets were selected based on age peaks identified by the AgePick macro and visual examination of the probability density plot. 25 grains from the 1788 Ma age peak were analyzed, and yielded a spread of $\varepsilon_{Hf(t)}$ from +5.0 to -10.9 (Figure 3a). An additional 25 grains from the 1849 Ma age peak were analyzed, and yielded a spread of $\varepsilon_{Hf(t)}$ from +11.1 to -3.6. Two grains from this age population yielded much lower $\varepsilon_{Hf(t)}$ of -13.9 at 1854 Ma, and -17.3 at 1853 Ma. Grains >2.0 Ga yield a similarly wide range of $\varepsilon_{Hf(t)}$, with the main population ranging from +6.5 to -8.2 at ~2.6 Ga.

K13-ASH-1

Sample K13-ASH-1 is a mica schist sampled from Ashford Canyon very close to sample LTG-344a from Ramo and Calzia (1998). The schist in Ashford Canyon has a locally distinct compositional layering which is defined by dismembered pods of more biotite-rich schist, interpreted as a relict bedding. This compositional layering is parallel to a folded tectonic layering, as well as similar quartzofeldspathic lenses with gradational contacts with micaceous layers. Thus, the Ashford Canyon schist was interpreted as a metaturbidite in the field.

Zircon grains from this sample range in size from ~50-200 μm with aspect ratios ranging from 1:1 to 3:1. Grain morphologies are primarily rounded to subhedral. Internal textures revealed by CL imaging show mostly oscillatory magmatic zoning and few homogenous or straight banded zonation. Several grains show distinct CL-bright overgrowths that were too small to be analyzed with a 30 μm beam.

U-Pb geochronology. We obtained 89 detrital zircon ages from 89 grains. Detrital zircon ages range from 1775 ± 19 Ma to 3188 ± 23 Ma. The probability density

distribution shows many discrete age peaks with the two most prominent peaks at 1856 Ma and 1878 Ma, and several distributed peaks defined by few grains ranging from 1913 Ma to 2699 Ma (Figure 3b).

Hf isotopes. Zircon grains from five age populations were analyzed for their Hf isotopic composition. Ten zircon grains from the 1.88 Ga population yielded $\varepsilon Hf_{(t)}$ ranging from +6.4 to -2.3 (Figure 3b). Nine zircon grains from the 2.0 Ga population yielded a range of $\varepsilon Hf_{(t)}$ from +2.7 to -7.6. Five grains ranging from 2.3-2.4 Ga yielded $\varepsilon Hf_{(t)}$ from +2.2 to -8.1. Thirteen zircon grains from the 2.65 Ga peak yield a range of $\varepsilon Hf_{(t)}$ from +4.2 to -3.2. The oldest population of zircon grains ranging from 2.9-3.1 Ga yielded $\varepsilon Hf_{(t)}$ from +4.6 to -5.0.

K13-NOP-4

Sample K13-NOP-4 was taken from the same location as the migmatite (LTG-337) sampled by Ramo and Calzia (1998) in the southern Nopah Range. Our sample was taken from a quartz rich layer within an area of migmatite schist similar in appearance to K13-NOP-1.

Zircon grains from this sample range from ~50 to 400 μm with aspect ratios ranging from 1:1 to 3:1. Grain morphologies vary from rounded to euhedral. Internal textures revealed by CL imaging show well-developed oscillatory zoning. However, many grains display homogenous or irregular CL textures.

U-Pb geochronology. We obtained 83 detrital zircon ages from 81 grains. Two analyses were interpreted as metamorphic ages based on CL texture and U/Th ratios, and are not considered here. Detrital zircon ages range from 1747 ± 27 Ma to 2810 ± 13 Ma. The probability density distribution shows a prominent peak at 1874 Ma as well as minor

peaks at 1838 Ma, 1908 Ma, 1974 Ma and 1995 Ma (Figure 3c). Additional older peaks occur at 2463 Ma and 2532 Ma, but are defined by few ages. Cores and rims from two complexly zoned zircon grains were analyzed. One pair yielded indistinguishable ages, but another yielded ages of 1883 ± 14 Ma and 1747 ± 47 Ma.

Hf isotopes. Zircon grains from the main age peaks of 1.87, 1.96, and 2.5 Ga were analyzed for their Hf isotopic composition. Ten zircon grains from the 1.87 Ga population yielded $\varepsilon Hf_{(t)}$ ranging from +1.3 to -5.2 (Figure 3c). Seven grains from the 1.96 Ga population yield more varied $\varepsilon Hf_{(t)}$ ranging from +4.6 to -7.9. Five grains from the 2.5 Ga population yield a range of $\varepsilon Hf_{(t)}$ from +3.7 to -4.0.

K13-NOP-1

Sample K13-NOP-1 is a sillimanite schist sampled from the southern end of the Nopah Range. The Nopah Range schist is penetratively deformed and locally migmatitic with abundant cm-scale tight to isoclinal folds present in micaceous layers. Lenses of quartzofeldspathic schist are present throughout and locally display both sharp and gradual transitions into the micaceous layers, which we interpreted in the field as relict graded bedding or Bouma sequences. We interpreted the protolith to be a turbidite in the field, and preferentially sampled quartz-rich lenses for detrital zircon geochronology. Zircon grains from this sample range in size from ~50 to 200 μm with aspect ratios ranging from 1:1 to 3:1. Grain morphologies are primarily rounded, with some subhedral grains. Internal textures revealed by CL-imaging display concentric growth zoning present in almost all grains. Many grains display complex zoning and clearly defined inherited cores that suggest some of the source rocks experienced complex magmatic histories.

U-Pb geochronology. We obtained 106 ages from 101 grains. Five grains were excluded based on high U/Th, including four of the rims overgrowing inherited cores. Detrital zircon ages range from 1760 ± 22 Ma to 3054 ± 15 Ma. The probability density distribution shows two main age peaks at 1859 Ma and 1868 Ma followed by a nearly continuous distribution of small age peaks from 1910-2740 Ma (Figure 3d). Complexly zoned zircon grains yielded core and rim age data. Two overgrowths yielded ages much younger than the pluton which intrudes this sample (K13-NOP-3; see below), and therefore cannot provide useful provenance information. These ages were interpreted as metamorphic based on their young age and high U/Th. One grain (K13-NOP-1-54) yielded a core age of 2148 ± 24 Ma and an overgrowth with a slightly discordant and high U/Th age of 1789 ± 12 Ma. Finally, one grain yielded indistinguishable core and rim age data.

Hf isotopes. Zircon grains from prominent age peaks at 1.86 and 1.98 Ga were analyzed for their Hf isotopic composition. Ten grains from a ~1.86 Ga age peak yielded $\varepsilon Hf_{(t)}$ from +2.9 to -3.5, with one outlier yielding a value of -9.9 (Figure 3d). Seven grains from the 1.98 Ga population yielded similar $\varepsilon Hf_{(t)}$ ranging from +3.4 to -2.9. $\varepsilon Hf_{(t)}$ from 2.1-2.6 Ga zircon grains yield a similar range from from +3.4 at 2.3 Ga to -5.4 at 2.4 Ga, however three grains yielded extremely low of -13.5 at 2.3 Ga, -16.1 at 2.1 Ga, and -17.3 at 2.4 Ga.

K14-BLFG-2

Sample K14-BLFG-2 was taken from an outcrop of somewhat ambiguous mica schist in the Bullfrog Hills at the same location sampled by Ramo and Calzia (1998). Grain morphologies are primarily rounded, with some subhedral grains. Internal textures

revealed by CL-imaging show concentric growth zoning, often disturbed or obscured by homogenous zones.

U-Pb geochronology. We obtained 75 ages from 75 grains. This sample appears to have experienced much more Pb loss and metamorphic overprinting than other detrital zircon samples in this study. Of the 75 ages we obtained only 23 were >90% concordant, and average concordance for the sample was 85%. Five analyses yielded U/Th >10 and four analyses yielded U concentrations >1000. Detrital zircon ages range from 1743 ± 18 Ma to 3253 ± 10 Ma. The probability density distribution shows several peaks defined by few grains, and one dominant peak at 1826 Ma (Figure 3e).

Hf isotopes. We obtained Hf isotopic data for 54 dated zircons. Hf targets were selected based on age peaks identified by the AgePick macro and visual examination of the probability density plot. Four grains from the youngest ~1.77 Ga population yield $\varepsilon_{Hf(t)}$ ranging from -0.9 to -4.7 (Figure 3e). 26 grains from the dominant 1.82 Ga population yielded $\varepsilon_{Hf(t)}$ ranging from +7.0 to -7.4, with two grains yielding much lower of -11.9 and -15.5 at ca. 1814 Ma and 1821 Ma respectively. Grains from the distributed population of Neoarchean to Paleoproterozoic ages (2.6-2.3 Ga) yielded a spread of $\varepsilon_{Hf(t)}$ ranging from +3.5 to -5.7.

K13-IBEX-1

Sample K13-IBEX-1 was taken from the southern Ibex Hills west of Ibex Spring. It was sampled very near the location of what Ramo and Calzia (1998) described as granitic gneiss (LTG-365), however our field and geochronologic data suggest that K13-IBEX-1 had a supracrustal protolith. K13-IBEX-1 was taken from a quartz rich layer

within a locally migmatitic siliminite schist that displayed rhythmic graded bedding interpreted as deposition in turbidity flows.

Zircons from this sample range in size from to ~50-250 μm in size, with aspect ratios ranging from 1:1 to 3:1. Grain morphologies are primarily rounded to subhedral, with few euhedral grains. Internal textures revealed by CL imaging show primarily oscillatory zoning, with some grains displaying convoluted zoning or homogenous CL texture.

U-Pb geochronology. We obtained 104 detrital zircon U-Pb ages from 104 grains. One age determination is excluded from consideration here; K13-IBEX-1-81 was taken from a CL homogeneous band within the grain, and yielded a 30% discordant age of 1680 ± 89 Ma. The high uncertainty, U/Th >10, discordance, and CL texture lead to the interpretation of a metamorphic age. Detrital zircon ages range from 1743 ± 28 Ma to 3050 ± 21 Ma. The probability density distributions shows that detrital zircon ages are dominated by a peak at 1856 Ma, with supplementary age peaks at 1812 Ma, 1844 Ma, 1881 Ma, and 1899 Ma (Figure 3f). Small peaks defined by few grains are distributed from 1945-2395 Ma.

Hf isotopes. Zircon grains from the prominent 1.85 Ga population as well as those ranging from 2.5-2.4 Ga were analyzed for their Hf isotopic composition. Nine zircon grains from the 1.85 Ga population yielded $\varepsilon Hf_{(t)}$ ranging from +1.1 to -4.3 (Figure 3f). Six zircon grains with ages from 2.5-2.4 Ga yielded $\varepsilon Hf_{(t)}$ ranging from +7.1 to +0.6.

Detrital zircon geochronology and Hf-isotope analysis summary

The detrital zircon age spectra of all six metasedimentary samples analyzed in this study are dominated by peaks at ~1.83-1.88 Ga (Figure 3, Table 1). Only one sample (K14-HH-

2) contained a robust population of >90% concordant zircon younger than 1.8 Ga (Figure 3, Table 1). Each sample also shows varied smaller peaks throughout the early Paleoproterozoic and late Archean; the total range of detrital zircon ages is from 3.25 to 1.75 Ga. These results are consistent with previous findings of Barth et al. (2000; 2001; 2009), Strickland (2012), and Shufeldt et al., (2010) who showed that the oldest micaceous gneisses in the Mojave province are dominated by 1.9-1.8 Ga detrital zircon ages, but yield ages as old as 3.3 Ga.

Hf-isotope data from detrital zircon grains yield a broad range of $^{176}Hf/^{177}Hf_{(t)}$ ranging from 0.281116 to 0.281904 ($\varepsilon_{Hf(t)}$ ~ -17 to +11) at 1.87 Ga (Figure 4), although most U-Pb-Hf analyses fall between $\varepsilon_{Hf(t)}$ of -5 to +5 at 1.87 Ga (>70%). A 2.0 Ga peak yielded a spread of $^{176}Hf/^{177}Hf_{(t)}$ ranging from 0.280980 to 0.281639 ($\varepsilon_{Hf\,(t)}$ ~ -8 to +5). The 1.79 Ga peak in sample K14-HH-2 yielded generally lower $^{176}Hf/^{177}Hf_{(t)}$ ratios than the ~1.87 Ga population, ranging from 0.281337 to 0.281673 ($\varepsilon_{Hf\,(t)}$ ~ -11 to +1). Neoarchean to earliest Paleoproterozoic 2.7-2.3 Ga detrital zircon grains yield a similar spread of $^{176}Hf/^{177}Hf_{(t)}$ ranging from 0.281418 to 0.280626 ($\varepsilon_{Hf\,(t)}$ ~ -17 to +7), with most grains yielding $\varepsilon_{Hf\,(t)}$ ranging from +5 to -5 at ~2.6 Ga. Finally, a minor component of Mesoarchean grains yield $^{176}Hf/^{177}Hf_{(t)}$ ranging from 0.280650 to 0.280983 ($\varepsilon_{Hf\,(t)}$ ~ -5 to +6). These data are similar to those presented by Wooden et al. (2012) from a garnet-bearing paragneiss in the New York Mountains, and the Vishnu Schist in Grand Canyon (Holland et al., 2015) (Figure 4).

Plutonic zircon samples

K14-WB

U-Pb geochronology. Sample K14-WB was taken from the World Beater Gneiss Complex in the southern Paniment range near the locality sampled by Ramo and Calzia (1998). Zircon grains from this sample range in size from 50-150 μm, with aspect ratios from 1:1 to 1:3. Internal textures as revealed by CL imaging revealed a population of CL-dark and pockmarked grains that were interpreted as metamict, and avoided during analysis. A CL-bright population of euhedral grains displayed well defined oscillatory zoning with rare homogeneous or convolute zones. Some grains appeared to have complex zoning, and multiple generations of zircon as indicated by truncation of oscillatory zoning, however we were unable to resolve multiple age domains in any zircon grains.

We obtained 32 dates from 30 zircon grains. Two grains that appeared to have distinct zircon domains yielded indistinguishable dates. Our results yield a range of dates from 1725 ± 18 Ma to 1803 ± 51 Ma, with one grain yielding a much older date of 1960 ± 25 Ma (Supplementary Figure 1A). With few exceptions, there is a direct correlation between age and concordance, with the youngest ages increasing in concordance towards the most concordant ages, as would be expected with some Pb loss. 31 dates yield a cord with an upper intercept at 1796 ± 6 Ma (Supplementary Figure 1A), however most dates overlap within analytical uncertainty, so the cord is not robust. A weighted mean of 18 >95% concordant ages yielded a weighted mean age of 1791 ± 15 Ma (MSWD = 0.8). Thus, the protolith of the World Beater gneiss complex is interpreted to have crystallized at 1791 Ma.

The one older date of 1960 ± 25 Ma was obtained from a grain with no discernable difference in internal textures from the main population. This date is 82%

concordant, and thus represents a minimum age. The grain, K14-WB-15 displays well defined oscillatory zoning with two thin (μm-scale) rims that disturb the internal oscillatory zoning. The outermost rim is CL-dark with one distinct protrusion into the oscillatory zoning. This is interpreted as a thin rim of fluid-induced alteration (Geisler et al., 2007; Kroner et al., 2014). A similarly thin CL-bright rim has an irregular contact with a darker zone of oscillatory zoning which may be the result of resorbtion and reprecipitation of new zircon in a melt. The older date obtained from this age clearly indicates that it is inherited, however there is minimal evidence for substantial resorbtion of the original grain.

Hf isotopes. Hf isotopic analyses were obtained from 13 dated zircon grains. 12 grains yielded a range of $^{176}Hf/^{177}Hf_i$ from 0.281445 ± 0.000034 to 0.281607 ± 0.000036, which correspond to a range of $\varepsilon Hf_{(t)}$ from -1.2 to -7.0 at 1.79 Ga. The one older inherited grain yielded a $^{176}Hf/^{177}Hf_i$ value of 0.281475 ± 0.000028 and a corresponding $\varepsilon Hf_{(t)}$ of -2.1 at 1.96 Ga, which due to the discordance of the date is a minimum estimate.

13H-060

U-Pb geochronology. Sample 13H-060 is a boitite + hornblende tonalitic orothogneiss with plagioclase phenocrysts from Ashford Canyon. Zircons from this sample range in size from 100-250 μm, with aspect ratios ranging from 1:1 to 1:4. Grain morphologies are primarily euhedral to subhedral, with some rounding and fracturing. Internal textures as revealed by CL imaging are ubiquitously magmatic, with concentric growth zoning present in all grains. In some grains, growth zoning is locally disturbed by CL-dark zones interpreted as the result of metamictization. Several zircons showed inherited cores, evident by the truncation of zoning and/or a change in CL signal.

A total of 56 dates were obtained from 50 zircons; several attempts were made to date inherited cores and magmatic overgrowths (see below). Ages range from 1750 ± 4 Ma to 2105 ± 19 Ma (Supplementary Figure 1B), and a group of 41 dates range from 1750 ± 4 to 1792 ± 15 Ma. The two youngest dates are also the least concordant, with age and concordance increasing towards a plateau of 39 >95% concordant ages that overlap within 2-sigma uncertainty. All dates combined define a cord with intercepts at 360 ± 61 and 1785 ± 2 Ma, and a weighted mean of 39 dates yields an age of 1784 ± 14 Ma (MSWD = 0.5). This is interpreted as the crystallization age of the sample.

A total of 15 analyses yielded dates much older than the interpreted 1784 Ma crystallization age of the sample. We obtained paired core and overgrowth analyses from 8 zircons. Two zircon crystals suspected to have inherited cores yielded indistinguishable core and overgrowth ages. 8 inherited core ages range from 1834 ± 22 Ma to 2105 ± 19 Ma, and all of their overgrowths were part of the main 1784 Ma population. In addition, 7 zircon grains that either did not display apparent cores, or had overgrowths that were too narrow to be analyzed by our 30 μm spot size yielded ages ranging from 1838 ± 20 Ma to 1876 ± 17 Ma.

Hf isotopes. We obtained 30 Hf isotopic analyses from selected grains of sample 13H-060. Results from 20 analyses on grains or overgrowths of the 1.78 Ga population yielded $^{176}Hf/^{177}Hf$ ranging from 0.281478 ± 0.000088 to 0.281759 ± 0.000052, which correspond to a range of $\varepsilon Hf_{(t)}$ from +0.5 to -7.3 at 1.784 Ga. The weighted mean

We obtained paired Hf isotopic analyses from 7 dated core and rim domains. Core domains were varied in both their age and Hf isotopic composition. $\varepsilon Hf_{(t)}$ obtained from

core domains ranged from +2.0 at 1.96 Ga to -5.2 at 1.91 Ga. The oldest core domain yielded an $\varepsilon Hf_{(t)}$ value of -1.3 at 2.1 Ga.

13H-080

U-Pb geochronology. Sample 13H-080 is a hornblende + biotite bearing granodiorite with megacrystic K-spar taken from Ashford Canyon. A heterogeneous zone of highly altered and brecciated tonalite and pelitic schist separated this sample from the main body of tonalite (13H-060), however our geochronologic data suggest that the two bodies may be genetically related (see below). Zircon grains from this sample range in size from 100-400 μm, with aspect ratios ranging from 1:1 to 6:1. Grain morphologies are predominantly euhedral to subhedral, with individual grains displaying varying degrees of fracture and/or rounding. Internal textures as revealed by CL imaging are predominantly magmatic, with concentric growth zoning present in almost every grain. Magmatic textures in some grains are disturbed by CL-dark zones and/or inclusions, and in some cases show irregular zoning or CL-homogenous zones. Several grains displayed inherited cores, evident by the truncation of magmatic growth zoning, and/or differences in CL intensity and texture.

We obtained 58 dates from 55 zircon grains. Dates ranged from 1768 ± 31 Ma to 2020 ± 29 Ma (Supplementary Figure 1C). A spread of 52 >95% concordant ages from 1768 ± 31 to 1817 ± 64 Ma yields a weighted mean of 1783 ± 16 Ma (MSWD = 0.9). Due to the relatively large uncertainties of these ages and their concordance, a cord could not be fit to the data. However, 22 of the most concordant ages (between 99-101%) yielded a concordia age of 1783 ± 2 Ma (MSWD = 0.019), in excellent agreement with the weighted mean age. The remaining 6 dates are older than the interpreted

crystallization age of the sample. Two of these grains do not have complementary overgrowth age data; one has rim that truncates internal CL-texture, but was too thin to be analyzed, and the other has no apparent overgrowth. Three older dates come from clearly defined inherited cores; analyses 13H-080-43C, 55C, and 56C yielded ages of 2020 ± 29 Ma, 1887 ± 31 Ma, and 1910 ± 22 Ma respectively. The overgrowths from 13H-080-55 and 56 yielded ages of 1784 ± 15 and 1800 ± 27 Ma and are interpreted to be related to 1783 Ma crystallization of the sample. The overgrowth of 13H-080-43 yields an age of 1830 ± 29 Ma. This age is statistically distinct from the interpreted crystallization of the sample, however after scrutinizing the CL-texture of the grain after analysis, it appears that the laser spot overlaps a portion of the inherited core. The date of 1830 ± 29 Ma is interpreted as a mixed age between the 2020 and 1783 Ma core and overgrowth. Because both the core and overgrowth are extremely concordant, and a mixing trend between 2020 and 1783 Ma is indistinguishable from the slope of concordia with these data, the mixed age is itself 100.6% concordant.

Hf isotopes. We obtained 20 Hf isotopic analyses from this sample. 16 analyses from the main population of zircon grains yielded $\varepsilon_{Hf(t)}$ ranging from -2.8 to +1.5 at 1.78 Ga. Hf isotopic analyses were conducted on all three zircon grains with multiple age domains. Grains 13H-080-55C and 56C each had overgrowths which were part of the main 1.78 Ga population, however $\varepsilon_{Hf(t)}$ from these inherited cores were quite different from the main population and each other. Grain 13H-080-55C yielded an $\varepsilon_{Hf(t)}$ value of +4.9 at 1.89 Ga, and 13H-080-56C yielded an $\varepsilon_{Hf(t)}$ value of -5.0 at 1.91 Ga. The zircon from which both age domains were older than the main population, (13H-080-43) yielded $\varepsilon_{Hf(t)}$ of -0.6 and -4.4 at 2.02 and 1.83 Ga respectively.

K13-NOP-3

U-Pb geochronology. Sample K13-NOP-3 is a garnet + biotite orthogneiss from below the nonconformity in the southern Nopah range. Zircon grains from this sample range in size from 100-300 μm, with aspect ratios ranging from 1:1 to 4:1. Grain morphologies are primarily elongate and subhedral with many rounded edges. Internal textures as revealed by CL-imaging are primarily magmatic, with concentric growth zoning present in most grains. Locally, CL-dark or homogenous zones disturb the magmatic zoning, and some grains display irregular zonation. Thin CL-dark rims are almost ubiquitous.

29 analyses were conducted on sample K13-NOP-3, however only ten analyses passed the data reduction process. Zircons were highly discordant, and pervasively affected by Pb loss. A model 2 solution (Ludwig, 2003) using all 29 analyses yielded a cord with an upper intercept of 1781 ± 34 Ma (MSWD = 3.8). A weighted mean of six >90% concordant ages yielded an age of 1782 ± 15 Ma (MSWD = 0.9) (Supplementary Figure 1D), which is our preferred age of crystallization for the sample.

Hf isotopes. Hf isotopic analysis of zircon grains from this sample yielded a tight cluster of $\varepsilon_{Hf(t)}$ ranging from -0.1 to -2.9 at 1.78 Ga.

(A) K14-WB - World Beater Gneiss Complex

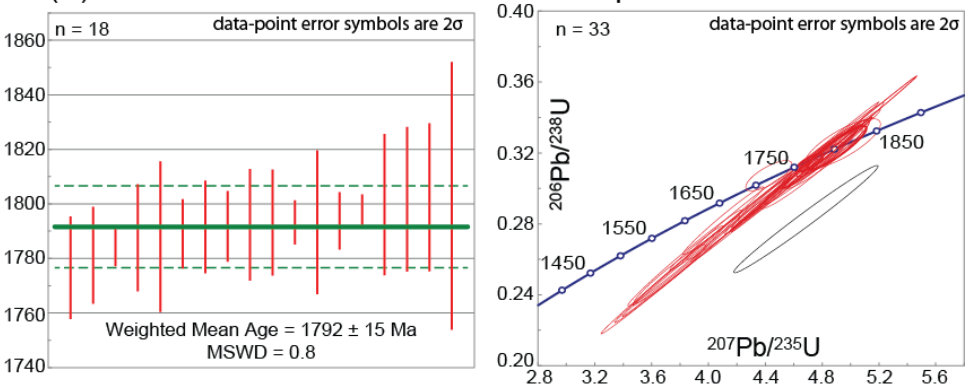

(B) 13H-060 - Ashford Canyon tonalitic orthogneiss

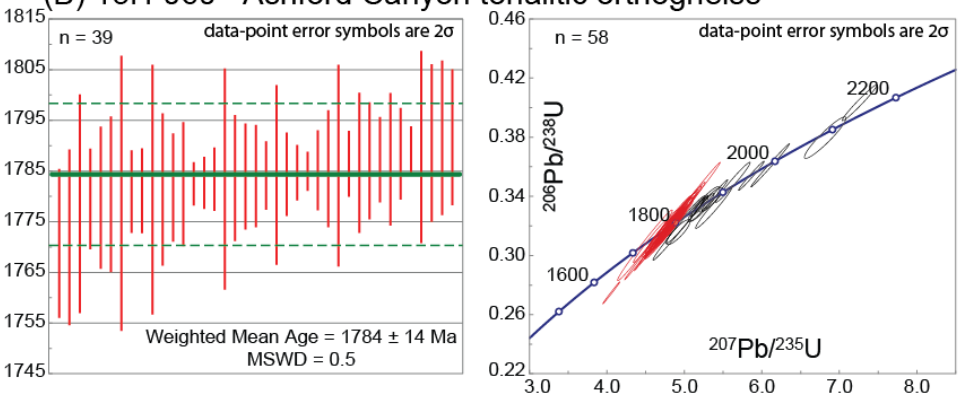

(C) 13H-080 - Megacrystic granodiorite

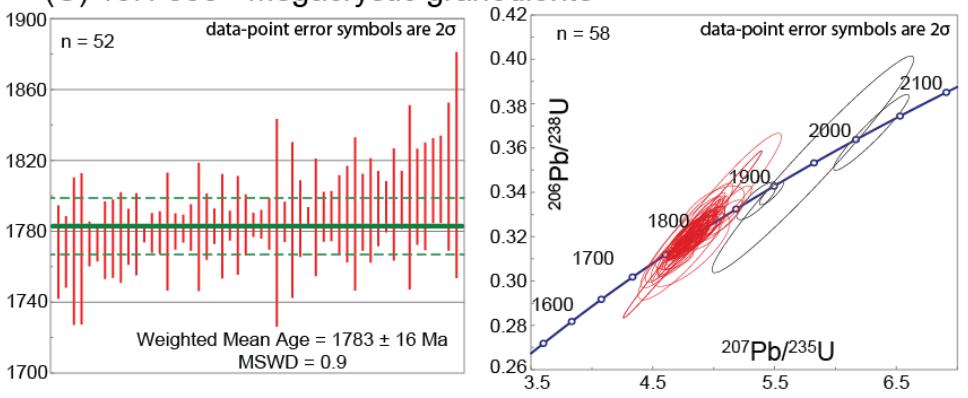

(D) K13-NOP-3 - Nopah Range orthogneiss

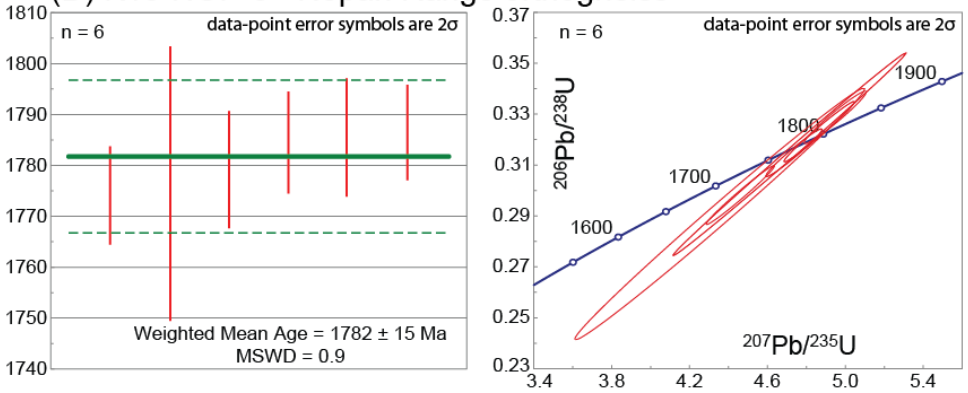

K14-HH-2

U-Pb geochronology. Sample K14-HH-2 was taken from an augen gneiss with large plagioclase phenocrysts intimately interlayered with the quartzite of sample K14-HH-1. Zircons from this sample range in size from 100-350 μm, with aspect ratios ranging from 1:1 to 1:3. Grain morphologies are varied, but primarily elongate and subhedral. Internal textures as revealed by CL imaging display igneous growth zoning, but it is commonly overprinted or disturbed by irregular homogenous zones, and many grains show CL-bright homogenous rims. These rims were avoided during spot analysis in favor of locally preserved igneous growth zoning.

We obtained 36 ages from as many zircon grains. Ages ranged from 1711 ± 44 Ma to 2292 ± 30 Ma (Supplementary Figure 1E). A weighted mean of 26 >90% concordant ages yielded an age of 1774 ± 17 (MSWD = 0.7), two ages were excluded based on discordance, and high U/Th. Five ages ranging from 1882 ± 27 Ma to 2292 ± 30 Ma were interpreted as inherited grains and excluded from the age determination. Of these five older grains, only one was identified as an older rim based on internal CL texture; analysis K14-HH-2-40C yielded the oldest age of 2292 ± 30 Ma. A separate analysis of another domain in the same grain did not pass the data reduction process.

Hf isotopes. Hf isotopic analyses conducted on 13 dated zircon grains yielded $\varepsilon Hf_{(t)}$ ranging from -3.9 to +4.4 at 1.77 Ga. In addition, the inherited core dated at 2292 ± 30 Ma yielded an $\varepsilon Hf_{(t)}$ value of -16.1.

K06-DV-37

U-Pb geochronology. Sample K06-DV-37 was taken from an augen gneiss in Jubilee Pass near the locality sampled by Ramo and Calzia (1998). Zircon grains from

this sample ranged in size from 100-200 μm with aspect ratios ranging from 1:1 to 3:1. Grain morphologies are primarily elongate subhedral to rounded with internal textures revealed by BSE images showing concentric growth zoning. Some core and rim domains were identified by BSE imaging and analyzed for both U-Pb age and Hf isotopic composition.

We obtained 49 dates from 46 zircon grains. The 49 dates ranged from 1750 ± 46 to 2164 ± 38 Ma, and 46 ages defined a continuous spread of ages from 1750 ± 46 to 1869 ± 46 Ma. All dates were >95% concordant, and most dates overlap within analytical uncertainty. A linearized probability plot of the data shows a clear break in slope between 38 dates ranging from 1750 ± 46 to 1798 ± 46 Ma and 8 dates ranging from 1813 ± 40 to 1869 ± 46 Ma. The population of 38 dates define a cord with an upper intercept of 1780 ± 8 Ma (MSWD = 0.71), however the cord is not robust due to the overlap in analytical uncertainties and concordance. A weighted mean of the same 38 dates yields an age of 1773 ± 8 Ma (MSWD = 0.24), which is perhaps a more conservative estimate of the crystallization age of the Jubilee Pass augen gneiss.

The population of 8 older dates yields a weighted mean of 1831 ± 15 Ma (MSWD = 0.75). These grains may be sampled from igneous crust in the subsurface similar in age to the Elves Chasm gneiss, or detrital grains.

Three paired core and rim analyses were conducted on zircon that appeared to have distinct domains as indicated by their internal textures. Because all three paired analyses yielded dates that overlap within analytical uncertainty, our interpretations of these core and rim data stem from the Hf isotopic data (see below), and the identification of two distinct age populations from the linearized probability plot.

Hf isotopes. Hf isotopic analyses conducted on 32 zircon grains from the main population yielded a range of $^{176}Hf/^{177}Hf$ isotopic ratios from 0.281537 to 0.281778, corresponding to $\varepsilon Hf_{(t)}$ values from -3.1 to +4.8 at 1.77 Ga (Supplementary Figure 1F).

Hf isotopic analysis of six of the eight grains that define the 1831 Ma population yield a range of $^{176}Hf/^{177}Hf$ isotopic ratios from 0.280994 to 0.281672. The difference in Hf isotopic composition suggests that they are not derived from the same source, however the large spread in Hf isotopic compositions from igneous rocks throughout the region and the abundance of ~1.8 Ga detrital zircon in the Mojave province makes this interpretation highly ambiguous.

Of the three grains interpreted to have distinct core and rim domains, two grains yielded both core and rim dates that fell in the same population; K06-DV-24 yielded dates that were both part of the 1773 Ma population, and K06-DV-30 yielded dates that were both part of the 1831 Ma population. The rim of K06-DV-30 was too thin to be analyzed with confidence of maintaining the correct age domain. However, the $^{176}Hf/^{177}Hf$ isotopic ratio of K06-DV-24R is markedly lower than those of the main population of grains, including K06-DV-24C. Although substantial isotopic heterogeneity is observed in almost all plutonic rocks of the Mojave province, these data may be the result of an incorrect age assignment of one of the core or rim analyses. Finally, K06-DV-25 yielded distinct core and rim Hf isotopic compositions. K06-DV-25C yielded a lower $^{176}Hf/^{177}Hf$ isotopic ratio of 0.281625 and K06-DV-25R yielded a higher $^{176}Hf/^{177}Hf$ isotopic ratio of 0.281709, corresponding to ~2 epsilon units.

K06-DV-31C

U-Pb geochronology. Sample K06-DV-31C was taken from a tonalite gneiss in the New York Mountains. Zircon grains from this sample range in size from 100-200 μm with aspect ratios rangingfrom 1:1 to 4:1. Grain morphologies were primarily rounded to subhedral, with some cracked grains and one anhedral grain. Internal textures revealed by BSE imaging show varied concentric zoning with many homogenous interiors.

We obtained 38 ages from as many zircon grains, with ages ranging from 1692 ± 56 to 2635 ± 42 Ma (Supplementary Figure 1G). The four oldest ages, ranging from 2076 ± 58 to 2635 ± 42 Ma are interpreted as inherited grains, however 29 younger ages define a nearly continuous spread of ages from 1692 ± 56 to 1880 ± 42 Ma. A comparison of age vs. concordance showed that concordance increased with age terminating in a cluster of ages at ~1.75 Ga. With increasing age, the >1.8 Ga population became slightly more discordant, thus a weighted mean age of 1748 ± 12 Ma (MSWD = 0.73) calculated from 21 of the youngest ages is taken to be the best approximation of the crystallization age of this sample. The remaining ages, ranging from 1802 ± 48 to 2635 ± 42 Ma, were obtained from grains that were not noticeably distinct in morphology or internal texture from the youngest population of grains, yet are interpreted as xenocrystic.

Hf isotopes. Hf isotopic analyses from 18 zircon grains used to determine the crystallization age of 1748 ± 12 Ma yielded $\varepsilon Hf_{(t)}$ ranging from -12.5 to +2.1. However, 16 of these zircon grains yielded a tighter cluster of from -3.3 to +2.1 at 1.75 Ga. Two zircon grains yielded significantly lower $\varepsilon Hf_{(t)}$ of -12.5 and -11.9 at 1.75 Ga. Given the abundance of older components in this sample, these may represent incorrect age assignment of Hf isotopic analysis.

With the exception of one grain, the 1800-1900 Ma inherited population of zircon grains yielded $\varepsilon Hf_{(t)}$ ranging from -3.6 to +1.3 at 1.85 Ga. One grain yielded an $\varepsilon Hf_{(t)}$ value of +7.2 at 1.81 Ga. The three oldest grains yielded $\varepsilon Hf_{(t)}$ of -1.0 at 2.1 Ga, +1.2 at 2.1 Ga, and +5.9 at 2.6 Ga.

K07-VIR1

U-Pb geochronology. Sample K07-VIR1 was taken from the Virgin Mountains. Zircon grains from this sample range in size from 50-200 μm with aspect ratios rangingfrom 1:1 to 2:1. Several grains were nearly equant and most are rounded. Internal textures revealed by BSE imaging show faint igneous growth zoning in most grains, and some had complex zoning, though our geochronologic results yielded no older ages indicative of inherited cores.

We obtained 22 ages from as many zircon grains, with ages ranging from 1642 ± 21 to 1777 ± 29 Ma. All but two ages were >95% concordant, but there was still a systematic increase in age with increasing concordance. A weighted mean of all 22 ages yields an age of 1734 ± 11 Ma, and the same ages define a cord with an upper intercept age of 1745 ± 4 Ma (Supplementary Figure 1H), which is taken as the best estimate of the age of emplacement.

Hf isotopes. Hf isotope analysis of 14 zircon grains yielded $^{176}Hf/^{177}Hf_{(t)}$ isotopic ratios ranging from 0.281793 to 0.281858 at 1745 Ma ($\varepsilon Hf_{(t)}$ ranging from ~ +4.3 to +10.3).

(E) K14-HH-2 - Augen gneiss

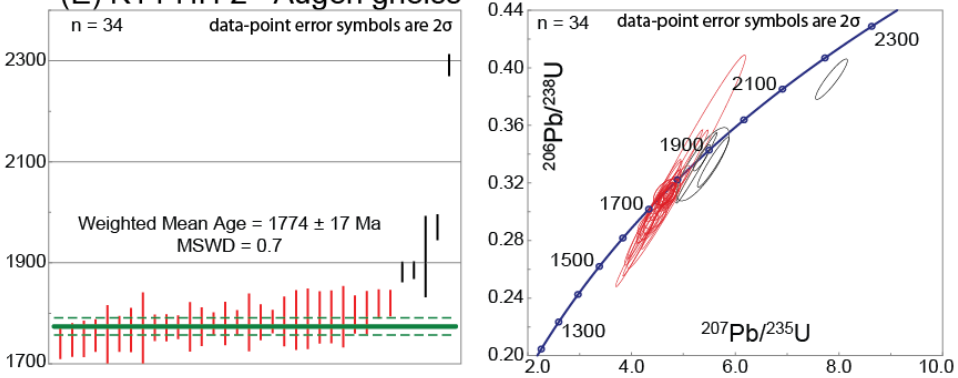

(F) K06-DV-37 - Jubilee Pass Augen Gneiss

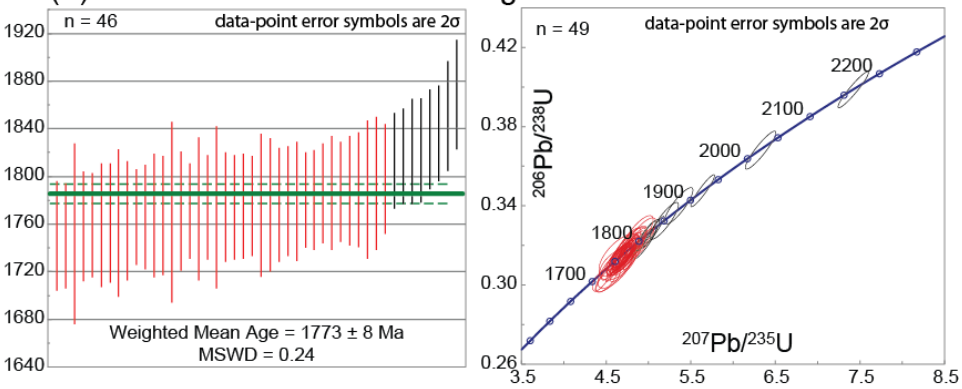

(G) K06-DV-31C - Tonalite Gneiss New York Mountains

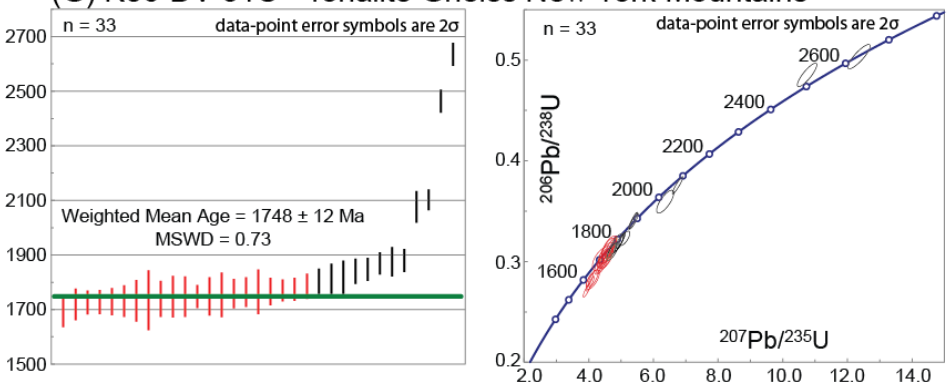

(H) K07-VIR1 - Granodiorite Virgin Mountains

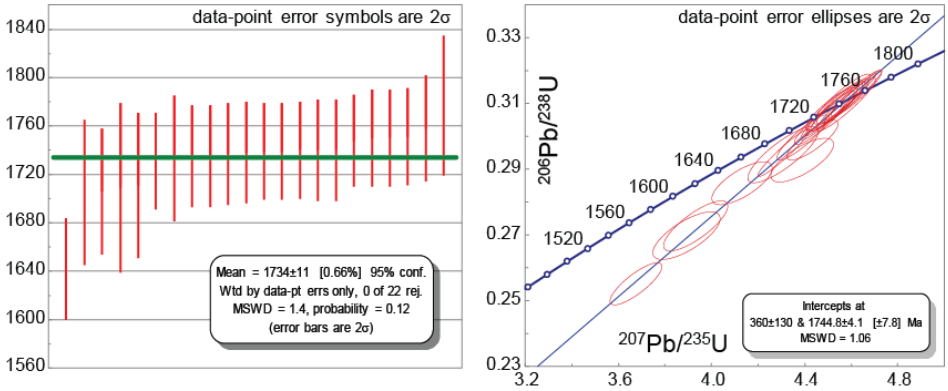

K06-DV-31A

U-Pb geochronology. Sample K06-DV-31A was taken from a gray gneiss in the New York Mountains. Zircon grains from this sample range in size from 100-200 μm with aspect ratios ranging from 1:1 to 1:3. Grain morphologies are primarily subhedral, with some rounded grains and fractured grains. Internal textures revealed by BSE imaging show some concentric growth zoning along with homogenous grains.

We obtained 18 ages from as many grains; ages ranged from 1656 ± 68 to 1818 ± 44 Ma (Supplementary Figure 1I). A weighted mean of 17 ages yields an age of 1732 ± 12 Ma (MSWD = 0.42). The oldest age of 1818 ± 44 Ma was obtained from a zoned zircon grain (K06-DV31A-21), and is interpreted as an older inherited core.

Hf isotopes. Hf isotopic analyses from 13 dated zircon grains yielded $\varepsilon Hf_{(t)}$ ranging from -4.0 to +7.8 at 1.73 Ga. Eight grains from the main population yielded a cluster of $\varepsilon Hf_{(t)}$ ranging from +4.9 to +7.8 at 1.73 Ga, however four grains yield lower and more scattered $\varepsilon Hf_{(t)}$ ranging from +2.5 to -4.0 at 1.73 Ga. The inherited core yielded an $\varepsilon Hf_{(t)}$ value of -1.0 at 1.82 Ga. The lower $\varepsilon Hf_{(t)}$ obtained from 1.73 Ga zircon grains may reflect an isotopically mixed source for this sample, or incorrect age assignments of Hf isotopic analyses.

K14-BLFG-1

U-Pb geochronology. Sample K14-BLFG-1 was taken from an augen gneiss with plagioclase phenocrysts in the Bullfrog Hills. Zircons from this sample range in size from 150-500 μm, with aspect ratios ranging from 1:2 to 1:3. Grain morphologies are predominantly euhedral to subhedral with some grains displaying moderate to extreme rounding and fractures. Internal zoning as revealed by CL imaging shows complex

zoning in almost all grains. Most grains preserve pristine magmatic textures at least locally. Internal textures of some grains have been completely obliterated, and others are locally disturbed by homogenous or convolute zones.

We obtained 37 ages from 34 zircon grains; attempts were made to date discrete age domains within zircons that displayed complex zoing, however our paired core and rim analyses yielded indistinguishable ages. Ages ranged from 1671 ± 22 Ma to 1720 ± 15 Ma (Supplementary Figure 4J). Comparing age and concordance showed that younger ages were more discordant, with a systematic increase in concordance with age. Four of the oldest ages obtained from domains which displayed pristine igneous zoning were between 99% and 100% concordant. These grains yielded a weighted mean age of 1716 ± 14 Ma (MSWD = 0.4), which is interpreted as the crystallization age of the sample.

Hf isotopes. Hf isotopic analyses from 12 dated zircon grains yielded a cluster of $\varepsilon Hf_{(t)}$ ranging from +0.2 to +4.5 at 1.71 Ga.

K06-DV-30

U-Pb geochronology. Sample K06-DV-30 was taken from the Fenner Gneiss in the Piute Mountains. Zircon grains from this sample range in size from 100-300 μm primarily with aspect ratios of 1:3. Grain morphologies are primarily subhedral with some rounded edges and fractures. Some grains display concentric zoning in BSE images, while many appear homogenous.

We obtained 22 ages from as many zircon grains from sample K06-DV-30, which ranged in age from 1659 ± 54 to 1719 ± 42 Ma (Supplementary Figure 4K). A weighted mean of all 22 ages yielded an age of 1691 ± 9 Ma (MSWD = 0.34). This age is in agreement with the age of 1685 ± 0.15 Ma reported by Bender (2008).

Hf isotopes. $\varepsilon Hf_{(t)}$ determined from 20 dated zircon grains from the Fenner Gneiss plot in a cluster ranging from +4.5 to +7.4 at 1.69 Ga.

K13-BL-1

U-Pb geochronology. Sample K13-BL-1 was taken from an island of basement rock at the southern edge of the Black Mountains at the same location as LTG-228 sampled by Ramo and Calzia (1998). Ramo and Calzia (1998) described their sample as granitic gneiss, however our field observations were that the sample was only weakly deformed, which is consistent with our geochronologic results and the known episodes of deformation in the Mojave province (Barth et al., 2009) (see below). Zircon grains from this sample range in size from 100-300 μm, with aspect ratios ranging from 2:1 to 4:1. Grain morphologies are primarily subhedral to euhedral and elongate. Internal textures revealed by CL imaging show concentric igneous growth zoning that is locally obscured by CL dark zones, particularly around the outside of grains. These potentially metamict zones were avoided whenever possible during analysis.

We conducted 24 analyses on 24 grains and obtained 19 ages. Ages ranged from 1607 ± 19 Ma to 1950 ± 97 Ma, and 89% to 102% concordant (Supplementary Figure 4L). Younger ages were more discordant showing a systematic increase in concordance with older ages, terminating with a cluster of precise and nearly perfectly concordant ages, as would be expected with ancient Pb loss. The data define a cord with intercepts at 527 ± 127 and 1687 ± 7.5 Ma, however the cord is not robust due to the overlap in analytical error between samples. The five most concordant ages (99-102%) yield a weighted mean age of 1691 ± 15 Ma (MSWD = 1.5), which is interpreted as the

crystallization age of this sample. Five additional zircon grains yield older and discordant ages, which are interpreted as inherited zircon grains.

Hf isotopes. Hf isotopic analysis of the most concordant zircon grains yielded initial $^{176}Hf/^{177}Hf$ ratios ranging from 0.281639 ± 0.000087 to 0.281735 ± 0.000069, corresponding to $\varepsilon_{Hf(t)}$ ranging from +0.3 to -3.3 at 1.69 Ga.

(I) K06-DV-31A - Gray Gneiss New York Mountains

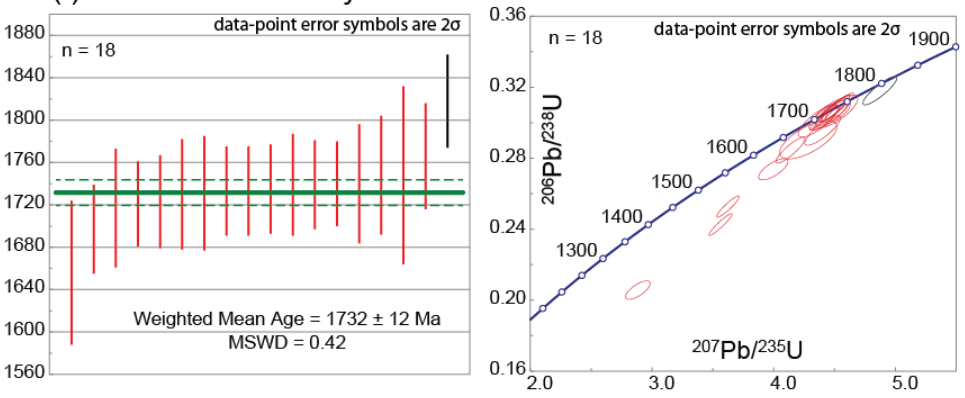

(J) K14-BLFG-1 - Augen gneiss Bullfrog Hills

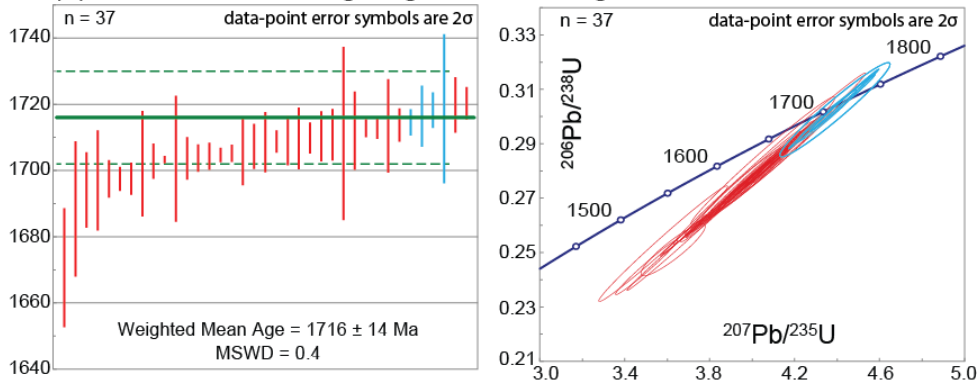

(K) K06-DV-30 - Fenner Gneiss Piute Mountains

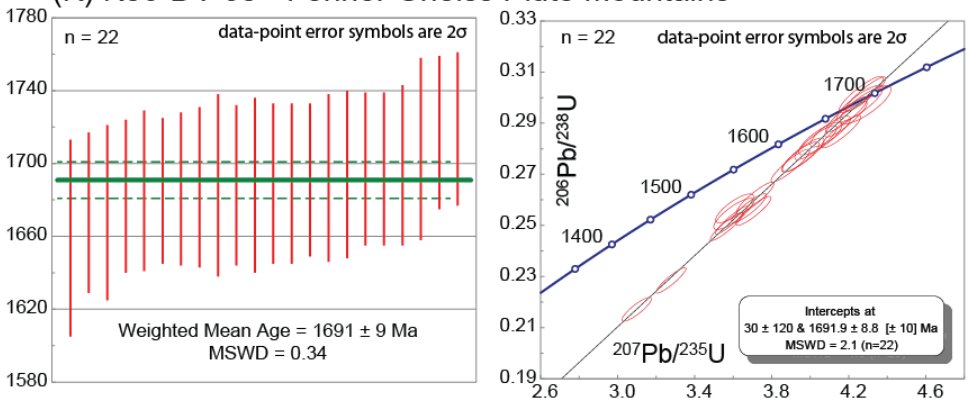

(L) K13-BL-1 - Granite Black Mountains

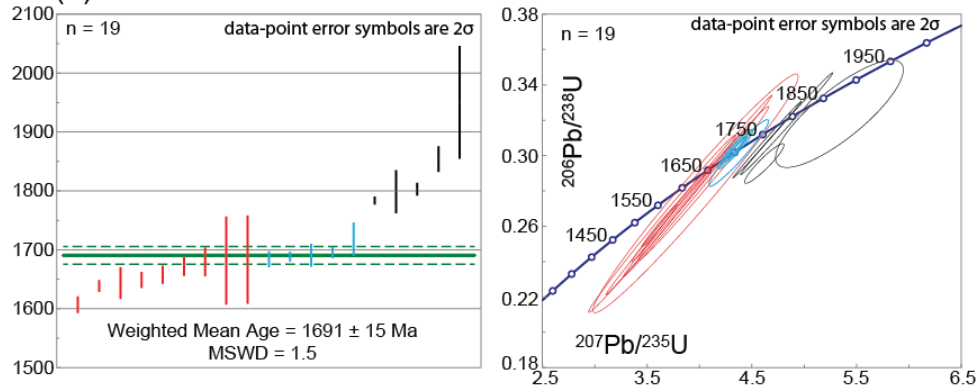

APPENDIX 2: Analytical data tables from Chapter 1

Table A2-1. ALC Detrital zircon U-Pb geochronologic data from Death Valley.

						Isotope ratios					Apparent ages (Ma)								
Analysis	U	206Pb	U/Th	206Pb*	±	207Pb*	±	206Pb*	±	error	206Pb*	±	207Pb*	±	206Pb*	±	Best age	±	Conc
	(ppm)	204Pb		207Pb*	(%)	235U*	(%)	238U	(%)	corr.	238U*	(Ma)	235U	(Ma)	207Pb*	(Ma)	(Ma)	(Ma)	(%)
K13ASH-1-94	477	5819	2.0	8.5771	0.6	4.1279	3.2	0.2568	3.1	0.98	1473.4	41.4	1659.8	26.2	1904.6	10.5	1904.6	10.5	77.4
K13ASH-1-10	354	14446	3.0	9.2144	0.4	3.7065	1.1	0.2477	1.1	0.94	1426.6	13.4	1572.8	8.9	1774.8	6.9	1774.8	6.9	80.4
K13ASH-1-105	477	8732	1.2	9.1742	0.4	3.7598	2.5	0.2502	2.4	0.99	1439.4	31.2	1584.2	19.7	1782.8	7.7	1782.8	7.7	80.7
K13ASH-1-5	285	22294	1.3	8.6709	0.6	4.2955	8.8	0.2701	8.8	1.00	1541.5	120.2	1692.5	72.5	1885.0	11.0	1885.0	11.0	81.8
K13ASH-1-103	359	8215	4.1	8.7376	1.0	4.2331	3.9	0.2683	3.8	0.97	1531.9	51.2	1680.5	31.9	1871.2	17.8	1871.2	17.8	81.9
K13ASH-1-32	315	20436	4.7	4.3225	0.3	15.2244	3.9	0.4773	3.9	1.00	2515.4	81.1	2829.4	37.2	3061.4	4.1	3061.4	4.1	82.2
K13ASH-1-65	268	16302	2.1	6.1025	0.5	8.5738	3.6	0.3795	3.6	0.99	2073.8	63.8	2293.8	33.0	2495.9	7.8	2495.9	7.8	83.1
K13ASH-1-55	360	24712	1.4	6.1631	1.0	8.4881	6.4	0.3794	6.4	0.99	2073.5	112.6	2284.6	58.5	2479.3	17.4	2479.3	17.4	83.6
K13ASH-1-68	203	9789	1.2	8.3489	0.7	4.7668	9.2	0.2886	9.2	1.00	1634.7	132.6	1779.1	77.4	1952.9	12.3	1952.9	12.3	83.7
K13ASH-1-104	326	24189	2.4	5.9862	1.3	9.2486	7.3	0.4015	7.1	0.98	2176.1	131.6	2362.9	66.5	2528.3	22.6	2528.3	22.6	86.1
K13ASH-1-6	215	54203	0.9	5.3993	0.6	11.2593	1.8	0.4409	1.7	0.95	2354.7	32.7	2544.8	16.3	2700.1	9.4	2700.1	9.4	87.2
K13ASH-1-44	147	52315	8.0	5.2673	2.9	11.9134	9.8	0.4551	9.3	0.95	2418.0	188.0	2597.6	91.8	2740.9	48.4	2740.9	48.4	88.2
K13ASH-1-17	138	13582	0.6	5.5268	0.3	11.1190	2.7	0.4457	2.7	0.99	2376.1	53.3	2533.2	25.1	2661.5	4.9	2661.5	4.9	89.3
K13ASH-1-51	379	14209	2.1	8.7461	0.6	4.7003	3.5	0.2982	3.5	0.99	1682.2	51.8	1767.3	29.7	1869.4	10.8	1869.4	10.8	90.0
K13ASH-1-24	263	62067	1.1	5.5813	0.8	11.2619	2.6	0.4559	2.4	0.95	2421.3	49.3	2545.1	24.1	2645.2	14.0	2645.2	14.0	91.5
K13ASH-1-88	406	15124	3.8	9.1065	0.7	4.4198	5.3	0.2919	5.2	0.99	1651.1	76.0	1716.1	43.6	1796.3	13.2	1796.3	13.2	91.9
K13ASH-1-70	109	25039	2.0	8.7986	0.6	4.7634	2.1	0.3040	2.0	0.95	1710.9	29.5	1778.5	17.2	1858.6	11.1	1858.6	11.1	92.1
K13ASH-1-4	166	3241	0.4	8.4622	1.9	5.1862	4.2	0.3183	3.7	0.89	1781.4	57.9	1850.4	35.6	1928.8	34.2	1928.8	34.2	92.4
K13ASH-1-28	178	28092	1.3	7.9399	0.3	5.9451	1.9	0.3424	1.9	0.99	1898.0	30.7	1967.8	16.4	2042.1	5.3	2042.1	5.3	92.9
K13ASH-1-27	246	26945	1.3	8.3876	0.3	5.3540	1.8	0.3257	1.7	0.99	1817.5	27.7	1877.5	15.2	1944.6	5.3	1944.6	5.3	93.5
K13ASH-1-77	345	53256	2.3	8.8301	0.3	4.8315	2.2	0.3094	2.2	0.99	1737.9	33.9	1790.4	18.9	1852.2	5.9	1852.2	5.9	93.8
K13ASH-1-36	132	27868	2.5	5.9115	1.5	10.4807	4.6	0.4493	4.4	0.94	2392.4	87.6	2478.2	43.0	2549.4	25.7	2549.4	25.7	93.8
K13ASH-1-49	63	30848	1.7	5.1790	0.3	13.2799	2.2	0.4988	2.2	0.99	2608.7	47.7	2699.8	21.2	2768.6	4.4	2768.6	4.4	94.2
K13ASH-1-60	147	48896	0.9	5.4695	0.4	12.1130	1.1	0.4805	1.0	0.92	2529.5	20.6	2613.2	10.1	2678.7	7.1	2678.7	7.1	94.4
K13ASH-1-15	308	25673	0.9	6.0823	0.4	10.1021	3.2	0.4456	3.2	0.99	2375.8	62.9	2444.2	29.5	2501.5	7.5	2501.5	7.5	95.0
K13ASH-1-23	172	55317	1.2	8.5573	0.4	5.2548	1.5	0.3261	1.4	0.96	1819.6	22.4	1861.5	12.6	1908.7	7.6	1908.7	7.6	95.3
K13ASH-1-82	187	64362	2.3	8.9302	0.4	4.8147	1.6	0.3118	1.6	0.97	1749.8	24.3	1787.5	13.8	1831.8	7.5	1831.8	7.5	95.5
K13ASH-1-57	318	9578	2.7	4.5452	0.4	16.8577	4.9	0.5557	4.9	1.00	2848.9	112.3	2926.8	46.9	2980.8	6.1	2980.8	6.1	95.6
K13ASH-1-11	180	35505	1.6	5.4888	0.1	12.3047	1.1	0.4898	1.1	0.99	2570.0	22.7	2627.9	10.1	2672.9	2.4	2672.9	2.4	96.1
K13ASH-1-26	309	27663	2.3	5.9351	0.2	10.7674	3.0	0.4635	3.0	1.00	2455.0	61.6	2503.3	28.1	2542.7	4.0	2542.7	4.0	96.6
K13ASH-1-81	155	10390	1.1	6.7404	0.4	8.5509	1.8	0.4180	1.8	0.98	2251.5	33.9	2291.4	16.6	2327.1	6.7	2327.1	6.7	96.8
K13ASH-1-99	244	12240	2.7	9.0223	0.6	4.7837	7.9	0.3130	7.9	1.00	1755.6	120.7	1782.0	66.2	1813.2	10.2	1813.2	10.2	96.8
K13ASH-1-74	32	46245	4.4	5.8063	0.8	11.2595	3.0	0.4742	2.8	0.96	2501.7	58.8	2544.9	27.5	2579.4	13.5	2579.4	13.5	97.0
K13ASH-1-73	169	40017	2.1	5.7735	0.2	11.3994	1.1	0.4773	1.1	0.99	2515.6	22.9	2556.4	10.4	2588.8	3.0	2588.8	3.0	97.2

K13ASH-1-84	126	44852	2.9	8.9496	0.4	4.8940	1.0	0.3177	0.9	0.93	1778.3	13.8	1801.2	8.1	1827.8	6.6	1827.8	6.6	97.3
K13ASH-1-19	377	40376	3.3	8.2023	0.2	5.9119	0.9	0.3517	0.9	0.97	1942.7	14.3	1963.0	7.7	1984.5	4.1	1984.5	4.1	97.9
K13ASH-1-80	237	164525	0.8	8.1406	0.9	6.0117	2.8	0.3549	2.7	0.95	1958.1	45.3	1977.5	24.5	1997.9	15.4	1997.9	15.4	98.0
K13ASH-1-16	178	48077	1.6	8.7303	0.5	5.2072	1.3	0.3297	1.3	0.93	1837.0	20.0	1853.8	11.5	1872.7	8.9	1872.7	8.9	98.1
K13ASH-1-50	105	328414	0.8	5.4915	0.1	12.6354	1.4	0.5032	1.3	0.99	2627.7	29.0	2652.9	12.7	2672.1	2.3	2672.1	2.3	98.3
K13ASH-1-39	219	175007	2.0	8.8242	0.3	5.1093	0.9	0.3270	0.9	0.96	1823.8	14.5	1837.6	8.1	1853.4	4.8	1853.4	4.8	98.4
K13ASH-1-7	113	304600	0.7	6.9628	0.9	8.2094	1.4	0.4146	1.1	0.77	2235.8	19.9	2254.4	12.3	2271.3	14.9	2271.3	14.9	98.4
K13ASH-1-41	50	161581	1.5	4.7849	0.4	16.0620	0.9	0.5574	0.8	0.88	2855.9	17.3	2880.5	8.2	2897.7	6.6	2897.7	6.6	98.6
K13ASH-1-48	312	133369	1.6	4.7443	0.3	16.3337	1.9	0.5620	1.8	0.98	2875.0	42.4	2896.5	17.8	2911.5	5.3	2911.5	5.3	98.7
K13ASH-1-59	27	29242	1.1	5.5178	1.0	12.6020	1.7	0.5043	1.3	0.80	2632.3	29.2	2650.4	16.0	2664.2	17.0	2664.2	17.0	98.8
K13ASH-1-20	135	7208	1.3	5.9465	0.6	11.0568	2.1	0.4769	2.0	0.96	2513.6	41.7	2527.9	19.5	2539.4	10.4	2539.4	10.4	99.0
K13ASH-1-25	84	11817	1.6	5.5405	0.2	12.5408	2.4	0.5039	2.4	1.00	2630.7	52.0	2645.8	22.8	2657.4	3.8	2657.4	3.8	99.0
K13ASH-1-72	215	97302	2.0	6.4696	0.2	9.4853	1.4	0.4451	1.3	0.99	2373.3	26.7	2386.1	12.5	2397.1	3.8	2397.1	3.8	99.0
K13ASH-1-67	143	245481	2.4	5.7223	0.5	11.8509	1.8	0.4918	1.7	0.96	2578.6	37.0	2592.7	17.0	2603.7	8.5	2603.7	8.5	99.0
K13ASH-1-95	207	187245	1.7	5.7744	0.3	11.6651	1.0	0.4885	0.9	0.96	2564.3	19.9	2577.9	9.1	2588.6	4.5	2588.6	4.5	99.1
K13ASH-1-22	112	24517	0.5	4.9423	1.1	15.3021	4.6	0.5485	4.4	0.97	2818.9	101.3	2834.2	43.7	2845.1	18.6	2845.1	18.6	99.1
K13ASH-1-47	116	70170	1.3	8.2151	0.5	5.9830	2.2	0.3565	2.1	0.97	1965.4	35.9	1973.4	19.0	1981.7	9.6	1981.7	9.6	99.2
K13ASH-1-8	195	161616	5.7	6.7378	0.3	8.8168	0.7	0.4309	0.6	0.93	2309.6	12.3	2319.2	6.2	2327.7	4.3	2327.7	4.3	99.2
K13ASH-1-31	280	270899	5.6	8.1525	0.3	6.0842	0.7	0.3597	0.7	0.93	1981.0	11.3	1988.0	6.2	1995.3	4.6	1995.3	4.6	99.3
K13ASH-1-64	127	223795	1.2	5.4460	0.2	12.9799	2.0	0.5127	2.0	1.00	2668.0	43.0	2678.2	18.6	2685.8	2.7	2685.8	2.7	99.3
K13ASH-1-85	99	213898	0.6	3.9919	0.2	21.9216	0.9	0.6347	0.9	0.98	3168.1	21.5	3180.3	8.5	3188.0	2.9	3188.0	2.9	99.4
K13ASH-1-43	80	20344	2.0	8.9330	0.6	5.0362	1.2	0.3263	1.0	0.87	1820.4	15.9	1825.4	9.8	1831.2	10.3	1831.2	10.3	99.4
K13ASH-1-87	161	285433	2.7	8.6928	0.4	5.3459	0.8	0.3370	0.7	0.90	1872.4	12.0	1876.2	7.0	1880.5	6.5	1880.5	6.5	99.6
K13ASH-1-62	37	68276	0.8	5.4668	0.5	12.9516	1.1	0.5135	0.9	0.86	2671.6	20.3	2676.1	10.1	2679.5	9.0	2679.5	9.0	99.7
K13ASH-1-40	63	150795	1.2	6.1468	1.5	10.5218	2.1	0.4691	1.4	0.68	2479.5	29.1	2481.8	19.4	2483.8	26.0	2483.8	26.0	99.8
K13ASH-1-92	276	201236	1.7	8.7114	0.2	5.3394	1.6	0.3373	1.6	0.99	1873.9	25.9	1875.2	13.7	1876.6	3.1	1876.6	3.1	99.9
K13ASH-1-9	138	234063	2.3	5.5373	0.1	12.6944	0.7	0.5098	0.7	0.98	2655.8	15.1	2657.2	6.7	2658.3	2.4	2658.3	2.4	99.9
K13ASH-1-76	53	117198	1.8	5.5613	0.4	12.5997	1.1	0.5082	1.0	0.93	2648.9	22.8	2650.2	10.6	2651.1	7.0	2651.1	7.0	99.9
K13ASH-1-1	62	188259	1.2	5.4042	0.3	13.2549	0.9	0.5195	0.8	0.94	2697.2	17.8	2698.0	8.2	2698.6	5.0	2698.6	5.0	99.9
K13ASH-1-61	77	217748	1.9	8.4613	0.7	5.6817	1.7	0.3487	1.6	0.91	1928.2	26.3	1928.6	15.0	1928.9	12.8	1928.9	12.8	100.0
K13ASH-1-46	165	235615	1.6	8.1252	0.3	6.1819	0.7	0.3643	0.6	0.88	2002.5	10.3	2001.9	6.0	2001.2	5.9	2001.2	5.9	100.1
K13ASH-1-3	106	126459	1.0	5.4553	0.2	13.0614	1.2	0.5168	1.2	0.98	2685.5	26.9	2684.1	11.8	2683.0	4.0	2683.0	4.0	100.1
K13ASH-1-38	92	99196	3.4	8.7008	0.2	5.3690	0.6	0.3388	0.5	0.90	1880.9	8.4	1879.9	4.9	1878.8	4.5	1878.8	4.5	100.1
K13ASH-1-63	241	266761	0.7	7.6755	0.2	6.9385	0.8	0.3863	0.7	0.97	2105.4	13.4	2103.6	6.9	2101.8	3.4	2101.8	3.4	100.2
K13ASH-1-12	306	513485	3.6	8.1461	0.2	6.1584	0.9	0.3638	0.9	0.97	2000.4	15.3	1998.6	8.0	1996.7	4.2	1996.7	4.2	100.2
K13ASH-1-45	206	108443	1.3	6.9081	0.2	8.5136	1.1	0.4265	1.1	0.99	2290.1	21.7	2287.4	10.4	2284.9	3.3	2284.9	3.3	100.2
K13ASH-1-86	164	355722	2.1	8.8549	0.4	5.1943	0.7	0.3336	0.6	0.81	1855.8	9.5	1851.7	6.2	1847.1	7.6	1847.1	7.6	100.5
K13ASH-1-14	169	176109	1.5	8.3670	0.4	5.8656	1.0	0.3559	0.9	0.90	1962.9	15.7	1956.2	8.9	1949.0	7.8	1949.0	7.8	100.7
K13ASH-1-56	81	194118	1.6	4.6814	0.2	17.1320	0.9	0.5817	0.9	0.97	2955.6	20.7	2942.3	8.7	2933.1	3.7	2933.1	3.7	100.8
K13ASH-1-90	39	129494	0.4	6.7065	0.7	9.0907	3.4	0.4422	3.3	0.98	2360.4	66.1	2347.2	31.3	2335.7	12.5	2335.7	12.5	101.1
K13ASH-1-66	135	177431	2.0	8.7442	0.5	5.3723	1.9	0.3407	1.8	0.96	1890.1	29.3	1880.4	15.9	1869.8	9.2	1869.8	9.2	101.1
K13ASH-1-101	229	220177	2.0	8.4046	0.2	5.8384	0.7	0.3559	0.7	0.97	1962.6	11.8	1952.1	6.2	1941.0	3.0	1941.0	3.0	101.1
K13ASH-1-30	221	191318	2.2	8.6902	0.3	5.4515	0.9	0.3436	0.9	0.96	1903.9	15.0	1893.0	8.1	1881.0	4.6	1881.0	4.6	101.2

K13ASH-1-102	237	306719	2.5	8.1530	0.3	6.2404	0.7	0.3690	0.6	0.92	2024.7	10.7	2010.1	5.9	1995.2	4.8	1995.2	4.8	101.5
K13ASH-1-54	220	251851	2.1	8.8054	0.3	5.3185	3.8	0.3397	3.7	1.00	1885.0	61.1	1871.8	32.1	1857.2	6.3	1857.2	6.3	101.5
K13ASH-1-2	158	308558	1.8	8.1007	0.4	6.3286	0.9	0.3718	0.8	0.88	2037.9	14.4	2022.4	8.2	2006.6	7.9	2006.6	7.9	101.6
K13ASH-1-37	314	469526	7.5	8.5379	0.1	5.6811	0.8	0.3518	0.8	0.99	1943.1	13.7	1928.5	7.1	1912.8	2.3	1912.8	2.3	101.6
K13ASH-1-21	97	64731	1.1	8.7014	0.5	5.4620	1.4	0.3447	1.3	0.94	1909.3	22.1	1894.6	12.3	1878.7	9.0	1878.7	9.0	101.6
K13ASH-1-69	140	289774	1.3	8.6977	0.4	5.4727	1.9	0.3452	1.9	0.98	1911.8	30.8	1896.3	16.4	1879.5	7.3	1879.5	7.3	101.7
K13ASH-1-34	217	190302	2.1	8.8064	0.2	5.3385	2.3	0.3410	2.3	1.00	1891.3	38.1	1875.0	19.9	1857.0	3.1	1857.0	3.1	101.8
K13ASH-1-33	183	290611	2.2	8.7084	0.2	5.4725	0.9	0.3456	0.8	0.97	1913.7	13.7	1896.3	7.3	1877.2	3.6	1877.2	3.6	101.9
K13ASH-1-78	145	238773	1.8	6.7825	0.2	8.9963	1.1	0.4425	1.1	0.98	2362.0	21.5	2337.6	10.2	2316.4	4.0	2316.4	4.0	102.0
K13ASH-1-89	128	104240	1.5	4.1896	1.1	20.9272	4.3	0.6359	4.2	0.97	3172.8	104.5	3135.2	41.9	3111.2	17.8	3111.2	17.8	102.0
K13ASH-1-71	410	41323	6.0	8.3400	1.2	6.0010	6.9	0.3630	6.8	0.98	1996.3	116.2	1976.0	60.0	1954.8	22.3	1954.8	22.3	102.1
K13ASH-1-42	175	51288	2.1	5.6846	0.5	12.7840	6.5	0.5271	6.5	1.00	2729.1	145.0	2663.9	61.6	2614.7	8.3	2614.7	8.3	104.4
K13-IBEX-1-81	859	3909	13.6	9.7022	2.4	2.8502	8.0	0.2006	7.6	0.95	1178.3	81.8	1368.9	60.0	1680.1	44.7	1680.1	44.7	70.1
K13-IBEX-1-91	499	3941	0.9	8.7207	0.6	3.6344	3.2	0.2299	3.2	0.98	1333.8	38.3	1557.1	25.7	1874.7	10.7	1874.7	10.7	71.1
K13-IBEX-1-11	590	6473	4.5	8.6437	0.4	3.7182	1.0	0.2331	0.9	0.91	1350.7	11.3	1575.3	8.2	1890.7	7.6	1890.7	7.6	71.4
K13-IBEX-1-57	451	4546	1.3	9.2461	0.5	3.3420	1.0	0.2241	0.8	0.86	1303.6	9.8	1490.9	7.5	1768.5	8.8	1768.5	8.8	73.7
K13-IBEX-1-99	389	8172	1.9	8.0780	0.3	4.5207	3.9	0.2649	3.8	1.00	1514.6	51.9	1734.8	32.1	2011.6	5.8	2011.6	5.8	75.3
K13-IBEX-1-42	455	4914	1.6	9.3755	0.8	3.3881	1.9	0.2304	1.7	0.92	1336.5	20.9	1501.6	14.8	1743.1	13.7	1743.1	13.7	76.7
K13-IBEX-1-73	473	11998	1.5	9.0365	0.2	3.7345	0.7	0.2448	0.7	0.95	1411.4	9.0	1578.8	6.0	1810.3	4.2	1810.3	4.2	78.0
K13-IBEX-1-50	175	6598	1.2	8.9120	0.8	3.8618	2.0	0.2496	1.8	0.91	1436.5	23.6	1605.7	16.2	1835.5	15.1	1835.5	15.1	78.3
K13-IBEX-1-27	305	17793	1.9	7.9502	5.4	4.8904	6.8	0.2820	4.2	0.61	1601.3	59.3	1800.6	57.7	2039.8	95.9	2039.8	95.9	78.5
K13-IBEX-1-36	419	7443	5.6	9.2675	0.4	3.5886	2.1	0.2412	2.0	0.98	1393.0	25.2	1547.0	16.3	1764.3	7.5	1764.3	7.5	79.0
K13-IBEX-1-32	284	6200	3.4	8.6760	1.2	4.1519	4.1	0.2613	4.0	0.96	1496.3	52.9	1664.6	33.9	1883.9	21.6	1883.9	21.6	79.4
K13-IBEX-1-15	368	12934	1.2	9.0521	0.4	3.9253	1.1	0.2577	1.1	0.94	1478.1	14.0	1618.9	9.1	1807.2	7.2	1807.2	7.2	81.8
K13-IBEX-1-96	326	21658	2.8	7.1607	0.2	6.3412	1.1	0.3293	1.1	0.97	1835.1	16.8	2024.2	9.5	2222.9	4.3	2222.9	4.3	82.6
K13-IBEX-1-109	330	14983	1.9	5.8848	0.2	9.3261	1.0	0.3980	1.0	0.99	2160.0	17.8	2370.6	9.0	2556.9	2.8	2556.9	2.8	84.5
K13-IBEX-1-43	69	31802	1.6	5.9160	0.4	9.2438	6.4	0.3966	6.3	1.00	2153.5	116.2	2362.5	58.4	2548.1	7.3	2548.1	7.3	84.5
K13-IBEX-1-69	388	73712	1.8	8.7748	0.7	4.4400	2.3	0.2826	2.2	0.96	1604.3	31.4	1719.8	19.1	1863.5	12.0	1863.5	12.0	86.1
K13-IBEX-1-39	287	47082	2.5	9.0187	0.3	4.2552	2.6	0.2783	2.6	0.99	1583.0	36.4	1684.7	21.4	1813.9	4.8	1813.9	4.8	87.3
K13-IBEX-1-85	363	17533	1.5	8.9638	0.6	4.3392	3.2	0.2821	3.1	0.98	1601.9	44.1	1700.8	26.2	1825.0	11.4	1825.0	11.4	87.8
K13-IBEX-1-35	180	5698	1.6	8.2310	0.6	5.3432	1.1	0.3190	0.9	0.85	1784.7	14.0	1875.8	9.0	1978.2	9.9	1978.2	9.9	90.2
K13-IBEX-1-51	477	16626	2.6	8.8282	0.2	4.6728	1.0	0.2992	1.0	0.98	1687.3	14.6	1762.4	8.4	1852.6	3.4	1852.6	3.4	91.1
K13-IBEX-1-44	197	58892	2.7	8.2265	0.4	5.4108	5.1	0.3228	5.1	1.00	1803.5	80.8	1886.6	44.2	1979.2	6.7	1979.2	6.7	91.1
K13-IBEX-1-8	194	16841	2.3	8.9062	0.5	4.6077	2.6	0.2976	2.5	0.98	1679.5	37.6	1750.7	21.5	1836.7	8.2	1836.7	8.2	91.4
K13-IBEX-1-14	252	18383	2.3	6.8298	1.3	7.8975	2.2	0.3912	1.7	0.79	2128.4	30.8	2219.4	19.4	2304.5	22.8	2304.5	22.8	92.4
K13-IBEX-1-4	276	61150	1.6	6.4820	0.3	8.8267	1.4	0.4150	1.4	0.98	2237.5	25.5	2320.3	12.6	2393.8	4.6	2393.8	4.6	93.5
K13-IBEX-1-18	185	14748	1.2	8.8865	0.3	4.7747	1.2	0.3077	1.2	0.97	1729.5	17.7	1780.5	10.1	1840.7	5.6	1840.7	5.6	94.0
K13-IBEX-1-103	229	34406	1.6	8.7520	0.5	4.9799	2.6	0.3161	2.6	0.98	1770.7	40.0	1815.9	22.3	1868.2	9.4	1868.2	9.4	94.8
K13-IBEX-1-105	297	34414	3.7	8.8537	0.3	4.8616	1.1	0.3122	1.1	0.97	1751.4	16.6	1795.6	9.4	1847.4	5.1	1847.4	5.1	94.8
K13-IBEX-1-54	219	181255	1.7	4.3546	0.7	17.9366	3.2	0.5665	3.1	0.98	2893.3	73.4	2986.3	30.9	3049.6	10.4	3049.6	10.4	94.9
K13-IBEX-1-74	268	17927	2.5	8.8203	0.4	4.9259	1.5	0.3151	1.5	0.97	1765.8	23.2	1806.7	13.1	1854.2	6.6	1854.2	6.6	95.2
K13-IBEX-1-17	219	53774	1.3	8.8125	0.3	4.9568	2.9	0.3168	2.9	0.99	1774.1	45.2	1812.0	24.8	1855.8	6.1	1855.8	6.1	95.6

K13-IBEX-1-26	306	16076	2.0	8.8343	1.0	4.9343	1.8	0.3162	1.5	0.82	1770.9	22.9	1808.1	15.2	1851.3	18.6	1851.3	18.6	95.7
K13-IBEX-1-94	269	22686	1.3	8.8781	0.3	4.9135	1.6	0.3164	1.6	0.98	1772.0	24.3	1804.6	13.5	1842.4	5.9	1842.4	5.9	96.2
K13-IBEX-1-13	213	29006	2.5	8.7941	0.3	5.0216	6.3	0.3203	6.3	1.00	1791.1	98.7	1823.0	53.5	1859.6	5.2	1859.6	5.2	96.3
K13-IBEX-1-55	43	52093	1.5	6.4339	0.5	9.2755	1.1	0.4328	1.0	0.90	2318.4	19.3	2365.6	10.1	2406.5	8.1	2406.5	8.1	96.3
K13-IBEX-1-9	133	226868	1.7	8.8252	0.5	4.9906	0.8	0.3194	0.6	0.77	1786.9	9.4	1817.7	6.6	1853.2	8.9	1853.2	8.9	96.4
K13-IBEX-1-66	107	113883	1.3	8.5849	0.3	5.3033	2.3	0.3302	2.3	0.99	1839.3	36.5	1869.4	19.6	1902.9	5.3	1902.9	5.3	96.7
K13-IBEX-1-108	217	27865	2.7	8.8401	0.6	4.9891	2.1	0.3199	2.0	0.96	1789.1	31.6	1817.5	17.9	1850.1	11.0	1850.1	11.0	96.7
K13-IBEX-1-77	371	76089	2.7	8.9099	0.2	4.9137	0.9	0.3175	0.8	0.96	1777.6	12.8	1804.6	7.3	1835.9	4.5	1835.9	4.5	96.8
K13-IBEX-1-92	193	149503	3.8	8.9114	0.3	4.9126	1.5	0.3175	1.5	0.98	1777.6	22.9	1804.4	12.7	1835.6	5.8	1835.6	5.8	96.8
K13-IBEX-1-56	81	41924	1.0	5.5551	0.5	12.1537	1.6	0.4897	1.5	0.94	2569.2	31.4	2616.3	14.8	2653.0	8.8	2653.0	8.8	96.8
K13-IBEX-1-65	225	36077	2.2	8.8390	0.6	5.0239	1.7	0.3221	1.6	0.93	1799.8	25.0	1823.4	14.4	1850.3	11.0	1850.3	11.0	97.3
K13-IBEX-1-16	382	27046	1.7	8.7536	0.2	5.1492	1.0	0.3269	1.0	0.98	1823.4	15.5	1844.3	8.5	1867.9	3.9	1867.9	3.9	97.6
K13-IBEX-1-95	253	351662	5.5	8.8678	0.1	5.0101	1.3	0.3222	1.3	1.00	1800.6	20.8	1821.0	11.2	1844.5	2.0	1844.5	2.0	97.6
K13-IBEX-1-104	74	168184	1.4	8.7480	0.7	5.1578	1.4	0.3272	1.2	0.85	1825.0	19.2	1845.7	12.1	1869.0	13.4	1869.0	13.4	97.6
K13-IBEX-1-62	256	38671	1.2	8.7604	0.3	5.1577	3.0	0.3277	3.0	0.99	1827.2	48.0	1845.7	25.8	1866.5	5.9	1866.5	5.9	97.9
K13-IBEX-1-71	249	130894	1.3	8.7810	0.3	5.1361	1.2	0.3271	1.2	0.98	1824.3	18.8	1842.1	10.3	1862.2	4.8	1862.2	4.8	98.0
K13-IBEX-1-52	56	17219	0.6	8.4270	1.7	5.6008	4.3	0.3423	4.0	0.92	1897.8	66.1	1916.2	37.5	1936.2	29.7	1936.2	29.7	98.0
K13-IBEX-1-61	141	29800	1.4	8.9934	0.6	4.8854	3.8	0.3187	3.7	0.99	1783.2	57.7	1799.7	31.7	1819.0	11.5	1819.0	11.5	98.0
K13-IBEX-1-12	314	38366	4.8	8.9138	0.4	4.9821	1.0	0.3221	1.0	0.93	1799.9	15.3	1816.3	8.8	1835.1	7.0	1835.1	7.0	98.1
K13-IBEX-1-76	230	91344	2.5	8.8084	0.3	5.1186	0.9	0.3270	0.8	0.95	1823.8	13.4	1839.2	7.5	1856.6	5.0	1856.6	5.0	98.2
K13-IBEX-1-59	208	91324	1.3	8.7801	0.3	5.1585	2.1	0.3285	2.1	0.99	1831.1	33.5	1845.8	18.1	1862.4	5.9	1862.4	5.9	98.3
K13-IBEX-1-21	312	47926	2.2	7.1077	0.6	7.8840	1.8	0.4064	1.6	0.93	2198.5	30.6	2217.8	15.8	2235.7	10.8	2235.7	10.8	98.3
K13-IBEX-1-5	373	26061	2.2	8.6141	0.3	5.3766	0.7	0.3359	0.7	0.92	1866.9	10.8	1881.1	6.2	1896.8	5.2	1896.8	5.2	98.4
K13-IBEX-1-89	184	83653	1.5	8.5233	0.3	5.4992	1.1	0.3399	1.1	0.97	1886.4	17.7	1900.5	9.6	1915.9	4.8	1915.9	4.8	98.5
K13-IBEX-1-58	153	113019	2.0	8.8574	0.5	5.0815	1.3	0.3264	1.2	0.92	1821.1	19.5	1833.0	11.4	1846.6	9.7	1846.6	9.7	98.6
K13-IBEX-1-70	113	16956	1.5	9.0747	1.3	4.8272	8.9	0.3177	8.8	0.99	1778.5	137.6	1789.7	75.3	1802.6	23.0	1802.6	23.0	98.7
K13-IBEX-1-47	223	76464	3.9	6.4789	0.2	9.4222	0.6	0.4427	0.5	0.91	2362.9	10.3	2380.0	5.3	2394.6	4.1	2394.6	4.1	98.7
K13-IBEX-1-20	146	121568	1.0	8.7648	0.3	5.2254	0.7	0.3322	0.7	0.93	1848.9	10.7	1856.8	6.1	1865.6	4.7	1865.6	4.7	99.1
K13-IBEX-1-53	99	16927	1.8	7.4363	0.5	7.3033	0.7	0.3939	0.6	0.77	2140.8	10.1	2149.2	6.5	2157.2	8.1	2157.2	8.1	99.2
K13-IBEX-1-86	206	136392	2.6	8.6134	0.3	5.4309	1.0	0.3393	0.9	0.95	1883.1	15.1	1889.7	8.3	1897.0	5.2	1897.0	5.2	99.3
K13-IBEX-1-46	199	58283	2.7	8.5775	0.3	5.4817	0.9	0.3410	0.8	0.94	1891.6	13.3	1897.7	7.4	1904.5	5.5	1904.5	5.5	99.3
K13-IBEX-1-82	123	183426	2.1	8.2207	0.4	5.9963	0.9	0.3575	0.8	0.86	1970.4	12.9	1975.3	7.6	1980.5	7.9	1980.5	7.9	99.5
K13-IBEX-1-84	217	20156	4.0	8.9527	0.4	5.0175	1.2	0.3258	1.2	0.95	1818.0	18.7	1822.3	10.4	1827.2	6.7	1827.2	6.7	99.5
K13-IBEX-1-102	178	34393	1.0	8.9382	0.5	5.0411	8.9	0.3268	8.9	1.00	1822.8	140.7	1826.3	75.3	1830.2	8.4	1830.2	8.4	99.6
K13-IBEX-1-48	116	61279	1.0	8.8024	0.7	5.2096	1.2	0.3326	0.9	0.82	1850.9	15.2	1854.2	9.9	1857.9	12.1	1857.9	12.1	99.6
K13-IBEX-1-72	86	98726	1.4	8.7539	0.5	5.2728	2.5	0.3348	2.4	0.98	1861.5	39.6	1864.5	21.3	1867.8	8.8	1867.8	8.8	99.7
K13-IBEX-1-93	159	181526	4.0	8.8895	0.4	5.1062	0.9	0.3292	0.7	0.86	1834.6	11.8	1837.1	7.3	1840.0	7.9	1840.0	7.9	99.7
K13-IBEX-1-60	177	64773	1.8	8.8102	0.2	5.2085	0.7	0.3328	0.7	0.96	1852.0	11.0	1854.0	6.0	1856.2	3.4	1856.2	3.4	99.8
K13-IBEX-1-45	336	210086	1.5	8.7157	0.1	5.3352	1.0	0.3373	1.0	1.00	1873.4	15.8	1874.5	8.3	1875.7	1.6	1875.7	1.6	99.9
K13-IBEX-1-31	160	231234	1.7	6.0633	0.2	10.8358	0.8	0.4765	0.7	0.95	2512.0	15.5	2509.1	7.3	2506.8	4.0	2506.8	4.0	100.2
K13-IBEX-1-101	190	215278	1.6	8.8037	0.3	5.2442	1.0	0.3348	0.9	0.95	1861.8	14.7	1859.8	8.2	1857.6	5.7	1857.6	5.7	100.2
K13-IBEX-1-83	204	273392	1.3	7.4866	0.2	7.2930	1.1	0.3960	1.0	0.98	2150.6	19.1	2148.0	9.6	2145.4	4.1	2145.4	4.1	100.2
K13-IBEX-1-87	216	304643	2.5	8.7500	0.2	5.3160	0.7	0.3374	0.7	0.97	1874.0	11.3	1871.4	6.1	1868.6	3.3	1868.6	3.3	100.3

K13-IBEX-1-79	264	114243	2.7	8.8265	0.2	5.2228	1.6	0.3343	1.6	0.99	1859.4	25.3	1856.4	13.5	1852.9	3.5	1852.9	3.5	100.3
K13-IBEX-1-100	144	129458	1.0	8.8107	0.4	5.2427	1.3	0.3350	1.3	0.96	1862.6	20.8	1859.6	11.5	1856.2	7.1	1856.2	7.1	100.3
K13-IBEX-1-90	172	132688	5.4	8.9182	0.3	5.1095	0.7	0.3305	0.6	0.91	1840.7	10.1	1837.7	5.9	1834.2	5.4	1834.2	5.4	100.4
K13-IBEX-1-24	75	180545	1.6	6.2371	0.6	10.3130	1.4	0.4665	1.2	0.90	2468.3	25.5	2463.3	12.8	2459.2	10.1	2459.2	10.1	100.4
K13-IBEX-1-10	105	196248	1.4	8.7987	0.8	5.2611	1.0	0.3357	0.6	0.63	1866.1	10.2	1862.6	8.5	1858.6	14.1	1858.6	14.1	100.4
K13-IBEX-1-110	81	132128	1.5	8.7718	0.5	5.2935	0.8	0.3368	0.6	0.79	1871.1	10.2	1867.8	6.8	1864.1	8.9	1864.1	8.9	100.4
K13-IBEX-1-67	64	73580	1.3	8.8770	0.9	5.1633	1.2	0.3324	0.7	0.62	1850.1	12.0	1846.6	10.2	1842.6	17.0	1842.6	17.0	100.4
K13-IBEX-1-38	192	215944	1.2	5.7378	0.1	11.9986	0.7	0.4993	0.7	0.99	2610.8	14.1	2604.3	6.2	2599.2	1.8	2599.2	1.8	100.4
K13-IBEX-1-64	93	174087	2.0	8.7658	0.5	5.3082	0.7	0.3375	0.4	0.57	1874.5	6.1	1870.2	5.7	1865.4	9.8	1865.4	9.8	100.5
K13-IBEX-1-88	156	346483	1.8	6.3529	0.2	9.9892	0.9	0.4603	0.9	0.98	2440.7	17.7	2433.8	8.2	2428.0	3.3	2428.0	3.3	100.5
K13-IBEX-1-106	175	211799	0.6	8.8981	0.3	5.1484	0.8	0.3323	0.8	0.93	1849.3	12.1	1844.1	6.9	1838.3	5.5	1838.3	5.5	100.6
K13-IBEX-1-80	107	192404	1.8	8.7727	0.6	5.3088	0.8	0.3378	0.6	0.73	1876.0	9.6	1870.3	7.0	1864.0	10.1	1864.0	10.1	100.6
K13-IBEX-1-68	54	307604	1.0	8.6932	0.7	5.4126	1.1	0.3413	0.9	0.79	1892.7	14.4	1886.9	9.6	1880.4	12.4	1880.4	12.4	100.7
K13-IBEX-1-30	201	186325	4.7	8.8955	0.3	5.1589	2.6	0.3328	2.6	0.99	1852.1	42.3	1845.9	22.5	1838.8	5.6	1838.8	5.6	100.7
K13-IBEX-1-22	140	77053	2.2	8.7611	0.4	5.3285	1.5	0.3386	1.5	0.97	1879.8	24.4	1873.4	13.2	1866.4	6.7	1866.4	6.7	100.7
K13-IBEX-1-2	123	37383	1.5	8.7760	0.6	5.3100	2.3	0.3380	2.2	0.97	1876.9	36.2	1870.5	19.7	1863.3	10.8	1863.3	10.8	100.7
K13-IBEX-1-3	183	156062	1.7	8.0687	0.2	6.3190	1.2	0.3698	1.2	0.99	2028.4	20.8	2021.1	10.6	2013.6	3.0	2013.6	3.0	100.7
K13-IBEX-1-75	50	60227	0.6	8.7634	1.0	5.3278	1.6	0.3386	1.3	0.80	1880.1	21.1	1873.3	13.8	1865.9	17.5	1865.9	17.5	100.8
K13-IBEX-1-23	197	422507	2.0	8.6850	0.1	5.4370	1.2	0.3425	1.2	1.00	1898.6	20.4	1890.7	10.7	1882.1	2.0	1882.1	2.0	100.9
K13-IBEX-1-41	205	382145	1.7	8.7706	0.4	5.3302	0.7	0.3391	0.6	0.85	1882.1	9.2	1873.7	5.7	1864.4	6.4	1864.4	6.4	101.0
K13-IBEX-1-6	191	286395	1.7	8.6648	0.5	5.4737	1.9	0.3440	1.9	0.96	1905.8	30.6	1896.5	16.6	1886.3	9.5	1886.3	9.5	101.0
K13-IBEX-1-25	72	90503	1.3	8.5383	0.7	5.6559	0.9	0.3502	0.6	0.62	1935.8	9.2	1924.7	7.7	1912.7	12.6	1912.7	12.6	101.2
K13-IBEX-1-49	74	161321	1.3	8.5977	0.4	5.5824	1.0	0.3481	0.9	0.93	1925.5	14.9	1913.4	8.4	1900.3	6.6	1900.3	6.6	101.3
K13-IBEX-1-40	151	450317	1.2	8.3837	0.3	5.8876	1.2	0.3580	1.1	0.97	1972.7	19.2	1959.4	10.1	1945.4	5.0	1945.4	5.0	101.4
K13-IBEX-1-19	181	210833	1.7	8.0333	0.2	6.4260	0.7	0.3744	0.7	0.95	2050.0	12.2	2035.8	6.4	2021.4	3.9	2021.4	3.9	101.4
K13-IBEX-1-37	282	102313	1.7	5.9654	0.3	11.3351	1.6	0.4904	1.5	0.98	2572.5	32.7	2551.1	14.7	2534.1	5.4	2534.1	5.4	101.5
K13-IBEX-1-29	89	89180	1.4	8.8305	0.4	5.2989	1.0	0.3394	0.9	0.91	1883.6	14.8	1868.7	8.5	1852.1	7.4	1852.1	7.4	101.7
K13-IBEX-1-34	97	116301	1.5	8.8640	0.7	5.2767	8.3	0.3392	8.3	1.00	1883.0	135.0	1865.1	70.9	1845.2	12.8	1845.2	12.8	102.0
K13-IBEX-1-1	100	264399	1.6	8.7610	0.4	5.4318	0.7	0.3451	0.6	0.83	1911.4	10.1	1889.9	6.3	1866.4	7.5	1866.4	7.5	102.4
K13-IBEX-1-28	104	308284	1.7	8.9690	0.5	5.1877	1.5	0.3375	1.4	0.94	1874.4	22.6	1850.6	12.5	1823.9	8.7	1823.9	8.7	102.8
K13-IBEX-1-107	438	16662	4.4	9.1197	2.7	5.1264	7.4	0.3391	6.9	0.93	1882.2	112.0	1840.5	62.8	1793.6	49.4	1793.6	49.4	104.9
K13-NOP-1-1	157	289538	1.6	6.1102	0.3	10.7274	1.0	0.4754	1.0	0.96	2507.2	20.0	2499.8	9.3	2493.8	4.7	2493.8	4.7	100.5
K13-NOP-1-2	98	133947	0.5	8.5662	0.4	5.4316	1.4	0.3375	1.4	0.96	1874.4	22.2	1889.9	12.2	1906.8	7.4	1906.8	7.4	98.3
K13-NOP-1-3	42	67069	0.8	7.6757	1.1	6.6606	1.7	0.3708	1.3	0.77	2033.1	22.2	2067.4	14.6	2101.7	18.5	2101.7	18.5	96.7
K13-NOP-1-4	256	9586	1.0	5.5683	0.3	11.9104	1.8	0.4810	1.8	0.98	2531.6	37.6	2597.4	17.1	2649.1	5.6	2649.1	5.6	95.6
K13-NOP-1-5	183	183863	1.8	8.8015	0.4	5.3353	1.2	0.3406	1.2	0.95	1889.4	19.3	1874.5	10.6	1858.0	6.7	1858.0	6.7	101.7
K13-NOP-1-6	436	46668	13.0	8.4536	0.3	5.4388	1.4	0.3335	1.4	0.98	1855.1	22.0	1891.0	11.9	1930.6	4.6	1930.6	4.6	96.1
K13-NOP-1-7c	186	689792	1.7	8.6971	0.3	5.3886	1.8	0.3399	1.8	0.98	1886.2	29.2	1883.0	15.6	1879.6	6.3	1879.6	6.3	100.4
K13-NOP-1-7r	710	23025	31.3	9.6760	0.2	3.4628	0.9	0.2430	0.9	0.98	1402.3	11.3	1518.8	7.2	1685.1	3.6	1685.1	3.6	83.2
K13-NOP-1-8	333	13853	2.8	7.6302	1.4	6.2915	2.6	0.3482	2.2	0.85	1925.8	36.3	2017.3	22.6	2112.2	24.0	2112.2	24.0	91.2
K13-NOP-1-9	339	70294	5.0	8.4415	0.2	5.6744	0.6	0.3474	0.5	0.94	1922.2	8.7	1927.5	4.8	1933.2	3.4	1933.2	3.4	99.4
K13-NOP-1-10c	103	4652	1.6	6.3316	0.7	9.0408	1.3	0.4152	1.1	0.83	2238.5	20.9	2342.1	12.1	2433.7	12.5	2433.7	12.5	92.0

K13-NOP-1-11	132	14054	2.8	5.2345	2.1	11.9507	5.2	0.4537	4.8	0.92	2411.7	97.1	2600.5	49.2	2751.1	33.9	2751.1	33.9	87.7
K13-NOP-1-12	320	217022	2.7	8.9616	0.6	5.1006	1.4	0.3315	1.3	0.90	1845.7	20.7	1836.2	12.2	1825.4	11.3	1825.4	11.3	101.1
K13-NOP-1-13	115	121208	1.3	8.8286	0.5	5.2139	0.8	0.3338	0.7	0.83	1857.0	10.9	1854.9	6.9	1852.5	8.2	1852.5	8.2	100.2
K13-NOP-1-14	253	165893	3.8	8.2936	0.2	5.9292	0.7	0.3566	0.6	0.96	1966.3	10.9	1965.5	5.8	1964.7	3.2	1964.7	3.2	100.1
K13-NOP-1-15	163	689690	0.8	8.8149	0.3	5.2605	0.6	0.3363	0.5	0.84	1868.9	8.2	1862.5	5.1	1855.3	5.8	1855.3	5.8	100.7
K13-NOP-1-16	153	83411	1.4	8.7388	0.4	5.3261	0.8	0.3376	0.7	0.88	1875.0	10.9	1873.1	6.5	1871.0	6.6	1871.0	6.6	100.2
K13-NOP-1-17	556	14156	4.4	9.1804	0.6	3.5624	2.7	0.2372	2.7	0.98	1372.1	33.0	1541.2	21.7	1781.5	10.9	1781.5	10.9	77.0
K13-NOP-1-18	473	257325	1.1	8.1957	0.1	6.0693	0.6	0.3608	0.6	0.99	1985.8	10.0	1985.9	5.2	1985.9	1.7	1985.9	1.7	100.0
K13-NOP-1-19	406	141626	1.8	8.7525	0.1	5.3257	0.9	0.3381	0.9	0.99	1877.4	14.5	1873.0	7.7	1868.1	1.8	1868.1	1.8	100.5
K13-NOP-1-21	289	80710	1.8	5.8536	0.2	11.0950	2.5	0.4710	2.5	1.00	2488.1	52.3	2531.1	23.7	2565.8	3.1	2565.8	3.1	97.0
K13-NOP-1-23	117	120519	0.7	8.6310	0.4	5.5091	0.6	0.3449	0.4	0.72	1910.0	6.7	1902.0	4.8	1893.3	7.1	1893.3	7.1	100.9
K13-NOP-1-23r	650	48679	124.5	9.7739	0.3	3.8257	3.1	0.2712	3.1	1.00	1546.8	43.0	1598.2	25.3	1666.5	5.5	1666.5	5.5	92.8
K13-NOP-1-25	134	5095	1.8	7.9105	1.6	6.1333	1.8	0.3519	0.7	0.41	1943.6	12.1	1995.0	15.4	2048.7	28.5	2048.7	28.5	94.9
K13-NOP-1-26	429	5832	9.7	5.2721	1.1	9.6426	5.4	0.3687	5.3	0.98	2023.3	92.6	2401.2	50.1	2739.3	18.2	2739.3	18.2	73.9
K13-NOP-1-27	312	316646	1.7	8.1475	0.1	6.2313	1.2	0.3682	1.2	1.00	2021.0	20.4	2008.8	10.3	1996.4	2.0	1996.4	2.0	101.2
K13-NOP-1-28	100	179403	1.4	8.7160	0.3	5.3711	0.7	0.3395	0.6	0.88	1884.4	10.0	1880.3	6.0	1875.7	5.9	1875.7	5.9	100.5
K13-NOP-1-29	185	177625	1.3	6.0384	0.2	10.9111	1.4	0.4778	1.4	0.99	2517.9	28.6	2515.6	13.0	2513.7	3.8	2513.7	3.8	100.2
K13-NOP-1-30	410	40155	2.0	8.4063	0.3	5.4305	2.9	0.3311	2.9	0.99	1843.6	46.5	1889.7	25.0	1940.6	5.7	1940.6	5.7	95.0
K13-NOP-1-31	499	74329	1.7	8.8457	0.4	4.8777	2.6	0.3129	2.6	0.99	1755.1	39.7	1798.4	22.1	1849.0	7.5	1849.0	7.5	94.9
K13-NOP-1-32	91	152134	1.1	6.8202	0.2	8.7564	1.8	0.4331	1.7	0.99	2319.8	33.9	2313.0	16.0	2306.9	3.8	2306.9	3.8	100.6
K13-NOP-1-33	215	14485	0.9	5.9758	0.3	10.4646	1.3	0.4535	1.2	0.96	2411.0	24.8	2476.8	11.9	2531.2	5.8	2531.2	5.8	95.2
K13-NOP-1-34	345	6632	1.4	6.2791	4.4	8.5873	7.5	0.3911	6.0	0.80	2127.8	108.9	2295.2	68.1	2447.8	75.1	2447.8	75.1	86.9
K13-NOP-1-35	538	31644	2.2	8.1856	0.1	5.9891	0.7	0.3556	0.6	0.98	1961.1	10.8	1974.3	5.7	1988.1	2.4	1988.1	2.4	98.6
K13-NOP-1-36	114	182093	1.1	8.7396	0.7	5.3291	0.9	0.3378	0.6	0.67	1876.0	9.9	1873.5	7.7	1870.8	12.0	1870.8	12.0	100.3
K13-NOP-1-37	635	94802	3.8	8.3113	0.2	5.4545	1.0	0.3288	0.9	0.97	1832.5	14.8	1893.5	8.2	1960.9	3.9	1960.9	3.9	93.5
K13-NOP-1-38	404	97616	1.6	8.1949	0.2	6.0208	0.7	0.3578	0.7	0.97	1972.0	11.8	1978.9	6.3	1986.1	3.3	1986.1	3.3	99.3
K13-NOP-1-39	519	7013	2.1	9.2846	0.4	3.8137	2.1	0.2568	2.1	0.98	1473.5	27.4	1595.6	17.0	1760.9	7.3	1760.9	7.3	83.7
K13-NOP-1-40	96	59020	0.8	6.6043	0.2	9.4104	2.8	0.4507	2.8	1.00	2398.6	55.5	2378.8	25.5	2362.0	3.6	2362.0	3.6	101.5
K13-NOP-1-40r	554	20303	16.4	8.7529	0.5	4.8819	1.4	0.3099	1.3	0.93	1740.3	19.3	1799.1	11.5	1868.0	9.0	1868.0	9.0	93.2
K13-NOP-1-41	286	129170	2.5	8.1515	1.2	6.1246	2.0	0.3621	1.6	0.80	1992.1	27.2	1993.8	17.4	1995.5	21.4	1995.5	21.4	99.8
K13-NOP-1-42	148	201796	1.8	8.8406	0.4	5.2009	0.7	0.3335	0.6	0.85	1855.2	10.2	1852.8	6.3	1850.0	7.1	1850.0	7.1	100.3
K13-NOP-1-43	445	30407	2.6	8.8339	0.4	4.6827	2.5	0.3000	2.4	0.98	1691.4	36.2	1764.2	20.7	1851.4	7.9	1851.4	7.9	91.4
K13-NOP-1-44	414	54943	0.9	6.3597	0.1	9.5471	1.2	0.4404	1.2	1.00	2352.2	23.7	2392.1	11.1	2426.2	1.5	2426.2	1.5	97.0
K13-NOP-1-45	125	268802	2.0	8.7270	0.4	5.3869	0.8	0.3410	0.7	0.84	1891.3	10.9	1882.8	6.7	1873.4	7.6	1873.4	7.6	101.0
K13-NOP-1-46	167	416234	1.5	6.8530	0.2	8.6612	0.7	0.4305	0.7	0.97	2307.9	14.0	2303.0	6.8	2298.7	3.4	2298.7	3.4	100.4
K13-NOP-1-47	151	13221	0.6	8.5886	0.5	5.2872	7.9	0.3293	7.9	1.00	1835.2	126.6	1866.8	67.9	1902.2	9.4	1902.2	9.4	96.5
K13-NOP-1-48	195	294055	0.3	8.7618	0.3	5.3525	1.2	0.3401	1.1	0.97	1887.3	18.6	1877.3	10.0	1866.2	5.1	1866.2	5.1	101.1
K13-NOP-1-49	489	100269	2.3	8.7160	0.1	5.2976	0.7	0.3349	0.7	0.98	1862.0	11.4	1868.5	6.2	1875.7	2.7	1875.7	2.7	99.3
K13-NOP-1-50	43	97137	1.0	5.2718	1.8	14.3386	4.6	0.5482	4.2	0.92	2817.8	95.5	2772.4	43.2	2739.4	29.5	2739.4	29.5	102.9
K13-NOP-1-51	379	256542	1.7	8.4298	0.2	5.7136	1.1	0.3493	1.1	0.99	1931.4	17.7	1933.4	9.3	1935.6	3.2	1935.6	3.2	99.8
K13-NOP-1-52	225	3625	1.8	8.6675	1.4	5.4312	3.7	0.3414	3.5	0.93	1893.5	57.1	1889.8	32.2	1885.7	25.0	1885.7	25.0	100.4
K13-NOP-1-53	259	90033	0.7	8.7481	0.2	5.2674	2.1	0.3342	2.1	1.00	1858.7	33.8	1863.6	17.9	1869.0	2.9	1869.0	2.9	99.4
K13-NOP-1-54c	145	31349	1.3	7.4759	0.7	6.7807	2.1	0.3677	2.0	0.95	2018.3	34.1	2083.2	18.4	2147.9	11.9	2147.9	11.9	94.0

K13-NOP-1-54r	740	13696	40.1	9.1424	0.3	3.9711	1.3	0.2633	1.3	0.97	1506.8	17.5	1628.3	10.9	1789.1	5.8	1789.1	5.8	84.2
K13-NOP-1-55	286	36264	2.6	7.6527	0.5	6.2989	1.4	0.3496	1.4	0.94	1932.7	22.6	2018.3	12.6	2107.0	8.8	2107.0	8.8	91.7
K13-NOP-1-56	89	103548	1.6	8.9426	0.7	5.0637	1.8	0.3284	1.7	0.93	1830.7	27.4	1830.0	15.6	1829.3	12.1	1829.3	12.1	100.1
K13-NOP-1-57	219	33132	2.6	8.9358	1.0	4.4891	1.7	0.2909	1.4	0.82	1646.2	20.5	1729.0	14.2	1830.6	17.7	1830.6	17.7	89.9
K13-NOP-1-58	188	508474	2.2	5.8634	0.2	11.4745	3.2	0.4880	3.2	1.00	2561.8	67.5	2562.5	29.9	2563.0	3.5	2563.0	3.5	100.0
K13-NOP-1-59	434	20404	6.3	8.8812	1.1	4.6034	4.6	0.2965	4.4	0.97	1674.0	65.3	1749.9	38.1	1841.7	20.2	1841.7	20.2	90.9
K13-NOP-1-60	323	139670	2.2	8.7575	0.5	4.7277	7.5	0.3003	7.5	1.00	1692.7	111.9	1772.2	63.2	1867.1	9.1	1867.1	9.1	90.7
K13-NOP-1-61	118	207125	2.0	8.7679	0.4	5.2052	1.0	0.3310	0.9	0.90	1843.3	14.5	1853.5	8.6	1864.9	8.1	1864.9	8.1	98.8
K13-NOP-1-62	173	2287	2.5	7.8339	3.9	5.4321	4.5	0.3086	2.4	0.52	1734.0	36.0	1889.9	38.9	2065.8	68.2	2065.8	68.2	83.9
K13-NOP-1-63	152	16019	2.5	8.6633	0.5	5.3821	1.2	0.3382	1.1	0.91	1877.9	18.2	1882.0	10.5	1886.6	9.1	1886.6	9.1	99.5
K13-NOP-1-63r	162	196605	2.6	8.6936	0.4	5.3771	1.2	0.3390	1.1	0.94	1882.0	17.9	1881.2	9.9	1880.3	6.8	1880.3	6.8	100.1
K13-NOP-1-64	117	17337	1.4	8.8002	0.6	5.2853	2.9	0.3373	2.8	0.98	1873.8	45.7	1866.5	24.5	1858.3	10.0	1858.3	10.0	100.8
K13-NOP-1-65	278	1023920	1.0	6.7225	0.2	9.0182	0.6	0.4397	0.5	0.92	2349.2	10.6	2339.8	5.4	2331.7	4.0	2331.7	4.0	100.8
K13-NOP-1-66	99	170425	1.3	8.1300	0.4	6.1547	0.8	0.3629	0.6	0.86	1995.9	11.1	1998.0	6.6	2000.2	6.9	2000.2	6.9	99.8
K13-NOP-1-67	592	128264	6.4	8.5491	0.1	5.4424	0.7	0.3375	0.7	0.99	1874.4	11.6	1891.6	6.2	1910.4	2.2	1910.4	2.2	98.1
K13-NOP-1-68	955	10172	2.9	9.2911	0.6	3.2168	4.2	0.2168	4.1	0.99	1264.8	47.6	1461.2	32.5	1759.6	10.8	1759.6	10.8	71.9
K13-NOP-1-69	128	216402	0.8	8.9329	0.4	5.0284	0.7	0.3258	0.5	0.79	1817.9	8.5	1824.1	5.7	1831.2	7.4	1831.2	7.4	99.3
K13-NOP-1-70	111	4551	2.3	6.3932	0.7	6.5115	5.4	0.3019	5.3	0.99	1700.9	79.4	2047.5	47.2	2417.3	12.3	2417.3	12.3	70.4
K13-NOP-1-71	219	435205	1.9	8.5630	0.2	5.6128	0.8	0.3486	0.8	0.97	1927.8	13.5	1918.1	7.2	1907.5	3.6	1907.5	3.6	101.1
K13-NOP-1-72	36	133680	1.1	4.3424	0.5	19.4645	1.1	0.6130	1.0	0.91	3082.1	25.0	3065.1	10.8	3054.0	7.5	3054.0	7.5	100.9
K13-NOP-1-73	248	21212	3.1	7.3251	2.5	5.1151	3.7	0.2717	2.8	0.74	1549.7	38.1	1838.6	31.7	2183.5	43.6	2183.5	43.6	71.0
K13-NOP-1-75	175	291013	2.9	7.6478	0.2	6.9946	1.8	0.3880	1.8	0.99	2113.4	31.6	2110.7	15.7	2108.1	3.4	2108.1	3.4	100.3
K13-NOP-1-76	320	189316	1.9	8.1219	0.1	6.2271	0.4	0.3668	0.4	0.95	2014.4	7.0	2008.3	3.7	2002.0	2.2	2002.0	2.2	100.6
K13-NOP-1-77	136	23382	1.4	6.3500	0.2	9.8405	1.2	0.4532	1.2	0.99	2409.5	23.6	2420.0	11.0	2428.8	3.3	2428.8	3.3	99.2
K13-NOP-1-78	77	239833	1.5	4.5164	0.2	18.1578	0.7	0.5948	0.6	0.94	3008.7	15.5	2998.1	6.6	2991.0	3.7	2991.0	3.7	100.6
K13-NOP-1-79	328	7611	2.1	5.9500	2.9	8.2830	3.5	0.3574	2.0	0.57	1970.0	34.0	2262.5	31.6	2538.5	47.8	2538.5	47.8	77.6
K13-NOP-1-80	292	316375	1.3	8.7060	0.3	5.3845	0.9	0.3400	0.9	0.95	1886.6	14.1	1882.4	7.8	1877.7	5.2	1877.7	5.2	100.5
K13-NOP-1-81	693	55106	2.5	8.9262	0.1	4.4246	2.7	0.2864	2.7	1.00	1623.7	39.4	1717.0	22.8	1832.6	2.1	1832.6	2.1	88.6
K13-NOP-1-82	68	74547	1.8	8.6841	0.8	5.5189	1.1	0.3476	0.8	0.68	1923.1	12.5	1903.5	9.5	1882.3	14.6	1882.3	14.6	102.2
K13-NOP-1-84	368	58714	1.6	8.7904	0.2	5.4331	2.0	0.3464	2.0	0.99	1917.3	33.4	1890.1	17.4	1860.3	4.0	1860.3	4.0	103.1
K13-NOP-1-85	214	10286	0.8	9.0226	1.0	4.8011	2.6	0.3142	2.4	0.92	1761.2	36.3	1785.1	21.6	1813.1	18.5	1813.1	18.5	97.1
K13-NOP-1-86	299	32842	0.7	6.6080	1.0	8.8556	1.7	0.4244	1.4	0.82	2280.5	27.5	2323.2	15.9	2361.0	17.0	2361.0	17.0	96.6
K13-NOP-1-87	343	64623	1.6	8.7534	0.1	5.4108	1.6	0.3435	1.6	1.00	1903.5	26.7	1886.6	13.9	1867.9	2.3	1867.9	2.3	101.9
K13-NOP-1-88	190	45089	1.4	8.7964	0.4	5.1462	6.8	0.3283	6.8	1.00	1830.2	108.2	1843.8	57.9	1859.1	7.4	1859.1	7.4	98.4
K13-NOP-1-89	724	10967	2.5	9.2652	1.3	4.1225	4.5	0.2770	4.3	0.96	1576.3	60.7	1658.8	37.0	1764.8	23.7	1764.8	23.7	89.3
K13-NOP-1-90	273	29502	1.3	8.9618	0.2	5.0271	1.0	0.3267	0.9	0.97	1822.6	14.8	1823.9	8.2	1825.4	4.5	1825.4	4.5	99.8
K13-NOP-1-91	115	173703	1.0	8.7383	0.4	5.2844	0.8	0.3349	0.7	0.83	1862.1	10.7	1866.3	6.8	1871.1	7.9	1871.1	7.9	99.5
K13-NOP-1-92	579	139795	2.9	8.1869	0.1	5.9967	0.8	0.3561	0.8	0.99	1963.5	13.1	1975.4	6.8	1987.8	1.6	1987.8	1.6	98.8
K13-NOP-1-93	564	14829	3.7	7.5626	4.8	5.1911	5.3	0.2847	2.3	0.43	1615.1	32.5	1851.2	45.6	2127.8	84.8	2127.8	84.8	75.9
K13-NOP-1-95	222	323602	2.0	8.1981	0.2	6.1500	0.6	0.3657	0.6	0.94	2009.0	9.6	1997.4	5.2	1985.4	3.6	1985.4	3.6	101.2
K13-NOP-1-96	295	498585	1.2	8.8197	0.2	5.2750	1.4	0.3374	1.4	0.99	1874.3	22.6	1864.8	12.0	1854.3	3.9	1854.3	3.9	101.1
K13-NOP-1-97	118	142631	0.8	5.7999	0.3	11.8977	0.8	0.5005	0.8	0.93	2615.8	16.9	2596.4	7.9	2581.2	5.2	2581.2	5.2	101.3
K13-NOP-1-98	242	41082	1.8	8.7305	0.2	5.3638	1.2	0.3396	1.2	0.98	1884.9	19.9	1879.1	10.6	1872.7	4.2	1872.7	4.2	100.7

K13-NOP-1-99	112	5771	2.2	5.7353	0.7	11.6885	1.2	0.4862	1.0	0.80	2554.2	20.0	2579.8	11.1	2599.9	11.9	2599.9	11.9	98.2
K13-NOP-1-100	396	9688	2.5	9.2501	0.5	3.9298	3.5	0.2636	3.5	0.99	1508.5	46.7	1619.8	28.4	1767.7	9.5	1767.7	9.5	85.3
K13-NOP-1-101	198	15937	1.2	8.8908	0.4	5.1769	1.8	0.3338	1.7	0.97	1856.9	27.8	1848.8	15.0	1839.8	7.2	1839.8	7.2	100.9
K13-NOP-1-102	110	281189	1.5	8.6029	0.5	5.4876	1.2	0.3424	1.1	0.90	1898.2	17.9	1898.7	10.4	1899.2	9.4	1899.2	9.4	99.9
K13-NOP-1-103	379	99009	5.1	8.9491	0.2	5.0645	0.9	0.3287	0.8	0.96	1832.1	13.1	1830.2	7.3	1827.9	4.4	1827.9	4.4	100.2
K13-NOP-1-104	136	81785	2.6	8.7807	0.3	5.4145	1.7	0.3448	1.7	0.98	1909.8	27.6	1887.1	14.6	1862.3	5.8	1862.3	5.8	102.5
K13-NOP-1-105	156	80871	4.1	6.2071	0.2	10.3571	0.7	0.4663	0.7	0.97	2467.1	13.8	2467.2	6.4	2467.3	3.0	2467.3	3.0	100.0
K13-NOP-1-106	21	29419	1.2	8.7156	2.1	5.4657	2.7	0.3455	1.8	0.65	1913.1	29.4	1895.2	23.3	1875.7	37.0	1875.7	37.0	102.0
K13-NOP-1-107	227	15109	2.9	8.2656	0.3	6.0845	1.3	0.3648	1.3	0.97	2004.7	21.8	1988.0	11.3	1970.8	5.5	1970.8	5.5	101.7
K13NOP-4-65	506	14798	2.7	8.7073	1.3	3.7128	2.0	0.2345	1.6	0.76	1357.9	19.1	1574.1	16.3	1877.4	23.8	1877.4	23.8	72.3
K13NOP-4-13r	544	4952	3.9	9.3553	0.7	3.5896	9.2	0.2436	9.2	1.00	1405.2	115.7	1547.2	73.1	1747.1	13.5	1747.1	13.5	80.4
K13NOP-4-25	211	41565	4.1	9.1684	0.4	3.7730	2.8	0.2509	2.8	0.99	1443.1	35.6	1587.0	22.4	1783.9	8.1	1783.9	8.1	80.9
K13NOP-4-7	44	33917	1.1	6.7628	1.1	6.9622	2.7	0.3415	2.4	0.91	1893.8	40.0	2106.6	23.8	2321.4	18.8	2321.4	18.8	81.6
K13NOP-4-30	629	12296	15.9	9.5751	0.5	3.5091	1.1	0.2437	1.0	0.89	1405.9	12.1	1529.3	8.5	1704.4	9.2	1704.4	9.2	82.5
K13NOP-4-99	548	8510	1.5	5.5937	0.2	10.0548	1.8	0.4079	1.8	0.99	2205.4	33.3	2439.8	16.6	2641.5	3.7	2641.5	3.7	83.5
K13NOP-4-31	219	1859	4.9	8.5531	3.2	4.5982	3.7	0.2852	1.8	0.49	1617.7	26.2	1748.9	31.0	1909.6	58.0	1909.6	58.0	84.7
K13NOP-4-58	266	15892	2.0	8.4864	0.6	4.7062	2.0	0.2897	1.9	0.96	1639.8	27.7	1768.3	16.7	1923.6	10.4	1923.6	10.4	85.2
K13NOP-4-68	319	24803	1.7	9.0826	0.2	4.0943	1.4	0.2697	1.4	0.98	1539.3	18.9	1653.2	11.5	1801.1	4.5	1801.1	4.5	85.5
K13NOP-4-87	236	31939	2.0	6.0529	0.6	9.0416	1.9	0.3969	1.9	0.95	2154.9	34.0	2342.2	17.8	2509.7	10.0	2509.7	10.0	85.9
K13NOP-4-49	520	43200	1.2	8.9014	0.2	4.3912	0.5	0.2835	0.5	0.91	1608.9	7.1	1710.7	4.5	1837.6	4.0	1837.6	4.0	87.6
K13NOP-4-92	561	46416	1.9	9.0174	0.4	4.3409	1.0	0.2839	0.9	0.92	1611.0	12.5	1701.2	7.9	1814.1	6.9	1814.1	6.9	88.8
K13NOP-4-62	466	25889	2.6	9.2691	1.0	4.1064	2.1	0.2761	1.8	0.88	1571.5	25.7	1655.6	17.0	1764.0	17.9	1764.0	17.9	89.1
K13NOP-4-54	205	12693	3.4	8.5710	6.5	4.8825	7.0	0.3035	2.5	0.36	1708.7	37.4	1799.2	59.1	1905.8	####	1905.8	####	89.7
K13NOP-4-21	196	30263	2.0	8.8180	0.3	4.6174	3.8	0.2953	3.8	1.00	1668.0	55.9	1752.4	31.9	1854.7	5.7	1854.7	5.7	89.9
K13NOP-4-27	503	37506	3.7	8.9467	0.3	4.5388	5.0	0.2945	5.0	1.00	1664.0	72.9	1738.1	41.5	1828.4	5.3	1828.4	5.3	91.0
K13NOP-4-38	41	417	0.8	7.9775	3.0	5.7734	4.3	0.3340	3.1	0.72	1857.9	49.9	1942.4	37.2	2033.8	52.8	2033.8	52.8	91.4
K13NOP-4-94	197	6343	4.1	8.9657	0.6	4.5439	3.4	0.2955	3.3	0.99	1668.8	49.0	1739.0	28.2	1824.6	10.4	1824.6	10.4	91.5
K13NOP-4-41	434	58156	37.5	8.6597	0.3	4.9671	2.1	0.3120	2.1	0.99	1750.4	32.6	1813.7	18.1	1887.3	4.6	1887.3	4.6	92.7
K13NOP-4-67	222	62380	2.1	8.8782	0.5	4.7415	1.4	0.3053	1.4	0.94	1717.6	20.5	1774.6	12.1	1842.3	8.9	1842.3	8.9	93.2
K13NOP-4-29	121	1383	2.7	8.0653	1.1	5.7906	1.7	0.3387	1.2	0.73	1880.5	19.7	1945.0	14.3	2014.4	20.0	2014.4	20.0	93.4
K13NOP-4-95	393	119073	2.2	8.8230	0.2	4.8333	2.0	0.3093	2.0	0.99	1737.2	29.8	1790.7	16.5	1853.6	3.6	1853.6	3.6	93.7
K13NOP-4-34	119	36303	1.0	5.9494	0.5	10.3543	1.4	0.4468	1.3	0.92	2380.9	24.9	2467.0	12.5	2538.7	8.7	2538.7	8.7	93.8
K13NOP-4-18	27	2310	1.1	8.6151	1.9	5.1535	2.3	0.3220	1.3	0.58	1799.5	21.2	1845.0	19.9	1896.6	34.3	1896.6	34.3	94.9
K13NOP-4-46	171	253946	1.8	8.8792	0.6	4.8371	5.4	0.3115	5.3	0.99	1748.1	81.5	1791.4	45.1	1842.2	10.2	1842.2	10.2	94.9
K13NOP-4-56	428	247074	6.5	8.6852	0.2	5.0767	1.0	0.3198	1.0	0.97	1788.7	15.2	1832.2	8.5	1882.0	4.4	1882.0	4.4	95.0
K13NOP-4-77	260	34636	1.1	8.6929	0.2	5.0820	1.7	0.3204	1.7	0.99	1791.7	26.1	1833.1	14.3	1880.4	3.9	1880.4	3.9	95.3
K13NOP-4-40	115	159960	2.3	6.4105	1.9	9.2696	6.6	0.4310	6.4	0.96	2310.1	123.3	2365.0	60.9	2412.7	32.7	2412.7	32.7	95.7
K13NOP-4-72	172	126384	1.6	5.0499	0.4	14.2258	1.1	0.5210	1.1	0.94	2703.5	23.4	2764.9	10.8	2810.0	6.6	2810.0	6.6	96.2
K13NOP-4-45	304	51260	1.9	8.4142	0.4	5.5605	1.3	0.3393	1.2	0.94	1883.5	19.5	1910.0	11.0	1938.9	8.0	1938.9	8.0	97.1
K13NOP-4-59	74	3249	0.6	8.6282	1.4	5.2834	1.8	0.3306	1.0	0.58	1841.4	16.4	1866.2	15.1	1893.9	25.9	1893.9	25.9	97.2
K13NOP-4-47	285	118994	1.5	8.5592	0.2	5.3785	1.3	0.3339	1.2	0.98	1857.2	20.1	1881.4	10.9	1908.3	4.3	1908.3	4.3	97.3
K13NOP-4-16	33	2110	1.7	5.3865	0.7	12.9185	1.3	0.5047	1.0	0.81	2633.9	22.2	2673.7	12.0	2704.0	12.4	2704.0	12.4	97.4

K13NOP-4-73	204	5650	0.7	8.7538	0.4	5.1377	1.3	0.3262	1.2	0.94	1819.9	18.7	1842.4	10.7	1867.9	8.0	1867.9	8.0	97.4
K13NOP-4-79	112	69695	1.0	9.1985	0.4	4.6301	1.1	0.3089	1.0	0.92	1735.2	15.3	1754.7	9.2	1778.0	7.9	1778.0	7.9	97.6
K13NOP-4-96	108	5308	1.4	8.7849	0.7	5.1119	1.2	0.3257	1.0	0.80	1817.5	15.2	1838.1	10.1	1861.5	12.8	1861.5	12.8	97.6
K13NOP-4-57	100	8868	1.4	8.4710	2.5	5.5427	2.8	0.3405	1.3	0.45	1889.2	20.9	1907.2	24.2	1926.9	44.9	1926.9	44.9	98.0
K13NOP-4-39	105	35143	1.1	8.0979	0.3	6.0932	0.9	0.3579	0.8	0.93	1972.0	14.3	1989.3	7.9	2007.2	6.0	2007.2	6.0	98.2
K13NOP-4-86	157	110090	1.3	8.0233	0.5	6.2104	0.9	0.3614	0.8	0.84	1988.8	13.0	2005.9	8.0	2023.6	8.9	2023.6	8.9	98.3
K13NOP-4-83	125	162476	1.3	8.3645	0.9	5.7076	1.3	0.3463	1.0	0.73	1916.7	16.0	1932.5	11.3	1949.5	15.9	1949.5	15.9	98.3
K13NOP-4-13c	341	45503	0.9	8.6789	0.4	5.2937	2.1	0.3332	2.0	0.98	1853.9	32.6	1867.8	17.6	1883.3	6.8	1883.3	6.8	98.4
K13NOP-4-74	282	7072	2.1	8.5605	0.6	5.4698	1.1	0.3396	0.9	0.83	1884.8	14.4	1895.9	9.1	1908.0	10.5	1908.0	10.5	98.8
K13NOP-4-20	134	91123	0.8	8.1434	0.3	6.0656	1.0	0.3582	0.9	0.94	1973.9	16.0	1985.3	8.7	1997.3	6.1	1997.3	6.1	98.8
K13NOP-4-14	351	18730	2.3	8.6998	0.4	5.3076	1.1	0.3349	1.0	0.94	1862.1	16.7	1870.1	9.4	1879.0	6.9	1879.0	6.9	99.1
K13NOP-4-1	38	71798	2.2	8.5896	0.9	5.4544	1.4	0.3398	1.1	0.75	1885.7	17.4	1893.4	12.1	1901.9	16.6	1901.9	16.6	99.1
K13NOP-4-55	127	187664	1.1	6.2244	0.2	10.2077	0.9	0.4608	0.9	0.98	2443.1	17.6	2453.8	8.2	2462.6	3.2	2462.6	3.2	99.2
K13NOP-4-42	201	269169	1.6	8.3616	0.3	5.7773	0.8	0.3504	0.7	0.93	1936.3	11.7	1943.0	6.5	1950.2	5.0	1950.2	5.0	99.3
K13NOP-4-8	123	347379	1.0	8.7460	0.4	5.2745	0.7	0.3346	0.6	0.82	1860.5	9.3	1864.7	6.0	1869.5	7.2	1869.5	7.2	99.5
K13NOP-4-15	155	3070	1.1	8.7086	1.7	5.3270	4.1	0.3365	3.7	0.91	1869.6	60.5	1873.2	34.9	1877.2	30.0	1877.2	30.0	99.6
K13NOP-4-3r	85	144975	1.1	8.7594	0.7	5.2638	1.2	0.3344	1.0	0.83	1859.7	16.2	1863.0	10.3	1866.7	12.0	1866.7	12.0	99.6
K13NOP-4-75	230	22948	1.3	8.3176	0.9	5.8633	1.2	0.3537	0.8	0.70	1952.3	14.3	1955.8	10.6	1959.6	15.7	1959.6	15.7	99.6
K13NOP-4-28	142	342347	1.6	8.7232	0.5	5.3106	3.0	0.3360	2.9	0.98	1867.3	47.8	1870.6	25.6	1874.2	9.8	1874.2	9.8	99.6
K13NOP-4-69	106	368056	1.3	8.1889	0.6	6.0684	1.4	0.3604	1.3	0.92	1984.1	22.6	1985.7	12.5	1987.4	10.0	1987.4	10.0	99.8
K13NOP-4-85	268	324953	1.5	5.9644	0.2	11.1173	1.5	0.4809	1.5	0.99	2531.3	31.5	2533.0	14.1	2534.4	2.8	2534.4	2.8	99.9
K13NOP-4-52	135	68123	1.0	8.5575	0.5	5.5445	0.9	0.3441	0.8	0.86	1906.5	12.8	1907.5	7.7	1908.7	8.2	1908.7	8.2	99.9
K13NOP-4-61	79	149582	1.7	7.4062	0.4	7.4228	1.0	0.3987	0.9	0.91	2163.1	17.1	2163.7	9.2	2164.3	7.5	2164.3	7.5	99.9
K13NOP-4-24	131	161110	1.0	8.5390	0.3	5.5768	0.9	0.3454	0.8	0.96	1912.5	14.0	1912.5	7.6	1912.6	4.7	1912.6	4.7	100.0
K13NOP-4-35	301	595635	1.4	8.7178	0.2	5.3445	1.3	0.3379	1.3	0.99	1876.7	21.6	1876.0	11.4	1875.3	3.0	1875.3	3.0	100.1
K13NOP-4-89	92	129172	0.8	8.7552	0.5	5.2998	0.9	0.3365	0.8	0.81	1870.0	12.2	1868.8	7.9	1867.6	9.9	1867.6	9.9	100.1
K13NOP-4-3	214	112763	1.2	8.7563	0.3	5.2984	1.0	0.3365	0.9	0.95	1869.7	14.9	1868.6	8.3	1867.3	5.3	1867.3	5.3	100.1
K13NOP-4-36	201	292594	2.3	5.9873	0.2	11.0765	0.9	0.4810	0.9	0.98	2531.6	18.6	2529.6	8.4	2528.0	2.7	2528.0	2.7	100.1
K13NOP-4-6	57	154148	1.0	5.7615	0.5	11.8751	1.6	0.4962	1.5	0.95	2597.5	32.0	2594.6	14.7	2592.3	8.1	2592.3	8.1	100.2
K13NOP-4-53	334	36746	2.6	8.5641	0.3	5.5571	0.7	0.3452	0.7	0.92	1911.5	10.8	1909.5	6.1	1907.3	4.9	1907.3	4.9	100.2
K13NOP-4-97	35	177518	1.3	6.2581	0.9	10.2319	8.2	0.4644	8.2	0.99	2459.0	166.7	2456.0	76.0	2453.5	14.6	2453.5	14.6	100.2
K13NOP-4-12	213	238021	2.3	8.7753	0.4	5.2873	1.2	0.3365	1.2	0.96	1869.8	18.9	1866.8	10.4	1863.4	6.3	1863.4	6.3	100.3
K13NOP-4-5	207	78364	1.5	7.7221	0.4	6.8727	1.6	0.3849	1.6	0.97	2099.2	28.4	2095.1	14.5	2091.2	7.5	2091.2	7.5	100.4
K13NOP-4-2	193	283868	2.5	8.6189	0.5	5.4952	1.5	0.3435	1.4	0.95	1903.5	23.3	1899.8	12.8	1895.8	8.3	1895.8	8.3	100.4
K13NOP-4-70	174	198477	2.4	8.2234	0.4	6.0564	0.9	0.3612	0.8	0.87	1987.9	13.5	1984.0	7.9	1979.9	8.0	1979.9	8.0	100.4
K13NOP-4-19	164	21975	1.1	7.0563	1.2	8.1967	4.8	0.4195	4.7	0.97	2258.1	89.3	2253.0	43.7	2248.3	20.0	2248.3	20.0	100.4
K13NOP-4-93	84	114903	1.5	8.7251	0.8	5.3587	2.4	0.3391	2.3	0.95	1882.3	37.5	1878.3	20.7	1873.8	14.0	1873.8	14.0	100.5
K13NOP-4-51	170	159810	3.5	8.2050	0.5	6.0953	0.8	0.3627	0.6	0.75	1995.1	10.7	1989.6	7.2	1983.9	9.6	1983.9	9.6	100.6
K13NOP-4-22	101	171330	2.0	8.7151	0.8	5.3815	1.3	0.3402	1.1	0.81	1887.4	17.5	1881.9	11.4	1875.8	14.2	1875.8	14.2	100.6
K13NOP-4-10	218	153251	1.2	8.7353	0.2	5.3619	0.9	0.3397	0.9	0.98	1885.2	15.0	1878.8	8.0	1871.7	3.7	1871.7	3.7	100.7
K13NOP-4-43	207	203696	1.7	8.6956	0.3	5.4169	0.8	0.3416	0.7	0.92	1894.5	12.0	1887.5	6.8	1879.9	5.7	1879.9	5.7	100.8
K13NOP-4-91	294	583189	1.0	8.2507	0.2	6.0492	0.8	0.3620	0.8	0.98	1991.6	13.1	1982.9	6.8	1974.0	3.1	1974.0	3.1	100.9
K13NOP-4-84	445	360246	2.4	8.7358	0.1	5.3790	0.7	0.3408	0.6	0.98	1890.5	10.5	1881.5	5.6	1871.6	2.6	1871.6	2.6	101.0

K13NOP-4-82	124	191295	1.8	8.7838	0.5	5.3195	0.9	0.3389	0.7	0.81	1881.3	11.9	1872.0	7.7	1861.7	9.6	1861.7	9.6	101.1
K13NOP-4-48	176	15164	3.2	8.8936	0.7	5.1970	2.8	0.3352	2.7	0.97	1863.6	43.5	1852.1	23.6	1839.2	12.2	1839.2	12.2	101.3
K13NOP-4-80	101	99012	2.0	8.7200	0.7	5.4207	1.1	0.3428	0.8	0.77	1900.2	13.5	1888.1	9.2	1874.8	12.4	1874.8	12.4	101.4
K13NOP-4-44	42	36401	1.0	8.8906	1.1	5.2026	2.1	0.3355	1.8	0.84	1864.8	28.5	1853.1	17.8	1839.8	20.5	1839.8	20.5	101.4
K13NOP-4-88	272	276497	0.9	7.7311	0.4	6.9449	1.4	0.3894	1.4	0.95	2120.1	24.7	2104.4	12.7	2089.1	7.8	2089.1	7.8	101.5
K13NOP-4-90	226	283456	1.9	8.7063	0.3	5.4889	1.4	0.3466	1.3	0.98	1918.3	22.2	1898.9	11.7	1877.7	4.6	1877.7	4.6	102.2
K13NOP-4-76	137	399367	1.8	8.7388	0.4	5.4936	1.6	0.3482	1.5	0.97	1925.9	25.6	1899.6	13.7	1870.9	7.3	1870.9	7.3	102.9
K14-BLFG-2-100	442	789553	1.0	8.1987	0.3	4.0541	8.9	0.2411	8.9	1.00	1392.2	111.0	1645.1	72.3	1985.2	5.3	1985.2	5.3	70.1
K14-BLFG-2-54	559	418182	2.7	8.9496	0.8	3.3903	9.0	0.2201	9.0	1.00	1282.2	104.6	1502.1	70.9	1827.8	13.8	1827.8	13.8	70.1
K14-BLFG-2-50	182	115714	2.2	6.2322	1.2	6.8849	3.9	0.3112	3.7	0.95	1746.6	56.9	2096.7	34.8	2460.5	21.0	2460.5	21.0	71.0
K14-BLFG-2-106	448	478154	5.8	9.2386	0.5	3.2145	3.3	0.2154	3.3	0.99	1257.4	37.7	1460.7	25.9	1770.0	9.8	1770.0	9.8	71.0
K14-BLFG-2-108	1374	83401	1.6	8.9680	0.1	3.4343	1.8	0.2234	1.8	1.00	1299.7	20.8	1512.3	13.9	1824.1	2.7	1824.1	2.7	71.2
K14-BLFG-2-92	1056	197393	3.0	9.1084	1.1	3.3703	1.5	0.2226	1.1	0.71	1295.8	12.6	1497.5	11.8	1795.9	19.2	1795.9	19.2	72.2
K14-BLFG-2-75	121	63118	1.8	8.9830	1.2	3.5002	2.9	0.2280	2.6	0.91	1324.2	31.1	1527.3	22.5	1821.1	21.4	1821.1	21.4	72.7
K14-BLFG-2-62	554	222390	13.2	9.3763	0.5	3.2336	2.8	0.2199	2.8	0.98	1281.3	32.2	1465.3	21.8	1743.0	9.1	1743.0	9.1	73.5
K14-BLFG-2-83	270	175543	2.5	8.8991	0.5	3.6191	5.3	0.2336	5.3	1.00	1353.3	64.5	1553.7	42.2	1838.1	8.4	1838.1	8.4	73.6
K14-BLFG-2-33	129	64295	2.2	9.0243	1.0	3.5273	9.7	0.2309	9.7	0.99	1339.0	116.7	1533.3	76.9	1812.7	18.4	1812.7	18.4	73.9
K14-BLFG-2-105	429	142926	5.6	7.3750	0.8	5.3176	2.6	0.2844	2.5	0.95	1613.6	35.6	1871.7	22.4	2171.6	14.4	2171.6	14.4	74.3
K14-BLFG-2-64	842	151658	2.0	6.0818	1.1	7.5859	4.0	0.3346	3.9	0.96	1860.7	62.9	2183.2	36.3	2501.7	18.2	2501.7	18.2	74.4
K14-BLFG-2-87	480	451498	2.4	9.2288	0.5	3.3993	4.5	0.2275	4.5	0.99	1321.5	53.7	1504.2	35.4	1772.0	8.6	1772.0	8.6	74.6
K14-BLFG-2-3	214	313599	4.5	6.9833	0.8	5.9336	4.7	0.3005	4.6	0.99	1693.9	68.3	1966.2	40.5	2266.2	13.5	2266.2	13.5	74.7
K14-BLFG-2-91	114	127138	4.0	6.6738	2.0	6.5124	8.0	0.3152	7.7	0.97	1766.3	119.7	2047.6	70.6	2344.1	34.7	2344.1	34.7	75.4
K14-BLFG-2-77	930	365879	2.6	8.4820	0.2	4.1217	1.3	0.2536	1.3	0.98	1456.8	16.5	1658.6	10.5	1924.6	4.0	1924.6	4.0	75.7
K14-BLFG-2-20	247	252868	18.8	6.6494	2.4	6.6042	4.4	0.3185	3.6	0.83	1782.4	56.6	2059.9	38.6	2350.3	41.8	2350.3	41.8	75.8
K14-BLFG-2-110	254	255330	1.1	5.6419	0.7	8.9039	2.4	0.3643	2.3	0.96	2002.7	39.7	2328.2	21.9	2627.2	11.3	2627.2	11.3	76.2
K14-BLFG-2-70	1200	238248	2.4	9.1237	0.2	3.5782	2.4	0.2368	2.3	0.99	1369.9	28.9	1544.7	18.7	1792.8	4.3	1792.8	4.3	76.4
K14-BLFG-2-97	1098	282340	3.9	9.2692	0.2	3.5179	3.4	0.2365	3.4	1.00	1368.5	41.5	1531.2	26.7	1764.0	4.3	1764.0	4.3	77.6
K14-BLFG-2-17	926	451093	2.2	9.0297	0.2	3.7482	2.1	0.2455	2.0	0.99	1415.1	26.0	1581.7	16.5	1811.7	3.9	1811.7	3.9	78.1
K14-BLFG-2-66	751	158526	7.9	9.0206	0.4	3.8863	7.7	0.2543	7.7	1.00	1460.4	100.2	1610.8	62.1	1813.5	6.9	1813.5	6.9	80.5
K14-BLFG-2-7	358	235034	3.7	9.2487	0.5	3.6874	2.0	0.2473	1.9	0.97	1424.8	24.3	1568.6	15.7	1768.0	9.0	1768.0	9.0	80.6
K14-BLFG-2-30	570	203746	1.9	9.0002	0.3	3.9194	1.4	0.2558	1.3	0.98	1468.5	17.6	1617.7	11.0	1817.6	4.6	1817.6	4.6	80.8
K14-BLFG-2-34	337	314190	0.8	6.5311	0.3	7.4295	7.0	0.3519	7.0	1.00	1943.8	117.6	2164.5	62.8	2381.0	5.8	2381.0	5.8	81.6
K14-BLFG-2-26	905	490854	3.7	9.1803	0.2	3.8307	3.8	0.2551	3.8	1.00	1464.5	49.7	1599.2	30.6	1781.6	2.9	1781.6	2.9	82.2
K14-BLFG-2-73	451	257459	11.0	8.9855	0.4	4.0179	4.0	0.2618	4.0	0.99	1499.3	53.0	1637.8	32.4	1820.6	7.8	1820.6	7.8	82.4
K14-BLFG-2-49	160	30824	1.5	8.5637	3.0	4.4684	6.3	0.2775	5.6	0.88	1578.9	77.8	1725.1	52.3	1907.4	53.1	1907.4	53.1	82.8
K14-BLFG-2-32	108	49726	3.5	9.0036	1.3	4.0804	4.3	0.2664	4.1	0.95	1522.8	55.4	1650.4	35.1	1816.9	24.2	1816.9	24.2	83.8
K14-BLFG-2-95	250	139551	8.3	8.5706	0.4	4.5360	2.6	0.2820	2.6	0.99	1601.2	36.6	1737.6	21.7	1905.9	7.3	1905.9	7.3	84.0
K14-BLFG-2-38	717	517019	3.1	9.0631	0.3	4.0513	1.9	0.2663	1.9	0.98	1522.0	25.8	1644.6	15.8	1805.0	6.2	1805.0	6.2	84.3
K14-BLFG-2-12	338	140666	1.7	7.0363	0.7	6.7250	2.7	0.3432	2.6	0.97	1902.0	42.7	2075.9	23.7	2253.2	12.0	2253.2	12.0	84.4
K14-BLFG-2-102	301	440442	3.1	6.4506	1.5	8.0371	1.9	0.3760	1.2	0.62	2057.6	20.6	2235.2	16.9	2402.1	24.9	2402.1	24.9	85.7
K14-BLFG-2-18	289	263569	1.7	7.1760	1.0	6.6023	3.7	0.3436	3.6	0.97	1904.0	58.7	2059.7	32.5	2219.2	16.7	2219.2	16.7	85.8
K14-BLFG-2-23	215	112704	1.1	5.7199	1.2	10.0085	1.7	0.4152	1.2	0.72	2238.6	22.8	2435.6	15.6	2604.4	19.7	2604.4	19.7	86.0

K14-BLFG-2-109	171	159409	2.2	5.8060	0.4	9.8233	3.0	0.4136	3.0	0.99	2231.6	56.3	2418.3	27.7	2579.5	6.4	2579.5	6.4	86.5
K14-BLFG-2-89	168	185227	2.3	6.0877	0.6	9.1073	2.1	0.4021	2.0	0.96	2178.7	36.8	2348.8	18.9	2500.0	9.4	2500.0	9.4	87.1
K14-BLFG-2-63	288	254571	2.3	8.8735	0.4	4.4007	3.4	0.2832	3.3	0.99	1607.5	47.6	1712.5	27.9	1843.3	7.5	1843.3	7.5	87.2
K14-BLFG-2-47	434	591416	1.8	8.3656	0.5	4.9952	2.5	0.3031	2.4	0.98	1706.5	36.7	1818.5	21.1	1949.3	8.3	1949.3	8.3	87.5
K14-BLFG-2-42	228	268786	1.2	6.4386	0.3	8.2837	4.1	0.3868	4.1	1.00	2108.1	73.7	2262.5	37.3	2405.2	5.7	2405.2	5.7	87.6
K14-BLFG-2-11	832	500014	5.2	8.4277	0.5	4.9368	4.2	0.3018	4.2	0.99	1700.0	62.7	1808.6	35.7	1936.1	9.5	1936.1	9.5	87.8
K14-BLFG-2-88	310	489926	3.7	8.9562	0.3	4.3568	1.8	0.2830	1.8	0.98	1606.5	25.8	1704.2	15.2	1826.5	5.8	1826.5	5.8	88.0
K14-BLFG-2-48	248	36669	1.9	5.9685	0.3	9.6156	2.9	0.4162	2.9	0.99	2243.4	54.7	2398.7	26.7	2533.3	5.4	2533.3	5.4	88.6
K14-BLFG-2-27	157	139212	1.5	8.9253	0.7	4.4388	2.4	0.2873	2.3	0.95	1628.2	33.4	1719.6	20.2	1832.8	13.4	1832.8	13.4	88.8
K14-BLFG-2-22	391	270140	2.1	5.7478	0.5	10.3198	2.2	0.4302	2.1	0.98	2306.6	41.0	2463.9	20.0	2596.3	7.9	2596.3	7.9	88.8
K14-BLFG-2-82	360	329419	1.8	8.9341	0.3	4.4380	1.3	0.2876	1.2	0.97	1629.4	17.6	1719.5	10.4	1831.0	5.3	1831.0	5.3	89.0
K14-BLFG-2-90	238	276018	2.0	7.1630	0.4	6.9408	2.3	0.3606	2.3	0.98	1984.9	39.4	2103.9	20.8	2222.3	7.2	2222.3	7.2	89.3
K14-BLFG-2-68	476	352897	2.3	6.2450	1.0	8.9781	2.2	0.4066	1.9	0.89	2199.6	36.2	2335.8	19.8	2457.0	16.4	2457.0	16.4	89.5
K14-BLFG-2-6	67	67768	1.7	5.8606	2.3	10.0739	4.8	0.4282	4.2	0.87	2297.5	81.1	2441.6	44.4	2563.8	39.0	2563.8	39.0	89.6
K14-BLFG-2-72	292	346741	8.4	8.5087	0.3	4.9680	2.2	0.3066	2.2	0.99	1723.8	32.9	1813.9	18.6	1918.9	5.8	1918.9	5.8	89.8
K14-BLFG-2-16	228	190094	1.2	6.7289	0.3	7.9153	2.7	0.3863	2.6	0.99	2105.6	47.4	2221.4	23.9	2330.0	4.7	2330.0	4.7	90.4
K14-BLFG-2-84	587	503096	2.4	8.9337	0.4	4.5170	2.6	0.2927	2.6	0.99	1654.9	38.1	1734.1	21.9	1831.1	6.6	1831.1	6.6	90.4
K14-BLFG-2-98	690	957755	2.6	9.0009	0.3	4.4665	1.7	0.2916	1.7	0.98	1649.4	24.6	1724.8	14.3	1817.5	5.9	1817.5	5.9	90.8
K14-BLFG-2-78	459	264075	3.0	8.9061	0.4	4.5898	8.0	0.2965	7.9	1.00	1673.8	117.0	1747.4	66.4	1836.7	7.8	1836.7	7.8	91.1
K14-BLFG-2-76	639	515247	3.3	6.3212	0.5	9.0218	1.5	0.4136	1.4	0.94	2231.4	26.3	2340.2	13.5	2436.5	8.3	2436.5	8.3	91.6
K14-BLFG-2-101	298	119355	1.0	8.9529	0.5	4.5657	3.4	0.2965	3.3	0.99	1673.7	48.9	1743.0	28.0	1827.2	9.5	1827.2	9.5	91.6
K14-BLFG-2-80	212	144029	2.5	9.0284	0.4	4.5042	2.5	0.2949	2.4	0.99	1666.2	35.8	1731.8	20.6	1811.9	7.5	1811.9	7.5	92.0
K14-BLFG-2-46	776	740799	1.4	8.7247	0.2	4.8521	1.3	0.3070	1.3	0.99	1726.1	19.0	1794.0	10.7	1873.9	2.8	1873.9	2.8	92.1
K14-BLFG-2-52	249	304716	1.9	6.2626	0.5	9.3434	4.2	0.4244	4.2	0.99	2280.3	80.0	2372.3	38.5	2452.2	8.9	2452.2	8.9	93.0
K14-BLFG-2-81	190	849679	1.6	6.1085	0.3	9.7945	1.7	0.4339	1.6	0.98	2323.4	31.8	2415.6	15.3	2494.3	5.8	2494.3	5.8	93.1
K14-BLFG-2-13	176	107078	1.4	3.8301	0.3	21.6178	2.3	0.6005	2.3	0.99	3031.9	55.9	3166.7	22.6	3253.3	5.0	3253.3	5.0	93.2
K14-BLFG-2-40	174	88650	1.5	8.7555	0.6	4.8963	2.2	0.3109	2.1	0.96	1745.2	31.9	1801.6	18.4	1867.5	11.3	1867.5	11.3	93.5
K14-BLFG-2-65	159	103853	1.4	8.9294	0.8	4.7134	2.9	0.3052	2.8	0.96	1717.3	41.6	1769.6	24.0	1831.9	13.6	1831.9	13.6	93.7
K14-BLFG-2-1	455	470866	1.9	6.9179	0.4	7.8670	5.8	0.3947	5.8	1.00	2144.6	106.0	2215.9	52.5	2282.4	6.6	2282.4	6.6	94.0
K14-BLFG-2-61	152	103195	0.6	8.2818	1.0	5.5354	2.0	0.3325	1.7	0.86	1850.4	27.4	1906.1	16.9	1967.3	17.6	1967.3	17.6	94.1
K14-BLFG-2-103	421	256349	1.7	8.9513	0.2	4.7074	1.6	0.3056	1.5	0.99	1719.1	23.4	1768.6	13.1	1827.5	3.1	1827.5	3.1	94.1
K14-BLFG-2-28	330	538701	1.8	5.5975	0.9	11.5919	2.1	0.4706	1.9	0.91	2486.2	39.6	2572.0	19.8	2640.4	14.8	2640.4	14.8	94.2
K14-BLFG-2-31	315	484495	0.9	6.7423	0.2	8.3965	4.0	0.4106	4.0	1.00	2217.6	75.5	2274.8	36.6	2326.6	4.3	2326.6	4.3	95.3
K14-BLFG-2-39	268	158725	2.6	9.0302	0.6	4.7312	2.3	0.3099	2.2	0.97	1740.0	33.4	1772.8	19.0	1811.6	10.4	1811.6	10.4	96.1
K14-BLFG-2-93	150	98270	1.8	8.9160	1.1	4.9147	6.6	0.3178	6.5	0.99	1779.0	101.4	1804.8	55.8	1834.7	19.1	1834.7	19.1	97.0
K14-BLFG-2-45	133	135345	0.9	5.7362	0.5	11.5311	2.9	0.4797	2.9	0.99	2526.1	60.1	2567.1	27.3	2599.7	8.3	2599.7	8.3	97.2
K14-BLFG-2-4	89	83019	1.6	8.1425	0.8	6.0384	5.0	0.3566	4.9	0.99	1966.0	83.1	1981.4	43.3	1997.5	14.0	1997.5	14.0	98.4
K14-BLFG-2-107	69	70022	2.7	8.9705	1.0	4.9925	2.6	0.3248	2.4	0.92	1813.2	37.3	1818.0	21.7	1823.6	18.1	1823.6	18.1	99.4
K14-HH-1-67	853	410590	2.3	9.4913	0.3	3.1769	1.2	0.2187	1.1	0.97	1274.9	13.0	1451.6	8.9	1720.6	4.8	1720.6	4.8	74.1
K14-HH-1-84	224	306505	1.6	9.3712	0.4	4.4302	1.0	0.3011	0.9	0.90	1696.8	13.5	1718.0	8.3	1744.0	8.0	1744.0	8.0	97.3
K14-HH-1-68	628	41493	2.9	9.3530	0.4	3.1126	7.4	0.2111	7.4	1.00	1234.9	83.3	1435.8	57.1	1747.5	7.4	1747.5	7.4	70.7
K14-HH-1-75	451	80148	2.2	9.3222	0.7	3.2024	1.9	0.2165	1.8	0.94	1263.5	20.8	1457.7	15.0	1753.5	12.3	1753.5	12.3	72.1

K14-HH-1-95	68	68962	1.4	9.2385	1.4	4.6652	2.2	0.3126	1.7	0.76	1753.4	25.4	1761.0	18.2	1770.0	25.7	1770.0	25.7	99.1
K14-HH-1-96	416	349444	4.4	9.2369	0.5	4.4244	0.8	0.2964	0.6	0.75	1673.4	8.7	1716.9	6.5	1770.3	9.4	1770.3	9.4	94.5
K14-HH-1-43	512	470356	1.7	9.2308	0.4	4.4974	1.0	0.3011	0.9	0.92	1696.7	14.1	1730.5	8.5	1771.6	7.3	1771.6	7.3	95.8
K14-HH-1-79	184	114931	2.5	9.2259	0.6	4.7717	0.8	0.3193	0.5	0.68	1786.3	8.2	1779.9	6.5	1772.5	10.3	1772.5	10.3	100.8
K14-HH-1-44	218	151609	2.4	9.2080	0.8	4.5552	0.9	0.3042	0.5	0.54	1712.2	7.6	1741.1	7.7	1776.1	14.2	1776.1	14.2	96.4
K14-HH-1-99	106	149776	1.6	9.1935	1.1	4.9454	1.4	0.3297	0.8	0.62	1837.1	13.6	1810.0	11.6	1779.0	19.7	1779.0	19.7	103.3
K14-HH-1-77	242	63369	1.4	9.1932	0.6	4.5991	0.8	0.3066	0.6	0.71	1724.2	9.0	1749.1	7.0	1779.0	10.8	1779.0	10.8	96.9
K14-HH-1-20	325	48643	3.0	9.1760	0.4	4.5745	2.5	0.3044	2.4	0.98	1713.3	36.8	1744.6	20.7	1782.4	8.1	1782.4	8.1	96.1
K14-HH-1-52	155	111716	1.1	9.1700	1.2	4.6620	3.9	0.3101	3.7	0.95	1741.0	56.0	1760.4	32.3	1783.6	22.1	1783.6	22.1	97.6
K14-HH-1-48	366	230834	0.9	9.1548	0.2	4.7855	1.3	0.3177	1.2	0.99	1778.7	19.3	1782.3	10.6	1786.6	3.6	1786.6	3.6	99.6
K14-HH-1-55	168	147263	2.2	9.1546	0.6	4.7332	1.2	0.3143	1.0	0.87	1761.7	15.8	1773.1	9.8	1786.7	10.3	1786.7	10.3	98.6
K14-HH-1-51	270	360802	2.5	9.1511	0.4	4.6171	0.7	0.3064	0.6	0.82	1723.1	8.7	1752.4	5.9	1787.4	7.3	1787.4	7.3	96.4
K14-HH-1-78	395	436246	0.8	9.1418	0.3	4.8458	0.7	0.3213	0.6	0.93	1796.0	10.0	1792.9	5.8	1789.2	4.7	1789.2	4.7	100.4
K14-HH-1-87	113	192741	2.8	9.1418	0.7	4.6221	5.6	0.3065	5.6	0.99	1723.2	84.5	1753.3	47.1	1789.2	13.4	1789.2	13.4	96.3
K14-HH-1-108	212	246164	2.3	9.1411	0.6	4.8577	1.2	0.3220	1.0	0.83	1799.7	15.2	1794.9	9.8	1789.4	11.8	1789.4	11.8	100.6
K14-HH-1-18	469	182820	2.7	9.1381	0.4	4.2312	1.1	0.2804	1.0	0.94	1593.5	14.6	1680.1	9.1	1790.0	7.1	1790.0	7.1	89.0
K14-HH-1-29	123	58596	1.4	9.1332	1.0	4.8270	1.4	0.3197	1.0	0.71	1788.5	15.2	1789.6	11.6	1790.9	17.8	1790.9	17.8	99.9
K14-HH-1-2	235	47624	1.6	9.1216	0.6	4.4952	1.1	0.2974	0.9	0.84	1678.3	13.3	1730.1	8.9	1793.3	10.7	1793.3	10.7	93.6
K14-HH-1-17	223	231755	1.9	9.1186	0.5	4.7277	0.9	0.3127	0.7	0.83	1753.8	11.4	1772.2	7.5	1793.9	9.0	1793.9	9.0	97.8
K14-HH-1-89	135	184646	1.3	9.1040	1.0	4.8459	1.1	0.3200	0.5	0.44	1789.6	7.8	1792.9	9.6	1796.8	18.6	1796.8	18.6	99.6
K14-HH-1-94	188	11826	3.0	9.0953	1.3	4.9969	3.4	0.3296	3.2	0.93	1836.5	51.0	1818.8	29.2	1798.5	23.6	1798.5	23.6	102.1
K14-HH-1-8	232	118560	1.8	9.0892	0.6	4.8111	0.8	0.3172	0.5	0.62	1775.8	7.9	1786.8	6.9	1799.7	11.8	1799.7	11.8	98.7
K14-HH-1-110	205	38379	1.5	9.0821	0.5	4.9337	0.9	0.3250	0.8	0.82	1814.0	11.9	1808.0	7.8	1801.2	9.6	1801.2	9.6	100.7
K14-HH-1-92	575	591461	1.0	9.0759	0.2	4.8817	0.5	0.3213	0.5	0.90	1796.3	7.2	1799.1	4.3	1802.4	4.1	1802.4	4.1	99.7
K14-HH-1-21	362	53650	3.3	9.0647	0.3	4.2070	1.4	0.2766	1.4	0.97	1574.1	19.2	1675.4	11.6	1804.6	6.3	1804.6	6.3	87.2
K14-HH-1-34	454	282696	1.2	9.0618	0.3	4.8947	1.9	0.3217	1.8	0.98	1798.0	28.9	1801.3	15.8	1805.2	6.1	1805.2	6.1	99.6
K14-HH-1-14	347	212183	1.3	9.0572	0.3	4.7126	0.7	0.3096	0.6	0.91	1738.6	9.8	1769.5	5.9	1806.1	5.2	1806.1	5.2	96.3
K14-HH-1-16	633	435110	2.4	9.0195	0.3	4.7719	1.0	0.3122	1.0	0.96	1751.3	14.7	1780.0	8.4	1813.7	5.0	1813.7	5.0	96.6
K14-HH-1-25	72	53478	2.8	9.0131	1.3	4.9202	1.6	0.3216	0.8	0.54	1797.7	13.3	1805.7	13.3	1815.0	24.2	1815.0	24.2	99.0
K14-HH-1-58	219	204392	1.9	9.0115	0.5	5.0912	1.6	0.3327	1.5	0.95	1851.7	24.9	1834.6	13.9	1815.3	9.4	1815.3	9.4	102.0
K14-HH-1-35	156	95014	4.6	9.0105	0.9	4.9819	2.4	0.3256	2.2	0.92	1816.9	34.6	1816.3	20.1	1815.5	16.9	1815.5	16.9	100.1
K14-HH-1-103	260	355186	1.3	8.9975	0.5	4.8611	1.3	0.3172	1.3	0.94	1776.1	19.6	1795.5	11.3	1818.1	8.4	1818.1	8.4	97.7
K14-HH-1-54	419	251995	1.1	8.9908	0.2	4.8291	0.5	0.3149	0.4	0.89	1764.7	6.6	1790.0	4.1	1819.5	4.0	1819.5	4.0	97.0
K14-HH-1-47	76	6556	1.5	8.9624	1.8	4.5951	2.4	0.2987	1.6	0.67	1684.8	23.7	1748.4	19.8	1825.2	32.0	1825.2	32.0	92.3
K14-HH-1-37	402	383779	1.0	8.9593	0.3	4.9667	1.1	0.3227	1.0	0.97	1803.0	16.4	1813.7	9.1	1825.9	5.1	1825.9	5.1	98.7
K14-HH-1-38	275	343804	1.9	8.9491	0.2	4.7751	0.8	0.3099	0.7	0.95	1740.3	11.2	1780.5	6.5	1827.9	4.4	1827.9	4.4	95.2
K14-HH-1-64	431	199261	2.4	8.9194	0.2	4.8265	1.3	0.3122	1.3	0.99	1751.6	19.4	1789.5	10.8	1834.0	3.6	1834.0	3.6	95.5
K14-HH-1-98	336	617091	1.9	8.9132	0.5	4.8530	0.9	0.3137	0.8	0.86	1759.0	12.1	1794.1	7.7	1835.2	8.5	1835.2	8.5	95.8
K14-HH-1-31	317	484303	1.2	8.9108	0.4	5.0798	0.9	0.3283	0.8	0.91	1830.1	13.2	1832.7	7.7	1835.7	6.8	1835.7	6.8	99.7
K14-HH-1-107	327	445989	4.8	8.8705	0.3	4.9679	0.8	0.3196	0.7	0.90	1787.8	11.3	1813.9	6.8	1843.9	6.2	1843.9	6.2	97.0
K14-HH-1-39	191	221758	1.4	8.8603	0.7	4.8893	1.3	0.3142	1.1	0.83	1761.3	16.4	1800.4	10.8	1846.0	12.8	1846.0	12.8	95.4
K14-HH-1-9	532	281671	1.0	8.8524	0.1	4.7631	1.3	0.3058	1.3	1.00	1720.0	19.2	1778.4	10.7	1847.6	2.3	1847.6	2.3	93.1
K14-HH-1-7	715	1013416	36.1	8.8418	0.3	4.7273	0.5	0.3031	0.4	0.85	1706.9	6.2	1772.1	4.1	1849.8	4.6	1849.8	4.6	92.3

K14-HH-1-60	207	115052	1.9	8.8367	0.3	5.0042	2.1	0.3207	2.1	0.99	1793.2	32.7	1820.0	17.9	1850.8	6.1	1850.8	6.1	96.9
K14-HH-1-69	317	307182	1.3	8.8282	0.4	5.1253	1.0	0.3282	1.0	0.92	1829.5	15.2	1840.3	8.8	1852.6	7.1	1852.6	7.1	98.8
K14-HH-1-63	118	76977	1.2	8.8266	0.8	4.9985	1.0	0.3200	0.6	0.61	1789.7	9.8	1819.1	8.7	1852.9	14.9	1852.9	14.9	96.6
K14-HH-1-65	431	432105	1.5	8.8239	0.2	4.8990	1.0	0.3135	1.0	0.97	1758.0	15.3	1802.1	8.6	1853.4	4.4	1853.4	4.4	94.9
K14-HH-1-76	62	76270	0.9	8.8213	2.5	4.5866	3.0	0.2934	1.6	0.55	1658.7	24.1	1746.8	24.8	1854.0	44.9	1854.0	44.9	89.5
K14-HH-1-101	152	75348	1.2	8.8210	0.6	5.2552	1.2	0.3362	1.0	0.86	1868.4	16.4	1861.6	10.0	1854.0	10.8	1854.0	10.8	100.8
K14-HH-1-109	477	195248	3.1	8.8183	0.3	4.6297	0.7	0.2961	0.7	0.91	1671.9	9.9	1754.6	6.2	1854.6	5.4	1854.6	5.4	90.1
K14-HH-1-30	727	799971	1.5	8.8112	0.2	4.8708	1.5	0.3113	1.5	0.99	1746.9	22.4	1797.2	12.4	1856.1	3.0	1856.1	3.0	94.1
K14-HH-1-46	349	125798	2.2	8.7897	0.4	5.1097	3.9	0.3257	3.9	1.00	1817.7	61.4	1837.7	33.1	1860.5	6.9	1860.5	6.9	97.7
K14-HH-1-91	602	340574	2.0	8.7863	0.2	4.9083	0.8	0.3128	0.7	0.96	1754.4	11.4	1803.7	6.6	1861.2	4.0	1861.2	4.0	94.3
K14-HH-1-74	108	82301	2.4	8.7782	0.9	5.2238	1.0	0.3326	0.5	0.50	1850.9	8.3	1856.5	8.8	1862.8	16.2	1862.8	16.2	99.4
K14-HH-1-105	570	868435	2.3	8.7770	0.1	5.1035	0.9	0.3249	0.9	0.99	1813.5	14.0	1836.7	7.6	1863.1	1.7	1863.1	1.7	97.3
K14-HH-1-42	94	82746	2.9	8.7765	0.9	5.2419	1.7	0.3337	1.4	0.85	1856.1	22.7	1859.5	14.2	1863.2	16.0	1863.2	16.0	99.6
K14-HH-1-22	56	59529	4.3	8.7690	1.0	5.3421	1.5	0.3398	1.1	0.74	1885.5	18.1	1875.6	12.9	1864.7	18.3	1864.7	18.3	101.1
K14-HH-1-23	382	248995	2.4	8.7641	0.3	4.9595	0.7	0.3152	0.6	0.90	1766.4	9.3	1812.4	5.7	1865.7	5.3	1865.7	5.3	94.7
K14-HH-1-88	132	194306	4.0	8.7495	0.5	5.4203	0.9	0.3440	0.7	0.81	1905.7	12.1	1888.1	7.7	1868.7	9.4	1868.7	9.4	102.0
K14-HH-1-66	563	599792	1.3	8.7411	0.2	5.1310	0.7	0.3253	0.6	0.95	1815.5	9.9	1841.3	5.6	1870.5	3.7	1870.5	3.7	97.1
K14-HH-1-61	164	166462	0.7	8.7337	0.6	5.1679	1.0	0.3273	0.7	0.77	1825.5	11.9	1847.3	8.3	1872.0	11.3	1872.0	11.3	97.5
K14-HH-1-13	224	232884	2.3	8.7177	0.7	5.2921	1.0	0.3346	0.7	0.74	1860.7	11.7	1867.6	8.3	1875.3	11.8	1875.3	11.8	99.2
K14-HH-1-15	284	728930	2.8	8.7139	0.3	4.9848	0.9	0.3150	0.8	0.93	1765.4	12.5	1816.7	7.3	1876.1	5.7	1876.1	5.7	94.1
K14-HH-1-28	119	85365	2.2	8.6945	0.7	5.3643	1.5	0.3383	1.4	0.89	1878.3	22.2	1879.2	13.2	1880.1	12.8	1880.1	12.8	99.9
K14-HH-1-6	557	565775	1.6	8.6778	0.2	5.2606	0.6	0.3311	0.5	0.92	1843.6	8.7	1862.5	5.0	1883.6	4.0	1883.6	4.0	97.9
K14-HH-1-27	106	73444	1.1	8.5426	0.5	5.6317	1.1	0.3489	0.9	0.87	1929.5	15.8	1921.0	9.4	1911.8	9.5	1911.8	9.5	100.9
K14-HH-1-41	184	209006	2.6	8.5363	0.7	5.5132	2.1	0.3413	2.0	0.95	1893.1	33.3	1902.7	18.4	1913.1	12.5	1913.1	12.5	99.0
K14-HH-1-86	152	180331	1.3	8.5315	0.9	5.5295	1.1	0.3421	0.6	0.58	1897.0	10.6	1905.2	9.5	1914.1	16.2	1914.1	16.2	99.1
K14-HH-1-36	355	284588	1.7	8.1443	0.3	5.9892	0.7	0.3538	0.6	0.88	1952.6	9.8	1974.3	5.7	1997.1	5.5	1997.1	5.5	97.8
K14-HH-1-40	572	614910	1.1	7.9178	0.2	6.4491	2.3	0.3703	2.3	0.99	2031.0	40.2	2039.0	20.4	2047.1	4.4	2047.1	4.4	99.2
K14-HH-1-73	376	447172	2.1	6.5822	0.4	9.3256	1.3	0.4452	1.3	0.96	2373.9	25.8	2370.5	12.4	2367.7	6.3	2367.7	6.3	100.3
K14-HH-1-62	495	435386	1.3	6.5778	1.1	7.9291	4.5	0.3783	4.4	0.97	2068.2	77.9	2223.0	40.9	2368.8	18.3	2368.8	18.3	87.3
K14-HH-1-5	557	38889	2.3	6.2388	1.5	7.8302	3.5	0.3543	3.2	0.90	1955.1	53.1	2211.7	31.5	2458.7	25.5	2458.7	25.5	79.5
K14-HH-1-100	723	698893	3.4	6.2158	1.6	8.5752	1.8	0.3866	0.8	0.43	2107.0	13.6	2293.9	16.0	2464.9	26.8	2464.9	26.8	85.5
K14-HH-1-81	380	282871	1.9	6.2077	0.6	9.1518	3.6	0.4120	3.5	0.99	2224.2	66.5	2353.3	32.8	2467.1	9.7	2467.1	9.7	90.2
K14-HH-1-11	127	87919	1.5	5.9028	0.6	9.9525	1.1	0.4261	0.9	0.83	2288.0	18.1	2430.4	10.4	2551.8	10.5	2551.8	10.5	89.7
K14-HH-1-19	294	245255	2.3	5.8026	0.2	11.3376	0.9	0.4771	0.9	0.98	2514.8	18.7	2551.3	8.5	2580.4	2.9	2580.4	2.9	97.5
K14-HH-1-90	312	334339	1.8	5.7672	0.2	11.3252	0.8	0.4737	0.8	0.97	2499.8	16.8	2550.3	7.8	2590.7	3.1	2590.7	3.1	96.5
K14-HH-1-93	241	323928	1.3	5.7097	0.2	11.8521	0.7	0.4908	0.7	0.96	2574.2	14.2	2592.8	6.5	2607.4	3.4	2607.4	3.4	98.7
K14-HH-1-1	387	95252	2.7	5.6909	1.0	10.3195	4.5	0.4259	4.4	0.97	2287.4	84.8	2463.9	41.9	2612.9	17.1	2612.9	17.1	87.5
K14-HH-1-10	80	105067	0.7	5.6906	0.9	11.2671	3.4	0.4650	3.2	0.96	2461.7	66.1	2545.5	31.3	2613.0	15.0	2613.0	15.0	94.2
K14-HH-1-102	239	273788	1.5	5.6787	0.4	10.8716	1.1	0.4478	1.1	0.94	2385.3	21.5	2512.2	10.7	2616.4	6.5	2616.4	6.5	91.2
K14-HH-1-26	319	379234	2.0	5.6322	0.7	11.9686	1.3	0.4889	1.2	0.87	2565.9	24.4	2602.0	12.4	2630.1	10.9	2630.1	10.9	97.6
K14-HH-1-80	117	127882	2.1	5.5982	0.4	12.4195	5.1	0.5043	5.1	1.00	2632.1	109.3	2636.7	47.7	2640.2	6.1	2640.2	6.1	99.7
K14-HH-1-59	113	73585	1.7	5.5968	0.6	11.6817	7.7	0.4742	7.6	1.00	2501.9	158.4	2579.2	71.8	2640.6	10.5	2640.6	10.5	94.7
K14-HH-1-70	353	318367	0.9	5.5260	0.4	12.6668	5.3	0.5077	5.3	1.00	2646.6	115.6	2655.2	50.3	2661.7	6.7	2661.7	6.7	99.4

K14-HH-1-85	134	304917	1.4	5.4662	0.2	13.3682	1.3	0.5300	1.3	0.99	2741.4	29.7	2706.0	12.7	2679.7	3.7	2679.7	3.7	102.3
K14-HH-1-12	109	182966	1.0	5.3778	0.5	12.9221	0.8	0.5040	0.6	0.76	2631.0	12.8	2674.0	7.4	2706.7	8.4	2706.7	8.4	97.2
K14-HH-1-50	304	490643	1.0	5.3557	0.2	13.1514	0.8	0.5108	0.8	0.97	2660.2	17.5	2690.6	7.8	2713.5	3.1	2713.5	3.1	98.0
K14-HH-1-104	133	142807	2.8	4.7211	0.4	16.8912	1.0	0.5784	1.0	0.93	2942.0	23.0	2928.7	10.1	2919.5	6.3	2919.5	6.3	100.8
K14-HH-1-49	340	202200	0.9	4.3082	1.7	17.3312	3.4	0.5415	2.9	0.87	2789.8	66.7	2953.3	32.5	3066.7	26.6	3066.7	26.6	91.0

Notes:
Analyses with >10% uncertainty (1-sigma) in 206Pb/238U age are not included.
Analyses with >10% uncertainty (1-sigma) in 206Pb/207Pb age are not included, unless 206Pb/238U age is <500 Ma.
Best age is determined from 206Pb/238U age for analyses with 206Pb/238U age < 900 Ma and from 206Pb/207Pb age for analyses with 206Pb/238Uage > 900 Ma.
Concordance is based on 206Pb/238U age / 206Pb/207Pb age. Value is not reported for 206Pb/238U ages <500 Ma because of large uncertainty in 206Pb/207Pb age.
Analyses with 206Pb/238U age > 500 Ma and with >20% discordance (<80% concordance) are not included.
Analyses with 206Pb/238U age > 500 Ma and with >5% reverse discordance (<105% concordance) are not included.
All uncertainties are reported at the 1-sigma level, and include only measurement errors.
Systematic errors are shown as 206Pb/238U uncertainty, 206Pb/207Pb uncertainty to the right of each sample (at 2-sigma level).
U concentration and U/Th are calibrated relative to Sri Lanka zircon and are accurate to ~20%.
Common Pb correction is from 204Pb, with composition interpreted from Stacey and Kramers (1975).
Uncertainties of 1.5 for 206Pb/ 204Pb, 0.3 for 207Pb/ 204Pb, and 2.0 for 208Pb/ 204Pb are applied to common Pb composition.
U/Pb and 206Pb/207Pb fractionation is calibrated relative to fragments of a large Sri Lanka zircon of 563.5 ± 3.2 Ma (2-sigma).
U decay constants and composition as follows: 238U = 9.8485 x 10-10, 235U = 1.55125 x 10-10, 238U/235U = 137.82
Analytical methods as described by Gehrels and Pecha (2014).

Table A2-2. Lu-Hf isotope data from detrital zircon ALC

Sample	(176Yb + 176Lu) / 176Hf (%)	Volts Hf	$^{176}Hf/^{177}Hf$	± (1s)	$^{176}Lu/^{177}Hf$	$^{176}Hf/^{177}Hf_{(t)}$	E-Hf (0)	E-Hf (0) ± (1s)	E-Hf (t)	Age (Ma)
K13-ASH-1-32	14.1	3.4	0.280718	0.000031	0.000909	0.280664	-73.1	1.1	-4.8	3061
K13-ASH-1-17	7.6	3.0	0.281116	0.000046	0.000590	0.281086	-59.0	1.6	0.7	2662
K13-ASH-1-24	17.8	2.9	0.281160	0.000031	0.001130	0.281102	-57.5	1.1	1.0	2645
K13-ASH-1-28	9.5	2.3	0.281409	0.000043	0.000672	0.281383	-48.7	1.5	-3.1	2042
K13-ASH-1-36	9.3	3.1	0.281114	0.000032	0.000597	0.281085	-59.1	1.1	-1.9	2549
K13-ASH-1-60	18.1	3.2	0.281237	0.000043	0.001602	0.281155	-54.7	1.5	3.6	2679
K13-ASH-1-23	8.7	2.9	0.281532	0.000037	0.000508	0.281514	-44.3	1.3	-1.5	1909
K13-ASH-1-57	12.1	3.6	0.281027	0.000023	0.000758	0.280983	-62.2	0.8	4.6	2981
K13-ASH-1-11	10.7	2.6	0.280999	0.000044	0.000633	0.280967	-63.1	1.6	-3.2	2673
K13-ASH-1-81	21.0	2.5	0.281106	0.000032	0.001341	0.281046	-59.4	1.1	-8.5	2327
K13-ASH-1-73	5.7	3.1	0.281234	0.000035	0.000351	0.281217	-54.8	1.2	3.7	2589
K13-ASH-1-19	10.3	3.6	0.281482	0.000032	0.000637	0.281457	-46.1	1.1	-1.8	1985

K13-ASH-1-80	11.5	2.7	0.281585	0.000027	0.000907	0.281551	-42.4	0.9	1.8	1998
K13-ASH-1-16	9.4	2.8	0.281536	0.000037	0.000580	0.281515	-44.2	1.3	-2.3	1873
K13-ASH-1-50	13.0	2.4	0.281223	0.000041	0.000896	0.281177	-55.2	1.5	4.2	2672
K13-ASH-1-7	8.0	3.2	0.281418	0.000028	0.000498	0.281396	-48.3	1.0	2.7	2271
K13-ASH-1-59	13.6	2.5	0.281157	0.000032	0.000848	0.281114	-57.6	1.1	1.8	2664
K13-ASH-1-25	23.8	2.8	0.281258	0.000032	0.001471	0.281184	-54.0	1.1	4.1	2657
K13-ASH-1-72	9.6	2.9	0.281205	0.000026	0.000584	0.281179	-55.9	0.9	-2.1	2397
K13-ASH-1-95	11.2	2.2	0.281248	0.000038	0.000901	0.281204	-54.3	1.4	3.2	2589
K13-ASH-1-47	18.0	3.0	0.281340	0.000042	0.001117	0.281297	-51.1	1.5	-7.6	1982
K13-ASH-1-8	13.4	2.3	0.281156	0.000043	0.000785	0.281121	-57.6	1.5	-5.8	2328
K13-ASH-1-87	9.0	3.0	0.281748	0.000041	0.000650	0.281725	-36.7	1.5	5.3	1881
K13-ASH-1-62	11.8	2.3	0.281083	0.000037	0.000732	0.281045	-60.2	1.3	-0.3	2680
K13-ASH-1-40	8.6	3.2	0.281165	0.000036	0.000501	0.281141	-57.3	1.3	-1.4	2484
K13-ASH-1-92	18.0	1.7	0.281721	0.000053	0.001088	0.281682	-37.6	1.9	3.7	1877
K13-ASH-1-9	14.5	3.1	0.281182	0.000035	0.000890	0.281136	-56.7	1.2	2.5	2658
K13-ASH-1-46	9.0	3.2	0.281348	0.000032	0.000580	0.281326	-50.8	1.1	-6.1	2001
K13-ASH-1-3	10.8	2.9	0.281139	0.000036	0.000595	0.281108	-58.2	1.3	2.0	2683
K13-ASH-1-38	5.2	2.8	0.281617	0.000037	0.000345	0.281604	-41.3	1.3	1.0	1879
K13-ASH-1-12	15.4	3.4	0.281405	0.000031	0.000902	0.281371	-48.8	1.1	-4.6	1997
K13-ASH-1-45	17.8	2.8	0.281423	0.000035	0.001115	0.281374	-48.2	1.2	2.2	2285
K13-ASH-1-56	10.2	3.1	0.280872	0.000036	0.000594	0.280838	-67.7	1.3	-1.7	2933
K13-ASH-1-66	11.6	2.6	0.281788	0.000033	0.000720	0.281762	-35.3	1.2	6.4	1870
K13-ASH-1-30	7.0	3.8	0.281556	0.000039	0.000441	0.281541	-43.4	1.4	-1.2	1881
K13-ASH-1-102	13.3	2.2	0.281497	0.000050	0.000948	0.281461	-45.5	1.8	-1.4	1995
K13-ASH-1-2	6.1	3.3	0.281343	0.000031	0.000371	0.281329	-51.0	1.1	-5.9	2007
K13-ASH-1-21	13.5	2.7	0.281553	0.000034	0.000819	0.281524	-43.6	1.2	-1.9	1879
K13-ASH-1-69	8.6	2.5	0.281649	0.000051	0.000516	0.281630	-40.2	1.8	1.9	1880
K13-ASH-1-33	8.1	3.0	0.281653	0.000034	0.000486	0.281635	-40.0	1.2	2.0	1877
K13-ASH-1-78	12.5	3.2	0.281333	0.000031	0.000786	0.281298	-51.4	1.1	0.2	2316
K13-ASH-1-89	3.4	3.1	0.280641	0.000035	0.000243	0.280626	-75.8	1.3	-5.0	3111
K13-ASH-1-42	11.8	3.0	0.281195	0.000033	0.000739	0.281158	-56.2	1.2	2.2	2615
K13-IBEX-1-100	18.7	3.0	0.281600	0.000026	0.001088	0.281562	-41.9	0.9	-1.1	1856

K13-IBEX-1-4	23.9	3.1	0.281420	0.000034	0.001489	0.281352	-48.3	1.2	4.0	2394
K13-IBEX-1-13	17.1	3.1	0.281505	0.000031	0.001040	0.281469	-45.3	1.1	-4.3	1860
K13-IBEX-1-55	23.6	2.2	0.281310	0.000040	0.001310	0.281250	-52.1	1.4	0.6	2407
K13-IBEX-1-71	16.8	2.7	0.281550	0.000035	0.001028	0.281514	-43.7	1.2	-2.6	1862
K13-IBEX-1-76	16.1	3.5	0.281586	0.000028	0.000980	0.281551	-42.4	1.0	-1.4	1857
K13-IBEX-1-59	17.7	3.1	0.281625	0.000033	0.001090	0.281586	-41.0	1.2	0.0	1862
K13-IBEX-1-47	10.6	3.1	0.281377	0.000040	0.000669	0.281347	-49.8	1.4	3.8	2395
K13-IBEX-1-48	12.9	2.8	0.281550	0.000032	0.000784	0.281522	-43.7	1.1	-2.4	1858
K13-IBEX-1-31	13.0	2.3	0.281293	0.000040	0.000802	0.281255	-52.8	1.4	3.1	2507
K13-IBEX-1-101	17.4	3.2	0.281633	0.000034	0.001068	0.281596	-40.7	1.2	0.2	1858
K13-IBEX-1-24	7.8	2.8	0.281357	0.000037	0.000516	0.281333	-50.5	1.3	4.8	2459
K13-IBEX-1-10	10.1	3.0	0.281642	0.000035	0.000621	0.281620	-40.4	1.2	1.1	1859
K13-IBEX-1-88	5.9	2.5	0.281435	0.000032	0.000372	0.281418	-47.7	1.1	7.1	2428
K13-IBEX-1-60	24.8	2.7	0.281646	0.000032	0.001662	0.281588	-40.3	1.1	-0.1	1856
K13-NOP-1-3	8.7	1.8	0.281003	0.000054	0.000577	0.280980	-63.0	1.9	-16.1	2102
K13-NOP-1-8	20.8	1.7	0.281442	0.000077	0.001596	0.281378	-47.5	2.7	-1.7	2112
K13-NOP-1-10c	23.1	2.0	0.281133	0.000053	0.001487	0.281063	-58.4	1.9	-5.4	2434
K13-NOP-1-16	8.5	2.1	0.281503	0.000048	0.000529	0.281484	-45.3	1.7	-3.5	1871
K13-NOP-1-18	12.4	2.7	0.281456	0.000046	0.000793	0.281426	-47.0	1.6	-2.9	1986
K13-NOP-1-19	12.0	2.7	0.281557	0.000048	0.000737	0.281531	-43.4	1.7	-1.9	1868
K13-NOP-1-21	11.4	2.4	0.281142	0.000043	0.000702	0.281107	-58.1	1.5	-0.7	2566
K13-NOP-1-32	14.0	2.0	0.281406	0.000064	0.001153	0.281355	-48.8	2.3	2.0	2307
K13-NOP-1-33	12.0	2.4	0.281218	0.000049	0.000765	0.281181	-55.4	1.7	1.1	2531
K13-NOP-1-35	24.3	2.6	0.281518	0.000036	0.001445	0.281463	-44.8	1.3	-1.5	1988
K13-NOP-1-36	14.4	2.4	0.281654	0.000053	0.000824	0.281625	-40.0	1.9	1.5	1871
K13-NOP-1-38	17.4	2.9	0.281478	0.000037	0.001130	0.281436	-46.2	1.3	-2.5	1986
K13-NOP-1-40	9.7	2.0	0.280801	0.000041	0.000555	0.280776	-70.2	1.4	-17.3	2362
K13-NOP-1-40r	14.1	2.8	0.281340	0.000032	0.000950	0.281306	-51.1	1.1	-9.9	1868
K13-NOP-1-41	24.3	1.3	0.281574	0.000052	0.001893	0.281502	-42.8	1.8	0.0	1996
K13-NOP-1-44	23.5	2.9	0.281377	0.000037	0.001736	0.281297	-49.8	1.3	2.8	2426
K13-NOP-1-46	15.2	2.3	0.281445	0.000052	0.001070	0.281398	-47.4	1.8	3.4	2299
K13-NOP-1-48	16.4	1.9	0.281646	0.000057	0.000941	0.281612	-40.3	2.0	1.0	1866

K13-NOP-1-53	4.6	3.2	0.281559	0.000040	0.000300	0.281549	-43.3	1.4	-1.2	1869
K13-NOP-1-55	19.5	3.9	0.281555	0.000027	0.001151	0.281508	-43.5	1.0	2.8	2107
K13-NOP-1-58	16.4	2.1	0.281186	0.000055	0.000947	0.281140	-56.5	1.9	0.4	2563
K13-NOP-1-60	15.5	1.9	0.281685	0.000055	0.000951	0.281651	-38.9	1.9	2.4	1867
K13-NOP-1-61	9.3	2.2	0.281681	0.000047	0.000560	0.281662	-39.0	1.7	2.7	1865
K13-NOP-1-63	7.3	2.5	0.281643	0.000038	0.000435	0.281628	-40.4	1.3	2.0	1887
K13-NOP-1-63r	6.0	2.3	0.281669	0.000055	0.000343	0.281657	-39.5	1.9	2.9	1880
K13-NOP-1-65	16.2	2.6	0.280943	0.000037	0.000903	0.280902	-65.2	1.3	-13.5	2332
K13-NOP-1-75	12.2	2.6	0.281490	0.000054	0.000772	0.281459	-45.8	1.9	1.1	2108
K13-NOP-1-77	16.3	2.0	0.281250	0.000045	0.000987	0.281204	-54.3	1.6	-0.5	2429
K13-NOP-1-87	15.9	3.1	0.281579	0.000038	0.000938	0.281545	-42.7	1.3	-1.4	1868
K13-NOP-1-92	15.4	3.3	0.281518	0.000036	0.000921	0.281484	-44.8	1.3	-0.8	1988
K13-NOP-1-95	13.8	2.2	0.281538	0.000049	0.000815	0.281507	-44.1	1.7	0.0	1985
K13-NOP-1-97	9.1	2.3	0.281208	0.000038	0.000573	0.281179	-55.8	1.3	2.2	2581
K13-NOP-1-99	11.1	2.9	0.281009	0.000034	0.000659	0.280976	-62.8	1.2	-4.6	2600
K13-NOP-1-105	13.4	2.8	0.281302	0.000038	0.000893	0.281260	-52.4	1.3	2.4	2467
K13-NOP-1-107	15.4	2.6	0.281651	0.000042	0.001053	0.281612	-40.1	1.5	3.4	1971
K13-NOP-4-34	11.9	2.7	0.281072	0.000037	0.000816	0.281032	-60.6	1.3	-4.0	2539
K13-NOP-4-83	5.0	2.9	0.281600	0.000036	0.000302	0.281589	-41.9	1.3	2.0	1950
K13-NOP-4-55	14.4	2.7	0.281331	0.000033	0.000938	0.281287	-51.4	1.2	3.2	2463
K13-NOP-4-42	4.0	3.2	0.281318	0.000032	0.000246	0.281309	-51.9	1.1	-7.9	1950
K13-NOP-4-15	14.1	2.7	0.281511	0.000032	0.000824	0.281482	-45.1	1.1	-3.4	1877
K13-NOP-4-75	13.9	2.8	0.281564	0.000031	0.000847	0.281533	-43.2	1.1	0.3	1960
K13-NOP-4-28	7.6	2.8	0.281518	0.000043	0.000482	0.281501	-44.8	1.5	-2.8	1874
K13-NOP-4-69	26.5	2.9	0.281679	0.000028	0.001670	0.281616	-39.1	1.0	3.9	1987
K13-NOP-4-85	9.5	3.5	0.281102	0.000033	0.000594	0.281073	-59.5	1.2	-2.7	2534
K13-NOP-4-35	9.7	2.7	0.281566	0.000028	0.000603	0.281545	-43.1	1.0	-1.2	1875
K13-NOP-4-36	10.1	3.4	0.281290	0.000034	0.000709	0.281256	-52.9	1.2	3.7	2528
K13-NOP-4-6	8.6	2.7	0.281073	0.000039	0.000606	0.281043	-60.5	1.4	-2.4	2592
K13-NOP-4-70	7.1	2.7	0.281470	0.000034	0.000439	0.281453	-46.5	1.2	-2.1	1980
K13-NOP-4-93	8.2	2.9	0.281482	0.000044	0.000492	0.281465	-46.1	1.5	-4.1	1874
K13-NOP-4-51	10.8	3.0	0.281664	0.000033	0.000668	0.281639	-39.6	1.2	4.6	1984

K13-NOP-4-22	7.6	3.1	0.281615	0.000040	0.000469	0.281598	-41.4	1.4	0.7	1876
K13-NOP-4-10	11.2	3.4	0.281527	0.000038	0.000732	0.281501	-44.5	1.3	-2.9	1872
K13-NOP-4-91	9.3	2.5	0.281644	0.000038	0.000558	0.281623	-40.3	1.3	3.8	1974
K13-NOP-4-84	7.5	2.3	0.281453	0.000054	0.000514	0.281434	-47.1	1.9	-5.2	1872
K13-NOP-4-80	14.4	2.6	0.281646	0.000031	0.000845	0.281616	-40.3	1.1	1.3	1875
K13-NOP-4-90	7.7	3.1	0.281590	0.000036	0.000446	0.281575	-42.2	1.3	-0.1	1878
K13-NOP-4-76	11.6	2.9	0.281541	0.000037	0.000650	0.281518	-44.0	1.3	-2.3	1871
K14-BLFG-2-54	22.7	2.6	0.281771	0.000032	0.001378	0.281724	-35.8	1.1	3.5	1828
K14-BLFG-2-50	21.5	2.3	0.281245	0.000040	0.001237	0.281187	-54.5	1.4	-0.9	2460
K14-BLFG-2-106	9.7	2.3	0.281650	0.000027	0.000573	0.281631	-40.1	1.0	-1.1	1770
K14-BLFG-2-108	50.6	2.1	0.281509	0.000045	0.002793	0.281412	-45.1	1.6	-7.6	1824
K14-BLFG-2-92	34.5	2.6	0.281581	0.000031	0.002044	0.281511	-42.6	1.1	-4.7	1796
K14-BLFG-2-75	17.7	1.9	0.281759	0.000037	0.001090	0.281721	-36.3	1.3	3.3	1821
K14-BLFG-2-83	24.9	2.4	0.281722	0.000034	0.001437	0.281672	-37.6	1.2	1.9	1838
K14-BLFG-2-33	16.7	2.4	0.281633	0.000034	0.000968	0.281600	-40.7	1.2	-1.2	1813
K14-BLFG-2-64	21.7	2.6	0.281239	0.000036	0.001347	0.281175	-54.7	1.3	-0.3	2502
K14-BLFG-2-87	16.6	2.5	0.281646	0.000037	0.000939	0.281614	-40.3	1.3	-1.6	1772
K14-BLFG-2-20	3.4	2.8	0.281262	0.000024	0.000204	0.281252	-53.9	0.8	-1.1	2350
K14-BLFG-2-70	19.8	2.4	0.281797	0.000035	0.001188	0.281757	-34.9	1.2	3.9	1793
K14-BLFG-2-97	44.2	2.9	0.281612	0.000034	0.002493	0.281528	-41.5	1.2	-4.9	1764
K14-BLFG-2-17	13.6	2.7	0.281598	0.000027	0.000802	0.281570	-42.0	0.9	-2.3	1812
K14-BLFG-2-66	29.7	1.8	0.281358	0.000045	0.001940	0.281291	-50.5	1.6	-12.1	1814
K14-BLFG-2-7	21.3	2.8	0.281603	0.000031	0.001309	0.281559	-41.8	1.1	-3.7	1768
K14-BLFG-2-30	9.3	2.7	0.281544	0.000030	0.000562	0.281525	-43.9	1.1	-3.8	1818
K14-BLFG-2-34	15.8	2.1	0.281398	0.000041	0.000925	0.281356	-49.0	1.5	3.3	2381
K14-BLFG-2-26	28.2	2.6	0.281688	0.000031	0.001653	0.281632	-38.8	1.1	-0.8	1782
K14-BLFG-2-73	7.7	2.9	0.281200	0.000027	0.000396	0.281187	-56.0	1.0	-15.7	1821
K14-BLFG-2-32	7.7	2.8	0.281660	0.000030	0.000491	0.281643	-39.8	1.1	0.4	1817
K14-BLFG-2-38	26.2	2.2	0.281739	0.000036	0.001541	0.281686	-37.0	1.3	1.7	1805
K14-BLFG-2-102	15.7	2.4	0.281180	0.000037	0.000945	0.281136	-56.8	1.3	-4.0	2402
K14-BLFG-2-23	6.1	2.4	0.280972	0.000031	0.000431	0.280951	-64.1	1.1	-5.9	2604
K14-BLFG-2-109	13.1	2.4	0.281251	0.000036	0.000768	0.281213	-54.2	1.3	2.9	2579

K14-BLFG-2-89	13.7	2.5	0.281253	0.000032	0.000950	0.281207	-54.2	1.1	0.8	2500
K14-BLFG-2-63	23.0	2.7	0.281681	0.000030	0.001324	0.281635	-39.0	1.1	0.7	1843
K14-BLFG-2-42	9.9	2.2	0.281323	0.000026	0.000606	0.281295	-51.7	0.9	1.7	2405
K14-BLFG-2-110	35.8	2.1	0.281060	0.000034	0.002026	0.280958	-61.0	1.2	-5.1	2627
K14-BLFG-2-88	19.1	2.6	0.281862	0.000030	0.001348	0.281815	-32.6	1.1	6.8	1827
K14-BLFG-2-48	12.7	2.3	0.281108	0.000033	0.000753	0.281071	-59.3	1.2	-3.3	2533
K14-BLFG-2-27	20.3	1.7	0.281688	0.000038	0.001179	0.281647	-38.8	1.4	0.9	1833
K14-BLFG-2-22	17.1	2.6	0.281163	0.000032	0.000965	0.281115	-57.4	1.1	-0.2	2596
K14-BLFG-2-82	10.9	2.7	0.281781	0.000035	0.000656	0.281759	-35.5	1.2	4.8	1831
K14-BLFG-2-68	22.1	2.4	0.281251	0.000035	0.001240	0.281193	-54.2	1.2	-0.7	2457
K14-BLFG-2-6	7.5	2.8	0.281208	0.000027	0.000430	0.281187	-55.8	1.0	1.6	2564
K14-BLFG-2-84	14.3	2.8	0.281636	0.000032	0.000897	0.281605	-40.6	1.1	-0.6	1831
K14-BLFG-2-98	13.8	2.3	0.281461	0.000034	0.000855	0.281431	-46.8	1.2	-7.1	1817
K14-BLFG-2-78	18.5	2.3	0.281697	0.000035	0.001084	0.281659	-38.5	1.3	1.4	1837
K14-BLFG-2-76	16.4	2.7	0.281317	0.000029	0.000956	0.281273	-51.9	1.0	1.6	2436
K14-BLFG-2-101	22.3	2.4	0.281517	0.000031	0.001248	0.281474	-44.8	1.1	-5.4	1827
K14-BLFG-2-80	8.5	2.6	0.281808	0.000033	0.000514	0.281790	-34.5	1.1	5.5	1812
K14-BLFG-2-46	11.6	2.9	0.281725	0.000029	0.000639	0.281702	-37.5	1.0	3.8	1874
K14-BLFG-2-52	8.1	2.3	0.281322	0.000027	0.000460	0.281301	-51.7	1.0	3.0	2452
K14-BLFG-2-81	19.5	2.0	0.281212	0.000046	0.001152	0.281157	-55.6	1.6	-1.1	2494
K14-BLFG-2-13	11.5	2.4	0.280696	0.000036	0.000735	0.280650	-73.9	1.3	-1.3	3253
K14-BLFG-2-40	15.4	2.3	0.281564	0.000031	0.001012	0.281528	-43.2	1.1	-2.5	1868
K14-BLFG-2-65	10.3	2.4	0.281611	0.000037	0.000602	0.281590	-41.5	1.3	-1.1	1832
K14-BLFG-2-103	26.1	2.3	0.281655	0.000022	0.001570	0.281601	-39.9	0.8	-0.8	1827
K14-BLFG-2-28	14.4	2.6	0.281132	0.000029	0.000824	0.281090	-58.5	1.0	-0.1	2640
K14-BLFG-2-39	26.5	2.4	0.281635	0.000032	0.001585	0.281580	-40.7	1.1	-1.9	1812
K14-BLFG-2-93	13.1	2.5	0.281623	0.000040	0.000838	0.281593	-41.1	1.4	-0.9	1835
K14-BLFG-2-45	20.1	2.0	0.281186	0.000033	0.001177	0.281127	-56.5	1.2	0.3	2600
K14-BLFG-2-107	21.0	1.6	0.281745	0.000040	0.001306	0.281699	-36.8	1.4	2.6	1824
K14-HH-1-1	23.1	2.3	0.281068	0.000046	0.001314	0.281002	-60.7	1.6	-3.9	2613
K14-HH-1-2	15.6	2.3	0.281452	0.000036	0.000871	0.281422	-47.1	1.3	-8.0	1793
K14-HH-1-11	17.2	2.1	0.281182	0.000042	0.000980	0.281134	-56.7	1.5	-0.6	2552

K14-HH-1-12	19.1	1.9	0.281099	0.000035	0.001136	0.281040	-59.6	1.2	-0.3	2707
K14-HH-1-15	12.4	1.9	0.281763	0.000039	0.000755	0.281736	-36.1	1.4	5.1	1876
K14-HH-1-13	17.7	2.3	0.281835	0.000035	0.001061	0.281797	-33.6	1.2	7.2	1875
K14-HH-1-9	19.7	2.2	0.281717	0.000042	0.001257	0.281673	-37.8	1.5	2.2	1848
K14-HH-1-10	18.0	2.0	0.281353	0.000043	0.001278	0.281289	-50.6	1.5	6.3	2613
K14-HH-1-14	26.0	1.9	0.281472	0.000040	0.001680	0.281415	-46.4	1.4	-7.9	1806
K14-HH-1-7	6.9	2.6	0.281851	0.000028	0.000657	0.281828	-33.0	1.0	7.8	1850
K14-HH-1-8	22.0	2.4	0.281698	0.000034	0.001254	0.281655	-38.4	1.2	0.5	1800
K14-HH-1-6	29.1	2.2	0.281747	0.000032	0.001742	0.281684	-36.7	1.1	3.4	1884
K14-HH-1-29	22.2	1.7	0.281611	0.000039	0.001239	0.281569	-41.5	1.4	-2.8	1791
K14-HH-1-30	42.8	1.8	0.281681	0.000038	0.002557	0.281591	-39.0	1.3	-0.5	1856
K14-HH-1-28	9.7	2.0	0.281871	0.000038	0.000597	0.281850	-32.3	1.4	9.2	1880
K14-HH-1-27	21.1	2.1	0.281627	0.000033	0.001290	0.281580	-41.0	1.2	0.4	1912
K14-HH-1-26	14.6	2.1	0.280964	0.000029	0.000841	0.280922	-64.4	1.0	-6.3	2630
K14-HH-1-21	11.0	2.0	0.281675	0.000039	0.000669	0.281652	-39.3	1.4	0.4	1805
K14-HH-1-22	15.9	2.2	0.281778	0.000037	0.000988	0.281743	-35.6	1.3	5.1	1865
K14-HH-1-23	25.2	2.5	0.281760	0.000031	0.001476	0.281708	-36.2	1.1	3.8	1866
K14-HH-1-20	28.8	2.6	0.281648	0.000038	0.001664	0.281592	-40.2	1.3	-2.2	1782
K14-HH-1-16	32.0	2.2	0.281830	0.000040	0.001810	0.281768	-33.8	1.4	4.8	1814
K14-HH-1-19	12.6	2.5	0.281223	0.000031	0.000710	0.281188	-55.2	1.1	2.0	2580
K14-HH-1-17	16.1	2.0	0.281538	0.000039	0.000883	0.281508	-44.1	1.4	-4.9	1794
K14-HH-1-18	15.5	2.7	0.281623	0.000041	0.001003	0.281589	-41.1	1.5	-2.1	1790
K14-HH-1-46	27.4	2.1	0.281687	0.000041	0.001645	0.281629	-38.8	1.5	0.9	1860
K14-HH-1-48	35.4	1.9	0.281422	0.000041	0.002295	0.281344	-48.2	1.4	-10.9	1787
K14-HH-1-49	13.2	2.6	0.280705	0.000030	0.000875	0.280654	-73.5	1.1	-5.6	3067
K14-HH-1-50	12.8	2.4	0.281133	0.000037	0.000865	0.281088	-58.4	1.3	1.5	2713
K14-HH-1-55	16.2	2.4	0.281626	0.000033	0.000932	0.281594	-41.0	1.2	-2.0	1787
K14-HH-1-51	10.9	2.3	0.281569	0.000035	0.000621	0.281548	-43.0	1.2	-3.6	1787
K14-HH-1-52	20.9	2.2	0.281451	0.000042	0.001080	0.281414	-47.2	1.5	-8.5	1784
K14-HH-1-44	17.8	2.3	0.281641	0.000037	0.000963	0.281609	-40.4	1.3	-1.7	1776
K14-HH-1-42	9.4	2.0	0.281739	0.000037	0.000562	0.281719	-37.0	1.3	4.2	1863
K14-HH-1-39	16.3	1.7	0.281742	0.000040	0.000984	0.281708	-36.9	1.4	3.4	1846
K14-HH-1-65	26.4	2.1	0.281844	0.000039	0.001661	0.281785	-33.3	1.4	6.3	1853

K14-HH-1-61	13.7	2.1	0.281517	0.000038	0.000789	0.281489	-44.8	1.4	-3.8	1872
K14-HH-1-62	14.0	2.7	0.281208	0.000029	0.000819	0.281171	-55.8	1.0	-3.6	2369
K14-HH-1-63	5.7	2.8	0.281127	0.000024	0.000339	0.281116	-58.6	0.8	-17.5	1853
K14-HH-1-70	30.6	2.2	0.281107	0.000035	0.001796	0.281015	-59.3	1.2	-2.3	2662
K14-HH-1-69	12.9	2.6	0.281843	0.000029	0.000720	0.281818	-33.3	1.0	7.4	1853
K14-HH-1-66	25.4	2.0	0.281592	0.000039	0.001641	0.281534	-42.2	1.4	-2.2	1870
K14-HH-1-73	6.8	2.7	0.281123	0.000030	0.000358	0.281107	-58.8	1.1	-5.9	2368
K14-HH-1-34	36.3	1.9	0.281461	0.000042	0.001934	0.281394	-46.8	1.5	-8.7	1805
K14-HH-1-59	10.6	2.1	0.280970	0.000036	0.000605	0.280940	-64.2	1.3	-5.4	2641
K14-HH-1-60	13.8	2.2	0.281894	0.000036	0.000853	0.281864	-31.5	1.3	9.1	1851
K14-HH-1-99	14.7	2.0	0.281459	0.000039	0.000808	0.281432	-46.9	1.4	-7.9	1779
K14-HH-1-100	21.8	2.7	0.280921	0.000030	0.001309	0.280860	-65.9	1.0	-12.4	2465
K14-HH-1-91	20.9	1.8	0.281712	0.000042	0.001201	0.281670	-37.9	1.5	2.4	1861
K14-HH-1-92	41.4	2.2	0.281696	0.000033	0.002231	0.281620	-38.5	1.2	-0.7	1802
K14-HH-1-93	21.3	2.2	0.281306	0.000043	0.001305	0.281241	-52.3	1.5	4.5	2607
K14-HH-1-94	16.6	2.3	0.281623	0.000029	0.000946	0.281591	-41.1	1.0	-1.8	1799
K14-HH-1-104	13.8	2.4	0.281013	0.000029	0.000806	0.280968	-62.7	1.0	2.1	2919
K14-HH-1-105	26.3	1.7	0.281766	0.000049	0.001713	0.281705	-36.0	1.7	3.7	1863
K14-HH-1-101	24.0	1.6	0.281662	0.000060	0.001271	0.281617	-39.7	2.1	0.3	1854
K14-HH-1-102	4.5	2.2	0.281230	0.000045	0.000292	0.281215	-55.0	1.6	3.8	2616
K14-HH-1-110	12.2	2.3	0.281362	0.000034	0.000680	0.281339	-50.3	1.2	-10.8	1801
K14-HH-1-109	12.4	2.4	0.281651	0.000032	0.000733	0.281625	-40.1	1.1	0.6	1855
K14-HH-1-108	16.1	2.3	0.281591	0.000031	0.000899	0.281561	-42.2	1.1	-3.1	1789
K14-HH-1-90	12.5	2.1	0.280924	0.000038	0.000703	0.280889	-65.8	1.3	-8.4	2591
K14-HH-1-89	21.7	1.8	0.281476	0.000049	0.001125	0.281437	-46.3	1.7	-7.3	1797
K14-HH-1-85	19.2	1.9	0.281071	0.000030	0.001065	0.281016	-60.6	1.0	-1.8	2680
K14-HH-1-88	8.1	2.3	0.281924	0.000036	0.000548	0.281904	-30.5	1.3	10.9	1869
K14-HH-1-87	15.9	1.9	0.281704	0.000044	0.000922	0.281673	-38.2	1.6	0.8	1789
K14-HH-1-80	19.0	1.9	0.281053	0.000033	0.001073	0.280998	-61.3	1.2	-3.4	2640
K14-HH-1-79	21.1	2.3	0.281628	0.000038	0.001180	0.281589	-40.9	1.3	-2.5	1773
K14-HH-1-78	36.4	2.0	0.281404	0.000037	0.001989	0.281337	-48.8	1.3	-11.1	1789
K14-HH-1-77	26.7	2.1	0.281554	0.000045	0.001556	0.281501	-43.5	1.6	-5.5	1779
K14-HH-1-76	14.1	2.0	0.281239	0.000036	0.000846	0.281209	-54.7	1.3	-14.1	1854

K14-HH-1-81	12.2	2.5	0.281130	0.000030	0.000679	0.281098	-58.5	1.1	-3.9	2467
Notes:										
Hf fractionation is corrected by comparing measured 179Hf/177Hf against known 179/177 (line by line). Beta Hf is applied as a power law.										
Yb fractionation is corrected by comparing measured 173Yb/171Yb against known 173/171 (line by line) if 171Yb intensity is more than ~1 mv. Beta Yb is applied as a power law.										
	If 171Yb intensity is less than can be measured reliably, Beta Hf is used to correct for Yb fractionation.									
	The actual cutoff used is determined from the analysis of standards during the same session as unknowns (see below).									
Data are filtered by intensity of Hf (removed if below cutoff value determined by monitoring the average offset of the standards from their known values, which is set at the minimum offset)										
Data are filtered by removing 1 max and 1 min value (out of 60).										
Data are aflso filtered by 95% filter (rejected if outside of 2-sigma std dev of full set)										
Uncertainties are standard error of the mean, expressed at 1-sigma										
Hf, Yb, Lu Sol "cocktails" behaved strangely during April 2013 session - same solutions run during different times in the session displayed variable interferrences. They also fractionated slightly different than the matrix matched in-run standards. Therefore, the Hf and Yb biases were determined by only looking at the in-run matrix matched standard analyses which was appropriate due to the large number of standards run during this session.										

Table A2-3. U-Pb geochronology of plutonic rocks ALC

						Isotope ratios					Apparent ages (Ma)								
Analysis	U	206Pb	U/Th	206Pb*	±	207Pb*	±	206Pb*	±	error	206Pb*	±	207Pb*	±	206Pb*	±	Best age	±	Conc
	(ppm)	204Pb		207Pb*	(%)	235U*	(%)	238U	(%)	corr.	238U*	(Ma)	235U	(Ma)	207Pb*	(Ma)	(Ma)	(Ma)	(%)
K14-WB-15	331	224833	1.6	8.3172	0.7	4.6861	4.4	0.2827	4.4	0.99	1604.8	62.2	1764.8	37.1	1959.7	12.4	1959.7	12.4	81.9
K14-WB-12	143	144123	1.4	9.3075	0.7	3.7290	2.8	0.2517	2.7	0.97	1447.3	35.0	1577.6	22.3	1756.4	12.2	1756.4	12.2	82.4
K14-WB-20C	225	215001	1.5	9.2961	0.4	3.8456	4.0	0.2593	4.0	1.00	1486.2	53.1	1602.4	32.4	1758.7	6.7	1758.7	6.7	84.5
K14-WB-23	411	20305	2.9	9.2591	0.5	3.9153	7.0	0.2629	7.0	1.00	1504.8	93.9	1616.8	56.8	1766.0	8.8	1766.0	8.8	85.2
K14-WB-31	157	103939	1.1	9.3782	0.6	3.8348	4.3	0.2608	4.3	0.99	1494.1	56.8	1600.1	34.6	1742.6	10.5	1742.6	10.5	85.7
K14-WB-3	234	74557	1.8	9.2542	0.4	4.0082	6.8	0.2690	6.8	1.00	1535.8	93.0	1635.9	55.5	1766.9	8.2	1766.9	8.2	86.9
K14-WB-9	221	139922	1.4	9.3735	0.4	3.9180	2.0	0.2664	1.9	0.98	1522.3	26.4	1617.4	16.0	1743.5	7.1	1743.5	7.1	87.3
K14-WB-21	170	208841	1.9	9.1871	0.3	4.2143	3.3	0.2808	3.3	0.99	1595.4	46.0	1676.8	26.9	1780.2	6.2	1780.2	6.2	89.6
K14-WB-28	107	130578	1.6	9.2994	0.7	4.2138	3.6	0.2842	3.5	0.98	1612.5	50.1	1676.7	29.3	1758.0	12.0	1758.0	12.0	91.7
K14-WB-1	550	98547	2.2	9.2489	0.3	4.2977	8.6	0.2883	8.6	1.00	1633.0	123.9	1692.9	70.9	1768.0	6.3	1768.0	6.3	92.4
K14-WB-30	236	706649	1.7	9.2009	0.2	4.3630	1.9	0.2911	1.9	0.99	1647.3	27.4	1705.4	15.7	1777.5	3.7	1777.5	3.7	92.7
K14-WB-24	601	88070	3.4	9.4697	0.5	4.1032	2.8	0.2818	2.8	0.98	1600.5	39.4	1654.9	23.1	1724.8	9.0	1724.8	9.0	92.8
K14-WB-22	209	148879	2.6	9.2175	0.4	4.3953	1.8	0.2938	1.7	0.97	1660.7	25.0	1711.5	14.5	1774.2	7.3	1774.2	7.3	93.6
K14-WB-14	290	260418	2.4	9.1570	0.3	4.5060	2.4	0.2993	2.4	0.99	1687.6	35.5	1732.1	20.0	1786.2	4.8	1786.2	4.8	94.5
K14-WB-17	167	38504	2.2	9.0893	0.7	4.6609	2.6	0.3073	2.5	0.96	1727.2	37.7	1760.2	21.7	1799.7	12.9	1799.7	12.9	96.0
K14-WB-4C	354	281257	1.8	9.1218	0.2	4.6330	4.1	0.3065	4.1	1.00	1723.5	62.6	1755.2	34.7	1793.2	4.0	1793.2	4.0	96.1

K14-WB-29	115	156932	1.4	9.1823	0.5	4.6752	4.9	0.3114	4.9	1.00	1747.4	74.6	1762.8	41.0	1781.2	8.9	1781.2	8.9	98.1
K14-WB-8	194	55962	1.6	9.0793	0.7	4.8125	2.3	0.3169	2.2	0.95	1774.6	34.0	1787.1	19.4	1801.7	13.3	1801.7	13.3	98.5
K14-WB-16C	126	255579	1.9	9.1261	0.6	4.7607	3.2	0.3151	3.1	0.98	1765.8	48.3	1778.0	26.6	1792.3	10.2	1792.3	10.2	98.5
K14-WB-13	164	266060	1.2	9.1219	0.5	4.7803	2.1	0.3163	2.1	0.97	1771.4	31.9	1781.5	17.9	1793.2	9.7	1793.2	9.7	98.8
K14-WB-18	94	244397	1.9	9.2052	0.5	4.7109	0.8	0.3145	0.6	0.78	1762.9	10.0	1769.2	6.9	1776.6	9.4	1776.6	9.4	99.2
K14-WB-19	102	119119	1.3	9.1302	0.5	4.7959	2.0	0.3176	1.9	0.97	1777.9	30.2	1784.2	16.8	1791.5	8.5	1791.5	8.5	99.2
K14-WB-5	63	94789	1.7	9.1482	0.8	4.7763	2.2	0.3169	2.1	0.94	1774.6	32.8	1780.7	18.9	1788.0	13.8	1788.0	13.8	99.3
K14-WB-16R	220	319819	2.2	9.1292	0.4	4.7991	1.1	0.3178	1.0	0.94	1778.8	15.5	1784.7	8.9	1791.7	6.5	1791.7	6.5	99.3
K14-WB-25	144	152445	1.8	9.1500	0.5	4.7832	2.4	0.3174	2.3	0.97	1777.1	35.8	1782.0	19.9	1787.6	9.8	1787.6	9.8	99.4
K14-WB-27	158	198482	1.7	9.1430	0.3	4.7973	2.3	0.3181	2.3	0.99	1780.5	35.9	1784.4	19.6	1789.0	6.3	1789.0	6.3	99.5
K14-WB-11	235	333861	1.6	9.1016	0.2	4.8531	2.5	0.3204	2.5	1.00	1791.5	39.6	1794.2	21.4	1797.2	3.1	1797.2	3.1	99.7
K14-WB-7	60	47158	1.2	9.0756	0.7	4.9043	1.7	0.3228	1.6	0.90	1803.4	24.6	1803.0	14.6	1802.4	13.5	1802.4	13.5	100.1
K14-WB-4R	373	64891	2.2	9.1664	0.2	4.8099	5.6	0.3198	5.6	1.00	1788.6	87.3	1786.6	47.0	1784.3	3.6	1784.3	3.6	100.2
K14-WB-26	115	214585	1.2	9.1217	0.7	4.8767	2.2	0.3226	2.0	0.94	1802.5	31.9	1798.2	18.1	1793.2	13.2	1793.2	13.2	100.5
K14-WB-20R	172	5349	2.0	9.0732	1.3	4.9446	2.2	0.3254	1.7	0.79	1815.9	27.7	1809.9	18.6	1802.9	24.5	1802.9	24.5	100.7
K14-WB-6	145	174791	1.8	9.1189	0.3	4.9323	2.3	0.3262	2.3	0.99	1820.0	36.4	1807.8	19.5	1793.8	5.3	1793.8	5.3	101.5
13H-060-20R	1109	522668	4.1	9.3390	0.1	4.0564	1.1	0.2748	1.1	1.00	1564.9	15.5	1645.6	9.1	1750.2	1.9	1750.2	1.9	89.4
13H-060-1R	1440	500737	9.2	9.2470	0.1	4.4417	2.0	0.2979	2.0	1.00	1680.8	29.3	1720.2	16.5	1768.4	2.6	1768.4	2.6	95.0
13H-060-51R	193	73912	2.1	9.1514	0.4	4.6553	0.8	0.3090	0.7	0.89	1735.7	10.6	1759.2	6.5	1787.3	6.5	1787.3	6.5	97.1
13H-060-29	280	478829	4.6	9.1758	0.1	4.6646	2.7	0.3104	2.7	1.00	1742.8	41.9	1760.9	23.0	1782.5	2.1	1782.5	2.1	97.8
13H-060-31	822	93742	5.5	9.1834	0.2	4.6622	2.2	0.3105	2.2	0.99	1743.3	33.6	1760.5	18.5	1780.9	4.1	1780.9	4.1	97.9
13H-060-13R	745	1025601	6.6	9.1432	0.1	4.7167	0.9	0.3128	0.9	0.99	1754.3	14.2	1770.2	7.8	1789.0	2.4	1789.0	2.4	98.1
13H-060-4	342	445071	2.8	9.1674	0.2	4.6964	1.8	0.3123	1.8	0.99	1751.8	27.3	1766.6	15.0	1784.1	3.4	1784.1	3.4	98.2
13H-060-9R	132	178266	1.4	9.1354	0.4	4.7396	2.2	0.3140	2.2	0.98	1760.5	33.3	1774.3	18.5	1790.5	7.8	1790.5	7.8	98.3
13H-060-15	137	172453	1.2	9.1896	0.4	4.7056	1.4	0.3136	1.3	0.96	1758.5	20.6	1768.2	11.6	1779.7	7.0	1779.7	7.0	98.8
13H-060-5	169	143377	2.0	9.1701	0.3	4.7344	2.0	0.3149	2.0	0.99	1764.6	30.2	1773.3	16.7	1783.6	6.2	1783.6	6.2	98.9
13H-060-43	273	365897	3.4	9.1711	0.2	4.7343	1.0	0.3149	1.0	0.99	1764.8	15.7	1773.3	8.6	1783.4	3.1	1783.4	3.1	99.0
13H-060-6	122	359650	1.2	9.1814	0.7	4.7239	1.5	0.3146	1.4	0.90	1763.1	21.0	1771.5	12.7	1781.3	12.3	1781.3	12.3	99.0
13H-060-24	201	416879	1.7	9.1529	0.3	4.7646	2.4	0.3163	2.4	0.99	1771.6	37.1	1778.7	20.3	1787.0	5.8	1787.0	5.8	99.1
13H-060-23R	281	105940	1.7	9.1748	0.1	4.7480	1.1	0.3159	1.1	0.99	1769.9	16.9	1775.8	9.2	1782.7	2.6	1782.7	2.6	99.3
13H-060-48	334	242839	4.4	9.1827	0.2	4.7450	0.6	0.3160	0.6	0.93	1770.2	9.0	1775.2	5.2	1781.1	4.2	1781.1	4.2	99.4
13H-060-27	177	359728	1.8	9.1709	0.6	4.7606	2.3	0.3166	2.2	0.97	1773.3	34.3	1778.0	19.2	1783.4	10.9	1783.4	10.9	99.4
13H-060-7R	156	202166	2.1	9.1392	0.5	4.7985	1.4	0.3181	1.3	0.93	1780.3	21.0	1784.6	12.2	1789.7	9.5	1789.7	9.5	99.5
13H-060-2	211	322367	3.1	9.1459	0.2	4.7919	0.9	0.3179	0.9	0.97	1779.3	14.2	1783.5	8.0	1788.4	4.5	1788.4	4.5	99.5
13H-060-25	185	36717	2.7	9.2291	0.5	4.7082	1.8	0.3151	1.8	0.97	1766.0	27.3	1768.7	15.3	1771.9	8.7	1771.9	8.7	99.7
13H-060-7C	114	148639	3.4	9.1297	0.4	4.8375	1.6	0.3203	1.6	0.97	1791.3	24.8	1791.4	13.7	1791.6	6.7	1791.6	6.7	100.0
13H-060-19	132	171047	1.4	9.1795	0.3	4.7820	1.9	0.3184	1.9	0.99	1781.8	29.1	1781.7	15.9	1781.7	5.3	1781.7	5.3	100.0
13H-060-26R	351	438493	3.0	9.1646	0.1	4.8052	1.5	0.3194	1.5	1.00	1786.7	23.5	1785.8	12.7	1784.7	2.7	1784.7	2.7	100.1
13H-060-10	161	222572	1.5	9.1548	0.4	4.8184	1.1	0.3199	1.1	0.94	1789.4	16.9	1788.1	9.6	1786.6	6.9	1786.6	6.9	100.2
13H-060-42	210	217071	2.5	9.1686	0.3	4.8068	1.1	0.3196	1.1	0.97	1788.0	16.7	1786.1	9.3	1783.9	5.2	1783.9	5.2	100.2
13H-060-35	224	241366	2.2	9.1623	0.2	4.8246	1.5	0.3206	1.5	0.99	1792.6	22.8	1789.2	12.4	1785.1	3.9	1785.1	3.9	100.4
13H-060-49	74	132277	0.8	9.1955	0.6	4.7955	1.0	0.3198	0.8	0.80	1788.8	12.3	1784.1	8.3	1778.6	10.8	1778.6	10.8	100.6

13H-060-12	134	419196	2.3	9.1300	0.4	4.8798	1.1	0.3231	1.0	0.92	1805.0	15.4	1798.8	9.0	1791.6	7.6	1791.6	7.6	100.7
13H-060-9C	231	207841	0.4	9.1558	0.2	4.8529	2.2	0.3223	2.2	1.00	1800.7	33.9	1794.1	18.2	1786.4	3.2	1786.4	3.2	100.8
13H-060-14	332	51445	2.0	9.2351	0.4	4.7707	2.7	0.3195	2.7	0.99	1787.5	41.4	1779.7	22.5	1770.7	7.3	1770.7	7.3	100.9
13H-060-32	423	519602	3.6	9.1633	0.1	4.8714	1.1	0.3237	1.1	1.00	1808.0	17.2	1797.3	9.2	1784.9	1.9	1784.9	1.9	101.3
13H-060-17R	311	581110	4.1	9.1518	0.2	4.9000	2.0	0.3252	1.9	0.99	1815.3	30.8	1802.3	16.5	1787.2	4.2	1787.2	4.2	101.6
13H-060-45	93	122209	0.7	9.1669	0.5	4.9078	1.7	0.3263	1.7	0.96	1820.4	26.4	1803.6	14.6	1784.2	8.9	1784.2	8.9	102.0
13H-060-50R	325	314128	5.1	9.1908	0.3	4.8837	1.2	0.3255	1.2	0.98	1816.7	19.1	1799.4	10.4	1779.5	5.0	1779.5	5.0	102.1
13H-060-36	196	161518	1.9	9.1813	0.4	4.8985	2.2	0.3262	2.1	0.98	1819.9	34.0	1802.0	18.4	1781.4	7.5	1781.4	7.5	102.2
13H-060-47R	206	255665	2.2	9.1760	0.3	4.9075	2.3	0.3266	2.3	0.99	1821.9	35.9	1803.6	19.3	1782.4	6.1	1782.4	6.1	102.2
13H-060-37	143	155883	1.9	9.1861	0.4	4.8981	2.1	0.3263	2.0	0.98	1820.6	32.3	1801.9	17.5	1780.4	7.7	1780.4	7.7	102.3
13H-060-52	122	131925	1.7	9.1851	0.7	4.9004	1.1	0.3264	0.8	0.71	1821.1	11.9	1802.3	8.9	1780.6	13.6	1780.6	13.6	102.3
13H-060-22	186	14549	0.9	9.1576	0.5	4.9367	1.5	0.3279	1.4	0.93	1828.1	22.6	1808.5	12.9	1786.1	10.0	1786.1	10.0	102.4
13H-060-8	249	356925	2.3	9.1662	0.2	4.9394	2.4	0.3284	2.4	1.00	1830.5	37.5	1809.0	20.0	1784.4	4.1	1784.4	4.1	102.6
13H-060-38	189	294111	3.4	9.1608	0.3	4.9706	2.4	0.3302	2.4	0.99	1839.6	38.7	1814.3	20.6	1785.4	5.8	1785.4	5.8	103.0
13H-060-18	253	193605	5.9	9.1680	0.3	4.9962	3.8	0.3322	3.8	1.00	1849.1	61.2	1818.7	32.3	1784.0	5.0	1784.0	5.0	103.6
13H-060-1C	216	74330	1.4	8.9174	0.5	5.0129	2.1	0.3242	2.1	0.97	1810.3	32.4	1821.5	17.8	1834.4	8.5	1834.4	8.5	98.7
13H-060-46	365	142368	1.9	8.9015	0.4	4.9276	2.8	0.3181	2.8	0.99	1780.5	42.8	1807.0	23.5	1837.6	6.6	1837.6	6.6	96.9
13H-060-16	477	806224	2.6	8.8553	0.2	5.1915	0.9	0.3334	0.9	0.98	1854.9	14.6	1851.2	7.9	1847.0	3.3	1847.0	3.3	100.4
13H-060-40	167	116351	3.0	8.8469	0.6	4.9222	1.3	0.3158	1.1	0.87	1769.3	17.1	1806.1	10.7	1848.7	11.5	1848.7	11.5	95.7
13H-060-30	128	192647	1.8	8.8375	0.3	5.2024	0.8	0.3335	0.8	0.93	1855.1	12.4	1853.0	7.1	1850.7	5.7	1850.7	5.7	100.2
13H-060-39	49	148699	0.9	8.7888	0.6	5.2501	1.6	0.3347	1.5	0.92	1860.9	23.7	1860.8	13.6	1860.7	11.4	1860.7	11.4	100.0
13H-060-26C	157	234262	0.8	8.7691	0.3	5.2326	1.2	0.3328	1.1	0.96	1851.9	18.4	1857.9	10.2	1864.7	5.9	1864.7	5.9	99.3
13H-060-21	116	176826	1.9	8.7205	0.6	5.3393	1.2	0.3377	1.0	0.87	1875.6	16.5	1875.2	9.9	1874.7	10.2	1874.7	10.2	100.0
13H-060-44	247	311929	1.6	8.7162	0.2	5.3899	1.3	0.3407	1.3	0.99	1890.2	20.8	1883.2	11.0	1875.6	3.4	1875.6	3.4	100.8
13H-060-20C	144	179710	0.9	8.5666	0.3	5.6247	1.6	0.3495	1.6	0.98	1932.0	26.7	1919.9	14.1	1906.8	5.8	1906.8	5.8	101.3
13H-060-23C	104	50309	0.8	8.5235	0.4	5.3807	1.8	0.3326	1.8	0.98	1851.1	28.5	1881.8	15.5	1915.8	7.0	1915.8	7.0	96.6
13H-060-51C	546	769856	3.5	8.3223	0.2	5.8635	1.2	0.3539	1.1	0.99	1953.3	19.4	1955.8	10.1	1958.6	3.2	1958.6	3.2	99.7
13H-060-17C	217	422846	1.6	8.1503	0.2	6.1069	1.7	0.3610	1.7	0.99	1986.9	28.6	1991.2	14.6	1995.8	3.0	1995.8	3.0	99.6
13H-060-13C	582	1044541	1.9	7.6807	0.6	6.8164	1.6	0.3797	1.5	0.94	2074.9	26.9	2087.9	14.3	2100.6	9.8	2100.6	9.8	98.8
13H-060-47C	131	157963	3.0	7.6607	0.3	7.2594	1.3	0.4033	1.2	0.98	2184.4	22.9	2143.8	11.3	2105.2	4.4	2105.2	4.4	103.8
13H-080-3	126	67419	1.3	9.2475	0.7	4.7701	1.6	0.3199	1.4	0.90	1789.4	22.6	1779.7	13.6	1768.3	13.1	1768.3	13.1	101.2
13H-080-1	168	99664	1.9	9.2469	0.6	4.7991	1.0	0.3219	0.9	0.84	1798.8	13.5	1784.7	8.6	1768.4	10.1	1768.4	10.1	101.7
13H-080-7	135	159432	1.4	9.2450	1.1	4.7978	3.1	0.3217	2.8	0.93	1798.0	44.7	1784.5	25.8	1768.7	20.8	1768.7	20.8	101.7
13H-080-37	106	66901	0.8	9.2381	1.2	4.7387	2.9	0.3175	2.7	0.92	1777.5	41.2	1774.1	24.3	1770.1	21.3	1770.1	21.3	100.4
13H-080-22	313	377077	4.9	9.2242	0.3	4.7964	1.5	0.3209	1.5	0.97	1794.0	23.3	1784.3	12.9	1772.9	6.3	1772.9	6.3	101.2
13H-080-44	534	421270	0.6	9.2221	0.3	4.7184	0.8	0.3156	0.8	0.94	1768.2	12.1	1770.5	6.9	1773.3	5.1	1773.3	5.1	99.7
13H-080-24	162	235366	1.8	9.2136	0.6	4.8722	1.9	0.3256	1.8	0.95	1816.9	28.3	1797.5	15.9	1775.0	10.9	1775.0	10.9	102.4
13H-080-11	133	171077	1.9	9.2094	0.6	4.8671	1.4	0.3251	1.2	0.89	1814.5	19.1	1796.6	11.4	1775.8	11.0	1775.8	11.0	102.2
13H-080-48	244	227102	4.2	9.2064	0.7	4.7890	1.5	0.3198	1.3	0.88	1788.6	20.1	1783.0	12.3	1776.4	12.8	1776.4	12.8	100.7
13H-080-9	286	363022	2.8	9.2038	0.4	4.7526	1.1	0.3172	1.0	0.92	1776.3	15.7	1776.6	9.2	1776.9	7.9	1776.9	7.9	100.0
13H-080-29	202	200902	1.5	9.1966	0.6	4.8149	1.2	0.3212	1.0	0.85	1795.3	15.7	1787.5	9.9	1778.3	11.5	1778.3	11.5	101.0
13H-080-2	743	589387	3.6	9.1963	0.1	4.8549	1.7	0.3238	1.7	1.00	1808.3	27.0	1794.5	14.4	1778.4	2.3	1778.4	2.3	101.7

13H-080-53	393	319242	6.2	9.1930	0.3	4.8568	1.7	0.3238	1.7	0.98	1808.4	26.4	1794.8	14.3	1779.0	5.6	1779.0	5.6	101.6
13H-080-8	290	299885	3.0	9.1924	0.3	4.7762	1.2	0.3184	1.2	0.96	1782.0	18.0	1780.7	10.1	1779.2	6.0	1779.2	6.0	100.2
13H-080-31	124	96235	2.2	9.1893	0.9	4.8084	1.3	0.3205	0.9	0.72	1792.0	14.6	1786.4	11.0	1779.8	16.6	1779.8	16.6	100.7
13H-080-45	462	522006	6.5	9.1889	0.3	4.6903	1.7	0.3126	1.7	0.99	1753.4	25.3	1765.5	14.0	1779.9	5.1	1779.9	5.1	98.5
13H-080-15	465	689865	4.3	9.1811	0.2	4.7808	1.0	0.3183	1.0	0.98	1781.6	15.4	1781.5	8.5	1781.4	3.9	1781.4	3.9	100.0
13H-080-46	420	304680	6.4	9.1774	0.4	4.6759	0.9	0.3112	0.8	0.92	1746.8	12.5	1762.9	7.5	1782.1	6.5	1782.1	6.5	98.0
13H-080-38	113	48829	2.2	9.1759	1.0	4.7905	1.5	0.3188	1.1	0.75	1783.9	17.4	1783.2	12.6	1782.4	18.1	1782.4	18.1	100.1
13H-080-34	134	82757	2.2	9.1751	0.5	4.8852	1.0	0.3251	0.9	0.87	1814.5	14.1	1799.7	8.6	1782.6	9.4	1782.6	9.4	101.8
13H-080-14	202	106933	2.5	9.1742	0.3	4.8418	0.8	0.3222	0.7	0.94	1800.3	11.5	1792.2	6.6	1782.8	5.0	1782.8	5.0	101.0
13H-080-42	158	77433	1.8	9.1741	0.8	4.9616	1.3	0.3301	1.0	0.79	1839.0	16.5	1812.8	11.1	1782.8	14.7	1782.8	14.7	103.2
13H-080-30	374	362216	6.6	9.1724	0.2	4.8306	0.6	0.3214	0.6	0.92	1796.3	8.7	1790.2	5.0	1783.1	4.2	1783.1	4.2	100.7
13H-080-32	187	129264	2.1	9.1718	0.8	4.8621	1.1	0.3234	0.8	0.72	1806.5	12.5	1795.7	9.3	1783.3	13.9	1783.3	13.9	101.3
13H-080-40	239	162263	3.6	9.1702	0.5	4.8272	4.8	0.3211	4.8	1.00	1794.9	75.3	1789.7	40.7	1783.6	8.6	1783.6	8.6	100.6
13H-080-18	342	280834	2.5	9.1699	0.2	4.6842	1.3	0.3115	1.2	0.99	1748.2	19.1	1764.4	10.5	1783.6	3.4	1783.6	3.4	98.0
13H-080-33	670	958698	6.9	9.1685	0.2	4.7672	0.6	0.3170	0.5	0.92	1775.1	8.2	1779.1	4.8	1783.9	4.0	1783.9	4.0	99.5
13H-080-55R	422	218147	6.1	9.1672	0.4	4.7169	0.9	0.3136	0.8	0.90	1758.5	12.8	1770.3	7.7	1784.2	7.3	1784.2	7.3	98.6
13H-080-13	80	63693	1.7	9.1644	1.6	4.9980	2.1	0.3322	1.3	0.63	1849.0	21.2	1819.0	17.6	1784.7	29.3	1784.7	29.3	103.6
13H-080-39	316	613534	5.8	9.1615	0.3	4.7533	0.7	0.3158	0.6	0.90	1769.3	9.8	1776.7	5.9	1785.3	5.6	1785.3	5.6	99.1
13H-080-51	145	83024	1.2	9.1560	1.2	4.6759	1.4	0.3105	0.7	0.49	1743.2	10.5	1762.9	11.6	1786.4	22.0	1786.4	22.0	97.6
13H-080-50	165	268631	1.8	9.1525	0.6	4.7758	0.8	0.3170	0.6	0.69	1775.1	8.8	1780.7	6.9	1787.1	10.8	1787.1	10.8	99.3
13H-080-10	707	684869	5.2	9.1493	0.2	4.8883	1.7	0.3244	1.7	1.00	1811.0	27.4	1800.2	14.7	1787.7	2.9	1787.7	2.9	101.3
13H-080-49	228	67575	2.2	9.1486	0.9	4.7167	1.6	0.3130	1.3	0.83	1755.3	20.5	1770.2	13.5	1787.9	16.6	1787.9	16.6	98.2
13H-080-16	203	187216	1.9	9.1471	0.4	4.9064	0.8	0.3255	0.7	0.89	1816.5	11.8	1803.4	7.1	1788.2	7.0	1788.2	7.0	101.6
13H-080-20	181	219359	1.7	9.1453	0.4	4.7726	0.7	0.3166	0.6	0.82	1772.9	8.7	1780.1	5.7	1788.5	7.1	1788.5	7.1	99.1
13H-080-27	151	233920	1.9	9.1411	0.6	4.8827	1.0	0.3237	0.8	0.78	1807.8	11.8	1799.3	8.2	1789.4	11.1	1789.4	11.1	101.0
13H-080-21	183	418400	2.3	9.1395	0.7	4.7938	1.0	0.3178	0.6	0.64	1778.8	9.6	1783.8	8.1	1789.7	13.6	1789.7	13.6	99.4
13H-080-47	288	23781	3.8	9.1391	1.2	5.0984	3.7	0.3379	3.5	0.95	1876.7	56.6	1835.8	31.2	1789.8	21.6	1789.8	21.6	104.9
13H-080-4	182	127797	2.1	9.1346	0.6	4.8522	0.8	0.3215	0.5	0.61	1796.8	7.2	1794.0	6.3	1790.7	10.8	1790.7	10.8	100.3
13H-080-19	135	171630	1.7	9.1292	0.8	4.7858	0.9	0.3169	0.4	0.43	1774.5	5.9	1782.4	7.5	1791.7	14.7	1791.7	14.7	99.0
13H-080-6	202	106419	2.6	9.1238	0.6	4.8144	1.8	0.3186	1.7	0.95	1782.8	27.1	1787.4	15.4	1792.8	10.6	1792.8	10.6	99.4
13H-080-26	202	301696	2.5	9.1185	0.4	4.9052	1.0	0.3244	0.9	0.91	1811.2	13.8	1803.2	8.1	1793.9	7.2	1793.9	7.2	101.0
13H-080-52	179	270511	2.1	9.1122	0.9	4.7254	1.6	0.3123	1.3	0.84	1752.0	20.4	1771.8	13.3	1795.1	15.8	1795.1	15.8	97.6
13H-080-54	228	205855	4.0	9.0993	0.4	4.8083	0.9	0.3173	0.8	0.87	1776.6	12.3	1786.4	7.6	1797.7	8.2	1797.7	8.2	98.8
13H-080-41	225	19156	3.1	9.0918	1.4	4.7362	3.1	0.3123	2.7	0.89	1752.0	41.8	1773.7	25.8	1799.2	26.0	1799.2	26.0	97.4
13H-080-56R	204	193126	2.1	9.0904	0.7	4.9063	1.1	0.3235	0.8	0.72	1806.7	12.1	1803.3	9.0	1799.5	13.5	1799.5	13.5	100.4
13H-080-36	158	133067	3.1	9.0894	0.8	4.9048	1.6	0.3233	1.3	0.85	1806.0	20.8	1803.1	13.2	1799.7	15.2	1799.7	15.2	100.4
13H-080-17	190	133708	3.0	9.0457	0.7	4.8864	1.0	0.3206	0.7	0.74	1792.5	11.5	1799.9	8.3	1808.4	12.0	1808.4	12.0	99.1
13H-080-23	160	174707	2.6	9.0417	0.7	4.9466	1.1	0.3244	0.9	0.79	1811.1	13.9	1810.2	9.4	1809.3	12.3	1809.3	12.3	100.1
13H-080-25	180	105832	2.2	9.0339	1.1	4.8834	1.4	0.3200	0.8	0.57	1789.5	12.5	1799.4	11.8	1810.8	20.8	1810.8	20.8	98.8
13H-080-28	139	170378	2.4	9.0016	1.8	4.8084	2.8	0.3139	2.1	0.77	1760.0	32.8	1786.4	23.2	1817.3	31.9	1817.3	31.9	96.8
13H-080-43R	245	240597	4.1	8.9408	0.8	5.0964	1.7	0.3305	1.5	0.89	1840.7	24.7	1835.5	14.7	1829.6	14.3	1829.6	14.3	100.6
13H-080-5	194	193890	4.5	8.9088	0.7	5.0865	1.2	0.3287	1.0	0.81	1831.9	15.6	1833.9	10.3	1836.1	12.9	1836.1	12.9	99.8
13H-080-55C	183	168880	2.0	8.6592	0.7	5.3526	1.3	0.3362	1.0	0.82	1868.1	16.8	1877.3	10.7	1887.4	12.8	1887.4	12.8	99.0

13H-080-56C	366	37748	2.3	8.5531	0.4	5.4745	0.7	0.3396	0.6	0.86	1884.7	10.4	1896.6	6.4	1909.6	6.9	1909.6	6.9	98.7
13H-080-35	281	30125	2.4	8.3612	1.3	5.8151	5.8	0.3526	5.7	0.97	1947.2	95.3	1948.7	50.5	1950.2	23.9	1950.2	23.9	99.8
13H-080-43C	201	700201	1.8	8.0409	0.6	6.2940	2.0	0.3671	1.9	0.95	2015.5	33.0	2017.6	17.6	2019.7	11.2	2019.7	11.2	99.8
K13-NOP-3-27	553	3350	2.5	9.4698	3.6	3.0653	6.1	0.2105	4.9	0.81	1231.6	55.4	1424.1	46.8	1724.8	65.9	1724.8	65.9	71.4
K13-NOP-3-5	705	1980	2.8	9.6357	3.1	3.0630	30.5	0.2141	30.3	0.99	1250.4	344.9	1423.5	237.5	1692.8	57.7	1692.8	57.7	73.9
K13-NOP-3-24	412	5380	4.4	9.3648	0.9	3.3072	16.1	0.2246	16.1	1.00	1306.3	190.3	1482.7	126.3	1745.2	16.1	1745.2	16.1	74.8
K13-NOP-3-16	752	900	2.1	9.8782	3.3	3.1009	18.1	0.2222	17.8	0.98	1293.3	209.1	1432.9	140.2	1646.8	61.3	1646.8	61.3	78.5
K13-NOP-3-19	444	2582	4.4	9.1309	5.4	3.6954	18.3	0.2447	17.5	0.96	1411.2	222.2	1570.4	147.6	1791.4	98.4	1791.4	98.4	78.8
K13-NOP-3-10	656	3455	4.6	9.6028	2.2	3.3767	11.1	0.2352	10.9	0.98	1361.5	133.4	1499.0	87.1	1699.1	41.4	1699.1	41.4	80.1
K13-NOP-3-15	335	3530	2.1	9.2676	0.9	3.7619	4.3	0.2529	4.2	0.98	1453.2	55.3	1584.7	34.9	1764.3	16.8	1764.3	16.8	82.4
K13-NOP-3-9	403	16646	8.2	9.2637	0.6	3.8535	10.3	0.2589	10.3	1.00	1484.2	136.6	1604.0	83.4	1765.1	11.7	1765.1	11.7	84.1
K13-NOP-3-23	413	4027	1.7	9.3265	0.5	3.8600	9.4	0.2611	9.4	1.00	1495.4	125.1	1605.3	75.8	1752.7	9.1	1752.7	9.1	85.3
K13-NOP-3-1	229	4901	3.0	9.2062	0.7	4.3553	7.0	0.2908	6.9	0.99	1645.5	100.9	1703.9	57.7	1776.4	13.5	1776.4	13.5	92.6
K13-NOP-3-17	258	14612	2.1	9.2180	0.3	4.4603	1.6	0.2982	1.6	0.99	1682.3	23.5	1723.6	13.4	1774.1	4.8	1774.1	4.8	94.8
K13-NOP-3-2	241	110080	2.0	9.1656	0.3	4.7359	1.3	0.3148	1.2	0.98	1764.4	18.8	1773.6	10.5	1784.5	5.0	1784.5	5.0	98.9
K13-NOP-3-7	299	16416	6.1	9.1924	0.3	4.7136	5.2	0.3143	5.2	1.00	1761.6	79.9	1769.7	43.5	1779.2	5.7	1779.2	5.7	99.0
K13-NOP-3-4	209	147556	1.6	9.1556	0.3	4.8658	1.5	0.3231	1.5	0.99	1804.9	23.6	1796.3	12.8	1786.5	4.7	1786.5	4.7	101.0
K13-NOP-3-6	157	433391	2.3	9.1605	0.3	4.9482	1.3	0.3287	1.3	0.97	1832.3	20.5	1810.5	11.2	1785.5	5.8	1785.5	5.8	102.6
K14-HH-2-35	275	50649	1.9	9.5431	1.1	3.7093	2.8	0.2567	2.5	0.91	1473.1	33.2	1573.4	22.1	1710.6	20.8	1710.6	20.8	86.1
K14-HH-2-20	167	10030	1.2	9.3831	0.9	4.4353	4.8	0.3018	4.7	0.98	1700.4	70.1	1719.0	39.5	1741.6	15.9	1741.6	15.9	97.6
K14-HH-2-16	165	163770	5.5	9.3553	0.9	4.4531	1.5	0.3021	1.2	0.80	1701.9	18.4	1722.3	12.7	1747.1	16.6	1747.1	16.6	97.4
K14-HH-2-27	133	75247	2.4	9.3442	1.0	4.2581	3.8	0.2886	3.7	0.97	1634.4	52.8	1685.3	31.2	1749.2	18.0	1749.2	18.0	93.4
K14-HH-2-10	111	49543	2.1	9.3104	0.9	4.5382	3.9	0.3064	3.8	0.97	1723.2	57.7	1738.0	32.6	1755.9	16.0	1755.9	16.0	98.1
K14-HH-2-30	123	100080	1.9	9.2977	1.6	4.3197	1.9	0.2913	1.1	0.57	1648.0	15.8	1697.1	15.8	1758.4	28.9	1758.4	28.9	93.7
K14-HH-2-28	133	56125	1.4	9.2930	1.0	4.2699	1.6	0.2878	1.3	0.80	1630.5	18.5	1687.6	13.2	1759.3	17.6	1759.3	17.6	92.7
K14-HH-2-39	117	62321	1.8	9.2548	1.2	4.5419	1.4	0.3049	0.7	0.48	1715.4	9.8	1738.7	11.3	1766.8	21.8	1766.8	21.8	97.1
K14-HH-2-8	108	145955	1.9	9.2341	1.9	4.6843	2.3	0.3137	1.2	0.53	1759.0	18.4	1764.4	18.9	1770.9	35.1	1770.9	35.1	99.3
K14-HH-2-36	109	44024	2.7	9.2317	0.7	4.0852	3.9	0.2735	3.8	0.98	1558.7	53.3	1651.4	31.9	1771.4	13.0	1771.4	13.0	88.0
K14-HH-2-14	131	82098	2.3	9.2316	0.7	4.6059	1.4	0.3084	1.2	0.86	1732.8	18.4	1750.3	11.8	1771.4	13.3	1771.4	13.3	97.8
K14-HH-2-6	275	194989	2.3	9.2254	0.6	4.5940	0.9	0.3074	0.7	0.73	1727.8	10.5	1748.2	7.9	1772.6	11.7	1772.6	11.7	97.5
K14-HH-2-2	91	94209	1.5	9.2216	1.3	4.5531	3.0	0.3045	2.7	0.89	1713.7	39.9	1740.7	24.7	1773.4	24.4	1773.4	24.4	96.6
K14-HH-2-7	174	94709	2.0	9.2213	1.0	4.6716	1.5	0.3124	1.0	0.69	1752.7	15.4	1762.2	12.1	1773.4	19.1	1773.4	19.1	98.8
K14-HH-2-3	212	182383	5.6	9.1910	0.6	4.7865	1.4	0.3191	1.3	0.91	1785.2	20.5	1782.5	12.2	1779.4	11.1	1779.4	11.1	100.3
K14-HH-2-31	123	85226	1.7	9.1879	1.2	4.6642	1.4	0.3108	0.7	0.51	1744.7	10.5	1760.9	11.4	1780.1	21.4	1780.1	21.4	98.0
K14-HH-2-19	99	91075	1.3	9.1804	0.7	4.6647	1.4	0.3106	1.2	0.88	1743.6	19.0	1760.9	11.8	1781.5	12.3	1781.5	12.3	97.9
K14-HH-2-18	99	43452	2.2	9.1773	1.6	4.6357	2.5	0.3086	1.9	0.78	1733.6	29.6	1755.7	20.8	1782.2	28.5	1782.2	28.5	97.3
K14-HH-2-38	99	46970	1.4	9.1769	1.0	4.6936	1.4	0.3124	1.1	0.74	1752.5	16.3	1766.1	12.0	1782.2	17.7	1782.2	17.7	98.3
K14-HH-2-37	176	182671	1.8	9.1693	0.6	4.6046	6.8	0.3062	6.8	1.00	1722.1	102.9	1750.1	57.1	1783.7	11.6	1783.7	11.6	96.5
K14-HH-2-22	101	137786	1.6	9.1680	1.4	4.3991	2.1	0.2925	1.7	0.78	1654.0	24.3	1712.2	17.8	1784.0	24.6	1784.0	24.6	92.7
K14-HH-2-26	99	127287	1.8	9.1551	1.6	4.4544	1.9	0.2958	1.0	0.54	1670.3	15.4	1722.5	16.0	1786.6	29.5	1786.6	29.5	93.5
K14-HH-2-34	104	77029	1.7	9.1431	1.6	4.6692	1.8	0.3096	0.7	0.39	1738.9	10.6	1761.7	14.9	1789.0	29.9	1789.0	29.9	97.2

K14-HH-2-21	89	43711	2.5	9.1285	1.4	4.6537	1.8	0.3081	1.0	0.60	1731.4	15.9	1759.0	14.7	1791.9	25.8	1791.9	25.8	96.6
K14-HH-2-13	86	53509	1.8	9.1234	1.4	4.4753	2.2	0.2961	1.6	0.75	1672.1	24.0	1726.4	18.0	1792.9	26.1	1792.9	26.1	93.3
K14-HH-2-25	104	24814	1.7	9.1210	1.7	5.0599	9.2	0.3347	9.1	0.98	1861.2	146.5	1829.4	78.3	1793.4	30.4	1793.4	30.4	103.8
K14-HH-2-32	145	47339	1.0	9.0987	1.0	4.7105	1.5	0.3108	1.1	0.74	1744.9	17.5	1769.1	12.9	1797.8	18.8	1797.8	18.8	97.1
K14-HH-2-29	117	54795	1.5	9.0822	1.2	4.7379	1.4	0.3121	0.8	0.54	1751.0	11.6	1774.0	11.7	1801.1	21.4	1801.1	21.4	97.2
K14-HH-2-17	113	65216	1.9	8.9954	0.8	4.9776	1.2	0.3247	0.9	0.76	1812.9	14.7	1815.5	10.3	1818.6	14.4	1818.6	14.4	99.7
K14-HH-2-23	208	130129	3.2	8.9879	0.7	4.8383	5.4	0.3154	5.4	0.99	1767.2	83.1	1791.6	45.7	1820.1	13.1	1820.1	13.1	97.1
K14-HH-2-1	378	156755	6.9	8.9273	0.3	4.8773	1.8	0.3158	1.8	0.99	1769.1	28.1	1798.3	15.5	1832.4	5.2	1832.4	5.2	96.5
K14-HH-2-15	120	88399	1.2	8.6849	0.6	5.3574	1.2	0.3375	1.1	0.89	1874.4	18.1	1878.1	10.7	1882.1	10.2	1882.1	10.2	99.6
K14-HH-2-41	497	803758	1.9	8.6684	0.5	5.2563	3.1	0.3305	3.0	0.99	1840.6	48.7	1861.8	26.3	1885.5	8.6	1885.5	8.6	97.6
K14-HH-2-11	123	144004	1.8	8.5394	2.2	5.3766	3.9	0.3330	3.1	0.81	1852.9	50.4	1881.1	33.0	1912.5	40.2	1912.5	40.2	96.9
K14-HH-2-9	173	119975	2.5	8.2663	0.7	5.5768	2.2	0.3343	2.1	0.95	1859.4	34.3	1912.5	19.3	1970.6	12.8	1970.6	12.8	94.4
K14-HH-2-40C	387	23690	1.4	6.8812	0.6	7.8558	1.6	0.3921	1.5	0.92	2132.4	26.7	2214.6	14.4	2291.6	10.9	2291.6	10.9	93.1
K14 BLFG-1-2	1793	111871	4.8	9.7520	0.5	3.5808	3.5	0.2533	3.4	0.99	1455.3	44.8	1545.3	27.5	1670.6	9.0	1670.6	9.0	87.1
K14 BLFG-1-7	1207	100671	8.7	9.6586	0.6	4.0511	3.4	0.2838	3.4	0.99	1610.4	48.3	1644.5	28.0	1688.4	10.2	1688.4	10.2	95.4
K14 BLFG-1-1	545	219382	3.3	9.6288	0.3	3.5025	1.7	0.2446	1.7	0.98	1410.5	21.4	1527.8	13.5	1694.1	5.7	1694.1	5.7	83.3
K14-BLGG-1-3C	357	522758	2.2	9.6137	0.4	4.0814	4.5	0.2846	4.5	1.00	1614.4	64.5	1650.6	37.0	1697.0	7.6	1697.0	7.6	95.1
K14 BLFG-1-11	846	687297	4.4	9.6114	0.2	4.0168	2.2	0.2800	2.2	1.00	1591.4	30.4	1637.6	17.6	1697.5	2.8	1697.5	2.8	93.8
K14-BLGG-1-35	1346	1259136	6.5	9.6112	0.1	3.6825	1.2	0.2567	1.2	1.00	1472.9	15.4	1567.6	9.4	1697.5	1.8	1697.5	1.8	86.8
K14 BLFG-1-15	815	297922	12.9	9.6111	0.1	3.6616	1.1	0.2552	1.1	0.99	1465.4	13.9	1563.0	8.5	1697.5	2.4	1697.5	2.4	86.3
K14 BLFG-1-13	735	272199	2.6	9.5873	0.4	3.9901	3.1	0.2775	3.1	0.99	1578.5	43.5	1632.2	25.4	1702.1	8.0	1702.1	8.0	92.7
K14 BLFG-1-10	842	1466992	8.5	9.5833	0.1	4.1233	0.6	0.2866	0.6	0.97	1624.5	8.9	1658.9	5.2	1702.8	2.6	1702.8	2.6	95.4
K14 BLFG-1-3R	1388	1709280	6.8	9.5809	0.0	4.1236	2.3	0.2865	2.3	1.00	1624.2	32.3	1659.0	18.4	1703.3	0.6	1703.3	0.6	95.4
K14 BLFG-1-8	184	83777	1.9	9.5796	0.5	3.9647	2.1	0.2755	2.0	0.97	1568.4	28.4	1627.0	17.1	1703.5	9.5	1703.5	9.5	92.1
K14-BLGG-1-38R	600	695482	4.5	9.5791	0.2	3.8857	2.1	0.2700	2.1	1.00	1540.6	28.5	1610.7	16.8	1703.6	3.2	1703.6	3.2	90.4
K14 BLFG-1-27	1225	868142	8.6	9.5786	0.1	4.0150	2.9	0.2789	2.9	1.00	1586.0	40.4	1637.2	23.4	1703.7	2.1	1703.7	2.1	93.1
K14-BLGG-1-39	1407	773286	5.8	9.5757	0.1	3.9899	1.0	0.2771	1.0	0.99	1576.7	14.0	1632.2	8.2	1704.3	2.0	1704.3	2.0	92.5
K14 BLFG-1-5	1239	877465	6.1	9.5736	0.1	4.1550	2.1	0.2885	2.1	1.00	1634.0	30.6	1665.2	17.4	1704.7	1.1	1704.7	1.1	95.9
K14 BLFG-1-29	1459	413409	4.6	9.5711	0.1	3.8066	1.1	0.2642	1.1	1.00	1511.5	14.6	1594.1	8.7	1705.2	1.3	1705.2	1.3	88.6
K14 BLFG-1-4	1014	931827	10.0	9.5688	0.3	4.0159	1.6	0.2787	1.6	0.99	1584.8	21.9	1637.4	12.9	1705.6	5.0	1705.6	5.0	92.9
K14 BLFG-1-23	662	394855	3.0	9.5601	0.2	3.8960	1.5	0.2701	1.5	0.99	1541.5	20.8	1612.9	12.3	1707.3	3.4	1707.3	3.4	90.3
K14 BLFG-1-28	403	425727	4.0	9.5535	0.2	3.7682	1.2	0.2611	1.1	0.98	1495.4	15.0	1586.0	9.2	1708.6	4.5	1708.6	4.5	87.5
K14 BLFG-1-26	1172	1585001	11.1	9.5527	0.1	3.8875	1.0	0.2693	1.0	1.00	1537.4	13.5	1611.1	8.0	1708.7	1.7	1708.7	1.7	90.0
K14-BLGG-1-36	438	108923	2.6	9.5515	0.2	4.0387	1.3	0.2798	1.3	0.99	1590.2	17.8	1642.0	10.4	1709.0	3.7	1709.0	3.7	93.1
K14 BLFG-1-19C	236	172563	3.9	9.5477	0.3	3.9448	0.7	0.2732	0.7	0.94	1556.8	9.7	1622.9	6.0	1709.7	4.6	1709.7	4.6	91.1
K14-BLGG-1-32	754	328174	2.9	9.5471	0.1	3.9086	2.3	0.2706	2.3	1.00	1544.0	31.7	1615.5	18.7	1709.8	2.4	1709.8	2.4	90.3
K14-BLGG-1-19R	348	192241	2.6	9.5443	0.2	4.0556	0.9	0.2807	0.8	0.97	1595.1	12.0	1645.4	7.1	1710.3	3.8	1710.3	3.8	93.3
K14-BLGG-1-34	439	149332	3.1	9.5421	0.2	3.6282	2.5	0.2511	2.5	1.00	1444.1	31.7	1555.7	19.6	1710.8	3.9	1710.8	3.9	84.4
K14 BLFG-1-21	381	19708	2.6	9.5402	0.7	3.6274	1.7	0.2510	1.6	0.91	1443.6	20.1	1555.6	13.6	1711.1	13.1	1711.1	13.1	84.4
K14 BLFG-1-16	362	507503	2.2	9.5355	0.3	4.0163	1.7	0.2778	1.7	0.98	1580.1	23.9	1637.5	14.1	1712.0	5.9	1712.0	5.9	92.3
K14 BLFG-1-24	848	541959	11.3	9.5315	0.1	4.0722	1.3	0.2815	1.3	1.00	1599.0	18.8	1648.8	10.8	1712.8	1.4	1712.8	1.4	93.4
K14 BLFG-1-22	1093	590938	15.0	9.5312	0.1	4.1375	1.6	0.2860	1.6	1.00	1621.6	22.5	1661.7	12.8	1712.9	1.7	1712.9	1.7	94.7

K14 BLFG-1-6	177	160896	2.3	9.5282	0.4	4.1204	2.8	0.2847	2.8	0.99	1615.2	39.3	1658.4	22.7	1713.4	7.0	1713.4	7.0	94.3
K14-BLGG-1-31	422	147602	2.6	9.5268	0.1	4.2134	1.2	0.2911	1.2	0.99	1647.2	17.5	1676.6	9.9	1713.7	2.5	1713.7	2.5	96.1
K14-BLGG-1-37	430	248252	2.5	9.5225	0.1	4.3841	2.0	0.3028	2.0	1.00	1705.1	29.7	1709.4	16.4	1714.5	2.0	1714.5	2.0	99.4
K14 BLFG-1-17	174	165620	0.3	9.5129	0.3	4.3506	1.3	0.3002	1.3	0.98	1692.1	19.4	1703.0	11.0	1716.4	4.6	1716.4	4.6	98.6
K14 BLFG-1-12	424	535616	1.2	9.5035	0.1	4.4255	1.4	0.3050	1.4	0.99	1716.2	21.3	1717.1	11.8	1718.2	2.7	1718.2	2.7	99.9
K14-BLGG-1-33	110	125780	0.7	9.5014	0.6	4.3894	2.4	0.3025	2.3	0.97	1703.6	35.1	1710.4	20.0	1718.6	11.2	1718.6	11.2	99.1
K14 BLFG-1-25	355	569231	2.1	9.4953	0.2	4.1146	1.7	0.2834	1.7	0.99	1608.2	23.9	1657.2	13.8	1719.8	4.2	1719.8	4.2	93.5
K14 BLFG-1-18	579	246701	2.7	9.4927	0.1	4.2335	2.2	0.2915	2.2	1.00	1648.8	32.2	1680.5	18.2	1720.3	2.4	1720.3	2.4	95.8
K13-BL1-22	512	68286	0.6	10.0936	0.4	3.3978	4.5	0.2487	4.5	1.00	1432.0	57.6	1503.9	35.3	1606.7	7.1	1606.7	7.1	89.1
K13-BL1-9	470	53883	0.5	9.9226	0.3	3.6167	1.9	0.2603	1.9	0.99	1491.3	25.0	1553.2	15.1	1638.5	5.1	1638.5	5.1	91.0
K13-BL1-16	313	26253	3.2	9.8958	0.7	3.6429	7.9	0.2615	7.9	1.00	1497.3	105.1	1558.9	63.0	1643.5	13.5	1643.5	13.5	91.1
K13-BL1-8	542	39197	0.6	9.8684	0.4	3.7402	4.3	0.2677	4.3	1.00	1529.1	57.9	1580.0	34.2	1648.7	6.7	1648.7	6.7	92.7
K13-BL1-20	336	55120	0.5	9.8198	0.4	3.8998	8.3	0.2777	8.3	1.00	1580.0	116.6	1613.6	67.4	1657.8	7.6	1657.8	7.6	95.3
K13-BL1-24	367	68163	0.5	9.7462	0.4	3.8657	6.3	0.2732	6.3	1.00	1557.3	86.9	1606.5	50.8	1671.7	8.0	1671.7	8.0	93.2
K13-BL1-4	386	84495	1.5	9.7060	0.7	4.0369	6.3	0.2842	6.3	0.99	1612.4	89.7	1641.7	51.5	1679.4	12.2	1679.4	12.2	96.0
K13-BL1-21	440	49633	0.6	9.6934	2.0	3.9632	10.1	0.2786	9.9	0.98	1584.4	139.2	1626.7	82.2	1681.8	37.4	1681.8	37.4	94.2
K13-BL1-12	559	20551	3.0	9.6856	2.0	3.5340	6.7	0.2483	6.4	0.95	1429.5	81.8	1534.9	53.0	1683.3	37.4	1683.3	37.4	84.9
K13-BL1-14	222	321218	1.8	9.6814	0.4	4.3565	1.0	0.3059	0.9	0.92	1720.5	13.2	1704.1	7.8	1684.1	6.8	1684.1	6.8	102.2
K13-BL1-15	328	434432	1.7	9.6597	0.2	4.3187	1.2	0.3026	1.2	0.98	1704.0	17.3	1696.9	9.7	1688.2	4.2	1688.2	4.2	100.9
K13-BL1-1	234	206504	2.6	9.6460	0.5	4.3401	1.6	0.3036	1.5	0.95	1709.3	22.7	1701.0	13.2	1690.8	9.6	1690.8	9.6	101.1
K13-BL1-13	452	502445	2.5	9.6240	0.3	4.3497	1.0	0.3036	1.0	0.97	1709.2	14.7	1702.8	8.4	1695.0	4.7	1695.0	4.7	100.8
K13-BL1-2	259	225660	6.6	9.5034	0.8	4.3730	2.7	0.3014	2.6	0.96	1698.3	38.3	1707.2	22.1	1718.2	14.1	1718.2	14.1	98.8
K13-BL1-3	344	81602	3.2	9.1703	0.2	4.6461	2.9	0.3090	2.9	1.00	1735.8	43.9	1757.6	24.2	1783.6	3.3	1783.6	3.3	97.3
K13-BL1-7	464	26568	3.6	9.0945	1.0	3.8436	8.4	0.2535	8.3	0.99	1456.6	108.8	1601.9	67.8	1798.7	18.1	1798.7	18.1	81.0
K13-BL1-17	263	477457	2.5	9.0732	0.3	4.8327	3.7	0.3180	3.7	1.00	1780.0	57.9	1790.6	31.4	1802.9	5.3	1802.9	5.3	98.7
K13-BL1-6	548	249518	6.2	8.8219	0.6	4.6183	1.7	0.2955	1.6	0.93	1668.9	22.9	1752.6	13.9	1853.9	10.9	1853.9	10.9	90.0
K13-BL1-18	426	27316	9.0	8.3621	2.7	5.3358	4.7	0.3236	3.8	0.82	1807.3	60.4	1874.6	40.0	1950.0	47.8	1950.0	47.8	92.7

Notes:

Analyses with >10% uncertainty (1-sigma) in 206Pb/238U age are not included.

Analyses with >10% uncertainty (1-sigma) in 206Pb/207Pb age are not included, unless 206Pb/238U age is <500 Ma.

Best age is determined from 206Pb/238U age for analyses with 206Pb/238U age < 900 Ma and from 206Pb/207Pb age for analyses with 206Pb/238Uage > 900 Ma.

Concordance is based on 206Pb/238U age / 206Pb/207Pb age. Value is not reported for 206Pb/238U ages <500 Ma because of large uncertainty in 206Pb/207Pb age.

Analyses with 206Pb/238U age > 500 Ma and with >20% discordance (<80% concordance) are not included.

Analyses with 206Pb/238U age > 500 Ma and with >5% reverse discordance (<105% concordance) are not included.

All uncertainties are reported at the 1-sigma level, and include only measurement errors.

Systematic errors are shown as 206Pb/238U uncertainty, 206Pb/207Pb uncertainty to the right of each sample (at 2-sigma level).

U concentration and U/Th are calibrated relative to Sri Lanka zircon and are accurate to ~20%.

Common Pb correction is from 204Pb, with composition interpreted from Stacey and Kramers (1975).

Uncertainties of 1.5 for 206Pb/ 204Pb, 0.3 for 207Pb/ 204Pb, and 2.0 for 208Pb/ 204Pb are applied to common Pb composition.

U/Pb and 206Pb/207Pb fractionation is calibrated relative to fragments of a large Sri Lanka zircon of 563.5 ± 3.2 Ma (2-sigma).

U decay constants and composition as follows: 238U = 9.8485 x 10-10, 235U = 1.55125 x 10-10, 238U/235U = 137.82

Analytical methods as described by Gehrels and Pecha (2014).

Table A2-4. Lu-Hf isotope data from plutonic zircon ALC													
Sample	(^{176}Yb+^{176}Lu) / ^{176}Hf (%)	Volts Hf	^{176}Hf/^{177}Hf	± (1s)	^{176}Lu/^{177}Hf	^{176}Hf/^{177}Hf $_{(t)}$	E-Hf (0)	± (1s)	E-Hf (t)	Age (Ma) grain	Age (Ma) pluton	^{176}Hf/^{177}Hf $_{(t)}$ pluton	E-Hf (t) pluton
K14-WB-9	25.1	2.5	0.281505	0.000035	0.001417	0.281458	-45.3	1.2	-7.6	1743	1791	0.281457	-6.6
K14-WB-12	26.2	2.1	0.281655	0.000036	0.001403	0.281608	-40.0	1.3	-2.0	1756	1791	0.281607	-1.3
K14-WB-20	24.3	2.2	0.281608	0.000042	0.001349	0.281563	-41.6	1.5	-3.6	1759	1791	0.281563	-2.8
K14-WB-21	15.0	2.3	0.281588	0.000032	0.000847	0.281559	-42.3	1.1	-3.2	1780	1791	0.281559	-3.0
K14-WB-29	18.6	2.4	0.281514	0.000043	0.001083	0.281477	-45.0	1.5	-6.1	1781	1791	0.281477	-5.9
K14-WB-5	10.3	2.3	0.281545	0.000047	0.000606	0.281524	-43.9	1.7	-4.3	1788	1791	0.281524	-4.2
K14-WB-16	10.8	2.4	0.281568	0.000031	0.000627	0.281547	-43.0	1.1	-3.4	1792	1791	0.281547	-3.4
K14-WB-4C	16.5	2.3	0.281542	0.000040	0.000941	0.281510	-43.9	1.4	-4.6	1793	1791	0.281510	-4.7
K14-WB-6	10.9	2.5	0.281620	0.000039	0.000633	0.281598	-41.2	1.4	-1.5	1794	1791	0.281598	-1.6
K14-WB-11	16.2	2.3	0.281523	0.000037	0.000927	0.281492	-44.6	1.3	-5.2	1797	1791	0.281492	-5.3
K14-WB-8	23.7	2.2	0.281492	0.000034	0.001356	0.281445	-45.7	1.2	-6.8	1802	1791	0.281445	-7.0
K14-WB-7	10.9	2.0	0.281568	0.000044	0.000627	0.281546	-43.0	1.6	-3.2	1802	1791	0.281546	-3.4
K14-WB-15	15.0	2.8	0.281505	0.000028	0.000815	0.281475	-45.2	1.0	-2.1	1960			
13H-060-20R	49.8	2.9	0.281611	0.000032	0.002865	0.281516	-41.5	1.1	-5.4	1750	1784	0.281514	-4.7
13H-060-1R	58.4	4.2	0.281759	0.000026	0.003720	0.281634	-36.3	0.9	-0.8	1768	1784	0.281633	-0.5
13H-060-49	14.6	2.5	0.281598	0.000027	0.000874	0.281568	-42.0	0.9	-2.9	1779	1784	0.281568	-2.8
13H-060-51R	21.9	2.8	0.281634	0.000042	0.001416	0.281586	-40.7	1.5	-2.3	1779	1784	0.281586	-2.2
13H-060-6	16.9	2.5	0.281595	0.000029	0.000988	0.281562	-42.1	1.0	-3.1	1781	1784	0.281561	-3.0
13H-060-47R	11.9	2.7	0.281574	0.000034	0.000754	0.281548	-42.8	1.2	-3.5	1782	1784	0.281548	-3.5
13H-060-23R	32.9	2.8	0.281729	0.000040	0.001952	0.281663	-37.4	1.4	0.5	1783	1784	0.281662	0.5
13H-060-5	18.8	2.8	0.281587	0.000035	0.001102	0.281550	-42.4	1.3	-3.5	1784	1784	0.281550	-3.5
13H-060-4	21.8	3.1	0.281706	0.000034	0.001304	0.281662	-38.2	1.2	0.5	1784	1784	0.281662	0.5
13H-060-45	15.6	3.1	0.281478	0.000044	0.001042	0.281443	-46.2	1.5	-7.3	1784	1784	0.281443	-7.3
13H-060-8	24.7	2.8	0.281699	0.000032	0.001408	0.281651	-38.4	1.1	0.2	1784	1784	0.281651	0.1
13H-060-26R	28.7	3.1	0.281624	0.000032	0.001659	0.281568	-41.0	1.1	-2.8	1785	1784	0.281568	-2.8
13H-060-32	41.0	3.3	0.281668	0.000027	0.002443	0.281586	-39.5	0.9	-2.2	1785	1784	0.281586	-2.2
13H-060-35	27.2	2.8	0.281665	0.000030	0.001577	0.281612	-39.6	1.1	-1.2	1785	1784	0.281612	-1.2
13H-060-38	23.8	2.9	0.281587	0.000031	0.001387	0.281539	-42.4	1.1	-3.8	1785	1784	0.281540	-3.8
13H-060-10	15.8	2.9	0.281647	0.000031	0.000933	0.281616	-40.2	1.1	-1.1	1787	1784	0.281616	-1.1
13H-060-24	22.5	2.8	0.281679	0.000037	0.001318	0.281634	-39.1	1.3	-0.4	1787	1784	0.281634	-0.5
13H-060-17R	40.1	3.1	0.281714	0.000037	0.002333	0.281625	-37.9	1.3	-0.4	1787	1784	0.281635	-0.4
13H-060-2	26.3	3.0	0.281673	0.000021	0.001554	0.281620	-39.3	0.7	-0.8	1788	1784	0.281620	-0.9
13H-060-7	32.3	2.7	0.281583	0.000033	0.001891	0.281519	-42.5	1.2	-4.4	1792	1784	0.281519	-4.5
13H-060-1C	18.5	2.7	0.281660	0.000031	0.001147	0.281620	-39.8	1.1	0.2	1834			
13H-060-46	27.8	2.9	0.281520	0.000038	0.001705	0.281460	-44.7	1.3	-5.4	1838			
13H-060-16	27.8	3.0	0.281705	0.000035	0.001701	0.281645	-38.2	1.2	1.4	1847			
13H-060-30	14.5	2.8	0.281566	0.000036	0.000856	0.281536	-43.1	1.3	-2.4	1851			

13H-060-26C	23.7	2.2	0.281588	0.000034	0.001323	0.281541	-42.3	1.2	-1.9	1865			
13H-060-20C	19.8	2.5	0.281462	0.000033	0.001171	0.281420	-46.8	1.2	-5.2	1907			
13H-060-23C	13.7	2.6	0.281527	0.000040	0.000810	0.281498	-44.5	1.4	-2.3	1916			
13H-060-51C	24.4	2.3	0.281646	0.000037	0.001509	0.281590	-40.3	1.3	2.0	1959			
13H-060-17C	26.6	2.1	0.281540	0.000042	0.001436	0.281491	-44.0	1.5	-0.9	1996			
13H-060-47C	8.3	3.2	0.281422	0.000035	0.000491	0.281402	-48.2	1.2	-1.3	2105			
13H-080-3	15.1	2.6	0.281648	0.000034	0.000902	0.281618	-40.2	1.2	-1.4	1768	1783	0.281618	-1.1
13H-080-11	19.2	2.7	0.281664	0.000036	0.001145	0.281625	-39.6	1.3	-1.0	1776	1783	0.281625	-0.8
13H-080-8	30.7	3.1	0.281699	0.000023	0.001830	0.281637	-38.4	0.8	-0.5	1779	1783	0.281637	-0.4
13H-080-34	20.2	2.8	0.281652	0.000035	0.001200	0.281612	-40.1	1.2	-1.3	1783	1783	0.281612	-1.3
13H-080-40	17.8	2.9	0.281610	0.000029	0.001163	0.281571	-41.5	1.0	-2.7	1784	1783	0.281571	-2.7
13H-080-18	28.3	2.8	0.281627	0.000033	0.001701	0.281569	-41.0	1.2	-2.8	1784	1783	0.281569	-2.8
13H-080-55R	27.5	3.1	0.281736	0.000033	0.001770	0.281676	-37.1	1.2	1.0	1784	1783	0.281676	1.0
13H-080-50	17.0	2.7	0.281713	0.000024	0.001023	0.281679	-37.9	0.9	1.2	1787	1783	0.281679	1.1
13H-080-16	19.5	2.7	0.281707	0.000033	0.001150	0.281668	-38.1	1.2	0.9	1788	1783	0.281668	0.7
13H-080-20	18.8	2.8	0.281639	0.000032	0.001126	0.281601	-40.5	1.1	-1.5	1789	1783	0.281601	-1.7
13H-080-27	20.0	2.9	0.281614	0.000031	0.001205	0.281573	-41.4	1.1	-2.5	1789	1783	0.281573	-2.7
13H-080-4	16.7	2.5	0.281648	0.000038	0.001013	0.281613	-40.2	1.4	-1.0	1791	1783	0.281614	-1.2
13H-080-19	18.6	2.8	0.281648	0.000026	0.001118	0.281610	-40.2	0.9	-1.1	1792	1783	0.281610	-1.3
13H-080-26	23.5	2.9	0.281691	0.000031	0.001396	0.281643	-38.7	1.1	0.1	1794	1783	0.281644	-0.1
13H-080-54	22.3	2.9	0.281607	0.000027	0.001356	0.281560	-41.7	0.9	-2.8	1798	1783	0.281561	-3.1
13H-080-56R	18.4	2.9	0.281718	0.000027	0.001114	0.281680	-37.7	0.9	1.5	1799	1783	0.281681	1.2
13H-080-43R	17.3	2.6	0.281531	0.000028	0.001105	0.281492	-44.4	1.0	-4.4	1830			
13H-080-55C	8.9	2.7	0.281736	0.000026	0.000527	0.281717	-37.1	0.9	4.9	1887			
13H-080-56C	14.7	3.0	0.281459	0.000023	0.000954	0.281424	-46.9	0.8	-5.0	1910			
13H-080-43C	21.1	2.2	0.281529	0.000041	0.001373	0.281476	-44.4	1.4	-0.6	2020			
K13-NOP-3-24	24.9	2.4	0.281698	0.000058	0.001408	0.281652	-38.4	2.0	-0.7	1745	1781	0.281651	0.1
K13-NOP-3-15	32.9	2.3	0.281654	0.000039	0.002093	0.281584	-40.0	1.4	-2.7	1764	1781	0.281583	-2.3
K13-NOP-3-23	37.8	2.3	0.281689	0.000044	0.002062	0.281620	-38.8	1.6	-1.7	1753	1781	0.281619	-1.1
K13-NOP-3-1	36.3	2.4	0.281660	0.000034	0.002159	0.281587	-39.8	1.2	-2.3	1776	1781	0.281587	-2.2
K13-NOP-3-17	17.7	2.6	0.281604	0.000034	0.000983	0.281571	-41.7	1.2	-2.9	1774	1781	0.281571	-2.8
K13-NOP-3-2	22.6	2.4	0.281605	0.000037	0.001400	0.281558	-41.7	1.3	-3.2	1785	1781	0.281558	-3.2
K13-NOP-3-7	13.6	2.8	0.281650	0.000042	0.000800	0.281623	-40.1	1.5	-1.0	1779	1781	0.281623	-0.9
K13-NOP-3-4	6.3	2.9	0.281622	0.000029	0.000293	0.281612	-41.1	1.0	-1.2	1787	1781	0.281612	-1.3
K13-NOP-3-6	17.2	2.5	0.281679	0.000030	0.001064	0.281643	-39.1	1.1	-0.1	1786	1781	0.281643	-0.2
K14-HH-2-27	16.2	2.5	0.281825	0.000036	0.000971	0.281793	-33.9	1.3	4.4	1749	1773	0.281792	4.9
K14-HH-2-10	13.8	2.7	0.281688	0.000025	0.000898	0.281658	-38.8	0.9	-0.2	1756	1773	0.281658	0.1
K14-HH-2-3	28.5	2.6	0.281642	0.000032	0.001670	0.281586	-40.4	1.1	-2.3	1779	1773	0.281586	-2.4
K14-HH-2-19	15.5	2.5	0.281751	0.000033	0.000933	0.281720	-36.6	1.2	2.5	1782	1773	0.281720	2.3
K14-HH-2-37	13.7	2.6	0.281604	0.000029	0.000825	0.281576	-41.8	1.0	-2.5	1784	1773	0.281576	-2.8

K14-HH-2-22	12.2	2.5	0.281723	0.000036	0.000740	0.281698	-37.5	1.3	1.8	1784	1773	0.281698	1.6
K14-HH-2-26	14.1	2.4	0.281760	0.000037	0.000824	0.281732	-36.2	1.3	3.1	1787	1773	0.281733	2.8
K14-HH-2-34	13.9	2.8	0.281710	0.000029	0.000896	0.281680	-38.0	1.0	1.3	1789	1773	0.281680	0.9
K14-HH-2-21	23.6	2.7	0.281580	0.000031	0.001405	0.281533	-42.6	1.1	-3.9	1792	1773	0.281533	-4.3
K14-HH-2-13	15.3	2.3	0.281727	0.000038	0.000908	0.281696	-37.4	1.3	2.0	1793	1773	0.281697	1.5
K14-HH-2-32	30.0	2.1	0.281696	0.000035	0.001660	0.281639	-38.5	1.2	0.0	1798	1773	0.281640	-0.5
K14-HH-2-29	15.7	2.6	0.281691	0.000031	0.000924	0.281660	-38.7	1.1	0.8	1801	1773	0.281660	0.2
K14-HH-2-17	10.2	2.7	0.281669	0.000023	0.000608	0.281648	-39.4	0.8	0.8	1819			
K14-HH-2-40C	8.8	2.5	0.280885	0.000036	0.000518	0.280862	-67.2	1.3	-16.1	2292			
K14-BLFG-1-8	7.2	2.4	0.281727	0.000032	0.000417	0.281713	-37.4	1.1	0.5	1704	1716	0.281713	0.8
K14-BLFG-1-23	13.0	4.1	0.281767	0.000024	0.000731	0.281743	-36.0	0.9	1.7	1707	1716	0.281743	1.9
K14-BLFG-1-36	10.5	4.0	0.281741	0.000023	0.000604	0.281722	-36.9	0.8	0.9	1709	1716	0.281722	1.1
K14-BLFG-1-19R	11.6	3.8	0.281780	0.000023	0.000643	0.281759	-35.6	0.8	2.3	1710	1716	0.281759	2.4
K14-BLFG-1-16	12.0	3.9	0.281788	0.000028	0.000662	0.281767	-35.2	1.0	2.6	1712	1716	0.281767	2.7
K14-BLFG-1-6	6.6	2.4	0.281765	0.000033	0.000399	0.281752	-36.1	1.2	2.1	1713	1716	0.281752	2.2
K14-BLFG-1-31	10.1	2.2	0.281837	0.000039	0.000569	0.281819	-33.5	1.4	4.5	1714	1716	0.281819	4.5
K14-BLFG-1-37	8.9	2.2	0.281735	0.000044	0.000510	0.281719	-37.1	1.6	0.9	1715	1716	0.281719	1.0
K14-BLFG-1-17	17.8	3.6	0.281801	0.000022	0.000928	0.281771	-34.8	0.8	2.8	1716	1716	0.281771	2.8
K14-BLFG-1-12	16.7	4.3	0.281728	0.000023	0.000960	0.281696	-37.4	0.8	0.2	1718	1716	0.281696	0.2
K14-BLFG-1-33	9.0	3.8	0.281773	0.000028	0.000487	0.281757	-35.8	1.0	2.4	1719	1716	0.281757	2.3
K14-BLFG-1-25	18.8	3.6	0.281779	0.000023	0.000988	0.281746	-35.6	0.8	2.0	1720	1716	0.281746	2.0
K13-BL1-24	11.7	3.0	0.281639	0.000044	0.000805	0.281614	-40.5	1.5	-3.8	1672	1691	0.281614	-3.3
K13-BL1-4	19.7	3.4	0.281722	0.000042	0.001243	0.281683	-37.6	1.5	-1.1	1679	1691	0.281682	-0.9
K13-BL1-21	9.3	3.1	0.281735	0.000035	0.000617	0.281715	-37.1	1.2	0.1	1682	1691	0.281715	0.3
K13-BL1-14	8.7	3.5	0.281673	0.000034	0.000488	0.281658	-39.3	1.2	-1.9	1684	1691	0.281658	-1.8
K13-BL1-15	10.3	3.8	0.281682	0.000034	0.000692	0.281660	-39.0	1.2	-1.7	1688	1691	0.281660	-1.7
K13-BL1-1	12.3	3.7	0.281644	0.000031	0.000784	0.281619	-40.4	1.1	-3.2	1691	1691	0.281619	-3.1
K13-BL1-13	11.5	4.1	0.281652	0.000031	0.000713	0.281629	-40.1	1.1	-2.7	1695	1691	0.281629	-2.8
Notes:													
The subscript "pluton" refers to the crystalization age interpreted from U-Pb geochronologic results. Time-integrated Hf-isotope ratios in columns with the subscript "pluton" have been recalculated based on the age assigned to the sample. Analyses from inherited zircon components have not been recalculated.													
Hf fractionation is corrected by comparing measured 179Hf/177Hf against known 179/177 (line by line). Beta Hf is applied as a power law.													
Yb fractionation is corrected by comparing measured 173Yb/171Yb against known 173/171 (line by line) if 171Yb intensity is more than ~1 mv. Beta Yb is applied as a power law.													
	If 171Yb intensity is less than can be measured reliably, Beta Hf is used to correct for Yb fractionation.												
	The actual cutoff used is determined from the analysis of standards during the same session as unknowns (see below).												
Data are filtered by intensity of Hf (removed if below cutoff value determined by monitoring the average offset of the standards from their known values, which is set at the minimum offset)													
Data are filtered by removing 1 max and 1 min value (out of 60).													
Data are aflso filtered by 95% filter (rejected if outside of 2-sigma std dev of full set)													
Uncertainties are standard error of the mean, expressed at 1-sigma													

	Hf, Yb, Lu Sol "cocktails" behaved strangely during April 2013 session - same solutions run during different times in the session displayed variable interferrences. They also fractionated slightly different than the matrix matched in-run standards. Therefore, the Hf and Yb biases were determined by only looking at the in-run matrix matched standard analyses which was appropriate due to the large number of standards run during this session.

Table A2-5. U-Pb zircon geochronologic data from GEMOC Key Centre.

				Corrected Isotopic Ratios										Corrected Ages (Ma)								
Analysis	**Th**	**U**	**U/Th**	**^{207}Pb/**	**1 σ**	**^{207}Pb/**	**1 σ**	**^{206}Pb/**	**1 σ**	**^{208}Pb/**	**1 σ**	**^{238}U/**	**1 σ**	**^{207}Pb/**	**1 σ**	**^{207}Pb/**	**1 σ**	**^{206}Pb/**	**1 σ**	**^{208}Pb/**	**1 σ**	**% Conc**
	ppm	**ppm**		**^{206}Pb**		**^{235}U**		**^{238}U**		**^{232}Th**		**^{232}Th**		**^{206}Pb**		**^{235}U**		**^{238}U**		**^{232}Th**		
K06-DV-30-15	75.11	233.43	3.11	0.10192	0.00146	3.60699	0.04021	0.25666	0.0023	0.0748	0.0007	4.16	0.26	1659	27	1551	9	1473	12	1458	13	88.8
K06-DV-30-06	534.22	701.18	1.31	0.10267	0.0012	4.26307	0.04694	0.30115	0.0029	0.08734	0.0018	1.26	0.08	1673	22	1686	9	1697	14	1692	34	101.4
K06-DV-30-11	130.10	191.30	1.47	0.10268	0.0013	3.60243	0.0426	0.25447	0.0025	0.0759	0.0019	1.41	0.09	1673	24	1550	9	1461	13	1479	36	87.3
K06-DV-30-22	129.47	144.47	1.12	0.10319	0.00114	4.28803	0.04247	0.30141	0.0027	0.08682	0.0016	1.49	0.09	1682	21	1691	8	1698	13	1683	29	101.0
K06-DV-30-03	111.16	254.93	2.29	0.10332	0.00118	3.71415	0.03986	0.26073	0.0025	0.07812	0.0015	2.19	0.14	1685	22	1574	9	1494	13	1520	28	88.7
K06-DV-30-14	441.67	237.48	0.54	0.10333	0.00111	3.59054	0.03403	0.25204	0.0022	0.0735	0.0011	0.72	0.04	1685	20	1547	8	1449	12	1434	20	86.0
K06-DV-30-04	245.22	347.62	1.42	0.10339	0.00116	3.89686	0.04118	0.27337	0.0026	0.08211	0.0016	1.36	0.08	1686	21	1613	9	1558	13	1595	30	92.4
K06-DV-30-08	191.75	281.62	1.47	0.10347	0.00122	4.02803	0.04464	0.28236	0.0027	0.0819	0.0019	1.4	0.09	1687	22	1640	9	1603	14	1591	35	95.0
K06-DV-30-17	58.66	483.50	8.24	0.1035	0.00139	3.0989	0.03133	0.21715	0.0019	0.06319	0.0006	11.03	0.69	1688	25	1432	8	1267	10	1238	11	75.1
K06-DV-30-34	301.79	647.54	2.15	0.10349	0.00121	3.94893	0.04025	0.27677	0.0024	0.0844	0.002	2.96	0.18	1688	22	1624	8	1575	12	1638	37	93.3
K06-DV-30-36	353.89	237.29	0.67	0.10351	0.0013	4.05175	0.04565	0.2839	0.0026	0.07883	0.0021	0.92	0.06	1688	24	1645	9	1611	13	1534	40	95.4
K06-DV-30-05	246.31	300.77	1.22	0.10357	0.00118	4.18942	0.04468	0.2934	0.0028	0.08651	0.0017	1.17	0.07	1689	22	1672	9	1658	14	1677	32	98.2
K06-DV-30-07	149.27	210.14	1.41	0.10355	0.00123	3.9634	0.04432	0.27762	0.0027	0.08027	0.0018	1.35	0.08	1689	22	1627	9	1579	14	1561	33	93.5
K06-DV-30-16	192.82	189.21	0.98	0.10366	0.00114	3.56617	0.03496	0.24953	0.0022	0.07195	0.0012	1.31	0.08	1691	21	1542	8	1436	12	1404	22	84.9
K06-DV-30-09	11.74	277.09	23.60	0.10373	0.00128	4.25796	0.04937	0.29772	0.0029	0.11076	0.0033	22.57	1.41	1692	23	1685	10	1680	14	2123	59	99.3
K06-DV-30-33	797.48	815.74	1.02	0.10382	0.00124	4.10415	0.04267	0.28674	0.0025	0.07937	0.002	1.41	0.09	1694	23	1655	8	1625	12	1544	38	95.9
K06-DV-30-05C	351.42	316.33	0.90	0.10403	0.00114	3.27733	0.03195	0.22849	0.0021	0.06584	0.001	1.2	0.08	1697	21	1476	8	1327	11	1289	18	78.2
K06-DV-30-28	244.36	194.11	0.79	0.10401	0.00117	3.68115	0.03734	0.25671	0.0023	0.07143	0.0014	1.06	0.07	1697	21	1567	8	1473	12	1395	27	86.8
K06-DV-30-02	992.17	759.26	0.77	0.10413	0.00119	4.1846	0.04498	0.29149	0.0028	0.0833	0.0015	0.73	0.05	1699	22	1671	9	1649	14	1617	28	97.1
K06-DV-30-38	517.49	429.46	0.83	0.10465	0.00137	4.28707	0.05407	0.29718	0.0031	0.08415	0.0026	1.14	0.07	1708	25	1691	10	1677	15	1633	48	98.2
K06-DV-30-23	121.62	128.53	1.06	0.10513	0.00118	3.70539	0.03735	0.25565	0.0023	0.07307	0.0014	1.41	0.09	1717	21	1573	8	1468	12	1425	26	85.5
K06-DV-30-24	86.74	105.16	1.21	0.10526	0.00118	4.16027	0.04182	0.28668	0.0026	0.08031	0.0016	1.62	0.1	1719	21	1666	8	1625	13	1561	29	94.5
K06_DV31A-16	81.20	499.87	6.16	0.10401	0.00115	3.62432	0.03793	0.25272	0.0025	0.06231	0.0017	9.54	0.6	1697	21	1555	8	1452	13	1222	31	85.6
K06_DV31A-03	74.99	138.51	1.85	0.10517	0.00154	4.36587	0.06716	0.30104	0.0038	0.09051	0.0038	3.19	0.2	1717	28	1706	13	1696	19	1751	70	98.8
K06_DV31A-13	139.30	457.36	3.28	0.10537	0.00111	4.40369	0.04447	0.30311	0.003	0.08442	0.0019	5.09	0.32	1721	20	1713	8	1707	15	1638	35	99.2
K06_DV31A-14	79.71	633.11	7.94	0.10548	0.00126	4.13773	0.04904	0.2845	0.003	0.08571	0.0028	12.31	0.77	1723	22	1662	10	1614	15	1662	52	93.7
K06_DV31A-17	74.25	296.41	3.99	0.10591	0.00147	3.99725	0.04952	0.27376	0.0025	0.05928	0.0026	6.19	0.39	1730	26	1634	10	1560	12	1164	49	90.2
K06_DV31A-07	202.40	505.59	2.50	0.10596	0.00152	4.45531	0.06723	0.30493	0.0037	0.09015	0.0042	4.32	0.27	1731	27	1723	13	1716	18	1745	78	99.1
K06_DV31A-01	159.22	298.09	1.87	0.10605	0.00118	4.50635	0.04956	0.30818	0.0032	0.09128	0.0022	3.24	0.2	1733	21	1732	9	1732	16	1766	40	99.9
K06_DV31A-18	35.77	171.77	4.80	0.10609	0.00117	4.51064	0.04761	0.30836	0.003	0.0934	0.0025	7.44	0.47	1733	21	1733	9	1733	15	1805	46	100.0
K06_DV31A-08	47.33	250.63	5.29	0.10621	0.00117	4.43443	0.04522	0.30279	0.0028	0.09215	0.0024	9.16	0.57	1735	21	1719	8	1705	14	1782	45	98.3
K06_DV31A-04	61.82	90.64	1.47	0.10643	0.00137	4.49641	0.05008	0.30643	0.0027	0.09494	0.0031	2.54	0.16	1739	24	1730	9	1723	13	1833	57	99.1
K06_DV31A-06	34.00	96.21	2.83	0.10642	0.00117	4.54069	0.04723	0.30943	0.003	0.09191	0.0022	4.89	0.31	1739	21	1738	9	1738	15	1777	41	99.9

K06_DV31A-02	1068.32	938.24	0.88	0.1065	0.00116	3.56307	0.03931	0.24263	0.0025	0.06953	0.0017	1.52	0.09	1740	20	1541	9	1400	13	1359	31	80.5
K06_DV31A-23	48.06	162.52	3.38	0.10646	0.00161	4.48147	0.06028	0.30544	0.0028	0.09499	0.0039	4.91	0.31	1740	28	1728	11	1718	14	1834	71	98.7
K06_DV31A-10	65.46	280.30	4.28	0.10697	0.00162	4.51892	0.07069	0.30637	0.0037	0.09432	0.0048	7.41	0.46	1748	28	1734	13	1723	18	1822	88	98.6
K06_DV31A-12	99.24	131.37	1.32	0.10696	0.00237	4.28403	0.09614	0.29044	0.0044	0.09313	0.0068	2.05	0.13	1748	42	1690	18	1644	22	1800	126	94.1
K06_DV31A-09	112.01	389.57	3.48	0.10801	0.00142	4.40219	0.06006	0.29557	0.0034	0.08579	0.0034	6.02	0.38	1766	25	1713	11	1669	17	1664	63	94.5
K06_DV31A-21	209.33	342.78	1.64	0.11111	0.00133	4.87239	0.0572	0.31806	0.0033	0.09432	0.0031	2.54	0.16	1818	22	1797	10	1780	16	1822	57	97.9
K06_DV_31C-09	75.82	304.95	4.02	0.10375	0.00156	4.02822	0.04622	0.28161	0.0028	0.08192	0.0009	6.32	0.4	1692	28	1640	9	1599	14	1592	16	94.5
K06_DV_31C-32	93.43	777.38	8.32	0.10405	0.00239	3.42148	0.06507	0.23849	0.0031	0.06936	0.001	10.96	0.68	1698	43	1509	15	1379	16	1355	18	81.2
K06_DV_31C-38	79.70	525.75	6.60	0.10528	0.00161	3.9371	0.04555	0.27123	0.0027	0.07878	0.0008	8.97	0.56	1719	29	1621	9	1547	14	1533	16	90.0
K06_DV_31C-24	124.71	627.93	5.03	0.10569	0.00124	4.04873	0.04885	0.27786	0.003	0.08366	0.0021	6.63	0.41	1726	22	1644	10	1581	15	1624	40	91.6
K06_DV_31C-39	97.17	360.68	3.71	0.10574	0.00126	4.40054	0.05173	0.30185	0.0031	0.09285	0.0026	5.05	0.32	1727	22	1712	10	1700	15	1795	49	98.4
K06_DV_31C-23	63.03	707.85	11.23	0.10582	0.00139	4.4096	0.0617	0.30228	0.0036	0.09463	0.0033	14.79	0.92	1729	25	1714	12	1703	18	1828	61	98.5
K06_DV_31C-30	67.86	569.18	8.39	0.10597	0.00163	4.13861	0.06609	0.28331	0.0035	0.09003	0.004	11.05	0.69	1731	29	1662	13	1608	18	1742	74	92.9
K06_DV_31C-41	78.06	455.26	5.83	0.10599	0.00212	4.12336	0.08527	0.28222	0.004	0.08728	0.0058	7.93	0.5	1732	38	1659	17	1603	20	1691	107	92.6
K06_DV_31C-07	54.53	189.40	3.47	0.10611	0.00313	4.42872	0.1293	0.3028	0.005	0.0872	0.009	5.46	0.34	1734	55	1718	24	1705	25	1690	168	98.3
K06_DV_31C-20	150.70	394.75	2.62	0.10644	0.00185	4.59779	0.0822	0.31333	0.0041	0.09666	0.0051	3.42	0.21	1739	33	1749	15	1757	20	1865	94	101.0
K06_DV_31C-29	54.63	237.37	4.35	0.10691	0.00219	4.54255	0.09527	0.30822	0.0044	0.09346	0.006	5.72	0.36	1747	38	1739	17	1732	22	1806	110	99.1
K06_DV_31C-31	69.73	274.85	3.94	0.10688	0.00212	4.6351	0.09483	0.3146	0.0044	0.1	0.0062	5.19	0.32	1747	37	1756	17	1763	22	1926	114	100.9
K06_DV_31C-16	81.55	307.38	3.77	0.10694	0.0012	4.35613	0.04831	0.29545	0.003	0.08682	0.002	4.92	0.31	1748	21	1704	9	1669	15	1683	36	95.5
K06_DV_31C-37	38.90	340.45	8.75	0.10694	0.002	4.38248	0.0851	0.29726	0.0041	0.09039	0.0054	11.9	0.74	1748	35	1709	16	1678	21	1749	100	96.0
K06_DV_31C-43	68.31	228.81	3.35	0.10728	0.00238	4.52345	0.08931	0.30582	0.0031	0.08866	0.001	4.55	0.28	1754	41	1735	16	1720	15	1717	18	98.1
K06_DV_31C-21	58.79	471.88	8.03	0.10754	0.00155	4.48345	0.06694	0.30241	0.0036	0.09161	0.0037	10.48	0.66	1758	27	1728	12	1703	18	1772	69	96.9
K06_DV_31C-17	77.92	408.77	5.25	0.10789	0.00157	4.67336	0.07049	0.31418	0.0038	0.09632	0.0039	6.85	0.43	1764	27	1762	13	1761	19	1859	72	99.8
K06_DV_31C-15	168.99	349.86	2.07	0.10794	0.00239	4.49013	0.08467	0.3017	0.0035	0.08741	0.0011	2.7	0.17	1765	41	1729	16	1700	17	1694	19	96.3
K06_DV_31C-02	216.83	339.34	1.57	0.10798	0.00147	4.56863	0.05535	0.30687	0.0027	0.09118	0.0036	2.46	0.15	1766	25	1744	10	1725	14	1764	66	97.7
K06_DV_31C-04	217.21	562.60	2.59	0.10822	0.0025	3.39313	0.0788	0.22752	0.0033	0.06738	0.0052	4.07	0.25	1770	43	1503	18	1321	17	1318	98	74.6
K06_DV_31C-13	94.88	210.58	2.22	0.10823	0.00117	4.47062	0.04267	0.29962	0.0027	0.08797	0.0017	2.9	0.18	1770	20	1726	8	1689	13	1704	31	95.4
K06_DV_31C-26	138.04	382.71	2.77	0.10847	0.00122	4.74711	0.05214	0.31743	0.0032	0.09132	0.002	3.65	0.23	1774	21	1776	9	1777	16	1766	37	100.2
K06_DV_31C-10	123.50	301.75	2.44	0.10914	0.00133	4.6532	0.05011	0.30923	0.0028	0.09157	0.003	3.84	0.24	1785	23	1759	9	1737	14	1771	55	97.3
K06_DV_31C-34	68.58	190.28	2.77	0.11014	0.00143	4.71777	0.0551	0.3107	0.0029	0.10401	0.0033	3.77	0.24	1802	24	1770	10	1744	14	2000	60	96.8
K06_DV_31C-14	67.10	414.68	6.18	0.11066	0.00159	3.78654	0.04389	0.24817	0.0021	0.07172	0.0007	8.07	0.5	1810	27	1590	9	1429	11	1400	13	79.0
K06_DV_31C-12	260.62	400.14	1.54	0.11076	0.00169	4.73354	0.07344	0.30999	0.0037	0.0932	0.0046	2.41	0.15	1812	28	1773	13	1741	18	1801	85	96.1
K06_DV_31C-05	75.57	235.18	3.11	0.11108	0.00188	4.86315	0.08439	0.31761	0.0041	0.09722	0.0052	4.89	0.31	1817	31	1796	15	1778	20	1875	95	97.9
K06_DV_31C-44	167.73	371.34	2.21	0.11247	0.00139	4.94195	0.06072	0.31872	0.0034	0.10134	0.0032	3.01	0.19	1840	23	1809	10	1783	16	1951	58	96.9
K06_DV_31C-35	51.70	265.00	5.13	0.11292	0.0013	4.99656	0.05733	0.32095	0.0034	0.09951	0.0025	6.97	0.44	1847	21	1819	10	1794	16	1917	47	97.1
K06_DV_31C-01	718.33	198.38	0.28	0.11428	0.00126	5.36422	0.05748	0.34047	0.0034	0.09754	0.0022	0.43	0.03	1869	20	1879	9	1889	16	1881	41	101.1
K06_DV_31C-18	211.16	868.34	4.11	0.11455	0.00145	3.81736	0.04925	0.24171	0.0027	0.07107	0.0022	5.37	0.34	1873	23	1596	10	1396	14	1388	42	74.5
K06_DV_31C-03	107.50	256.56	2.39	0.11467	0.00166	5.10698	0.06659	0.32302	0.003	0.09554	0.0042	3.75	0.23	1875	27	1837	11	1804	14	1844	78	96.2
K06_DV_31C-22	153.03	181.87	1.19	0.11501	0.00131	5.39137	0.05693	0.34002	0.0032	0.09791	0.0023	1.55	0.1	1880	21	1883	9	1887	15	1888	42	100.4
K06_DV_31C-28	155.36	454.81	2.93	0.11627	0.00215	4.19223	0.06657	0.2615	0.0025	0.07519	0.0008	3.85	0.24	1900	34	1673	13	1498	13	1465	15	78.8
K06_DV_31C-06	322.18	466.54	1.45	0.12842	0.0021	6.36383	0.10858	0.35946	0.0047	0.10369	0.0054	2.28	0.14	2076	29	2027	15	1980	22	1994	99	95.4
K06_DV_31C-25	134.67	289.38	2.15	0.13028	0.00141	6.7494	0.06739	0.37576	0.0035	0.10983	0.0021	2.83	0.18	2102	19	2079	9	2056	16	2106	39	97.8

K06_DV_31C-19	62.04	105.65	1.70	0.16069	0.00196	10.7526	0.12357	0.48532	0.0048	0.13589	0.0037	2.22	0.14	2463	21	2502	11	2550	21	2575	65	103.5
K06_DV_31C-40	110.40	231.94	2.10	0.17804	0.00215	12.3571	0.14162	0.50345	0.005	0.14574	0.0043	2.86	0.18	2635	21	2632	11	2629	21	2750	76	99.8
K06DV-37-17	1031.85	1291.06	1.25	0.10709	0.00134	4.59497	0.06103	0.31122	0.0036	0.08352	0.0021	1.13	0.07	1750	23	1748	11	1747	18	1621	38	99.8
K06DV-37-32	128.48	996.90	7.76	0.10704	0.00123	4.49372	0.05039	0.30451	0.0031	0.09521	0.0019	6.94	0.43	1750	22	1730	9	1714	15	1838	35	97.9
K06DV-37-10	178.13	987.20	5.54	0.1072	0.0022	4.65564	0.09869	0.315	0.0044	0.09562	0.0051	5.02	0.31	1752	38	1759	18	1765	21	1846	95	100.7
K06DV-37-07	170.48	1550.60	9.10	0.10755	0.0013	4.64393	0.05688	0.31322	0.0033	0.09808	0.0023	8.24	0.52	1758	23	1757	10	1757	16	1891	43	99.9
K06DV-37-02	187.71	375.78	2.00	0.10758	0.00124	4.6416	0.05544	0.31298	0.0034	0.09412	0.0019	1.81	0.11	1759	22	1757	10	1755	17	1818	35	99.8
K06DV-37-39	126.07	343.27	2.72	0.1076	0.00152	4.64977	0.06177	0.31345	0.0032	0.09372	0.0027	2.45	0.15	1759	26	1758	11	1758	16	1811	51	99.9
K06DV-37-05	134.93	492.77	3.65	0.10768	0.00145	4.7445	0.06771	0.31961	0.0038	0.09476	0.0028	3.31	0.21	1761	25	1775	12	1788	19	1830	51	101.5
K06DV-37-55	90.20	298.74	3.31	0.10772	0.0018	4.50031	0.06738	0.30311	0.0027	0.08003	0.0032	3.01	0.19	1761	31	1731	12	1707	13	1556	60	96.9
K06DV-37-37	62.05	307.52	4.96	0.10785	0.00147	4.66494	0.05828	0.31374	0.003	0.10114	0.0029	4.46	0.28	1763	25	1761	10	1759	15	1947	53	99.8
K06DV-37-01	938.24	842.23	0.90	0.10799	0.00116	4.69676	0.04938	0.31548	0.0032	0.09238	0.0015	0.81	0.05	1766	20	1767	9	1768	15	1786	27	100.1
K06DV-37-03	293.28	364.76	1.24	0.10798	0.00127	4.6999	0.0496	0.31568	0.0029	0.0869	0.0018	1.13	0.07	1766	22	1767	9	1769	14	1684	33	100.2
K06DV-37-24R	100.07	644.63	6.44	0.10808	0.0015	4.67603	0.06687	0.31381	0.0036	0.09212	0.0028	5.8	0.36	1767	26	1763	12	1759	18	1781	52	99.5
K06DV-37-43	135.97	444.66	3.27	0.10804	0.00143	4.50622	0.05152	0.30255	0.0026	0.09263	0.0025	2.94	0.18	1767	25	1732	10	1704	13	1791	46	96.4
K06DV-37-36	18.90	146.80	7.77	0.10825	0.00222	4.63555	0.08756	0.31075	0.0034	0.07656	0.0041	6.99	0.44	1770	38	1756	16	1744	17	1491	78	98.5
K06DV-37-42	195.45	1474.39	7.54	0.10828	0.00142	4.72841	0.06484	0.31674	0.0037	0.09533	0.0026	6.79	0.42	1771	25	1772	11	1774	18	1840	49	100.2
K06DV-37-49	260.42	1132.54	4.35	0.10829	0.00118	4.61712	0.04975	0.30926	0.0031	0.09559	0.0016	3.96	0.25	1771	20	1752	9	1737	15	1845	30	98.1
K06DV-37-19	146.93	870.46	5.92	0.10842	0.00176	4.72754	0.0815	0.31628	0.0041	0.09435	0.0038	5.33	0.33	1773	30	1772	14	1772	20	1822	69	99.9
K06DV-37-09	130.49	335.05	2.57	0.10849	0.00126	4.73187	0.05128	0.31636	0.003	0.09429	0.0019	2.33	0.15	1774	22	1773	9	1772	15	1821	36	99.9
K06DV-37-31	170.37	480.73	2.82	0.10848	0.00197	4.61043	0.08617	0.30827	0.0041	0.093	0.0041	2.52	0.16	1774	34	1751	16	1732	20	1797	76	97.6
K06DV-37-45	107.98	316.87	2.93	0.10848	0.00131	4.74612	0.05601	0.31733	0.0033	0.09782	0.0022	2.64	0.17	1774	23	1775	10	1777	16	1886	40	100.2
K06DV-37-52	245.72	446.84	1.82	0.10846	0.00127	4.72017	0.05355	0.31568	0.0032	0.0937	0.0019	1.65	0.1	1774	22	1771	10	1769	16	1810	35	99.7
K06DV-37-51	62.18	438.88	7.06	0.10852	0.00125	4.70056	0.05176	0.31418	0.0031	0.09527	0.0019	6.42	0.4	1775	22	1767	9	1761	15	1839	35	99.2
K06DV-37-53	129.05	298.39	2.31	0.10854	0.00124	4.66723	0.0505	0.31189	0.003	0.09198	0.0017	2.1	0.13	1775	21	1761	9	1750	15	1779	32	98.6
K06DV-37-18	137.85	304.55	2.21	0.1086	0.00172	4.77553	0.07994	0.31898	0.0041	0.09377	0.0034	1.99	0.12	1776	30	1781	14	1785	20	1812	63	100.5
K06DV-37-41	405.19	1527.88	3.77	0.1086	0.00162	4.86545	0.07754	0.32499	0.0041	0.09547	0.0033	3.39	0.21	1776	28	1796	13	1814	20	1843	61	102.1
K06DV-37-54	158.20	287.79	1.82	0.10859	0.00138	4.70035	0.05214	0.31399	0.0027	0.08448	0.0021	1.66	0.1	1776	24	1767	9	1760	13	1639	38	99.1
K06DV-37-06	204.27	507.52	2.48	0.1088	0.00132	4.6848	0.05333	0.31235	0.003	0.09472	0.0022	2.25	0.14	1779	23	1765	10	1752	15	1829	40	98.5
K06DV-37-23	303.55	511.00	1.68	0.10875	0.00147	4.82585	0.06209	0.32189	0.0033	0.09141	0.0026	1.52	0.09	1779	25	1789	11	1799	16	1768	48	101.1
K06DV-37-25R	173.89	1012.15	5.82	0.10881	0.00116	4.72929	0.04843	0.31526	0.0031	0.0922	0.0014	5.21	0.33	1780	20	1772	9	1767	15	1783	26	99.3
K06DV-37-28	128.47	338.47	2.63	0.10881	0.00121	4.76533	0.04892	0.31765	0.003	0.0948	0.0016	2.36	0.15	1780	21	1779	9	1778	15	1831	30	99.9
K06DV-37-48	151.41	301.88	1.99	0.10917	0.00122	4.76402	0.04745	0.31654	0.0028	0.10004	0.0017	1.81	0.11	1786	21	1779	8	1773	14	1927	31	99.3
K06DV-37-50	242.57	267.39	1.10	0.1092	0.00138	4.7171	0.05537	0.31334	0.003	0.09905	0.0023	1	0.06	1786	24	1770	10	1757	15	1909	43	98.4
K06DV-37-47	383.02	595.57	1.55	0.10925	0.00123	4.77183	0.05074	0.31682	0.003	0.09479	0.0018	1.4	0.09	1787	21	1780	9	1774	15	1830	33	99.3
K06DV-37-44	153.20	251.40	1.64	0.1093	0.00133	4.82538	0.0525	0.32022	0.0029	0.08874	0.002	1.48	0.09	1788	23	1789	9	1791	14	1718	37	100.2
K06DV-37-08	131.77	384.11	2.92	0.10938	0.00141	4.82897	0.06409	0.32026	0.0036	0.09569	0.0025	2.64	0.17	1789	24	1790	11	1791	18	1847	46	100.1
K06DV-37-24C	62.48	379.67	6.08	0.10935	0.00172	4.7428	0.07833	0.3146	0.004	0.0918	0.0034	5.47	0.34	1789	29	1775	14	1763	19	1775	63	98.5
K06DV-37-27	179.39	509.89	2.84	0.10967	0.00163	4.89682	0.07776	0.32385	0.0041	0.09569	0.0032	2.54	0.16	1794	28	1802	13	1809	20	1847	58	100.8
K06DV-37-15	181.54	355.50	1.96	0.10993	0.00137	4.67722	0.05332	0.30861	0.0029	0.09573	0.0022	1.76	0.11	1798	23	1763	10	1734	14	1848	41	96.4
K06DV-37-12	145.76	509.35	3.49	0.1108	0.00122	4.94828	0.05557	0.32394	0.0034	0.09502	0.0017	3.15	0.2	1813	20	1811	9	1809	17	1835	30	99.8
K06DV-37-35	141.32	357.12	2.53	0.11105	0.00119	4.82206	0.0488	0.31497	0.003	0.09353	0.0014	2.27	0.14	1817	20	1789	9	1765	15	1807	26	97.1

K06DV-37-33	696.46	728.74	1.05	0.11134	0.00129	4.99107	0.05602	0.32514	0.0033	0.0853	0.0017	0.94	0.06	1821	22	1818	9	1815	16	1655	32	99.7
K06DV-37-26	88.71	519.96	5.86	0.11138	0.00129	4.93505	0.05292	0.32139	0.003	0.09326	0.0018	5.24	0.33	1822	22	1808	9	1797	15	1802	34	98.6
K06DV-37-13	797.98	1402.95	1.76	0.11194	0.00127	4.95884	0.05724	0.32134	0.0034	0.09369	0.0018	1.58	0.1	1831	21	1812	10	1796	17	1810	33	98.1
K06DV-37-25C	74.31	259.83	3.50	0.11225	0.00119	5.06105	0.05101	0.32704	0.0031	0.097	0.0014	3.13	0.2	1836	20	1830	9	1824	15	1871	26	99.3
K06DV-37-30R	279.68	940.97	3.36	0.1132	0.00142	5.18747	0.06816	0.33239	0.0038	0.09894	0.0025	3.01	0.19	1851	23	1851	11	1850	18	1907	45	99.9
K06DV-37-30	186.91	421.04	2.25	0.11428	0.00144	5.35588	0.06935	0.33993	0.0038	0.09895	0.0024	2.02	0.13	1869	23	1878	11	1886	18	1907	44	100.9
K06DV-37-11	58.75	1088.47	18.53	0.11769	0.00127	5.63994	0.0574	0.34758	0.0033	0.10429	0.0017	16.68	1.04	1921	20	1922	9	1923	16	2005	31	100.1
K06DV-37-38	111.81	184.69	1.65	0.12462	0.00143	6.32452	0.07387	0.3681	0.0039	0.10618	0.002	1.49	0.09	2023	21	2022	10	2020	19	2040	36	99.9
K06DV-37-04	137.72	225.88	1.64	0.13501	0.00144	7.41998	0.07393	0.39863	0.0038	0.1164	0.0018	1.49	0.09	2164	19	2163	9	2163	17	2226	32	100.0
K07VIR1-04	137.13	147.00	1.07	0.10635	0.0012	4.52973	0.04888	0.30892	0.003	0.08996	0.0015	0.95	0.06	1738	21	1736	9	1735	15	1741	27	99.9
K07VIR1-06	234.26	495.55	2.12	0.10705	0.00112	4.60695	0.05021	0.31215	0.0033	0.0921	0.0012	1.88	0.12	1750	20	1751	9	1751	16	1781	23	100.0
K07VIR1-08	241.88	413.10	1.71	0.10692	0.0011	4.59386	0.04621	0.31164	0.0031	0.09148	0.0011	1.52	0.1	1748	19	1748	8	1749	15	1769	20	100.1
K07VIR1-10	233.44	1125.13	4.82	0.10447	0.00167	3.67559	0.04541	0.25517	0.0026	0.07418	0.0008	4.29	0.27	1705	30	1566	10	1465	13	1446	15	93.6
K07VIR1-11	569.64	1168.33	2.05	0.10598	0.00113	4.31079	0.04541	0.29503	0.003	0.08543	0.0013	1.83	0.11	1731	20	1695	9	1667	15	1657	23	98.3
K07VIR1-12	68.72	253.51	3.69	0.10643	0.00112	4.51764	0.04734	0.30789	0.0031	0.0925	0.0013	3.29	0.21	1739	20	1734	9	1730	15	1788	23	99.8
K07VIR1-15	388.16	2695.63	6.94	0.10096	0.00109	2.7882	0.02807	0.20031	0.0019	0.04825	0.0008	6.19	0.39	1642	21	1352	8	1177	10	952	14	87.1
K07VIR1-18	944.74	1205.89	1.28	0.10714	0.00117	4.5774	0.05185	0.30987	0.0033	0.09153	0.0015	1.14	0.07	1751	20	1745	9	1740	16	1770	28	99.7
K07VIR1-21	574.43	883.09	1.54	0.10649	0.00115	4.54072	0.04766	0.30927	0.0031	0.08545	0.0012	1.3	0.08	1740	20	1738	9	1737	15	1657	23	99.9
K07VIR1-20	161.40	447.66	2.77	0.10644	0.00115	4.49839	0.04696	0.30653	0.003	0.08795	0.0013	2.35	0.15	1739	20	1731	9	1724	15	1704	23	99.6
K07VIR1-23	431.97	591.49	1.37	0.10705	0.00115	4.62248	0.04478	0.31319	0.0028	0.08864	0.0013	1.16	0.07	1750	20	1753	8	1756	14	1717	23	100.2
K07VIR1-24	136.60	342.74	2.51	0.10756	0.00128	4.43305	0.04491	0.29893	0.0025	0.08439	0.0016	2.13	0.13	1758	22	1719	8	1686	12	1638	30	98.1
K07VIR1-25	632.04	1161.61	1.84	0.10607	0.00145	4.30638	0.0619	0.29447	0.0035	0.08419	0.0023	1.56	0.1	1733	26	1695	12	1664	17	1634	43	98.2
K07VIR1-26	149.37	474.83	3.18	0.10618	0.00119	4.55952	0.04971	0.31145	0.0031	0.0934	0.0016	2.69	0.17	1735	21	1742	9	1748	15	1805	29	100.3
K07VIR1-27	155.98	376.36	2.41	0.10621	0.00121	4.51583	0.04494	0.3084	0.0027	0.07921	0.0014	2.05	0.13	1735	21	1734	8	1733	13	1541	26	99.9
K07VIR1-28	303.98	784.38	2.58	0.1065	0.00118	4.56352	0.04566	0.3108	0.0028	0.09314	0.0016	2.19	0.14	1740	21	1743	8	1745	14	1800	29	100.1
K07VIR1-29	178.46	456.07	2.56	0.10629	0.0012	4.39293	0.04534	0.29978	0.0028	0.09058	0.0016	2.17	0.14	1737	21	1711	9	1690	14	1753	30	98.8
K07VIR1-34	296.18	961.01	3.24	0.10868	0.0017	4.38868	0.0555	0.29287	0.0027	0.0848	0.0008	2.9	0.18	1777	29	1710	10	1656	13	1645	15	96.8
K07VIR1-40	137.98	506.92	3.67	0.10646	0.00118	4.46365	0.04347	0.30411	0.0027	0.09476	0.0016	3.28	0.21	1740	21	1724	8	1712	13	1830	29	99.3
K07VIR1-42	273.06	713.12	2.61	0.1048	0.00166	4.13028	0.05304	0.28584	0.0026	0.08307	0.0008	2.34	0.15	1711	30	1660	10	1621	13	1613	15	97.7
K07VIR1-43	156.13	1351.21	8.65	0.10467	0.00197	3.89355	0.05921	0.26978	0.003	0.07841	0.0009	7.74	0.48	1709	35	1612	12	1540	15	1526	17	95.5
K07VIR1-44	105.61	1061.85	10.05	0.1045	0.00146	3.93133	0.05595	0.27286	0.0031	0.07461	0.0023	8.99	0.56	1706	26	1620	12	1555	16	1454	43	96.0

Table A2-6. Lu-Hf isotopic data from GEMOC Key Centre.

Analysis	**$^{176}Hf/^{177}Hf$**	**1 S.D.**	**$^{176}Lu/^{177}Hf$**	**$^{176}Yb/^{177}Hf$**	**$^{176}Hf/^{177}Hf$ (T)**	**E Hf (T)**	**1s**	**Age (Ma)**	**Age (Ma)**	**176Hf/177Hf (t)**	**E-Hf (t)**
								grain	pluton	pluton	pluton
KO6-DV-30-15	0.281905	0.000006	0.001034	0.046875	0.281872	5.8	0.2	1659	1691	0.281872	5.8
KO6-DV-30-06	0.281897	0.000009	0.001077	0.048307	0.281863	5.5	0.3	1673	1691	0.281862	5.5

KO6-DV-30-22	0.281875	0.000008	0.000881	0.039294	0.281847	4.9	0.3	1682	1691	0.281847	5.0
KO6-DV-30-03	0.281872	0.000013	0.000716	0.032674	0.281849	5.0	0.5	1685	1691	0.281849	5.0
KO6-DV-30-14	0.281880	0.000014	0.000806	0.037719	0.281854	5.2	0.5	1685	1691	0.281854	5.2
KO6-DV-30-04	0.281909	0.000007	0.000880	0.041038	0.281881	6.1	0.2	1686	1691	0.281881	6.2
KO6-DV-30-08	0.281874	0.000005	0.000739	0.033330	0.281850	5.0	0.2	1687	1691	0.281850	5.1
KO6-DV-30-17	0.281899	0.000014	0.001395	0.062679	0.281854	5.2	0.5	1688	1691	0.281854	5.2
KO6-DV-30-34	0.281904	0.000009	0.000991	0.046781	0.281872	5.8	0.3	1688	1691	0.281872	5.9
KO6-DV-30-36	0.281900	0.000009	0.001066	0.050795	0.281866	5.6	0.3	1688	1691	0.281866	5.6
KO6-DV-30-05	0.281958	0.000009	0.001325	0.058658	0.281916	7.4	0.3	1689	1691	0.281916	7.4
KO6-DV-30-07	0.281899	0.000011	0.001329	0.062981	0.281856	5.3	0.4	1689	1691	0.281856	5.3
KO6-DV-30-16	0.281870	0.000010	0.001049	0.048217	0.281836	4.5	0.3	1691	1691	0.281836	4.6
KO6-DV-30-09	0.281872	0.000015	0.000995	0.045642	0.281840	4.7	0.5	1692	1691	0.281840	4.7
KO6-DV-30-33	0.281919	0.000009	0.001045	0.050153	0.281886	6.3	0.3	1694	1691	0.281885	6.3
KO6-DV-30-28	0.281892	0.000008	0.000790	0.035320	0.281867	5.6	0.3	1697	1691	0.281867	5.7
KO6-DV-30-02	0.281906	0.000008	0.001342	0.060757	0.281863	5.5	0.3	1699	1691	0.281863	5.5
KO6-DV-30-38	0.281907	0.000011	0.001292	0.056656	0.281866	5.6	0.4	1708	1691	0.281866	5.6
KO6-DV-30-23	0.281899	0.000010	0.000732	0.032840	0.281876	5.9	0.3	1717	1691	0.281876	6.0
KO6-DV-30-24	0.281889	0.000013	0.000731	0.032452	0.281866	5.6	0.5	1719	1691	0.281866	5.6
K06-DV-31A-03a	0.281863	0.000011	0.000350	0.006607	0.281851	6.1	0.4	1717	1732	0.281851	6.1
K06-DV-31A-13	0.281881	0.000012	0.000345	0.007164	0.281870	6.7	0.4	1721	1732	0.281870	6.7
K06-DV-31A-14	0.281881	0.000009	0.000661	0.014956	0.281859	6.4	0.3	1723	1732	0.281859	6.3
K06-DV-31A-17	0.281747	0.000013	0.000458	0.011997	0.281732	1.8	0.5	1730	1732	0.281732	1.8
K06-DV-31A-07	0.281879	0.000014	0.000568	0.011488	0.281860	6.4	0.5	1731	1732	0.281860	6.4
K06-DV-31A-08	0.281912	0.000011	0.000378	0.007781	0.281900	7.8	0.4	1735	1732	0.281900	7.8
K06-DV-31A-04a	0.281853	0.000013	0.000430	0.010009	0.281839	5.6	0.5	1739	1732	0.281839	5.6
K06-DV-31A-06	0.281755	0.000009	0.000170	0.003656	0.281749	2.5	0.3	1739	1732	0.281749	2.4
K06-DV-31A-01	0.281893	0.000010	0.000269	0.005040	0.281884	7.2	0.3	1740	1732	0.281884	7.2
K06-DV-31A-10	0.281602	0.000012	0.001033	0.027449	0.281568	-4.0	0.4	1748	1732	0.281568	-4.0
K06-DV-31A-12	0.281701	0.000018	0.000388	0.008119	0.281688	0.3	0.6	1748	1732	0.281688	0.3
K06-DV-31A-09	0.281850	0.000011	0.001000	0.027853	0.281817	4.9	0.4	1766	1732	0.281817	4.8
K06-DV-31A-21	0.281678	0.000010	0.000827	0.024232	0.281651	-1.0	0.3	1818			

K06-DV-31C-09	0.281634	0.000016	0.000471	0.014136	0.281618	-2.0	0.6	1692	1748	0.281618	-1.8
K06-DV-31C-24	0.281639	0.000023	0.000223	0.008300	0.281632	-1.9	0.8	1726	1748	0.281632	-1.4
K06-DV-31C-23	0.281702	0.000015	0.000486	0.020157	0.281686	0.1	0.5	1729	1748	0.281686	0.6
K06-DV-31C-07	0.281354	0.000014	0.000445	0.011762	0.281339	-11.9	0.5	1734	1748	0.281339	-11.8
K06-DV-31C-20	0.281717	0.000013	0.000884	0.035692	0.281688	0.4	0.5	1739	1748	0.281688	0.6
K06-DV-31C-29	0.281784	0.000023	0.001606	0.062696	0.281731	2.1	0.8	1747	1748	0.281731	2.1
K06-DV-31C-31	0.281725	0.000009	0.001240	0.043948	0.281684	0.4	0.3	1747	1748	0.281684	0.5
K06-DV-31C-16	0.281345	0.000014	0.000785	0.027147	0.281319	-12.5	0.5	1748	1748	0.281319	-12.5
K06-DV-31C-37	0.281594	0.000015	0.000483	0.017290	0.281578	-3.3	0.5	1748	1748	0.281578	-3.3
K06-DV-31C-21	0.281689	0.000012	0.000220	0.011323	0.281682	0.6	0.4	1758	1748	0.281682	0.4
K06-DV-31C-17	0.281644	0.000011	0.000219	0.009784	0.281637	-0.9	0.4	1764	1748	0.281637	-1.2
K06-DV-31C-15	0.281690	0.000013	0.000347	0.012840	0.281678	0.6	0.5	1765	1748	0.281678	0.3
K06-DV-31C-02	0.281605	0.000011	0.000397	0.012948	0.281592	-2.9	0.4	1766	1748	0.281592	-2.8
K06-DV-31C-13	0.281676	0.000014	0.000741	0.026484	0.281651	-0.2	0.5	1770	1748	0.281651	-0.7
K06-DV-31C-26	0.281698	0.000013	0.001040	0.040235	0.281663	0.3	0.5	1774	1748	0.281664	-0.2
K06-DV-31C-10	0.281706	0.000015	0.000613	0.022633	0.281685	1.3	0.5	1785	1748	0.281686	0.5
K06-DV-31C-34	0.281705	0.000018	0.000770	0.021228	0.281679	1.5	0.6	1802			
K06-DV-31C-14	0.281618	0.000013	0.000910	0.035857	0.281587	-1.6	0.5	1810			
K06-DV-31C-12	0.281855	0.000018	0.000592	0.022225	0.281835	7.2	0.6	1812			
K06-DV-31C-44	0.281573	0.000011	0.000517	0.019394	0.281555	-2.1	0.4	1840			
K06-DV-31C-35	0.281662	0.000018	0.000487	0.016334	0.281645	1.3	0.6	1847			
K06-DV-31C-01	0.281563	0.000011	0.001476	0.040950	0.281511	-3.0	0.4	1869			
K06-DV-31C-03	0.281580	0.000012	0.000687	0.021190	0.281556	-1.2	0.4	1875			
K06-DV-31C-22	0.281516	0.000014	0.000864	0.032746	0.281485	-3.6	0.5	1880			
K06-DV-31C-28	0.281605	0.000014	0.000823	0.024067	0.281575	0.0	0.5	1900			
K06-DV-31C-06	0.281467	0.000014	0.000855	0.026244	0.281433	-1.0	0.5	2076			
K06-DV-31C-25	0.281499	0.000017	0.000544	0.020578	0.281477	1.2	0.6	2102			
K06-DV-31C-40	0.281317	0.000019	0.001011	0.036989	0.281266	5.9	0.7	2635			
K06-DV-37-17	0.281807	0.000017	0.002003	0.075734	0.281741	2.5	0.6	1750	1773	0.281740	3.0
K06-DV-37-32	0.281770	0.000013	0.001495	0.061548	0.281720	1.8	0.5	1750	1773	0.281720	2.3
K06-DV-37-10	0.281700	0.000017	0.001279	0.051076	0.281658	-0.4	0.6	1752	1773	0.281657	0.1
K06-DV-37-07	0.281835	0.000022	0.002345	0.092083	0.281757	3.2	0.8	1758	1773	0.281756	3.6

K06-DV-37-02	0.281715	0.000014	0.000925	0.035160	0.281684	0.7	0.5	1759	1773	0.281684	1.1
K06-DV-37-39	0.281666	0.000018	0.000973	0.039998	0.281634	-1.1	0.6	1759	1773	0.281633	-0.7
K06-DV-37-05	0.281687	0.000019	0.001294	0.049355	0.281644	-0.7	0.7	1761	1773	0.281643	-0.4
K06-DV-37-55	0.281746	0.000014	0.001194	0.046090	0.281706	1.5	0.5	1761	1773	0.281706	1.8
K06-DV-37-01	0.281699	0.000019	0.001384	0.055507	0.281653	-0.3	0.7	1766	1773	0.281652	-0.1
K06-DV-37-03	0.281715	0.000017	0.001535	0.054301	0.281664	0.1	0.6	1766	1773	0.281663	0.3
K06-DV-37-24R	0.281608	0.000012	0.001053	0.038550	0.281573	-3.1	0.4	1767	1773	0.281573	-2.9
K06-DV-37-43	0.281748	0.000015	0.001602	0.058713	0.281694	1.2	0.5	1767	1773	0.281694	1.4
K06-DV-37-42	0.281772	0.000023	0.002175	0.087886	0.281699	1.5	0.8	1771	1773	0.281699	1.6
K06-DV-37-49	0.281738	0.000013	0.001255	0.047078	0.281696	1.4	0.5	1771	1773	0.281696	1.5
K06-DV-37-31	0.281756	0.000024	0.001540	0.061208	0.281704	1.7	0.8	1774	1773	0.281704	1.8
K06-DV-37-45	0.281705	0.000020	0.001682	0.059125	0.281648	-0.2	0.7	1774	1773	0.281648	-0.2
K06-DV-37-52	0.281754	0.000023	0.001269	0.051946	0.281711	2.0	0.8	1774	1773	0.281711	2.0
K06-DV-37-51	0.281700	0.000021	0.001459	0.058272	0.281651	-0.1	0.7	1775	1773	0.281651	-0.1
K06-DV-37-53	0.281693	0.000016	0.001087	0.042481	0.281656	0.1	0.6	1775	1773	0.281656	0.1
K06-DV-37-41	0.281846	0.000028	0.003167	0.116897	0.281739	3.0	1.0	1776	1773	0.281739	3.0
K06-DV-37-54	0.281725	0.000017	0.000981	0.037646	0.281692	1.4	0.6	1776	1773	0.281692	1.3
K06-DV-37-06	0.281753	0.000018	0.002107	0.084255	0.281682	1.1	0.6	1779	1773	0.281682	1.0
K06-DV-37-23	0.281756	0.000019	0.001419	0.056981	0.281708	2.0	0.7	1779	1773	0.281708	1.9
K06-DV-37-25R	0.281785	0.000015	0.002267	0.082557	0.281708	2.0	0.5	1780	1773	0.281709	1.9
K06-DV-37-28	0.281726	0.000015	0.000947	0.036996	0.281694	1.5	0.5	1780	1773	0.281694	1.4
K06-DV-37-48	0.281751	0.000018	0.001340	0.051160	0.281706	2.1	0.6	1786	1773	0.281706	1.8
K06-DV-37-47	0.281719	0.000024	0.000966	0.034132	0.281686	1.4	0.8	1787	1773	0.281686	1.1
K06-DV-37-44	0.281716	0.000014	0.001013	0.038142	0.281682	1.3	0.5	1788	1773	0.281682	1.0
K06-DV-37-08	0.281765	0.000019	0.001481	0.061864	0.281715	2.5	0.7	1789	1773	0.281715	2.2
K06-DV-37-24C	0.281696	0.000012	0.001229	0.045566	0.281654	0.3	0.4	1789	1773	0.281655	0.0
K06-DV-37-27	0.281835	0.000021	0.001700	0.065783	0.281777	4.8	0.7	1794	1773	0.281778	4.4
K06-DV-37-15	0.281702	0.000023	0.001423	0.056507	0.281653	0.5	0.8	1798	1773	0.281654	0.0
K06-DV-37-12	0.281589	0.000023	0.001353	0.054587	0.281542	-3.1	0.8	1813	1773	0.281543	-3.9
K06-DV-37-33	0.281718	0.000021	0.001672	0.061535	0.281660	1.2	0.7	1821	1773	0.281662	0.3
K06-DV-37-26	0.281021	0.000016	0.000788	0.027248	0.280994	-22.4	0.6	1822	1773	0.280994	-23.4
K06-DV-37-13	0.281716	0.000017	0.001278	0.051400	0.281672	1.9	0.6	1831			
K06-DV-37-25C	0.281693	0.000015	0.001971	0.073178	0.281624	0.3	0.5	1836			

K06-DV-37-30	0.281504	0.000016	0.000534	0.021277	0.281485	-3.9	0.6	1869			
K06-DV-37-11	0.281643	0.000015	0.001333	0.049560	0.281594	1.2	0.5	1921			
K06-DV-37-38	0.281695	0.000016	0.001050	0.039040	0.281655	5.7	0.6	2023			
K06-DV-37-04	0.281587	0.000019	0.000894	0.035427	0.281550	5.2	0.7	2164			
K07VIR1-04	0.281831	0.000019	0.000510	0.015528	0.281814	5.1	0.7	1738	1754	0.281814	5.2
K07VIR1-06	0.281879	0.000017	0.000945	0.030605	0.281847	6.3	0.6	1750	1754	0.281847	6.4
K07VIR1-08	0.281849	0.000014	0.000776	0.026184	0.281823	5.4	0.5	1748	1754	0.281823	5.6
K07VIR1-10	0.281881	0.000019	0.001217	0.039857	0.281841	6.0	0.7	1705	1754	0.281840	6.2
K07VIR1-11	0.281916	0.000018	0.000632	0.021568	0.281895	7.9	0.6	1731	1754	0.281895	8.1
K07VIR1-12	0.281818	0.000018	0.000755	0.023780	0.281793	4.3	0.6	1739	1754	0.281793	4.5
K07VIR1-18	0.282055	0.000021	0.002848	0.098813	0.281960	10.3	0.7	1751	1754	0.281960	10.4
K07VIR1-21	0.281946	0.000017	0.002302	0.078903	0.281870	9.6	0.7	1740	1754	0.281869	7.2
K07VIR1-20	0.281979	0.000021	0.001087	0.032950	0.281943	7.0	0.6	1739	1754	0.281942	9.8
K07VIR1-23	0.281921	0.000022	0.001173	0.037687	0.281882	7.5	0.8	1750	1754	0.281882	7.6
K07VIR1-24	0.281965	0.000021	0.001201	0.039970	0.281925	9.0	0.7	1758	1754	0.281925	9.2
K07VIR1-25	0.281868	0.000019	0.001104	0.034419	0.281831	5.7	0.7	1733	1754	0.281831	5.8
K07VIR1-26	0.281851	0.000020	0.000742	0.024375	0.281826	5.5	0.7	1735	1754	0.281826	5.7
K07VIR1-27	0.281883	0.000015	0.000950	0.029581	0.281851	6.4	0.5	1735	1754	0.281851	6.6
NOTE:											
The subscript "pluton" refers to the crystalization age interpreted from U-Pb geochronologic results. Time-integrated Hf-isotope ratios in columns with the subscript "pluton" have been recalculated based on the age assigned to the sample. Analyses from inherited zircon components have not been recalculated.											

CHAPTER 2 U-Pb geochronologic and Lu-Hf isotopic record of Proterozoic igneous and detrital zircon from northern New Mexico: Formation of the Mazatzal crustal province in an extended continental margin arc

Mark E. Holland[1], Tyler A. Grambling[2], Karl E. Karlstrom[1], George Gehrels[3]

[1]Department of Earth and Planetary Sciences, University of New Mexico, Northrop Hall, 221 Yale Boulevard NE, Albuquerque, New Mexico 87131, USA;

[2]University of Tennessee

[3]Arizona LaserChron Center, Department of Geoscience, University of Arizona, Tucson, Arizona 85721, USA

ABSTRACT

Proterozoic lithosphere of southern Laurentia is underlain by accretionary orogens that developed during lithospheric growth from ~1.8-1.0 Ga. Paleoproterozoic crust in the southwestern United States has been divided into two main crustal provinces composed of arc-related plutonic and supracrustal successions. The Yavapai and Mazatzal provinces were successively accreted to the margin of southern Laurentia during the 1.74-1.68 Ga Yavapai and 1.65-1.60 Ga Mazatzal orogenies respectively. Recent discoveries of older crust locally within dominantly juvenile provinces and 1.5-1.45 Ga Mesoproterozoic sedimentary successions require a re-evaluation of the lithospheric structure and tectonic evolution of the Mazatzal province. Here we present 1,914 new U-Pb dates and 282 new Lu-Hf geochronologic analyses from plutonic, volcanic, and detrital zircon from the Proterozoic crust of northern New Mexico. Our results show that plutonic and associated metavolcanics rocks throughout northern New Mexico yield εHf(t) values ranging from +6 to +12 at ~1.65 Ga. These data suggest that

plutonic and volcanic rocks of the Mazatzal province were derived from mixing of a juvenile depleted mantle source with partial melts of crustal components as old as ~2.0 Ga. Detrital zircon grains in 1.70-1.65 Ga ultramature quartzite successions in northern New Mexico share the same age and Hf-isotope composition as the underlying plutonic and metavolcanics substrate upon which they were deposited, indicating first cycle deposition of ultramature quartzites across both the Yavapai and Mazatzal provinces. Minor populations of 2.0-1.7 Ga (23%) and >2.0 Ga detrital zircon grains (1%) with evolved Hf-isotope compositions suggests that these basins developed in a tectonic environment where they received far-traveled older Laurentian detritus. Mesoproterozoic plutonic rocks that intrude the Mazatzal province have Hf-isotope compositions consistent with melting of dominantly juvenile Paleoproterozoic Yavapai and/or Mazatzal province crust driven by heat from and mixing with underplated juvenile 1.4 Ga mafic mantle melts. The combined evidence suggests Mazatzal province was a 1.65 Ga continental margin arc system that formed on top of older (2.0-1.7 Ga) Yavapai province crust. This continental arc system experienced periodic slab rollback that formed intra and backarc basins in which 1.7-1.65 Ga quartzite basins developed. Episodic slab shallowing caused shortening of quartzite successions during the 1.65-1.60 Ga Mazatzal orogeny. Intense deformation of 1.5-1.45 Ga basins of the Trampas Group and variable deformation of 1.46-1.43 Ga plutons indicate that the final geometry of fabrics and major structures in northern New Mexico developed during the 1.45-1.35 Ga Picuris orogeny.

INTRODUCTION

Proterozoic crust of southern Laurentia has been regarded as an example of lithospheric growth through accretionary tectonic processes for over 30 years (Condie,

1982; Karlstrom and Houston, 1984; Karlstrom and Bowring, 1988; Cawood et al., 2009). These and other structural, metamorphic, geochronologic, and isotopic studies have given rise to a broadly accepted model for lithospheric formation involving the accretion of distinct crustal provinces during successive orogenic episodes (Whitmeyer and Karlstrom, 2007). Two major crustal provinces exposed in northern New Mexico, the Yavapai and Maztaztal provinces, are the focus of this paper.

The Yavapai province is characterized by 1.8-1.7 Ga metavolcanic and immature clastic metasedimentary rocks intruded by calk-alkaline granodiorite plutonic bodies. This lithotectonic association varies locally, but has been consistently interpreted as representing the mid-crustal remnants of at least one, and likely multiple arc systems (Condie, 1982; Jessup et al., 2005, 2006; Whitmeyer and Karlstrom, 2007). The Yavapai province is also characterized by juvenile Nd-isotope compositions, with Nd model ages ≤100 Ma of crystallization and/or depositional ages (Bennett and DePaolo, 1987). Hf-isotope analyses of zircon from the Yavapai province yield similar results (Bickford et al., 2008; Holland et al., 2015). Rocks of the Yavapai crustal province were deformed and metamorphosed during the 1.74-1.68 Ga Yavapai orogeny (Ilg et al., 1996), which is interpreted to represent the amalgamation and accretion of Yavapai province arcs onto the margin of southwestern Laurentia.

The Mazatzal crustal province is characterized by 1.7-1.6 Ga metavolcanic and metasedimentary rocks intruded by calc-alkaline granodiorite plutons in a similar lithotectonic assemblage as the Yavapai province. However, clastic metasedimentary rocks of the Mazatzal province are generally more mature than those of the Yavapai province, with several distinctive quartzite successions prevalent throughout the province

(Jones et al., 2009; Doe, 2014). The Mazatzal province is characterized by similarly juvenile Nd and Hf-isotope compositions (Bennett and DePaolo, 1987; Mako et al., 2015). The Mazatzal crustal province has been interpreted to have formed as one or more arc terranes that accreted onto the margin of the Yavapai province during the 1.65-1.60 Mazatzal orogeny (Karlstrom and Bowring, 1988, 1993; Whitmeyer and Karlstrom, 2007). Numerous questions remain about whether arcs were continental or oceanic, timing of deformation(s), and overall tectonic evolution.

Following protracted crustal growth from 1.8-1.6 Ga, a conspicuous lack of tectonism from 1.6-1.5 Ga has been inferred to represent a period of lithospheric stability and erosion of highlands termed the North American tectonic gap (Karlstrom et al., 2004; Doe et al., 2012). Paleoproterozoic crust of southwestern Laurentia was interpreted to have experienced long-term mid crustal residence after Paleoproterozoic accretionary orogenesis (Williams and Karlstrom, 1996) such that the major structural fabrics in northern New Mexico formed between 1.70-1.65 Ga (Karlstrom et al., 1997), followed by variable but locally penetrative reactivation during intracratonic deformation at ~1.45 Ga (Williams et al., 1999). The discovery of previously unrecognized 1.50-1.45 Ga sedimentary successions that are apparently structurally conformable with underlying Paleoproterozoic successions has called long-standing tectonic models into question (Jones et al., 2011; Doe et al., 2012; Daniel et al., 2013; Mako et al., 2015). Geochronologic evidence now indicates that many structural elements thought to have formed during the 1.65-1.60 Mazatzal orogeny may have formed during the 1.49-1.45 Ga Picuris orogeny (Daniel et al., 2013; Mako et al., 2015). However, exposed rocks of the Mazatzal province include belts of 1.65 Ga granodioritic plutons and 1.7-1.6 Ga mixed

volcanic-metasedimentary basins that seem to require a main pulse of crust formation at ~1.65 Ga (Karlstrom et al., 2004). Thus, the tectonic setting of crust formation in the Mazatzal province needs to be reevaluated both in terms of timing of multiple accretion events and timing of multiple deformation events.

Paired application of the U-Pb and Lu-Hf isotope systems in zircon from intrusive and supracrustal rocks from convergent margins provides detailed insight into processes of crust formation (Holland et al., 2018). Specifically, detrital zircon age distributions are indicative of the tectonic environment in which they form (Cawood et al., 2012), and secular variation in Hf-isotope composition of plutonic rocks can be attributed to alternating magma sources due to changes in tectonic setting (Kemp et al., 2009). Combined Hf-isotope analysis of detrital and plutonic zircon therefore provide both a "top-down," and "bottom-up" perspective on crustal formation: detrital grain analysis provides a top-down view of sedimentary basins and their provenance; and the Hf-isotope analyses provide a snapshot of the composition and evolution of melt-source regions for plutons.

In this paper, we present 1,914 new U-Pb ages and 282 new Lu-Hf isotope analyses from plutonic and supracrustal rocks in New Mexico. New U-Pb geochronologic data were obtained from 9 plutonic rocks, and 4 associated metavolcanics rocks, as well as detrital zircon geochronology from 7 metasedimentary rocks. Lu-Hf isotope analyses were conducted on all 9 plutonic rocks, 3 metarhyolites, and 6 out of 7 metasedimentary rocks. Our interpretation is that crust of the Mazatzal Province of New Mexico formed in a continental margin arc system that was built atop the newly accreted Yavapai province. The upper plate of the arc system was periodically extended due to slab rollback (Jones et

al., 2009), accommodating deposition of locally derived quartzite and rhyolite successions in intra and/or rear arc basins. These basins were partially deformed during periodic slab shallowing events in the Paleoproterozoic, but the final geometry of the Proterozoic crust in southwestern Laurentia was achieved during the Picuris orogeny.

GEOLOGIC BACKGROUND

Reviews of the geologic history of Proterozoic rocks in New Mexico are in Karlstrom et al. (2004), Daniel and Pyle, (2006), Amato et al., (2008, 2011), Jones et al. (2011), and Daniel et al. (2013). This paper builds on these studies and also presents a brief summary of the rocks of northern and central New Mexico. Proterozoic rocks in New Mexico are exposed in a series of semi-continuous basement-cored uplifts attributed to the Ancestral Rocky Mountain and Laramide orogenies (Karlstrom et al., 2004). The uplifts sampled in this study are shown in Figure 2-1. These include the Tusas, Picuris, Nacimiento, and Zuni uplifts. In central New Mexico, we sampled in the 100-km-long Sandia-Manzano-Los Pinos mountains.

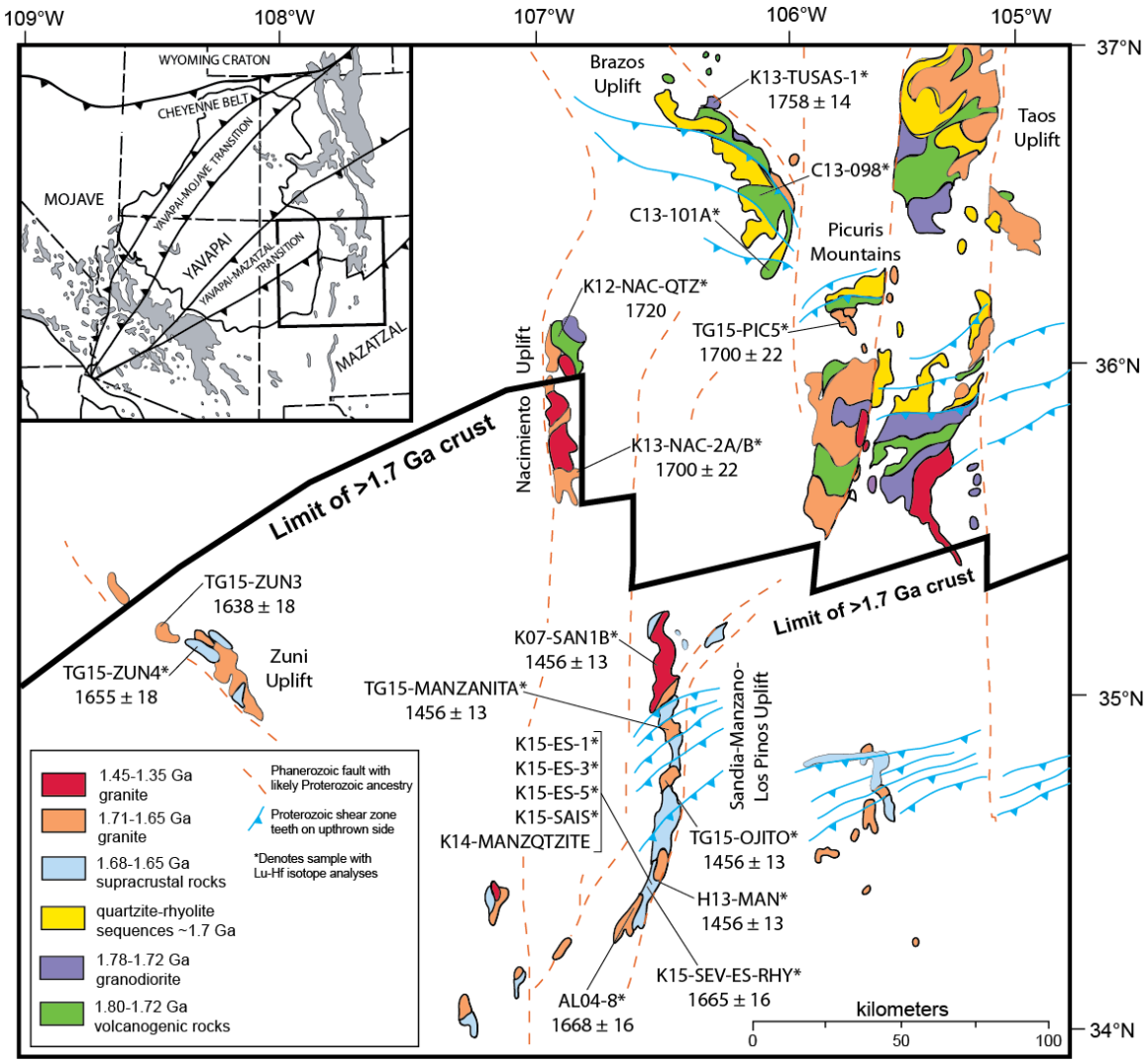

Figure 2-1. Simplified geologic map of northern New Mexico with sample locations and U-Pb geochronologic results for plutonic and metavolcanic samples shown with 2-sigma uncertainty.

Northern New Mexico

The oldest rocks in northern New Mexico are the Moppin, Pecos, and Gold Hill complexes. These rocks consist of complexly interlayered and dominantly mafic metavolcanic rocks, though intermediate schists and immature metasedimentary rocks are also present (Karlstrom et al., 2004). Relict primary structures such as pillow basalts and Bouma sequences are preserved locally, and suggest submarine depositional environments. Geochemical data from these deposits show both thoeleiitic and calc-

alkaline trends, with incompatible element signatures typical of modern arc-related rocks (Condie and McCrink, 1982). A suite of 1.76-1.75 Ga calc-alkaline plutons intrudes the supracrustal package, suggesting that the entire suite of rocks represents a mid-crustal exposure of an arc system.

Overlying the Moppin, Pecos, and Gold-Hill complexes is the Vadito Group, which is composed of a younger package of metavolcanic and metasedimentary rocks. In contrast to older basement complexes, the Vadito Group is dominated by the felsic metavolcanic rocks and metasedimentary rocks ranging from pelitic schists to pebble conglomerates (Bauer and Williams, 1988). Felsic metavolcanic rocks in the Vadito Group range in age from 1.71-1.70 Ga (Bauer and Williams, 1989), and a suite of ~1.69-1.63 Ga plutonic rocks intrudes the Vadito Group and older basement complexes (Karlstrom et al., 2004). Mawer et al. (1990) interpreted the Vadito Group to represent rift-related volcanism and sedimentation along a continental margin. Abundant regional evidence for synchronous and subsequent arc-related sedimentation, volcanism, and plutonism seems to require that any such rifting would have occurred in the broader context of convergent margin tectonism (Jones et al., 2009).

The Vadito Group is overlain by the Hondo Group, a >2.5 km thick section of siliciclastic metasedimentary rocks. Across northern New Mexico, the contact between the Vadito and Hondo groups is variably tectonized, however it has been interpreted as a conformable section in the Tusas Mountains and Rio Mora area (Bauer and Williams, 1989; Mawer et al., 1990). The most prominent formation in the Hondo Group is the 0.8-1.5 km thick Ortega orthoquartzite, which preserves abundant primary depositional features, and was interpreted to represent tide and storm dominated deposition in a stable

continental shelf (Soegarrd and Eriksson, 1986). Overlying the Ortega Formation is the Rinconada Formation, which transitions into interbedded phylitic schists and quartzites interpreted to represent inner-shelf and deltaic deposits (Soegaard and Ericksson, 1986). Similar to the Vadito Group, it is likely that these deposits were not deposited along a passive margin, but rather in syn-tectonic rear-arc basins associated with slab rollback in a subduction zone setting (Jones et al., 2009).

Above the Rinconada Formation is the recently defined Trampas Group (Daniel et al., 2013). At the base of the Trampas Group is the Pilar Formation, a phyllite-schist unit with centimeter to meter scale meta-tuff beds dated at 1488 ± 6 Ma (Daniel et al., 2013). The Pilar Formation has a gradational contact with the overlying Piedra Lumbre Formation, which grades upward into schist and quartzite including local graded beds. Detrital zircon grains from a quartzite layer in the Piedra Lumbre Formation yield abundant exotic 1.6-1.5 Ga ages with no known southern Laurentian source (Daniel et al., 2013). These detrital zircon grains are interpreted to have been derived from Australian sources (Doe et al., 2012, 2013; Daniel et al., 2013).

Finally, the Marquenas Formation is juxtaposed against the underlying Trampas and Vadito Groups by a ductile shear zone and tectonized unconformity respectively (Bauer, 1993; Jones et al., 2011). The Marquenas Formation consist of a basal polymictic boulder-to-cobble conglomerate, with a cross-bedded quartzite layer sandwiched between another quartz pebble conglomerate (Bauer, 1993). Detrital zircon geochronology from the Marquenas Formation yields maximum depositional ages from 1457-1472 Ma (Jones et al., 2011; Daniel et al., 2013).

Central New Mexico

The oldest rocks in the Sandia-Manzano-Los Pinos uplift are bimodal metavolcanic and minor intercalated metasedimentary deposits locally exposed throughout the transect which range in age back to ~1680-1660 Ma (Unruh, unpubl.). Exposures of these "greenstone" rocks occur in and to the south of Tijeras Pass in the Manzanita Mountains (Brown et al., 1999), and likely correlate with a greenstone basement sequence found in several places in the uplift, including the interlayered amphibolite, quartzofeldspathic, and pelitic schists of the Bootleg Canyon sequence in the Los Pinos Mountains (Luther, 2006). The first distinctive marker unit in the Manzano Group is the 1662 ± 2 Ma Sevilleta metarhyolite (Shastri, 1992; Luther, 2006), which consists of a thin lower unit interlayerd with amphibolite, and a ~1 km thick upper metarhyolite layer. Overlying the Sevilleta metarhyolite is the Abajo Formation, which consists of meta-lithic arenite at its base grading upward into cleaner micaceous quartzite and meta-quartz arenite, and finally the White Ridge quartzite (Bauer et al., 1993; Baer, 2004). The White Ridge quartzite is a clean quartzite capped by a distinctive aluminous horizon. Overlying the White Ridge quartzite is the Estadio Schist, a garnet + staurolite + biotite schist which preserves multiple deformational fabrics (Thompson, 1996). The micaceous Sais quartzite overlies the Estadio Schist. Finally, the Blue Springs Formation consists of interbedded quartzites, garnet + chlorite + quartz + muscovite schist, and the 1601 ± 4 Ma Blue Springs rhyolite (Jones, unpubl.).

Several Paleo-and-Mesoproterozoic granitic bodies intrude the Manzano Group along the Sandia-Manzano-Los Pinos uplift. Paleoproterozoic plutons from north to south include the 1653 ± 21 Cibola gneiss (Unruh, unpubl., in Karlstrom et al., 2004), the 1645

± 16 Ma Manzanita pluton (Brown et al., 1999), the 1659 ± 5 Ma Ojito pluton (Unruh, unpubl., in Karlstrom et al., 2004), the 1656 Ma Monte Largo pluton (Bauer et al., 1993), and the 1655 ± 3 Ma Los Pinos pluton (Shastri, 1992). The Manzanita and Ojito plutons display contact aureoles that elevate the regional greenschist facies metamorphism to amphibolite grade in the pluton margins, with emplacement conditions of both plutons estimated at 0.2-0.3 GPa and 600-620°C (Parchman, 1980; Brown et al., 1999; Karlstrom et al., 1999). The Manzanita pluton was interpreted to have been emplaced syntectonically with top-NW thrust-sense ductile shearing (Brown et al., 1999) and the Los Pino pluton was also interpreted to have been emplaced syntectonically with respect to NW-SE contraction and formation of the NE-SW subvertical regional cleavage (Shastri, 1992).

Mesoproterozoic plutons which intrude the Manzano Group include the 1437 ± 47 Ma Sandia granite (Kirby et al., 1995), and the 1450 Ma 1427 ± 10 Ma Priest pluton (Bauer et al., 1993). Mesoproterozoic intrusions are generally much less deformed than the earlier suite of plutons, however they record locally intense fabric development in their margins (Nyman et al., 1994). The Sandia granite dominates the northern part of the uplift (the Sandia Mountains), and was interpreted by Kirby et al. (1995) to preserve the regional strain field as induced by far field stresses along the thermally softened margins of the intrusion; this conclusion was based on folding of pegmatite dikes associated with the pluton, evidence for synchronous magmatic and solid state fabric development, and syndeformational andalusite growth in the contact aureole. Similarly, the margin of the Priest pluton is intensely strained and porphyroblast-matrix textures in the contact aureole have been interpreted as syntectonic (Thompson, 1996).

METHODS

The methods used in this study are similar to those described in Holland et al (2015; 2018). However, U-Pb geochronologic analyses from 11 samples presented in this study used different analytical procedures from those described by Holland et al. (2015; 2018), and are described below.

Six plutonic/metavolcanic samples (TG14-ZUN3, TG-14ZUN4, TG15-PIC5, TG15-OJITO, K15-SEV-ES-RHY, and K14-MANZANITA) and five detrital zircon samples (K14-MANZQTZITE, K15-ES-1, K15-ES-3, K15-ES-5, and K15-SAIS) were analyzed at the Arizona Laserchron Center using a Thermo Element2 single-collector inductively-coupled-plasma mass spectrometer (SC-ICP-MS) coupled to a Photon Analtye G2 excimer laser following the methods of (Pullen et al., 2014). Sample targeting was conducted using the Photon Machines Offline Targeting program. Sample locations were selected using back-scattered electron images of grain mounts, then location coordinates were exported as a .csv file and re-coordinated once mounted in the sample chamber. A 10 μm beam size was used during U-Pb analysis on the Element2. The difference in beam-size between the Element2 single-collector ICP-MS (10 μm) and the Nu Plasma HR multi-collector ICP-MS (30 μm) used for U-Pb geochronologic analysis by Holland et al. (2015; 2018) raises a few complexities for the interpretation of paired U-Pb and Lu-Hf isotope data, as discussed below.

RESULTS

A summary of geochronologic results from metavolcanic and plutonic rocks is shown in Table 2-1. Detrital zircon geochronologic results are shown in Table 2-2.

Sample	Lat and long (°N, °W)	Weighted mean age (this study)	MSWD	Previously published ages	Citation
K13-TUSAS-1		1758 ± 14	0.3	1751 ± 6	Davis et al., 2001
C13-098	36.570616 -106.085136	1705 ± 18	0.3	1700 ± 25	Silver, 1984
TG15-PIC5		1700 ± 22	0.3	1673 ± 5	Bell (1985)
C13-101A	36.307878 -106.053081	1699 ± 14	0.4	1700 ± 25	Silver, 1984
K15-SEV-ES-RHY	34.513221, -106.498492	1665 ± 16	1.0	1662 ± 1	Shastri, 1993
AL04-8		1662 ± 14	0.4	1655 ± 3	Shastri, 1993
TG15-OJITO		1661 ± 17	0.5	1659 ± 5	Unruh, unpublished data
K14-MANZANITA	34.946787 -106.439193	1655 ± 14	0.8	1645 ± 16	Unruh, unpublished data
TG15-ZUN4		1655 ± 18	0.2	1655 ± 20	Bowring and Condie, 1982
TG15-ZUN3		1638 ± 18	1.4	1655 ± 20	Bowring and Condie, 1982
H13-MAN	34.515941 -106.483344	1456 ± 13	1.1	1427 ± 10	Bauer et al., 1992
K07-SAN1B		1453 ± 12	0.2	1437 ± 47	Kirby et al., 1995
K13-NAC-2A/B	35.731482 -106.763740	1450 ± 12	0.4	1460 ± 10	Silver, 1984

Table 2-1. Igneous zircon geochronologic results.

Sample	Lat and long (°N, °W)	n_{total}	Minimum Age (Ma)	Maximum Age (Ma)	Peak Age (Ma)	n_{peak}
K12-NAC-QTZ		107	1698 ± 40	2681 ± 11	1720	106
K15-ES-1	34.514209 -106.496754	285	1610 ± 54	2609 ± 24	1666	241
					1853	3
K15-ES-3	34.513534 -106.494910	297	1626 ± 25	3231 ± 15	1666	201
K15-ES-5	34.514468 -106.493841	285	1606 ± 43	2642 ± 37	1673	184
					1825	12
K15-SAIS	34.515956 -106.487138	289	1627 ± 39	2545 ± 46	1660	210
					1867	6
					1979	3
K14-Manzqtzite	34.515362 -106.492157	302	1602 ± 80	2470 ± 48	1667	239

Table 2-2. Detrital zircon geochronologic results.

Tusas Mountains

Igneous Samples

K13-Tusas-1 Sample K13-Tusas-1 was taken from the Maquanita granodiorite in the Tusas Mountains. We obtained 23 U-Pb ages from individual zircons from this sample. Ages ranged from 1746 ± 26 to 1765 ± 12 Ma. 22 out of 23 ages were >90% concordant, and a weighted mean of all 23 ages yields an age of 1758 ± 14 Ma (MSWD = 0.3) (Figure 2-2A). This is within error of an earlier U-Pb analysis of 1755 Ma (Silver, 1984; in Karlstrom et al., 2004).

Hf-isotope analyses were conducted on 15 dated zircon grains. εHf(t) values ranged from +2.8 to +11.7 at 1758 Ma. A weighted mean of all 15 analyses yields an εHf(t) value of 9.0 ± 1.4 (MSWD = 2.8) (Figure 2-2A). The MSWD value suggests that the Maquanita granodiorite was derived from an isotopically heterogeneous source, or that mixing of multiple source components was involved in its genesis.

C13-098 Sample C13-098 was taken from the Posos Lake metarhyolite. The Posos Lake metarhyolite is part of the Vadito Group in the central Tusas Mountains. We obtained 21 U-Pb ages from this sample. Ages range from 1685 ± 30 Ma to 1750 ± 125 Ma. A weighted mean of all 21 ages yields an age of 1705 ± 18 Ma (MSWD = 0.3) (Figure 2-2B). This age is in excellent agreement with the often quoted age of the Burned Mountain Formation of the Vadito Group at 1700 Ma (Karlstrom et al., 2004; Daniel et al., 2013; Jones et al., 2011; where the original citation for this date was personal communication from Lee Silver (Bauer and Williams, 1989).

Hf-isotope analyses were conducted on 12 dated zircon grains. $^{176}Hf/^{177}Hf_{(i)}$ values ranged from 0.281912 to 0.282012, equating to εHf(t) values of +7.6 to +11.1 at 1.7 Ga. A weighted mean of initial Hf-isotope values yielded an εHf(t) value of +10.0 at 1705 (MSWD = 0.7) (Figure 2-2B). This value is slightly higher than but within error of the coeval depleted mantle value of +8.4.

C13-101A Sample C13-101A was taken from the Cerro Colorado metarhyolite. We obtained 88 zircon U-Pb ages from this sample. Ages range from 1679 ± 17 to 1741 ± 110 Ma, and 77 ages were >95% concordant. A weighted mean of all 88 $^{207}Pb/^{206}Pb$ ages yields an age of 1699 ± 14 Ma (MSWD = 0.4) (Figure 2-2C).

Hf-isotope analyses were conducted on 30 dated zircon grains. $^{176}Hf/^{177}Hf_{(i)}$ values from 0.281856 to 0.282038, equating to εHf(t) values ranging from +5.5 to +11.9 at 1.7 Ga (Figure 2-2C).

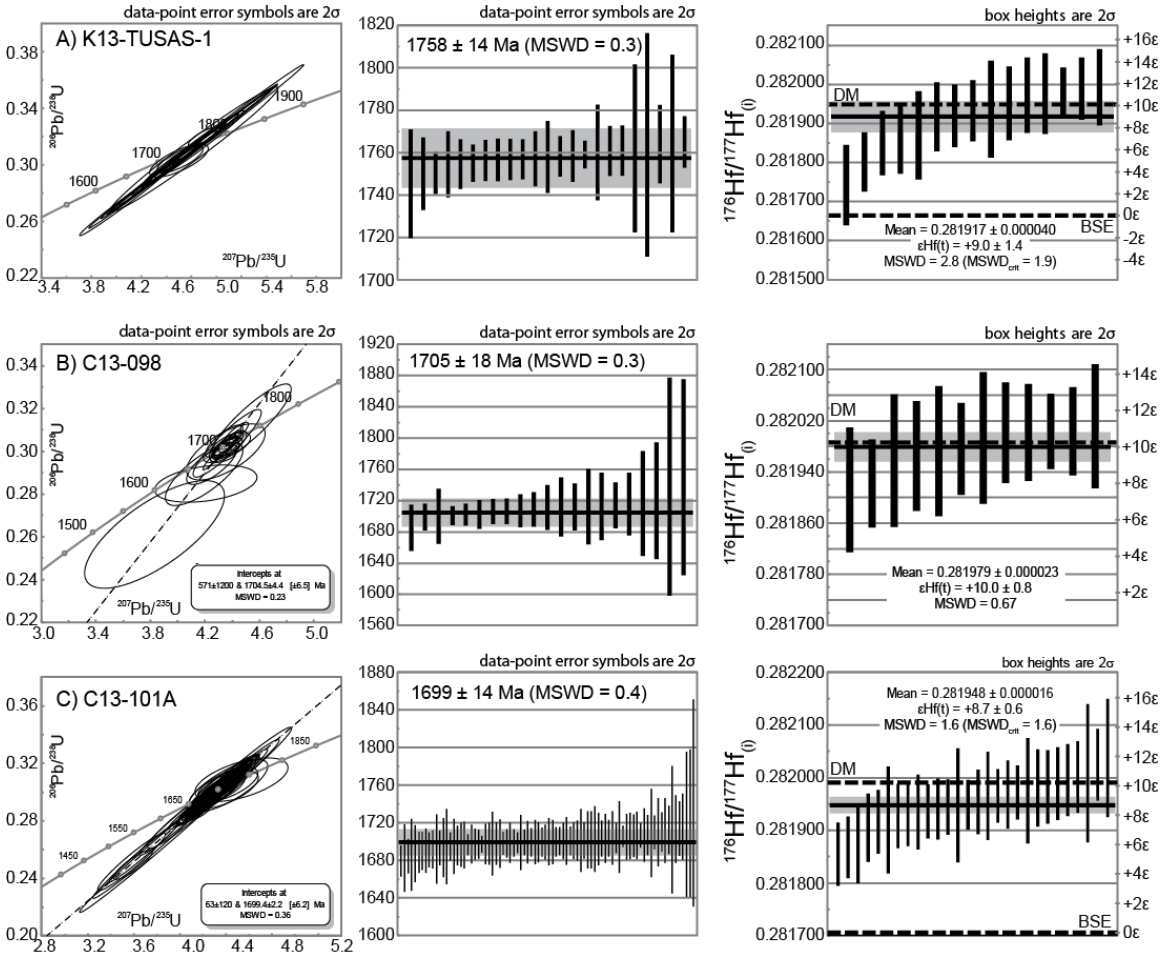

Figure 2-2. Summary of U-Pb and Lu-Hf isotope data from the Tusas Mountains. Each plutonic or metavolcanic sample shows three panels. Left, U-Pb concordia diagram. Middle, weighted mean with each zircon analysis shown as vertical black bars. Horizontal black bar is the weighted mean age, with the gray band representing 2-sigma uncertainty. Right, weighted mean of 176Hf/177Hf(i) values, with horizontal black and gray bands as in middle diagram. Equivalent εHf(t) values are shown on the right y-axis, and concurrent depleted mantle and bulk silicate earth values are shown as dashed black lines. A) Maquanita granodiorite. B) Posos Lake metarhyolite. C) Cerro Colorado metarhyolite.

Nacimiento Uplift

Igneous Samples

K13-NAC-2A/B Two samples with marked textural differences were collected from the monzogranite of the Guadalupe Box. K13-NAC-2A was taken from a pink monzogranite with abundant potassium feldspar megacrysts. K13-NAC-2B was taken

from the same location, but in an area with abundant 5-10 cm mafic enclaves. There was no statistical difference between the U-Th-Pb and Lu-Hf isotopic results, and so they are reported here as one composite sample.

We obtained a total of 41 U-Pb ages from the composite sample, which yielded ages from 1376 ± 82 to 1476 ± 109 Ma. All but one age was >90% concordant, and a weighted mean of all 41 analyses yielded an age of 1450 ± 12 Ma (MSWD = 0.4) (Figure 2-3). This is interpreted as the age of crystallization of the monzogranite of the Guadalupe Box.

Hf-isotope analyses were conducted on 30 dated zircon grains from this sample. εHf(t) values define a continuous spread from +2.6 to +7.8 at 1.45 Ga (Figure 2-3). A single zircon grain (K13-NAC-2A-12) yielded a higher value of +10.5 at 1.45 Ga.

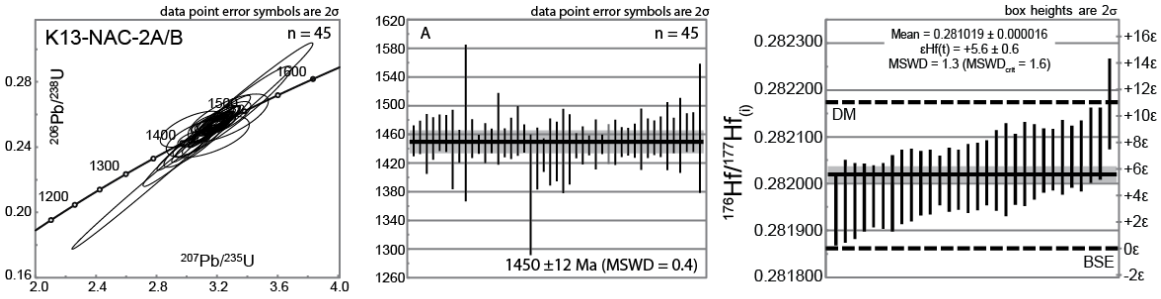

Figure 2-3. Summary of U-Pb and Lu-Hf data from the Nacimiento Uplift. Diagrams and symbols as in Figure 2.

Detrital Samples

K12-NAC-QTZ Sample K12-NAC-QTZ was taken from a fine grained micaceous quartzite with well-preserved crossed bedding and a penetrative NW-striking foliation. The quartzite is interlayered with quartzofeldspathic schists interpreted as metarhyolites, and is cross cut by the 1696 Ma Clear Creek monzongranite (Premo and Kellog, 2005). We obtained 107 U-Pb detrital zircon ages from this sample, with the dominant

population (106 grains) ranging from 1698 ± 40 to 1760 ± 60 Ma. One grain yielded an Archean age of 2681 ± 11 Ma. The strongly unimodal detrital zircon population yields a peak age of 1720 Ma (Figure 2-4).

Hf-isotope analyses were conducted on 28 dated zircon grains. εHf(t) values from the unimodal population ranged from +7.1 to +14.2 at 1.72 Ga. The single Archean grain yielded an εHf(t) value of +6.4 at 2.68 Ga. The highest values are greater than, though within 2-sigma uncertainty of the depleted mantle model array (Figure 2-4).

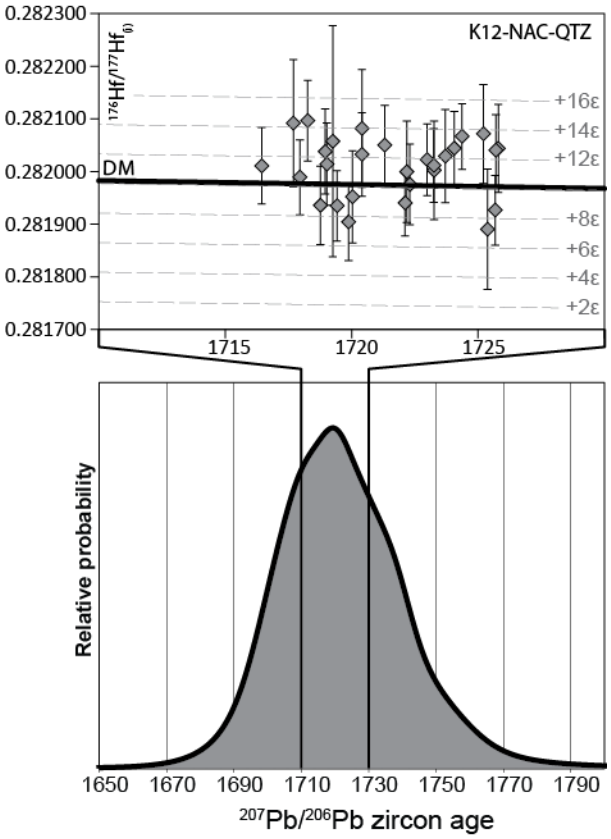

Figure 2-4. Detrital zircon results from the San Pedro quartzite, Nacimiento Uplift. Probability density distribution (PDD) of main population of detrital zircon (bottom). One Archean age is excluded. Hf-isotope data from dated detrital zircon are shown above. Each diamond represents a single zircon with age and initial Hf-isotope composition. Error bars are 2-sigma. Dashed gray lines show εHf values relative to the bulk silicate earth in increments of 2 epsilon units. Solid black line is the depleted mantle array.

Picuris Mountains

Igneous Samples

TG15-PIC5 Sample TG15-PIC5 was taken from the Rana quartz monzonite in the Picuris Mountains. We obtained 20 U-Pb ages from as many zircon grains. U-Pb ages ranged from 1681 ± 42 to 1927 ± 34 Ma. We interpret six ages ranging from 1746 ± 44 to 1927 ± 34 Ma to reflect inherited xenocrystic zircon grains. A weighted mean of 14 >95% concordant ages yields an age of 1700 ± 22 Ma (MSWD = 0.3) that approximates the crystallization age of the Rana pluton (Figure 2-5). This age is older than, but just within 2 sigma error of, the 1673 ± 5 Ma U-Pb zircon age reported by Bell (1985). Given the presence and interesting age range of xenocrystic grains, likely higher precision of the older TIMS age, and field observations that the 1700 Ma Rana intrudes the 1700 Ma Vadito Group, we favor 1673 ± 5 Ma as the crystallization age.

Hf-isotope analyses were obtained from 15 dated zircon grains from the Rana pluton, including five xenocrystic grains. Hf-isotope analyses from 10 zircon grains from the main magmatic population yield a cluster of $^{176}Hf/^{177}Hf_{(i)}$ values ranging from 0.281889 to 0.281974, yielding a weighted mean equivalent to an $\varepsilon Hf_{(t)}$ value of +8.0 at 1.7 Ga (MSWD = 0.89) (Figure 2-4). Inherited zircon grains yield almost identical $^{176}Hf/^{177}Hf_{(i)}$ values as primary magmatic grains, despite being, in some cases, >200 Ma older than the Rana pluton itself. Two >1.9 Ga zircon grains yielded $^{176}Hf/^{177}Hf_{(i)}$ values that plot above the depleted mantle array (Figure 2-5). These $^{176}Hf/^{177}Hf_{(i)}$ values are almost identical to the mean $^{176}Hf/^{177}Hf_{(i)}$ value of the primary magmatic population.

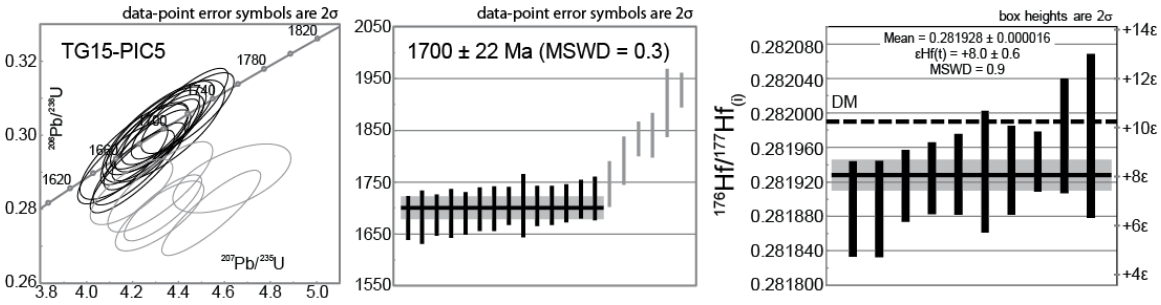

Figure 2-5. Summary of U-Pb and Lu-Hf isotope data from the Picuris Mountains. Diagram and symbols as in Figure 2.

Zuni Uplift

Igneous Samples

TG15-ZUN4 Sample TG15-ZUN4 was taken from a metarhyolite near the center of the Zuni Uplift. We obtained 24 U-Pb ages from this sample, ranging from 1644 ± 40 to 1891 ± 40 Ma. The oldest age was interpreted to represent an inherited xenocrystic zircon grain, and a weighted mean of the remaining 23 ages yielded an age of 1655 ± 18 Ma (MSWD = 0.2), which is interpreted as the age of deposition of the metarhyolite (Figure 2-6A).

Hf-isotope analyses were conducted on 11 dated zircon grains from this sample, including one inherited zircon grain. $^{176}Hf/^{177}Hf_{(i)}$ values of the primary magmatic population of zircon range from 0.281913 to 0.282062, equating to εHf(t) values of +6.5 to +11.8 (Figure 2-6A). The inherited zircon grain yielded an initial $^{176}Hf/^{177}Hf$ value of 0.281909 at 1.89 Ga. This equates to an εHf(t) value of +11.8 at 1.89 Ga, which is barely within 2-sigma uncertainty of the depleted mantle array.

TG15-ZUN3 Sample TG15-ZUN3 was taken from a granitoid at the northwestern end of the Zuni Uplift. We obtained 13 U-Pb ages from this sample. Ages ranged from 1595 ± 37 to 1695 ± 40 Ma, and together define a weighted mean age of 1638 ± 18 (MSWD = 1.4) (Figure 2-6B).

No Hf-isotope analyses were conducted on this sample.

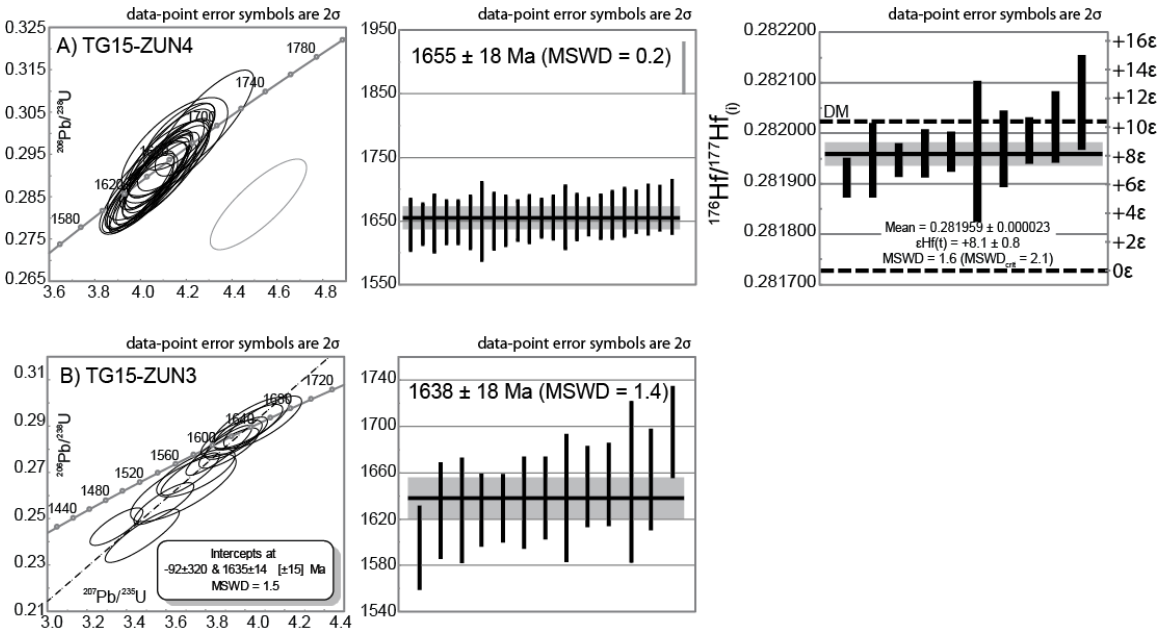

Figure 2-6. Summary of U-Pb and Lu-Hf geochronologic data from the Zuni Mountains. Diagram and symbols as in Figure 2.

Sandia-Manzano-Los Pinos uplift

Igneous Samples

AL04-8 Sample AL04-8 was taken from the Los Pinos pluton in the Los Pinos Mountains where it intrudes the 1665 Ma Sevilleta metarhyolite in the Los Pinos anticline. The Los Pinos pluton ranges in texture from nearly aplitic to somewhat coarser grained granite dominated by K-feldspar. The margin of the pluton is marked by locally brecciated zones, and miarolitic cavities throughout the pluton suggest shallow emplacement (Luther, 2006). We obtained 15 ages from this sample, ranging from 1639 ± 66 to 1703 ± 58 Ma. Individual zircon analyses ranged from 72-99% concordant, allowing for regression of a discordia age of 1668 ± 13 Ma (MSWD = 1.4) (Figure 2-7A). This age is older than the 1655 ± 3 Ma age obtained by Shastri (1992), and older than the 1662 ± 1 Ma age of the Sevilleta metarhyolite (Shastri, 1992) into which the Los Pinos

pluton intrudes. However, we note that the uncertainties on LA-ICP-MS data presented in this study are much larger and overlap within the 2-sigma confidence level of the ages reported by Shastri (1992). Luther (2006) highlighted the geochemical similarities between the Los Pinos pluton and the Sevilleta metarhyolite, and suggested that the Los Pinos pluton may represent an intrusive equivalent to the Sevilleta metarhyolite. This is supported by the fine-grained nature of the pluton and miarolitic cavities that indicate shallow emplacement. In this case, overlapping ages may be expected if volcanism, plutonism, and sedimentation was occuring synchronously.

Hf-isotope analyses were conducted on 10 dated zircon grains. $^{176}Hf/^{177}Hf_{(i)}$ values from dated zircon grains ranged from 0.281980 to 0.282068, equating to εHf(t) values of +9.1 to +12.2 at 1.67 Ga (Figure 2-7A).

K15-SEV-RHY-ES A sample of the Sevilleta metarhyolite was collected from near the base of the Abajo formation at the mouth of Estadio Canyon. We obtained 19 near concordant ages from this sample. A weighted mean of all 19 ages yields an age of 1665 ± 16 Ma (MSWD = 1.0) (Figure 2-7B). This age is in good agreement with the more precise ID-TIMS age presented by Shastri (1993) of 1662 ± 1 Ma. A wider range of rhyolite ages in the Sandia-Manzanos was reported by Karlsrom et al (2004) based on TIMS dating and it is unclear if that broad range is real or represents mixed ages in rhyolites with older inherited grains.

Hf-isotope analyses were conducted on 10 dated zircon grains from the Sevilleta metarhyolite. $^{176}Hf/^{177}Hf_{(i)}$ values from dated zircon grains yielded a remarkably tight cluster with a weighted mean equal to 0.282006 (MSWD = 0.19) equating to εHf(t) value of +10.0 at 1.66 Ga (Figure 2-7B).

TG15-OJITO A sample of the Ojito pluton was taken from near the southern margin of the intrusion. We obtained 27 ages ranging from 1646 ± 35 to 2073 ± 91 Ma (Figure 2-7C). A weighted mean of the 20 youngest ages yields an age of 1661 ± 17 Ma. This age is in good agreement with the ID-TIMS age from Dan Unrue of 1659 ± 5 Ma (in Karlstrom et al., 2004). The older population of grains were not obtained from texturally distinct zircon domains, however they were excluded from our age determination based on a marked change in concordance towards more discordant (<90% concordant) ages.

Hf-isotope analyses were conducted on 7 dated zircon grains, including 2 inherited zircon grains. $^{176}Hf/^{177}Hf_{(i)}$ values from the primary magmatic population of zircon grains ranged from 0.281935 to 0.281977, equating to εHf(t) values of +7.4 to +9.1. at 1.66 Ga (Figure 2-7C). Inherited zircon grains yielded $^{176}Hf/^{177}Hf_{(i)}$ values nearly identical to those of the main magmatic population of zircon grains,

K14-MANZANITA A relatively undeformed sample of Manzanita granite was collected from within the Manzanita shear zone. We obtained 41 ages ranging from 1750 ± 48 to 1634 ± 33 Ma. A weighted mean of the 30 youngest grains yields an age of 1655 ± 14 Ma (MSWD = 0.8) (Figure 2-7D). This age is in good agreement with the unpublished age of 1645 ± 16 age from Dan Unrue ID-TIMS dating (in Karlstrom et al., 2004). The older population of grains was excluded based on a marked change in concordance towards more discordant (<90% concordant) ages. 11 ages define a separate cord with an upper-intercept age of 1733 Ma. A weighted mean of the same 11 ages yields an age of 1723 ± 11 Ma.

Hf-isotope analyses were conducted on 14 dated zircon grains, including 5 inherited zircon grains. $^{176}Hf/^{177}Hf_{(i)}$ values from the primary magmatic population of

zircon grains ranged from 0.281910 to 0.281984, equating to εHf(t) values of +6.4 to +9.0. at 1.66 Ga (Figure 2-7D). Five of the most concordant inherited zircon grains

H13-MAN Sample H13-MAN was taken from the Priest pluton in Estadio Canyon. The Priest pluton is primarily quartz monzonite with K-feldspar megacrysts. This sample yielded extremely complex U-Pb and Lu-Hf results. The results of this sample are discussed below after a discussion of potential complexities in isotope systematics.

K07-SAN1B Sample K07-SAN1B was taken from the Sandia granite and analyzed at the GEMOC Key Centre. We obtained 24 ages ranging from 1409 ± 72 to 1495 ± 70 Ma (Figure 2-7F). A weighted mean of all analyses yields an age of 1453 ± 12. This is within error of the 1437 ± 47 Ma age presented by Kirby et al. (1995), but more precise and is likely a more robust estimate of the age of crystallization.

Hf-isotope analyses were conducted on 12 zircon grains from the Sandia pluton. $^{176}Hf/^{177}Hf(i)$ values ranged from 0.282017 to 0.282185, equating to εHf(t) values of +5.5 to +11.5 (Figure 2-7F). The zircon grain that yielded the +11.5 value is an outlier, however even when it is excluded the variation in Hf-isotope composition of the other 11 grains is greater than can be explained by analytical uncertainties alone (Figure 2-7E).

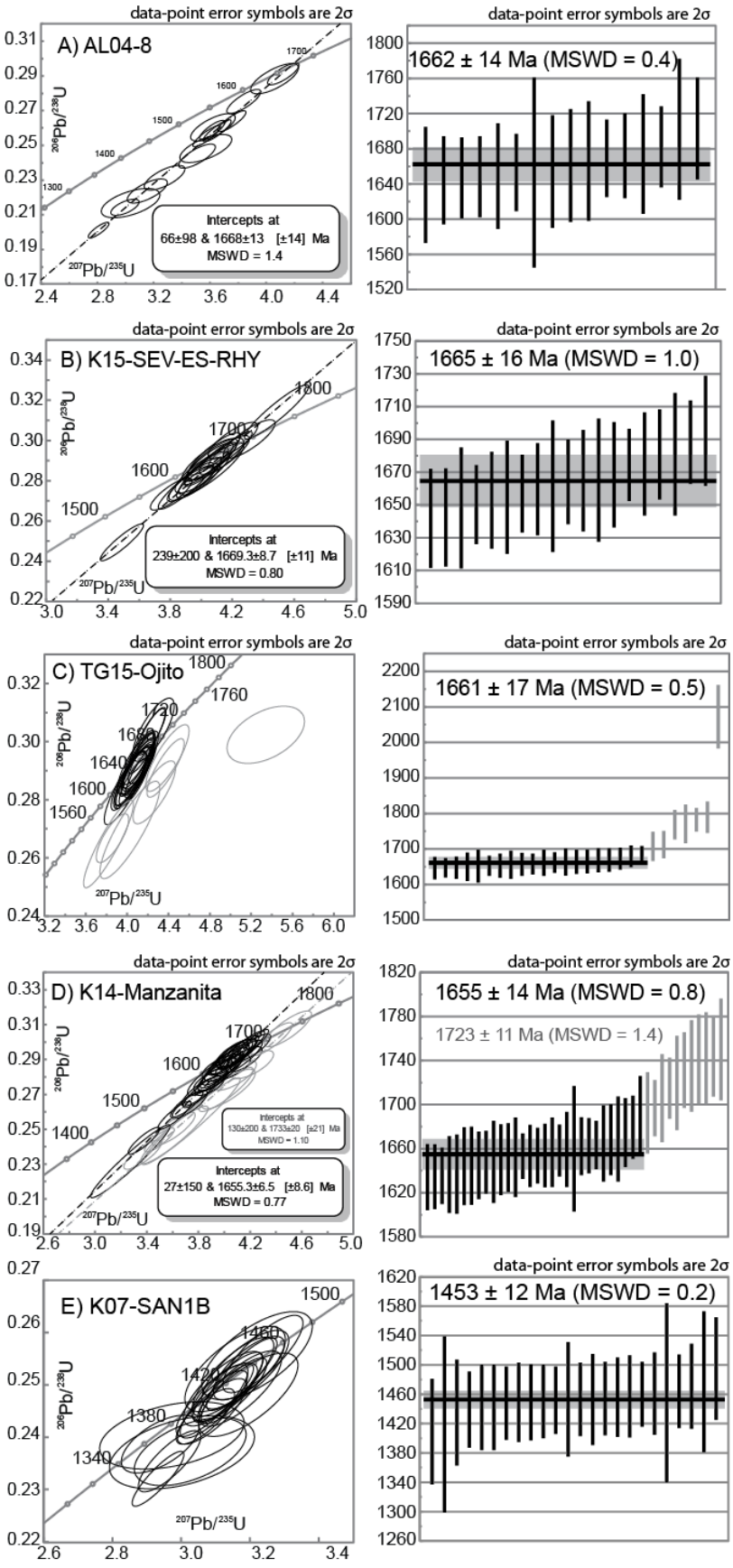
data-point error symbols are 2σ
A) AL04-8
Intercepts at
66±98 & 1668±13 [±14] Ma
MSWD = 1.4
1662 ± 14 Ma (MSWD = 0.4)
B) K15-SEV-ES-RHY
Intercepts at
239±200 & 1669.3±8.7 [±11] Ma
MSWD = 0.80
1665 ± 16 Ma (MSWD = 1.0)
C) TG15-Ojito
1661 ± 17 Ma (MSWD = 0.5)
D) K14-Manzanita
Intercepts at
130±200 & 1733±20 [±21] Ma
MSWD = 1.10
Intercepts at
27±150 & 1655.3±6.5 [±8.6] Ma
MSWD = 0.77
1655 ± 14 Ma (MSWD = 0.8)
1723 ± 11 Ma (MSWD = 1.4)
E) K07-SAN1B
1453 ± 12 Ma (MSWD = 0.2)
206Pb/238U
207Pb/235U

Figure 2-7. U-Pb and Lu-Hf geochronologic summary of the Sandia-Manzano-Los Pinos Uplift. Diagram and symbols as in Figure 2.

Detrital Samples

We collected five detrital zircon samples from course grained quartzofeldspathic members of the Manzano Group. Our sampling began at the base of the Abajo Formation in Estadio Canyon and proceeded up-section to the White Ridge quartzite.

K15-ES-1 Sample K15-ES-1 is a sample of the meta-lithic arenite at the base of the Abajo Group. This unit records a transition from bimodal metavolcanic rocks to clastic and volcaniclastic sedimentary rocks of the Abajo Formation. We obtained 285 detrital zircon U-Pb ages from this sample (Figure 2-8). In total, ages range from 1609 ± 54 to 2609 ±24 Ma, however the oldest age of 2609 ±24 Ma is the only Archean age obtained from this sample. 254 ages (89%) fall between 1700-1600 Ma, and 26 ages spread from 1705 ± 34 to 1791 ± 31 Ma. The peak age defined by the AgePick routine is defined by 241 ages at 1666 Ma. Three grains ranging from 1835 ± 29 to 1864 ±28 Ma define a peak at 1853 Ma.

K15-ES-3 Sample K15-ES-3 is a sample of meta-feldspathic arenite from the Abajo Group. This unit is transitional between the immature lithic sediments at the base of the Abajo Group and the mature orthoquartzites further up-section. We obtained 297 detrital zircon U-Pb ages from this sample (Figure 2-8). In total, ages range from 1626 ± 25 to 3231 ±15 Ma. Similar to the underlying K15-ES-1, detrital zircon ages from this sample are predominantly between 1700-1600 Ma (72%), with 75 ages spreading from 1800-1700 (25%). 8 grains yield ages that range from 1801 ± 29 to 3231 ±15 Ma. Two grains yielded ages of 1585 ± 38 and 1414 ± 42 Ma, however these are younger than cross cutting relationships with the Ojito pluton, and a 1643 Ma granodioritic dike in

Estadio Canyon (Unruh, unpubl. in Karlstorm et al., 2004)allow and are interpreted as grains with disturbed U-Pb systematics. The age peak defined by the AgePick routine is defined by 201 ages at 1666 Ma, identical to that of K15-ES-1.

K15-ES-5 Sample K15-ES-5 is a micaceous quartzite taken from the top of the Abajo Formation. We obtained 285 detrital zircon U-Pb ages from this sample (Figure 2-8). In total, ages range from 1606 ± 43 to 2642 ± 37 Ma. This sample contains the greatest abundance of >1700 Ma grains, with only 165 grains yielding ages from 1700-1600 Ma (58%), and 95 grains yielding ages from 1800-1700 Ma (33%). This sample also contains a robust population of >1800 Ma grains, with the AgePick routine defining a peak at 1825 Ma (12 grains). Four grains yielded ages >2000 Ma including two Archean ages.

K15-SAIS Sample K15-SAIS was taken from the Sais quartzite in Estadio Canyon. We obtained 289 detrital zircon U-Pb ages from this sample (Figure 2-8). In total, ages range from 1627 ± 39 to 2545 ± 46 Ma. Detrital zircon ages in the Sais quartzite are predominantly 1700-1600 Ma (78%), although 51 grains (18%) yield ages between 1800-1700 Ma. Similar to the underlying Abajo Formation quartzite, K15-SAIS contains a robust population of >1800 Ma detrital zircon, with two peaks defined by the AgePick routine at 1867 and 1979 Ma. The sample also yielded 4 ages >2000 Ma.

K14-MANZQTZITE Sample K14-MANZQTZITE was taken from the White Ledges quartzite in the upper-middle Manzano Group in Estadio Canyon. We obtained 302 detrital zircon U-Pb ages from this sample (Figure 2-8). In total, ages range from 1602 ± 80 to 2470 ± 48 Ma. Of the 302 ages we obtained, 236 (78%) of them range from

1700-1600 Ma, and 60 of them (20%) range from 1800-1700 Ma. There is also a minor population of >1800 Ma grains; 6 grains range in age from 2470 ± 41 to 1816 ± 47 Ma.

No Hf-isotope data were collected from this sample.

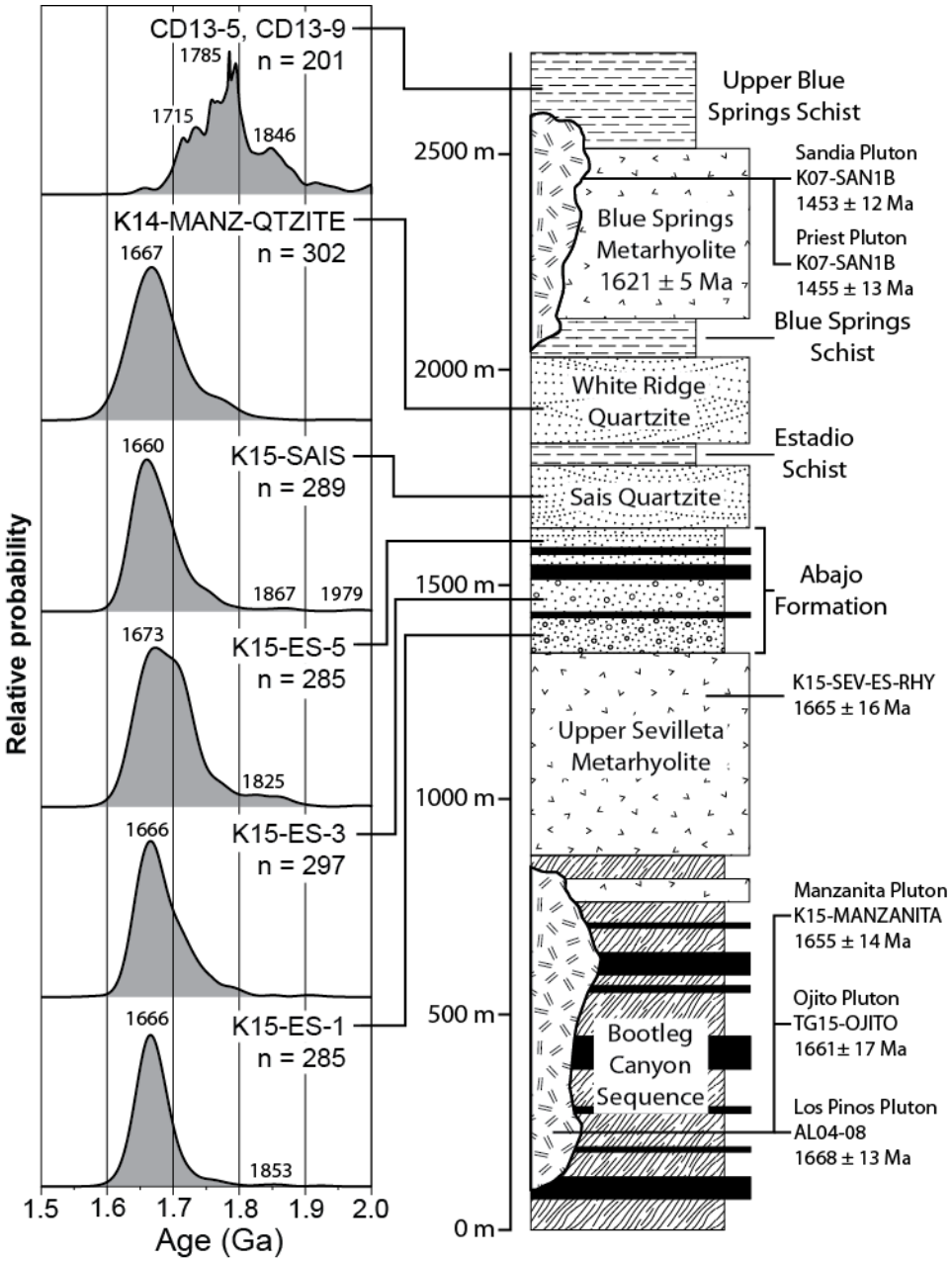

Figure 2-8. Detrital zircon geochronologic summary of the Manzano Group. PDDs of each sample are shown to the left of a schematic stratigraphic section (modified after Luther, 2006). Samples CD13-5 and CD13-9 are from (Wallace, 2014).

DISCUSSION

Hf-isotope systematics of New Mexico Proterozoic Rocks

An essential aspect in the use of paired U-Pb and Lu-Hf isotope analyses in zircon is ensuring that the Hf-isotope composition measured in a zircon is placed in a robust geochronologic context (Vervoort and Kemp, 2016). This is not always a straightforward task because zircon is well known to retain geochronologic information through multiple episodes of metamorphism, magmatism, and/or fluid alteration (Gerdes and Zeh, 2009). Almost all samples analyzed in this study had complex U-Pb and/or Lu-Hf isotope systematics. Of the ten igneous samples reported herein, five samples contained inherited zircon components. In addition, the $^{176}Hf/^{177}Hf_{(i)}$ values from magmatic zircon (excluding inherited zircon components) in three samples varied more than could be explained by analytical uncertainties alone (e.g. K13-TUSAS-1, H13-MAN, and K07-SAN1B). Finally, three igneous samples and three detrital zircon samples contained zircon grains which yielded $^{176}Hf/^{177}Hf_{(i)}$ values significantly higher than that of the coeval depleted mantle model (Vervoort and Blichert-Toft, 1999). In this section we discuss complex isotope systematics and discuss possible interpretations in individual samples, and groups of samples with similar complexities.

Four Paleoproterozoic samples contained inherited zircon components with $^{207}Pb/^{206}Pb$ ages much older than the interpreted crystallization age of the sample (Figure 2-9). Inherited zircon cores and xenocrystic grains can be transported from the melt source region, or assimilated from wallrocks. In the case of the former, inherited zircon can provide a wealth of information concerning the melt-source region of igneous rocks, although such interpretations are often non-unique (Corfu et al., 2003). Combined Hf-

isotope analysis of inherited and primary zircon components can help mediate the ambiguities of interpreting complex zircon crystals because 1) the formation of new zircon from material represented by inherited components should yield a Hf-isotope composition consistent with radiogenic growth of ^{176}Hf from an assumed or known $^{176}Lu/^{177}Hf$ ratio (Flowerdew et al., 2006; Ibanez-Mejia et al., 2015), and 2) alteration processes that disrupt U-Pb isotope systematics in zircon should leave the Hf-isotope composition unchanged (Gerdes and Zeh, 2009). Furthermore, characterization of the age and isotope composition of wallrocks can help rule out or confirm the source of inherited grains (Holland et al., 2015; 2018).

Xenocrystic zircon grains in Paleoproterozoic plutonic and volcanic rocks in central and northern New Mexico yield a wide range of ages from 2.0-1.7 Ga (Figure 2-9). However, most of the inherited zircon grains in the four Paleoproterozoic samples yielded $^{176}Hf/^{177}Hf_{(i)}$ values that plot above the coeval depleted mantle array (Figure 2-9). Such analyses are problematic because the depleted mantle should have a higher Lu/Hf ratio than primitive mantle or crustal reservoirs. In some cases, individual zircon grains may yield $^{176}Hf/^{177}Hf_{(i)}$ values that are greater than, but within analytical uncertainty of, the depleted mantle array. This case is allowable given the uncertainty in the depleted mantle array itself (Vervoort and Blichert-Toft, 1999). Furthermore, at present, the upper mantle is highly varied in its isotopic composition, and includes anomalously depleted segments which may give rise to particularly radiogenic Hf-isotope values (Stracke et al., 2011; Salters et al., 2011). In this case, the $^{176}Hf/^{177}Hf_{(i)}$ values from inherited grains are nearly identical to the $^{176}Hf/^{177}Hf_{(i)}$ values of main magmatic population of zircon (Figure 2-8). Recalculating the $^{176}Hf/^{177}Hf_{(i)}$ values of inherited grains at the age of crystallization

of their host rocks yields $^{176}Hf/^{177}Hf_{(i)}$ values that match the main population (Figure 2-9). In light of this observation, the most likely explanation for these isotopic systematics is a miss-match between the measured Hf-isotope composition and the age assigned to that composition. It is possible that the difference in beam size used for U-Pb (10 μm) vs. Lu-Hf (40 μm) isotope analysis resulted in mixing of different zircon domains with distinct U-Pb and Lu-Hf isotope compositions.

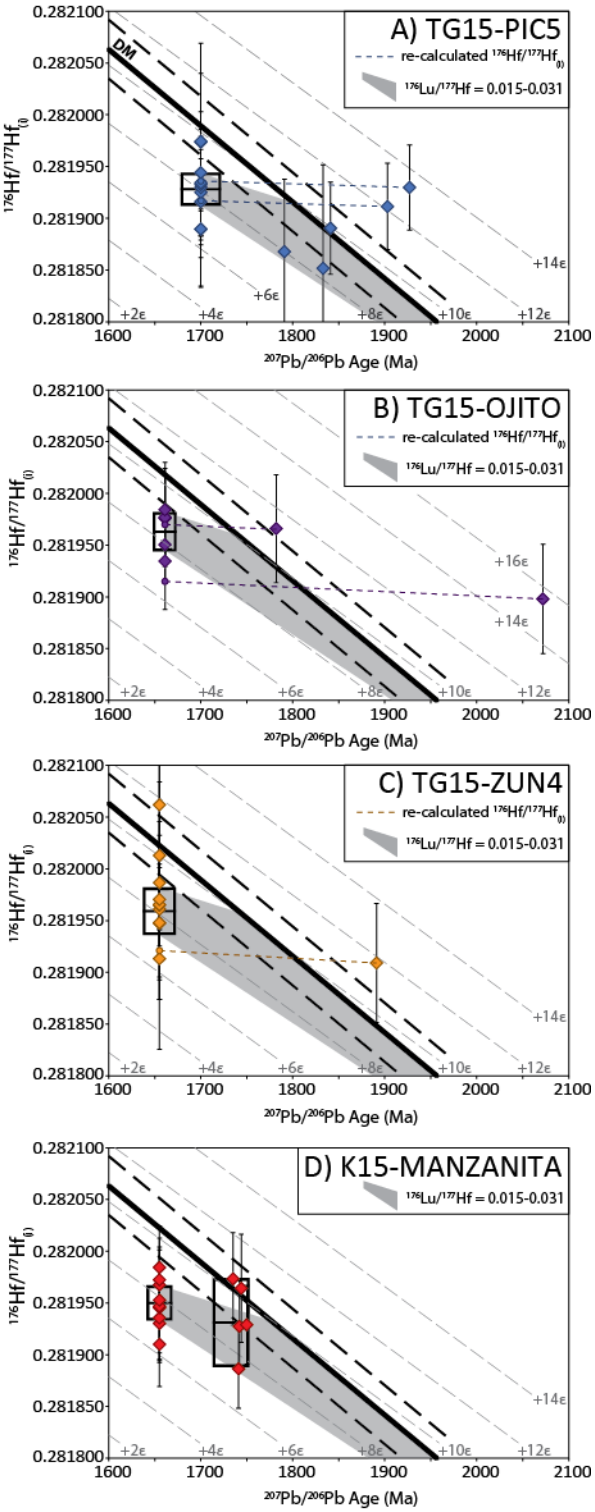

Figure 2-9. Summary of geochronologic data from samples with complex U-Pb and Hf-isotope systematics. Initial Hf-isotope values from plutonic or metavolcanic rocks are shown as diamonds with error bars showing the 2-sigma uncertainty in Hf-isotope composition. The primary magmatic populations are shown with a box outlining the

uncertainty in the weighted means of both crystallization ages (width) and Hf-isotope composition (height) expressed at 2-sigma. Solid black line represents the depleted mantle model array. Dashed gray lines show εHf values relative to the bulk silicate earth in increments of 2 epsilon units. Dashed black lines show the ~1 epsilon unit uncertainty in the depleted mantle array. Gray fields represent the range of possible evolution paths for sources with 176Lu/177Hf between 0.015-0.031 projected from the weighted mean of primary magmatic grains. Evolutions paths suggest the involvement of pre-existing crustal material (at least ~1.8 Ga) in the petrogenesis of these samples.

Similar issues were found in three detrital zircon samples from the Manzano Group. Four detrital zircon grains from the main Paleoproterozoic population of detrital zircon, and four detrital zircon from the minor >2.2 Ga population yielded $^{176}Hf/^{177}Hf_{(i)}$ values greater than coeval depleted mantle (Figure 2-10). The $^{176}Hf/^{177}Hf_{(i)}$ values from the <2.2 Ga detrital zircon grains are in good agreement with $^{176}Hf/^{177}Hf_{(i)}$ values of the peak ~1660 Ma population of detrital zircon (Figure 2-10), however the nature of detrital zircon precludes choosing an age to recalculate $^{176}Hf/^{177}Hf_{(i)}$ values. Ultimately, we can conclude that age and Hf-isotope compositions of detrital zircon from the Manzano Group consist primarily of locally derived detritus, and include some older grains with age and Hf-isotope compositions typical of Yavapai and Mojave province crust (Figure 2-11).

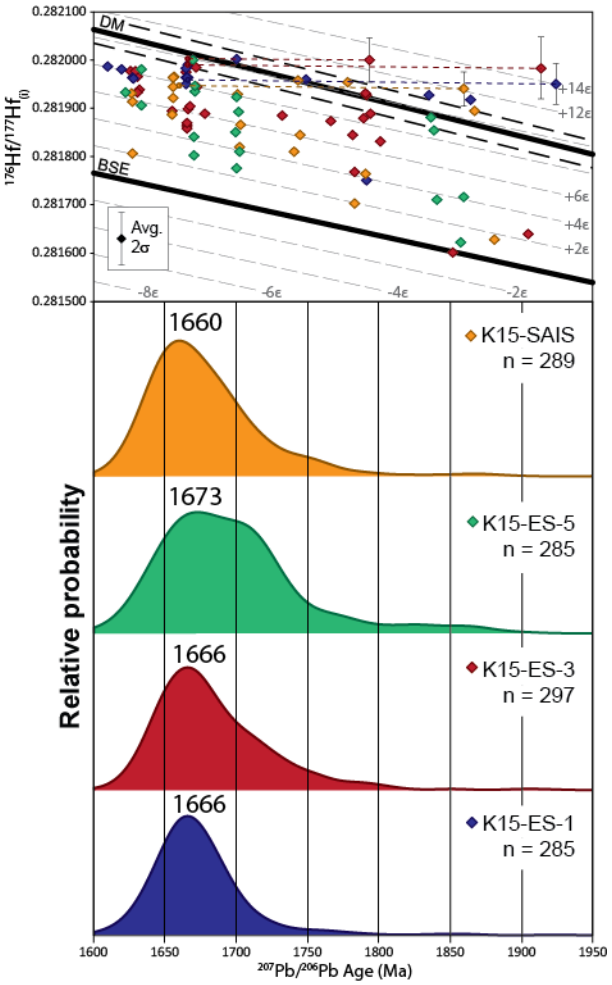

Figure 2-10. Summary of Hf-isotope data from the Manzano Group. Diagram and symbols as in Figure 9. Grains with initial Hf-isotope values the plot above the depleted mantle are shown with 2-sigma uncertainty.

The potential age-Hf miss-matches in this dataset makes the interpretation of inherited zircon grains very difficult. Some grains plot above, but within uncertainty of the depleted mantle array. Whether these grains represent miss-matches or sample juvenile crust characteristic of older Laurentian crustal provinces (Figure 2-11) is impossible to answer with the current dataset. However, the Hf-isotope composition of primary magmatic zircon suggests that partial melting of older crustal components was an important part of magmatism in the Mazatzal province (Figure 2-8). Inherited grains in some samples (e.g. K15-MANZANITA) may represent sampling of this older crust, and

have Hf-isotope compositions consistent with older Yavapai province basement (Figure 2-11).

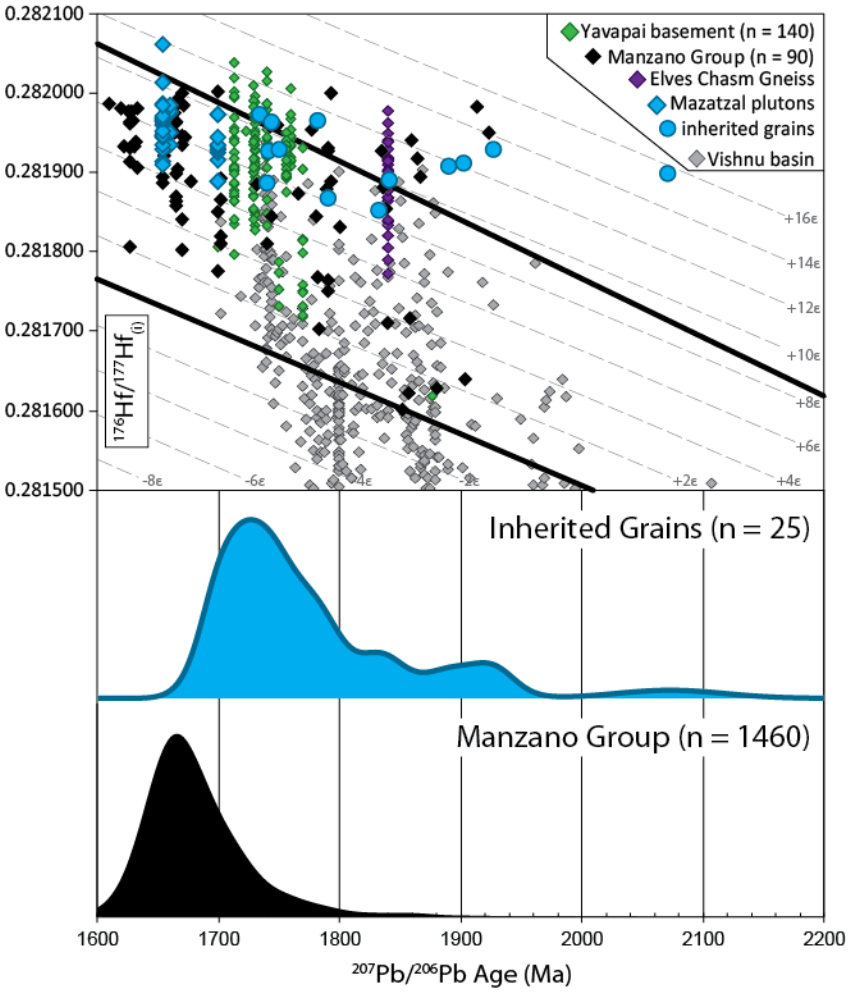

Figure 2-11. Comparison of plutonic and metavolcanic samples with inheritance and potential sources of inherited grains. Diagram and symbols as in Figures 9, 10. Yavapai province basement zircon data from Bickford et al. (2008), and Holland et al. (2015). Elves Chasm Gneiss data from Holland et al. (2015), and Vishnu basin detrital zircon grains from Holland et al. (2018).

The Priest Pluton

U-Pb and Lu-Hf isotope systematics in the Priest pluton are very complex, and warrant a focused discussion. Sample H13-MAN was taken from the Priest pluton in Estadio Canyon. We analyzed 40 zircon grains from this sample, yet only 11 passed the data reduction process. Many analyses yielded highly discordant (>20%) ages and very

high common Pb, which is consistent with the blotchy and disturbed internal textures revealed by CL imaging. The ages obtained from these grains range from 1673 ± 55 to 1452 ± 14 Ma (Figure 2-12). Four of the youngest and most concordant ages yield an upper intercept age of 1466 ±15 Ma, and a weighted mean age of 1455 ± 13 Ma (MSWD = 1.2), which is interpreted as the age of crystallization of the Priest pluton. One slightly older and more discordant grain yielded an age of 1484 ± 57 which we exclude from the weighted mean calculation due to its discordance and large uncertainty.

Four concordant Paleoproterozoic ages obtained texturally distinct zircon cores yield a weighted mean age of 1658 ± 21 Ma (MSWD = 0.2). The Paleoproterozoic zircon cores are similar in age to the age of a thin 1643 ± 20 granite dike in Estadio Canyon and also similar in age to other ~1660 Ma Paleoproterozoic plutons and hence these are interpreted as inherited zircon grains. Thompson (1996) determined that the Priest pluton was geochemically similar to “S-type” granites interpreted to be derived from the partial melting of supracrustal source rocks (Chappell and White, 2001). This is supported by the similarity between the age and Hf-isotope composition of inherited zircon grains in the Priest pluton, and detrital zircon grains from quartzites of the Manzano Group into which the Priest pluton intrudes (Figure 2-12). Hf-isotope analysis may provide insight into the nature of the two discordant ages of 1558 ± 103 and 1587 ± 46 Ma.

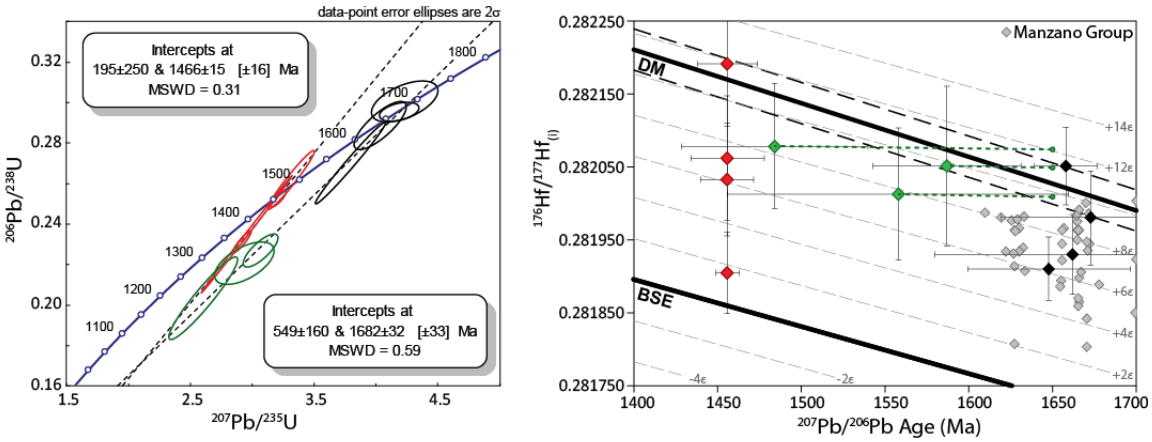

Figure 2-12. Summary of U-Pb and Lu-Hf data from the Priest pluton. >90% concordant analyses used to calculate the crystallization age of the Priest pluton are shown in red. >90% concordant inherited zircon cores are shown in black. Discordant analyses are shown in green. The Hf-isotope composition of discordant grains is recalculated and projected at 1650 Ma (dashed green lines).

The U-Th-Pb isotope system in zircon can be disturbed if crystals experience metamictization followed by diffusion or fluid-driven alteration that mobilizes Pb (Mezger, 1997). However, diffusion of Hf is extremely slow in zircon (Cherniak and Watson, 2003), so Pb-loss events should leave the Hf-isotope composition of zircon unaffected unless there is dissolution and reprecipitation of newly formed zircon (Amelin et al., 2000). The result of Pb-loss in $^{207}Pb^*/^{206}Pb^*$ vs. $^{176}Hf/^{177}Hf(i)$ space is a series of analyses that fall on a line with a slope ≈ 0 (Amelin et al., 2000; Ibanez-Mejia, 2015). The Hf-isotope composition of four discordant grains from the Priest pluton define a horizontal trend originating at the depleted mantle at ~1650 Ma (Figure 2-12). As juvenile 1650 Ma detrital zircon grains are the most abundant population in the Manzano Group, it is likely that these discordant grains are Paleoproterozoic detrital zircon grains that were either entrained in the Priest pluton during partial melting of Manzano Group-like sedimentary rocks at a deeper crustal level, or from the Manzano Group wallrocks during emplacement.

Interpretations and Tectonic Implications from U-Pb and Hf-isotope Data

Regional Correlations

Detrital zircon geochronology and Hf-isotope studies of Proterozoic sedimentary successions in southwestern Laurentia have identified several distinct basin systems (Doe, 2014; Holland et al., 2018). In this section, we expand on these regional correlations and include new data from New Mexico. In our proposed correlations, we do not mean to suggest that the successions described were necessarily deposited in the same basins, we only intend to highlight similar lithologic, geochronologic, and isotopic packages of rock to work towards a comprehensive tectonic model for the formation of Paleoproterozoic crust in southwestern Laurentia.

1.75- 1.72 Ga Basement Complexes Zircon grains from our oldest plutonic sample from the Maquanita granodiorite in the Tusas Mountains yields a range of Hf-isotope compositions, indicating that multiple sources contributed to its genesis. However, 12 of the 15 Hf-isotope analyses conducted on 1758 Ma zircon grains yielded Hf-isotope compositions that overlap within 2-sigma uncertainty, and indicate that the Maquanita granodiorite was derived from a predominantly juvenile source with minor older crustal contamination. This Hf-isotope composition is typical of Yavapai province crust (Bickford et al., 2008; Holland et al., 2015), and supports that the correlation between the 1.76-1.73 Ga basement complexes of northern New Mexico and basement complexes of the Yavapai province of Arizona, such as the Yavapai Supergroup and Grand Canyon Metamorphic Suite (Doe, 2014; Holland et al., 2015), and southern Colorado (Bickford et al., 2008) (Figure 2-13). Overall, northern New Mexico basement

is interpreted to made up of 1760 to 1720 Ma, dominantly juvenile, volcanic and plutonic arc rocks with local >1.8 Ga lower crustal components (Bickford et al., 2008).

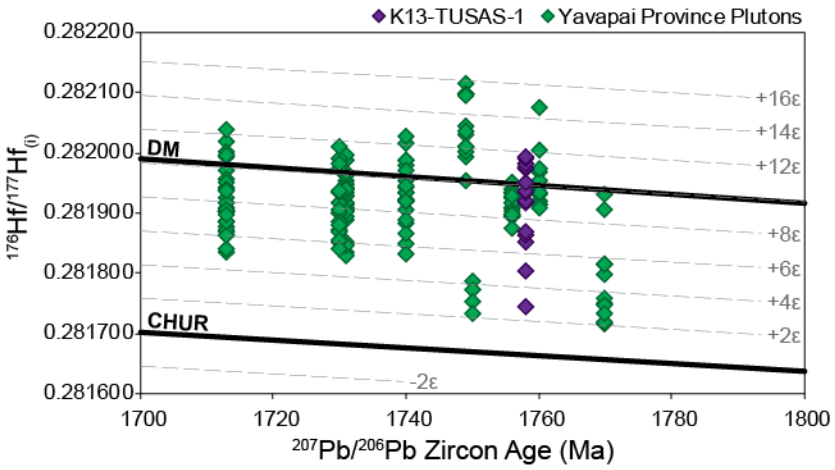

Figure 2-13. Comparison of U-Pb and Hf-isotope data from the Maquanita granodiorite (Tusas Mountains) with Yavapai province basement (Bickford et al., 2008; Holland et al., 2015). Diagram and symbols as in Figure 9.

1.72-1.70 Ga Vadito Group The contact between the Mopin/Maquinita complex and the overlying Vadito Group is unconformable or tectonic in nature. Metasedimentary rocks in the Vadito Group are characterized by strongly unimodal detrital zircon signatures from within a mixed lithotectonic package of primarily rhyolites and quartzites (Jones et al., 2011; Daniel et al., 2013). The supracrustal rocks in the San Pedro Mountains are lithologically similar to the Vadito Group (Bauer and Williams, 1989), with felsic metavolcanics and quartzofeldspathic metasedimentary rocks being the predominant lithologies. Our sample of quartzite from the San Pedro Mountains yielded a dramatically unimodal detrital zircon age population, with a peak age at 1720 Ma. Hf-isotope analysis of detrital zircon from the San Pedro quartzite are overwhelmingly juvenile, with a spread of εHf(t) values ranging from +14.2 to +6.4 at 1.72 Ga. Some of the highest values barely plot within 2-sigma uncertainty of the coeval depleted mantle model array value of +10.0, suggesting that the sample was derived almost exclusively

from juvenile Yavapai province crust. We suggest that the supracrustal rocks in the San Pedro Mountains correlate with the Vadito Group, expanding on the inferred depositional area of the Pilar basin (Jones et al., 2011) (Figure 2-14). Hf-isotopes indicate that detrital zircon grains were derived from local juvenile 1.72 Ga volcano-plutonic basement, likely from basement complexes of northern New Mexico or even the underlying San Pedro Park basement (Karlstrom et al., 2004).

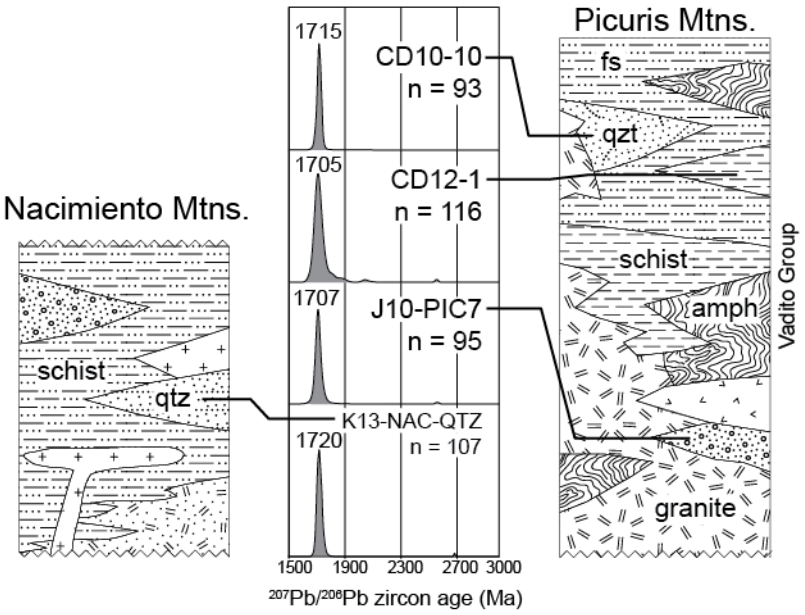

Figure 2-14. Correlation diagram between the San Pedro and Picuris Mountains. Schematic stratigraphic section of Paleoproterozoic supracrustal rocks in the northern Nacimiento Mountains based on lithologic descriptions by Woodward (1974). Schematic stratigraphic section of the Vadito Group in the Picuris Mountains modified after Daniel et al. (2013). Detrital zircon age populations in the San Pedro quartzite (K13-NAC-QTZ) and the Vadito Group are markedly similar. Both locations are characterized by strongly unimodal age peaks with minor components of >1.8 Ga zircon.

Our new geochronologic results from the Posos Lake and Cerro Colorado metarhyolites constrain deposition of the Vadito Group between 1705-1699 Ma. Furthermore, the Hf-isotope composition of Vadito Group metarhyolites is juvenile at 1.7 Ga, similar to underlying basement complexes. This suggests protracted juvenile magmatism in the Yavapai province from at least 1.76-1.70 Ga. The high silica – high

alkali rhyolites of the Vadito Group have been interpreted to be related to eruptions of voluminous ash flow tuffs from calderas, including an interpreted caldera at Cerro Colorado. Hf-isotope compositions in zircon grains from metarhyolites in the Vadito Group indicate a juvenile source (Figure 2-2).

1.70 Hondo Group The 1.70 Ga Hondo Group is also characterized by prominent unimodal detrital zircon age populations (Jones et al., 2009; 2011; Daniel et al., 2013). However, the range of ages present in the Ortega and Rinconada formations expands up-section such that probability density distributions show broader age peaks (see Figure 5 in Daniel et al., 2013). This progressive change in detrital zircon populations is coupled with a lithologic shift from immature felsic schists and interbedded metarhyolites of the Vaditio Group to the distinctive ultramature Ortega quartzite, and interlayered schists and quartzites of the Rinconada Formation.

Summary of Northern New Mexico U-Pb and Hf-isotope Data

Paired U-Pb and Lu-Hf isotope data from plutonic, volcanic, and detrital zircon in northern New Mexico suggest the following sequence of events: 1) formation of 1.76-1.72 Ga juvenile arc-related basement represented by the Moppin, Gold Hill, and Pecos complexes, 2) eruption of extensive caldera-related juvenile rhyolites, and deposition of intercalated immature siliciclastic metasedimentary rocks derived almost exclusively from crust of the same age and Hf-isotope composition of underlying basement and interlayered metarhyolites, 3) continued deposition of siliciclastic sedimentary rocks with a shift towards more compositionally mature sediments, possible basin deepening indicated by schist and phyllitic rocks in the Rinconada Formation, and a wider

provenance indicated by up-section broadening probability density distributions of detrital zircon geochronologic data.

Central New Mexico

An apparently separate but similar succession of basement complexes, metarhyolites, siliciclastic metasedimentary rocks, and plutonic rocks exists in central New Mexico, and is exemplified by the Sandia-Manzano-Los Pinos uplift. Similar to the regional extent of the Vadito and Hondo Groups, the central New Mexico succession extends as far west as the Zuni Mountains, east to the Pedernal Hills, and may include successions in the San Andres and Burro Mountains of southern New Mexico.

Zuni Mountains. The Zuni Mountains are dominated by metarhyolite and quartz monzonite that are proposed to be part of an extensive batholith-rhyolite complex system correlative with similar rocks in the Sandia-Manzano-Los Pinos uplift (Bowring and Condie, 1982; Strickland et al., 2003). Our new U-Pb and Hf-isotope further strengthen this correlation, and suggest the presence of a >1.8 Ga crustal component involved in the genesis of the Zuni Mountains metarhyolite (Figure 2-9C).

The Sandia-Manzano-Los Pinos Mountains. The lower Manzano Group in central New Mexico is displays a similar succession of lithologies, and isotopic compositions as the northern New Mexico cover sequences, yet is ~15 Ma younger. Overlying the greenstone complex throughout the Sandia, Manzano, and Los Pinos mountains is the 1665 Ma Sevilleta metarhyolite. Hf-isotope compositions of zircon from the Sevilleta metarhyolite are identical to that of coeval depleted mantle, indicating a juvenile source for rhyolite volcanism similar to the Zuni Mountains, and Vadito Group. Immature clastic metasedimentary rocks of the Manzano Group grade up-section into

mature quartzites, and eventually interlayered schists and quartzites of the Blue Springs Formation which are interlayered with 1621 and 1602 Ma rhyolite flows (Wallace, 2014; Jones, unpubl.). Detrital zircon populations in the Manzano group are strongly unimodal, similar to the Vadito and Hondo groups, and display a similar broadening of probability density distributions. Two samples of quartzites within the Blue Springs Formation are dominated by 1.8-1.7 Ga detritus (Wallace, 2014; Nagotko, 2015), and include several Archean detrital zircons similar in age to those described in the Vishnu Basin of the Mojave crustal province (Holland et al., 2018). Hf-isotope data from the lower Manzano Group support derivation of much of the detritus in the Manzano Group from underlying juvenile plutonic and rhyolitic rocks (Figure 2-11).

Supracrustal rocks of the Manzano Group have been correlated across the entire Sandia-Manzano-Los Pinos uplift (Luther, 2006) and metasedimentary rocks with similar characteristics also exist in southern New Mexico (Amato et al., 2008). Quartzofeldspathic schists in the Burro Mountains and a quartzite from the San Andres Mountains yield detrital zircon age populations similar to those of the Manzano Group (Figure 2-15). Maximum depositional ages determined from the youngest detrital zircon grains in the Burro and San Andres Mountains are nearly identical to the Manzano Group, with maximum depositional ages of 1670-1646 Ma (Figure 2-15). These data suggest widespread deposition of locally derived quartz-rich metasedimentary rocks throughout the Mazatzal province at ~1.65 Ga.

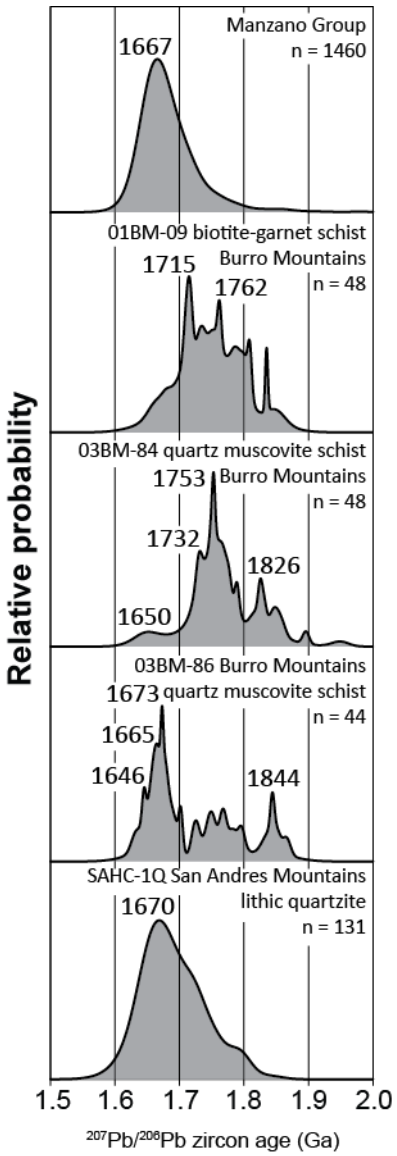

Figure 2-15. PDD plots of Paleoproterozoic metasedimentary rocks from central and southern New Mexico.

Summary of Central New Mexico

Paired U-Pb and Lu-Hf isotope data from plutonic, volcanic, and detrital zircon in central New Mexico suggest the following sequence of events: 1) formation of ≥1.65 Ga greenstone belts capped by the 1.65 Ga Sevilleta metarhyolite, 2) deposition of immature siliciclastic sedimentary rocks derived almost entirely from crust of the same age and Hf-isotope composition of underlying metarhyolite and intrusive plutonic bodies, 3)

continued deposition of siliciclastic sedimentary rocks with a shift towards more compositionally mature sediments, possible basin deepening indicated by schist and phyllitic rocks in the Blue Springs Formation, and a wider provenance indicated by up-section broadening probability density distributions of detrital zircon geochronologic data.

Mesoproterozoic Plutons

1.45 Ga plutons that intrude Paleoproterozoic crust of the Yavapai and Mazatzal provinces have been interpreted as the result of partial melting of the lower crust during extensive intracratonic tectonism (Shawl et al., 2005; Goodge and Vervoort, 2006). The Hf-isotope composition of most zircon separated from the Guadalupe Box, Sandia, and Priest plutons fall between εHf(t) values of +8 to +4 at ~1.45 Ga. These values are similar to the averages reported by Goodge and Vervoort for ~1.48-1.42 Ga plutons much further north in the Yavapai province. Regionally, there is no discernable difference in Hf-isotope compositon between the Mesoproterozoic plutons that intrude the Yavapai vs. Mazatzal crustal provinces. This may indicate that there is >1.7 Ga crustal material underlying much of the Mazatzal province, as also suggested by Paleoproterozoic pluton Hf data.

Interestingly, each Mesoproterozoic plutonic sample analyzed in this study yielded a single Hf-isotope analysis nearly equal to the coeval depleted mantle array (Figure 2-16). A distinctive feature of the 1.4 Ga magmatic suite in New Mexico and elsewhere is the abundance of mafic enclaves (e.g. sample K13-NAC-2B). These enclaves have been interpreted as the result of magma mixing due to injection of basaltic melts into the granitic magma chambers. Systematic differences in Hf-isotope

composition between mafic envlaves and host rocks indicating a juvenile mafic component have been documented (Yang et al., 2007). However, sample K13-NAC-2A and K13-NAC-2B were analyzed separately specifically to test for Hf-isotope variation due to textural and compositional differences, and yielded indistinguishable Hf-isotope compositions. In fact, the single zircon grain that yielded a depleted mantle like value came from sample K13-NAC-2A, which contained fewer mafic enclaves.

Lower crustal xenoliths from the Four Corners region contain igneous zircon grains with εHf(t) values ranging from +4 to +7 at 1.43 Ga, typical of similarly aged granitic rocks (Figure 2-16), however abundant metamorphic zircon yield εHf(t) values ranging from -0.7 to +13.6 at ~1.4 Ga (Crowley et al., 2006). These data suggest that lower crustal metamorphic zircon grew from extremely heterogeneous sources, likely involving a variety of fluid compositions and rock types (Crowley et al., 2006). Recent Sm-Nd isotope analysis of mantle xenoliths from the Four Corners region also suggested mantle melt extraction and/or metasomatic event at 1.4 Ga (Marshall et al., 2017), consistent with the petrogenetic model of lower crustal anataxis due to mafic underplating (Shaw et al., 2005; Crowley et al., 2006). It is possible that minor components of mantle derived melts were mixed into 1.4 Ga plutonic rocks and manifested by zircons with high $^{176}Hf/^{177}Hf_{(i)}$ values.

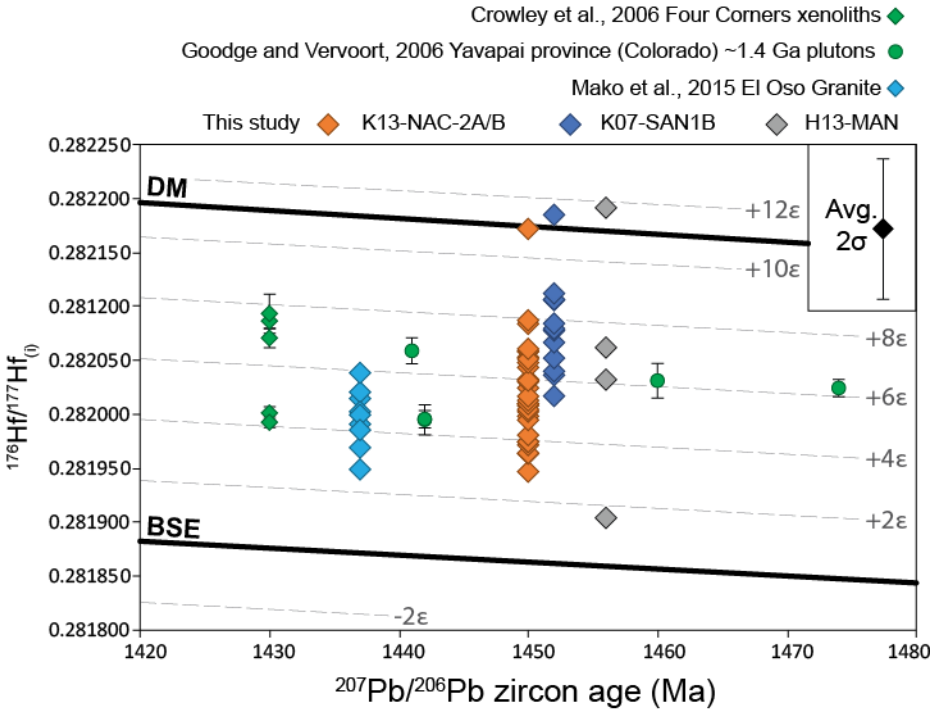

Figure 2-16. Regional summary of Hf-isotope data from 1.48-1.43 Ga plutonic rocks from southwestern Laurentia. Diagram and symbols as in Figure 9.

Towards a Refined Tectonic Model

The Yavapai and Mazatzal provinces have been viewed as juvenile oceanic arc terranes that developed outboard of the Laurentian continent before accretion during the Yavapai and Mazatzal orogenies (Whitmeyer and Karlstrom 2007). However, aspects of this model need refinement in light of recent geochronologic and isotopic studies (Jones et al., 2011; Doe et al., 2012; Daniel et al., 2013; Mako et al., 2015). Based on new U-Pb and Lu-Hf isotope data presented in this paper, we present a refined model for the formation of the Mazatzal crustal province that builds upon the work of Jones et al. (2009).

New insights from this study include: 1) Hf-isotope compositions and inherited zircon grains in plutonic rocks that suggest the presence of >1.8 Ga lower crust in the Mazatzal province, and 2) recognition of repeated cycles of rhyolite volcanism and

sedimentation in the Yavapai and Mazatzal provinces. In conjunction with previous regional structural, metamorphic, and geochronologic studies, these two features lead us to interpret the formation of the Mazatzal as a continental margin arc. The Mazatzal arc formed atop the recently accreted arc terrane(s) of the Yavapai province, and rhyolite-quartzite-schist successions of the Yavapai and Mazatzal provinces were deposited during opening of continental back arc basins on the upper plate of the Mazatzal arc system. These basins were episodically inverted before the North American tectonic gap and subsequent reactivation during the Picuris orogeny. Our model is shown in time-slice cross sectional views in Figure 2-17. In each time-slice, the crustal substrate for each stage is recorded by the Hf isotopic composition of the nearly coeval plutonic and volcanic rocks, basin setting is recorded by detrital zircon data, and tectonic setting is recorded by field and geochronologic constraints on deformation and metamorphism.

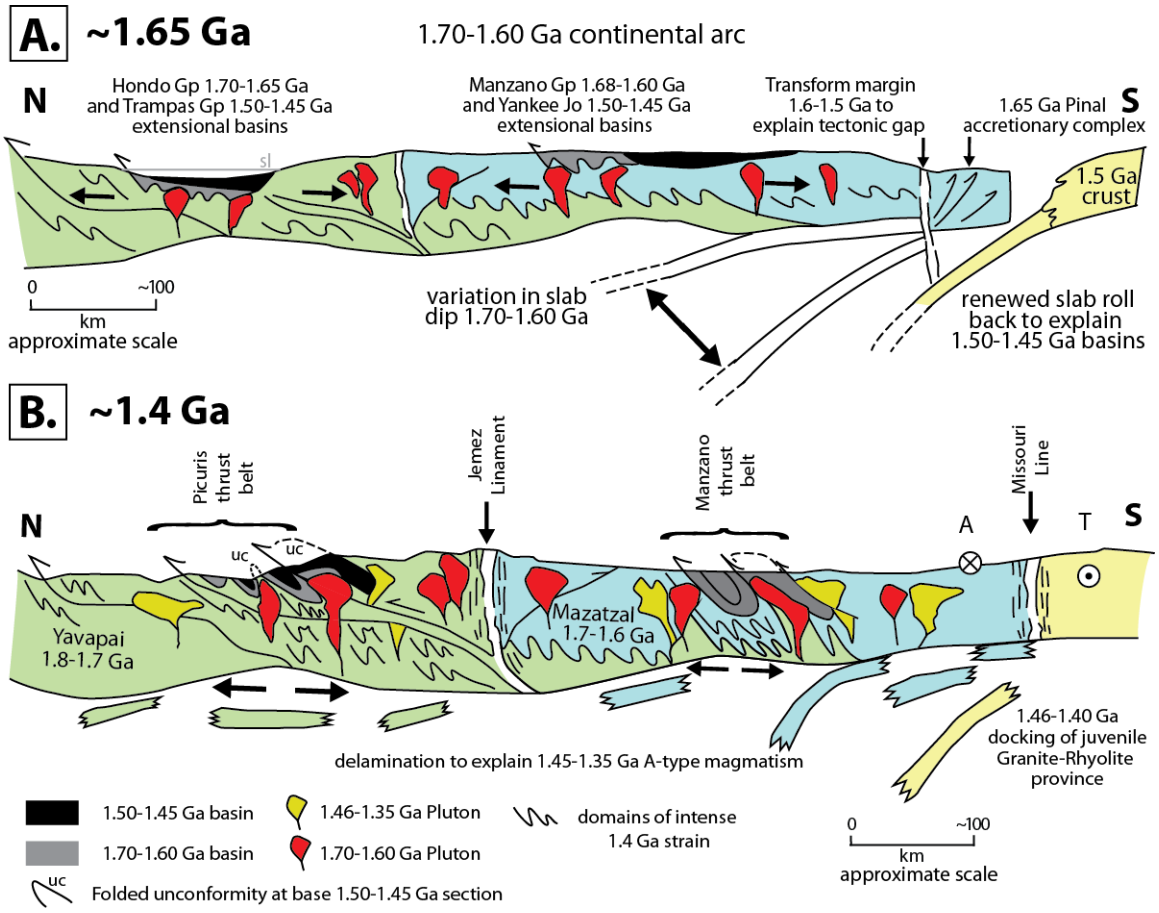

Figure 2-17. Tectonic model for the Proterozoic evolution of the Mazatzal crustal province. A) The Mazatzal province forms as a continental margin arc atop of the recently accreted Yavapai province. The composite Yavapai-Mazatzal arc system is extended due to slab rollback, and locally derived quartzite basins are deposited in an intra and/or rear arc basin setting(s). Plutonic rocks in the Manzano Mountains are emplaced at 0.2-0.3 GPa (~8-12 km depths) with field evidence suggesting syn-tectonic emplacement. Episodic slab shallowing or coupling with the overriding plate may have caused some solid-state fabric development. B) Following the North American tectonic gap, flat slab subduction along the margin of the Granite-Rhyolite province causes intracratonic deformation of the Mazatzal and Yavapai provinces. Voluminous Mesoproterozoic granitic magmatism is the result of delamination after flat slab subduction.

Paleoproterozoic basement in norther New Mexico formed during accretion of arc terranes during the Yavapai orogeny (Karlstrom and Bowring, 1988). Hf-isotope data from the Maquanita granodiorite in the Tusas Mountains strengthen the correlation

between northern New Mexico basement complexes and those of the Yavapai province in Arizona and Colorado (Holland et al., 2015; Bickford et al., 2008).

After the accretion of the Yavapai province, deposition of the Vadito Group took place between 1705-1699 Ma. Hf-isotope compositions from the Posos Lake and Cerro Colorado metarhyolites are juvenile at 1.7 Ga. Immature metasedimentary rocks in the Vadito Group were derived almost exclusively from local Yavapai basement and interlayered metarhyolites, as indicated by their prominent unimodal detrital zircon age peaks from 1720-1705 Ma, and juvenile Hf-isotope compositions. The Vadito Group grades conformably into the ultramature Ortega quartzite. The Ortega quartzite yields strongly unimodal detrital zircon populations, however displays a wider range of ages, as indicated by broadening probability density distributions. This trend continues into interlayered schists and quartzite of the Rinconada Formation, which has a maximum depositional age of 1679 Ma (Daniel et al., 2013). We interpret this sequence of juvenile rhyolite magmatism, followed by locally derived immature sedimentary rocks that grade into mature quartzites and schists as the opening of a continental margin back arc basin. Deformation of the Vadito Group involved refolded folds that may record more than one basin closure, and the details of the relative importance of Mazatzal versus Picuris orogeny fabrics has been difficult to evaluate because of the intense fabric formation at triple point conditions at 1.4 Ga in the Picuris and southern Tusas Mountains. The northern Tusas Moutains may preserve 1.69 Ga fabrics recorded by the 1693 Ma Tusas Mountain orthogneiss (Davis et al., 2011), and 1680-1670 Ma monazite growth (Kopera et al., 2002).

A second cycle of rhyolite volcanism and sedimentation is recorded in central New Mexico. Rhyolite volcanism in the Zuni Mountains, Pedernal Hills, and the Sandia-Manzano-Los Pinos uplift was active from 1665-1655 Ma, and in the Manzano Moutains, is characterized by juvenile Hf-isotope compositions. The 1665 Ma Sevilleta metarhyolite forms the base of the Manzano Group, grades from lithic arenite of the Abajo Formation into mature quartzites of the White Ledge and Sais Formations, and ultimately interlayered quartzite and schist of the Blue Springs Formation. Detrital zircon populations in the Manzano Group are unimodal, and suggest derivation from the underlying metarhyolite. Similar to the Vadito and Hondo Groups, detrital zircon age populations in the Manzano Group broaden to include more far-travelled detritus in the Blue Springs Formation (Wallace, 2014; Nagotko, 2015). Archean detrital zircon grains in the Blue Springs Formation are similar to those preserved in the Vishnu basin (Holland et al., 2015; 2018), and may have been recycled from portions of the Vishnu basin uplifted during the Yavapai orogeny. These data suggest that the Mazatzal province formed in a tectonic environment that was able to receive detritus from Laurentian highlands, and thus could not have evolved as an outboard oceanic arc terrane. Hence we favor an extended continental margin arc, and associated back arc basins model to accommodate the presence of older Laurentian detritus in the Mazatzal province. Plutonic rocks that intrude the Manzano Group yield Hf-isotope compositions consistent with their derivation from >1.8 Ga crustal material, which is supported by the presence of xenocrystic zircon grains in several plutonic rocks throughout the Sandia-Manzano-Los Pinos uplift, supporting a continental margin arc built atop the recently accreted Yavapai province.

Our model for variable older crustal components in the Mazatzal province also is compatible with Nd-isotope data from migmatites and orthogneisses in the Burro Mountains, southern New Mexico, which yield model ages ranging from 2.0-1.78 Ga (Amato et al., 2008). This model is also in agreement with Hf-isotope data from 1.68-1.65 Ga plutons in the Four Peaks region, AZ that suggest the involvement of 2.0-1.7 Ga lower crust in their genesis, including the presence of >1.7 Ga xenocrystic zircon grains in orthogneisses (Mako et al., 2015). Similarities between quartzites of the Manzano Group and quartzites in southern New Mexico (Amato et al., 2008 (Figure 2-15), suggest that the entire Mazatzal province developed in a tectonic setting that allowed Laurentian detritus to be shed into Mazatzal province basins.

Deformation in the Sandia-Manzano-Los Pinos uplift is similar in style to that of the Tusas Mountains. Three generations of fabric development and folding are recording the Manzano and Los Pinos mountains, although the precise timing of their development is uncertain. The 1.66-1.65 Ga Manzanita, Ojito, and Los Pinos plutons were interpreted to have been emplaced syn-tectonically (Brown et al., 1999; Luther, 2006), and the 1.45 Ga Priest pluton cross cuts a km-scale syncline and axial planar cleavage. The Blue Springs metarhyolite in the core of this syncline was dated at 1621 ±5 Ma (Wallace, 2014), suggesting that the fold and axial planar fabric developed between 1621-1452 Ma during either the Mazatzal or Picuris orogenies.

The North American tectonic gap represents a protracted period of tectonic quiescence (Karlstrom et al., 2004). The tectonic gap remains an enigmatic feature of southern Laurentia, but likely represents the first lengthy period of lithospheric stability. In southern Arizona, the Pinal province has been interpreted as an accretionary complex

that experienced an ocean spreading center subduction event at ~1.65 Ga (Meijer, 2014), although the timing of this event is poorly constrained. It is possible that the subduction of a mid ocean ridge or other mechanisms that shifted the locus of subduction farther outboard could have converted the previously long-lived 1.8-1.6 Ga convergent margin responsible for the growth of the Mojave, Yavapai, and Mazatzal crustal provinces into a trans-current plate margin analogous to the subduction of the East Pacific Rise beneath western North America in the Oligocene (Atwater, 1970) (Figure 2-17).

After the 1.6-1.5 Ga North American tectonic gap, the Paleoproterozoic crust of the Mazatzal province was deformed and metamorphosed during the 1.49-1.45 Ga Picuris orogeny (Daniel et al., 2013; Mako et al., 2015). During and outlasting the Picuris orogeny, voluminous Mesoproterozoic plutonic rocks intruded into Paleoproterozoic crust of southern Laurentia from 1.49-1.34 Ga (Bickford et al., 2015). These plutons were derived from lower crustal anataxis in response to mantle-derived melts ponding at the base of the crust (Shaw et al., 2005; Marshall et al., 2017). A possible analogue for such intracratonic tectonism is the Laramide orogeny. During the Laramide orogeny, flat slab subduction drove deformation over 1000 km inboard of the North American plate boundary (Yonkee and Weil, 2015) (Figure 2-17). The Laramide slab then delaminated from the base of the North American plate (Humphreys, 1995), and gave rise to the voluminous ignimbrite flare-up in the western United States (Farmer et al., 2008).

CONCLUSIONS

In conjunction with previous structural, metamorphic, and geochronologic studies, paired U-Pb and Lu-Hf data from northern and central New Mexico help refine models for the origin and evolution of the southern Yavapai and Mazatzal crustal

provinces. Regional sampling of plutonic, metavolcanic, and metasedimentary rocks from the Yavapai and Mazatzal provinces have identified two major cycles of rhyolite volcanism and sedimentation. The tectonic evolution of southern Laurentia involved recurring pulses of magmatism, basin formation, and deformation involving alternating extensional opening of basins during slab rollback and their contractional closure due plate convergence. Hf-isotope compositions of igneous and detrital zircon in the Mazatzal province support a model where slab rollback allowed upwelling of asthenospheric mantle, giving rise to extensive juvenile magmatism from 1.7-1.6 Ga and mixing of juvenile melts with older crust.

Following crustal growth from 1.7-1.6 Ga, a spreading center subduction event, or alternative mechanisms to shift from contractional to transcurrent plate margin tectonism terminated subduction by converting the convergent margin into a trans current margin. The North American tectonic gap represents a period of relative lithospheric stability due to the cessation of subduction and a period of erosion of Mazatzal highlands.

The Mesoproterozoic Picuris orogeny resulted in intense intracratonic deformation from 1.49-1.45 Ga, and resulted in the formation of many major structures and fabrics in the Mazatzal province. Synchronous with and outlasting the Picuris orogeny, Paleoproterozoic crust of southwestern Laurentia was perforated with voluminous granitic intrusions from 1.48-1.35 Ga (Bickford et al., 2015). These magmas were the result of lower crustal melting driven by slab delamination and basaltic underplating of Laurentian crust. The Hf-isotope composition of Mesoproterozoic plutonic rocks supports their derivation from juvenile Paleoproterozoic crust typical of the Yavapai and Mazatzal crustal provinces.

This tectonic model represents a synthesis of decades of geologic investigation into the Proterozoic crust of southwestern Laurentia. The model presented herein offers comparisons to Phanerozoic orogenic systems, and provides new testable hypotheses to further evaluate the origin and evolution of Paleoproterozoic lithosphere in the southwestern United States.

REFERENCES CITED

Amato, J.M., Boullion, A.O., Serna, A.M., Sanders, A.E., Farmer, G.L., Gehrels, G.E., and Wooden, J.L., 2008, Evolution of the Mazatzal province and the timing of the Mazatzal orogeny: Insights from U-Pb geochronology and geochemistry of igneous and metasedimentary rocks in southern New Mexico: Bulletin of the Geological Society of America, v. 120, p. 328–346, doi: 10.1130/B26200.1.

Amato, J.M., Heizler, M.T., Boullion, A.O., Sanders, A.E., Toro, J., Virginia, T., and Andronicos, C.L., 2011, Syntectonic 1 . 46 Ga magmatism and rapid cooling of a gneiss dome in the southern Mazatzal Province : Burro Mountains , New Mexico: , p. 1–25, doi: 10.1130/B30337.1.

Amelin, Y., Lee, D., and Halliday, A.N., 2000, Early-middle Archaean crustal evolution deduced from Lu-Hf and U-Pb isotopic studies of single zircon grains: Geochimica et Cosmochimica Acta, v. 64, p. 4205–4225, doi: 10.1016/S0016-7037(00)00493-2.

Atwater, T., 1970, Implications of Plate Tectonics for the Cenozoic Tectonic Evolution of Western North America: Geological Society of America Bulletin, v. 81, p. 3513–3536.

Baer, S., 2004, Geologic and tectonic evolution of the Manzano Peak Quadrangle, central New Mexico: University of New Mexico, 78 p.

Bauer, P.W., Karlstrom, K.E., Bowring, S.A., Smith, A.G., and Goodwin, L.B., 1993, Proterozoic plutonism and regional deformation—new constraints from the southern Manzano Mountains, central New Mexico: New Mexico Geology Science and Service, v. 15, p. 49–77.

Bauer, P.W., and Williams, M.L., 1988, Stratigraphic nomenclature of Proterozoic rocks, northern New Mexico - revisions, redefinitions, and formalization: New Mexico Geology Science and Service, v. 11, p. 45–52.

Bennett, V.C., and DePaolo, D.J., 1987, Proterozoic crustal history of the western United States as determined by Nd mapping: Geological Society of America Bulletin, v. 99, p. 674–685, doi: 10.1130/0016-7606(1987)99<674:PCHOTW>2.0.CO;2.

Bickford, M.E., Mueller, P.A., Kamenov, G.D., and Hill, B.M., 2008, Crustal evolution of southern Laurentia during the Paleoproterozoic: Insights from zircon Hf isotopic studies of ca. 1.75 Ga rocks in central Colorado: Geology, v. 36, p. 555–558, doi: 10.1130/G24700A.1.

Bickford, M.E., Van Schmus, W.R., Karlstrom, K.E., Mueller, P.A., and Kamenov, G.D., 2015, Mesoproterozoic-trans-Laurentian magmatism: A synthesis of continent-wide age distributions, new SIMS U-Pb ages, zircon saturation temperatures, and Hf and Nd isotopic compositions: Precambrian Research, v. 265, p. 286–312, doi: 10.1016/j.precamres.2014.11.024.

Brown, C.L., Karlstrom, K.E., Heizler, M., and Unruh, D., 1999, New Mexico Geological Society of the 1 . 65 GA Manzanita Pluton , Manzanita Mountains , New Mexico: , p. 255–268.

Cawood, P.A., Hawkesworth, C.J., and Dhuime, B., 2012, Detrital zircon record and

tectonic setting: Geology, v. 40, p. 875–878, doi: 10.1130/G32945.1.

Cawood, P. a., Kroner, a., Collins, W.J., Kusky, T.M., Mooney, W.D., and Windley, B.F., 2009, Accretionary orogens through Earth history: Geological Society, London, Special Publications, v. 318, p. 1–36, doi: 10.1144/SP318.1.

Chappell, B.W., and White, A.J.R., 2001, Two contrasting granite types: 25 years later: Australian Journal of Earth Sciences, v. 48, p. 489–500, doi: 10.1046/j.1440-0952.2001.00882.x.

Cherniak, D.J., and Watson, B.E., 2003, Diffusion in Zircon: Reviews in Mineralogy and Geochemistry, v. 53, p. 113–143.

Condie, K.C., 1982, Plate-tectonics model for Proterozoic continental accretion in the southwestern United States: Geology, v. 10, p. 37–42, doi: 10.1130/0091-7613(1982)10<37.

Condie, K.C., and McCrink, T.P., 1982, Geochemistry of Proterozoic volcanic and granitic rocks from the Gold Hill-Wheeler Peak area, northern New Mexico: Precambrian Research, v. 19, p. 141–166, doi: 10.1016/0301-9268(82)90056-0.

Corfu, F., Hanchar, J.M., Hoskin, P.W.O., and Kinny, P., 2003, Atlas of Zircon Textures: Reviews in Mineralogy and Geochemistry, v. 53, p. 469–500, doi: 10.2113/0530469.

Crowley, J.L., Schmitz, M.D., Bowring, S.A., Williams, M.L., and Karlstrom, K.E., 2006, U-Pb and Hf isotopic analysis of zircon in lower crustal xenoliths from the Navajo volcanic field: 1.4 Ga mafic magmatism and metamorphism beneath the Colorado Plateau: Contributions to Mineralogy and Petrology, v. 151, p. 313–330, doi: 10.1007/s00410-006-0061-z.

Daniel, C.G., Pfeifer, L.S., Jones, J. V., and McFarlane, C.M., 2013, Detrital zircon evidence for non-laurentian provenance, mesoproterozoic (ca. 1490-1450 ma) deposition and orogenesis in a reconstructed orogenic belt, northern new mexico, USA: Defining the picuris orogeny: Bulletin of the Geological Society of America, v. 125, p. 1423–1441, doi: 10.1130/B30804.1.

Daniel, C.G., and Pyle, J.M., 2006, Monazite-Xenotime thermochronometry and Al2SiO5 reaction textures in the Picuris range, Northern New Mexico, USA: New evidence for a 1450-1400 Ma orogenic event: Journal of Petrology, v. 47, p. 97–118, doi: 10.1093/petrology/egi069.

Davis, P., Williams, M., and Karlstrom, K., 2011, New Mexico Geological Society Structural evolution and timing of deformation along the Proterozoic Spring Creek shear zone of the northern Tusas Mountains, New Mexico: New Mexico Geological Society Guidebook, 62nd Field Conference, p. 177–190.

Doe, M.F., Jones, J. V., Karlstrom, K.E., Dixon, B., Gehrels, G., and Pecha, M., 2013, Using detrital zircon ages and Hf isotopes to identify 1.48-1.45Ga sedimentary basins and fingerprint sources of exotic 1.6-1.5Ga grains in southwestern Laurentia: Precambrian Research, v. 231, p. 409–421, doi: 10.1016/j.precamres.2013.03.002.

Doe, M.F., Jones, J. V., Karlstrom, K.E., Thrane, K., Frei, D., Gehrels, G., and Pecha, M., 2012, Basin formation near the end of the 1.60-1.45 Ga tectonic gap in southern Laurentia: Mesoproterozoic Hess Canyon Group of Arizona and implications for ca. 1.5 Ga supercontinent configurations: Lithosphere, v. 4, p. 77–88, doi: 10.1130/L160.1.

Farmer, G.L., Bailley, T., and Elkins-Tanton, L.T., 2008, Mantle source volumes and the

origin of the mid-Tertiary ignimbrite flare-up in the southern Rocky Mountains, western U.S.: Lithos, v. 102, p. 279–294, doi: 10.1016/j.lithos.2007.08.014.

Flowerdew, M.J., Millar, I.L., Vaughan, A.P.M., Horstwood, M.S.A., and Fanning, C.M., 2006, The source of granitic gneisses and migmatites in the Antarctic Peninsula: A combined U-Pb SHRIMP and laser ablation Hf isotope study of complex zircons: Contributions to Mineralogy and Petrology, v. 151, p. 751–768, doi: 10.1007/s00410-006-0091-6.

Gerdes, A., and Zeh, A., 2009, Zircon formation versus zircon alteration - New insights from combined U-Pb and Lu-Hf in-situ LA-ICP-MS analyses, and consequences for the interpretation of Archean zircon from the Central Zone of the Limpopo Belt: Chemical Geology, v. 261, p. 230–243, doi: 10.1016/j.chemgeo.2008.03.005.

Goodge, J.W., and Vervoort, J.D., 2006, Origin of Mesoproterozoic A-type granites in Laurentia: Hf isotope evidence: Earth and Planetary Science Letters, v. 243, p. 711–731, doi: 10.1016/j.epsl.2006.01.040.

Holland, M.E., Karlstrom, K.E., Doe, M.F., Gehrels, G.E., Pecha, M., Shufeldt, O.P., Begg, G., Griffin, W.L., and Belousova, E., 2015, An imbricate midcrustal suture zone: The mojave-yavapai province boundary in grand canyon, arizona: Bulletin of the Geological Society of America, v. 127, p. 1391–1410, doi: 10.1130/B31232.1.

Holland, M.E., Karlstrom, K.E., Gehrels, G., Shufeldt, O.P., Begg, G., Gri, W., and Belousova, E., 2018, The Paleoproterozoic Vishnu basin in southwestern Laurentia : Implications for supercontinent reconstructions , crustal growth , and the origin of the Mojave crustal province: v. 308, p. 1–17, doi: 10.1016/j.precamres.2018.02.001.

Humphreys, E.D., 1995, Post-Laramide removal of the Farallon slab,western United

States: Geology, v. 23, p. 987–990, doi: 10.1130/0091-7613(1995)023<0987.

Ibanez-Mejia, M., Pullen, A., Arenstein, J., Gehrels, G.E., Valley, J., Ducea, M.N., Mora, A.R., Pecha, M., and Ruiz, J., 2015, Unraveling crustal growth and reworking processes in complex zircons from orogenic lower-crust: The Proterozoic Putumayo Orogen of Amazonia: Precambrian Research, v. 267, p. 285–310, doi: 10.1016/j.precamres.2015.06.014.

Ilg, B.R., Karlstrom, K.E., Hawkins, D.P., and Williams, M.L., 1996, Tectonic evolution of Paleoproterozoic rocks in the Grand Canyon: Insights into middle-crustal processes: Bulletin of the Geological Society of America, v. 108, p. 1149–1166, doi: 10.1130/0016-7606(1996)108<1149:TEOPRI>2.3.CO;2.

Jessup, M.J., Jones III, J.V., Karlstrom, K.E., Williams, M.L., Connelly, J.N., and Heizler, M.T., 2006, Three Proterozoic Orogenic Episodes and an Intervening Exhumation Event in the Black Canyon of the Gunnison Region, Colorado: The Journal of Geology, v. 114, p. 555–576, doi: 10.1086/506160.

Jessup, M.J., Karlstrom, K.E., Connelly, J., Williams, M., Livaccari, R., Tyson, A., and Rogers, S.A., 2005, Complex proterozoic crustal assembly of southwestern North America in an arcuate subduction system: The Black Canyon of the Gunnison, Southwestern Colorado, *in* Karlstrom, K.E. and Randy Keller, G. eds., Geophysical Monograph Series, p. 21–38.

Jones, J. V., Connelly, J.N., Karlstrom, K.E., Williams, M.L., and Doe, M.F., 2009, Age, provenance, and tectonic setting of Paleoproterozoic quartzite successions in the southwestern United States: Bulletin of the Geological Society of America, v. 121, p. 247–264, doi: 10.1130/B26351.1.

Jones, J. V., Daniel, C.G., Frei, D., and Thrane, K., 2011, Revised regional correlations and tectonic implications of Paleoproterozoic and Mesoproterozoic metasedimentary rocks in northern New Mexico, USA: New findings from detrital zircon studies of the Hondo Group, Vadito Group, and Marquenas Formation: Geosphere, v. 7, p. 974, doi: 10.1130/GES00614.1.

Karlstrom, K.E., Amato, J.M., Williams, M.L., Heizler, M.T., Shaw, C.A., Read, A.S., and Bauer, P.W., 2004, Proterozoic tectonic evolution of the New Mexico region, *in* Mack, G.H. and Giles, K.A. eds., The Geology of New Mexico: A geologic history, New Mexico Geological Society Special Publication 11, p. 1–34.

Karlstrom, K.E., and Bowring, S.A., 1988, Early Proterozoic Assembly of Tectonostratigraphic Terranes in Southwestern North America: The Journal of Geology, v. 96, p. 561–576, doi: 10.1086/629252.

Karlstrom, K.E., and Bowring, S. a, 1993, Proterozoic orogenic history of Arizona, *in* Reed, J.C. ed., Precambrian: Conterminous US: Boulder, Colorado, Geological Society of America, Geology of North America, Boulder, Colorado, Geological Society of America, p. 188–211.

Karlstrom, K.E., Dallmeyer, R.D., and Grambling, J.A., 1997, 40Ar/39Ar Evidence For 1.4 Ga Regional Metamorphism in New Mexico: Implications For Thermal Evolution of Lithosphere in the Southwestern USA: Journal of Geology, v. 105, p. 205–224.

Karlstrom, K.E., and Houston, R.S., 1984, The Cheyenne Belt: Analysis of a Proterozoic suture in southern Wyoming: Precambrian Research, v. 25, p. 415–446.

Kemp, A.I.S., Hawkesworth, C.J., Collins, W.J., Gray, C.M., and Blevin, P.L., 2009,

Isotopic evidence for rapid continental growth in an extensional accretionary orogen: The Tasmanides, eastern Australia: Earth and Planetary Science Letters, v. 284, p. 455–466, doi: 10.1016/j.epsl.2009.05.011.

Kirby, E., Karlstrom, K.E., Andronicos, C.L., and Dallmeyer, R.D., 1995, Tectonic setting of the Sandia pluton: An orogenic 1.4 Ga granite in New Mexico: Tectonics, v. 14, p. 185–201, doi: 10.1029/94TC02699.

Luther, A., 2006, History and timing of polyphase Proterozoic deformation in the Manzano thrust belt, central New Mexico: University of New Mexico, 117 p.

Mako, C.A., Williams, M.L., Karlstrom, K.E., Doe, M.F., Powicki, D., Holland, M.E., Gehrels, G., and Pecha, M., 2015, Polyphase Proterozoic deformation in the Four Peaks area, central Arizona, and relevance for the Mazatzal orogeny: Geosphere, v. 11, p. 1975–1995, doi: 10.1130/GES01196.1.

Marshall, E.W., Lassiter, J.C., Barnes, J.D., Luguet, A., and Lissner, M., 2017, Mantle melt production during the 1 . 4 Ga Laurentian magmatic event : Isotopic constraints from Colorado Plateau mantle xenoliths: v. 45, p. 519–522, doi: 10.1130/G38891.1.

Mawer, C., Grambling, J., Williams, M., Bauer, P., and Robertson, J., 1990, The relationship of the Proterozoic Hondo Group to older rocks, southern Picuris Mountains and adjacent areas, northern New Mexico: New Mexico Geological Society Guidebook: Southern Sangre de Cristo Mountains, v. 41, p. 171–177.

Meijer, A., 2014, The Pinal Schist of southern Arizona: A paleoproterozoic forearc complex with evidence of spreading ridge-trench interaction at ca. 1.65 Ga and a proterozoic arc obduction event: Bulletin of the Geological Society of America, v. 126, p. 1145–1163, doi: 10.1130/B31002.1.

Nagotko, K.N., 2015, Depositional Age Constraints and Provenance of Detrital Zircon Age Populations From the Paleoproterozoic (1650 Ma) Manzano Group, Central New Mexico: Bucknell University, 80 p.

Nyman, M.W., Karlstrom, K.E., Kirby, E., and Graubard, C.M., 1994, Mesoproterozoic contractional orogeny in western North America : Evidence from Mesoproterozoic contractional orogeny in western North America : Evidence from ca . 1 . 4 Ga plutons: Geology, v. 22, p. 901–904, doi: 10.1130/0091-7613(1994)022<0901.

Pullen, A., Ibanez-Mejia, M., Gehrels, G.E., Ibanez-Mejia, J.C., and Pecha, M., 2014, What happens when n= 1000? Creating large-n geochronological datasets with LA-ICP-MS for geologic investigations: Journal of Analytical Atomic Spectrometry, v. 29, p. 971–980, doi: 10.1039/C4JA00024B.

Salters, V.J.M., Mallick, S., Hart, S.R., Langmuir, C.E., and Stracke, A., 2011, Domains of depleted mantle: New evidence from hafnium and neodymium isotopes: Geochemistry, Geophysics, Geosystems, v. 12, doi: 10.1029/2011GC003617.

Shawl, C.A., Heizler, M.T., and Karlstrom, K.E., 2005, Intracontinental Tectonism in the Southern Rocky Mountains : Interplay of Conductive and Advective Heating with Intracontinental Deformation:

Soegarrd, K., and Eriksson, K., 1986, Transition from Arc Volcanism to Stable-Shelf and Subsequent Convergent-Margin Sedimentation in Northern New Mexico from 1 . 76 Ga Author (s): Kristian Soegaard and Kenneth A . Eriksson Source : The Journal of Geology , Vol . 94 , No . 1 (Jan ., 1986): Journal of Geology, v. 94, p. 47–66.

Stracke, A., Snow, J.E., Hellebrand, E., von der Handt, A., Bourdon, B., Birbaum, K., and Günther, D., 2011, Abyssal peridotite Hf isotopes identify extreme mantle

depletion: Earth and Planetary Science Letters, v. 308, p. 359–368, doi: 10.1016/j.epsl.2011.06.012.

Strickland, D., Heizler, M.T., Selverstone, J., and Karlstrom, K.E., 2003, Proterozoic evolution of the Zuni Mountains, western New Mexico: Relationship to the Jemez Lineament and implications for a complex cooling history: New Mexico Geological Society Guidebook, 54th Field Conference, p. 109–117.

Thompson, A.G., 1996, Proterozoic thermal and deformational history and geochemical evolution of hte 1.4 Ga Priest pluton and its aureole: University of New Mexico, 135 p.

Vervoort, J.D., and Blichert-Toft, J., 1999, Evolution of the depleted mantle: Hf isotope evidence from juvenile rocks through time: Geochimica et Cosmochimica Acta, v. 63, p. 533–556, doi: 10.1016/S0016-7037(98)00274-9.

Vervoort, J.D., and Kemp, A.I.S., 2016, Clarifying the zircon Hf isotope record of crust-mantle evolution: Chemical Geology, v. 425, p. 65–75, doi: 10.1016/j.chemgeo.2016.01.023.

Wallace, D.P., 2014, Detrital Zircon Evidence for Mixing of Mazatzal Province Age Detritus with Yavapai Age (ca . 1700-1740 Ma) and Older Detritus in the ca. 1650 Ma Mazatzal Province of Central New Mexico, USA: 54 p.

Whitmeyer, S.J., and Karlstrom, K.E., 2007, Tectonic model for the Proterozoic growth of North America: Geosphere, v. 3, p. 220–259, doi: 10.1130/GES00055.1.

Williams, M.L., and Karlstrom, K.E., 1996, Looping P-T paths and high-T, low-P middle crustal metamorphism: Proterozoic evolution of the southwestern United States: Geology, v. 24, p. 1119–1122, doi: 10.1130/0091-

7613(1996)024<1119:LPTPAH>2.3.CO;2.

Williams, M.L., Karlstrom, K.E., Lanzirotti, A., Read, A.S., Bishop, J.L., Lombardi, C.E., Pedrick, J.N., and Wingsted, M.B., 1999, New Mexico middle-crustal cross sections: 1.65-Ga macroscopic geometry, 1.4-Ga thermal structure, and continued problems in understanding crustal evolution: Rocky Mountain Geology, v. 34, p. 53–66, doi: 10.2113/34.1.53.

Yang, J.H., Wu, F.Y., Wilde, S.A., Xie, L.W., Yang, Y.H., and Liu, X.M., 2007, Tracing magma mixing in granite genesis: In situ U - Pb dating and Hf-isotope analysis of zircons: Contributions to Mineralogy and Petrology, v. 153, p. 177–190, doi: 10.1007/s00410-006-0139-7.

Yonkee, W.A., and Weil, A.B., 2015, Tectonic evolution of the Sevier and Laramide belts within the North American Cordillera orogenic system: Earth-Science Reviews, v. 150, p. 531–593, doi: 10.1016/j.earscirev.2015.08.001.

APPENDIX 3: Analytical data from Chapter 2.

Table A3-1. U-Pb geochronologic results from igneous rocks in New Mexico

						Isotope ratios					Apparent ages (Ma)								
Analysis	U	206Pb	U/Th	206Pb*	±	207Pb*	±	206Pb*	±	error	206Pb*	±	207Pb*	±	206Pb*	±	Best age	±	Conc
	(ppm)	204Pb		207Pb*	(%)	235U*	(%)	238U	(%)	corr.	238U*	(Ma)	235U	(Ma)	207Pb*	(Ma)	(Ma)	(Ma)	(%)
TG14-ZUN4 Spot 17	64	112816	1.3	9.8920	1.1	4.1720	1.5	0.2993	1.1	0.70	1687.9	16.0	1668.5	12.5	1644.2	20.2	1644.2	20.2	102.7
TG14-ZUN4 Spot 16	194	182152	1.5	9.8871	0.9	3.9913	1.6	0.2862	1.4	0.85	1622.5	19.7	1632.4	13.1	1645.2	15.8	1645.2	15.8	98.6
TG14-ZUN4 Spot 23	74	47499	1.6	9.8808	1.2	4.0317	1.8	0.2889	1.3	0.74	1636.1	19.1	1640.6	14.6	1646.3	22.4	1646.3	22.4	99.4
TG14-ZUN4 Spot 7	169	54003	1.9	9.8723	0.9	4.0692	1.6	0.2914	1.3	0.82	1648.3	19.2	1648.2	13.1	1647.9	17.0	1647.9	17.0	100.0
TG14-ZUN4 Spot 26	242	50583	1.5	9.8722	0.9	3.9973	1.6	0.2862	1.3	0.81	1622.5	18.1	1633.6	12.6	1648.0	16.9	1648.0	16.9	98.5
TG14-ZUN4 Spot 13	68	51507	1.3	9.8720	1.1	3.9915	1.8	0.2858	1.4	0.78	1620.4	19.7	1632.5	14.3	1648.0	20.5	1648.0	20.5	98.3
TG14-ZUN4 Spot 14	52	46705	1.6	9.8650	1.6	4.1493	2.3	0.2969	1.6	0.70	1675.8	23.5	1664.1	18.7	1649.3	30.5	1649.3	30.5	101.6
TG14-ZUN4 Spot 1	191	1212952	1.4	9.8614	1.2	4.1292	1.9	0.2953	1.4	0.77	1668.1	21.1	1660.1	15.2	1650.0	22.0	1650.0	22.0	101.1
TG14-ZUN4 Spot 27	300	143320	1.7	9.8613	1.0	4.1372	1.9	0.2959	1.5	0.83	1670.9	22.7	1661.7	15.2	1650.0	19.4	1650.0	19.4	101.3
TG14-ZUN4 Spot 21	232	1149389	1.7	9.8568	0.8	4.0426	1.8	0.2890	1.6	0.89	1636.5	23.3	1642.8	14.8	1650.8	15.4	1650.8	15.4	99.1
TG14-ZUN4 Spot 25	343	188909	1.6	9.8462	1.0	4.0283	1.8	0.2877	1.5	0.83	1629.9	21.1	1639.9	14.4	1652.8	18.4	1652.8	18.4	98.6
TG14-ZUN4 Spot 6	128	134548	1.4	9.8397	0.8	4.0699	1.4	0.2904	1.2	0.83	1643.8	17.3	1648.3	11.8	1654.1	14.9	1654.1	14.9	99.4
TG14-ZUN4 Spot 12	112	58494	1.3	9.8327	0.9	4.0561	1.8	0.2893	1.5	0.86	1637.8	21.9	1645.5	14.3	1655.4	16.8	1655.4	16.8	98.9
TG14-ZUN4 Spot 20	50	56432	1.7	9.8301	1.3	4.1130	1.9	0.2932	1.4	0.71	1657.7	19.8	1656.9	15.5	1655.9	24.6	1655.9	24.6	100.1
TG14-ZUN4 Spot 5	267	930374	1.3	9.8277	1.0	3.9973	1.5	0.2849	1.1	0.76	1616.1	16.3	1633.6	12.1	1656.3	17.8	1656.3	17.8	97.6
TG14-ZUN4 Spot 10	231	81106	1.6	9.8251	0.8	4.0426	1.8	0.2881	1.6	0.91	1631.9	23.7	1642.8	14.8	1656.8	14.2	1656.8	14.2	98.5
TG14-ZUN4 Spot 19	250	160199	1.5	9.8249	0.9	4.1075	1.7	0.2927	1.4	0.84	1654.9	21.0	1655.8	14.0	1656.9	17.1	1656.9	17.1	99.9
TG14-ZUN4 Spot 22	104	112584	1.4	9.8110	1.0	4.1437	1.5	0.2949	1.2	0.76	1665.7	17.2	1663.0	12.6	1659.5	18.5	1659.5	18.5	100.4
TG14-ZUN4 Spot 15	142	89746	1.6	9.7877	1.0	4.1188	1.8	0.2924	1.6	0.84	1653.4	22.7	1658.0	15.1	1663.9	18.5	1663.9	18.5	99.4
TG14-ZUN4 Spot 8	111	972589	1.5	9.7849	0.9	4.0746	1.8	0.2892	1.6	0.86	1637.4	22.6	1649.2	14.9	1664.4	17.3	1664.4	17.3	98.4
TG14-ZUN4 Spot 24	202	206364	1.2	9.7676	1.1	4.1076	1.9	0.2910	1.5	0.81	1646.5	22.3	1655.8	15.4	1667.7	20.2	1667.7	20.2	98.7
TG14-ZUN4 Spot 2	167	115845	1.3	9.7539	1.0	4.0836	1.6	0.2889	1.3	0.80	1635.9	18.8	1651.0	13.3	1670.3	18.1	1670.3	18.1	97.9
TG14-ZUN4 Spot 11	60	87330	1.1	9.7431	1.2	4.2796	2.1	0.3024	1.7	0.82	1703.2	25.3	1689.4	17.0	1672.3	21.9	1672.3	21.9	101.8
TG14-ZUN4 Spot 9	412	47385	1.7	8.6432	1.1	4.5176	1.9	0.2832	1.5	0.81	1607.4	22.0	1734.2	15.9	1890.8	20.2	1890.8	20.2	85.0
TG15-PIC-5 Spot 42	189	60732	2.3	9.6995	1.1	4.1578	1.9	0.2925	1.5	0.80	1654.0	22.4	1665.8	15.7	1680.6	21.2	1680.6	21.2	98.4
TG15-PIC-5 Spot 46	88	56522	2.1	9.6934	1.4	4.2074	2.3	0.2958	1.8	0.79	1670.4	26.7	1675.5	18.8	1681.8	25.7	1681.8	25.7	99.3
TG15-PIC-5 Spot 48	69	151133	1.4	9.6681	1.1	4.2737	1.6	0.2997	1.2	0.74	1689.7	17.8	1688.3	13.3	1686.6	19.9	1686.6	19.9	100.2
TG15-PIC-5 Spot 62	93	72203	1.5	9.6556	1.3	4.3022	2.1	0.3013	1.6	0.78	1697.6	24.1	1693.8	17.0	1689.0	23.5	1689.0	23.5	100.5
TG15-PIC-5 Spot 40	121	169848	2.0	9.6556	1.1	4.2763	2.1	0.2995	1.7	0.84	1688.6	25.8	1688.8	17.0	1689.0	20.4	1689.0	20.4	100.0
TG15-PIC-5 Spot 63	94	114453	2.0	9.6101	1.1	4.3525	1.9	0.3034	1.5	0.80	1708.0	22.7	1703.4	15.6	1697.7	21.0	1697.7	21.0	100.6
TG15-PIC-5 Spot 39	164	103959	1.9	9.6032	1.2	4.3165	1.8	0.3006	1.4	0.77	1694.5	21.2	1696.5	15.2	1699.0	21.5	1699.0	21.5	99.7
TG15-PIC-5 Spot 37	157	80046	2.1	9.5770	1.0	4.3021	1.8	0.2988	1.5	0.84	1685.4	22.4	1693.8	14.9	1704.1	18.3	1704.1	18.3	98.9
TG15-PIC-5 Spot 61	64	92605	1.3	9.5764	1.7	4.3355	2.5	0.3011	1.9	0.75	1696.9	28.0	1700.1	20.6	1704.2	30.5	1704.2	30.5	99.6
TG15-PIC-5 Spot 54	140	51388	1.7	9.5764	1.0	4.4050	1.9	0.3060	1.6	0.84	1720.7	24.7	1713.3	16.1	1704.2	19.3	1704.2	19.3	101.0

TG15-PIC-5 Spot 56	159	122740	1.6	9.5731	1.0	4.2657	1.8	0.2962	1.5	0.82	1672.3	21.9	1686.8	14.9	1704.8	18.9	1704.8	18.9	98.1
TG15-PIC-5 Spot 43	211	62934	2.3	9.5527	1.0	4.2054	1.7	0.2914	1.4	0.82	1648.3	20.5	1675.1	14.2	1708.7	18.3	1708.7	18.3	96.5
TG15-PIC-5 Spot 47	158	184097	1.8	9.5099	1.0	4.2231	2.0	0.2913	1.7	0.86	1647.9	24.9	1678.5	16.4	1717.0	18.8	1717.0	18.8	96.0
TG15-PIC-5 Spot 52	204	1737286	1.9	9.5036	1.1	4.4401	1.9	0.3060	1.5	0.79	1721.2	22.1	1719.9	15.4	1718.2	21.0	1718.2	21.0	100.2
TG15-PIC-5 Spot 60	89	2973393	1.5	9.3588	1.2	4.1960	1.7	0.2848	1.3	0.73	1615.5	18.2	1673.2	14.3	1746.4	21.8	1746.4	21.8	92.5
TG15-PIC-5 Spot 58	166	45535	1.5	9.1306	1.3	4.3203	2.2	0.2861	1.7	0.81	1622.0	25.0	1697.3	17.8	1791.5	23.3	1791.5	23.3	90.5
TG15-PIC-5 Spot 49	257	35998	2.0	8.9226	0.9	4.3332	1.6	0.2804	1.3	0.81	1593.4	18.3	1699.7	13.1	1833.3	16.7	1833.3	16.7	86.9
TG15-PIC-5 Spot 38	235	35997	2.0	8.8855	1.2	4.3175	1.8	0.2782	1.4	0.76	1582.5	19.5	1696.7	15.0	1840.9	21.4	1840.9	21.4	86.0
TG15-PIC-5 Spot 59	116	66451	1.1	8.5844	1.8	4.6322	2.3	0.2884	1.3	0.58	1633.5	19.0	1755.1	18.9	1903.0	33.0	1903.0	33.0	85.8
TG15-PIC-5 Spot 36	127	29221	1.8	8.4684	0.9	4.5433	1.9	0.2790	1.7	0.87	1586.5	23.7	1738.9	16.1	1927.4	16.8	1927.4	16.8	82.3
K15-SEV-ES-RHY Spot 3	981	201125	1.9	9.6228	0.9	4.3083	1.6	0.3007	1.3	0.82	1694.7	19.5	1695.0	13.1	1695.3	16.8	1695.3	16.8	100.0
K15-SEV-ES-RHY Spot 4	340	60139	3.1	9.8101	0.8	3.9000	1.9	0.2775	1.7	0.91	1578.7	23.8	1613.7	15.1	1659.6	14.1	1659.6	14.1	95.1
K15-SEV-ES-RHY Spot 5	1150	650132	1.2	9.6593	0.7	4.4853	1.9	0.3142	1.8	0.93	1761.4	27.1	1728.3	15.7	1688.3	12.7	1688.3	12.7	104.3
K15-SEV-ES-RHY Spot 7	448	151920	1.2	9.6985	0.7	3.9812	1.5	0.2800	1.3	0.86	1591.6	17.6	1630.4	11.8	1680.8	13.7	1680.8	13.7	94.7
K15-SEV-ES-RHY Spot 8	404	395705	1.7	9.8364	0.9	4.2043	1.6	0.2999	1.2	0.80	1691.0	18.5	1674.9	12.7	1654.7	17.3	1654.7	17.3	102.2
K15-SEV-ES-RHY Spot 9	647	78589	2.3	9.7639	0.9	3.9386	1.5	0.2789	1.3	0.82	1585.9	17.7	1621.7	12.4	1668.4	16.1	1668.4	16.1	95.1
K15 SEV-ES-RHYSpot 10	224	238033	2.0	9.8007	1.1	4.0921	1.8	0.2909	1.5	0.80	1645.9	21.3	1652.7	14.9	1661.4	20.1	1661.4	20.1	99.1
K15-SEV-ES-RHY Spot 11	116	1026795	1.7	9.7812	1.0	4.0068	1.8	0.2842	1.5	0.83	1612.7	21.2	1635.6	14.6	1665.1	18.8	1665.1	18.8	96.9
K15-SEV-ES-RHY Spot 12	217	207659757	2.4	9.8247	0.6	4.0313	1.5	0.2873	1.3	0.90	1627.8	18.8	1640.5	11.8	1656.9	11.9	1656.9	11.9	98.2
K15-SEV-ES-RHY Spot 13	624	458117	1.7	9.6976	1.0	4.0648	2.1	0.2859	1.9	0.88	1621.0	26.5	1647.3	17.2	1681.0	18.7	1681.0	18.7	96.4
K15-SEV-ES-RHY Spot 14	699	56006	1.7	9.8601	0.7	3.4876	1.6	0.2494	1.5	0.92	1435.4	19.4	1524.4	12.9	1650.2	12.1	1650.2	12.1	87.0
K15-SEV-ES-RHY Spot 15	625	2227938	1.5	9.9049	0.8	3.8061	1.4	0.2734	1.2	0.83	1558.2	16.5	1594.0	11.6	1641.8	15.1	1641.8	15.1	94.9
K15-SEV-ES-RHY Spot 16	390	196042	1.4	9.7867	0.7	4.0601	1.7	0.2882	1.5	0.91	1632.5	22.2	1646.3	13.8	1664.1	12.9	1664.1	12.9	98.1
K15-SEV-ES-RHY Spot 17	239	144921	2.1	9.9015	0.8	4.0850	1.7	0.2934	1.5	0.88	1658.3	21.5	1651.3	13.7	1642.5	15.0	1642.5	15.0	101.0
K15-SEV-ES-RHY Spot 18	320	179877	3.1	9.7321	0.6	4.1871	1.4	0.2955	1.2	0.90	1669.2	18.3	1671.5	11.3	1674.4	11.0	1674.4	11.0	99.7
K15-SEV-ES-RHY Spot 19	259	87013	1.8	9.7288	0.8	4.1493	1.6	0.2928	1.3	0.85	1655.4	19.6	1664.1	13.0	1675.0	15.7	1675.0	15.7	98.8
K15-SEV-ES-RHY Spot 20	254	143812	2.1	9.8713	1.0	4.0547	1.8	0.2903	1.5	0.83	1643.0	21.7	1645.3	14.7	1648.1	18.4	1648.1	18.4	99.7
K15-SEV-ES-RHY Spot 21	752	116167	2.3	9.7829	0.8	3.9552	1.8	0.2806	1.6	0.89	1594.5	22.5	1625.1	14.6	1664.8	15.5	1664.8	15.5	95.8
K15-SEV-ES-RHY Spot 22	247	225415	1.9	9.8462	0.8	4.0548	1.5	0.2896	1.3	0.85	1639.3	18.9	1645.3	12.5	1652.9	14.8	1652.9	14.8	99.2
TG15-OJITO Spot 51	153	584307	2.5	9.8742	0.8	4.1129	1.5	0.2945	1.3	0.84	1664.2	19.0	1656.9	12.6	1647.6	15.6	1647.6	15.6	101.0
TG15-OJITO Spot 52	299	64347	1.9	9.7974	0.8	4.0929	1.3	0.2908	1.0	0.79	1645.7	14.7	1652.9	10.4	1662.1	14.5	1662.1	14.5	99.0
TG15-OJITO Spot 53	161	82811	2.1	9.8609	1.1	4.0875	1.8	0.2923	1.5	0.81	1653.2	21.5	1651.8	14.9	1650.1	19.8	1650.1	19.8	100.2
TG15-OJITO Spot 54	361	397691	1.6	9.7067	0.8	4.0639	1.4	0.2861	1.2	0.82	1622.0	16.8	1647.1	11.7	1679.2	15.1	1679.2	15.1	96.6
TG15-OJITO Spot 55	227	82340	1.9	9.6828	0.7	4.1217	1.4	0.2895	1.2	0.88	1638.8	18.1	1658.6	11.5	1683.8	12.2	1683.8	12.2	97.3
TG15-OJITO Spot 56	257	150526	1.3	9.7892	1.0	4.0523	1.8	0.2877	1.5	0.83	1630.1	22.1	1644.8	15.0	1663.6	18.9	1663.6	18.9	98.0
TG15-OJITO Spot 57	274	1265638	1.8	9.8221	0.8	4.0988	1.7	0.2920	1.5	0.89	1651.4	22.1	1654.1	13.9	1657.4	14.6	1657.4	14.6	99.6
TG15-OJITO Spot 58	407	41454	1.4	9.1774	0.9	4.3714	1.7	0.2910	1.4	0.84	1646.3	20.6	1706.9	13.9	1782.1	16.5	1782.1	16.5	92.4
TG15-OJITO Spot 60	287	136218	2.1	9.8462	0.8	4.1124	1.5	0.2937	1.3	0.87	1659.9	19.6	1656.8	12.6	1652.8	14.0	1652.8	14.0	100.4
TG15-OJITO Spot 61	205	22266	1.1	7.8046	2.5	5.3416	2.9	0.3024	1.3	0.46	1703.0	19.9	1875.6	24.5	2072.5	44.7	2072.5	44.7	82.2
TG15-OJITO Spot 62	151	52792	1.8	9.7647	0.9	4.0629	1.8	0.2877	1.5	0.85	1630.2	21.8	1646.9	14.5	1668.2	17.1	1668.2	17.1	97.7
TG15-OJITO Spot 64	286	65514	1.8	9.5350	1.0	3.8579	1.7	0.2668	1.3	0.78	1524.5	17.5	1604.9	13.4	1712.1	19.2	1712.1	19.2	89.0

TG15-OJITO Spot 65	428	48750	1.4	9.1398	1.2	4.2625	2.0	0.2826	1.6	0.79	1604.2	22.2	1686.2	16.3	1789.6	22.0	1789.6	22.0	89.6
TG15-OJITO Spot 66	317	139116	2.2	9.7830	0.9	4.1058	1.6	0.2913	1.3	0.83	1648.1	19.3	1655.5	13.1	1664.8	16.8	1664.8	16.8	99.0
TG15-OJITO Spot 67	308	177132	1.7	9.8018	1.0	4.1259	1.7	0.2933	1.4	0.83	1658.0	21.0	1659.4	14.2	1661.2	18.1	1661.2	18.1	99.8
TG15-OJITO Spot 68	359	70172	1.6	9.5594	1.1	3.8192	2.6	0.2648	2.3	0.90	1514.3	31.4	1596.8	20.8	1707.4	20.7	1707.4	20.7	88.7
TG15-OJITO Spot 69	286	81943	1.9	9.8759	0.7	4.2384	1.3	0.3036	1.1	0.83	1709.1	16.6	1681.5	10.9	1647.3	13.7	1647.3	13.7	103.8
TG15-OJITO Spot 71	321	363828	1.8	9.8451	0.9	4.0143	1.7	0.2866	1.5	0.85	1624.7	21.0	1637.1	14.0	1653.0	17.1	1653.0	17.1	98.3
TG15-OJITO Spot 72	290	149807	1.2	9.7887	0.9	4.0796	1.9	0.2896	1.7	0.87	1639.7	24.1	1650.2	15.5	1663.7	17.1	1663.7	17.1	98.6
TG15-OJITO Spot 73	340	44457	1.7	9.2461	1.1	4.3898	2.0	0.2944	1.6	0.82	1663.3	23.4	1710.4	16.2	1768.5	20.6	1768.5	20.6	94.1
TG15-OJITO Spot 74	293	47352	1.4	9.2337	1.5	4.0261	2.9	0.2696	2.5	0.86	1538.9	34.8	1639.5	24.0	1771.0	27.1	1771.0	27.1	86.9
TG15-OJITO Spot 75	397	182170	1.8	9.7616	0.9	4.0989	1.5	0.2902	1.2	0.81	1642.5	18.0	1654.1	12.4	1668.8	16.4	1668.8	16.4	98.4
TG15-OJITO Spot 76	397	60345	1.4	9.8252	0.9	4.0324	1.6	0.2873	1.3	0.84	1628.3	18.9	1640.8	12.8	1656.8	16.1	1656.8	16.1	98.3
TG15-OJITO Spot 77	223	80463	1.9	9.7398	0.8	4.1450	1.3	0.2928	1.0	0.77	1655.5	14.8	1663.2	10.7	1672.9	15.5	1672.9	15.5	99.0
TG15-OJITO Spot 78	205	158000	1.3	9.8296	1.1	3.9824	2.1	0.2839	1.8	0.86	1611.0	25.6	1630.6	17.0	1656.0	19.8	1656.0	19.8	97.3
TG15-OJITO Spot 79	333	80769	1.9	9.8812	0.8	4.1889	1.7	0.3002	1.5	0.87	1692.3	22.7	1671.8	14.3	1646.3	15.7	1646.3	15.7	102.8
TG15-OJITO Spot 80	138	206743	2.1	9.8538	1.2	4.2548	1.9	0.3041	1.5	0.76	1711.5	22.0	1684.7	15.8	1651.4	23.1	1651.4	23.1	103.6
TG15-ZUN3 Spot 110	79	56619	1.0	10.1558	1.0	3.3483	1.7	0.2466	1.3	0.81	1421.0	17.0	1492.4	12.9	1595.3	18.3	1595.3	18.3	89.1
TG15-ZUN3 Spot 113	76	64631	1.4	9.9833	1.1	3.9315	1.6	0.2847	1.2	0.72	1614.8	16.6	1620.2	13.1	1627.2	20.8	1627.2	20.8	99.2
TG15-ZUN3 Spot 120	81	48589	1.6	9.9811	1.2	4.0282	2.0	0.2916	1.5	0.78	1649.5	22.5	1639.9	16.1	1627.6	22.9	1627.6	22.9	101.3
TG15-ZUN3 Spot 115	148	105703	1.0	9.9796	0.9	3.7221	1.6	0.2694	1.4	0.85	1537.8	18.8	1576.1	13.0	1627.9	15.9	1627.9	15.9	94.5
TG15-ZUN3 Spot 111	163	151789	1.5	9.9710	0.8	3.8670	1.8	0.2796	1.6	0.89	1589.6	22.2	1606.8	14.3	1629.5	14.8	1629.5	14.8	97.6
TG15-ZUN3 Spot 106	118	197435	1.3	9.9460	1.1	4.0152	1.8	0.2896	1.4	0.80	1639.7	20.3	1637.3	14.4	1634.1	19.9	1634.1	19.9	100.3
TG15-ZUN3 Spot 122	113	71003	1.4	9.9239	1.0	3.9565	1.6	0.2848	1.3	0.81	1615.3	18.8	1625.3	13.2	1638.3	17.8	1638.3	17.8	98.6
TG15-ZUN3 Spot 119	48	141580	1.2	9.9235	1.5	3.7501	2.2	0.2699	1.6	0.73	1540.3	21.6	1582.1	17.4	1638.3	27.7	1638.3	27.7	94.0
TG15-ZUN3 Spot 121	162	247261	1.6	9.8723	0.9	3.9179	1.6	0.2805	1.3	0.80	1594.0	17.9	1617.4	12.8	1647.9	17.5	1647.9	17.5	96.7
TG15-ZUN3 Spot 114	146	113689	1.1	9.8608	1.0	3.5877	1.7	0.2566	1.4	0.83	1472.4	19.0	1546.8	13.8	1650.1	18.0	1650.1	18.0	89.2
TG15-ZUN3 Spot 117	27	24694	0.9	9.8498	1.9	3.6869	2.9	0.2634	2.3	0.77	1507.1	30.5	1568.5	23.5	1652.2	34.8	1652.2	34.8	91.2
TG15-ZUN3 Spot 118	118	207329	0.9	9.8383	1.2	4.0878	2.0	0.2917	1.6	0.80	1649.9	23.1	1651.9	16.1	1654.3	22.0	1654.3	22.0	99.7
TG15-ZUN3 Spot 105	121	148516	1.3	9.6219	1.1	3.4783	2.2	0.2427	1.9	0.87	1400.9	24.2	1522.3	17.4	1695.4	19.9	1695.4	19.9	82.6
K14-MANZANITA Spot 42	348	58971	3.3	9.9455	0.8	4.0314	1.6	0.2908	1.3	0.86	1645.5	19.5	1640.6	12.7	1634.2	15.0	1634.2	15.0	100.7
K14-MANZANITA Spot 36	340	160119	2.2	9.9438	0.8	4.0042	1.2	0.2888	1.0	0.77	1635.4	13.8	1635.1	10.1	1634.5	14.7	1634.5	14.7	100.1
K14-MANZANITA Spot 18	580	99973	2.8	9.9394	0.7	3.3779	1.5	0.2435	1.3	0.88	1404.9	16.5	1499.3	11.6	1635.4	12.8	1635.4	12.8	85.9
K14-MANZANITA Spot 35	117	208815	1.1	9.9330	0.9	4.0762	1.4	0.2937	1.1	0.76	1659.8	16.1	1649.6	11.8	1636.6	17.4	1636.6	17.4	101.4
K14-MANZANITA Spot 17	257	73085	2.1	9.9313	1.0	3.8881	1.8	0.2801	1.5	0.85	1591.7	21.8	1611.2	14.7	1636.9	17.9	1636.9	17.9	97.2
K14-MANZANITA Spot 41	258	54168	2.2	9.8930	0.9	4.1014	1.4	0.2943	1.1	0.75	1662.9	15.9	1654.6	11.8	1644.1	17.6	1644.1	17.6	101.1
K14-MANZANITA Spot 33	142	56187	1.6	9.8907	1.0	4.0956	1.5	0.2938	1.2	0.78	1660.4	17.5	1653.4	12.5	1644.5	17.7	1644.5	17.7	101.0
K14-MANZANITA Spot 45	628	104672	2.3	9.8889	0.8	4.0452	1.5	0.2901	1.3	0.84	1642.2	18.4	1643.3	12.3	1644.8	15.4	1644.8	15.4	99.8
K14-MANZANITA Spot 34	273	93694	1.9	9.8737	0.8	4.1095	1.6	0.2943	1.4	0.87	1662.9	20.0	1656.2	12.8	1647.7	14.3	1647.7	14.3	100.9
K14-MANZANITA Spot 24	127	53637	1.3	9.8716	1.0	4.0156	1.7	0.2875	1.4	0.81	1629.0	19.9	1637.4	13.9	1648.1	18.6	1648.1	18.6	98.8
K14-MANZANITA Spot 58	315	182036	3.5	9.8619	0.9	3.9880	1.6	0.2852	1.4	0.85	1617.7	19.9	1631.8	13.3	1649.9	16.0	1649.9	16.0	98.0
K14-MANZANITA Spot 39	485	184358	2.6	9.8509	0.8	3.9543	1.5	0.2825	1.2	0.83	1604.0	17.6	1624.9	12.1	1652.0	15.6	1652.0	15.6	97.1
K14-MANZANITA Spot 8	497	93720	2.8	9.8502	1.0	3.8945	1.4	0.2782	1.0	0.71	1582.4	13.9	1612.5	11.2	1652.1	18.0	1652.1	18.0	95.8

K14-MANZANITA Spot 68	585	380813	2.2	9.8444	0.6	4.1364	1.1	0.2953	1.0	0.86	1668.1	14.1	1661.5	9.1	1653.2	10.3	1653.2	10.3	100.9
K14-MANZANITA Spot 64	697	2665525	2.2	9.8432	0.8	4.1419	1.7	0.2957	1.5	0.89	1669.9	22.3	1662.6	13.9	1653.4	14.1	1653.4	14.1	101.0
K14-MANZANITA Spot 14	515	93846	2.3	9.8423	0.7	3.6152	1.5	0.2581	1.3	0.88	1479.9	17.1	1552.9	11.6	1653.6	12.6	1653.6	12.6	89.5
K14-MANZANITA Spot 50	661	71679	3.2	9.8415	0.8	3.8041	1.4	0.2715	1.2	0.84	1548.5	16.5	1593.6	11.5	1653.7	14.4	1653.7	14.4	93.6
K14-MANZANITA Spot 54	569	57824	2.1	9.8262	0.8	3.9220	1.4	0.2795	1.1	0.78	1588.9	14.9	1618.2	11.0	1656.6	15.7	1656.6	15.7	95.9
K14-MANZANITA Spot 63	521	72945	2.5	9.8171	0.6	3.7169	1.3	0.2646	1.1	0.87	1513.6	15.5	1575.0	10.5	1658.3	11.8	1658.3	11.8	91.3
K14-MANZANITA Spot 11	244	57036	2.2	9.8124	0.9	3.9707	1.7	0.2826	1.5	0.85	1604.3	21.1	1628.2	14.2	1659.2	17.0	1659.2	17.0	96.7
K14-MANZANITA Spot 21	350	98995	2.7	9.8088	1.5	4.0159	1.9	0.2857	1.1	0.59	1620.0	16.1	1637.4	15.5	1659.9	28.4	1659.9	28.4	97.6
K14-MANZANITA Spot 60	426	70641	12.1	9.7962	0.7	3.8249	1.5	0.2718	1.4	0.89	1549.7	19.0	1598.0	12.5	1662.3	13.1	1662.3	13.1	93.2
K14-MANZANITA Spot 69	319	231146	1.6	9.7937	0.7	4.0408	1.1	0.2870	0.9	0.79	1626.6	12.6	1642.5	9.0	1662.7	12.5	1662.7	12.5	97.8
K14-MANZANITA Spot 4	596	896773	2.3	9.7907	0.6	4.1800	1.6	0.2968	1.5	0.93	1675.5	21.9	1670.1	13.1	1663.3	10.9	1663.3	10.9	100.7
K14-MANZANITA Spot 5	259	109918	1.9	9.7835	0.9	3.7268	1.6	0.2644	1.3	0.80	1512.5	17.0	1577.1	12.5	1664.7	17.2	1664.7	17.2	90.9
K14-MANZANITA Spot 23	307	334681	2.6	9.7654	0.9	3.8855	1.2	0.2752	0.8	0.69	1567.1	11.4	1610.7	9.6	1668.1	16.0	1668.1	16.0	93.9
K14-MANZANITA Spot 40	338	81364	1.9	9.7616	1.0	3.2723	3.8	0.2317	3.7	0.96	1343.3	44.9	1474.5	29.9	1668.8	19.3	1668.8	19.3	80.5
K14-MANZANITA Spot 3	199	109434	2.4	9.7316	0.8	4.1359	1.6	0.2919	1.3	0.84	1651.1	19.4	1661.4	12.9	1674.5	15.6	1674.5	15.6	98.6
K14-MANZANITA Spot 22	296	515804	2.3	9.7056	0.8	4.2217	1.3	0.2972	1.1	0.81	1677.3	15.9	1678.3	10.9	1679.5	14.3	1679.5	14.3	99.9
K14-MANZANITA Spot 53	182	111123	2.3	9.6457	0.9	4.1505	1.4	0.2904	1.0	0.74	1643.3	15.0	1664.3	11.5	1690.9	17.5	1690.9	17.5	97.2
K14-MANZANITA Spot 51	280	204227	2.1	9.6373	1.0	3.3681	1.8	0.2354	1.5	0.82	1362.8	17.9	1497.0	13.8	1692.5	18.4	1692.5	18.4	80.5
K14-MANZANITA Spot 26	555	122791	3.3	9.6150	0.7	3.4979	1.3	0.2439	1.2	0.86	1407.1	14.6	1526.7	10.6	1696.8	12.7	1696.8	12.7	82.9
K14-MANZANITA Spot 1	236	152618	3.3	9.5676	1.1	3.6066	1.9	0.2503	1.6	0.82	1439.8	20.1	1551.0	15.1	1705.9	20.0	1705.9	20.0	84.4
K14-MANZANITA Spot 10	354	218500	1.7	9.5205	0.8	4.3694	1.5	0.3017	1.3	0.86	1699.7	19.1	1706.6	12.2	1714.9	13.9	1714.9	13.9	99.1
K14-MANZANITA Spot 56	327	138433	2.0	9.4960	1.2	4.0786	1.7	0.2809	1.2	0.73	1595.9	17.6	1650.0	13.9	1719.7	21.4	1719.7	21.4	92.8
K14-MANZANITA Spot 65	442	368426	2.4	9.4361	0.9	4.4938	1.7	0.3075	1.4	0.82	1728.6	20.7	1729.8	13.8	1731.3	17.2	1731.3	17.2	99.8
K14-MANZANITA Spot 37	471	77043	1.7	9.4164	1.1	3.6138	3.0	0.2468	2.7	0.92	1422.0	34.9	1552.6	23.5	1735.1	20.8	1735.1	20.8	82.0
K14-MANZANITA Spot 9	105	115423	1.5	9.3855	1.1	4.2180	1.6	0.2871	1.1	0.72	1627.1	16.5	1677.5	13.1	1741.1	20.2	1741.1	20.2	93.5
K14-MANZANITA Spot 13	290	118021	1.6	9.3803	1.1	3.7423	4.2	0.2546	4.0	0.96	1462.1	52.4	1580.5	33.4	1742.2	20.7	1742.2	20.7	83.9
K14-MANZANITA Spot 44	646	52688	2.1	9.3718	1.0	4.0142	2.1	0.2728	1.9	0.88	1555.2	26.2	1637.1	17.4	1743.8	18.3	1743.8	18.3	89.2
K14-MANZANITA Spot 20	515	68062	2.3	9.3400	1.3	4.0313	2.1	0.2731	1.7	0.80	1556.4	23.5	1640.5	17.2	1750.1	23.1	1750.1	23.1	88.9
K13-TUSAS-1-1	320	301763	3.1	9.3031	0.4	4.7281	0.7	0.3190	0.7	0.88	1784.9	10.2	1772.2	6.2	1757.3	6.5	1757.3	6.5	101.6
K13-TUSAS-1-4	253	97591	1.9	9.2843	0.3	4.5980	5.7	0.3096	5.7	1.00	1738.8	86.7	1748.9	47.5	1761.0	5.9	1761.0	5.9	98.7
K13-TUSAS-1-5	194	23668	2.8	9.2698	1.4	4.5024	2.1	0.3027	1.6	0.74	1704.7	23.7	1731.4	17.8	1763.9	26.3	1763.9	26.3	96.6
K13-TUSAS-1-6	247	40208	2.9	9.2988	0.5	4.7624	6.4	0.3212	6.3	1.00	1795.5	99.4	1778.3	53.4	1758.1	8.5	1758.1	8.5	102.1
K13-TUSAS-1-9	207	46840	1.3	9.2962	0.3	4.3714	4.6	0.2947	4.6	1.00	1665.1	67.6	1706.9	38.2	1758.7	6.1	1758.7	6.1	94.7
K13-TUSAS-1-10	290	19583	2.3	9.2838	0.3	4.1468	3.6	0.2792	3.6	1.00	1587.4	50.9	1663.6	29.7	1761.1	5.9	1761.1	5.9	90.1
K13-TUSAS-1-11	267	71803	2.0	9.3049	0.3	4.7090	5.1	0.3178	5.1	1.00	1778.9	79.0	1768.8	42.7	1756.9	4.9	1756.9	4.9	101.3
K13-TUSAS-1-13	215	30938	1.4	9.2631	0.3	4.4458	2.3	0.2987	2.3	0.99	1684.8	34.0	1720.9	19.2	1765.2	6.1	1765.2	6.1	95.4
K13-TUSAS-1-15	294	40079	1.0	9.2880	0.6	4.6525	3.3	0.3134	3.3	0.98	1757.4	50.2	1758.7	27.8	1760.3	11.3	1760.3	11.3	99.8
K13-TUSAS-1-16	148	189429	2.0	9.3059	0.3	4.6252	1.6	0.3122	1.5	0.98	1751.3	23.5	1753.8	13.0	1756.7	5.0	1756.7	5.0	99.7
K13-TUSAS-1-17	203	237801	2.4	9.3136	0.2	4.7415	0.9	0.3203	0.9	0.96	1791.1	13.6	1774.6	7.6	1755.2	4.4	1755.2	4.4	102.0
K13-TUSAS-1-18	99	165861	4.6	9.3633	0.7	4.7092	1.1	0.3198	0.9	0.79	1788.7	14.0	1768.9	9.5	1745.5	12.8	1745.5	12.8	102.5
K13-TUSAS-1-19	228	128431	2.5	9.2970	0.3	4.6055	2.1	0.3105	2.1	0.99	1743.4	32.2	1750.3	17.7	1758.5	4.8	1758.5	4.8	99.1
K13-TUSAS-1-20	295	250675	2.0	9.3043	0.3	4.5530	2.9	0.3072	2.9	1.00	1727.1	43.7	1740.7	24.1	1757.1	4.8	1757.1	4.8	98.3

K13-TUSAS-1-21	289	56844	2.3	9.3163	0.4	4.3446	1.0	0.2936	1.0	0.91	1659.3	13.9	1701.9	8.6	1754.7	7.8	1754.7	7.8	94.6
K13-TUSAS-1-22	225	78266	1.7	9.3075	0.3	4.5970	3.4	0.3103	3.4	1.00	1742.3	52.4	1748.7	28.7	1756.4	4.8	1756.4	4.8	99.2
K13-TUSAS-1-23	184	140333	3.5	9.2932	0.2	4.6067	6.1	0.3105	6.1	1.00	1743.1	92.6	1750.5	50.6	1759.2	3.3	1759.2	3.3	99.1
K13-TUSAS-1-24	122	4036	1.6	9.2780	1.1	4.5113	1.7	0.3036	1.3	0.76	1709.0	19.1	1733.1	13.9	1762.2	19.8	1762.2	19.8	97.0
K13-TUSAS-1-25	248	299748	3.4	9.3159	0.3	4.6737	1.7	0.3158	1.7	0.98	1769.1	26.1	1762.5	14.4	1754.8	5.9	1754.8	5.9	100.8
K13-TUSAS-1-26	259	16799	2.5	9.2664	1.1	4.6233	6.0	0.3107	5.8	0.98	1744.2	89.3	1753.5	49.8	1764.5	20.9	1764.5	20.9	98.9
K13-TUSAS-1-27	270	72486	3.1	9.3371	0.3	4.5280	1.4	0.3066	1.4	0.98	1724.1	20.6	1736.1	11.6	1750.6	5.1	1750.6	5.1	98.5
K13-TUSAS-1-28	159	78104	1.9	9.3387	0.5	4.4414	2.0	0.3008	2.0	0.97	1695.4	29.5	1720.1	16.8	1750.3	8.5	1750.3	8.5	96.9
K13-TUSAS-1-30	423	20192	1.1	9.2679	0.5	4.0609	3.6	0.2730	3.5	0.99	1555.8	49.0	1646.5	29.2	1764.2	9.3	1764.2	9.3	88.2
H13-MAN-26R	859	10482	3.1	10.9575	0.2	2.9553	5.0	0.2349	5.0	1.00	1359.9	61.8	1396.2	38.3	1452.1	3.6	1452.1	3.6	93.7
H13-MAN-37R	593	16953	2.5	10.9347	0.4	2.9154	1.0	0.2312	1.0	0.92	1340.8	11.6	1385.9	7.9	1456.0	8.0	1456.0	8.0	92.1
H13-MAN-18C	128	126067	1.2	10.8883	0.6	3.3164	2.3	0.2619	2.3	0.97	1499.5	30.1	1484.9	18.1	1464.1	10.8	1464.1	10.8	102.4
H13-MAN-4C	156	149517	1.7	10.8659	0.5	3.2059	0.8	0.2526	0.7	0.82	1452.1	8.7	1458.6	6.3	1468.0	9.0	1468.0	9.0	98.9
H13-MAN-3C	310	3243	1.9	10.7740	1.5	2.6032	4.4	0.2034	4.1	0.94	1193.6	44.9	1301.5	32.1	1484.1	27.9	1484.1	27.9	80.4
H13-MAN-2C	130	3337	3.0	10.3578	2.7	2.9388	3.3	0.2208	1.9	0.58	1285.9	22.6	1392.0	25.3	1558.4	51.0	1558.4	51.0	82.5
H13-MAN-8C	155	5438	2.2	10.2015	1.2	3.0685	1.9	0.2270	1.5	0.78	1318.9	17.3	1424.9	14.3	1586.9	22.1	1586.9	22.1	83.1
H13-MAN-16C	77	7097	1.3	9.8717	1.3	4.0350	2.1	0.2889	1.7	0.79	1636.0	24.2	1641.3	17.3	1648.1	24.3	1648.1	24.3	99.3
H13-MAN-12C	233	7554	1.0	9.8194	0.5	3.7943	3.1	0.2702	3.0	0.99	1541.9	41.7	1591.5	24.8	1657.9	9.5	1657.9	9.5	93.0
H13-MAN-1C	149	6471	0.7	9.7959	2.2	4.2316	2.6	0.3006	1.4	0.53	1694.5	20.8	1680.2	21.5	1662.3	41.1	1662.3	41.1	101.9
H13-MAN-17C	99	9515	1.2	9.7385	1.4	4.1863	1.6	0.2957	0.6	0.41	1669.9	9.5	1671.3	13.0	1673.2	26.7	1673.2	26.7	99.8
K13-NAC-2A-1	119	94218	1.4	10.9639	0.6	3.1995	1.1	0.2544	1.0	0.87	1461.2	12.8	1457.0	8.8	1450.9	10.7	1450.9	10.7	100.7
K13-NAC-2A-3	109	111327	1.3	10.9366	0.6	3.1922	0.8	0.2532	0.5	0.61	1455.0	6.1	1455.3	5.9	1455.7	11.6	1455.7	11.6	100.0
K13-NAC-2A-4	81	15397	2.8	10.9888	1.1	3.0349	1.7	0.2419	1.3	0.77	1396.4	16.5	1416.4	13.0	1446.6	20.8	1446.6	20.8	96.5
K13-NAC-2A-6	125	134783	1.5	10.9446	0.8	3.1534	1.5	0.2503	1.3	0.85	1440.1	16.4	1445.8	11.5	1454.3	14.8	1454.3	14.8	99.0
K13-NAC-2A-7	178	14445	1.6	10.8992	0.7	3.2483	1.6	0.2568	1.4	0.91	1473.3	18.9	1468.8	12.3	1462.2	12.7	1462.2	12.7	100.8
K13-NAC-2A-9	167	6978	1.7	10.9048	0.7	2.7737	7.8	0.2194	7.8	1.00	1278.5	90.6	1348.5	58.6	1461.2	12.9	1461.2	12.9	87.5
K13-NAC-2A-12	116	67206	1.2	11.0341	1.4	3.1562	1.6	0.2526	0.7	0.43	1451.8	8.9	1446.5	12.4	1438.8	27.6	1438.8	27.6	100.9
K13-NAC-2A-14	125	105059	1.5	11.0076	0.6	3.0881	1.0	0.2465	0.8	0.79	1420.6	9.7	1429.7	7.4	1443.4	11.4	1443.4	11.4	98.4
K13-NAC-2A-16	130	6161	1.3	10.8217	2.9	3.1388	3.6	0.2464	2.1	0.59	1419.6	27.0	1442.3	27.5	1475.8	54.6	1475.8	54.6	96.2
K13-NAC-2A-19	137	76994	1.2	10.9457	0.7	3.2313	1.1	0.2565	0.8	0.74	1472.0	10.3	1464.7	8.2	1454.1	13.5	1454.1	13.5	101.2
K13-NAC-2A-20	151	35938	1.3	10.9922	0.3	3.0994	0.7	0.2471	0.6	0.87	1423.5	7.7	1432.5	5.3	1446.0	6.6	1446.0	6.6	98.4
K13-NAC-2A-21	107	21305	1.6	10.9825	0.7	3.2705	1.0	0.2605	0.7	0.71	1492.4	9.8	1474.1	8.1	1447.7	14.0	1447.7	14.0	103.1
K13-NAC-2A-23	106	19002	1.1	10.9656	0.4	3.0991	1.2	0.2465	1.1	0.93	1420.3	14.4	1432.5	9.4	1450.6	8.6	1450.6	8.6	97.9
K13-NAC-2A-25	99	9740	1.1	10.8679	1.3	3.3307	4.4	0.2625	4.2	0.95	1502.8	56.7	1488.3	34.6	1467.7	25.0	1467.7	25.0	102.4
K13-NAC-2A-26	181	88923	1.1	10.9800	0.5	3.1885	0.8	0.2539	0.5	0.72	1458.6	7.1	1454.4	5.9	1448.1	10.1	1448.1	10.1	100.7
K13-NAC-2A-28	109	10233	1.3	10.9445	0.8	3.2252	1.2	0.2560	0.9	0.78	1469.4	12.4	1463.2	9.4	1454.3	14.3	1454.3	14.3	101.0
K13-NAC-2A-29	138	386393	1.4	10.8844	0.9	3.2260	1.2	0.2547	0.8	0.67	1462.5	10.7	1463.4	9.4	1464.8	17.2	1464.8	17.2	99.8
K13-NAC-2A-30	180	64241	1.8	10.9457	0.5	3.2160	0.7	0.2553	0.5	0.72	1465.8	6.9	1461.0	5.7	1454.1	9.8	1454.1	9.8	100.8
K13-NAC-2B-1	43	39925	1.5	10.8636	2.4	3.2738	3.3	0.2579	2.3	0.70	1479.3	30.6	1474.9	25.8	1468.4	45.0	1468.4	45.0	100.7
K13-NAC-2B-2	127	155245	1.5	10.9764	0.8	3.2427	1.4	0.2581	1.1	0.79	1480.4	14.2	1467.4	10.5	1448.8	15.8	1448.8	15.8	102.2

K13-NAC-2B-4	32	22335	1.2	11.4030	2.2	3.0346	2.8	0.2510	1.8	0.63	1443.5	23.2	1416.4	21.6	1375.8	42.1	1375.8	42.1	104.9
K13-NAC-2B-5	171	237642	1.0	11.0033	0.5	3.1617	2.0	0.2523	1.9	0.97	1450.4	25.0	1447.9	15.3	1444.1	8.7	1444.1	8.7	100.4
K13-NAC-2B-6	79	137572	1.0	11.0453	1.5	3.1746	1.9	0.2543	1.1	0.59	1460.7	14.5	1451.0	14.7	1436.8	29.3	1436.8	29.3	101.7
K13-NAC-2B-7	310	84678	1.2	10.9388	0.6	3.1845	2.2	0.2526	2.1	0.96	1452.1	27.2	1453.4	16.9	1455.3	12.0	1455.3	12.0	99.8
K13-NAC-2B-8	127	67701	2.0	10.9221	0.6	3.2108	1.2	0.2543	1.0	0.84	1460.8	13.0	1459.8	9.2	1458.2	12.3	1458.2	12.3	100.2
K13-NAC-2B-9	194	165523	1.9	10.9998	0.4	3.1725	0.9	0.2531	0.8	0.91	1454.4	10.6	1450.5	6.9	1444.7	6.9	1444.7	6.9	100.7
K13-NAC-2B-10	209	39378	2.0	10.9921	0.4	3.2119	0.8	0.2561	0.7	0.88	1469.6	8.9	1460.0	5.9	1446.0	6.8	1446.0	6.8	101.6
K13-NAC-2B-11	104	118072	1.3	10.9308	0.7	3.0147	1.1	0.2390	0.9	0.76	1381.5	10.9	1411.3	8.7	1456.7	14.1	1456.7	14.1	94.8
K13-NAC-2B-12	80	50424	1.1	11.1077	1.1	3.0431	1.4	0.2452	0.8	0.58	1413.4	10.2	1418.5	10.6	1426.1	21.5	1426.1	21.5	99.1
K13-NAC-2B-13	95	95593	1.6	10.8979	0.7	3.1986	1.2	0.2528	0.9	0.79	1453.0	12.0	1456.8	9.0	1462.4	13.4	1462.4	13.4	99.4
K13-NAC-2B-14	87	98494	1.5	11.0498	1.1	3.1990	1.8	0.2564	1.5	0.80	1471.2	19.1	1456.9	14.0	1436.1	20.7	1436.1	20.7	102.4
K13-NAC-2B-15	109	77412	1.3	10.9928	0.9	3.2270	2.5	0.2573	2.3	0.93	1475.9	30.2	1463.7	19.1	1445.9	17.4	1445.9	17.4	102.1
K13-NAC-2B-16	122	39099	1.0	10.9512	1.1	3.2722	7.0	0.2599	6.9	0.99	1489.3	92.1	1474.5	54.6	1453.1	21.3	1453.1	21.3	102.5
K13-NAC-2B-17	106	35718	1.4	11.0795	0.6	2.9392	1.9	0.2362	1.8	0.95	1366.8	22.2	1392.1	14.4	1431.0	11.6	1431.0	11.6	95.5
K13-NAC-2B-19	103	67516	1.9	11.0329	1.3	3.1665	1.5	0.2534	0.7	0.50	1455.9	9.7	1449.0	11.4	1439.0	24.5	1439.0	24.5	101.2
K13-NAC-2B-20	165	134780	1.5	10.9626	0.6	3.2022	1.0	0.2546	0.8	0.78	1462.2	10.2	1457.7	7.7	1451.2	11.8	1451.2	11.8	100.8
K13-NAC-2B-21	129	71507	1.5	10.8941	0.7	3.1975	1.1	0.2526	0.8	0.74	1452.1	10.4	1456.6	8.4	1463.1	13.9	1463.1	13.9	99.2
K13-NAC-2B-22	101	69936	1.4	10.9715	0.5	3.1502	1.3	0.2507	1.2	0.92	1441.9	15.5	1445.1	10.0	1449.6	9.6	1449.6	9.6	99.5
K13-NAC-2B-23	39	37557	1.3	11.0542	1.2	3.1780	1.4	0.2548	0.7	0.52	1463.1	9.7	1451.8	11.1	1435.3	23.4	1435.3	23.4	101.9
K13-NAC-2B-24	133	147531	1.4	10.9737	0.5	3.2277	1.2	0.2569	1.1	0.89	1473.9	14.0	1463.8	9.2	1449.2	10.3	1449.2	10.3	101.7
K13-NAC-2B-25	81	91680	1.4	10.9198	1.4	3.2563	2.1	0.2579	1.6	0.76	1479.1	21.0	1470.7	16.3	1458.6	26.1	1458.6	26.1	101.4
K13-NAC-2B-27	95	79396	1.1	10.9894	0.7	3.1917	1.4	0.2544	1.2	0.86	1461.1	15.9	1455.2	10.9	1446.5	13.8	1446.5	13.8	101.0
K13-NAC-2B-27	81	16552	1.9	10.9426	0.7	3.1014	2.7	0.2461	2.6	0.96	1418.5	32.6	1433.0	20.4	1454.6	13.8	1454.6	13.8	97.5
K13-NAC-2B-29	121	270575	1.4	11.0009	0.7	3.2012	1.3	0.2554	1.1	0.85	1466.3	14.6	1457.4	10.2	1444.5	13.2	1444.5	13.2	101.5
K13-NAC-2B-30	100	24257	1.5	10.9262	1.2	3.0373	2.5	0.2407	2.2	0.87	1390.3	27.7	1417.0	19.4	1457.5	23.7	1457.5	23.7	95.4
C13-098-28	192	62969	2.7	9.6745	0.8	4.3419	1.3	0.3047	1.0	0.78	1714.4	15.2	1701.4	10.7	1685.4	14.9	1685.4	14.9	101.7
C13-098-32	344	84309	2.8	9.6012	0.5	4.4251	0.9	0.3081	0.7	0.84	1731.6	11.1	1717.1	7.2	1699.4	8.7	1699.4	8.7	101.9
C13-098-4	181	196094	2.3	9.5989	1.0	4.3628	2.3	0.3037	2.1	0.91	1709.8	32.1	1705.3	19.3	1699.8	17.6	1699.8	17.6	100.6
C13-098-25	264	284947	1.9	9.5926	0.3	4.3246	1.3	0.3009	1.3	0.97	1695.6	19.2	1698.1	10.9	1701.1	6.0	1701.1	6.0	99.7
C13-098-18	495	20496	2.2	9.5864	0.4	4.3442	0.8	0.3020	0.7	0.88	1701.4	11.1	1701.8	6.9	1702.2	7.2	1702.2	7.2	100.0
C13-098-1	300	308018	2.9	9.5861	0.5	4.3402	0.7	0.3018	0.5	0.72	1700.0	7.6	1701.0	5.9	1702.3	9.1	1702.3	9.1	99.9
C13-098-9	487	314889	2.3	9.5658	0.4	4.3329	0.9	0.3006	0.8	0.87	1694.3	11.3	1699.6	7.2	1706.2	7.9	1706.2	7.9	99.3
C13-098-5	319	91583	2.2	9.5647	0.4	4.3727	0.7	0.3033	0.5	0.75	1707.8	7.7	1707.2	5.6	1706.4	8.2	1706.4	8.2	100.1
C13-098-21	243	47820	2.2	9.5609	0.6	4.4062	0.7	0.3055	0.4	0.59	1718.7	6.4	1713.5	5.9	1707.1	10.6	1707.1	10.6	100.7
C13-098-17	314	170887	2.3	9.5512	0.6	4.3576	0.9	0.3019	0.7	0.75	1700.5	10.1	1704.3	7.4	1709.0	11.0	1709.0	11.0	99.5
C13-098-11	433	27359	2.4	9.5405	0.8	4.3797	1.2	0.3031	0.9	0.76	1706.4	13.6	1708.5	9.9	1711.1	14.4	1711.1	14.4	99.7
C13-098-10	222	24832	2.1	9.5366	1.0	4.3067	1.1	0.2979	0.5	0.40	1680.8	6.7	1694.7	9.2	1711.8	18.8	1711.8	18.8	98.2
C13-098-16	339	4407	2.6	9.5360	0.8	4.3680	1.0	0.3021	0.6	0.59	1701.7	8.9	1706.3	8.3	1711.9	15.0	1711.9	15.0	99.4
C13-098-22	419	25490	1.9	9.5332	1.3	4.5313	2.7	0.3133	2.4	0.87	1756.9	36.4	1736.7	22.5	1712.5	24.2	1712.5	24.2	102.6
C13-098-20	213	6753	1.6	9.5318	1.2	4.2510	1.8	0.2939	1.3	0.75	1660.9	19.3	1683.9	14.5	1712.8	21.7	1712.8	21.7	97.0
C13-098-14	167	205584	3.3	9.5257	0.8	4.3579	0.9	0.3011	0.4	0.46	1696.6	6.3	1704.4	7.5	1713.9	14.7	1713.9	14.7	99.0
C13-098-15	136	67147	2.2	9.5167	1.1	4.3895	1.4	0.3030	0.8	0.59	1706.0	11.9	1710.4	11.2	1715.7	20.2	1715.7	20.2	99.4

C13-098-31	214	6491	1.8	9.5143	1.8	4.1951	2.8	0.2895	2.1	0.75	1638.9	30.2	1673.1	22.7	1716.1	33.5	1716.1	33.5	95.5
C13-098-27	201	22854	2.3	9.4940	2.0	4.3532	2.7	0.2997	1.8	0.66	1690.1	26.5	1703.5	22.3	1720.1	37.3	1720.1	37.3	98.3
C13-098-34	83	1978	1.1	9.4035	3.8	3.8295	5.5	0.2612	3.9	0.72	1495.8	52.6	1599.0	44.1	1737.6	69.7	1737.6	69.7	86.1
C13-098-6	204	4546	1.6	9.3408	3.4	4.2066	3.6	0.2850	1.2	0.34	1616.4	17.8	1675.3	29.9	1749.9	62.6	1749.9	62.6	92.4
C13-101A-2	120	159082	2.1	9.6593	0.6	4.3199	0.9	0.3026	0.6	0.72	1704.4	9.2	1697.2	7.0	1688.3	10.9	1688.3	10.9	101.0
C13-101A-3	114	199803	1.9	9.5831	0.8	4.3719	2.2	0.3039	2.1	0.94	1710.4	31.6	1707.0	18.5	1702.9	13.9	1702.9	13.9	100.4
C13-101A-4	86	169659	2.2	9.6240	0.8	4.2119	1.7	0.2940	1.5	0.88	1661.4	21.8	1676.3	13.8	1695.0	14.7	1695.0	14.7	98.0
C13-101A-6	130	34445	2.1	9.6783	0.5	4.0439	1.5	0.2839	1.4	0.94	1610.7	19.9	1643.1	12.0	1684.7	9.1	1684.7	9.1	95.6
C13-101A-7	69	15115	2.6	9.4959	2.1	4.3821	2.8	0.3018	1.8	0.64	1700.2	26.8	1709.0	23.0	1719.7	39.2	1719.7	39.2	98.9
C13-101A-8	66	19303	1.9	9.5645	0.7	4.3149	1.1	0.2993	0.9	0.80	1687.9	13.6	1696.2	9.4	1706.5	12.7	1706.5	12.7	98.9
C13-101A-9	83	107622	2.6	9.5660	0.6	4.3837	1.2	0.3041	1.0	0.85	1711.8	15.0	1709.3	9.7	1706.2	11.2	1706.2	11.2	100.3
C13-101A-10	96	82320	2.6	9.5778	0.8	4.3269	1.7	0.3006	1.5	0.89	1694.1	22.8	1698.5	14.1	1703.9	14.2	1703.9	14.2	99.4
C13-101A-11	81	10432	1.9	9.5329	1.8	4.4159	2.4	0.3053	1.6	0.65	1717.6	24.0	1715.3	20.2	1712.5	33.9	1712.5	33.9	100.3
C13-101A-12	136	237837	2.3	9.5440	0.6	4.3289	1.3	0.2996	1.1	0.90	1689.6	16.9	1698.9	10.5	1710.4	10.4	1710.4	10.4	98.8
C13-101A-13	86	154784	2.3	9.5681	0.7	4.4050	3.3	0.3057	3.3	0.98	1719.4	49.3	1713.3	27.6	1705.8	12.3	1705.8	12.3	100.8
C13-101A-15	122	183975	3.1	9.6418	0.5	4.2798	1.2	0.2993	1.1	0.89	1687.7	16.0	1689.5	9.9	1691.6	10.1	1691.6	10.1	99.8
C13-101A-17	82	213930	2.7	9.6012	0.6	4.2932	1.3	0.2990	1.1	0.89	1686.1	16.9	1692.1	10.5	1699.4	10.7	1699.4	10.7	99.2
C13-101A-18	84	48489	2.0	9.5465	1.0	4.3224	2.0	0.2993	1.8	0.87	1687.7	26.2	1697.6	16.6	1709.9	18.1	1709.9	18.1	98.7
C13-101A-19	162	140870	1.8	9.6077	0.4	4.3710	2.4	0.3046	2.4	0.99	1714.0	36.1	1706.9	20.1	1698.1	7.6	1698.1	7.6	100.9
C13-101A-20	76	7749	1.7	9.5848	0.9	3.5897	1.9	0.2495	1.7	0.87	1436.1	21.5	1547.3	15.3	1702.5	17.5	1702.5	17.5	84.4
C13-101A-21	94	158126	2.3	9.6088	0.7	4.3390	1.1	0.3024	0.8	0.77	1703.1	12.5	1700.8	9.0	1697.9	12.9	1697.9	12.9	100.3
C13-101A-22	156	159698	2.3	9.6029	0.4	4.2688	0.6	0.2973	0.4	0.77	1677.9	6.6	1687.4	4.8	1699.1	6.8	1699.1	6.8	98.8
C13-101A-23	81	22127	1.6	9.6391	1.0	4.0106	3.0	0.2804	2.8	0.94	1593.3	39.9	1636.4	24.4	1692.1	18.5	1692.1	18.5	94.2
C13-101A-25	134	158117	2.3	9.6122	0.2	4.3680	1.0	0.3045	0.9	0.97	1713.7	13.9	1706.3	7.9	1697.3	4.6	1697.3	4.6	101.0
C13-101A-26	65	86257	2.2	9.6267	1.1	4.3732	3.0	0.3053	2.8	0.93	1717.7	41.8	1707.3	24.6	1694.5	20.0	1694.5	20.0	101.4
C13-101A-27	85	98162	2.5	9.6000	0.7	4.3723	1.0	0.3044	0.7	0.71	1713.2	10.2	1707.1	7.9	1699.6	12.5	1699.6	12.5	100.8
C13-101A-28	132	83599	1.8	9.5925	0.6	4.2932	1.5	0.2987	1.3	0.92	1684.8	20.0	1692.1	12.1	1701.1	10.7	1701.1	10.7	99.0
C13-101A-29	132	53600	2.4	9.5262	0.8	3.8384	7.6	0.2652	7.5	0.99	1516.4	101.7	1600.8	61.0	1713.8	14.6	1713.8	14.6	88.5
C13-101A-30	49	111800	2.0	9.7062	0.5	4.3073	2.9	0.3032	2.8	0.99	1707.3	42.3	1694.8	23.5	1679.3	8.3	1679.3	8.3	101.7
C13-101A-31	117	7965	1.8	9.6899	1.0	3.5793	3.4	0.2515	3.2	0.96	1446.4	41.9	1545.0	26.8	1682.4	18.1	1682.4	18.1	86.0
C13-101A-32	84	21351	1.8	9.6095	0.9	4.2056	1.3	0.2931	0.9	0.71	1657.0	13.4	1675.1	10.6	1697.8	16.9	1697.8	16.9	97.6
C13-101A-33	96	137775	2.5	9.6103	0.6	4.3596	1.8	0.3039	1.7	0.94	1710.5	25.1	1704.7	14.6	1697.7	10.7	1697.7	10.7	100.8
C13-101A-34	180	9537	2.6	9.6446	0.5	4.1106	0.9	0.2875	0.8	0.84	1629.2	11.3	1656.4	7.6	1691.1	9.2	1691.1	9.2	96.3
C13-101A-35	122	71063	2.1	9.6054	0.6	4.3366	1.3	0.3021	1.2	0.90	1701.7	17.5	1700.3	10.8	1698.6	10.8	1698.6	10.8	100.2
C13-101A-36	98	134567	2.2	9.6344	0.5	4.3505	1.3	0.3040	1.2	0.92	1711.1	17.4	1703.0	10.4	1693.0	9.2	1693.0	9.2	101.1
C13-101A-37	126	62069	2.4	9.6014	0.6	4.2981	2.5	0.2993	2.4	0.97	1687.8	35.1	1693.0	20.2	1699.4	11.8	1699.4	11.8	99.3
C13-101A-38	154	9681	1.9	9.5737	1.0	4.3252	3.2	0.3003	3.0	0.95	1692.9	44.4	1698.2	26.0	1704.7	19.0	1704.7	19.0	99.3
C13-101A-39	147	284395	1.8	9.6012	0.4	4.3252	1.0	0.3012	0.9	0.91	1697.2	13.9	1698.2	8.4	1699.4	7.7	1699.4	7.7	99.9
C13-101A-40	85	82945	2.4	9.6012	0.5	4.3936	1.1	0.3059	1.0	0.89	1720.7	14.6	1711.1	9.0	1699.4	9.2	1699.4	9.2	101.3
C13-101A-42	119	186821	2.5	9.6039	0.3	4.3682	2.9	0.3043	2.9	0.99	1712.4	43.8	1706.3	24.2	1698.9	5.5	1698.9	5.5	100.8
C13-101A-43	77	11189	2.2	9.5500	1.3	4.3688	1.8	0.3026	1.3	0.70	1704.2	19.0	1706.5	14.9	1709.3	23.6	1709.3	23.6	99.7
C13-101A-45	102	107583	1.9	9.6327	0.8	4.3105	2.7	0.3011	2.6	0.95	1697.0	38.4	1695.4	22.3	1693.4	15.6	1693.4	15.6	100.2

C13-101A-46	117	4204	2.7	9.5332	0.7	4.3796	1.2	0.3028	0.9	0.80	1705.2	13.9	1708.5	9.6	1712.5	12.9	1712.5	12.9	99.6
C13-101A-47	72	47832	2.5	9.6092	0.6	4.3705	3.0	0.3046	2.9	0.98	1714.0	43.6	1706.8	24.5	1697.9	11.3	1697.9	11.3	101.0
C13-101A-48	165	163731	1.7	9.6151	0.3	4.3697	2.4	0.3047	2.4	0.99	1714.7	36.4	1706.6	20.2	1696.7	5.7	1696.7	5.7	101.1
C13-101A-49	123	104410	2.4	9.6207	0.6	4.3841	1.1	0.3059	0.9	0.85	1720.5	13.6	1709.4	8.8	1695.7	10.5	1695.7	10.5	101.5
C13-101A-50	118	14197	1.9	9.6503	0.6	3.6920	3.4	0.2584	3.3	0.99	1481.7	44.1	1569.6	27.0	1690.0	10.2	1690.0	10.2	87.7
C13-101A-51	59	14837	2.4	9.5027	2.1	4.4148	3.2	0.3043	2.4	0.76	1712.4	36.8	1715.1	26.7	1718.4	38.5	1718.4	38.5	99.7
C13-101A-52	106	158050	2.2	9.6164	0.7	4.3715	1.4	0.3049	1.2	0.88	1715.5	18.7	1707.0	11.7	1696.5	12.4	1696.5	12.4	101.1
C13-101A-53	100	136005	2.1	9.6028	0.6	4.4294	2.4	0.3085	2.3	0.97	1733.3	34.8	1717.8	19.6	1699.1	11.3	1699.1	11.3	102.0
C13-101A-54	79	11145	2.0	9.5891	0.8	4.1704	1.5	0.2900	1.3	0.84	1641.7	18.4	1668.2	12.4	1701.7	15.2	1701.7	15.2	96.5
C13-101A-55	110	9963	2.0	9.6667	0.8	4.0636	4.2	0.2849	4.1	0.98	1616.0	58.9	1647.0	34.2	1686.9	15.1	1686.9	15.1	95.8
C13-101A-56	108	141505	1.8	9.6102	0.6	4.2468	2.9	0.2960	2.8	0.98	1671.4	41.5	1683.1	23.7	1697.7	11.2	1697.7	11.2	98.5
C13-101A-57	172	373660	2.2	9.6081	0.3	4.3711	0.5	0.3046	0.4	0.73	1714.1	5.4	1706.9	4.0	1698.1	6.2	1698.1	6.2	100.9
C13-101A-59	144	266451	2.1	9.6124	0.4	4.3065	1.4	0.3002	1.3	0.94	1692.4	19.1	1694.6	11.2	1697.2	8.2	1697.2	8.2	99.7
C13-101A-63	119	9710	2.1	9.5999	0.6	4.2242	1.4	0.2941	1.2	0.89	1662.0	17.8	1678.7	11.3	1699.7	11.8	1699.7	11.8	97.8
C13-101A-64	82	8381	2.1	9.5884	0.8	4.1830	2.1	0.2909	1.9	0.92	1646.0	27.9	1670.7	17.2	1701.9	15.4	1701.9	15.4	96.7
C13-101A-65	121	149656	2.1	9.6168	0.6	4.4336	1.8	0.3092	1.7	0.93	1737.0	25.5	1718.6	14.8	1696.4	11.7	1696.4	11.7	102.4
C13-101A-66	142	88120	2.4	9.6124	0.4	4.3078	0.7	0.3003	0.5	0.77	1692.9	7.4	1694.8	5.4	1697.2	7.7	1697.2	7.7	99.7
C13-101A-67	145	222169	2.2	9.5932	0.5	4.3571	1.7	0.3031	1.6	0.95	1706.9	24.3	1704.2	14.1	1700.9	9.9	1700.9	9.9	100.3
C13-101A-68	125	152689	2.1	9.5919	0.9	4.4703	4.6	0.3110	4.5	0.98	1745.6	68.9	1725.5	38.1	1701.2	16.6	1701.2	16.6	102.6
C13-101A-69	69	39354	2.1	9.5374	0.9	4.1385	1.3	0.2863	0.8	0.66	1622.8	11.9	1661.9	10.3	1711.7	17.3	1711.7	17.3	94.8
C13-101A-70	121	93657	1.7	9.6261	0.4	4.3478	1.0	0.3035	1.0	0.92	1708.9	14.5	1702.5	8.6	1694.6	7.5	1694.6	7.5	100.8
C13-101A-71	141	100185	2.5	9.5717	0.3	4.2887	0.9	0.2977	0.8	0.94	1680.0	12.5	1691.2	7.4	1705.1	5.7	1705.1	5.7	98.5
C13-101A-73	65	55660	2.4	9.6706	1.0	4.3402	1.9	0.3044	1.6	0.84	1713.1	24.0	1701.0	15.7	1686.1	19.1	1686.1	19.1	101.6
C13-101A-74	93	30719	2.2	9.5631	0.8	4.4220	4.1	0.3067	4.0	0.98	1724.5	60.6	1716.5	33.8	1706.7	14.1	1706.7	14.1	101.0
C13-101A-75	152	91109	2.3	9.5166	1.0	4.3345	1.6	0.2992	1.2	0.79	1687.2	18.3	1699.9	12.9	1715.7	17.6	1715.7	17.6	98.3
C13-101A-76	136	123150	2.4	9.5908	0.5	4.2617	1.7	0.2964	1.6	0.95	1673.6	24.0	1686.0	14.1	1701.4	9.7	1701.4	9.7	98.4
C13-101A-77	70	136053	3.0	9.5291	1.0	4.3964	2.1	0.3038	1.8	0.88	1710.3	27.4	1711.7	17.2	1713.3	18.1	1713.3	18.1	99.8
C13-101A-78	121	88211	2.3	9.5935	0.4	4.3863	1.1	0.3052	1.0	0.92	1717.0	15.1	1709.8	9.0	1700.9	7.6	1700.9	7.6	100.9
C13-101A-80	79	93775	2.1	9.5708	0.7	4.3593	1.6	0.3026	1.4	0.91	1704.2	21.4	1704.7	13.0	1705.2	12.2	1705.2	12.2	99.9
C13-101A-81	109	119412	1.9	9.5480	0.5	4.2871	1.8	0.2969	1.7	0.96	1675.8	24.9	1690.9	14.4	1709.6	8.9	1709.6	8.9	98.0
C13-101A-82	134	144263	1.8	9.5817	0.5	4.3322	1.6	0.3011	1.5	0.94	1696.6	22.3	1699.5	13.0	1703.1	9.6	1703.1	9.6	99.6
C13-101A-83	108	322198	2.5	9.5626	0.6	4.2808	0.8	0.2969	0.6	0.73	1675.9	9.1	1689.7	7.0	1706.8	10.7	1706.8	10.7	98.2
C13-101A-84	94	117520	1.9	9.6138	0.6	4.2942	1.0	0.2994	0.8	0.82	1688.4	11.8	1692.2	8.0	1697.0	10.3	1697.0	10.3	99.5
C13-101A-85	100	9879	2.5	9.3874	3.0	4.5345	3.6	0.3087	2.0	0.56	1734.4	30.8	1737.3	30.2	1740.8	55.1	1740.8	55.1	99.6
C13-101A-86	111	119969	2.4	9.5797	0.5	4.3662	0.9	0.3034	0.7	0.82	1707.9	11.2	1706.0	7.5	1703.5	9.6	1703.5	9.6	100.3
C13-101A-87	172	152083	2.2	9.6027	0.4	4.3350	0.7	0.3019	0.6	0.82	1700.8	8.8	1700.0	5.9	1699.1	7.6	1699.1	7.6	100.1
C13-101A-88	109	7020	2.0	9.6030	0.8	3.7144	5.2	0.2587	5.1	0.99	1483.2	68.0	1574.5	41.6	1699.1	14.7	1699.1	14.7	87.3
C13-101A-89	128	133182	2.3	9.6052	0.4	4.3170	0.9	0.3007	0.8	0.90	1695.0	11.9	1696.6	7.4	1698.6	7.3	1698.6	7.3	99.8
C13-101A-90	180	98428	2.2	9.5954	0.4	4.3579	0.9	0.3033	0.8	0.90	1707.5	12.5	1704.4	7.7	1700.5	7.6	1700.5	7.6	100.4
C13-101A-91	149	202386	2.4	9.5641	0.4	4.4498	1.0	0.3087	0.9	0.93	1734.1	13.5	1721.7	7.9	1706.5	6.6	1706.5	6.6	101.6
C13-101A-92	94	79054	2.5	9.6495	0.6	4.3547	1.2	0.3048	1.0	0.84	1714.9	14.8	1703.8	9.7	1690.2	11.8	1690.2	11.8	101.5
C13-101A-93	74	114358	2.3	9.5936	0.7	4.3619	2.2	0.3035	2.0	0.95	1708.6	30.7	1705.2	17.8	1700.9	12.6	1700.9	12.6	100.5
C13-101A-94	154	240338	2.4	9.5764	0.4	4.3689	1.2	0.3034	1.1	0.93	1708.4	16.7	1706.5	9.9	1704.2	8.1	1704.2	8.1	100.2

C13-101A-96	185	220395	2.4	9.5980	0.4	4.3233	1.6	0.3009	1.5	0.96	1696.0	22.2	1697.8	12.8	1700.0	7.9	1700.0	7.9	99.8
C13-101A-98	73	67728	2.5	9.5807	0.7	4.3593	1.8	0.3029	1.7	0.92	1705.7	25.5	1704.7	15.3	1703.3	13.2	1703.3	13.2	100.1

Table A3-2. Lu-Hf isotope results from igneous zircon (ALC)

Sample	(176Yb+176Lu) / 176Hf (%)	Volts Hf	176Hf/177Hf	± (1s)	176Lu/177Hf	176Hf/177Hf (T)	E-Hf (0)	± (1s)	E-Hf (T)	Age (Ma) zircon	Age (Ma) pluton	176Hf/177Hf(t) pluton
TG15-ZUN4 9	41.6	6.2	0.282001	0.000029	0.002562	0.281909	-27.7	1.0	11.8	1891	1891	0.281909
TG15-ZUN4 5	25.1	7.0	0.281960	0.000020	0.001494	0.281913	-29.2	0.7	6.5	1656	1655	0.281913
TG15-ZUN4 22	29.9	3.5	0.282018	0.000037	0.002239	0.281947	-27.1	1.3	7.8	1659	1655	0.281947
TG15-ZUN4 12	17.5	7.0	0.281982	0.000017	0.001089	0.281948	-28.4	0.6	7.7	1655	1655	0.281948
TG15-ZUN4 10	22.3	7.5	0.282003	0.000024	0.001344	0.281961	-27.6	0.8	8.2	1657	1655	0.281961
TG15-ZUN4 25	27.0	7.3	0.282015	0.000020	0.001602	0.281965	-27.2	0.7	8.3	1653	1655	0.281965
TG15-ZUN4 19	43.8	3.1	0.282070	0.000070	0.003321	0.281965	-25.3	2.5	8.4	1657	1655	0.281965
TG15-ZUN4 27	34.2	3.6	0.282041	0.000038	0.002258	0.281971	-26.3	1.3	8.4	1650	1655	0.281970
TG15-ZUN4 20	21.4	7.2	0.282032	0.000023	0.001441	0.281987	-26.6	0.8	9.1	1656	1655	0.281987
TG15-ZUN4 21	27.3	3.8	0.282069	0.000035	0.001797	0.282013	-25.3	1.3	9.9	1651	1655	0.282013
TG15-ZUN4 6	29.3	2.1	0.282132	0.000047	0.002243	0.282062	-23.1	1.7	11.7	1654	1655	0.282062
TG15-PIC-5 61	18.8	3.7	0.281928	0.000028	0.001190	0.281889	-30.3	1.0	6.8	1704	1700	0.281889
TG15-PIC-5 52	34.2	6.0	0.281968	0.000028	0.002427	0.281889	-28.9	1.0	7.1	1718	1700	0.281890
TG15-PIC5 48	24.5	4.1	0.281985	0.000021	0.002144	0.281917	-28.3	0.7	7.3	1687	1700	0.281916
TG15-PIC-5 62	16.6	5.6	0.281958	0.000021	0.001009	0.281925	-29.3	0.7	7.7	1689	1700	0.281925
TG15-PIC5 42	21.2	6.4	0.281972	0.000024	0.001312	0.281930	-28.7	0.8	7.7	1681	1700	0.281930
TG15-PIC-5 56	24.5	3.6	0.281993	0.000035	0.001867	0.281932	-28.0	1.2	8.3	1705	1700	0.281932
TG15-PIC5 46	23.6	2.9	0.281992	0.000026	0.001799	0.281935	-28.0	0.9	7.9	1682	1700	0.281934
TG15-PIC5 37	20.5	6.9	0.281984	0.000017	0.001233	0.281944	-28.3	0.6	8.7	1704	1700	0.281944
TG15-PIC5 39	21.6	4.5	0.282029	0.000033	0.001721	0.281974	-26.7	1.2	9.6	1699	1700	0.281974
TG15-PIC5 40	22.8	2.7	0.282029	0.000048	0.001699	0.281974	-26.7	1.7	9.4	1689	1700	0.281974
TG15-PIC-5 58	32.7	5.2	0.281945	0.000035	0.002264	0.281868	-29.7	1.2	8.0	1791	1791	0.281868
TG15-PIC5 49	42.0	4.4	0.281945	0.000050	0.002675	0.281852	-29.7	1.8	8.4	1833	1833	0.281852
TG15-PIC5 38	24.4	6.4	0.281959	0.000022	0.001973	0.281890	-29.2	0.8	10.0	1841	1841	0.281890
TG15-PIC-5 59	24.4	5.7	0.281963	0.000021	0.001436	0.281911	-29.1	0.7	12.1	1903	1903	0.281911
TG15-PIC5-36	24.4	5.9	0.281984	0.000021	0.001468	0.281930	-28.3	0.7	13.4	1927	1927	0.281930
K15-SEV-ES-RHY 20	22.4	5.8	0.282048	0.000023	0.001284	0.282008	-26.1	0.8	9.7	1648	1665	0.282008

K15-SEV-ES-RHY 22	21.9	5.4	0.282056	0.000025	0.001181	0.282019	-25.8	0.9	10.2	1653	1665	0.282018
K15-SEV-ES-RHY 21	47.3	6.2	0.282078	0.000020	0.002710	0.281993	-25.0	0.7	9.5	1665	1665	0.281993
K15-SEV-ES-RHY 19	21.5	6.0	0.282035	0.000026	0.001221	0.281996	-26.5	0.9	9.9	1675	1665	0.281997
K15-SEV-ES-RHY 18	33.8	4.6	0.282063	0.000025	0.002025	0.281999	-25.5	0.9	10.0	1674	1665	0.281999
k15-SEV-ES-RHY 10	19.9	5.9	0.282036	0.000022	0.001151	0.282000	-26.5	0.8	9.7	1661	1665	0.281999
k15-SEV-ES-RHY 12	13.9	6.2	0.282027	0.000018	0.000818	0.282002	-26.8	0.6	9.7	1657	1665	0.282001
k15-SEV-ES-RHY 16	28.2	5.0	0.282062	0.000022	0.001590	0.282012	-25.6	0.8	10.2	1664	1665	0.282012
k15-SEV-ES-RHY 9	35.4	5.2	0.282081	0.000024	0.002070	0.282016	-24.9	0.8	10.4	1668	1665	0.282016
k15-SEV-ES-RHY 11	16.4	5.0	0.282054	0.000026	0.000967	0.282024	-25.8	0.9	10.6	1665	1665	0.282024
TG15-OJITO 60	18.0	5.8	0.281969	0.000023	0.001108	0.281935	-28.8	0.8	7.2	1653	1661	0.281935
TG15-OJITO 57	17.0	5.9	0.281983	0.000018	0.001043	0.281950	-28.4	0.7	7.9	1657	1661	0.281950
TG15-OJITO 52	16.4	6.1	0.282008	0.000021	0.001013	0.281976	-27.5	0.7	8.9	1662	1661	0.281976
TG15-OJITO 56	22.6	5.6	0.282019	0.000024	0.001356	0.281977	-27.1	0.8	8.9	1664	1661	0.281977
TG15-OJITO 62	14.9	6.0	0.282012	0.000023	0.000890	0.281984	-27.3	0.8	9.3	1668	1661	0.281984
TG15-OJITO 58	26.7	5.1	0.282021	0.000026	0.001634	0.281966	-27.0	0.9	11.3	1782	1782	0.281966
TG15-OJITO 61	36.4	4.9	0.281981	0.000026	0.002102	0.281898	-28.4	0.9	15.6	2072	2072	0.281898
K14-MANZANITA 35	37.1	6.8	0.281980	0.000020	0.002229	0.281911	-28.5	0.7	6.0	1637	1655	0.281910
K14-MANZANITA 64	31.8	7.1	0.281993	0.000018	0.001987	0.281930	-28.0	0.6	7.1	1653	1655	0.281930
K14-MANZANITA 4	36.8	7.1	0.282005	0.000020	0.002201	0.281935	-27.6	0.7	7.5	1663	1655	0.281936
K14-MANZANITA 42	48.1	7.2	0.282040	0.000022	0.003001	0.281947	-26.4	0.8	7.2	1634	1655	0.281945
K14-MANZANITA 34	15.6	8.2	0.281979	0.000027	0.001033	0.281947	-28.5	1.0	7.5	1648	1655	0.281947
K14-MANZANITA 36	20.0	6.9	0.281991	0.000014	0.001210	0.281953	-28.1	0.5	7.4	1635	1655	0.281953
K14-MANZANITA 68	21.0	6.7	0.282008	0.000018	0.001279	0.281967	-27.5	0.6	8.4	1653	1655	0.281967
K14-MANZANITA 41	24.8	7.4	0.282031	0.000020	0.001853	0.281973	-26.7	0.7	8.3	1644	1655	0.281972
K14-MANZANITA 33	34.3	5.9	0.282047	0.000020	0.001989	0.281985	-26.1	0.7	8.8	1645	1655	0.281984
K14-MANZANITA 37	31.1	5.9	0.282034	0.000022	0.001836	0.281973	-26.6	0.8	10.5	1735	1735	0.281973
K14-MANZANITA 9	16.5	6.3	0.281920	0.000019	0.001009	0.281886	-30.6	0.7	7.5	1741	1741	0.281886
K14-MANZANITA 13	25.0	6.1	0.281978	0.000022	0.001522	0.281927	-28.5	0.8	9.0	1742	1742	0.281927
K14-MANZANITA 44	23.4	6.1	0.282011	0.000026	0.001426	0.281964	-27.4	0.9	10.3	1744	1744	0.281964
K14-MANZANITA 20	22.1	6.4	0.281974	0.000019	0.001362	0.281929	-28.7	0.7	9.2	1750	1750	0.281929
K13-TUSAS-1-23	29.2	1.8	0.281807	0.000051	0.001891	0.281744	-34.6	1.8	2.9	1759	1758	0.281744
K13-TUSAS-1-17	25.7	1.8	0.281856	0.000038	0.001593	0.281803	-32.8	1.3	4.9	1755	1758	0.281803
K13-TUSAS-1-22	27.4	1.9	0.281910	0.000041	0.001744	0.281852	-30.9	1.5	6.6	1756	1758	0.281852
K13-TUSAS-1-6	28.0	1.9	0.281924	0.000044	0.001832	0.281862	-30.5	1.6	7.1	1758	1758	0.281862

K13-TUSAS-1-4	81.9	1.6	0.282026	0.000056	0.004667	0.281870	-26.8	2.0	7.4	1761	1758	0.281871
K13-TUSAS-1-27	25.7	1.7	0.281974	0.000044	0.001666	0.281919	-28.7	1.6	8.9	1751	1758	0.281918
K13-TUSAS-1-11	21.4	2.0	0.281968	0.000040	0.001413	0.281921	-28.9	1.4	9.1	1757	1758	0.281921
K13-TUSAS-1-28	30.1	1.9	0.281995	0.000039	0.001855	0.281934	-27.9	1.4	9.4	1750	1758	0.281933
K13-TUSAS-1-19	58.9	1.6	0.282042	0.000062	0.003112	0.281938	-26.3	2.2	9.7	1758	1758	0.281938
K13-TUSAS-1-20	29.7	1.9	0.282016	0.000047	0.001895	0.281953	-27.2	1.7	10.2	1757	1758	0.281953
K13-TUSAS-1-9	56.4	1.7	0.282078	0.000048	0.003133	0.281973	-25.0	1.7	11.0	1759	1758	0.281973
K13-TUSAS-1-25	35.8	1.8	0.282050	0.000051	0.002187	0.281977	-26.0	1.8	11.1	1755	1758	0.281977
K13-TUSAS-1-16	11.1	2.2	0.282008	0.000031	0.000766	0.281983	-27.5	1.1	11.3	1757	1758	0.281983
K13-TUSAS-1-1	28.1	2.0	0.282054	0.000040	0.001909	0.281990	-25.8	1.4	11.6	1757	1758	0.281990
K13-TUSAS-1-21	32.2	1.9	0.282061	0.000049	0.002038	0.281993	-25.6	1.7	11.6	1755	1758	0.281993
H13-MAN-4C	20.1	2.9	0.281939	0.000028	0.001290	0.281904	-29.9	1.0	1.9	1468	1456	0.281904
H13-MAN-26R	23.4	2.9	0.282068	0.000039	0.001302	0.282032	-25.4	1.4	6.0	1452	1456	0.282032
H13-MAN-18C	27.3	2.5	0.282109	0.000043	0.001697	0.282062	-23.9	1.5	7.4	1464	1456	0.282062
H13-MAN-37R	19.0	1.7	0.282222	0.000043	0.001138	0.282191	-19.9	1.5	11.8	1456	1456	0.282191
H13-MAN-3C	18.3	1.6	0.282113	0.000043	0.001225	0.282078	-23.8	1.5	8.4	1484	1484	0.282078
H13-MAN-2C	28.0	1.8	0.282072	0.000046	0.002012	0.282012	-25.2	1.6	7.8	1558	1558	0.282012
H13-MAN-8C	32.4	1.6	0.282112	0.000055	0.002000	0.282052	-23.8	1.9	9.8	1587	1587	0.282052
H13-MAN-16C	23.9	3.4	0.281953	0.000022	0.001389	0.281910	-29.4	0.8	6.2	1648	1648	0.281910
H13-MAN-12C	28.6	3.1	0.282106	0.000027	0.001742	0.282051	-24.0	0.9	11.4	1658	1658	0.282051
H13-MAN-1C	37.2	2.9	0.281997	0.000027	0.002114	0.281930	-27.9	1.0	7.2	1662	1662	0.281930
H13-MAN-17C	22.1	2.9	0.282021	0.000032	0.001299	0.281980	-27.0	1.1	9.3	1673	1673	0.281980
K13-NAC-2A-14	14.4	2.6	0.281970	0.000038	0.000854	0.281947	-28.8	1.4	2.8	1443	1450	0.281947
K13-NAC-2A-4	36.3	2.5	0.282025	0.000044	0.002244	0.281964	-26.9	1.6	3.5	1447	1450	0.281963
K13-NAC-2A-29	22.2	2.5	0.282034	0.000039	0.001289	0.281998	-26.6	1.4	5.1	1465	1450	0.281998
K13-NAC-2A-19	22.7	2.4	0.282044	0.000026	0.001313	0.282008	-26.2	0.9	5.2	1454	1450	0.282008
K13-NAC-2A-30	19.9	2.5	0.282041	0.000032	0.001146	0.282010	-26.3	1.1	5.3	1454	1450	0.282010
K13-NAC-2A-7	19.4	2.6	0.282056	0.000035	0.001151	0.282024	-25.8	1.2	6.0	1462	1450	0.282024
K13-NAC-2A-9	19.0	1.9	0.282063	0.000043	0.001220	0.282030	-25.5	1.5	6.2	1461	1450	0.282030
K13-NAC-2A-28	27.5	2.0	0.282079	0.000038	0.001693	0.282032	-25.0	1.3	6.1	1454	1450	0.282032
K13-NAC-2A-1	21.8	2.3	0.282079	0.000045	0.001289	0.282043	-25.0	1.6	6.4	1451	1450	0.282043
K13-NAC-2A-6	21.0	2.7	0.282089	0.000033	0.001315	0.282053	-24.6	1.2	6.8	1454	1450	0.282053
K13-NAC-2A-20	20.9	2.3	0.282092	0.000040	0.001231	0.282058	-24.5	1.4	6.8	1446	1450	0.282058
K13-NAC-2A-21	25.6	2.4	0.282099	0.000033	0.001483	0.282059	-24.2	1.2	6.9	1448	1450	0.282059
K13-NAC-2A-3	19.5	2.5	0.282115	0.000040	0.001139	0.282084	-23.7	1.4	8.0	1456	1450	0.282084

K13-NAC-2A-23	29.6	2.3	0.282133	0.000038	0.001691	0.282087	-23.0	1.4	8.0	1451	1450	0.282087
K13-NAC-2A-12	22.8	2.1	0.282204	0.000048	0.001195	0.282172	-20.5	1.7	10.7	1439	1450	0.282172
K13-NAC-2B-2	15.7	2.5	0.282042	0.000036	0.000918	0.282016	-26.3	1.3	5.4	1449	1450	0.282016
K13-NAC-2B-05	20.9	2.1	0.282006	0.000033	0.001172	0.281974	-27.5	1.2	3.8	1444	1450	0.281974
K13-NAC-2B-07	31.6	2.2	0.282100	0.000034	0.001799	0.282051	-24.2	1.2	6.8	1455	1450	0.282051
K13-NAC-2B-08	16.4	2.4	0.282007	0.000041	0.000959	0.281980	-27.5	1.4	4.4	1458	1450	0.281981
K13-NAC-2B-09	22.3	2.2	0.282007	0.000036	0.001286	0.281972	-27.5	1.3	3.7	1445	1450	0.281972
K13-NAC-2B-10	39.8	2.3	0.282108	0.000040	0.002206	0.282048	-23.9	1.4	6.5	1446	1450	0.282048
K13-NAC-2B-11	32.3	2.1	0.282052	0.000035	0.001728	0.282004	-25.9	1.2	5.2	1457	1450	0.282004
K13-NAC-2B-13	18.8	2.3	0.282090	0.000038	0.001058	0.282060	-24.6	1.3	7.3	1462	1450	0.282060
K13-NAC-2B-17	26.0	2.3	0.282054	0.000037	0.001495	0.282013	-25.9	1.3	4.9	1431	1450	0.282013
K13-NAC-2B-20	17.3	2.7	0.282059	0.000049	0.001026	0.282031	-25.7	1.8	6.0	1451	1450	0.282031
K13-NAC-2B-21	18.8	2.6	0.281994	0.000040	0.001086	0.281964	-28.0	1.4	3.9	1463	1450	0.281964
K13-NAC-2B-22	22.1	2.2	0.282030	0.000040	0.001273	0.281995	-26.7	1.4	4.7	1450	1450	0.281995
K13-NAC-2B-24	22.0	2.4	0.282044	0.000034	0.001259	0.282010	-26.2	1.2	5.2	1449	1450	0.282009
K13-NAC-2B-27	12.8	2.3	0.282022	0.000035	0.000731	0.282002	-27.0	1.2	4.9	1447	1450	0.282002
K13-NAC-2B-29	22.6	2.4	0.282010	0.000035	0.001280	0.281975	-27.4	1.2	3.8	1445	1450	0.281974
C13-098-1	21.5	2.5	0.282017	0.000036	0.001244	0.281977	-27.2	1.3	9.8	1702	1705	0.281977
C13-098-4	27.3	2.1	0.282018	0.000043	0.001623	0.281965	-27.1	1.5	9.4	1700	1705	0.281965
C13-098-5	35.8	2.2	0.282070	0.000034	0.002049	0.282003	-25.3	1.2	10.9	1706	1705	0.282003
C13-098-9	33.5	2.2	0.281983	0.000034	0.001890	0.281922	-28.3	1.2	8.0	1706	1705	0.281922
C13-098-11	37.7	2.1	0.281980	0.000049	0.002083	0.281912	-28.5	1.7	7.7	1711	1705	0.281912
C13-098-15	41.5	1.7	0.282067	0.000052	0.002275	0.281993	-25.4	1.8	10.7	1716	1705	0.281993
C13-098-17	36.6	2.1	0.282079	0.000048	0.002090	0.282011	-25.0	1.7	11.2	1709	1705	0.282012
C13-098-18	34.0	2.1	0.282066	0.000038	0.001985	0.282002	-25.4	1.3	10.7	1702	1705	0.282002
C13-098-21	37.6	2.0	0.282046	0.000051	0.002269	0.281973	-26.1	1.8	9.8	1707	1705	0.281973
C13-098-25	51.2	2.0	0.282050	0.000052	0.002855	0.281958	-26.0	1.8	9.1	1701	1705	0.281958
C13-098-28	25.0	2.2	0.282048	0.000039	0.001436	0.282002	-26.1	1.4	10.3	1685	1705	0.282002
C13-098-32	18.8	2.7	0.282040	0.000029	0.001119	0.282004	-26.4	1.0	10.7	1699	1705	0.282003
C13-101A-2	20.7	3.1	0.281976	0.000026	0.001216	0.281937	-28.6	0.9	8.1	1688	1699	0.281937
C13-101A-17	20.6	2.7	0.281914	0.000038	0.001159	0.281877	-30.8	1.3	6.2	1699	1699	0.281877
C13-101A-22	24.2	2.9	0.281988	0.000026	0.001329	0.281946	-28.2	0.9	8.6	1699	1699	0.281946
C13-101A-27	14.4	3.1	0.281969	0.000029	0.000851	0.281941	-28.9	1.0	8.5	1700	1699	0.281941
C13-101A-29	25.7	1.8	0.282018	0.000042	0.001571	0.281967	-27.1	1.5	9.7	1714	1699	0.281967

C13-101A-30	29.8	1.4	0.282004	0.000054	0.001748	0.281948	-27.6	1.9	8.3	1679	1699	0.281947
C13-101A-31	33.9	2.5	0.282088	0.000034	0.001944	0.282026	-24.7	1.2	11.1	1682	1699	0.282025
C13-101A-35	29.3	2.6	0.281908	0.000030	0.001601	0.281856	-31.0	1.1	5.5	1699	1699	0.281856
C13-101A-37	26.7	2.7	0.282021	0.000032	0.001601	0.281969	-27.0	1.1	9.5	1699	1699	0.281969
C13-101A-39	37.8	1.5	0.282082	0.000065	0.002226	0.282010	-24.9	2.3	10.9	1699	1699	0.282010
C13-101A-40	67.1	1.8	0.282165	0.000056	0.003919	0.282038	-21.9	2.0	11.9	1699	1699	0.282038
C13-101A-42	19.2	3.1	0.282010	0.000025	0.001126	0.281973	-27.4	0.9	9.6	1699	1699	0.281973
C13-101A-51	28.4	2.9	0.282005	0.000036	0.002124	0.281936	-27.6	1.3	8.7	1718	1699	0.281937
C13-101A-53	24.0	2.9	0.282026	0.000036	0.001379	0.281981	-26.9	1.3	9.9	1699	1699	0.281981
C13-101A-55	37.1	2.6	0.282059	0.000034	0.001931	0.281997	-25.7	1.2	10.2	1687	1699	0.281996
C13-101A-57	25.3	3.0	0.282013	0.000025	0.001441	0.281967	-27.3	0.9	9.4	1698	1699	0.281967
C13-101A-60	22.4	3.0	0.282032	0.000034	0.001311	0.281990	-26.6	1.2	9.9	1685	1699	0.281989
C13-101A-63	23.5	3.0	0.281912	0.000029	0.001344	0.281868	-30.9	1.0	5.9	1700	1699	0.281868
C13-101A-73	24.4	2.7	0.282029	0.000035	0.001426	0.281984	-26.7	1.2	9.7	1686	1699	0.281983
C13-101A-75	21.2	1.5	0.281969	0.000051	0.001465	0.281921	-28.9	1.8	8.2	1716	1699	0.281922
C13-101A-85	20.0	3.0	0.281994	0.000031	0.001167	0.281955	-28.0	1.1	10.0	1741	1699	0.281956
C13-101A-87	27.8	2.9	0.281979	0.000030	0.001572	0.281928	-28.5	1.1	8.0	1699	1699	0.281928
C13-101A-88	29.0	2.6	0.281955	0.000032	0.001518	0.281906	-29.3	1.1	7.2	1699	1699	0.281906
C13-101A-89	19.9	3.0	0.281987	0.000024	0.001156	0.281950	-28.2	0.8	8.8	1699	1699	0.281950
C13-101A-90	23.9	2.9	0.282048	0.000034	0.001429	0.282002	-26.1	1.2	10.7	1701	1699	0.282002
C13-101A-93	20.8	2.8	0.281971	0.000031	0.001218	0.281932	-28.8	1.1	8.2	1701	1699	0.281932
C13-101A-96	28.1	3.2	0.281971	0.000030	0.001675	0.281917	-28.8	1.1	7.7	1700	1699	0.281917
C13-101A-99	59.3	3.1	0.282070	0.000050	0.002905	0.281976	-25.3	1.8	9.8	1701	1699	0.281976

Table A3-3. Igneous U-Pb zircon geochronologic data from GEMOC Key Centre.

	Concentratin (ppm)			Corrected Isotopic Ratios										Corrected Ages (Ma)								
Analysis	U	U/	$^{207}Pb/$	1σ	$^{207}Pb/$	1σ	$^{206}Pb/$	1σ	$^{208}Pb/$	1σ	ρr	$^{238}U/$	1σ	$^{207}Pb/$	1σ	$^{207}Pb/$	1σ	$^{206}Pb/$	1σ	$^{208}Pb/$	1σ	% Conc
	ppm	Th	^{206}Pb		^{235}U		^{238}U		^{232}Th			^{232}Th		^{206}Pb		^{235}U		^{238}U		^{232}Th		
AL04_8-18	406	1.4	0.10122	0.00122	2.80694	0.03017	0.20115	0.00182	0.04485	0.00091	0.27	1.37	0.09	1647	23	1357	8	1181	10	887	18	72
AL04_8-15	325	1.8	0.10135	0.00158	2.99537	0.04185	0.21437	0.00194	0.04438	0.00161	0.13	1.67	0.1	1649	30	1406	11	1252	10	878	31	76
AL04_8-39	396	0.7	0.10159	0.00289	3.03495	0.0855	0.2167	0.00342	0.03196	0.0026	0.26	0.71	0.04	1653	54	1416	22	1264	18	636	51	76
AL04_8-09R	617	1.6	0.10226	0.00185	3.15502	0.05797	0.22379	0.00287	0.03771	0.00167	0.37	1.55	0.1	1666	34	1446	14	1302	15	748	33	78
AL04_8-04	205	0.9	0.10272	0.00185	3.27552	0.05925	0.23129	0.00295	0.02138	0.00085	0.36	0.84	0.05	1674	34	1475	14	1341	15	428	17	80
AL04_8-27	156	1.5	0.10435	0.00159	3.50728	0.05329	0.24379	0.00281	0.03503	0.00112	0.38	1.45	0.09	1703	29	1529	12	1406	15	696	22	83

AL04_8-12	102	1.3	0.10431	0.00223	3.56993	0.07519	0.24822	0.00337	0.03488	0.00168	0.3	1.21	0.08	1702	40	1543	17	1429	17	693	33	84
AL04_8-06R	217	0.7	0.10158	0.0012	3.57632	0.04017	0.25536	0.00252	0.02177	0.00042	0.38	0.63	0.04	1653	22	1544	9	1466	13	435	8	89
AL04_8-23	97	1.2	0.10243	0.00121	3.65071	0.04099	0.25852	0.00255	0.04525	0.00081	0.38	1.17	0.07	1669	22	1561	9	1482	13	895	16	89
AL04_8-17	198	1.4	0.10317	0.00123	3.75509	0.04083	0.26399	0.00245	0.06474	0.00124	0.31	1.31	0.08	1682	23	1583	9	1510	12	1268	24	90
AL04_8-01	121	1.4	0.10127	0.00122	3.61531	0.03712	0.25895	0.0022	0.05574	0.00106	0.19	1.37	0.09	1648	23	1553	8	1484	11	1096	20	90
AL04_8-38	531	1.2	0.10083	0.00174	3.62052	0.06411	0.26044	0.00327	0.05528	0.00237	0.39	1.19	0.07	1639	33	1554	14	1492	17	1088	45	91
AL04_8-13	167	1.6	0.1011	0.00135	3.84017	0.04957	0.27549	0.00285	0.07206	0.00187	0.36	1.47	0.09	1644	25	1601	10	1569	14	1406	35	95
AL04_8-36	299	1.7	0.10199	0.00171	4.05881	0.06938	0.28862	0.00357	0.07781	0.00309	0.39	1.58	0.1	1661	32	1646	14	1635	18	1515	58	98
AL04_8-16	70	1.8	0.10261	0.0013	4.12061	0.04572	0.29126	0.0026	0.07083	0.00144	0.21	1.68	0.11	1672	24	1658	9	1648	13	1383	27	99
K07SAN1B-02	55		0.09144	0.00126	3.08766	0.04084	0.24491	0.00256	0.07577	0.0021	0.34	6.71	0.42	1456	27	1430	10	1412	13	1476	39	97
K07SAN1B-03	289	7.5	0.09183	0.00116	3.15111	0.03897	0.24888	0.00257	0.07547	0.00178	0.39	2.75	0.17	1464	25	1445	10	1433	13	1471	33	98
K07SAN1B-04	313	3.1	0.09162	0.00105	2.93121	0.03072	0.23205	0.00214	0.06864	0.00128	0.33	1.79	0.11	1460	22	1390	8	1345	11	1342	24	92
K07SAN1B-06C	259	2.0	0.09584	0.00123	3.40925	0.04062	0.258	0.00247	0.0789	0.00194	0.3	1 . 3	0.08	1545	25	1507	9	1480	13	1535	36	96
K07SAN1B-06R	486	1.5	0.09132	0.00181	3.21834	0.0656	0.2556	0.00343	0.07578	0.00375	0.37	1.98	0.12	1453	39	1462	16	1467	18	1476	70	101
K07SAN1B-07	255	2.2	0.09171	0.00131	3.23521	0.04748	0.25587	0.003	0.07948	0.00221	0.43	1.79	0.11	1461	28	1466	11	1469	15	1546	41	101
K07SAN1B-08	363	2.0	0.09219	0.00138	3.16899	0.04874	0.24931	0.00294	0.07632	0.00246	0.42	1.64	0.1	1471	29	1450	12	1435	15	1487	46	98
K07SAN1B-11	327	1.8	0.09078	0.00134	3.14863	0.04858	0.25156	0.00308	0.07593	0.00234	0.45	2.81	0.18	1442	29	1445	12	1447	16	1479	44	100
K07SAN1B-12	92	3.1	0.09151	0.00131	3.19451	0.04225	0.25322	0.00249	0.07983	0.00258	0.26	9.77	0.61	1457	28	1456	10	1455	13	1552	48	100
K07SAN1B-14	356	10.7	0.09334	0.00169	3.19295	0.05911	0.24811	0.00325	0.07589	0.00318	0.38	2.16	0.14	1495	35	1455	14	1429	17	1478	60	96
K07SAN1B-17	394	2.4	0.09175	0.00286	2.99936	0.0861	0.2371	0.00286	0.06987	0.00085	0.53	1.92	0.12	1462	61	1407	22	1372	15	1365	16	94
K07SAN1B-18	220	2.1	0.09109	0.00119	3.09267	0.04018	0.24626	0.00264	0.07794	0.00191	0.41	1.99	0.12	1448	25	1431	10	1419	14	1517	36	98
K07SAN1B-19	568	2.2	0.09045	0.00166	3.1548	0.05939	0.25298	0.00332	0.07547	0.00339	0.38	1.43	0.09	1435	36	1446	15	1454	17	1471	64	101
K07SAN1B-21	180	1.6	0.0911	0.00128	3.12308	0.03934	0.24862	0.00228	0.07682	0.0022	0.2	2.38	0.15	1449	27	1438	10	1431	12	1496	41	99
K07SAN1B-23	292	2.6	0.09118	0.00117	3.06776	0.03478	0.24398	0.00217	0.07203	0.00177	0.21	1.34	0.08	1450	25	1425	9	1407	11	1406	33	97
K07SAN1B-24	318	1.5	0.09133	0.00119	2.96385	0.03721	0.2354	0.00239	0.06855	0.00176	0.36	2.03	0.13	1453	25	1398	10	1363	12	1340	33	94
K07SAN1B-26	407	2.2	0.08924	0.00163	2.93657	0.04601	0.23867	0.00226	0.07053	0.00068	0.58	1.97	0.12	1409	36	1391	12	1380	12	1378	13	98
K07SAN1B-27	276	2.1	0.09065	0.00123	3.08709	0.04266	0.24702	0.00281	0.07869	0.00208	0.43	3.08	0.19	1439	26	1429	11	1423	15	1531	39	99
K07SAN1B-29	285	3.3	0.09135	0.00117	3.17385	0.0417	0.25201	0.00282	0.07999	0.00195	0.46	3.27	0.2	1454	25	1451	10	1449	15	1555	36	100
K07SAN1B-30	233	3.5	0.09111	0.0012	3.13412	0.04152	0.24951	0.00274	0.08323	0.00208	0.42	2.33	0.15	1449	26	1441	10	1436	14	1616	39	99
K07SAN1B-35	316	2.5	0.09126	0.00108	3.12626	0.03312	0.24846	0.00223	0.07707	0.00153	0.28	1.12	0.07	1452	23	1439	8	1431	12	1501	29	99
K07SAN1B-40	186	1.2	0.09078	0.00136	3.11939	0.04707	0.24924	0.0029	0.07745	0.00235	0.39	0.98	0.06	1442	29	1437	12	1435	15	1508	44	100

K07SAN1B-41	325	1.1	0.09133	0.00145	3.18418	0.05148	0.25289	0.00306	0.08127	0.00292	0 . 4	2 . 2 8	0.14	1453	31	1453	12	1453	16	1579	55	100
K07SAN1B-43	203	2.5	0.08967	0.00277	2.97115	0.08569	0.24031	0.00262	0.07098	0.00082	0.32	2 . 8 9	0.18	1419	60	1400	22	1388	14	1386	16	98
K07SAN1B-44	617	3.1	0.09246	0.00227	3.02428	0.06603	0.23723	0.00264	0.06985	0.00079	0.52	2 . 2 6	0.14	1477	48	1414	17	1372	14	1365	15	93

Table A3-4. Lu-Hf isotope results from igneous rocks (GEMOC Key Centre)								
Analysis N	Hf176/Hf177	1 S.D.	Lu176/Hf177	Yb176/Hf177	Hf176/Hf177 (i)	εHf(t)	1σ	AGE
AL04_8-01	0.282112	0.000023	0.00145	0.044498	0.282066	12.13909	0.805	1666
AL04_8-02	0.282181	0.000021	0.003677	0.127236	0.282065	12.09335	0.735	1666
AL04_8-03C	0.282265	0.000035	0.008364	0.283877	0.282001	9.824453	1.225	1666
AL04_8-04	0.282058	0.000025	0.000957	0.028443	0.282028	10.77473	0.875	1666
AL04_8-06R	0.282079	0.000018	0.001067	0.032832	0.282045	11.39667	0.63	1666
AL04_8-12	0.282077	0.000022	0.001203	0.04012	0.282039	11.17285	0.77	1666
AL04_8-13	0.282027	0.000023	0.000887	0.028891	0.281999	9.752101	0.805	1666
AL04_8-15	0.282135	0.000018	0.002263	0.080169	0.282064	12.04475	0.63	1666
AL04_8-16	0.282014	0.000021	0.001062	0.0348	0.28198	9.094939	0.735	1666
AL04_8-17	0.282132	0.000026	0.002023	0.072115	0.282068	12.20753	0.91	1666
K07SAN1B-02	0.282082	0.000022	0.001088	0.029776	0.282052	6.781183	0.77	1452
K07SAN1B-03	0.282111	0.000016	0.000972	0.028373	0.282084	7.922906	0.56	1452
K07SAN1B-04	0.28204	0.000011	0.000825	0.024642	0.282017	5.546847	0.385	1452
K07SAN1B-06Core	0.282128	0.000019	0.000795	0.023482	0.282106	8.698456	0.665	1452
K07SAN1B-07	0.282134	0.000023	0.001001	0.030143	0.282106	8.710404	0.805	1452
K07SAN1B-08	0.282233	0.000014	0.001743	0.054655	0.282185	11.5006	0.49	1452
K07SAN1B-11	0.282122	0.000021	0.001543	0.041925	0.282079	7.757472	0.735	1452
K07SAN1B-12	0.282108	0.000014	0.001099	0.032296	0.282077	7.692902	0.49	1452
K07SAN1B-14	0.282072	0.000016	0.001295	0.037753	0.282036	6.225272	0.56	1452
K07SAN1B-17	0.282148	0.000024	0.001305	0.037987	0.282112	8.911862	0.84	1452
K07SAN1B-18	0.282066	0.000019	0.000942	0.027523	0.28204	6.356112	0.665	1452
K07SAN1B-19	0.282096	0.000015	0.001062	0.030314	0.282067	7.302706	0.525	1452

Table A3-5. Detrital zircon U-Pb geochronologic analyses (ALC).

						Isotope ratios					Apparent ages (Ma)								
Analysis	U	206Pb	U/Th	206Pb*	±	207Pb*	±	206Pb*	±	error	206Pb*	±	207Pb*	±	206Pb*	±	Best age	±	Conc
	(ppm)	204Pb		207Pb*	(%)	235U*	(%)	238U	(%)	corr.	238U*	(Ma)	235U	(Ma)	207Pb*	(Ma)	(Ma)	(Ma)	(%)
K14-MANZQTZITE-Spot 2	138	50652	0.9	9.9138	1.1	3.9624	1.6	0.2849	1.2	0.73	1616.0	17.0	1626.5	13.2	1640.2	20.8	1640.2	20.8	98.5
K14-MANZQTZITE-Spot 3	42	16805	2.2	9.8147	2.2	4.1289	3.8	0.2939	3.1	0.82	1661.0	45.8	1660.0	31.2	1658.8	40.4	1658.8	40.4	100.1
K14-MANZQTZITE-Spot 4	71	47298	2.2	9.5933	1.8	4.1864	3.5	0.2913	3.1	0.87	1647.9	44.7	1671.4	29.0	1700.9	32.4	1700.9	32.4	96.9
K14-MANZQTZITE-Spot 5	121	118634	1.6	9.6833	1.7	4.0650	3.0	0.2855	2.5	0.82	1618.9	35.1	1647.3	24.3	1683.7	31.5	1683.7	31.5	96.2
K14-MANZQTZITE-Spot 6	158	166212	1.0	9.9101	1.1	4.1023	3.7	0.2949	3.5	0.96	1665.7	51.3	1654.8	29.9	1640.9	20.1	1640.9	20.1	101.5
K14-MANZQTZITE-Spot 7	76	33278	1.3	9.5969	1.6	4.1420	2.6	0.2883	2.0	0.79	1633.0	29.4	1662.6	21.2	1700.2	29.6	1700.2	29.6	96.0
K14-MANZQTZITE-Spot 8	163	79839	0.8	9.9537	1.3	3.7907	2.2	0.2737	1.8	0.82	1559.3	25.5	1590.8	18.0	1632.7	23.6	1632.7	23.6	95.5
K14-MANZQTZITE-Spot 10	128	111145	2.5	9.7370	1.2	4.3354	1.9	0.3062	1.4	0.76	1721.8	21.5	1700.1	15.4	1673.5	22.3	1673.5	22.3	102.9
K14-MANZQTZITE-Spot 11	306	229003	3.3	9.4103	1.4	4.4458	2.4	0.3034	1.9	0.81	1708.3	29.0	1720.9	19.8	1736.3	25.7	1736.3	25.7	98.4
K14-MANZQTZITE-Spot 12	232	251941	0.6	9.7311	1.3	3.3010	4.8	0.2330	4.6	0.96	1350.1	56.2	1481.3	37.3	1674.6	23.3	1674.6	23.3	80.6
K14-MANZQTZITE-Spot 13	65	31227	1.5	9.9428	1.8	3.9363	2.4	0.2839	1.6	0.67	1610.7	22.6	1621.2	19.2	1634.7	32.7	1634.7	32.7	98.5
K14-MANZQTZITE-Spot 14	227	99683	1.7	9.5280	0.9	4.2500	1.8	0.2937	1.6	0.88	1659.9	23.5	1683.7	15.0	1713.5	16.2	1713.5	16.2	96.9
K14-MANZQTZITE-Spot 15	128	58275	1.5	9.8421	1.7	4.0574	2.3	0.2896	1.5	0.65	1639.7	21.6	1645.8	18.7	1653.6	32.3	1653.6	32.3	99.2
K14-MANZQTZITE-Spot 17	154	128822	1.2	9.8141	1.0	3.9001	2.2	0.2776	1.9	0.88	1579.3	26.8	1613.7	17.6	1658.9	19.4	1658.9	19.4	95.2
K14-MANZQTZITE-Spot 18	462	170722	1.2	9.7835	1.4	3.4489	4.5	0.2447	4.3	0.95	1411.2	54.1	1515.6	35.3	1664.7	25.1	1664.7	25.1	84.8
K14-MANZQTZITE-Spot 19	130	44685	4.8	9.4292	1.4	4.5654	2.5	0.3122	2.0	0.82	1751.6	31.2	1743.0	20.8	1732.6	26.4	1732.6	26.4	101.1
K14-MANZQTZITE-Spot 20	174	53526	0.9	9.8558	1.1	4.0090	2.3	0.2866	2.0	0.87	1624.3	28.6	1636.0	18.5	1651.0	20.5	1651.0	20.5	98.4
K14-MANZQTZITE-Spot 22	233	74613	1.7	9.7212	0.9	4.1502	3.9	0.2926	3.8	0.97	1654.6	54.8	1664.3	31.7	1676.5	17.3	1676.5	17.3	98.7
K14-MANZQTZITE-Spot 24	106	60391	2.6	9.6664	1.6	4.2429	2.8	0.2975	2.3	0.83	1678.7	34.4	1682.4	23.1	1686.9	28.9	1686.9	28.9	99.5
K14-MANZQTZITE-Spot 25	357	180483	1.7	9.6433	1.1	4.2575	2.1	0.2978	1.7	0.85	1680.2	25.9	1685.2	16.9	1691.3	20.1	1691.3	20.1	99.3
K14-MANZQTZITE-Spot 26	82	45859	2.1	9.1797	2.0	4.5240	2.9	0.3012	2.2	0.74	1697.2	32.1	1735.4	24.3	1781.7	36.1	1781.7	36.1	95.3
K14-MANZQTZITE-Spot 28	214	112706	1.7	9.8125	1.2	4.0766	2.3	0.2901	1.9	0.85	1642.1	27.8	1649.6	18.4	1659.2	22.0	1659.2	22.0	99.0
K14-MANZQTZITE-Spot 29	197	133547	2.0	9.7960	1.0	4.1217	1.6	0.2928	1.2	0.78	1655.7	18.2	1658.6	13.1	1662.3	18.5	1662.3	18.5	99.6
K14-MANZQTZITE-Spot 30	223	73669	1.2	9.9197	1.8	3.2661	2.9	0.2350	2.2	0.78	1360.5	27.5	1473.0	22.3	1639.1	33.0	1639.1	33.0	83.0
K14-MANZQTZITE-Spot 31	679	89836	1.5	9.1690	1.2	3.7568	2.4	0.2498	2.1	0.87	1437.6	26.8	1583.6	19.1	1783.8	21.0	1783.8	21.0	80.6
K14-MANZQTZITE-Spot 32	281	128613	0.9	9.6300	1.3	3.7077	2.9	0.2590	2.7	0.90	1484.5	35.2	1573.0	23.5	1693.9	23.1	1693.9	23.1	87.6
K14-MANZQTZITE-Spot 35	36	15924	0.6	9.3263	2.4	3.7074	5.2	0.2508	4.7	0.89	1442.5	60.3	1573.0	41.8	1752.7	43.2	1752.7	43.2	82.3
K14-MANZQTZITE-Spot 36	420	562834	3.7	9.1824	1.3	4.7946	3.6	0.3193	3.3	0.93	1786.3	52.1	1784.0	30.2	1781.1	24.3	1781.1	24.3	100.3
K14-MANZQTZITE-Spot 37	233	141238	4.1	9.2236	1.4	4.6204	3.3	0.3091	3.0	0.91	1736.2	46.4	1753.0	27.9	1773.0	24.9	1773.0	24.9	97.9
K14-MANZQTZITE-Spot 38	139	248601	0.8	9.7347	1.5	3.4848	4.0	0.2460	3.7	0.93	1418.0	47.1	1523.8	31.4	1673.9	27.1	1673.9	27.1	84.7
K14-MANZQTZITE-Spot 39	197	35519	1.2	9.7874	0.9	3.9872	3.3	0.2830	3.2	0.96	1606.6	44.9	1631.6	26.8	1663.9	17.4	1663.9	17.4	96.6
K14-MANZQTZITE-Spot 40	145	66811	1.8	9.7681	1.1	4.3752	2.0	0.3100	1.7	0.85	1740.5	25.9	1707.7	16.5	1667.6	19.5	1667.6	19.5	104.4
K14-MANZQTZITE-Spot 41	337	57401	1.1	9.1941	1.3	4.0868	1.7	0.2725	1.1	0.66	1553.5	15.8	1651.7	14.1	1778.8	23.5	1778.8	23.5	87.3
K14-MANZQTZITE-Spot 42	74	36546	1.8	9.7226	1.7	4.0678	2.3	0.2868	1.5	0.65	1625.7	21.2	1647.9	18.5	1676.2	31.9	1676.2	31.9	97.0

K14-MANZQTZITE-Spot 43	561	931673	8.5	9.2137	0.9	4.5192	2.5	0.3020	2.3	0.94	1701.2	34.3	1734.5	20.4	1774.9	15.8	1774.9	15.8	95.8
K14-MANZQTZITE-Spot 44	72	77155	1.0	9.7257	2.0	3.8990	3.1	0.2750	2.3	0.75	1566.2	32.6	1613.5	25.1	1675.6	37.7	1675.6	37.7	93.5
K14-MANZQTZITE-Spot 45	208	119854	1.2	9.9365	1.5	4.1008	2.5	0.2955	2.0	0.80	1669.1	28.9	1654.5	20.1	1635.9	27.6	1635.9	27.6	102.0
K14-MANZQTZITE-Spot 47	130	180314	2.0	9.7451	1.6	4.1537	3.0	0.2936	2.5	0.84	1659.4	36.4	1664.9	24.3	1671.9	29.8	1671.9	29.8	99.2
K14-MANZQTZITE-Spot 48	128	62739	2.1	9.7598	1.5	4.0339	3.5	0.2855	3.2	0.91	1619.2	45.6	1641.1	28.5	1669.2	27.0	1669.2	27.0	97.0
K14-MANZQTZITE-Spot 49	169	98259	2.3	9.6601	1.4	4.4392	5.3	0.3110	5.1	0.96	1745.7	77.6	1719.7	43.6	1688.1	25.8	1688.1	25.8	103.4
K14-MANZQTZITE-Spot 50	207	62205	1.7	9.7978	1.5	4.0865	5.2	0.2904	5.0	0.96	1643.5	72.3	1651.6	42.5	1662.0	27.7	1662.0	27.7	98.9
K14-MANZQTZITE-Spot 51	113	112694	1.5	9.7642	1.2	4.1109	2.1	0.2911	1.8	0.83	1647.1	25.7	1656.5	17.4	1668.3	21.8	1668.3	21.8	98.7
K14-MANZQTZITE-Spot 52	96	26620	1.7	9.6634	1.9	4.1862	6.0	0.2934	5.7	0.95	1658.5	83.1	1671.3	49.2	1687.5	35.9	1687.5	35.9	98.3
K14-MANZQTZITE-Spot 53	261	152071	0.9	9.7397	1.0	3.8991	1.8	0.2754	1.5	0.84	1568.3	20.9	1613.5	14.4	1673.0	17.8	1673.0	17.8	93.7
K14-MANZQTZITE-Spot 54	170	176795	1.0	9.7110	1.1	3.8160	2.2	0.2688	1.9	0.87	1534.5	26.4	1596.1	17.9	1678.4	20.2	1678.4	20.2	91.4
K14-MANZQTZITE-Spot 55	413	73035	2.0	9.5243	1.0	4.4161	2.3	0.3051	2.1	0.90	1716.3	31.7	1715.4	19.3	1714.2	18.5	1714.2	18.5	100.1
K14-MANZQTZITE-Spot 56	303	125875	1.0	9.7879	1.2	3.8787	3.2	0.2753	3.0	0.93	1567.9	41.3	1609.3	25.7	1663.8	21.3	1663.8	21.3	94.2
K14-MANZQTZITE-Spot 57	186	56623	1.0	9.8293	1.4	3.5232	1.7	0.2512	1.1	0.63	1444.5	14.0	1532.4	13.7	1656.0	25.0	1656.0	25.0	87.2
K14-MANZQTZITE-Spot 58	117	62162	1.7	9.7670	1.7	4.0529	2.4	0.2871	1.8	0.73	1627.0	25.8	1644.9	19.9	1667.8	30.7	1667.8	30.7	97.6
K14-MANZQTZITE-Spot 59	80	68852	1.6	9.6416	1.6	4.2464	2.1	0.2969	1.3	0.61	1676.1	18.6	1683.0	17.0	1691.7	30.4	1691.7	30.4	99.1
K14-MANZQTZITE-Spot 60	204	116902	2.1	9.6893	1.4	4.2350	2.7	0.2976	2.2	0.84	1679.4	33.0	1680.8	21.8	1682.6	26.4	1682.6	26.4	99.8
K14-MANZQTZITE-Spot 61	242	157699	1.3	9.5614	1.0	4.2640	3.7	0.2957	3.6	0.96	1669.9	52.4	1686.4	30.5	1707.0	18.6	1707.0	18.6	97.8
K14-MANZQTZITE-Spot 62	108	133365	1.2	9.7330	1.4	4.1309	2.1	0.2916	1.6	0.76	1649.5	23.7	1660.4	17.6	1674.2	25.9	1674.2	25.9	98.5
K14-MANZQTZITE-Spot 63	222	80688	1.6	9.8906	1.1	4.1378	1.9	0.2968	1.5	0.81	1675.5	22.7	1661.8	15.5	1644.5	20.5	1644.5	20.5	101.9
K14-MANZQTZITE-Spot 64	431	180151	3.4	9.4203	1.0	4.2619	2.2	0.2912	2.0	0.90	1647.4	28.9	1686.0	18.2	1734.4	17.5	1734.4	17.5	95.0
K14-MANZQTZITE-Spot 65	144	42438	3.0	9.8146	1.3	4.0060	2.3	0.2852	1.9	0.83	1617.3	27.0	1635.4	18.6	1658.8	23.8	1658.8	23.8	97.5
K14-MANZQTZITE-Spot 66	139	77361	1.8	9.6759	1.3	3.9675	4.4	0.2784	4.2	0.96	1583.4	59.4	1627.6	35.9	1685.1	23.5	1685.1	23.5	94.0
K14-MANZQTZITE-Spot 67	294	965375	1.1	9.6843	1.1	4.0785	3.0	0.2865	2.8	0.93	1623.8	40.5	1650.0	24.7	1683.5	20.4	1683.5	20.4	96.5
K14-MANZQTZITE-Spot 68	336	221518	2.5	9.2191	0.9	4.0274	1.6	0.2693	1.3	0.81	1537.1	17.6	1639.7	12.9	1773.9	17.0	1773.9	17.0	86.7
K14-MANZQTZITE-Spot 69	287	458042	1.4	9.4625	1.3	4.1956	2.7	0.2879	2.4	0.87	1631.2	34.6	1673.2	22.5	1726.2	24.5	1726.2	24.5	94.5
K14-MANZQTZITE-Spot 70	122	73248	1.0	9.7511	1.4	3.4721	2.8	0.2456	2.5	0.88	1415.5	31.2	1520.9	22.1	1670.8	25.0	1670.8	25.0	84.7
K14-MANZQTZITE-Spot 71	251	119000	0.7	9.6435	1.1	3.5072	2.8	0.2453	2.6	0.92	1414.2	33.1	1528.8	22.4	1691.3	20.3	1691.3	20.3	83.6
K14-MANZQTZITE-Spot 72	123	200754	1.9	9.7996	1.7	3.8917	3.9	0.2766	3.5	0.90	1574.2	49.0	1612.0	31.6	1661.6	32.3	1661.6	32.3	94.7
K14-MANZQTZITE-Spot 73	324	143433	1.1	9.6778	1.3	3.9696	2.7	0.2786	2.4	0.88	1584.4	33.8	1628.0	22.1	1684.8	23.8	1684.8	23.8	94.0
K14-MANZQTZITE-Spot 74	182	543440	1.6	9.9594	1.4	4.0081	2.5	0.2895	2.1	0.83	1639.1	29.7	1635.8	20.1	1631.6	25.4	1631.6	25.4	100.5
K14-MANZQTZITE-Spot 75	101	81071	1.7	9.7098	1.7	4.3505	2.9	0.3064	2.4	0.82	1722.8	36.4	1703.0	24.2	1678.7	30.8	1678.7	30.8	102.6
K14-MANZQTZITE-Spot 76	244	61760	1.0	9.6814	1.3	3.3916	2.0	0.2381	1.5	0.75	1377.0	18.9	1502.4	15.9	1684.1	24.7	1684.1	24.7	81.8
K14-MANZQTZITE-Spot 77	234	70894	2.8	9.3413	1.4	4.4677	2.5	0.3027	2.1	0.82	1704.6	30.7	1725.0	20.8	1749.8	26.4	1749.8	26.4	97.4
K14-MANZQTZITE-Spot 78	163	152034	2.2	9.8622	1.3	4.1140	2.1	0.2943	1.6	0.78	1662.8	23.9	1657.1	17.0	1649.8	24.0	1649.8	24.0	100.8
K14-MANZQTZITE-Spot 79	289	97099	1.5	9.8858	1.1	4.0748	2.3	0.2922	2.0	0.89	1652.3	29.4	1649.3	18.5	1645.4	19.5	1645.4	19.5	100.4
K14-MANZQTZITE-Spot 80	174	381034	1.6	9.6664	1.5	4.1358	2.3	0.2900	1.7	0.75	1641.3	25.0	1661.4	18.8	1686.9	28.0	1686.9	28.0	97.3
K14-MANZQTZITE-Spot 81	167	131597	2.0	9.6712	1.2	4.1821	2.3	0.2933	2.0	0.85	1658.2	28.9	1670.5	19.1	1686.0	23.0	1686.0	23.0	98.4
K14-MANZQTZITE-Spot 82	43	72089	1.6	9.6034	1.7	4.0759	3.0	0.2839	2.5	0.83	1610.9	36.0	1649.5	24.7	1699.0	30.8	1699.0	30.8	94.8
K14-MANZQTZITE-Spot 83	88	47844	1.2	9.8580	1.6	4.0576	2.5	0.2901	1.9	0.78	1642.0	27.9	1645.8	20.2	1650.6	28.9	1650.6	28.9	99.5
K14-MANZQTZITE-Spot 86	250	89790	1.4	9.8797	1.4	4.0971	3.6	0.2936	3.3	0.92	1659.3	48.6	1653.7	29.4	1646.6	26.0	1646.6	26.0	100.8
K14-MANZQTZITE-Spot 88	253	1698231	1.6	9.7606	1.0	3.6233	1.9	0.2565	1.6	0.84	1471.9	20.6	1554.7	14.8	1669.0	18.7	1669.0	18.7	88.2
K14-MANZQTZITE-Spot 89	165	219932	1.5	9.9420	1.9	4.0871	3.1	0.2947	2.5	0.80	1665.0	36.1	1651.7	25.1	1634.9	34.4	1634.9	34.4	101.8

K14-MANZQTZITE-Spot 91	280	90483	1.2	9.7770	1.2	4.0131	1.9	0.2846	1.5	0.78	1614.3	21.6	1636.9	15.7	1665.9	22.3	1665.9	22.3	96.9
K14-MANZQTZITE-Spot 92	157	45313	1.9	9.6955	1.5	4.2992	2.1	0.3023	1.5	0.71	1702.8	21.9	1693.2	17.1	1681.4	27.1	1681.4	27.1	101.3
K14-MANZQTZITE-Spot 93	37	181907	4.7	8.3766	1.6	5.7499	2.6	0.3493	2.1	0.78	1931.3	34.4	1938.9	22.8	1947.0	29.4	1947.0	29.4	99.2
K14-MANZQTZITE-Spot 95	144	123125	3.0	9.2827	1.2	4.8167	1.7	0.3243	1.3	0.74	1810.6	20.1	1787.8	14.5	1761.3	21.1	1761.3	21.1	102.8
K14-MANZQTZITE-Spot 96	127	85928	2.3	9.8454	1.2	4.0701	2.4	0.2906	2.1	0.86	1644.7	29.9	1648.3	19.4	1653.0	22.3	1653.0	22.3	99.5
K14-MANZQTZITE-Spot 97	124	99935	0.9	9.3541	1.3	3.7267	2.8	0.2528	2.5	0.88	1453.0	32.7	1577.1	22.8	1747.3	24.4	1747.3	24.4	83.2
K14-MANZQTZITE-Spot 98	182	95464	2.7	6.2267	1.4	10.2726	4.9	0.4639	4.7	0.96	2456.8	95.4	2459.6	45.2	2461.9	24.1	2461.9	24.1	99.8
K14-MANZQTZITE-Spot 100	113	49314	1.2	10.1168	2.1	3.8787	2.9	0.2846	2.0	0.68	1614.5	27.9	1609.3	23.1	1602.4	39.1	1602.4	39.1	100.8
K14-MANZQTZITE-Spot 101	90	48882	1.8	9.8442	1.2	4.0414	2.6	0.2885	2.3	0.88	1634.3	32.9	1642.6	21.1	1653.2	22.8	1653.2	22.8	98.9
K14-MANZQTZITE-Spot 102	264	126012	1.2	9.8822	1.6	3.9986	2.6	0.2866	2.0	0.78	1624.5	29.2	1633.9	21.2	1646.1	30.4	1646.1	30.4	98.7
K14-MANZQTZITE-Spot 103	470	219410	2.8	9.1524	1.2	4.8281	2.5	0.3205	2.2	0.88	1792.1	34.7	1789.8	21.2	1787.1	21.7	1787.1	21.7	100.3
K14-MANZQTZITE-Spot 104	242	213504	0.6	9.6494	1.5	3.8024	2.3	0.2661	1.7	0.74	1521.0	22.9	1593.3	18.4	1690.2	28.6	1690.2	28.6	90.0
K14-MANZQTZITE-Spot 106	147	95332	1.2	9.7964	1.0	5.0821	2.0	0.3611	1.8	0.88	1987.3	30.3	1833.1	17.1	1662.2	17.6	1662.2	17.6	119.6
K14-MANZQTZITE-Spot 107	225	115222	1.5	9.8934	1.3	3.9799	2.0	0.2856	1.5	0.74	1619.4	21.4	1630.1	16.3	1644.0	25.0	1644.0	25.0	98.5
K14-MANZQTZITE-Spot 108	213	205083	2.4	9.8273	1.4	4.0523	2.2	0.2888	1.7	0.76	1635.7	24.5	1644.8	18.2	1656.4	26.8	1656.4	26.8	98.7
K14-MANZQTZITE-Spot 109	143	126969	2.6	9.8255	1.0	4.1260	2.0	0.2940	1.7	0.86	1661.6	24.9	1659.5	16.2	1656.8	19.0	1656.8	19.0	100.3
K14-MANZQTZITE-Spot 110	219	106406	0.6	9.7781	1.4	4.0766	2.3	0.2891	1.8	0.80	1637.0	26.2	1649.6	18.5	1665.7	25.2	1665.7	25.2	98.3
K14-MANZQTZITE-Spot 111	138	82282	1.5	9.8830	1.2	4.0536	1.7	0.2906	1.2	0.71	1644.3	17.7	1645.0	14.0	1645.9	22.4	1645.9	22.4	99.9
K14-MANZQTZITE-Spot 112	146	74233	1.7	9.5514	1.3	4.4303	3.3	0.3069	3.0	0.92	1725.4	45.7	1718.0	27.3	1709.0	24.2	1709.0	24.2	101.0
K14-MANZQTZITE-Spot 113	138	59334	1.3	9.6645	1.2	4.2336	3.8	0.2968	3.7	0.95	1675.2	53.9	1680.6	31.5	1687.3	21.5	1687.3	21.5	99.3
K14-MANZQTZITE-Spot 114	239	326029	2.0	9.8526	1.1	4.0310	1.9	0.2880	1.6	0.83	1631.8	22.6	1640.5	15.5	1651.6	19.8	1651.6	19.8	98.8
K14-MANZQTZITE-Spot 115	123	69793	1.7	9.8745	1.1	4.0207	2.0	0.2879	1.6	0.83	1631.3	23.6	1638.4	16.0	1647.5	20.2	1647.5	20.2	99.0
K14-MANZQTZITE-Spot 116	148	658349	1.7	9.7034	1.2	4.1590	2.1	0.2927	1.8	0.82	1655.0	25.6	1666.0	17.4	1679.9	22.3	1679.9	22.3	98.5
K14-MANZQTZITE-Spot 117	171	216007	1.5	9.8623	1.0	3.8215	2.3	0.2733	2.1	0.89	1557.7	28.7	1597.3	18.7	1649.8	19.2	1649.8	19.2	94.4
K14-MANZQTZITE-Spot 118	270	140568	1.8	10.0319	1.0	3.9757	2.2	0.2893	2.0	0.89	1637.8	28.4	1629.2	18.0	1618.1	19.1	1618.1	19.1	101.2
K14-MANZQTZITE-Spot 119	439	60523	1.2	9.5724	0.9	3.6048	1.7	0.2503	1.5	0.86	1439.8	19.1	1550.6	13.6	1704.9	16.0	1704.9	16.0	84.5
K14-MANZQTZITE-Spot 120	210	279852	1.9	9.4453	1.4	4.2751	2.5	0.2929	2.0	0.83	1655.8	29.9	1688.6	20.4	1729.5	25.5	1729.5	25.5	95.7
K14-MANZQTZITE-Spot 121	217	82888	2.3	9.7428	1.2	4.1409	2.1	0.2926	1.7	0.81	1654.5	24.7	1662.4	17.1	1672.4	22.7	1672.4	22.7	98.9
K14-MANZQTZITE-Spot 122	283	129855	1.8	9.2059	1.1	4.5801	2.2	0.3058	1.9	0.86	1720.0	29.2	1745.7	18.7	1776.5	20.8	1776.5	20.8	96.8
K14-MANZQTZITE-Spot 123	94	46111	2.5	9.7570	1.5	4.2150	2.7	0.2983	2.2	0.82	1682.7	32.6	1676.9	22.0	1669.7	28.3	1669.7	28.3	100.8
K14-MANZQTZITE-Spot 125	231	62135	2.1	9.9693	1.3	4.1038	1.9	0.2967	1.5	0.76	1675.0	21.7	1655.1	15.7	1629.8	23.2	1629.8	23.2	102.8
K14-MANZQTZITE-Spot 126	152	78800	1.2	9.7698	1.5	4.0210	2.5	0.2849	1.9	0.78	1616.1	27.5	1638.4	20.0	1667.3	28.4	1667.3	28.4	96.9
K14-MANZQTZITE-Spot 128	217	128105	2.3	9.9380	1.5	4.0350	2.6	0.2908	2.2	0.83	1645.7	31.8	1641.3	21.6	1635.6	27.6	1635.6	27.6	100.6
K14-MANZQTZITE-Spot 129	132	80087	1.5	9.6621	1.1	4.2179	3.8	0.2956	3.6	0.96	1669.3	53.6	1677.5	31.3	1687.8	20.9	1687.8	20.9	98.9
K14-MANZQTZITE-Spot 130	114	92267	2.1	9.7729	1.4	4.1078	2.4	0.2912	1.9	0.81	1647.3	28.0	1655.8	19.4	1666.7	25.6	1666.7	25.6	98.8
K14-MANZQTZITE-Spot 131	91	31136	1.6	9.8857	1.1	4.0772	2.4	0.2923	2.1	0.88	1653.2	30.1	1649.8	19.2	1645.4	21.2	1645.4	21.2	100.5
K14-MANZQTZITE-Spot 132	112	39434	1.0	9.4627	1.3	3.9937	2.4	0.2741	2.0	0.83	1561.5	27.2	1632.9	19.2	1726.1	24.1	1726.1	24.1	90.5
K14-MANZQTZITE-Spot 133	200	110989	1.3	9.8733	0.9	4.0877	1.9	0.2927	1.7	0.88	1655.1	25.0	1651.9	15.8	1647.8	16.9	1647.8	16.9	100.4
K14-MANZQTZITE-Spot 134	266	80089	2.1	9.6544	1.2	3.9599	2.7	0.2773	2.4	0.89	1577.6	33.5	1626.0	21.9	1689.2	22.9	1689.2	22.9	93.4
K14-MANZQTZITE-Spot 135	334	2547610	2.1	9.7918	1.4	4.1696	2.0	0.2961	1.4	0.72	1672.0	20.9	1668.1	16.1	1663.1	25.1	1663.1	25.1	100.5
K14-MANZQTZITE-Spot 136	333	1790705	1.3	9.8166	0.9	3.9836	3.5	0.2836	3.4	0.97	1609.6	47.8	1630.9	28.2	1658.4	16.2	1658.4	16.2	97.1
K14-MANZQTZITE-Spot 137	142	59843	1.6	9.8023	1.6	4.0433	2.2	0.2875	1.6	0.72	1628.8	23.3	1643.0	18.3	1661.1	28.7	1661.1	28.7	98.1
K14-MANZQTZITE-Spot 138	92	125915	2.1	9.8425	1.4	4.2468	2.6	0.3032	2.1	0.82	1706.9	31.7	1683.1	21.0	1653.5	26.9	1653.5	26.9	103.2

K14-MANZQTZITE-Spot 139	254	50272	1.2	9.8204	1.0	4.2453	1.4	0.3024	1.1	0.75	1703.1	16.2	1682.8	11.9	1657.7	17.8	1657.7	17.8	102.7
K14-MANZQTZITE-Spot 140	247	149190	1.9	9.7065	1.0	4.2499	2.0	0.2992	1.7	0.87	1687.3	25.7	1683.7	16.3	1679.3	17.8	1679.3	17.8	100.5
K14-MANZQTZITE-Spot 141	140	157789	2.1	9.7330	0.7	4.1694	1.7	0.2943	1.6	0.90	1663.1	23.1	1668.0	14.3	1674.2	13.7	1674.2	13.7	99.3
K14-MANZQTZITE-Spot 142	376	66220	2.1	9.8724	1.1	4.0932	2.2	0.2931	1.9	0.87	1656.9	27.8	1653.0	17.9	1647.9	20.2	1647.9	20.2	100.5
K14-MANZQTZITE-Spot 144	157	169487	1.5	9.6929	1.5	4.1434	3.1	0.2913	2.7	0.87	1647.9	39.9	1662.9	25.7	1681.9	28.3	1681.9	28.3	98.0
K14-MANZQTZITE-Spot 145	158	131942	3.1	9.2150	1.2	4.6912	2.2	0.3135	1.8	0.83	1758.0	28.4	1765.7	18.5	1774.7	22.4	1774.7	22.4	99.1
K14-MANZQTZITE-Spot 146	371	64926	1.1	9.6931	0.8	3.3736	2.5	0.2372	2.3	0.94	1372.0	28.9	1498.3	19.4	1681.8	15.0	1681.8	15.0	81.6
K14-MANZQTZITE-Spot 147	266	86858	5.0	9.8824	1.2	4.0591	4.5	0.2909	4.4	0.97	1646.2	63.4	1646.1	36.8	1646.0	21.5	1646.0	21.5	100.0
K14-MANZQTZITE-Spot 148	263	115340	1.5	9.9333	1.1	4.0592	2.0	0.2924	1.7	0.83	1653.7	24.5	1646.2	16.5	1636.5	20.9	1636.5	20.9	101.1
K14-MANZQTZITE-Spot 150	376	199766	3.8	9.6952	1.0	4.0206	1.7	0.2827	1.3	0.80	1605.0	19.0	1638.4	13.5	1681.4	18.4	1681.4	18.4	95.5
K14-MANZQTZITE-Spot 151	63	87059	1.5	9.8705	1.6	4.0467	2.4	0.2897	1.8	0.74	1640.0	26.1	1643.6	19.8	1648.3	30.2	1648.3	30.2	99.5
K14-MANZQTZITE-Spot 152	238	166801	6.9	9.7560	1.3	4.3150	3.8	0.3053	3.6	0.94	1717.6	53.5	1696.2	31.2	1669.9	24.1	1669.9	24.1	102.9
K14-MANZQTZITE-Spot 153	176	69664	2.2	9.8113	1.1	4.1384	2.8	0.2945	2.6	0.92	1663.9	37.7	1661.9	22.9	1659.4	20.7	1659.4	20.7	100.3
K14-MANZQTZITE-Spot 154	128	46134	1.4	9.9099	1.5	3.9357	3.0	0.2829	2.6	0.88	1605.8	37.6	1621.1	24.4	1640.9	27.1	1640.9	27.1	97.9
K14-MANZQTZITE-Spot 155	204	85088	1.4	9.7140	1.2	4.2949	2.7	0.3026	2.4	0.90	1704.1	36.4	1692.4	22.3	1677.8	21.9	1677.8	21.9	101.6
K14-MANZQTZITE-Spot 156	136	107938	1.6	9.9922	1.2	3.9404	2.0	0.2856	1.6	0.79	1619.3	22.5	1622.0	16.1	1625.5	22.5	1625.5	22.5	99.6
K14-MANZQTZITE-Spot 157	308	166262	0.8	9.8162	1.1	4.0580	1.6	0.2889	1.3	0.77	1636.1	18.4	1645.9	13.4	1658.5	19.5	1658.5	19.5	98.6
K14-MANZQTZITE-Spot 158	115	177259	1.9	9.7614	1.3	4.0604	3.4	0.2875	3.1	0.92	1628.8	45.2	1646.4	27.8	1668.9	24.9	1668.9	24.9	97.6
K14-MANZQTZITE-Spot 159	107	245910	1.7	9.5720	1.4	4.3571	2.1	0.3025	1.5	0.72	1703.6	22.6	1704.3	17.3	1705.0	26.6	1705.0	26.6	99.9
K14-MANZQTZITE-Spot 160	311	124777	1.1	9.8263	1.4	4.0951	2.3	0.2918	1.8	0.78	1650.7	26.2	1653.3	18.7	1656.6	26.4	1656.6	26.4	99.6
K14-MANZQTZITE-Spot 161	180	65405	1.6	9.9096	1.0	4.0963	2.7	0.2944	2.4	0.92	1663.5	35.8	1653.6	21.7	1640.9	19.4	1640.9	19.4	101.4
K14-MANZQTZITE-Spot 162	393	128873	2.1	9.6252	0.9	4.1966	2.3	0.2930	2.1	0.91	1656.3	30.8	1673.3	18.9	1694.8	17.3	1694.8	17.3	97.7
K14-MANZQTZITE-Spot 163	511	196127	1.1	9.7876	1.1	3.9331	2.1	0.2792	1.8	0.85	1587.3	25.5	1620.5	17.3	1663.9	20.8	1663.9	20.8	95.4
K14-MANZQTZITE-Spot 164	142	124545	1.6	9.7682	0.9	4.2036	2.1	0.2978	1.9	0.90	1680.4	27.4	1674.7	16.9	1667.6	16.9	1667.6	16.9	100.8
K14-MANZQTZITE-Spot 165	279	51736	1.4	9.5001	1.4	3.5166	2.6	0.2423	2.3	0.85	1398.6	28.3	1531.0	20.9	1718.9	25.3	1718.9	25.3	81.4
K14-MANZQTZITE-Spot 166	525	101772	2.0	9.6493	0.9	3.9889	2.3	0.2792	2.1	0.91	1587.1	29.5	1631.9	18.6	1690.2	17.1	1690.2	17.1	93.9
K14-MANZQTZITE-Spot 167	308	158563	3.6	9.3787	0.9	4.6020	1.8	0.3130	1.6	0.88	1755.6	24.7	1749.6	15.2	1742.5	15.9	1742.5	15.9	100.8
K14-MANZQTZITE-Spot 168	291	65911	1.5	9.8827	1.1	4.1412	1.8	0.2968	1.4	0.78	1675.5	20.6	1662.5	14.7	1646.0	20.8	1646.0	20.8	101.8
K14-MANZQTZITE-Spot 170	298	120837	1.4	9.7881	1.0	3.8835	2.4	0.2757	2.1	0.90	1569.6	29.8	1610.3	19.1	1663.8	18.7	1663.8	18.7	94.3
K14-MANZQTZITE-Spot 171	402	32974	1.0	8.9341	1.5	4.3303	2.2	0.2806	1.6	0.71	1594.3	22.0	1699.1	18.1	1831.0	27.9	1831.0	27.9	87.1
K14-MANZQTZITE-Spot 172	435	192166	1.2	9.6104	1.1	3.5174	3.0	0.2452	2.9	0.94	1413.5	36.2	1531.1	24.0	1697.6	19.5	1697.6	19.5	83.3
K14-MANZQTZITE-Spot 173	292	8917061	1.8	9.8516	1.2	4.0987	1.7	0.2929	1.2	0.70	1655.8	17.6	1654.1	14.1	1651.8	22.9	1651.8	22.9	100.2
K14-MANZQTZITE-Spot 174	227	2948905	2.6	9.5829	0.9	4.3762	1.8	0.3042	1.6	0.86	1711.9	23.7	1707.9	15.1	1702.9	16.9	1702.9	16.9	100.5
K14-MANZQTZITE-Spot 175	361	60443	8.1	9.3217	1.2	4.7489	2.2	0.3211	1.9	0.86	1794.9	30.2	1775.9	18.8	1753.6	21.1	1753.6	21.1	102.4
K14-MANZQTZITE-Spot 176	390	52461	1.8	9.2888	1.0	3.6975	2.2	0.2491	1.9	0.88	1433.8	24.5	1570.8	17.2	1760.1	18.4	1760.1	18.4	81.5
K14-MANZQTZITE-Spot 177	292	55948	2.2	8.8558	1.5	5.1955	4.0	0.3337	3.7	0.93	1856.3	59.7	1851.9	33.9	1846.9	26.4	1846.9	26.4	100.5
K14-MANZQTZITE-Spot 178	30	56117	1.7	9.7239	1.6	4.2346	2.9	0.2986	2.4	0.83	1684.6	35.3	1680.8	23.6	1676.0	29.9	1676.0	29.9	100.5
K14-MANZQTZITE-Spot 179	133	9343135	1.7	9.7989	0.9	4.1231	2.0	0.2930	1.8	0.89	1656.6	25.7	1658.9	16.1	1661.8	16.6	1661.8	16.6	99.7
K14-MANZQTZITE-Spot 180	213	61481	1.4	9.7640	1.1	4.1757	3.5	0.2957	3.3	0.95	1670.0	49.0	1669.3	28.8	1668.4	20.8	1668.4	20.8	100.1
K14-MANZQTZITE-Spot 181	48	162087	0.8	9.7583	1.9	4.0638	5.2	0.2876	4.8	0.93	1629.6	69.6	1647.1	42.2	1669.5	34.4	1669.5	34.4	97.6
K14-MANZQTZITE-Spot 182	122	63421	1.5	9.9170	1.2	4.1156	2.2	0.2960	1.9	0.84	1671.5	27.9	1657.4	18.4	1639.6	22.4	1639.6	22.4	101.9
K14-MANZQTZITE-Spot 183	60	73000	1.1	9.7350	1.2	4.2863	2.2	0.3026	1.8	0.83	1704.3	27.3	1690.7	18.0	1673.9	22.5	1673.9	22.5	101.8
K14-MANZQTZITE-Spot 184	271	178002	1.6	9.4578	0.9	4.6041	3.6	0.3158	3.5	0.97	1769.3	54.1	1750.0	30.2	1727.1	16.8	1727.1	16.8	102.4

K14-MANZQTZITE-Spot 186	341	70500	0.8	9.7029	1.4	3.4601	2.5	0.2435	2.1	0.83	1404.8	26.6	1518.2	20.0	1680.0	26.0	1680.0	26.0	83.6
K14-MANZQTZITE-Spot 187	368	212689	2.2	9.4893	1.2	4.0692	1.6	0.2801	1.1	0.70	1591.6	16.0	1648.2	13.2	1721.0	21.3	1721.0	21.3	92.5
K14-MANZQTZITE-Spot 188	272	191584	2.7	9.5143	1.3	4.3665	2.1	0.3013	1.6	0.79	1697.8	24.4	1706.0	17.2	1716.1	23.7	1716.1	23.7	98.9
K14-MANZQTZITE-Spot 189	125	60004	1.0	9.6899	1.1	4.3085	2.4	0.3028	2.1	0.88	1705.1	31.1	1695.0	19.6	1682.4	21.2	1682.4	21.2	101.3
K14-MANZQTZITE-Spot 190	191	62415	1.0	9.8847	1.0	4.2554	2.0	0.3051	1.7	0.85	1716.4	25.2	1684.8	16.2	1645.6	19.3	1645.6	19.3	104.3
K14-MANZQTZITE-Spot 191	119	30167	1.5	10.0680	1.0	3.9075	2.3	0.2853	2.0	0.89	1618.1	28.7	1615.2	18.3	1611.4	19.5	1611.4	19.5	100.4
K14-MANZQTZITE-Spot 192	322	515906	1.9	9.6474	1.1	4.4215	4.1	0.3094	4.0	0.96	1737.6	60.4	1716.4	34.1	1690.6	20.4	1690.6	20.4	102.8
K14-MANZQTZITE-Spot 193	64	28792	27.9	9.2425	1.5	4.7381	3.3	0.3176	2.9	0.89	1778.0	45.4	1774.0	27.4	1769.2	26.8	1769.2	26.8	100.5
K14-MANZQTZITE-Spot 194	217	37866657	1.6	9.8072	1.2	4.1303	2.2	0.2938	1.8	0.83	1660.4	26.8	1660.3	18.1	1660.2	23.1	1660.2	23.1	100.0
K14-MANZQTZITE-Spot 195	266	169741	5.8	9.5243	1.0	4.5728	2.2	0.3159	1.9	0.89	1769.5	30.1	1744.3	18.2	1714.2	18.2	1714.2	18.2	103.2
K14-MANZQTZITE-Spot 196	102	30383	1.6	9.7683	1.6	4.0900	2.1	0.2898	1.4	0.65	1640.3	20.1	1652.3	17.5	1667.6	30.2	1667.6	30.2	98.4
K14-MANZQTZITE-Spot 197	106	25124	1.7	9.8098	1.5	4.0628	2.2	0.2891	1.7	0.76	1636.8	24.5	1646.9	18.3	1659.7	27.2	1659.7	27.2	98.6
K14-MANZQTZITE-Spot 198	305	113477	1.4	9.8744	1.0	4.0922	3.4	0.2931	3.2	0.96	1656.9	46.9	1652.8	27.4	1647.5	18.4	1647.5	18.4	100.6
K14-MANZQTZITE-Spot 199	85	42444	1.6	9.8902	1.5	4.0697	2.6	0.2919	2.1	0.80	1651.1	29.9	1648.3	20.9	1644.6	28.7	1644.6	28.7	100.4
K14-MANZQTZITE-Spot 200	281	57988	1.4	9.9590	1.1	4.1914	1.8	0.3027	1.5	0.81	1704.9	21.8	1672.3	14.8	1631.7	19.6	1631.7	19.6	104.5
K14-MANZQTZITE-Spot 201	187	132521	2.6	6.1986	1.2	10.5076	4.1	0.4724	4.0	0.96	2494.0	81.9	2480.6	38.4	2469.6	20.5	2469.6	20.5	101.0
K14-MANZQTZITE-Spot 202	114	102322	1.4	9.6348	1.3	4.2230	3.2	0.2951	2.9	0.91	1666.9	42.2	1678.5	25.9	1693.0	23.8	1693.0	23.8	98.5
K14-MANZQTZITE-Spot 203	156	58298	2.2	9.8162	1.4	3.9885	4.0	0.2840	3.8	0.94	1611.3	54.2	1631.9	32.9	1658.5	25.6	1658.5	25.6	97.2
K14-MANZQTZITE-Spot 204	326	286080	2.2	9.2077	1.2	4.8342	1.9	0.3228	1.5	0.79	1803.5	23.8	1790.9	16.0	1776.1	21.2	1776.1	21.2	101.5
K14-MANZQTZITE-Spot 205	326	228791	0.9	9.6456	1.2	3.4518	2.9	0.2415	2.6	0.90	1394.4	32.4	1516.3	22.5	1690.9	22.6	1690.9	22.6	82.5
K14-MANZQTZITE-Spot 206	165	95835	1.3	9.7230	1.4	3.9013	2.1	0.2751	1.6	0.75	1566.7	21.9	1613.9	16.9	1676.1	25.5	1676.1	25.5	93.5
K14-MANZQTZITE-Spot 207	47	33260	1.0	9.7880	1.4	4.0481	3.0	0.2874	2.6	0.88	1628.4	37.8	1643.9	24.3	1663.8	26.4	1663.8	26.4	97.9
K14-MANZQTZITE-Spot 208	106	54600	2.7	9.7322	1.2	4.1244	2.0	0.2911	1.6	0.81	1647.1	23.8	1659.1	16.5	1674.4	21.7	1674.4	21.7	98.4
K14-MANZQTZITE-Spot 209	176	130302	2.1	9.6889	1.1	4.4825	2.2	0.3150	1.9	0.86	1765.2	29.2	1727.7	18.2	1682.6	20.4	1682.6	20.4	104.9
K14-MANZQTZITE-Spot 210	270	251149	1.3	9.7068	1.6	4.3757	2.5	0.3080	1.9	0.77	1731.1	29.5	1707.8	20.7	1679.2	29.3	1679.2	29.3	103.1
K14-MANZQTZITE-Spot 211	29	25950	2.2	9.4876	1.9	4.3795	3.4	0.3014	2.8	0.83	1698.0	42.3	1708.5	28.1	1721.3	34.5	1721.3	34.5	98.6
K14-MANZQTZITE-Spot 212	167	46701	2.3	9.7767	1.2	4.2626	2.1	0.3023	1.8	0.83	1702.5	26.6	1686.2	17.7	1666.0	22.4	1666.0	22.4	102.2
K14-MANZQTZITE-Spot 213	167	39583	1.1	10.0315	1.6	4.0933	2.6	0.2978	2.1	0.79	1680.4	30.3	1653.0	21.2	1618.2	29.9	1618.2	29.9	103.8
K14-MANZQTZITE-Spot 214	251	124488	2.4	9.6405	1.1	4.3587	1.8	0.3048	1.5	0.82	1714.8	22.4	1704.5	15.0	1691.9	19.4	1691.9	19.4	101.4
K14-MANZQTZITE-Spot 215	164	87683	1.3	9.8755	1.4	4.1702	2.4	0.2987	2.0	0.81	1684.8	29.2	1668.2	19.9	1647.3	26.3	1647.3	26.3	102.3
K14-MANZQTZITE-Spot 216	179	63017	1.2	9.6858	1.7	3.3877	3.3	0.2380	2.8	0.86	1376.2	35.3	1501.6	26.1	1683.2	31.8	1683.2	31.8	81.8
K14-MANZQTZITE-Spot 217	253	207947	1.6	9.7981	1.1	4.2658	2.0	0.3031	1.7	0.84	1706.8	25.3	1686.8	16.5	1661.9	20.2	1661.9	20.2	102.7
K14-MANZQTZITE-Spot 218	233	56902	1.2	9.7059	0.9	4.1588	2.1	0.2928	1.9	0.91	1655.3	28.4	1665.9	17.5	1679.4	16.5	1679.4	16.5	98.6
K14-MANZQTZITE-Spot 219	110	191045	1.4	9.9302	1.3	3.9797	2.0	0.2866	1.5	0.75	1624.6	21.1	1630.1	16.0	1637.1	24.2	1637.1	24.2	99.2
K14-MANZQTZITE-Spot 220	383	87705	1.5	9.7024	1.0	3.8190	2.1	0.2687	1.8	0.87	1534.4	24.8	1596.8	16.7	1680.1	18.7	1680.1	18.7	91.3
K14-MANZQTZITE-Spot 221	169	44564	1.4	9.7606	1.4	4.1943	2.0	0.2969	1.5	0.73	1676.0	21.5	1672.9	16.4	1669.0	25.5	1669.0	25.5	100.4
K14-MANZQTZITE-Spot 222	229	54947	3.3	9.1704	1.5	4.7579	2.5	0.3164	2.0	0.81	1772.4	31.7	1777.5	21.1	1783.5	26.8	1783.5	26.8	99.4
K14-MANZQTZITE-Spot 223	125	88762	1.5	9.9516	1.6	4.0521	2.4	0.2925	1.7	0.72	1653.8	25.1	1644.7	19.4	1633.1	30.5	1633.1	30.5	101.3
K14-MANZQTZITE-Spot 224	412	80929	1.1	9.6805	1.0	4.1328	3.2	0.2902	3.0	0.95	1642.3	43.7	1660.8	26.0	1684.2	19.0	1684.2	19.0	97.5
K14-MANZQTZITE-Spot 225	342	77203	0.9	9.9976	1.0	4.1406	3.6	0.3002	3.5	0.96	1692.4	51.4	1662.3	29.5	1624.5	19.1	1624.5	19.1	104.2
K14-MANZQTZITE-Spot 226	179	84863	1.5	9.7981	1.1	4.1811	2.6	0.2971	2.3	0.91	1677.0	34.3	1670.3	21.0	1661.9	19.8	1661.9	19.8	100.9
K14-MANZQTZITE-Spot 227	314	105770	1.4	9.9224	0.8	4.0866	1.7	0.2941	1.5	0.89	1661.9	21.9	1651.6	13.7	1638.6	14.4	1638.6	14.4	101.4
K14-MANZQTZITE-Spot 228	316	73497	1.7	9.8485	1.2	4.1707	2.0	0.2979	1.7	0.82	1680.9	24.6	1668.3	16.6	1652.4	21.3	1652.4	21.3	101.7

K14-MANZQTZITE-Spot 229	236	206572	1.0	9.8561	1.1	3.8188	2.2	0.2730	1.9	0.87	1555.9	26.8	1596.7	18.0	1651.0	20.5	1651.0	20.5	94.2
K14-MANZQTZITE-Spot 231	150	49337	1.5	10.0260	1.1	4.0274	1.4	0.2929	0.8	0.61	1655.8	12.2	1639.7	11.2	1619.2	20.4	1619.2	20.4	102.3
K14-MANZQTZITE-Spot 232	109	47200	0.7	10.0210	1.1	4.0506	2.0	0.2944	1.7	0.84	1663.5	24.5	1644.4	16.2	1620.2	20.0	1620.2	20.0	102.7
K14-MANZQTZITE-Spot 233	158	72279	1.7	9.7385	0.9	4.2544	2.4	0.3005	2.2	0.92	1693.7	32.3	1684.6	19.4	1673.2	17.5	1673.2	17.5	101.2
K14-MANZQTZITE-Spot 234	304	70415	0.9	9.9167	1.3	3.9234	4.4	0.2822	4.2	0.95	1602.3	59.2	1618.5	35.4	1639.6	24.3	1639.6	24.3	97.7
K14-MANZQTZITE-Spot 235	443	93827	3.4	9.4138	1.2	4.1225	3.8	0.2815	3.6	0.95	1598.7	51.2	1658.8	31.2	1735.6	22.3	1735.6	22.3	92.1
K14-MANZQTZITE-Spot 236	399	206457	2.0	10.0442	0.9	4.0434	1.8	0.2945	1.5	0.86	1664.2	22.3	1643.0	14.4	1615.9	16.8	1615.9	16.8	103.0
K14-MANZQTZITE-Spot 237	145	35990	1.4	9.8574	1.2	4.1517	2.4	0.2968	2.0	0.85	1675.5	30.0	1664.5	19.5	1650.7	23.0	1650.7	23.0	101.5
K14-MANZQTZITE-Spot 238	230	106048	1.4	9.9011	1.3	4.0435	2.1	0.2904	1.7	0.78	1643.3	24.2	1643.0	17.4	1642.5	24.9	1642.5	24.9	100.0
K14-MANZQTZITE-Spot 240	337	792261	1.9	9.8532	1.6	4.0481	2.3	0.2893	1.7	0.73	1638.0	24.1	1643.9	18.6	1651.5	28.9	1651.5	28.9	99.2
K14-MANZQTZITE-Spot 241	379	70259	2.2	9.0069	1.3	4.9326	2.0	0.3222	1.5	0.77	1800.6	24.2	1807.9	17.0	1816.3	23.5	1816.3	23.5	99.1
K14-MANZQTZITE-Spot 242	275	138919	2.2	9.6886	1.4	4.2322	2.5	0.2974	2.1	0.83	1678.4	30.9	1680.3	20.6	1682.7	25.5	1682.7	25.5	99.7
K14-MANZQTZITE-Spot 243	372	143305	1.4	9.8484	1.3	4.0836	2.0	0.2917	1.5	0.75	1649.9	22.0	1651.0	16.4	1652.4	24.7	1652.4	24.7	99.8
K14-MANZQTZITE-Spot 244	240	131501	1.8	9.7258	1.1	4.3115	3.1	0.3041	2.9	0.93	1711.7	43.6	1695.6	25.6	1675.6	20.4	1675.6	20.4	102.2
K14-MANZQTZITE-Spot 245	559	89066	1.4	9.7310	1.0	3.4911	2.7	0.2464	2.5	0.93	1419.8	32.3	1525.2	21.6	1674.6	18.9	1674.6	18.9	84.8
K14-MANZQTZITE-Spot 246	221	118813	1.5	9.8354	1.0	4.1293	1.8	0.2946	1.5	0.82	1664.3	22.2	1660.1	15.0	1654.9	19.3	1654.9	19.3	100.6
K14-MANZQTZITE-Spot 247	558	56385	1.8	9.5202	0.8	4.2850	2.3	0.2959	2.2	0.93	1670.8	32.2	1690.5	19.3	1715.0	15.5	1715.0	15.5	97.4
K14-MANZQTZITE-Spot 248	121	32882	2.0	9.6881	1.8	4.2143	2.5	0.2961	1.7	0.68	1672.0	24.6	1676.8	20.1	1682.8	33.2	1682.8	33.2	99.4
K14-MANZQTZITE-Spot 249	320	63309	2.4	9.4793	1.5	4.3691	4.2	0.3004	3.9	0.93	1693.2	58.6	1706.5	34.9	1722.9	28.0	1722.9	28.0	98.3
K14-MANZQTZITE-Spot 250	174	45086	2.1	9.6639	1.4	4.1347	3.2	0.2898	2.9	0.90	1640.5	41.6	1661.2	26.1	1687.4	25.8	1687.4	25.8	97.2
K14-MANZQTZITE-Spot 251	418	218277	2.2	9.7492	1.1	4.0293	3.2	0.2849	2.9	0.93	1616.0	42.2	1640.1	25.7	1671.2	20.9	1671.2	20.9	96.7
K14-MANZQTZITE-Spot 252	355	58162	0.8	9.9331	1.1	4.0915	2.3	0.2948	2.0	0.88	1665.3	29.4	1652.6	18.6	1636.5	20.3	1636.5	20.3	101.8
K14-MANZQTZITE-Spot 253	335	112348	1.1	9.8252	1.2	4.2912	2.7	0.3058	2.4	0.90	1719.9	36.8	1691.7	22.3	1656.8	21.5	1656.8	21.5	103.8
K14-MANZQTZITE-Spot 255	219	59145	1.5	9.9501	0.9	4.1088	1.7	0.2965	1.4	0.84	1674.0	20.8	1656.0	13.7	1633.4	16.7	1633.4	16.7	102.5
K14-MANZQTZITE-Spot 256	158	38310	2.2	9.7079	1.2	4.2672	2.2	0.3004	1.8	0.83	1693.5	26.9	1687.1	17.8	1679.0	22.1	1679.0	22.1	100.9
K14-MANZQTZITE-Spot 257	127	125971	2.1	9.5670	1.2	4.2584	2.3	0.2955	2.0	0.86	1668.9	29.1	1685.4	18.9	1706.0	21.6	1706.0	21.6	97.8
K14-MANZQTZITE-Spot 259	335	107301	3.7	9.2971	0.9	4.7364	1.7	0.3194	1.4	0.84	1786.7	22.3	1773.7	14.3	1758.5	17.0	1758.5	17.0	101.6
K14-MANZQTZITE-Spot 260	97	49844	1.3	9.8255	1.1	4.0593	2.4	0.2893	2.1	0.88	1637.9	31.0	1646.2	19.8	1656.7	21.2	1656.7	21.2	98.9
K14-MANZQTZITE-Spot 261	402	118889	1.4	9.7488	0.9	4.1530	4.1	0.2936	4.0	0.98	1659.7	58.9	1664.8	33.8	1671.3	16.6	1671.3	16.6	99.3
K14-MANZQTZITE-Spot 262	616	618456	1.7	9.7364	0.8	3.9663	2.8	0.2801	2.7	0.95	1591.8	37.5	1627.3	22.6	1673.6	15.4	1673.6	15.4	95.1
K14-MANZQTZITE-Spot 263	120	28214	1.8	9.4831	1.4	4.4302	2.4	0.3047	1.9	0.79	1714.6	28.2	1718.0	19.6	1722.2	26.6	1722.2	26.6	99.6
K14-MANZQTZITE-Spot 264	201	74561	1.8	9.7486	1.2	4.2459	2.3	0.3002	2.0	0.85	1692.3	29.7	1682.9	19.3	1671.3	23.0	1671.3	23.0	101.3
K14-MANZQTZITE-Spot 265	99	63970	0.8	9.8055	1.9	4.0886	2.2	0.2908	1.3	0.57	1645.3	18.5	1652.0	18.3	1660.5	34.3	1660.5	34.3	99.1
K14-MANZQTZITE-Spot 266	332	99103	3.5	9.6268	1.2	4.1456	1.7	0.2894	1.3	0.72	1638.8	18.1	1663.3	14.3	1694.5	22.5	1694.5	22.5	96.7
K14-MANZQTZITE-Spot 267	406	175672	2.1	9.6521	1.5	4.3552	3.9	0.3049	3.6	0.93	1715.5	54.5	1703.9	32.2	1689.6	27.0	1689.6	27.0	101.5
K14-MANZQTZITE-Spot 268	236	214485	1.6	9.6952	1.2	4.1274	4.0	0.2902	3.8	0.95	1642.6	54.6	1659.7	32.4	1681.4	22.8	1681.4	22.8	97.7
K14-MANZQTZITE-Spot 269	164	94334	1.8	9.8171	1.8	4.1327	4.7	0.2942	4.3	0.93	1662.7	63.5	1660.8	38.3	1658.3	32.6	1658.3	32.6	100.3
K14-MANZQTZITE-Spot 270	253	204680	2.5	9.5267	1.2	4.2241	2.2	0.2919	1.8	0.83	1650.8	26.4	1678.7	18.0	1713.7	22.7	1713.7	22.7	96.3
K14-MANZQTZITE-Spot 271	166	140847	1.6	9.4686	1.4	4.2754	2.5	0.2936	2.1	0.83	1659.5	30.0	1688.6	20.4	1725.0	25.4	1725.0	25.4	96.2
K14-MANZQTZITE-Spot 272	85	119679	1.4	9.8853	1.1	3.9641	2.3	0.2842	2.0	0.88	1612.5	28.9	1626.9	18.6	1645.5	20.1	1645.5	20.1	98.0
K14-MANZQTZITE-Spot 273	575	54186	6.0	9.5131	1.2	4.4992	2.1	0.3104	1.7	0.82	1742.8	25.8	1730.8	17.2	1716.4	21.9	1716.4	21.9	101.5
K14-MANZQTZITE-Spot 274	451	214558	0.9	9.9992	0.8	3.9673	1.7	0.2877	1.5	0.88	1630.1	21.5	1627.5	13.8	1624.2	15.1	1624.2	15.1	100.4
K14-MANZQTZITE-Spot 275	236	226106	1.3	9.9321	1.4	4.1208	2.2	0.2968	1.7	0.78	1675.6	24.8	1658.4	17.7	1636.7	25.4	1636.7	25.4	102.4

K14-MANZQTZITE-Spot 276	254	384078	1.5	9.7451	1.3	4.1743	2.9	0.2950	2.5	0.89	1666.6	37.4	1669.0	23.4	1672.0	23.8	1672.0	23.8	99.7
K14-MANZQTZITE-Spot 277	321	57553	1.6	9.6852	1.0	3.7827	2.9	0.2657	2.8	0.94	1519.0	37.3	1589.1	23.4	1683.3	17.8	1683.3	17.8	90.2
K14-MANZQTZITE-Spot 278	221	60013	1.2	9.8449	1.2	3.2982	2.0	0.2355	1.6	0.79	1363.3	19.6	1480.6	15.7	1653.1	22.8	1653.1	22.8	82.5
K14-MANZQTZITE-Spot 279	139	32338	1.8	9.8024	1.5	4.1139	3.5	0.2925	3.2	0.91	1653.9	46.2	1657.1	28.5	1661.1	26.9	1661.1	26.9	99.6
K14-MANZQTZITE-Spot 280	466	126226	3.8	9.2043	1.1	4.8266	1.7	0.3222	1.3	0.77	1800.5	20.8	1789.5	14.6	1776.8	20.3	1776.8	20.3	101.3
K14-MANZQTZITE-Spot 281	52	766513	1.3	9.8853	1.5	4.0948	2.2	0.2936	1.5	0.70	1659.4	22.0	1653.3	17.6	1645.5	28.6	1645.5	28.6	100.8
K14-MANZQTZITE-Spot 282	316	62894	2.6	9.1793	1.2	4.7098	2.5	0.3136	2.2	0.88	1758.2	33.4	1769.0	20.8	1781.8	21.8	1781.8	21.8	98.7
K14-MANZQTZITE-Spot 283	111	55259	1.6	9.6038	1.4	4.2722	4.1	0.2976	3.9	0.94	1679.3	57.5	1688.0	34.0	1698.9	25.5	1698.9	25.5	98.8
K14-MANZQTZITE-Spot 284	526	112535	2.0	9.2970	1.4	4.7266	2.1	0.3187	1.6	0.75	1783.4	24.2	1772.0	17.3	1758.5	24.7	1758.5	24.7	101.4
K14-MANZQTZITE-Spot 285	242	124235	1.7	9.9487	1.4	4.0488	2.2	0.2921	1.7	0.77	1652.2	24.8	1644.0	17.9	1633.6	26.0	1633.6	26.0	101.1
K14-MANZQTZITE-Spot 286	275	69062	1.8	9.8602	1.0	4.0607	1.8	0.2904	1.6	0.85	1643.5	22.5	1646.4	14.8	1650.2	17.7	1650.2	17.7	99.6
K14-MANZQTZITE-Spot 287	307	113107	1.0	9.6046	1.3	3.8161	1.8	0.2658	1.3	0.70	1519.6	17.1	1596.2	14.5	1698.7	23.8	1698.7	23.8	89.5
K14-MANZQTZITE-Spot 288	259	164912	1.2	9.8207	1.2	4.0595	2.1	0.2891	1.7	0.81	1637.2	25.0	1646.2	17.4	1657.7	23.1	1657.7	23.1	98.8
K14-MANZQTZITE-Spot 289	352	87910	3.1	9.6417	1.1	4.3548	1.7	0.3045	1.3	0.75	1713.7	19.2	1703.8	14.0	1691.7	20.6	1691.7	20.6	101.3
K14-MANZQTZITE-Spot 291	294	52436	1.0	9.9280	1.1	4.0299	1.8	0.2902	1.4	0.78	1642.4	20.3	1640.2	14.7	1637.5	21.1	1637.5	21.1	100.3
K14-MANZQTZITE-Spot 292	143	47433	1.0	9.9401	1.4	3.9105	2.7	0.2819	2.3	0.85	1601.0	32.8	1615.9	21.9	1635.2	26.1	1635.2	26.1	97.9
K14-MANZQTZITE-Spot 293	187	153205	1.5	9.8180	1.3	4.0331	2.3	0.2872	1.9	0.82	1627.4	27.4	1640.9	19.0	1658.2	24.9	1658.2	24.9	98.1
K14-MANZQTZITE-Spot 294	163	33018	2.5	9.5317	1.1	4.3332	2.1	0.2996	1.8	0.87	1689.1	27.4	1699.7	17.5	1712.8	19.4	1712.8	19.4	98.6
K14-MANZQTZITE-Spot 295	118	109739	1.5	9.6606	1.0	4.2925	2.5	0.3008	2.3	0.91	1695.1	33.8	1691.9	20.5	1688.0	19.1	1688.0	19.1	100.4
K14-MANZQTZITE-Spot 296	211	90238	1.6	9.7847	1.4	4.0349	2.6	0.2863	2.1	0.83	1623.2	30.6	1641.3	20.9	1664.5	26.4	1664.5	26.4	97.5
K14-MANZQTZITE-Spot 297	456	116899	4.4	9.7332	1.0	4.1396	1.9	0.2922	1.7	0.87	1652.6	24.5	1662.2	15.8	1674.2	17.7	1674.2	17.7	98.7
K14-MANZQTZITE-Spot 298	211	74231	2.0	9.8632	0.9	4.0296	1.7	0.2883	1.5	0.86	1632.8	21.1	1640.2	13.9	1649.6	16.1	1649.6	16.1	99.0
K14-MANZQTZITE-Spot 299	449	71149	1.3	9.9330	1.2	3.6814	3.0	0.2652	2.8	0.92	1516.5	37.7	1567.4	24.3	1636.6	22.7	1636.6	22.7	92.7
K14-MANZQTZITE-Spot 300	597	79921	3.1	9.5202	1.2	4.5033	2.5	0.3109	2.1	0.87	1745.3	32.8	1731.6	20.5	1715.0	22.4	1715.0	22.4	101.8
K14-MANZQTZITE-Spot 301	446	175732	1.7	9.4791	1.1	4.4760	2.0	0.3077	1.7	0.84	1729.5	25.0	1726.5	16.4	1722.9	19.8	1722.9	19.8	100.4
K14-MANZQTZITE-Spot 302	215	78265	2.0	9.7641	1.2	4.2461	1.6	0.3007	1.0	0.66	1694.8	15.2	1683.0	12.8	1668.3	21.7	1668.3	21.7	101.6
K14-MANZQTZITE-Spot 303	372	86021	2.7	9.5397	1.0	4.4384	1.8	0.3071	1.5	0.83	1726.4	22.4	1719.5	14.8	1711.2	18.5	1711.2	18.5	100.9
K14-MANZQTZITE-Spot 304	491	55658	1.6	9.8483	0.9	4.2001	1.9	0.3000	1.6	0.86	1691.3	24.1	1674.0	15.4	1652.4	17.6	1652.4	17.6	102.4
K14-MANZQTZITE-Spot 305	221	114594	1.7	9.7174	1.1	4.1320	2.4	0.2912	2.1	0.88	1647.6	31.0	1660.7	19.7	1677.2	20.8	1677.2	20.8	98.2
K14-MANZQTZITE-Spot 306	266	78167	2.1	9.6438	1.1	4.2887	2.1	0.3000	1.8	0.85	1691.1	26.3	1691.2	17.2	1691.2	20.6	1691.2	20.6	100.0
K14-MANZQTZITE-Spot 308	159	56712	1.5	10.0399	1.6	4.0363	3.9	0.2939	3.5	0.91	1661.0	51.4	1641.5	31.4	1616.7	30.1	1616.7	30.1	102.7
K14-MANZQTZITE-Spot 309	219	135527	1.9	9.8430	1.8	4.0427	3.3	0.2886	2.8	0.85	1634.5	40.8	1642.8	27.2	1653.5	32.9	1653.5	32.9	98.9
K14-MANZQTZITE-Spot 310	151	155721	2.8	9.5574	1.8	4.3440	2.7	0.3011	2.0	0.76	1696.8	30.3	1701.8	22.2	1707.8	32.4	1707.8	32.4	99.4
K14-MANZQTZITE-Spot 311	186	161567	1.6	9.6243	1.0	4.0806	3.8	0.2848	3.6	0.96	1615.7	52.2	1650.4	30.9	1695.0	18.9	1695.0	18.9	95.3
K14-MANZQTZITE-Spot 312	380	221194	1.7	9.7358	1.0	3.8983	1.9	0.2753	1.5	0.83	1567.4	21.4	1613.3	15.0	1673.7	19.4	1673.7	19.4	93.7
K14-MANZQTZITE-Spot 313	616	168630	1.6	9.6761	1.0	4.3089	1.8	0.3024	1.5	0.82	1703.1	21.9	1695.1	14.7	1685.1	18.9	1685.1	18.9	101.1
K14-MANZQTZITE-Spot 314	184	56258	1.4	9.7053	1.5	4.2177	2.4	0.2969	1.9	0.78	1675.8	28.0	1677.5	20.0	1679.5	28.3	1679.5	28.3	99.8
K14-MANZQTZITE-Spot 315	261	170285	1.4	9.8148	1.1	3.9757	3.0	0.2830	2.8	0.93	1606.5	39.8	1629.3	24.4	1658.8	20.1	1658.8	20.1	96.8
K14-MANZQTZITE-Spot 316	182	213150	1.5	9.6706	1.2	4.1321	3.2	0.2898	3.0	0.93	1640.6	43.5	1660.7	26.3	1686.1	21.3	1686.1	21.3	97.3
K14-MANZQTZITE-Spot 317	103	45416	1.5	9.6518	1.6	4.2116	3.2	0.2948	2.7	0.87	1665.6	40.2	1676.3	25.9	1689.7	29.2	1689.7	29.2	98.6
K14-MANZQTZITE-Spot 318	318	197240	1.7	9.7234	1.1	4.2509	1.7	0.2998	1.3	0.75	1690.2	19.6	1683.9	14.4	1676.1	21.2	1676.1	21.2	100.8
K14-MANZQTZITE-Spot 319	235	172017	2.3	9.8338	1.4	4.2130	2.0	0.3005	1.4	0.70	1693.7	20.8	1676.6	16.3	1655.2	26.2	1655.2	26.2	102.3
K14-MANZQTZITE-Spot 320	298	80912	1.9	9.6654	1.1	4.2830	2.2	0.3002	1.9	0.87	1692.5	28.9	1690.1	18.4	1687.1	20.5	1687.1	20.5	100.3

K14-MANZQTZITE-Spot 321	385	56031	1.6	9.8477	0.9	3.9316	4.0	0.2808	3.9	0.98	1595.4	55.4	1620.2	32.5	1652.6	16.1	1652.6	16.1	96.5
K14-MANZQTZITE-Spot 322	285	110127	1.3	10.0345	1.4	4.1140	2.6	0.2994	2.2	0.85	1688.4	32.6	1657.1	21.2	1617.7	25.6	1617.7	25.6	104.4
K14-MANZQTZITE-Spot 323	394	65842	0.9	9.3880	1.3	3.7441	2.0	0.2549	1.5	0.75	1463.8	19.5	1580.8	15.8	1740.7	23.8	1740.7	23.8	84.1
K14-MANZQTZITE-Spot 324	384	153092	2.9	9.7115	1.2	4.3557	2.3	0.3068	2.0	0.84	1724.9	29.8	1704.0	19.2	1678.3	23.1	1678.3	23.1	102.8
K14-MANZQTZITE-Spot 325	181	27738	1.7	10.0357	1.5	3.9512	2.2	0.2876	1.6	0.73	1629.5	23.6	1624.2	18.2	1617.4	28.6	1617.4	28.6	100.7
K14-MANZQTZITE-Spot 326	156	55801	2.2	9.7451	1.2	4.0941	3.3	0.2894	3.1	0.93	1638.3	44.4	1653.1	26.8	1671.9	21.9	1671.9	21.9	98.0
K14-MANZQTZITE-Spot 327	171	147867	1.9	9.5928	1.5	4.1935	2.4	0.2918	1.9	0.79	1650.3	28.0	1672.8	19.9	1701.0	27.3	1701.0	27.3	97.0
K14-MANZQTZITE-Spot 328	220	121770	1.1	9.7496	0.9	4.1664	2.0	0.2946	1.8	0.89	1664.5	25.9	1667.4	16.3	1671.1	17.0	1671.1	17.0	99.6
K14-MANZQTZITE-Spot 329	267	199214	2.8	9.9083	1.3	4.1231	2.1	0.2963	1.7	0.80	1672.9	24.5	1658.9	17.0	1641.2	23.4	1641.2	23.4	101.9
K14-MANZQTZITE-Spot 330	182	66281	1.3	9.7970	1.3	4.1020	2.3	0.2915	1.9	0.81	1648.8	26.9	1654.7	18.7	1662.1	24.9	1662.1	24.9	99.2
K15-ES-1-Spot 1	225	172307	2.2	9.7302	0.7	4.1157	1.5	0.2904	1.3	0.87	1643.8	18.5	1657.4	12.0	1674.8	13.4	1674.8	13.4	98.1
K15-ES-1-Spot 2	106	170701	1.9	9.7050	0.8	4.1231	1.4	0.2902	1.2	0.84	1642.6	17.6	1658.9	11.7	1679.6	14.2	1679.6	14.2	97.8
K15-ES-1-Spot 3	294	113104	2.0	9.8346	0.7	4.1442	1.3	0.2956	1.0	0.82	1669.4	15.3	1663.1	10.4	1655.0	13.3	1655.0	13.3	100.9
K15-ES-1-Spot 4	211	140865	1.2	9.6821	1.0	4.0759	1.7	0.2862	1.5	0.84	1622.6	20.8	1649.5	14.2	1683.9	17.6	1683.9	17.6	96.4
K15-ES-1-Spot 5	455	97118	1.6	9.7051	0.7	3.9019	1.3	0.2746	1.1	0.83	1564.4	14.7	1614.1	10.3	1679.5	13.2	1679.5	13.2	93.1
K15-ES-1-Spot 6	251	64876	1.2	9.8049	0.7	4.0965	1.3	0.2913	1.1	0.84	1648.1	15.8	1653.6	10.5	1660.6	12.7	1660.6	12.7	99.2
K15-ES-1-Spot 7	48	45479	1.9	9.8802	1.1	4.0863	1.8	0.2928	1.4	0.78	1655.6	20.5	1651.6	14.7	1646.4	21.0	1646.4	21.0	100.6
K15-ES-1-Spot 8	43	106033	1.7	9.9837	1.3	3.9865	1.6	0.2887	1.0	0.60	1634.8	13.9	1631.5	13.0	1627.1	23.8	1627.1	23.8	100.5
K15-ES-1-Spot 9	591	103779	3.5	9.2747	0.7	4.0202	1.4	0.2704	1.2	0.86	1543.0	15.9	1638.3	11.0	1762.9	12.6	1762.9	12.6	87.5
K15-ES-1-Spot 10	156	121199	1.1	9.7931	0.9	4.0331	1.6	0.2865	1.4	0.85	1623.8	19.8	1640.9	13.2	1662.9	15.9	1662.9	15.9	97.7
K15-ES-1-Spot 11	206	154124	1.1	9.8017	0.8	4.0606	1.6	0.2887	1.4	0.86	1634.8	19.8	1646.4	13.0	1661.2	15.0	1661.2	15.0	98.4
K15-ES-1-Spot 12	81	85450	1.2	9.8396	1.0	4.1213	1.6	0.2941	1.2	0.78	1662.0	18.1	1658.5	12.9	1654.1	18.3	1654.1	18.3	100.5
K15-ES-1-Spot 13	84	120776	2.3	9.6247	0.9	4.2327	1.6	0.2955	1.4	0.84	1668.8	20.3	1680.4	13.4	1694.9	16.2	1694.9	16.2	98.5
K15-ES-1-Spot 14	191	141418	3.3	9.6211	0.8	4.1704	1.3	0.2910	1.0	0.78	1646.6	14.1	1668.2	10.3	1695.6	14.6	1695.6	14.6	97.1
K15-ES-1-Spot 15	134	93777	2.8	9.3444	1.0	4.2686	1.6	0.2893	1.3	0.80	1638.0	18.6	1687.3	13.2	1749.2	17.8	1749.2	17.8	93.6
K15-ES-1-Spot 16	147	195400	2.2	9.7405	1.0	4.1823	1.7	0.2955	1.4	0.80	1668.7	20.3	1670.6	14.2	1672.8	19.1	1672.8	19.1	99.8
K15-ES-1-Spot 17	69	121109	2.3	9.7018	1.1	4.1825	1.6	0.2943	1.1	0.71	1662.9	16.5	1670.6	12.9	1680.2	20.3	1680.2	20.3	99.0
K15-ES-1-Spot 18	156	220796	1.8	9.7813	1.0	4.0701	1.7	0.2887	1.4	0.79	1635.2	19.6	1648.3	14.0	1665.1	19.4	1665.1	19.4	98.2
K15-ES-1-Spot 19	125	64086	1.0	9.8917	0.8	3.9575	1.4	0.2839	1.2	0.84	1611.1	17.1	1625.5	11.5	1644.3	14.2	1644.3	14.2	98.0
K15-ES-1-Spot 20	193	60136	3.4	9.8280	0.8	3.9980	1.6	0.2850	1.4	0.86	1616.4	19.7	1633.8	12.9	1656.3	14.8	1656.3	14.8	97.6
K15-ES-1-Spot 21	205	100700	2.4	9.7206	0.8	4.1510	1.5	0.2926	1.3	0.84	1654.7	18.3	1664.4	12.1	1676.6	14.7	1676.6	14.7	98.7
K15-ES-1-Spot 22	576	53744	2.7	9.6350	0.7	3.9638	1.7	0.2770	1.6	0.91	1576.2	21.7	1626.8	13.9	1692.9	13.1	1692.9	13.1	93.1
K15-ES-1-Spot 24	117	70449	2.4	9.7216	1.0	4.1437	1.7	0.2922	1.4	0.81	1652.3	19.8	1663.0	13.7	1676.4	18.3	1676.4	18.3	98.6
K15-ES-1-Spot 27	121	84216	2.9	9.5467	0.9	4.4151	1.3	0.3057	1.0	0.76	1719.5	15.3	1715.2	11.0	1709.9	15.8	1709.9	15.8	100.6
K15-ES-1-Spot 28	105	82053	2.0	9.8697	1.0	4.0847	1.6	0.2924	1.2	0.77	1653.5	18.0	1651.3	13.1	1648.4	19.0	1648.4	19.0	100.3
K15-ES-1-Spot 29	134	106445	1.2	9.8166	0.7	4.0303	1.5	0.2869	1.3	0.87	1626.3	18.5	1640.3	12.0	1658.4	13.4	1658.4	13.4	98.1
K15-ES-1-Spot 30	84	120550	0.9	9.7623	0.8	4.0425	1.4	0.2862	1.1	0.80	1622.6	15.7	1642.8	11.2	1668.7	15.4	1668.7	15.4	97.2
K15-ES-1-Spot 31	212	124045	2.2	9.8131	0.8	4.1524	1.5	0.2955	1.3	0.86	1669.1	18.9	1664.7	12.3	1659.1	14.2	1659.1	14.2	100.6
K15-ES-1-Spot 32	271	65145	2.2	9.7360	0.7	4.1858	1.6	0.2956	1.4	0.89	1669.3	20.8	1671.2	13.1	1673.7	13.7	1673.7	13.7	99.7
K15-ES-1-Spot 34	182	105219	2.1	9.6905	0.8	4.2135	1.4	0.2961	1.2	0.81	1672.1	17.2	1676.7	11.8	1682.3	15.4	1682.3	15.4	99.4
K15-ES-1-Spot 35	164	108951	1.6	9.8815	0.9	4.1012	1.3	0.2939	1.0	0.75	1661.1	14.8	1654.5	11.0	1646.2	16.4	1646.2	16.4	100.9
K15-ES-1-Spot 36	176	192780	2.0	9.7327	0.8	4.1999	1.4	0.2965	1.2	0.81	1673.8	17.1	1674.0	11.7	1674.3	15.4	1674.3	15.4	100.0
K15-ES-1-Spot 37	78	72736	1.7	9.9431	1.1	3.9678	1.7	0.2861	1.3	0.75	1622.2	18.0	1627.6	13.6	1634.7	20.5	1634.7	20.5	99.2

K15-ES-1-Spot 38	191	90113	1.4	9.6804	0.8	4.1424	1.2	0.2908	1.0	0.78	1645.7	14.0	1662.7	10.1	1684.3	14.3	1684.3	14.3	97.7
K15-ES-1-Spot 39	351	487616	1.9	9.7000	0.7	4.1840	1.6	0.2944	1.5	0.92	1663.2	22.1	1670.9	13.5	1680.5	12.1	1680.5	12.1	99.0
K15-ES-1-Spot 40	301	168634	1.8	8.7717	0.8	5.3307	1.5	0.3391	1.3	0.86	1882.5	21.3	1873.8	13.0	1864.2	14.0	1864.2	14.0	101.0
K15-ES-1-Spot 43	477	72001	1.1	9.5351	0.8	4.4058	1.3	0.3047	1.0	0.79	1714.5	15.2	1713.4	10.5	1712.1	14.2	1712.1	14.2	100.1
K15-ES-1-Spot 44	120	61143	2.0	9.7188	0.8	4.2711	1.4	0.3011	1.1	0.78	1696.5	16.0	1687.8	11.2	1676.9	15.7	1676.9	15.7	101.2
K15-ES-1-Spot 45	92	52378	2.5	9.8764	1.0	4.1420	1.7	0.2967	1.3	0.81	1674.9	19.9	1662.6	13.6	1647.2	18.2	1647.2	18.2	101.7
K15-ES-1-Spot 46	76	86217	1.6	9.8078	0.8	4.1389	1.4	0.2944	1.2	0.84	1663.5	17.5	1662.0	11.6	1660.1	14.2	1660.1	14.2	100.2
K15-ES-1-Spot 47	58	129952	1.8	9.8878	1.0	4.0685	1.3	0.2918	0.9	0.68	1650.3	13.2	1648.0	10.9	1645.0	18.1	1645.0	18.1	100.3
K15-ES-1-Spot 48	129	115809	1.5	9.7610	1.4	4.3141	2.0	0.3054	1.5	0.74	1718.1	22.8	1696.1	16.9	1668.9	25.5	1668.9	25.5	102.9
K15-ES-1-Spot 49	93	120677	1.5	9.8955	0.8	4.0645	1.6	0.2917	1.3	0.85	1650.0	19.5	1647.2	12.8	1643.6	15.3	1643.6	15.3	100.4
K15-ES-1-Spot 50	236	165527	1.2	9.6871	1.1	4.1701	1.7	0.2930	1.3	0.77	1656.4	19.2	1668.2	14.0	1683.0	20.2	1683.0	20.2	98.4
K15-ES-1-Spot 51	167	74743	1.9	8.9143	0.8	4.9716	1.4	0.3214	1.1	0.82	1796.7	17.9	1814.5	11.8	1835.0	14.6	1835.0	14.6	97.9
K15-ES-1-Spot 52	51	97787	1.5	9.9791	1.1	4.1085	1.5	0.2974	1.0	0.68	1678.2	14.9	1656.0	12.2	1628.0	20.5	1628.0	20.5	103.1
K15-ES-1-Spot 53	142	47167	1.4	8.4856	0.9	4.7477	1.6	0.2922	1.3	0.80	1652.5	18.4	1775.7	13.2	1923.8	16.7	1923.8	16.7	85.9
K15-ES-1-Spot 54	136	88308	2.6	9.8404	0.9	4.1337	1.6	0.2950	1.3	0.84	1666.6	19.5	1661.0	12.9	1653.9	15.8	1653.9	15.8	100.8
K15-ES-1-Spot 55	230	117209	2.1	9.9126	0.7	4.1241	1.2	0.2965	1.0	0.81	1673.9	14.5	1659.1	9.9	1640.4	13.2	1640.4	13.2	102.0
K15-ES-1-Spot 56	202	118344	3.6	9.7761	0.8	4.1695	1.3	0.2956	1.0	0.78	1669.6	14.9	1668.0	10.6	1666.1	14.8	1666.1	14.8	100.2
K15-ES-1-Spot 57	316	132837	2.0	9.6779	1.1	3.8555	1.8	0.2706	1.4	0.81	1543.9	19.7	1604.4	14.4	1684.7	19.5	1684.7	19.5	91.6
K15-ES-1-Spot 58	60	221136	1.5	10.0049	1.0	4.0566	1.6	0.2944	1.2	0.78	1663.3	18.3	1645.6	13.1	1623.2	18.8	1623.2	18.8	102.5
K15-ES-1-Spot 59	291	66742	2.8	9.4862	0.9	4.4392	1.7	0.3054	1.4	0.84	1718.1	21.8	1719.7	14.3	1721.6	17.4	1721.6	17.4	99.8
K15-ES-1-Spot 60	76	201459	2.7	9.7924	1.3	4.2842	1.9	0.3043	1.4	0.73	1712.4	20.5	1690.3	15.4	1663.0	23.6	1663.0	23.6	103.0
K15-ES-1-Spot 62	136	112860	2.3	9.7195	1.1	4.1969	1.8	0.2958	1.4	0.79	1670.7	20.7	1673.4	14.6	1676.8	20.0	1676.8	20.0	99.6
K15-ES-1-Spot 63	80	182232	1.2	9.7181	0.9	4.2422	1.4	0.2990	1.0	0.74	1686.3	15.0	1682.2	11.2	1677.1	16.8	1677.1	16.8	100.6
K15-ES-1-Spot 64	302	170803	2.0	9.6036	0.8	4.3015	1.4	0.2996	1.1	0.83	1689.4	16.9	1693.6	11.3	1699.0	14.2	1699.0	14.2	99.4
K15-ES-1-Spot 65	157	187409	2.7	9.8468	1.0	4.0632	1.7	0.2902	1.3	0.78	1642.4	19.2	1646.9	13.8	1652.7	19.4	1652.7	19.4	99.4
K15-ES-1-Spot 66	183	91392	1.2	9.7824	1.0	4.0597	1.5	0.2880	1.2	0.78	1631.7	17.0	1646.2	12.4	1664.9	17.7	1664.9	17.7	98.0
K15-ES-1-Spot 67	76	99826	1.9	9.7522	1.0	4.1348	1.6	0.2925	1.3	0.80	1653.8	18.9	1661.2	13.3	1670.6	18.1	1670.6	18.1	99.0
K15-ES-1-Spot 68	126	96731	2.2	9.7479	0.8	4.1197	1.4	0.2913	1.2	0.82	1647.8	16.9	1658.2	11.6	1671.4	15.0	1671.4	15.0	98.6
K15-ES-1-Spot 69	132	258500	2.0	9.7272	0.9	4.1969	1.6	0.2961	1.4	0.82	1671.9	19.9	1673.4	13.5	1675.3	17.4	1675.3	17.4	99.8
K15-ES-1-Spot 70	185	214979	1.7	9.8157	0.8	4.0614	1.5	0.2891	1.2	0.83	1637.2	17.4	1646.6	11.8	1658.6	15.0	1658.6	15.0	98.7
K15-ES-1-Spot 71	229	87573	2.0	9.7760	1.0	4.1789	1.6	0.2963	1.3	0.78	1672.9	18.7	1669.9	13.4	1666.1	19.1	1666.1	19.1	100.4
K15-ES-1-Spot 72	139	56503	1.9	9.8793	1.0	4.1032	1.5	0.2940	1.1	0.73	1661.5	15.8	1654.9	12.1	1646.6	18.6	1646.6	18.6	100.9
K15-ES-1-Spot 73	102	174186	1.7	9.7711	1.0	4.1386	1.8	0.2933	1.5	0.83	1658.0	21.8	1662.0	14.7	1667.0	18.4	1667.0	18.4	99.5
K15-ES-1-Spot 74	63	71749	1.8	9.8021	1.0	4.1549	1.5	0.2954	1.1	0.74	1668.4	16.4	1665.2	12.3	1661.2	18.7	1661.2	18.7	100.4
K15-ES-1-Spot 75	49	92160	1.2	9.9019	1.0	4.1123	1.6	0.2953	1.2	0.75	1668.1	17.6	1656.8	13.0	1642.4	19.3	1642.4	19.3	101.6
K15-ES-1-Spot 76	108	68279	2.4	9.8622	1.0	4.1821	1.5	0.2991	1.2	0.78	1687.0	17.9	1670.5	12.6	1649.8	17.7	1649.8	17.7	102.3
K15-ES-1-Spot 77	108	136065	2.8	9.7626	0.9	4.2262	1.7	0.2992	1.4	0.84	1687.5	21.4	1679.1	14.0	1668.6	17.0	1668.6	17.0	101.1
K15-ES-1-Spot 78	240	61346	3.3	9.4896	0.7	4.4256	1.2	0.3046	1.0	0.84	1714.1	15.1	1717.2	9.9	1720.9	12.0	1720.9	12.0	99.6
K15-ES-1-Spot 79	264	153218	1.9	9.7888	0.8	4.0975	1.4	0.2909	1.1	0.81	1646.0	16.0	1653.8	11.1	1663.7	14.7	1663.7	14.7	98.9
K15-ES-1-Spot 80	143	70799	2.1	9.7147	0.9	4.2099	1.5	0.2966	1.2	0.81	1674.5	17.6	1676.0	12.1	1677.7	15.8	1677.7	15.8	99.8
K15-ES-1-Spot 81	72	4506811	1.8	9.8125	1.0	4.1033	1.6	0.2920	1.3	0.81	1651.6	19.4	1655.0	13.4	1659.2	17.8	1659.2	17.8	99.5
K15-ES-1-Spot 82	71	35504	1.7	9.8294	0.9	4.1347	1.8	0.2948	1.5	0.85	1665.3	22.2	1661.2	14.5	1656.0	17.3	1656.0	17.3	100.6
K15-ES-1-Spot 84	142	1744852	1.7	9.8451	1.0	4.1726	1.5	0.2979	1.1	0.74	1681.1	16.9	1668.7	12.6	1653.1	19.2	1653.1	19.2	101.7

K15-ES-1-Spot 85	63	53599	1.9	9.8164	1.0	4.1402	1.4	0.2948	1.0	0.73	1665.3	15.1	1662.3	11.5	1658.5	17.8	1658.5	17.8	100.4
K15-ES-1 Spot 86	34	49869	1.6	10.0762	1.5	4.0584	1.9	0.2966	1.3	0.66	1674.4	18.9	1646.0	15.8	1609.9	27.1	1609.9	27.1	104.0
K15-ES-1-Spot 87	59	92349	1.7	9.8491	1.1	4.1560	1.7	0.2969	1.3	0.75	1675.8	19.0	1665.4	14.0	1652.3	21.0	1652.3	21.0	101.4
K15-ES-1-Spot 88	141	149670	1.1	9.7889	0.7	4.1333	1.4	0.2934	1.2	0.84	1658.7	17.3	1660.9	11.4	1663.6	13.9	1663.6	13.9	99.7
K15-ES-1-Spot 89	139	436975	2.3	9.1321	0.9	4.8974	1.6	0.3244	1.3	0.83	1811.0	20.6	1801.8	13.2	1791.2	15.7	1791.2	15.7	101.1
K15-ES-1-Spot 90	49	38894	1.7	9.8478	1.1	4.1727	1.7	0.2980	1.3	0.76	1681.5	19.2	1668.7	13.9	1652.6	20.4	1652.6	20.4	101.8
K15-ES-1-Spot 91	172	1953078	1.6	9.8243	1.0	4.2629	1.8	0.3037	1.4	0.81	1709.9	21.3	1686.2	14.4	1657.0	19.2	1657.0	19.2	103.2
K15-ES-1-Spot 92	93	98016	3.4	9.6116	1.3	4.3476	1.8	0.3031	1.2	0.67	1706.5	17.6	1702.4	14.6	1697.4	24.3	1697.4	24.3	100.5
K15-ES-1-Spot 93	210	106327	2.0	9.7843	1.0	4.1539	1.6	0.2948	1.2	0.78	1665.3	17.9	1665.0	12.8	1664.5	18.3	1664.5	18.3	100.0
K15-ES-1-Spot 94	223	78578	2.0	9.8890	1.0	4.2087	1.4	0.3019	1.1	0.73	1700.5	15.8	1675.7	11.8	1644.8	18.2	1644.8	18.2	103.4
K15-ES-1-Spot 95	42	72707	2.0	9.9286	1.4	4.1010	2.2	0.2953	1.7	0.78	1668.0	24.8	1654.5	17.7	1637.4	25.3	1637.4	25.3	101.9
K15-ES-1-Spot 96	88	129222	2.2	9.7989	0.9	4.2101	1.4	0.2992	1.1	0.77	1687.4	16.2	1676.0	11.7	1661.8	16.9	1661.8	16.9	101.5
K15-ES-1-Spot 97	67	114345	1.9	9.8208	1.2	4.1289	1.6	0.2941	1.0	0.66	1661.9	15.1	1660.0	12.8	1657.6	21.8	1657.6	21.8	100.3
K15-ES-1-Spot 98	162	133452	2.1	9.6116	0.8	4.4280	1.5	0.3087	1.3	0.84	1734.2	19.1	1717.6	12.4	1697.4	15.0	1697.4	15.0	102.2
K15-ES-1-Spot 99	167	209850	1.7	9.7908	0.6	4.2347	1.5	0.3007	1.3	0.90	1694.8	19.4	1680.8	11.9	1663.3	11.8	1663.3	11.8	101.9
K15-ES-1-Spot 100	165	161305	1.7	9.8053	0.7	4.1555	1.2	0.2955	1.0	0.80	1669.1	14.5	1665.3	10.0	1660.5	13.6	1660.5	13.6	100.5
K15-ES-1-Spot 101	126	76515	1.9	9.8835	0.9	4.1239	1.6	0.2956	1.3	0.83	1669.5	19.5	1659.0	13.1	1645.8	16.8	1645.8	16.8	101.4
K15-ES-1-Spot 102	191	135613	1.6	9.7544	0.9	4.0843	1.7	0.2889	1.5	0.86	1636.3	21.7	1651.2	14.2	1670.2	16.5	1670.2	16.5	98.0
K15-ES-1-Spot 103	59	92151	1.9	9.7686	1.3	4.2029	2.0	0.2978	1.5	0.76	1680.2	22.6	1674.6	16.5	1667.5	24.3	1667.5	24.3	100.8
K15-ES-1-Spot 104	453	437625	1.9	5.7047	0.7	11.8712	1.6	0.4912	1.4	0.89	2575.7	29.5	2594.3	14.6	2608.8	11.9	2608.8	11.9	98.7
K15-ES-1-Spot 105	275	91566	2.5	9.7902	0.9	4.0603	1.3	0.2883	1.0	0.74	1633.0	13.8	1646.4	10.5	1663.4	16.1	1663.4	16.1	98.2
K15-ES-1-Spot 106	82	297519	2.5	9.6136	1.0	4.4824	1.6	0.3125	1.2	0.75	1753.2	17.9	1727.7	12.9	1697.0	19.0	1697.0	19.0	103.3
K15-ES-1-Spot 107	65	108861	1.8	9.8384	1.0	4.1156	1.7	0.2937	1.4	0.80	1659.8	20.2	1657.4	14.0	1654.3	19.1	1654.3	19.1	100.3
K15-ES-1-Spot 108	102	152987	1.5	9.8372	0.9	4.0160	1.5	0.2865	1.2	0.79	1624.1	16.6	1637.4	11.9	1654.5	16.6	1654.5	16.6	98.2
K15-ES-1-Spot 109	173	415419	3.0	9.6245	0.7	4.2275	1.1	0.2951	0.8	0.74	1666.9	11.8	1679.4	8.9	1694.9	13.3	1694.9	13.3	98.3
K15-ES-1-Spot 110	210	167547	2.1	9.7798	1.0	4.2380	1.8	0.3006	1.4	0.82	1694.3	21.5	1681.4	14.5	1665.4	18.7	1665.4	18.7	101.7
K15-ES-1-Spot 111	262	338285	2.2	9.7934	0.7	4.1353	1.2	0.2937	1.0	0.83	1660.1	14.4	1661.3	9.7	1662.8	12.4	1662.8	12.4	99.8
K15-ES-1-Spot 112	47	97682	2.1	9.9096	1.1	4.0575	1.7	0.2916	1.2	0.73	1649.6	17.9	1645.8	13.7	1640.9	21.3	1640.9	21.3	100.5
K15-ES-1-Spot 113	251	162940	1.5	9.7719	0.9	4.1698	1.7	0.2955	1.5	0.85	1669.1	21.6	1668.1	14.1	1666.9	16.7	1666.9	16.7	100.1
K15-ES-1-Spot 114	68	88510	2.4	9.5210	1.0	4.3710	1.7	0.3018	1.3	0.80	1700.4	20.1	1706.9	13.9	1714.8	18.5	1714.8	18.5	99.2
K15-ES-1-Spot 115	202	94709	1.3	9.8217	0.9	4.1065	1.6	0.2925	1.3	0.82	1654.1	18.8	1655.6	12.9	1657.5	16.8	1657.5	16.8	99.8
K15-ES-1-Spot 116	359	51709	3.3	9.7023	0.7	3.8174	1.7	0.2686	1.6	0.92	1533.8	21.6	1596.4	13.8	1680.1	12.3	1680.1	12.3	91.3
K15-ES-1-Spot 117	248	50431	1.8	9.8130	0.9	4.1695	1.6	0.2967	1.3	0.81	1675.2	18.6	1668.1	12.8	1659.1	17.1	1659.1	17.1	101.0
K15-ES-1-Spot 118	76	54648	1.6	9.7685	1.1	4.1222	1.7	0.2921	1.3	0.76	1651.8	18.4	1658.7	13.6	1667.5	20.0	1667.5	20.0	99.1
K15-ES-1-Spot 119	54	55897	1.6	9.6661	1.4	4.1334	1.8	0.2898	1.1	0.61	1640.4	15.7	1660.9	14.5	1687.0	26.0	1687.0	26.0	97.2
K15-ES-1-Spot 120	174	167616	1.7	9.8324	0.8	4.0905	1.6	0.2917	1.4	0.86	1650.0	20.3	1652.4	13.2	1655.4	15.1	1655.4	15.1	99.7
K15-ES-1-Spot 121	281	245760	2.0	9.7571	0.8	4.2764	1.5	0.3026	1.2	0.84	1704.3	18.3	1688.8	12.0	1669.7	14.7	1669.7	14.7	102.1
K15-ES-1-Spot 123	97	95725	1.7	9.8467	0.9	4.0357	1.7	0.2882	1.4	0.83	1632.6	19.8	1641.4	13.5	1652.7	17.3	1652.7	17.3	98.8
K15-ES-1-Spot 124	280	378390	2.2	9.8109	0.6	4.1970	1.1	0.2986	0.9	0.84	1684.6	13.4	1673.4	8.9	1659.5	10.9	1659.5	10.9	101.5
K15-ES-1-Spot 125	132	123839	3.0	9.7900	0.8	4.1578	1.5	0.2952	1.3	0.87	1667.6	19.5	1665.7	12.5	1663.4	14.0	1663.4	14.0	100.2
K15-ES-1-Spot 126	96	174571	1.5	9.7118	1.0	4.1556	1.4	0.2927	1.1	0.75	1655.0	15.7	1665.3	11.8	1678.3	17.7	1678.3	17.7	98.6
K15-ES-1-Spot 127	46	75659	1.6	9.8961	1.3	4.0167	1.8	0.2883	1.2	0.69	1633.0	17.9	1637.6	14.7	1643.5	24.3	1643.5	24.3	99.4
K15-ES-1-Spot 128	73	1118129	2.2	9.8521	0.9	4.0604	1.3	0.2901	0.9	0.72	1642.2	13.7	1646.4	10.6	1651.7	16.6	1651.7	16.6	99.4

K15-ES-1-Spot 129	70	59494	2.0	9.8020	1.0	4.1006	1.6	0.2915	1.2	0.77	1649.1	18.0	1654.4	13.2	1661.2	19.2	1661.2	19.2	99.3
K15-ES-1-Spot 130	224	175204	1.6	9.7328	0.7	4.1289	1.3	0.2915	1.0	0.81	1648.8	14.8	1660.0	10.3	1674.3	13.7	1674.3	13.7	98.5
K15-ES-1-Spot 132	102	107539	1.5	9.7106	0.8	4.2991	1.4	0.3028	1.1	0.80	1705.1	17.0	1693.2	11.7	1678.5	15.6	1678.5	15.6	101.6
K15-ES-1-Spot 133	78	80371	2.1	9.8097	1.0	4.1790	1.5	0.2973	1.2	0.77	1678.0	17.6	1669.9	12.7	1659.7	18.2	1659.7	18.2	101.1
K15-ES-1-Spot 134	80	92181	1.6	10.0233	1.1	3.9995	1.5	0.2907	1.1	0.73	1645.2	16.2	1634.1	12.5	1619.7	19.7	1619.7	19.7	101.6
K15-ES-1-Spot 135	116	64901	1.9	9.8160	1.0	4.1012	1.6	0.2920	1.2	0.78	1651.4	17.9	1654.5	12.9	1658.5	18.2	1658.5	18.2	99.6
K15-ES-1-Spot 137	286	296278	2.0	9.7649	0.7	4.0889	1.4	0.2896	1.2	0.87	1639.5	18.0	1652.1	11.7	1668.2	13.3	1668.2	13.3	98.3
K15-ES-1-Spot 138	250	175253	1.8	9.6240	0.8	4.2325	1.3	0.2954	1.0	0.78	1668.6	14.8	1680.3	10.7	1695.0	15.1	1695.0	15.1	98.4
K15-ES-1-Spot 139	185	74673	3.3	9.8741	0.8	4.1589	1.3	0.2978	1.0	0.76	1680.5	14.6	1666.0	10.6	1647.6	15.5	1647.6	15.5	102.0
K15-ES-1-Spot 141	50	69095	2.1	9.9078	1.0	4.0049	1.7	0.2878	1.4	0.80	1630.4	19.6	1635.2	13.8	1641.3	19.1	1641.3	19.1	99.3
K15-ES-1-Spot 142	274	106908	1.8	9.3638	0.8	4.4007	1.3	0.2989	1.0	0.76	1685.7	14.1	1712.5	10.4	1745.4	15.1	1745.4	15.1	96.6
K15-ES-1-Spot 143	196	960163	1.4	9.5567	0.8	4.3624	1.5	0.3024	1.3	0.84	1703.0	19.3	1705.2	12.7	1708.0	15.5	1708.0	15.5	99.7
K15-ES-1-Spot 144	94	48440	1.2	9.8751	1.2	3.9701	1.8	0.2843	1.4	0.78	1613.2	20.4	1628.1	14.9	1647.4	21.3	1647.4	21.3	97.9
K15-ES-1-Spot 145	57	157150	1.4	9.8108	1.0	4.0490	1.6	0.2881	1.3	0.78	1632.1	18.1	1644.1	13.1	1659.5	18.8	1659.5	18.8	98.3
K15-ES-1-Spot 147	147	184456	1.4	9.7400	0.9	3.9677	1.6	0.2803	1.3	0.81	1592.8	18.8	1627.6	13.3	1672.9	17.5	1672.9	17.5	95.2
K15-ES-1-Spot 148	124	120790	1.3	9.7364	1.1	4.0169	1.7	0.2837	1.3	0.76	1609.7	18.2	1637.6	13.6	1673.6	20.0	1673.6	20.0	96.2
K15-ES-1-Spot 149	200	132989	1.6	9.8093	0.6	4.0696	1.4	0.2895	1.3	0.91	1639.2	18.6	1648.2	11.6	1659.8	11.1	1659.8	11.1	98.8
K15-ES-1-Spot 150	69	76776	2.3	9.8260	0.8	4.3131	2.0	0.3074	1.8	0.91	1727.8	26.8	1695.9	16.1	1656.6	15.2	1656.6	15.2	104.3
K15-ES-1-Spot 151	101	162603	1.1	9.8549	1.3	4.0408	1.8	0.2888	1.2	0.68	1635.6	17.3	1642.4	14.4	1651.2	24.1	1651.2	24.1	99.1
K15-ES-1-Spot 152	76	226856	1.6	9.8200	1.3	4.1254	2.1	0.2938	1.7	0.80	1660.6	25.1	1659.3	17.5	1657.8	23.8	1657.8	23.8	100.2
K15-ES-1-Spot 153	262	83733	1.7	9.7838	0.9	4.2380	1.8	0.3007	1.5	0.86	1694.9	22.6	1681.4	14.5	1664.6	16.7	1664.6	16.7	101.8
K15-ES-1-Spot 154	108	75080	1.9	9.4926	1.4	4.2706	1.9	0.2940	1.2	0.67	1661.6	18.2	1687.7	15.3	1720.3	25.4	1720.3	25.4	96.6
K15-ES-1-Spot 155	195	133543	4.4	9.8541	1.0	3.3994	1.6	0.2429	1.3	0.80	1402.0	16.7	1504.3	12.9	1651.4	18.3	1651.4	18.3	84.9
K15-ES-1-Spot 156	130	123578	1.7	9.7973	0.9	4.0846	1.7	0.2902	1.5	0.84	1642.7	21.2	1651.2	14.2	1662.1	17.5	1662.1	17.5	98.8
K15-ES-1-Spot 157	309	63671	1.1	9.6739	0.8	4.0879	1.7	0.2868	1.5	0.88	1625.6	21.0	1651.9	13.6	1685.5	14.7	1685.5	14.7	96.4
K15-ES-1-Spot 158	336	193053	3.1	9.7023	0.8	4.1989	1.2	0.2955	1.0	0.77	1668.8	14.2	1673.8	10.2	1680.1	14.7	1680.1	14.7	99.3
K15-ES-1-Spot 159	195	204794	1.7	9.7900	0.9	4.0623	1.5	0.2884	1.2	0.80	1633.7	16.9	1646.8	11.9	1663.4	16.1	1663.4	16.1	98.2
K15-ES-1-Spot 160	353	139135	1.9	9.6084	0.7	4.0412	1.3	0.2816	1.1	0.84	1599.5	15.2	1642.5	10.4	1698.0	12.9	1698.0	12.9	94.2
K15-ES-1-Spot 161	81	123453	2.7	9.7904	0.8	4.1525	1.3	0.2949	1.1	0.80	1665.7	15.6	1664.7	10.9	1663.4	14.7	1663.4	14.7	100.1
K15-ES-1-Spot 162	83	239390	1.9	9.7353	1.3	4.0760	1.6	0.2878	1.0	0.63	1630.5	14.8	1649.5	13.2	1673.8	23.2	1673.8	23.2	97.4
K15-ES-1-Spot 164	86	121381	2.0	9.7493	1.1	4.2606	1.7	0.3013	1.3	0.77	1697.5	19.6	1685.8	14.0	1671.2	19.9	1671.2	19.9	101.6
K15-ES-1-Spot 166	103	106007	1.5	9.6843	0.9	4.1591	1.4	0.2921	1.1	0.78	1652.1	16.2	1666.0	11.6	1683.5	16.3	1683.5	16.3	98.1
K15-ES-1-Spot 167	157	118567	2.1	9.7067	0.9	4.1854	1.3	0.2947	1.0	0.72	1664.7	14.1	1671.2	11.0	1679.2	17.4	1679.2	17.4	99.1
K15-ES-1-Spot 168	117	130676	2.0	9.7124	0.9	4.0272	1.7	0.2837	1.5	0.84	1609.9	20.7	1639.7	14.1	1678.1	17.5	1678.1	17.5	95.9
K15-ES-1-Spot 169	230	681025	7.8	9.3965	1.0	4.4236	1.5	0.3015	1.1	0.73	1698.6	16.0	1716.8	12.2	1739.0	18.6	1739.0	18.6	97.7
K15-ES-1-Spot 170	353	60837	1.1	9.8077	0.7	3.9902	1.4	0.2838	1.2	0.87	1610.6	17.4	1632.2	11.4	1660.1	12.8	1660.1	12.8	97.0
K15-ES-1-Spot 171	175	200722	1.4	9.7168	0.9	4.0960	1.5	0.2887	1.1	0.77	1634.8	16.2	1653.5	11.9	1677.3	17.1	1677.3	17.1	97.5
K15-ES-1-Spot 172	283	134924	2.8	9.7205	0.9	3.6577	1.8	0.2579	1.5	0.87	1478.9	20.4	1562.2	14.1	1676.6	16.0	1676.6	16.0	88.2
K15-ES-1-Spot 173	57	62549	1.6	9.8849	1.3	4.0099	1.9	0.2875	1.3	0.70	1628.9	18.9	1636.2	15.3	1645.6	24.9	1645.6	24.9	99.0
K15-ES-1-Spot 174	297	63339	2.3	9.6891	0.8	4.0599	1.4	0.2853	1.1	0.81	1618.0	16.1	1646.3	11.3	1682.6	15.2	1682.6	15.2	96.2
K15-ES-1-Spot 175	77	236972	2.1	9.7868	1.2	4.1322	2.1	0.2933	1.7	0.83	1658.0	25.3	1660.7	17.1	1664.1	21.9	1664.1	21.9	99.6
K15-ES-1-Spot 176	246	709250	1.6	9.8129	0.9	4.0680	1.4	0.2895	1.1	0.77	1639.1	15.5	1647.9	11.3	1659.1	16.3	1659.1	16.3	98.8
K15-ES-1-Spot 177	147	99574	2.4	9.6815	1.0	4.2280	2.0	0.2969	1.7	0.85	1675.8	24.7	1679.5	16.1	1684.0	18.8	1684.0	18.8	99.5

K15-ES-1-Spot 178	39	144322	2.3	9.8215	1.2	4.1309	1.8	0.2943	1.3	0.73	1662.7	19.1	1660.4	14.6	1657.5	22.6	1657.5	22.6	100.3
K15-ES-1-Spot 179	165	74397	1.4	9.6887	1.1	4.0690	1.7	0.2859	1.3	0.78	1621.1	18.8	1648.1	13.8	1682.7	19.6	1682.7	19.6	96.3
K15-ES-1-Spot 180	157	1149881	1.9	9.7060	1.1	4.0629	1.9	0.2860	1.5	0.80	1621.5	21.6	1646.9	15.4	1679.4	20.8	1679.4	20.8	96.6
K15-ES-1-Spot 182	163	78918	3.6	8.8301	0.9	5.1409	1.6	0.3292	1.4	0.84	1834.6	22.0	1842.9	13.8	1852.2	15.8	1852.2	15.8	99.1
K15-ES-1-Spot 183	299	1227998	1.9	9.7269	0.6	4.2100	1.6	0.2970	1.5	0.93	1676.4	22.3	1676.0	13.4	1675.4	11.3	1675.4	11.3	100.1
K15-ES-1-Spot 184	120	63853	5.1	9.6463	0.9	4.2261	1.7	0.2957	1.5	0.84	1669.8	21.4	1679.1	14.2	1690.8	17.0	1690.8	17.0	98.8
K15-ES-1-Spot 185	202	90609	2.6	9.7433	0.7	4.0952	1.5	0.2894	1.3	0.86	1638.5	18.1	1653.4	11.9	1672.3	13.8	1672.3	13.8	98.0
K15-ES-1-Spot 186	245	3104815	2.0	9.6413	0.6	4.1807	1.3	0.2923	1.2	0.90	1653.2	17.1	1670.2	10.7	1691.7	10.7	1691.7	10.7	97.7
K15-ES-1-Spot 187	72	48071	2.8	9.7898	1.0	4.0859	1.4	0.2901	1.1	0.73	1642.1	15.3	1651.5	11.7	1663.5	18.2	1663.5	18.2	98.7
K15-ES-1-Spot 188	53	161182	2.2	9.7861	1.1	4.0740	1.5	0.2892	1.0	0.69	1637.3	15.0	1649.1	12.3	1664.2	20.2	1664.2	20.2	98.4
K15-ES-1-Spot 189	256	151221	2.9	9.7132	0.7	4.1847	1.4	0.2948	1.2	0.86	1665.5	17.3	1671.0	11.2	1678.0	12.7	1678.0	12.7	99.3
K15-ES-1-Spot 190	62	60453	1.7	9.8828	1.1	4.0333	1.9	0.2891	1.5	0.81	1637.0	21.8	1640.9	15.2	1646.0	20.3	1646.0	20.3	99.5
K15-ES-1-Spot 191	103	76161	1.2	9.7273	0.9	4.0254	1.4	0.2840	1.1	0.77	1611.4	15.1	1639.3	11.2	1675.3	16.3	1675.3	16.3	96.2
K15-ES-1-Spot 192	185	91582	2.5	9.8431	0.8	4.1867	1.5	0.2989	1.3	0.83	1685.8	18.7	1671.4	12.4	1653.4	15.6	1653.4	15.6	102.0
K15-ES-1-Spot 193	210	87247	1.4	9.3741	0.9	4.3440	1.4	0.2953	1.1	0.78	1668.1	16.0	1701.8	11.5	1743.4	15.9	1743.4	15.9	95.7
K15-ES-1-Spot 194	146	70290	4.9	9.5431	0.7	4.4452	1.3	0.3077	1.1	0.84	1729.2	16.8	1720.8	10.9	1710.6	13.0	1710.6	13.0	101.1
K15-ES-1-Spot 195	140	156836	2.4	9.6934	0.9	4.2697	1.7	0.3002	1.4	0.82	1692.2	20.4	1687.5	13.7	1681.8	17.5	1681.8	17.5	100.6
K15-ES-1-Spot 198	179	840004	1.9	9.8519	1.0	3.6615	1.6	0.2616	1.3	0.79	1498.2	16.9	1563.0	12.7	1651.8	17.9	1651.8	17.9	90.7
K15-ES-1-Spot 199	102	132420	1.8	9.6749	1.1	4.2758	1.8	0.3000	1.4	0.80	1691.5	21.5	1688.7	14.9	1685.3	19.9	1685.3	19.9	100.4
K15-ES-1-Spot 200	169	263683	1.8	9.7752	0.8	4.1566	1.3	0.2947	1.0	0.77	1664.9	14.6	1665.5	10.6	1666.2	15.5	1666.2	15.5	99.9
K15-ES-1-Spot 201	130	261676	1.7	9.6287	0.7	4.2379	1.3	0.2959	1.1	0.85	1671.2	15.9	1681.4	10.5	1694.1	12.6	1694.1	12.6	98.6
K15-ES-1-Spot 202	112	190679	2.1	9.6472	1.0	4.3172	1.5	0.3021	1.1	0.76	1701.6	16.9	1696.7	12.3	1690.6	18.0	1690.6	18.0	100.6
K15-ES-1-Spot 205	57	41087	1.6	9.8887	1.0	4.0251	1.6	0.2887	1.2	0.75	1634.9	17.1	1639.3	12.8	1644.9	19.3	1644.9	19.3	99.4
K15-ES-1-Spot 206	77	32360	1.5	9.8637	0.9	4.0444	1.5	0.2893	1.2	0.80	1638.2	17.6	1643.2	12.4	1649.5	17.0	1649.5	17.0	99.3
K15-ES-1-Spot 208	96	241262	1.3	9.8202	1.2	4.1045	1.8	0.2923	1.4	0.77	1653.2	20.7	1655.2	15.0	1657.7	21.6	1657.7	21.6	99.7
K15-ES-1-Spot 209	213	112457	2.1	9.6090	0.9	4.1001	1.5	0.2857	1.2	0.80	1620.2	17.5	1654.3	12.4	1697.9	16.9	1697.9	16.9	95.4
K15-ES-1-Spot 210	36	49634	2.5	9.7291	1.3	4.1808	1.9	0.2950	1.4	0.75	1666.5	20.9	1670.3	15.5	1675.0	23.1	1675.0	23.1	99.5
K15-ES-1-Spot 211	323	161202	1.8	9.6439	0.8	4.1169	1.5	0.2880	1.3	0.85	1631.3	18.7	1657.7	12.5	1691.2	14.8	1691.2	14.8	96.5
K15-ES-1-Spot 212	180	123324	1.1	9.8120	1.0	3.9155	1.8	0.2786	1.5	0.82	1584.5	20.6	1616.9	14.5	1659.3	19.0	1659.3	19.0	95.5
K15-ES-1-Spot 214	65	65995	1.4	9.8472	1.0	4.0582	1.4	0.2898	1.0	0.73	1640.7	15.1	1645.9	11.7	1652.6	18.3	1652.6	18.3	99.3
K15-ES-1-Spot 215	139	52512	1.3	9.7062	1.0	4.1695	1.6	0.2935	1.3	0.80	1659.1	19.1	1668.0	13.4	1679.3	18.1	1679.3	18.1	98.8
K15-ES-1-Spot 216	168	98880	1.5	9.8648	0.9	4.1718	1.4	0.2985	1.1	0.75	1683.7	15.6	1668.5	11.5	1649.3	17.0	1649.3	17.0	102.1
K15-ES-1-Spot 217	292	71571	2.1	9.6782	0.7	4.1588	1.4	0.2919	1.1	0.84	1651.1	16.7	1665.9	11.2	1684.7	13.7	1684.7	13.7	98.0
K15-ES-1-Spot 218	311	90100	1.8	9.7355	0.7	4.0747	1.1	0.2877	0.9	0.76	1630.1	12.6	1649.2	9.3	1673.8	13.6	1673.8	13.6	97.4
K15-ES-1-Spot 219	167	129271	2.6	9.8707	0.7	4.2658	1.5	0.3054	1.4	0.89	1718.0	20.5	1686.8	12.6	1648.2	12.9	1648.2	12.9	104.2
K15-ES-1-Spot 220	197	463826	1.7	9.7333	1.0	4.0703	1.5	0.2873	1.1	0.75	1628.2	15.9	1648.4	12.0	1674.2	17.8	1674.2	17.8	97.3
K15-ES-1-Spot 221	193	191873	1.8	9.8482	0.9	4.0787	1.7	0.2913	1.5	0.86	1648.2	21.5	1650.1	14.1	1652.5	16.5	1652.5	16.5	99.7
K15-ES-1-Spot 224	109	62466	1.7	9.7473	0.9	4.1286	1.6	0.2919	1.3	0.81	1650.9	19.0	1660.0	13.1	1671.5	17.1	1671.5	17.1	98.8
K15-ES-1-Spot 225	226	114376	1.7	9.7940	0.9	4.1052	1.3	0.2916	0.9	0.71	1649.5	13.7	1655.3	10.8	1662.7	17.4	1662.7	17.4	99.2
K15-ES-1-Spot 226	332	142869	1.8	9.8000	0.8	4.0766	1.7	0.2897	1.5	0.88	1640.3	21.3	1649.6	13.6	1661.6	14.8	1661.6	14.8	98.7
K15-ES-1-Spot 227	144	116272	1.6	9.7663	1.0	4.1483	1.5	0.2938	1.1	0.72	1660.7	15.7	1663.9	12.2	1667.9	19.1	1667.9	19.1	99.6
K15-ES-1-Spot 228	125	101545	1.7	9.7274	0.9	4.0631	1.7	0.2866	1.4	0.83	1624.8	20.0	1646.9	13.7	1675.3	17.3	1675.3	17.3	97.0
K15-ES-1-Spot 229	330	148403	1.6	9.7138	0.9	3.9215	1.8	0.2763	1.6	0.87	1572.6	21.8	1618.1	14.4	1677.9	16.0	1677.9	16.0	93.7

K15-ES-1-Spot 230	190	54191	1.7	9.7968	0.8	4.1157	1.6	0.2924	1.3	0.85	1653.7	19.5	1657.4	12.9	1662.2	15.5	1662.2	15.5	99.5
K15-ES-1-Spot 231	103	126984	2.2	9.6876	1.0	4.2293	1.5	0.2972	1.2	0.77	1677.2	17.5	1679.7	12.7	1682.9	18.2	1682.9	18.2	99.7
K15-ES-1-Spot 232	83	57847	2.2	9.8174	1.2	4.1083	1.9	0.2925	1.4	0.76	1654.1	20.8	1655.9	15.3	1658.3	22.6	1658.3	22.6	99.7
K15-ES-1-Spot 233	143	87110	1.8	9.7328	0.9	4.1866	1.6	0.2955	1.3	0.80	1669.1	18.5	1671.4	12.8	1674.3	17.2	1674.3	17.2	99.7
K15-ES-1-Spot 234	81	182758	1.9	9.7483	0.8	4.1316	1.2	0.2921	0.9	0.75	1652.1	13.4	1660.6	10.0	1671.3	15.0	1671.3	15.0	98.8
K15-ES-1-Spot 235	154	205189	2.0	9.6966	1.1	4.3232	1.4	0.3040	0.9	0.66	1711.3	13.9	1697.8	11.6	1681.2	19.5	1681.2	19.5	101.8
K15-ES-1-Spot 236	73	134592	1.2	9.3285	2.1	4.2508	2.5	0.2876	1.4	0.55	1629.5	20.0	1683.9	20.8	1752.3	38.6	1752.3	38.6	93.0
K15-ES-1-Spot 237	589	177522	2.4	9.7930	0.9	3.8638	1.8	0.2744	1.5	0.84	1563.3	20.6	1606.2	14.2	1662.9	17.5	1662.9	17.5	94.0
K15-ES-1-Spot 238	248	76170	2.4	9.8067	0.7	4.1392	1.4	0.2944	1.3	0.88	1663.5	18.6	1662.1	11.8	1660.3	12.7	1660.3	12.7	100.2
K15-ES-1-Spot 239	184	81271	1.7	9.8005	1.2	4.1378	1.9	0.2941	1.5	0.79	1662.1	22.7	1661.8	15.9	1661.5	21.9	1661.5	21.9	100.0
K15-ES-1-Spot 240	93	64779	1.9	9.8245	1.1	4.0751	1.9	0.2904	1.6	0.83	1643.4	22.8	1649.3	15.5	1656.9	19.8	1656.9	19.8	99.2
K15-ES-1-Spot 241	144	147975	2.3	9.7254	1.1	4.0934	1.7	0.2887	1.4	0.78	1635.2	19.6	1653.0	14.2	1675.7	20.1	1675.7	20.1	97.6
K15-ES-1-Spot 244	64	88518	2.0	9.7548	1.1	4.1816	1.4	0.2958	0.9	0.63	1670.7	12.7	1670.4	11.3	1670.1	19.8	1670.1	19.8	100.0
K15-ES-1-Spot 245	395	63712	1.6	9.7043	0.8	4.0492	1.6	0.2850	1.4	0.87	1616.5	20.2	1644.1	13.2	1679.7	14.6	1679.7	14.6	96.2
K15-ES-1-Spot 246	65	63060	1.8	9.7874	1.1	4.0947	1.5	0.2907	0.9	0.63	1644.8	13.3	1653.3	12.0	1663.9	21.2	1663.9	21.2	98.9
K15-ES-1-Spot 247	69	105002	2.5	9.7334	1.2	4.1544	1.5	0.2933	0.9	0.61	1657.9	13.2	1665.1	12.0	1674.2	21.4	1674.2	21.4	99.0
K15-ES-1-Spot 248	45	92971	1.4	9.8978	1.2	4.0953	1.7	0.2940	1.2	0.73	1661.4	18.2	1653.4	14.0	1643.2	21.8	1643.2	21.8	101.1
K15-ES-1-Spot 249	217	52835	3.3	9.8535	0.8	4.1515	1.4	0.2967	1.1	0.82	1674.9	16.8	1664.5	11.4	1651.5	14.9	1651.5	14.9	101.4
K15-ES-1-Spot 250	55	27749	1.7	9.8540	1.0	4.0594	1.6	0.2901	1.2	0.76	1642.1	17.4	1646.2	12.8	1651.4	18.7	1651.4	18.7	99.4
K15-ES-1-Spot 251	159	257973	2.0	9.8387	0.9	4.1360	1.4	0.2951	1.1	0.78	1667.1	16.0	1661.4	11.5	1654.3	16.4	1654.3	16.4	100.8
K15-ES-1-Spot 252	68	93380	2.0	9.7343	1.1	4.2945	1.6	0.3032	1.1	0.71	1707.1	16.6	1692.3	12.9	1674.0	20.3	1674.0	20.3	102.0
K15-ES-1-Spot 253	444	402811	2.9	9.7261	0.9	3.9769	1.6	0.2805	1.4	0.83	1594.0	19.3	1629.5	13.3	1675.6	16.7	1675.6	16.7	95.1
K15-ES-1-Spot 254	166	129144	2.0	9.7973	0.9	4.1055	1.6	0.2917	1.3	0.83	1650.1	19.6	1655.4	13.3	1662.1	16.9	1662.1	16.9	99.3
K15-ES-1-Spot 255	128	79508	1.5	9.7806	1.2	4.0954	1.9	0.2905	1.5	0.76	1644.1	21.1	1653.4	15.5	1665.2	22.8	1665.2	22.8	98.7
K15-ES-1-Spot 256	222	776478	2.2	9.2125	1.2	4.5516	1.7	0.3041	1.2	0.70	1711.7	17.9	1740.4	14.3	1775.2	22.5	1775.2	22.5	96.4
K15-ES-1-Spot 257	156	152274	2.2	9.7065	0.9	4.2343	1.4	0.2981	1.1	0.77	1681.8	16.3	1680.7	11.7	1679.3	16.7	1679.3	16.7	100.1
K15-ES-1-Spot 258	275	143623	1.5	9.8520	0.7	3.7687	2.0	0.2693	1.8	0.93	1537.2	24.9	1586.1	15.8	1651.7	13.7	1651.7	13.7	93.1
K15-ES-1-Spot 259	224	68164	2.2	9.8040	0.9	4.1211	1.5	0.2930	1.2	0.81	1656.7	18.2	1658.5	12.6	1660.8	16.8	1660.8	16.8	99.8
K15-ES-1-Spot 260	128	94554	1.4	9.5262	0.8	4.3201	1.4	0.2985	1.1	0.82	1683.8	16.5	1697.2	11.2	1713.8	14.1	1713.8	14.1	98.2
K15-ES-1-Spot 261	60	264992	1.8	9.7834	1.2	4.0987	1.8	0.2908	1.3	0.75	1645.7	19.6	1654.1	14.8	1664.7	22.3	1664.7	22.3	98.9
K15-ES-1-Spot 262	169	76354	2.3	9.7118	0.9	4.0489	1.5	0.2852	1.3	0.83	1617.4	18.2	1644.1	12.6	1678.3	16.1	1678.3	16.1	96.4
K15-ES-1-Spot 263	410	1927699	3.4	9.5135	0.7	4.3549	1.3	0.3005	1.1	0.85	1693.7	16.6	1703.8	10.9	1716.3	12.9	1716.3	12.9	98.7
K15-ES-1-Spot 264	190	536644	1.5	9.7999	0.7	4.1059	1.3	0.2918	1.1	0.83	1650.7	15.6	1655.5	10.6	1661.6	13.5	1661.6	13.5	99.3
K15-ES-1-Spot 265	281	851368	2.0	9.7488	0.7	4.0507	1.6	0.2864	1.4	0.89	1623.5	20.8	1644.4	13.2	1671.3	13.3	1671.3	13.3	97.1
K15-ES-1-Spot 266	121	185595	1.9	9.6926	0.9	4.3254	1.7	0.3041	1.4	0.83	1711.4	20.7	1698.2	13.7	1681.9	17.1	1681.9	17.1	101.8
K15-ES-1-Spot 267	161	202536	3.1	9.6197	0.9	4.2475	1.6	0.2963	1.3	0.82	1673.1	19.8	1683.2	13.4	1695.9	17.1	1695.9	17.1	98.7
K15-ES-1-Spot 268	170	125841	1.6	9.7353	0.9	4.0487	1.5	0.2859	1.1	0.78	1620.8	16.4	1644.0	11.9	1673.8	17.0	1673.8	17.0	96.8
K15-ES-1-Spot 269	317	71098	2.8	9.3208	0.9	4.6632	1.9	0.3152	1.7	0.87	1766.4	26.0	1760.7	16.1	1753.8	17.3	1753.8	17.3	100.7
K15-ES-1-Spot 270	78	113763	1.9	9.8654	0.8	4.1082	1.4	0.2939	1.1	0.80	1661.2	16.6	1655.9	11.5	1649.2	15.6	1649.2	15.6	100.7
K15-ES-1-Spot 271	78	87044	2.2	9.8136	0.9	4.1242	1.8	0.2935	1.5	0.86	1659.2	22.1	1659.1	14.4	1659.0	16.7	1659.0	16.7	100.0
K15-ES-1-Spot 272	220	244028	2.3	9.6692	1.1	4.2317	1.7	0.2968	1.3	0.78	1675.2	19.7	1680.2	14.0	1686.4	19.5	1686.4	19.5	99.3
K15-ES-1-Spot 273	62	122613	1.3	9.8547	1.3	4.0952	2.1	0.2927	1.6	0.77	1655.0	23.7	1653.3	17.1	1651.2	24.7	1651.2	24.7	100.2
K15-ES-1-Spot 274	186	185963	1.2	9.5557	0.9	4.1575	1.4	0.2881	1.1	0.77	1632.2	16.0	1665.7	11.8	1708.1	16.8	1708.1	16.8	95.6

K15-ES-1-Spot 275	96	131785	2.2	9.8527	1.0	4.0275	1.6	0.2878	1.2	0.79	1630.5	17.7	1639.8	12.7	1651.6	17.9	1651.6	17.9	98.7
K15-ES-1-Spot 276	72	45475	1.8	9.9014	0.9	4.0435	1.6	0.2904	1.4	0.84	1643.4	19.7	1643.0	13.2	1642.5	16.4	1642.5	16.4	100.1
K15-ES-1-Spot 277	132	1130262	2.3	9.7653	0.8	4.2338	1.5	0.2999	1.2	0.83	1690.6	18.0	1680.6	12.0	1668.1	15.3	1668.1	15.3	101.3
K15-ES-1-Spot 278	118	119025	2.5	9.5698	0.9	4.3646	1.7	0.3029	1.4	0.84	1705.8	21.2	1705.7	14.0	1705.4	17.2	1705.4	17.2	100.0
K15-ES-1-Spot 279	299	127125	6.8	9.6805	0.9	4.2230	1.5	0.2965	1.2	0.82	1673.9	18.1	1678.5	12.3	1684.2	15.9	1684.2	15.9	99.4
K15-ES-1-Spot 280	51	57354	1.7	9.7966	1.2	4.1377	1.9	0.2940	1.5	0.77	1661.5	21.4	1661.8	15.6	1662.2	22.8	1662.2	22.8	100.0
K15-ES-1-Spot 281	298	100568	3.7	9.4545	0.6	4.2494	1.7	0.2914	1.6	0.94	1648.4	23.0	1683.6	13.8	1727.7	10.7	1727.7	10.7	95.4
K15-ES-1-Spot 282	196	163456	2.6	9.5282	1.1	4.4330	1.7	0.3063	1.3	0.77	1722.7	20.2	1718.5	14.3	1713.4	20.0	1713.4	20.0	100.5
K15-ES-1-Spot 284	178	72223	1.6	9.6751	1.3	3.9906	2.2	0.2800	1.8	0.82	1591.5	25.9	1632.3	18.3	1685.3	23.9	1685.3	23.9	94.4
K15-ES-1-Spot 285	180	147956	1.8	9.6483	1.0	4.3811	1.5	0.3066	1.2	0.77	1723.8	17.9	1708.8	12.7	1690.4	18.2	1690.4	18.2	102.0
K15-ES-1-Spot 286	98	88132	1.4	9.7993	1.1	4.1796	1.8	0.2971	1.4	0.80	1676.7	21.0	1670.0	14.6	1661.7	19.8	1661.7	19.8	100.9
K15-ES-1-Spot 287	403	211456	1.9	9.2480	0.8	4.5506	1.5	0.3052	1.3	0.84	1717.1	19.3	1740.3	12.7	1768.2	15.2	1768.2	15.2	97.1
K15-ES-1-Spot 288	245	103801	1.4	9.9475	0.8	4.2045	1.5	0.3033	1.3	0.85	1707.8	19.2	1674.9	12.4	1633.8	14.8	1633.8	14.8	104.5
K15-ES-1-Spot 289	213	107692	1.5	9.8185	0.8	4.1610	1.4	0.2963	1.2	0.85	1673.0	18.1	1666.4	11.8	1658.1	14.0	1658.1	14.0	100.9
K15-ES-1-Spot 291	290	56075	2.6	9.4603	1.0	4.5352	1.5	0.3112	1.1	0.74	1746.5	17.2	1737.5	12.6	1726.6	18.7	1726.6	18.7	101.2
K15-ES-1-Spot 292	240	101789	2.3	9.8615	0.9	4.0756	1.2	0.2915	0.8	0.69	1649.0	11.8	1649.4	9.7	1650.0	15.9	1650.0	15.9	99.9
K15-ES-1-Spot 293	167	136607	1.2	9.8345	0.9	4.1607	1.4	0.2968	1.1	0.78	1675.3	16.0	1666.3	11.4	1655.1	16.3	1655.1	16.3	101.2
K15-ES-1-Spot 294	36	441740	2.1	9.7449	1.3	4.1656	1.7	0.2944	1.2	0.69	1663.5	17.7	1667.3	14.3	1672.0	23.3	1672.0	23.3	99.5
K15-ES-1-Spot 295	145	120826	2.0	9.8619	1.0	4.1173	1.5	0.2945	1.1	0.74	1663.9	16.2	1657.7	12.2	1649.9	18.7	1649.9	18.7	100.8
K15-ES-1-Spot 296	83	97913	1.6	9.8123	1.1	4.1416	1.8	0.2947	1.5	0.81	1665.2	21.6	1662.6	15.0	1659.2	20.1	1659.2	20.1	100.4
K15-ES-1-Spot 297	75	223237	2.0	9.7169	1.1	4.2235	1.6	0.2976	1.1	0.73	1679.6	17.0	1678.6	13.0	1677.3	20.1	1677.3	20.1	100.1
K15-ES-1-Spot 298	198	65269	2.1	9.6862	1.1	4.0912	1.6	0.2874	1.1	0.71	1628.6	16.0	1652.5	12.7	1683.1	20.2	1683.1	20.2	96.8
K15-ES-1-Spot 299	235	146125	2.1	9.6387	1.0	4.2128	1.7	0.2945	1.4	0.83	1664.0	21.1	1676.5	14.3	1692.2	18.0	1692.2	18.0	98.3
K15-ES-1-Spot 300	231	155320	2.1	9.7576	0.9	4.2651	1.5	0.3018	1.2	0.79	1700.4	17.9	1686.6	12.5	1669.6	17.4	1669.6	17.4	101.8
K15-ES-1-Spot 301	252	208279	3.5	9.2183	1.0	4.3919	1.8	0.2936	1.5	0.82	1659.7	22.3	1710.8	15.3	1774.0	19.1	1774.0	19.1	93.6
K15-ES-1-Spot 302	89	199622	2.2	9.7680	0.7	4.1844	1.4	0.2964	1.2	0.86	1673.6	17.7	1671.0	11.5	1667.6	13.4	1667.6	13.4	100.4
K15-ES-1-Spot 303	283	79924	1.8	9.7434	0.8	4.1558	1.5	0.2937	1.2	0.84	1659.9	18.2	1665.4	12.0	1672.3	14.6	1672.3	14.6	99.3
K15-ES-1-Spot 304	75	65635	1.5	9.9846	0.9	4.0018	1.5	0.2898	1.2	0.80	1640.5	17.8	1634.6	12.5	1626.9	17.2	1626.9	17.2	100.8
K15-ES-1-Spot 305	104	155593	1.8	9.8871	0.8	4.1632	1.6	0.2985	1.4	0.86	1684.0	20.4	1666.8	13.2	1645.2	15.4	1645.2	15.4	102.4
K15-ES-1-Spot 306	42	40441	2.0	9.8947	1.1	4.0703	1.8	0.2921	1.4	0.77	1652.0	19.8	1648.4	14.4	1643.7	20.8	1643.7	20.8	100.5
K15-ES-1-Spot 307	92	49544	1.8	9.8187	0.9	4.1947	1.5	0.2987	1.2	0.80	1684.9	18.1	1673.0	12.6	1658.0	17.3	1658.0	17.3	101.6
K15-ES-1-Spot 309	128	715990	2.1	9.7867	1.1	4.1257	1.9	0.2928	1.5	0.81	1655.7	22.2	1659.4	15.3	1664.1	20.2	1664.1	20.2	99.5
K15-ES-1-Spot 310	468	69071	4.7	9.6375	0.7	4.2397	1.8	0.2963	1.7	0.93	1673.2	24.9	1681.7	14.9	1692.5	12.2	1692.5	12.2	98.9
K15-ES-1-Spot 312	85	126807	1.8	9.7301	1.0	4.1373	1.6	0.2920	1.2	0.76	1651.4	17.4	1661.7	12.8	1674.8	18.7	1674.8	18.7	98.6
K15-ES-1-Spot 313	248	172264	1.9	9.9325	0.8	4.1180	1.5	0.2966	1.2	0.82	1674.7	18.1	1657.9	12.2	1636.7	15.7	1636.7	15.7	102.3
K15-ES-1-Spot 314	281	271733	2.2	9.8073	0.8	4.1585	1.3	0.2958	1.0	0.77	1670.4	14.4	1665.9	10.4	1660.2	15.0	1660.2	15.0	100.6
K15-ES-1-Spot 315	259	797220	2.4	9.6350	0.8	4.2943	1.3	0.3001	1.0	0.77	1691.7	14.4	1692.3	10.4	1692.9	14.9	1692.9	14.9	99.9

K15-Estadio-3-Spot 1	180	194777	1.7	9.5138	0.7	4.3214	1.3	0.2982	1.1	0.83	1682.3	16.2	1697.5	10.9	1716.2	13.6	1716.2	13.6	98.0
K15-Estadio-3-Spot 2	98	58089	2.2	9.6865	0.9	4.1462	1.3	0.2913	0.9	0.71	1647.9	13.2	1663.5	10.4	1683.1	16.5	1683.1	16.5	97.9
K15-Estadio-3-Spot 4	119	195640	2.3	9.2960	0.8	4.5977	1.3	0.3100	1.0	0.76	1740.6	15.3	1748.9	10.9	1758.7	15.5	1758.7	15.5	99.0
K15-Estadio-3-Spot 5	65	51125	1.6	9.8375	1.0	4.0959	1.7	0.2922	1.4	0.82	1652.7	20.5	1653.5	13.9	1654.5	17.9	1654.5	17.9	99.9

K15-Estadio-3-Spot 6	230	510423	1.6	9.5646	0.7	4.2181	1.0	0.2926	0.8	0.78	1654.5	12.0	1677.5	8.6	1706.4	12.1	1706.4	12.1	97.0
K15-Estadio-3-Spot 7	102	68383	1.2	9.7979	0.8	4.1080	1.2	0.2919	0.9	0.74	1651.1	13.4	1655.9	10.2	1662.0	15.4	1662.0	15.4	99.3
K15-Estadio-3-Spot 9	146	88885	1.2	9.7779	0.9	4.1490	1.4	0.2942	1.0	0.74	1662.6	15.0	1664.0	11.2	1665.7	17.0	1665.7	17.0	99.8
K15-Estadio-3-Spot 10	291	86805	1.9	9.8143	0.7	4.0222	1.3	0.2863	1.1	0.83	1623.0	15.3	1638.7	10.5	1658.8	13.4	1658.8	13.4	97.8
K15-Estadio-3-Spot 11	196	70917	2.0	9.5782	0.7	4.2199	1.3	0.2931	1.1	0.82	1657.2	15.4	1677.9	10.5	1703.8	13.4	1703.8	13.4	97.3
K15-Estadio-3-Spot 12	149	235944	1.0	9.7725	0.9	4.0633	1.5	0.2880	1.2	0.81	1631.5	17.4	1647.0	12.2	1666.7	16.3	1666.7	16.3	97.9
K15-Estadio-3-Spot 14	883	226333	11.7	9.7355	0.6	4.0456	2.2	0.2857	2.1	0.96	1619.8	30.6	1643.4	18.1	1673.8	11.5	1673.8	11.5	96.8
K15-Estadio-3-Spot 15	157	74282	1.8	9.3957	0.9	4.3724	1.5	0.2980	1.3	0.83	1681.2	18.9	1707.1	12.8	1739.2	15.8	1739.2	15.8	96.7
K15-Estadio-3-Spot 16	355	67414	1.1	9.6277	1.0	3.7240	1.7	0.2600	1.3	0.79	1490.0	17.5	1576.5	13.3	1694.3	18.7	1694.3	18.7	87.9
K15-Estadio-3-Spot 17	226	1990777	2.1	9.7178	0.8	4.1748	1.2	0.2942	0.9	0.75	1662.7	13.4	1669.1	10.0	1677.1	15.0	1677.1	15.0	99.1
K15-Estadio-3-Spot 18	138	192651	1.4	9.8978	0.8	3.9482	1.3	0.2834	1.0	0.75	1608.6	13.6	1623.6	10.3	1643.1	15.7	1643.1	15.7	97.9
K15-Estadio-3-Spot 19	171	255696	0.9	9.6515	0.8	4.2959	1.3	0.3007	1.0	0.77	1694.8	15.3	1692.6	11.0	1689.8	15.6	1689.8	15.6	100.3
K15-Estadio-3-Spot 20	138	116889	1.6	9.8716	0.8	3.9908	1.3	0.2857	1.0	0.78	1620.1	14.9	1632.3	10.9	1648.1	15.5	1648.1	15.5	98.3
K15-Estadio-3-Spot 21	104	187289	0.9	9.8024	0.7	4.0321	1.3	0.2867	1.0	0.82	1624.8	15.0	1640.7	10.4	1661.1	13.5	1661.1	13.5	97.8
K15-Estadio-3-Spot 22	161	136261	1.9	9.7771	0.8	4.0745	1.2	0.2889	0.9	0.72	1636.1	12.4	1649.2	9.7	1665.9	15.2	1665.9	15.2	98.2
K15-Estadio-3-Spot 23	159	54047	1.4	9.7363	0.8	4.0759	1.2	0.2878	0.9	0.77	1630.6	13.6	1649.5	10.0	1673.6	14.6	1673.6	14.6	97.4
K15-Estadio-3-Spot 24	21	936265	1.8	9.5392	1.3	4.3030	1.8	0.2977	1.3	0.69	1679.9	18.5	1693.9	15.1	1711.3	24.5	1711.3	24.5	98.2
K15-Estadio-3-Spot 25	362	86982	4.4	9.6388	0.7	4.2547	1.4	0.2974	1.2	0.85	1678.6	17.3	1684.6	11.3	1692.2	13.5	1692.2	13.5	99.2
K15-Estadio-3-Spot 26	109	33792	1.3	9.8964	0.6	4.0753	1.0	0.2925	0.8	0.78	1654.0	11.4	1649.4	8.1	1643.4	11.4	1643.4	11.4	100.6
K15-Estadio-3-Spot 27	343	69001	3.6	9.4670	0.8	4.0585	1.4	0.2787	1.1	0.80	1584.6	15.8	1646.0	11.4	1725.3	15.3	1725.3	15.3	91.8
K15-Estadio-3-Spot 28	181	84422	1.3	9.7932	0.7	3.9672	1.1	0.2818	0.9	0.79	1600.3	12.1	1627.5	8.8	1662.8	12.3	1662.8	12.3	96.2
K15-Estadio-3-Spot 29	139	94172	3.1	9.7217	0.8	4.1535	1.4	0.2929	1.1	0.83	1655.8	16.3	1664.9	11.1	1676.4	14.1	1676.4	14.1	98.8
K15-Estadio-3-Spot 30	77	205024	1.5	9.8654	1.3	4.0197	1.8	0.2876	1.2	0.66	1629.6	17.1	1638.2	14.6	1649.2	25.0	1649.2	25.0	98.8
K15-Estadio-3-Spot 31	188	185017	3.4	9.7210	0.6	4.1256	1.2	0.2909	1.0	0.85	1645.9	15.2	1659.4	10.1	1676.5	12.0	1676.5	12.0	98.2
K15-Estadio-3-Spot 32	374	124909	3.0	9.5937	0.8	4.2521	1.5	0.2959	1.3	0.84	1670.8	18.5	1684.1	12.3	1700.8	14.7	1700.8	14.7	98.2
K15-Estadio-3-Spot 33	126	171519	3.8	9.5789	1.0	4.2697	1.6	0.2966	1.2	0.76	1674.6	17.6	1687.5	12.9	1703.7	18.8	1703.7	18.8	98.3
K15-Estadio-3-Spot 34	301	140059	1.7	9.8666	0.6	3.9717	1.2	0.2842	1.1	0.89	1612.5	15.6	1628.4	10.0	1649.0	10.5	1649.0	10.5	97.8
K15-Estadio-3-Spot 35	173	171097	1.8	9.5399	0.8	4.2773	1.1	0.2959	0.8	0.74	1671.2	12.5	1689.0	9.4	1711.2	14.2	1711.2	14.2	97.7
K15-Estadio-3-Spot 36	237	72659	2.8	9.5019	1.0	4.5110	1.4	0.3109	1.0	0.73	1745.0	15.6	1733.0	11.6	1718.5	17.6	1718.5	17.6	101.5
K15-Estadio-3-Spot 37	136	111786	1.2	9.9089	0.8	4.0853	1.4	0.2936	1.1	0.80	1659.5	16.5	1651.4	11.5	1641.1	15.6	1641.1	15.6	101.1
K15-Estadio-3-Spot 38	109	164208	1.6	9.7788	0.7	4.1227	1.3	0.2924	1.1	0.82	1653.5	15.3	1658.8	10.5	1665.6	13.7	1665.6	13.7	99.3
K15-Estadio-3-Spot 39	106	52816	1.5	9.6008	0.7	4.2177	1.3	0.2937	1.1	0.86	1659.9	16.8	1677.5	10.9	1699.5	12.5	1699.5	12.5	97.7
K15-Estadio-3-Spot 40	76	120368	2.0	9.8858	1.0	4.0075	1.5	0.2873	1.1	0.74	1628.2	16.4	1635.7	12.5	1645.4	19.2	1645.4	19.2	99.0
K15-Estadio-3-Spot 41	120	61106	0.9	9.7433	0.9	4.0943	1.4	0.2893	1.1	0.77	1638.1	15.5	1653.2	11.4	1672.3	16.5	1672.3	16.5	98.0
K15-Estadio-3-Spot 42	101	715657	2.4	9.8393	1.0	4.0240	1.6	0.2872	1.2	0.77	1627.3	17.9	1639.1	13.1	1654.2	18.9	1654.2	18.9	98.4
K15-Estadio-3-Spot 45	258	705495	2.0	9.6480	0.8	4.1795	1.3	0.2925	1.0	0.79	1653.8	14.6	1670.0	10.4	1690.4	14.5	1690.4	14.5	97.8
K15-Estadio-3-Spot 46	184	56956	1.8	9.6336	0.6	4.1868	1.2	0.2925	1.1	0.86	1654.1	15.3	1671.4	10.0	1693.2	11.6	1693.2	11.6	97.7
K15-Estadio-3-Spot 47	229	61751	1.5	9.7374	0.8	4.0160	1.3	0.2836	1.0	0.80	1609.6	14.6	1637.4	10.4	1673.4	14.1	1673.4	14.1	96.2
K15-Estadio-3-Spot 48	126	142787	1.6	9.5381	0.8	4.2526	1.2	0.2942	0.9	0.72	1662.4	12.6	1684.2	9.8	1711.5	15.1	1711.5	15.1	97.1
K15-Estadio-3-Spot 49	206	59926	1.6	9.5615	0.7	4.1343	1.2	0.2867	1.0	0.81	1625.0	13.7	1661.1	9.6	1707.0	12.9	1707.0	12.9	95.2
K15-Estadio-3-Spot 50	254	60114	3.1	9.1849	0.9	4.6202	1.5	0.3078	1.2	0.80	1729.8	17.9	1752.9	12.3	1780.6	16.0	1780.6	16.0	97.1
K15-Estadio-3-Spot 51	183	67223	2.7	9.6720	0.9	4.1516	1.3	0.2912	1.0	0.76	1647.6	14.7	1664.5	10.9	1685.9	16.0	1685.9	16.0	97.7
K15-Estadio-3-Spot 52	889	228226	2.8	9.5010	0.8	4.5274	1.7	0.3120	1.5	0.88	1750.4	22.8	1736.0	14.1	1718.7	15.0	1718.7	15.0	101.8

K15-Estadio-3-Spot 53	155	395692	3.0	9.4815	0.8	4.3521	1.3	0.2993	1.0	0.78	1687.7	15.4	1703.3	10.9	1722.5	15.2	1722.5	15.2	98.0
K15-Estadio-3-Spot 54	104	28094520	1.2	9.8953	1.0	4.0281	1.4	0.2891	1.0	0.69	1637.0	14.1	1639.9	11.4	1643.6	18.8	1643.6	18.8	99.6
K15-Estadio-3-Spot 55	96	111756	1.8	9.7324	0.8	4.1011	1.5	0.2895	1.2	0.82	1638.9	17.6	1654.5	12.1	1674.4	15.7	1674.4	15.7	97.9
K15-Estadio-3-Spot 56	92	97637	1.6	9.9097	0.7	3.9623	1.3	0.2848	1.1	0.83	1615.4	16.0	1626.5	10.9	1640.9	13.9	1640.9	13.9	98.4
K15-Estadio-3-Spot 57	176	228716	1.8	9.7859	1.0	4.1077	1.4	0.2915	1.1	0.75	1649.2	15.6	1655.8	11.7	1664.2	17.7	1664.2	17.7	99.1
K15-Estadio-3-Spot 58	232	59695	1.0	9.7944	0.9	3.9791	1.5	0.2827	1.2	0.82	1604.7	17.5	1629.9	12.2	1662.6	16.0	1662.6	16.0	96.5
K15-Estadio-3-Spot 59	191	136083	1.7	9.7440	0.8	4.1001	1.2	0.2898	0.9	0.73	1640.3	13.0	1654.3	10.0	1672.2	15.4	1672.2	15.4	98.1
K15-Estadio-3-Spot 60	86	195071	1.6	3.8858	0.5	22.4278	1.1	0.6321	1.0	0.90	3157.8	24.1	3202.4	10.5	3230.5	7.5	3230.5	7.5	97.7
K15-Estadio-3-Spot 61	172	151531	1.7	9.6647	0.8	4.2483	1.2	0.2978	0.8	0.69	1680.3	11.9	1683.4	9.5	1687.2	15.4	1687.2	15.4	99.6
K15-Estadio-3-Spot 62	167	105697	1.1	9.8940	0.8	4.0100	1.3	0.2877	1.0	0.79	1630.3	14.7	1636.2	10.4	1643.9	14.5	1643.9	14.5	99.2
K15-Estadio-3-Spot 63	285	186093	7.1	9.5880	0.8	4.2446	1.2	0.2952	0.9	0.74	1667.3	12.6	1682.7	9.5	1701.9	14.3	1701.9	14.3	98.0
K15-Estadio-3-Spot 64	102	121314	1.5	9.7290	1.0	4.1460	1.6	0.2926	1.3	0.77	1654.3	18.3	1663.4	13.2	1675.0	19.0	1675.0	19.0	98.8
K15-Estadio-3-Spot 65	190	57476	5.8	9.3969	0.7	4.4616	1.4	0.3041	1.2	0.87	1711.5	18.5	1723.9	11.7	1738.9	12.7	1738.9	12.7	98.4
K15-Estadio-3-Spot 66	174	156266	2.1	9.4204	0.8	4.6238	1.4	0.3159	1.2	0.84	1769.7	18.8	1753.6	12.0	1734.4	14.1	1734.4	14.1	102.0
K15-Estadio-3-Spot 67	247	170280	1.5	9.7539	0.9	4.2167	1.8	0.2983	1.6	0.87	1682.8	23.2	1677.3	14.8	1670.3	16.3	1670.3	16.3	100.8
K15-Estadio-3-Spot 68	137	304520	3.8	6.2127	0.7	10.2567	1.2	0.4622	1.0	0.80	2449.1	20.0	2458.2	11.3	2465.8	12.3	2465.8	12.3	99.3
K15-Estadio-3-Spot 69	112	167630	1.7	9.9911	0.7	3.9357	1.3	0.2852	1.1	0.84	1617.4	15.2	1621.0	10.2	1625.7	12.6	1625.7	12.6	99.5
K15-Estadio-3-Spot 70	87	77949	2.2	9.8795	0.9	4.0590	1.4	0.2908	1.1	0.76	1645.7	15.6	1646.1	11.5	1646.6	17.0	1646.6	17.0	99.9
K15-Estadio-3-Spot 71	114	135627	1.0	9.8050	1.0	4.0327	1.3	0.2868	0.9	0.70	1625.4	13.6	1640.8	11.0	1660.6	17.8	1660.6	17.8	97.9
K15-Estadio-3-Spot 72	193	168306	1.1	9.7473	0.9	4.1121	1.5	0.2907	1.1	0.77	1645.0	16.6	1656.7	12.0	1671.5	17.2	1671.5	17.2	98.4
K15-Estadio-3-Spot 73	158	299495	2.7	9.6326	0.7	4.2350	1.3	0.2959	1.1	0.82	1670.8	15.6	1680.8	10.6	1693.4	13.5	1693.4	13.5	98.7
K15-Estadio-3-Spot 74	197	176602	1.7	9.8708	0.7	3.9591	1.2	0.2834	1.0	0.80	1608.6	13.7	1625.9	9.8	1648.2	13.6	1648.2	13.6	97.6
K15-Estadio-3-Spot 75	260	211643	2.3	9.6525	0.9	3.6888	1.3	0.2582	1.0	0.75	1480.8	13.2	1568.9	10.6	1689.6	16.1	1689.6	16.1	87.6
K15-Estadio-3-Spot 76	106	120633	1.3	9.7045	1.1	4.2159	1.7	0.2967	1.3	0.78	1675.1	19.4	1677.1	13.8	1679.7	19.5	1679.7	19.5	99.7
K15-Estadio-3-Spot 77	141	170879	2.0	9.7631	1.0	4.0327	1.3	0.2855	0.9	0.69	1619.2	13.1	1640.8	10.8	1668.5	18.0	1668.5	18.0	97.0
K15-Estadio-3-Spot 78	87	69645	1.4	9.6679	0.9	4.1938	1.7	0.2941	1.4	0.84	1661.8	21.2	1672.8	14.1	1686.6	17.4	1686.6	17.4	98.5
K15-Estadio-3-Spot 79	213	99026	1.7	9.3687	0.8	4.4785	1.4	0.3043	1.1	0.81	1712.6	16.8	1727.0	11.5	1744.4	14.9	1744.4	14.9	98.2
K15-Estadio-3-Spot 80	110	109700	1.2	9.8771	0.8	4.0844	1.3	0.2926	1.1	0.79	1654.5	15.4	1651.2	10.9	1647.0	15.1	1647.0	15.1	100.5
K15-Estadio-3-Spot 81	166	186533	1.9	9.8496	0.7	4.0027	1.2	0.2859	1.0	0.83	1621.2	14.5	1634.7	9.8	1652.2	12.4	1652.2	12.4	98.1
K15-Estadio-3-Spot 82	112	159196	1.5	9.7764	0.8	4.0895	1.4	0.2900	1.1	0.79	1641.4	15.7	1652.2	11.2	1666.0	15.6	1666.0	15.6	98.5
K15-Estadio-3-Spot 83	752	152605	8.8	9.5095	0.7	4.6471	1.5	0.3205	1.4	0.90	1792.2	21.7	1757.8	12.9	1717.1	12.4	1717.1	12.4	104.4
K15-Estadio-3-Spot 84	111	117658	1.4	9.7141	0.8	4.1080	1.4	0.2894	1.1	0.80	1638.6	15.9	1655.9	11.2	1677.8	15.3	1677.8	15.3	97.7
K15-Estadio-3-Spot 85	106	74802	1.6	9.9658	0.8	3.8939	1.4	0.2814	1.1	0.82	1598.7	16.0	1612.4	11.2	1630.4	14.9	1630.4	14.9	98.1
K15-Estadio-3-Spot 86	80	74858	2.4	9.8541	0.9	4.0788	1.4	0.2915	1.0	0.73	1649.0	14.6	1650.1	11.2	1651.4	17.4	1651.4	17.4	99.9
K15-Estadio-3-Spot 87	97	526075	1.7	9.8547	1.0	4.0214	1.5	0.2874	1.2	0.77	1628.6	17.2	1638.5	12.6	1651.2	18.2	1651.2	18.2	98.6
K15-Estadio-3-Spot 88	32	144649	1.6	9.9177	1.1	4.0816	1.7	0.2936	1.3	0.75	1659.5	19.2	1650.6	14.2	1639.4	21.3	1639.4	21.3	101.2
K15-Estadio-3-Spot 90	447	135948	2.7	9.5465	0.6	4.4017	1.5	0.3048	1.3	0.91	1714.9	19.9	1712.7	12.0	1709.9	10.9	1709.9	10.9	100.3
K15-Estadio-3-Spot 91	179	217373	1.7	9.7244	0.7	4.1504	1.1	0.2927	0.9	0.77	1655.1	12.7	1664.3	9.2	1675.9	13.4	1675.9	13.4	98.8
K15-Estadio-3-Spot 92	108	116732	1.5	9.8103	1.2	4.0518	1.7	0.2883	1.2	0.71	1633.0	17.1	1644.7	13.5	1659.6	21.6	1659.6	21.6	98.4
K15-Estadio-3-Spot 93	83	51931	1.4	9.8605	1.2	4.0894	1.6	0.2925	1.1	0.68	1653.8	15.6	1652.2	12.8	1650.2	21.4	1650.2	21.4	100.2
K15-Estadio-3-Spot 94	790	70186	11.6	9.3980	0.6	3.5747	1.3	0.2437	1.1	0.89	1405.7	14.3	1543.9	10.2	1738.7	10.9	1738.7	10.9	80.8
K15-Estadio-3-Spot 95	443	119588	2.0	9.7965	0.9	3.5853	2.2	0.2547	2.0	0.92	1462.9	26.0	1546.3	17.2	1662.2	15.9	1662.2	15.9	88.0
K15-Estadio-3-Spot 97	75	74076	1.4	9.7224	1.0	4.1496	1.4	0.2926	1.0	0.70	1654.5	14.4	1664.1	11.5	1676.3	18.5	1676.3	18.5	98.7

K15-Estadio-3-Spot 98	130	595489	1.7	9.8178	0.7	4.0435	1.4	0.2879	1.2	0.85	1631.1	16.7	1643.0	11.2	1658.2	13.6	1658.2	13.6	98.4
K15-Estadio-3-Spot 99	107	137042	1.2	9.6687	0.9	4.3273	1.2	0.3034	0.9	0.70	1708.4	13.1	1698.6	10.3	1686.5	16.5	1686.5	16.5	101.3
K15-Estadio-3-Spot 100	281	378160	2.1	9.8587	1.0	4.0838	1.4	0.2920	1.0	0.71	1651.5	14.1	1651.1	11.1	1650.5	17.6	1650.5	17.6	100.1
K15-Estadio-3-Spot 102	257	182307	1.7	9.9655	0.8	4.0473	1.3	0.2925	1.0	0.77	1654.1	14.5	1643.8	10.5	1630.5	15.1	1630.5	15.1	101.5
K15-Estadio-3-Spot 103	701	96196	14.9	9.6352	0.5	3.8839	1.3	0.2714	1.2	0.91	1548.0	16.6	1610.3	10.7	1692.9	9.9	1692.9	9.9	91.4
K15-Estadio-3-Spot 104	255	65317	1.8	9.9337	0.8	3.9783	1.5	0.2866	1.3	0.87	1624.6	18.8	1629.8	12.3	1636.4	14.0	1636.4	14.0	99.3
K15-Estadio-3-Spot 106	127	66239	1.9	9.7421	0.7	4.1441	1.2	0.2928	1.0	0.80	1655.6	14.0	1663.1	9.8	1672.5	13.4	1672.5	13.4	99.0
K15-Estadio-3-Spot 107	65	62354	1.2	9.7694	1.1	4.0978	1.6	0.2903	1.2	0.72	1643.3	16.8	1653.9	13.1	1667.3	20.8	1667.3	20.8	98.6
K15-Estadio-3-Spot 108	208	64490	1.9	9.7996	0.8	4.0459	1.5	0.2876	1.2	0.85	1629.3	17.8	1643.5	11.9	1661.6	14.3	1661.6	14.3	98.1
K15-Estadio-3-Spot 109	202	129383	1.6	9.9003	0.7	4.0269	1.1	0.2891	0.9	0.77	1637.3	12.7	1639.6	9.2	1642.7	13.3	1642.7	13.3	99.7
K15-Estadio-3-Spot 110	91	55485	1.1	9.7606	0.8	4.1071	1.4	0.2907	1.1	0.79	1645.3	15.7	1655.7	11.2	1669.0	15.6	1669.0	15.6	98.6
K15-Estadio-3-Spot 111	643	150195	1.3	9.4325	0.7	4.5426	1.1	0.3108	0.9	0.77	1744.5	13.4	1738.8	9.5	1732.0	13.5	1732.0	13.5	100.7
K15-Estadio-3-Spot 112	311	124683	2.8	9.0819	0.8	4.8072	1.2	0.3166	0.9	0.76	1773.3	14.3	1786.2	10.2	1801.2	14.3	1801.2	14.3	98.5
K15-Estadio-3-Spot 113	233	238066	1.4	9.7469	0.6	4.1625	1.2	0.2943	1.1	0.86	1662.8	15.5	1666.7	10.0	1671.6	11.3	1671.6	11.3	99.5
K15-Estadio-3-Spot 114	66	38842	1.4	9.9006	1.0	4.0145	1.7	0.2883	1.3	0.77	1632.8	18.5	1637.1	13.4	1642.6	19.4	1642.6	19.4	99.4
K15-Estadio-3-Spot 115	100	148977	1.4	9.7735	0.7	4.2808	1.2	0.3034	1.0	0.81	1708.3	14.7	1689.7	9.9	1666.6	13.0	1666.6	13.0	102.5
K15-Estadio-3-Spot 116	238	203166	4.1	9.3383	0.8	4.6202	1.1	0.3129	0.7	0.69	1755.0	11.2	1752.9	8.8	1750.4	14.1	1750.4	14.1	100.3
K15-Estadio-3-Spot 117	286	75413	1.7	9.9551	0.8	3.9973	1.3	0.2886	1.0	0.76	1634.6	14.0	1633.6	10.4	1632.4	15.4	1632.4	15.4	100.1
K15-Estadio-3-Spot 119	474	63297	1.7	9.2563	2.1	4.4848	3.2	0.3011	2.4	0.75	1696.7	35.6	1728.2	26.4	1766.5	38.4	1766.5	38.4	96.0
K15-Estadio-3-Spot 120	144	154855	1.0	9.8346	0.8	4.0542	1.3	0.2892	1.0	0.80	1637.4	14.6	1645.1	10.3	1655.0	14.1	1655.0	14.1	98.9
K15-Estadio-3-Spot 121	189	51115	2.3	9.7131	0.9	4.1760	1.3	0.2942	1.0	0.76	1662.4	15.1	1669.3	11.0	1678.0	16.0	1678.0	16.0	99.1
K15-Estadio-3-Spot 122	248	553533	1.3	9.7698	0.8	4.1719	1.3	0.2956	1.1	0.81	1669.5	16.0	1668.5	11.0	1667.3	14.3	1667.3	14.3	100.1
K15-Estadio-3-Spot 123	154	608586	1.9	9.5826	0.8	4.2100	1.6	0.2926	1.4	0.86	1654.5	20.6	1676.0	13.5	1703.0	15.3	1703.0	15.3	97.2
K15-Estadio-3-Spot 124	104	165993	3.1	9.7015	1.0	4.2388	1.5	0.2983	1.1	0.75	1682.6	16.4	1681.6	12.1	1680.2	18.0	1680.2	18.0	100.1
K15-Estadio-3-Spot 125	128	66840	1.0	9.1330	1.1	4.3583	1.5	0.2887	1.1	0.71	1635.0	15.6	1704.5	12.6	1791.0	19.7	1791.0	19.7	91.3
K15-Estadio-3-Spot 126	160	78102	1.2	9.8315	0.9	4.0320	1.8	0.2875	1.5	0.86	1629.0	22.0	1640.7	14.5	1655.6	17.1	1655.6	17.1	98.4
K15-Estadio-3-Spot 127	88	92126	2.3	9.4605	0.9	4.4574	1.6	0.3058	1.3	0.81	1720.2	19.7	1723.1	13.3	1726.6	17.2	1726.6	17.2	99.6
K15-Estadio-3-Spot 128	93	71222	1.9	9.7223	0.8	4.0468	1.1	0.2853	0.7	0.69	1618.2	10.7	1643.7	8.8	1676.3	14.5	1676.3	14.5	96.5
K15-Estadio-3-Spot 129	183	59272	1.7	9.7831	0.8	4.1553	1.3	0.2948	1.0	0.76	1665.7	14.2	1665.3	10.4	1664.7	15.3	1664.7	15.3	100.1
K15-Estadio-3-Spot 130	371	158118	1.3	9.4580	0.8	4.1261	1.6	0.2830	1.4	0.88	1606.6	20.0	1659.5	13.1	1727.0	13.9	1727.0	13.9	93.0
K15-Estadio-3-Spot 131	105	218229	1.4	9.8108	1.0	4.0804	1.4	0.2903	1.0	0.70	1643.2	13.8	1650.4	11.0	1659.5	17.8	1659.5	17.8	99.0
K15-Estadio-3-Spot 132	173	195389	1.2	9.7168	1.0	4.2183	1.5	0.2973	1.2	0.77	1677.8	17.4	1677.6	12.6	1677.3	18.2	1677.3	18.2	100.0
K15-Estadio-3-Spot 133	77	119436	1.5	9.8917	0.7	4.1340	1.3	0.2966	1.1	0.84	1674.3	15.7	1661.0	10.4	1644.3	12.7	1644.3	12.7	101.8
K15-Estadio-3-Spot 134	521	107935	8.1	9.6247	0.7	4.5197	2.0	0.3155	1.9	0.94	1767.7	28.7	1734.6	16.4	1694.9	12.2	1694.9	12.2	104.3
K15-Estadio-3-Spot 135	167	227586	3.1	9.2452	1.1	4.4605	1.5	0.2991	1.0	0.69	1686.8	15.3	1723.7	12.4	1768.7	19.8	1768.7	19.8	95.4
K15-Estadio-3-Spot 136	121	138049	1.9	9.6626	1.0	4.1993	1.8	0.2943	1.5	0.83	1662.9	21.6	1673.9	14.6	1687.7	18.5	1687.7	18.5	98.5
K15-Estadio-3-Spot 137	124	102539	1.3	9.8421	0.9	4.0130	1.3	0.2865	1.0	0.76	1623.8	14.6	1636.8	10.9	1653.6	16.0	1653.6	16.0	98.2
K15-Estadio-3-Spot 138	939	53489	4.8	9.4822	0.6	3.6407	1.6	0.2504	1.4	0.92	1440.4	18.5	1558.5	12.4	1722.4	11.5	1722.4	11.5	83.6
K15-Estadio-3-Spot 139	187	3041143	2.1	9.7922	1.0	4.0947	1.4	0.2908	1.0	0.71	1645.5	14.9	1653.2	11.8	1663.0	18.9	1663.0	18.9	98.9
K15-Estadio-3-Spot 140	259	54433	2.3	9.8696	0.8	4.0698	1.3	0.2913	1.1	0.81	1648.1	15.5	1648.3	10.7	1648.4	14.2	1648.4	14.2	100.0
K15-Estadio-3-Spot 141	79	48223	1.7	9.8529	0.8	4.1427	1.3	0.2960	1.0	0.79	1671.6	15.4	1662.8	10.9	1651.6	15.1	1651.6	15.1	101.2
K15-Estadio-3-Spot 142	277	117914	2.9	9.5402	0.5	4.3210	0.9	0.2990	0.7	0.83	1686.2	11.0	1697.4	7.3	1711.1	9.0	1711.1	9.0	98.5
K15-Estadio-3-Spot 143	178	56156	1.5	9.7608	0.9	3.8858	1.5	0.2751	1.2	0.81	1566.6	17.3	1610.7	12.4	1669.0	16.8	1669.0	16.8	93.9

K15-Estadio-3-Spot 144	79	96295	1.6	9.7782	0.9	4.1324	1.3	0.2931	0.9	0.69	1656.8	12.7	1660.7	10.3	1665.7	16.8	1665.7	16.8	99.5
K15-Estadio-3-Spot 145	89	63744	1.6	9.6261	1.0	4.3066	1.6	0.3007	1.2	0.75	1694.6	17.5	1694.6	12.9	1694.6	18.9	1694.6	18.9	100.0
K15-Estadio-3-Spot 146	188	100073	1.2	9.8512	0.9	4.1050	1.5	0.2933	1.2	0.78	1658.0	17.1	1655.3	12.3	1651.9	17.4	1651.9	17.4	100.4
K15-Estadio-3-Spot 148	105	52678	1.4	9.6803	1.0	4.2422	1.5	0.2978	1.2	0.77	1680.6	17.1	1682.2	12.4	1684.3	17.9	1684.3	17.9	99.8
K15-Estadio-3-Spot 149	70	33431	1.6	9.9442	1.0	4.0647	1.5	0.2932	1.1	0.75	1657.3	16.4	1647.3	12.2	1634.5	18.6	1634.5	18.6	101.4
K15-Estadio-3-Spot 150	337	300312	1.5	9.8724	0.8	4.1028	1.3	0.2938	1.0	0.78	1660.3	14.9	1654.9	10.7	1647.9	15.3	1647.9	15.3	100.8
K15-Estadio-3-Spot 151	98	58383	1.5	9.8034	1.0	4.0806	1.5	0.2901	1.1	0.72	1642.2	15.3	1650.4	11.9	1660.9	18.6	1660.9	18.6	98.9
K15-Estadio-3-Spot 152	273	100448	2.5	9.8906	0.8	3.5660	1.3	0.2558	1.1	0.80	1468.3	14.1	1542.0	10.6	1644.5	14.8	1644.5	14.8	89.3
K15-Estadio-3-Spot 153	418	161845	2.4	9.4002	0.6	4.4756	1.2	0.3051	1.0	0.84	1716.7	15.3	1726.5	10.0	1738.3	11.9	1738.3	11.9	98.8
K15-Estadio-3-Spot 154	31	42816	3.6	9.7506	1.0	4.2416	1.4	0.3000	0.9	0.70	1691.1	14.1	1682.1	11.2	1670.9	18.1	1670.9	18.1	101.2
K15-Estadio-3-Spot 155	92	132277	3.4	10.2093	1.0	3.4501	1.5	0.2555	1.1	0.74	1466.6	14.6	1515.9	11.8	1585.4	18.8	1585.4	18.8	92.5
K15-Estadio-3-Spot 156	462	72018	1.0	9.7827	0.7	4.1940	1.4	0.2976	1.2	0.87	1679.2	17.6	1672.9	11.2	1664.8	12.3	1664.8	12.3	100.9
K15-Estadio-3-Spot 157	158	174080	1.0	9.9299	0.8	3.9384	1.3	0.2836	1.0	0.77	1609.6	14.0	1621.6	10.3	1637.1	15.0	1637.1	15.0	98.3
K15-Estadio-3-Spot 158	123	153484	3.0	9.4632	0.7	4.4426	1.2	0.3049	0.9	0.78	1715.6	13.7	1720.3	9.6	1726.0	13.2	1726.0	13.2	99.4
K15-Estadio-3-Spot 159	423	256663	1.3	9.8867	0.7	4.0963	1.4	0.2937	1.2	0.86	1660.1	17.8	1653.6	11.6	1645.2	13.5	1645.2	13.5	100.9
K15-Estadio-3-Spot 160	110	432769	3.1	9.7326	1.2	4.2305	1.5	0.2986	1.0	0.64	1684.4	14.6	1680.0	12.7	1674.3	22.1	1674.3	22.1	100.6
K15-Estadio-3-Spot 161	155	196426	0.8	9.7913	1.1	3.8613	1.6	0.2742	1.1	0.69	1562.1	14.8	1605.6	12.5	1663.2	20.9	1663.2	20.9	93.9
K15-Estadio-3-Spot 162	346	50758	1.2	9.8626	0.9	4.1391	1.4	0.2961	1.1	0.80	1671.8	16.8	1662.1	11.7	1649.8	15.9	1649.8	15.9	101.3
K15-Estadio-3-Spot 163	121	34341850	1.3	9.7494	0.9	4.1864	1.5	0.2960	1.2	0.81	1671.5	17.5	1671.4	12.0	1671.1	15.8	1671.1	15.8	100.0
K15-Estadio-3-Spot 164	69	50885	2.2	9.8669	1.2	4.0915	1.5	0.2928	1.0	0.65	1655.5	14.6	1652.6	12.5	1648.9	21.6	1648.9	21.6	100.4
K15-Estadio-3-Spot 165	306	211122	1.2	9.7988	0.8	4.0780	1.3	0.2898	1.0	0.80	1640.6	14.8	1649.9	10.4	1661.8	14.0	1661.8	14.0	98.7
K15-Estadio-3-Spot 166	328	174491	1.4	9.8121	0.6	4.1172	1.3	0.2930	1.1	0.87	1656.5	16.3	1657.7	10.4	1659.3	11.5	1659.3	11.5	99.8
K15-Estadio-3-Spot 167	112	35979	1.1	9.1401	1.6	4.3472	2.0	0.2882	1.2	0.60	1632.4	16.9	1702.4	16.2	1789.6	28.5	1789.6	28.5	91.2
K15-Estadio-3-Spot 168	91	60778	1.7	9.7131	1.2	4.2003	1.6	0.2959	1.0	0.67	1670.9	15.4	1674.1	12.8	1678.0	21.4	1678.0	21.4	99.6
K15-Estadio-3-Spot 169	181	57990	2.9	9.7525	0.9	4.1769	1.4	0.2954	1.1	0.75	1668.7	15.5	1669.5	11.5	1670.5	17.2	1670.5	17.2	99.9
K15-Estadio-3-Spot 170	243	10881303	1.7	9.9051	0.9	4.0014	1.7	0.2875	1.4	0.84	1628.8	20.4	1634.5	13.7	1641.8	17.2	1641.8	17.2	99.2
K15-Estadio-3-Spot 171	117	54562	2.4	9.6742	1.1	4.2480	1.4	0.2981	1.0	0.68	1681.7	14.3	1683.4	11.7	1685.4	19.4	1685.4	19.4	99.8
K15-Estadio-3-Spot 172	201	193364	1.6	9.9262	0.8	4.0732	1.5	0.2932	1.3	0.85	1657.7	19.3	1648.9	12.6	1637.8	15.0	1637.8	15.0	101.2
K15-Estadio-3-Spot 173	178	76982	1.5	9.8516	0.7	4.0149	1.0	0.2869	0.7	0.69	1625.9	10.1	1637.2	8.3	1651.8	13.8	1651.8	13.8	98.4
K15-Estadio-3-Spot 174	101	212894	1.5	9.6844	0.9	4.2601	1.1	0.2992	0.7	0.60	1687.4	9.9	1685.7	9.2	1683.5	16.5	1683.5	16.5	100.2
K15-Estadio-3-Spot 175	309	86441	2.2	9.5270	0.6	4.2519	1.2	0.2938	1.0	0.86	1660.4	14.8	1684.1	9.6	1713.7	10.8	1713.7	10.8	96.9
K15-Estadio-3-Spot 176	563	63006	1.9	9.6944	0.6	4.2227	1.4	0.2969	1.2	0.90	1675.9	18.2	1678.4	11.2	1681.6	11.0	1681.6	11.0	99.7
K15-Estadio-3-Spot 177	278	170795	6.1	9.5459	0.7	4.3433	1.1	0.3007	0.9	0.80	1694.8	13.0	1701.6	9.0	1710.0	12.2	1710.0	12.2	99.1
K15-Estadio-3-Spot 178	266	144298	1.6	9.8567	0.5	3.8679	0.9	0.2765	0.8	0.85	1573.7	10.8	1607.0	7.3	1650.9	8.8	1650.9	8.8	95.3
K15-Estadio-3-Spot 179	252	66625	1.4	9.7730	0.6	4.1771	1.1	0.2961	1.0	0.85	1671.8	14.2	1669.5	9.4	1666.7	11.3	1666.7	11.3	100.3
K15-Estadio-3-Spot 180	245	130932	2.0	9.4744	0.8	4.5071	1.4	0.3097	1.2	0.82	1739.2	17.6	1732.3	11.6	1723.9	14.5	1723.9	14.5	100.9
K15-Estadio-3-Spot 181	131	86423	2.8	9.1810	1.0	4.7627	1.6	0.3171	1.2	0.76	1775.7	18.4	1778.3	13.1	1781.4	18.4	1781.4	18.4	99.7
K15-Estadio-3-Spot 182	111	95617	1.5	9.8204	0.8	4.0880	1.4	0.2912	1.1	0.78	1647.3	15.5	1651.9	11.1	1657.7	15.7	1657.7	15.7	99.4
K15-Estadio-3-Spot 183	184	73848	1.7	9.6921	0.8	4.2002	1.2	0.2952	1.0	0.78	1667.7	14.0	1674.1	10.1	1682.0	14.3	1682.0	14.3	99.1
K15-Estadio-3-Spot 184	223	53187	1.2	9.5551	1.3	4.1255	1.8	0.2859	1.3	0.72	1621.0	18.8	1659.4	14.8	1708.3	23.2	1708.3	23.2	94.9
K15-Estadio-3-Spot 185	132	210373	1.5	9.7354	0.8	4.0696	1.5	0.2873	1.2	0.82	1628.2	17.4	1648.2	12.0	1673.8	15.5	1673.8	15.5	97.3
K15-Estadio-3-Spot 186	588	96841	2.2	9.2916	0.6	4.7309	1.3	0.3188	1.1	0.88	1783.9	17.4	1772.7	10.6	1759.6	10.8	1759.6	10.8	101.4
K15-Estadio-3-Spot 187	102	57484	1.4	9.9062	0.9	4.1513	1.5	0.2983	1.2	0.81	1682.7	17.9	1664.5	12.2	1641.6	16.4	1641.6	16.4	102.5

K15-Estadio-3-Spot 188	97	75002	2.0	9.6443	1.1	4.2660	1.7	0.2984	1.3	0.74	1683.3	18.7	1686.8	14.0	1691.2	21.0	1691.2	21.0	99.5
K15-Estadio-3-Spot 189	392	5575825	1.6	9.8334	0.7	3.9658	1.3	0.2828	1.1	0.83	1605.6	15.4	1627.2	10.6	1655.3	13.7	1655.3	13.7	97.0
K15-Estadio-3-Spot 190	191	202842	1.8	9.1335	0.8	4.7415	1.3	0.3141	1.1	0.81	1760.8	16.2	1774.6	10.9	1790.9	13.9	1790.9	13.9	98.3
K15-Estadio-3-Spot 191	104	52001	1.0	9.7852	1.0	4.1481	1.6	0.2944	1.2	0.76	1663.4	18.1	1663.8	13.2	1664.4	19.4	1664.4	19.4	99.9
K15-Estadio-3-Spot 192	202	232816	1.7	9.7475	1.0	3.8039	1.8	0.2689	1.5	0.84	1535.3	20.7	1593.6	14.5	1671.5	18.0	1671.5	18.0	91.9
K15-Estadio-3-Spot 193	93	162189	1.2	9.8162	0.9	4.1153	1.7	0.2930	1.4	0.83	1656.4	20.4	1657.3	13.8	1658.5	17.5	1658.5	17.5	99.9
K15-Estadio-3-Spot 194	147	217682	1.8	9.7907	0.8	4.0611	1.4	0.2884	1.1	0.83	1633.4	16.5	1646.5	11.2	1663.3	14.2	1663.3	14.2	98.2
K15-Estadio-3-Spot 195	109	41427	1.3	9.5347	0.8	4.3084	1.4	0.2979	1.1	0.79	1681.1	15.8	1695.0	11.2	1712.2	15.4	1712.2	15.4	98.2
K15-Estadio-3-Spot 196	334	57793	2.1	9.7901	0.5	3.8875	0.9	0.2760	0.7	0.79	1571.3	9.6	1611.1	7.0	1663.4	9.8	1663.4	9.8	94.5
K15-Estadio-3-Spot 197	168	219393	2.1	9.3201	1.2	4.6089	1.9	0.3115	1.4	0.76	1748.3	22.1	1750.9	15.7	1754.0	22.3	1754.0	22.3	99.7
K15-Estadio-3-Spot 198	119	72902	2.3	9.5920	0.8	4.2591	1.3	0.2963	1.0	0.77	1672.9	14.3	1685.5	10.4	1701.2	14.8	1701.2	14.8	98.3
K15-Estadio-3-Spot 199	112	140243	1.3	9.8856	0.6	4.0853	1.1	0.2929	0.9	0.82	1656.0	13.3	1651.4	9.0	1645.4	11.6	1645.4	11.6	100.6
K15-Estadio-3-Spot 200	86	60686	1.3	9.7332	1.0	4.1400	1.3	0.2923	0.9	0.65	1652.8	12.6	1662.2	10.9	1674.2	18.6	1674.2	18.6	98.7
K15-Estadio-3-Spot 201	76	67455	0.8	9.7769	1.1	4.1202	1.7	0.2922	1.3	0.78	1652.3	19.4	1658.3	14.0	1665.9	19.9	1665.9	19.9	99.2
K15-Estadio-3-Spot 202	529	89617	2.3	9.6009	0.7	4.0161	1.3	0.2797	1.1	0.85	1589.6	15.4	1637.5	10.5	1699.5	12.6	1699.5	12.6	93.5
K15-Estadio-3-Spot 203	214	73689	4.1	8.5786	0.8	5.4940	1.5	0.3418	1.2	0.82	1895.4	19.5	1899.7	12.5	1904.3	15.1	1904.3	15.1	99.5
K15-Estadio-3-Spot 204	79	86690	2.6	9.6403	1.0	4.2602	1.3	0.2979	0.9	0.66	1680.7	13.2	1685.7	11.1	1691.9	18.7	1691.9	18.7	99.3
K15-Estadio-3-Spot 205	53	235807	1.9	9.8211	1.0	4.0928	1.3	0.2915	0.8	0.62	1649.2	11.7	1652.9	10.5	1657.6	18.7	1657.6	18.7	99.5
K15-Estadio-3-Spot 206	239	134723	1.6	8.8305	0.6	5.1491	1.3	0.3298	1.1	0.86	1837.3	17.3	1844.2	10.7	1852.1	11.4	1852.1	11.4	99.2
K15-Estadio-3-Spot 207	889	308632	3.4	9.5970	0.9	4.1189	1.6	0.2867	1.3	0.83	1625.0	19.0	1658.1	13.0	1700.2	16.2	1700.2	16.2	95.6
K15-Estadio-3-Spot 208	325	144775	11.1	9.1731	0.8	4.7552	1.6	0.3164	1.4	0.87	1771.9	21.3	1777.0	13.2	1783.0	14.1	1783.0	14.1	99.4
K15-Estadio-3-Spot 209	334	133229	2.8	9.4851	0.6	4.2916	1.2	0.2952	1.0	0.86	1667.6	15.1	1691.8	9.8	1721.8	11.3	1721.8	11.3	96.9
K15-Estadio-3-Spot 210	95	113851	1.4	9.7113	0.8	4.0658	1.5	0.2864	1.3	0.86	1623.3	18.0	1647.5	12.0	1678.4	14.0	1678.4	14.0	96.7
K15-Estadio-3-Spot 211	109	223934	2.0	9.7892	0.9	4.2002	1.4	0.2982	1.1	0.79	1682.4	16.8	1674.1	11.8	1663.6	16.5	1663.6	16.5	101.1
K15-Estadio-3-Spot 212	329	156184	1.3	9.8806	0.6	4.0861	1.4	0.2928	1.2	0.89	1655.6	17.9	1651.5	11.2	1646.4	11.4	1646.4	11.4	100.6
K15-Estadio-3-Spot 213	81	51890	1.4	9.7765	0.9	4.1615	1.2	0.2951	0.8	0.69	1666.9	12.4	1666.5	10.1	1666.0	16.6	1666.0	16.6	100.1
K15-Estadio-3-Spot 214	110	74902	1.9	9.7573	0.9	4.0318	1.5	0.2853	1.2	0.80	1618.1	17.2	1640.6	12.2	1669.6	16.5	1669.6	16.5	96.9
K15-Estadio-3-Spot 216	126	2823229	1.8	9.7769	0.9	4.0032	1.3	0.2839	0.9	0.70	1610.8	12.6	1634.8	10.3	1665.9	16.7	1665.9	16.7	96.7
K15-Estadio-3-Spot 217	192	56734	2.2	9.8525	0.8	4.1103	1.4	0.2937	1.1	0.80	1660.0	16.3	1656.3	11.3	1651.7	15.3	1651.7	15.3	100.5
K15-Estadio-3-Spot 218	141	132279	1.5	9.5853	0.7	4.2039	1.3	0.2923	1.0	0.83	1652.8	15.1	1674.8	10.3	1702.4	13.0	1702.4	13.0	97.1
K15-Estadio-3-Spot 219	736	119858	2.3	9.3169	0.6	3.9164	1.0	0.2646	0.8	0.82	1513.5	11.0	1617.1	8.0	1754.6	10.3	1754.6	10.3	86.3
K15-Estadio-3-Spot 220	191	142076	1.0	9.8510	0.8	4.0516	1.2	0.2895	0.9	0.77	1638.9	13.5	1644.6	9.9	1651.9	14.5	1651.9	14.5	99.2
K15-Estadio-3-Spot 221	315	271804	2.2	9.6836	0.8	4.2433	1.3	0.2980	1.1	0.82	1681.5	15.7	1682.4	10.7	1683.6	13.9	1683.6	13.9	99.9
K15-Estadio-3-Spot 223	151	102760	1.9	9.9113	0.9	4.0311	1.4	0.2898	1.0	0.75	1640.4	15.0	1640.5	11.3	1640.6	17.0	1640.6	17.0	100.0
K15-Estadio-3-Spot 224	265	133196	1.6	9.7397	0.6	4.1794	1.2	0.2952	1.0	0.86	1667.6	14.6	1670.0	9.4	1673.0	10.7	1673.0	10.7	99.7
K15-Estadio-3-Spot 225	352	167407	0.9	9.8636	0.7	4.0286	1.2	0.2882	1.0	0.83	1632.5	14.5	1640.0	9.8	1649.6	12.5	1649.6	12.5	99.0
K15-Estadio-3-Spot 226	96	139357	1.9	9.5687	1.0	4.3693	1.5	0.3032	1.1	0.73	1707.3	16.2	1706.6	12.1	1705.7	18.4	1705.7	18.4	100.1
K15-Estadio-3-Spot 227	200	151123	4.0	9.3357	0.7	4.6370	1.2	0.3140	1.0	0.82	1760.2	15.7	1755.9	10.4	1750.9	13.1	1750.9	13.1	100.5
K15-Estadio-3-Spot 228	1032	60460	1.0	9.4041	0.7	3.7139	1.2	0.2533	0.9	0.78	1455.5	12.1	1574.4	9.5	1737.5	13.5	1737.5	13.5	83.8
K15-Estadio-3-Spot 229	69	92212	1.8	11.1785	1.1	2.9177	1.5	0.2365	1.1	0.69	1368.7	13.0	1386.5	11.6	1413.9	21.4	1413.9	21.4	96.8
K15-Estadio-3-Spot 230	141	153625	1.5	9.4263	0.7	4.3904	1.4	0.3002	1.2	0.88	1692.1	18.2	1710.5	11.6	1733.2	12.4	1733.2	12.4	97.6
K15-Estadio-3-Spot 231	803	180804	2.0	9.4288	0.6	4.3473	1.2	0.2973	1.0	0.87	1677.8	15.1	1702.4	9.7	1732.7	10.8	1732.7	10.8	96.8
K15-Estadio-3-Spot 232	241	89297	2.4	9.6518	0.6	4.2759	1.1	0.2993	0.9	0.85	1687.9	13.5	1688.7	8.8	1689.7	10.3	1689.7	10.3	99.9

K15-Estadio-3-Spot 233	64	47900	1.3	9.7723	1.2	4.1439	1.6	0.2937	1.1	0.66	1660.0	15.4	1663.0	13.0	1666.8	22.0	1666.8	22.0	99.6
K15-Estadio-3-Spot 234	84	157368	2.0	9.5193	1.0	4.2836	1.4	0.2957	1.0	0.72	1670.1	14.9	1690.2	11.5	1715.2	17.7	1715.2	17.7	97.4
K15-Estadio-3-Spot 235	423	158743	6.8	9.3042	0.9	4.7494	1.6	0.3205	1.3	0.83	1792.1	21.0	1776.0	13.5	1757.1	16.3	1757.1	16.3	102.0
K15-Estadio-3-Spot 236	442	119853	3.1	9.6577	0.7	4.2291	1.2	0.2962	1.0	0.83	1672.6	14.7	1679.7	9.9	1688.6	12.2	1688.6	12.2	99.1
K15-Estadio-3-Spot 237	143	173347	2.7	9.6195	0.9	4.2296	1.5	0.2951	1.3	0.82	1666.9	18.5	1679.8	12.6	1695.9	16.3	1695.9	16.3	98.3
K15-Estadio-3-Spot 238	83	198907	1.1	6.0974	0.8	10.4216	1.4	0.4609	1.0	0.78	2443.4	21.4	2473.0	12.5	2497.4	14.3	2497.4	14.3	97.8
K15-Estadio-3-Spot 239	248	171837	1.1	9.7865	0.8	3.9833	1.3	0.2827	1.1	0.81	1605.1	15.3	1630.8	10.8	1664.1	14.5	1664.1	14.5	96.5
K15-Estadio-3-Spot 240	30	44790	1.3	9.6620	1.1	4.3142	1.4	0.3023	0.9	0.66	1702.8	13.9	1696.1	11.6	1687.8	19.6	1687.8	19.6	100.9
K15-Estadio-3-Spot 241	469	36236	1.0	9.1181	0.9	4.1150	1.3	0.2721	1.0	0.73	1551.6	13.4	1657.3	10.9	1794.0	16.7	1794.0	16.7	86.5
K15-Estadio-3-Spot 242	158	90616	1.4	9.8192	1.0	3.8639	1.9	0.2752	1.6	0.84	1567.0	22.6	1606.2	15.6	1657.9	19.2	1657.9	19.2	94.5
K15-Estadio-3-Spot 243	373	315044	1.4	9.9729	0.8	4.0276	1.5	0.2913	1.3	0.86	1648.1	18.7	1639.8	12.1	1629.1	14.1	1629.1	14.1	101.2
K15-Estadio-3-Spot 244	257	85331	1.5	9.7075	0.8	4.1117	1.3	0.2895	0.9	0.75	1639.0	13.6	1656.6	10.2	1679.1	15.3	1679.1	15.3	97.6
K15-Estadio-3-Spot 245	90	49693	2.1	8.5338	1.3	4.8171	1.6	0.2981	1.0	0.60	1682.1	14.1	1787.9	13.3	1913.6	22.7	1913.6	22.7	87.9
K15-Estadio-3-Spot 246	155	99476	1.6	9.7454	0.8	4.2113	1.5	0.2977	1.3	0.84	1679.7	19.1	1676.2	12.7	1671.9	15.7	1671.9	15.7	100.5
K15-Estadio-3-Spot 247	175	52540	1.9	9.6847	0.6	4.2195	1.0	0.2964	0.8	0.77	1673.3	11.3	1677.8	8.2	1683.4	11.7	1683.4	11.7	99.4
K15-Estadio-3-Spot 248	109	118951	1.6	9.6905	1.1	4.1848	1.6	0.2941	1.2	0.75	1662.1	17.6	1671.1	13.2	1682.3	19.7	1682.3	19.7	98.8
K15-Estadio-3-Spot 249	267	73104	1.3	9.7411	0.8	4.0923	1.2	0.2891	0.9	0.76	1637.1	13.4	1652.8	9.9	1672.7	14.4	1672.7	14.4	97.9
K15-Estadio-3-Spot 251	246	243178	1.9	9.7684	0.7	4.2858	1.3	0.3036	1.2	0.86	1709.3	17.5	1690.6	11.1	1667.5	12.7	1667.5	12.7	102.5
K15-Estadio-3-Spot 252	115	126600	1.5	9.8293	0.8	4.0793	1.4	0.2908	1.1	0.79	1645.6	15.6	1650.2	11.1	1656.0	15.5	1656.0	15.5	99.4
K15-Estadio-3-Spot 253	97	38019	0.8	9.8368	0.7	4.0404	1.4	0.2883	1.2	0.86	1632.8	17.4	1642.4	11.3	1654.6	13.0	1654.6	13.0	98.7
K15-Estadio-3-Spot 254	92	59776	3.2	9.2253	0.9	4.7642	1.6	0.3188	1.3	0.82	1783.7	19.9	1778.6	13.1	1772.6	16.2	1772.6	16.2	100.6
K15-Estadio-3-Spot 255	227	515086	2.5	9.5481	0.6	4.4130	1.1	0.3056	0.9	0.83	1719.0	13.5	1714.8	8.9	1709.6	11.1	1709.6	11.1	100.5
K15-Estadio-3-Spot 256	118	237005	1.7	9.8515	0.8	4.1318	1.3	0.2952	1.0	0.80	1667.6	15.2	1660.6	10.5	1651.8	14.1	1651.8	14.1	101.0
K15-Estadio-3-Spot 257	209	101046	2.7	9.5102	0.8	4.3439	1.5	0.2996	1.2	0.82	1689.4	18.3	1701.7	12.4	1716.9	15.6	1716.9	15.6	98.4
K15-Estadio-3-Spot 258	198	37215	1.2	9.1193	2.5	4.5059	2.7	0.2980	1.2	0.43	1681.5	17.4	1732.1	22.8	1793.7	45.2	1793.7	45.2	93.7
K15-Estadio-3-Spot 259	65	70165	1.7	9.8166	1.0	4.0403	1.5	0.2877	1.1	0.75	1629.8	15.8	1642.4	12.0	1658.4	18.1	1658.4	18.1	98.3
K15-Estadio-3-Spot 260	52	48477	0.7	9.8049	1.4	4.0772	2.0	0.2899	1.4	0.70	1641.2	20.1	1649.8	16.1	1660.6	26.1	1660.6	26.1	98.8
K15-Estadio-3-Spot 261	93	245594	1.9	9.7119	1.1	4.1568	1.5	0.2928	1.1	0.70	1655.5	15.6	1665.5	12.6	1678.3	20.3	1678.3	20.3	98.6
K15-Estadio-3-Spot 262	211	55002	2.0	9.7978	0.7	4.0089	1.3	0.2849	1.1	0.82	1615.8	15.1	1636.0	10.5	1662.0	13.7	1662.0	13.7	97.2
K15-Estadio-3-Spot 263	549	55759	7.2	9.6053	0.9	3.7546	2.2	0.2616	2.0	0.92	1497.8	26.7	1583.1	17.5	1698.6	16.1	1698.6	16.1	88.2
K15-Estadio-3-Spot 264	184	126556	1.7	9.6726	0.9	4.1255	1.3	0.2894	1.0	0.73	1638.6	14.0	1659.4	10.8	1685.7	16.8	1685.7	16.8	97.2
K15-Estadio-3-Spot 265	406	59939	1.7	9.3484	0.6	4.4647	1.1	0.3027	0.9	0.82	1704.7	13.6	1724.4	9.1	1748.4	11.4	1748.4	11.4	97.5
K15-Estadio-3-Spot 266	106	67034	2.0	9.7688	0.8	4.1112	1.4	0.2913	1.2	0.84	1647.9	17.5	1656.5	11.7	1667.4	14.3	1667.4	14.3	98.8
K15-Estadio-3-Spot 267	166	72600	1.0	9.8726	0.9	4.0078	1.3	0.2870	0.9	0.74	1626.3	13.4	1635.8	10.3	1647.9	15.9	1647.9	15.9	98.7
K15-Estadio-3-Spot 268	103	51608	2.1	9.5208	0.9	4.4393	1.5	0.3065	1.2	0.80	1723.7	17.8	1719.7	12.1	1714.9	16.0	1714.9	16.0	100.5
K15-Estadio-3-Spot 269	158	673195	3.2	9.5115	0.9	4.3243	1.4	0.2983	1.1	0.78	1682.9	16.0	1698.0	11.5	1716.7	16.1	1716.7	16.1	98.0
K15-Estadio-3-Spot 270	168	223792	1.7	9.8375	0.8	4.1708	1.2	0.2976	0.9	0.76	1679.3	13.4	1668.3	9.7	1654.5	14.2	1654.5	14.2	101.5
K15-Estadio-3-Spot 271	266	113471	2.0	9.7180	0.7	4.1828	1.3	0.2948	1.1	0.85	1665.5	16.2	1670.6	10.7	1677.1	12.8	1677.1	12.8	99.3
K15-Estadio-3-Spot 273	494	188485	10.3	9.4583	0.7	4.2325	2.3	0.2903	2.2	0.96	1643.2	31.9	1680.3	18.9	1727.0	12.1	1727.0	12.1	95.2
K15-Estadio-3-Spot 274	76	86707	2.0	9.8515	1.0	4.0443	1.4	0.2890	1.0	0.72	1636.4	14.5	1643.2	11.4	1651.8	18.0	1651.8	18.0	99.1
K15-Estadio-3-Spot 275	163	109601	0.9	9.7427	0.6	4.0922	1.1	0.2892	0.9	0.82	1637.3	13.0	1652.7	9.0	1672.4	11.8	1672.4	11.8	97.9
K15-Estadio-3-Spot 276	182	126436	3.1	9.5145	0.8	4.3533	1.3	0.3004	1.1	0.81	1693.3	15.7	1703.5	10.8	1716.1	14.2	1716.1	14.2	98.7
K15-Estadio-3-Spot 277	344	143758	1.7	9.7689	0.6	3.7344	1.1	0.2646	0.9	0.83	1513.3	12.4	1578.8	8.9	1667.4	11.4	1667.4	11.4	90.8

K15-Estadio-3-Spot 278	346	154203	1.5	9.7027	0.8	4.2225	1.5	0.2971	1.3	0.84	1677.1	18.8	1678.4	12.4	1680.0	15.0	1680.0	15.0	99.8
K15-Estadio-3-Spot 279	84	79986	1.3	9.6430	0.9	4.2724	1.4	0.2988	1.2	0.81	1685.4	17.4	1688.1	11.9	1691.4	15.7	1691.4	15.7	99.6
K15-Estadio-3-Spot 280	234	700814	1.5	9.8805	0.9	3.8980	1.7	0.2793	1.4	0.84	1588.0	19.6	1613.3	13.4	1646.4	16.5	1646.4	16.5	96.5
K15-Estadio-3-Spot 281	295	166030	1.6	9.6204	0.5	4.1821	1.1	0.2918	1.0	0.89	1650.5	14.3	1670.5	9.1	1695.7	9.4	1695.7	9.4	97.3
K15-Estadio-3-Spot 282	340	76271	4.2	9.3051	0.5	4.7551	0.9	0.3209	0.8	0.83	1794.2	12.2	1777.0	7.9	1756.9	9.7	1756.9	9.7	102.1
K15-Estadio-3-Spot 283	245	209523	1.7	9.7581	0.7	4.1188	1.5	0.2915	1.3	0.86	1649.0	18.4	1658.0	12.0	1669.5	13.7	1669.5	13.7	98.8
K15-Estadio-3-Spot 284	580	67036	2.9	9.5454	0.7	3.7498	1.2	0.2596	0.9	0.78	1487.8	12.0	1582.1	9.2	1710.1	13.2	1710.1	13.2	87.0
K15-Estadio-3-Spot 285	141	240498	1.5	9.7364	0.9	4.1286	1.5	0.2915	1.2	0.79	1649.2	16.8	1660.0	12.0	1673.6	16.7	1673.6	16.7	98.5
K15-Estadio-3-Spot 286	102	103573	1.5	9.8013	0.8	4.1049	1.4	0.2918	1.1	0.82	1650.5	16.7	1655.3	11.4	1661.3	14.9	1661.3	14.9	99.4
K15-Estadio-3-Spot 287	120	98873	1.6	9.6306	0.8	4.2669	1.3	0.2980	1.1	0.81	1681.6	15.6	1687.0	10.7	1693.8	14.1	1693.8	14.1	99.3
K15-Estadio-3-Spot 288	150	229278	0.9	9.7563	0.7	4.0138	1.1	0.2840	0.9	0.76	1611.6	12.5	1637.0	9.3	1669.8	13.7	1669.8	13.7	96.5
K15-Estadio-3-Spot 289	192	160841	0.7	5.8982	0.9	11.5289	1.4	0.4932	1.1	0.78	2584.4	23.6	2566.9	13.4	2553.1	15.1	2553.1	15.1	101.2
K15-Estadio-3-Spot 290	293	584751	15.2	9.4704	0.7	4.3857	1.3	0.3012	1.1	0.87	1697.4	17.1	1709.6	10.9	1724.6	12.1	1724.6	12.1	98.4
K15-Estadio-3-Spot 291	249	219828	1.9	9.5866	0.9	4.2314	1.4	0.2942	1.1	0.78	1662.5	15.6	1680.1	11.3	1702.2	15.9	1702.2	15.9	97.7
K15-Estadio-3-Spot 292	193	196668	2.3	9.7400	0.9	4.0882	1.5	0.2888	1.1	0.76	1635.5	16.0	1651.9	11.8	1672.9	17.3	1672.9	17.3	97.8
K15-Estadio-3-Spot 293	166	53653	1.2	9.7958	0.6	3.9803	1.4	0.2828	1.3	0.89	1605.4	17.9	1630.2	11.5	1662.4	11.9	1662.4	11.9	96.6
K15-Estadio-3-Spot 294	237	322918	1.3	9.7381	0.9	4.1277	1.3	0.2915	0.9	0.71	1649.1	13.0	1659.8	10.3	1673.3	16.6	1673.3	16.6	98.6
K15-Estadio-3-Spot 295	240	146459	2.3	9.7217	0.8	3.8466	1.2	0.2712	0.8	0.71	1547.0	11.3	1602.6	9.4	1676.4	15.1	1676.4	15.1	92.3
K15-Estadio-3-Spot 296	366	99039	1.8	9.8808	0.7	3.9609	1.2	0.2838	1.0	0.82	1610.7	14.5	1626.2	10.0	1646.3	13.1	1646.3	13.1	97.8
K15-Estadio-3-Spot 297	292	323681	1.9	9.7089	0.5	4.1356	1.0	0.2912	0.8	0.85	1647.6	12.3	1661.4	8.1	1678.8	9.8	1678.8	9.8	98.1
K15-Estadio-3-Spot 298	127	50314	2.0	9.7413	0.8	4.1257	1.5	0.2915	1.2	0.83	1648.9	18.0	1659.4	12.2	1672.7	15.2	1672.7	15.2	98.6
K15-Estadio-3-Spot 299	77	79682	2.0	9.6779	0.9	4.2362	1.4	0.2973	1.0	0.74	1678.1	15.4	1681.1	11.5	1684.7	17.4	1684.7	17.4	99.6
K15-Estadio-3-Spot 300	120	65252	1.2	9.8592	0.9	4.0331	1.3	0.2884	1.0	0.76	1633.5	14.8	1640.9	11.0	1650.4	16.2	1650.4	16.2	99.0
K15-Estadio-3-Spot 301	322	176540	0.6	9.7863	0.7	4.0423	1.4	0.2869	1.2	0.85	1626.0	16.8	1642.7	11.2	1664.1	13.4	1664.1	13.4	97.7
K15-Estadio-3-Spot 302	56	62579	1.1	9.6034	0.9	4.1968	1.4	0.2923	1.1	0.78	1653.1	16.0	1673.4	11.5	1699.0	16.2	1699.0	16.2	97.3
K15-Estadio-3-Spot 303	109	76671	1.2	9.8460	1.0	4.0234	1.5	0.2873	1.1	0.75	1628.1	16.4	1638.9	12.4	1652.9	18.7	1652.9	18.7	98.5
K15-Estadio-3-Spot 304	101	139716	1.8	9.7054	0.6	4.2678	1.2	0.3004	1.1	0.86	1693.3	15.7	1687.2	10.1	1679.5	11.5	1679.5	11.5	100.8
K15-Estadio-3-Spot 305	133	138964	1.5	9.7220	0.9	4.0479	1.2	0.2854	0.8	0.65	1618.6	11.6	1643.9	10.2	1676.3	17.5	1676.3	17.5	96.6
K15-Estadio-3-Spot 306	77	80534	1.7	9.8081	0.7	4.3625	1.2	0.3103	0.9	0.79	1742.3	14.0	1705.3	9.6	1660.0	13.4	1660.0	13.4	105.0
K15-Estadio-3-Spot 307	261	175072	2.0	9.8843	0.7	4.0444	1.1	0.2899	0.8	0.75	1641.2	11.8	1643.2	8.8	1645.7	13.2	1645.7	13.2	99.7
K15-Estadio-3-Spot 309	104	128791	2.5	9.4400	1.0	4.4501	1.5	0.3047	1.2	0.76	1714.5	17.5	1721.7	12.7	1730.5	18.4	1730.5	18.4	99.1
K15-Estadio-3-Spot 310	214	248474	1.9	9.8279	0.8	4.0239	1.3	0.2868	1.0	0.76	1625.6	14.4	1639.0	10.6	1656.3	15.7	1656.3	15.7	98.1
K15-Estadio-3-Spot 311	128	129505	1.7	9.8010	0.9	4.0885	1.4	0.2906	1.0	0.74	1644.7	14.5	1652.0	11.1	1661.4	17.0	1661.4	17.0	99.0
K15-Estadio-3-Spot 312	226	55524	1.2	9.8863	0.9	4.0076	1.3	0.2874	0.9	0.71	1628.3	13.2	1635.7	10.5	1645.3	16.9	1645.3	16.9	99.0
K15-Estadio-3-Spot 313	213	226860	3.3	9.4923	0.9	4.3325	1.3	0.2983	1.0	0.74	1682.7	14.7	1699.6	11.1	1720.4	16.7	1720.4	16.7	97.8
K15-Estadio-3-Spot 314	113	4361790	1.4	9.7921	1.0	4.1388	1.4	0.2939	1.0	0.72	1661.2	14.9	1662.0	11.5	1663.0	18.1	1663.0	18.1	99.9
K15-Estadio-3-Spot 315	297	122561	2.8	9.5269	0.7	4.3666	1.1	0.3017	0.9	0.81	1699.8	13.7	1706.0	9.4	1713.7	12.3	1713.7	12.3	99.2

K13-ES-5-Spot 1	220	125867	2.3	8.9500	0.7	5.0903	1.5	0.3304	1.3	0.89	1840.4	21.5	1834.5	12.8	1827.8	12.5	1827.8	12.5	100.7
K13-ES-5-Spot 2	305	91875	0.9	9.8562	0.8	4.0409	1.3	0.2889	1.0	0.77	1635.8	15.0	1642.5	10.9	1651.0	15.7	1651.0	15.7	99.1
K13-ES-5-Spot 3	482	150562	6.6	8.2014	1.1	4.7002	1.7	0.2796	1.3	0.77	1589.2	17.9	1767.3	13.8	1984.6	18.8	1984.6	18.8	80.1
K13-ES-5-Spot 5	77	49156	1.3	9.7045	1.2	4.2123	1.6	0.2965	1.1	0.68	1673.8	16.0	1676.4	13.2	1679.7	21.8	1679.7	21.8	99.7

K13-ES-5-Spot 7	328	94473	1.8	9.6024	0.9	4.2125	1.6	0.2934	1.3	0.83	1658.4	19.3	1676.5	13.1	1699.2	16.6	1699.2	16.6	97.6
K13-ES-5-Spot 8	75	86166	1.8	9.7532	1.3	4.1711	1.6	0.2950	0.8	0.54	1666.7	12.4	1668.4	12.8	1670.4	24.4	1670.4	24.4	99.8
K13-ES-5-Spot 9	585	58902	2.2	9.3949	0.8	4.5353	1.3	0.3090	1.1	0.81	1735.9	16.5	1737.5	11.2	1739.3	14.5	1739.3	14.5	99.8
K13-ES-5-Spot 10	54	69609	0.7	9.9206	1.5	4.0190	1.9	0.2892	1.3	0.66	1637.4	18.5	1638.1	15.7	1638.9	27.0	1638.9	27.0	99.9
K13-ES-5-Spot 11	483	212609	1.1	9.6834	0.9	4.0983	1.5	0.2878	1.2	0.79	1630.7	16.8	1654.0	12.0	1683.7	16.6	1683.7	16.6	96.9
K13-ES-5-Spot 12	498	54560	1.3	9.8793	0.8	3.6781	1.4	0.2635	1.2	0.82	1507.9	15.6	1566.6	11.3	1646.6	14.9	1646.6	14.9	91.6
K13-ES-5-Spot 13	209	66660	2.6	9.8021	0.8	4.1283	1.2	0.2935	0.9	0.77	1658.9	13.6	1659.9	9.9	1661.2	14.2	1661.2	14.2	99.9
K13-ES-5-Spot 14	237	113115	3.0	9.3393	0.9	4.6645	1.5	0.3159	1.2	0.80	1769.9	18.6	1760.9	12.6	1750.2	16.6	1750.2	16.6	101.1
K13-ES-5-Spot 15	314	195289	4.7	9.6255	1.0	4.0160	2.4	0.2804	2.2	0.91	1593.2	30.7	1637.4	19.5	1694.7	18.6	1694.7	18.6	94.0
K13-ES-5-Spot 16	572	97169	1.6	9.7717	0.9	4.1006	1.5	0.2906	1.3	0.82	1644.6	18.5	1654.4	12.6	1666.9	16.2	1666.9	16.2	98.7
K13-ES-5-Spot 18	724	155477	2.3	9.5454	0.6	3.9308	1.4	0.2721	1.3	0.90	1551.6	17.6	1620.0	11.5	1710.1	11.4	1710.1	11.4	90.7
K13-ES-5-Spot 19	218	104533	2.5	9.5216	0.8	3.9033	1.4	0.2696	1.2	0.82	1538.5	16.2	1614.4	11.7	1714.7	15.3	1714.7	15.3	89.7
K13-ES-5-Spot 20	120	198320	2.2	8.9470	0.9	5.0448	1.6	0.3274	1.3	0.82	1825.6	20.9	1826.9	13.6	1828.4	16.7	1828.4	16.7	99.8
K13-ES-5-Spot 22	105	86478	1.1	9.6128	1.2	4.2699	1.7	0.2977	1.2	0.70	1679.9	17.3	1687.6	13.8	1697.2	22.1	1697.2	22.1	99.0
K13-ES-5-Spot 23	112	65694	2.1	10.0981	1.2	4.0680	1.7	0.2979	1.2	0.73	1681.0	18.4	1647.9	13.8	1605.9	21.6	1605.9	21.6	104.7
K13-ES-5-Spot 25	126	68480	2.3	9.7803	0.9	4.1234	1.7	0.2925	1.4	0.82	1653.9	20.0	1659.0	13.6	1665.3	17.5	1665.3	17.5	99.3
K13-ES-5-Spot 26	228	85364	1.5	9.7908	1.0	4.1165	1.6	0.2923	1.2	0.79	1653.1	18.1	1657.6	12.8	1663.3	17.9	1663.3	17.9	99.4
K13-ES-5-Spot 27	367	151070	1.7	9.5320	0.8	4.4088	1.5	0.3048	1.3	0.83	1715.0	19.1	1714.0	12.6	1712.7	15.5	1712.7	15.5	100.1
K13-ES-5-Spot 28	190	237612	2.3	9.4995	0.9	4.5023	1.5	0.3102	1.2	0.81	1741.7	19.1	1731.4	12.8	1719.0	16.6	1719.0	16.6	101.3
K13-ES-5-Spot 29	257	249257	3.5	9.6444	0.9	4.1964	1.4	0.2935	1.1	0.79	1659.1	16.7	1673.3	11.8	1691.1	16.2	1691.1	16.2	98.1
K13-ES-5-Spot 30	113	135015	1.6	9.4979	1.2	4.4278	2.0	0.3050	1.5	0.79	1716.1	23.2	1717.6	16.2	1719.3	22.1	1719.3	22.1	99.8
K13-ES-5-Spot 31	945	62065	2.8	9.4076	0.7	3.5825	1.5	0.2444	1.3	0.89	1409.7	17.0	1545.7	12.0	1736.8	12.7	1736.8	12.7	81.2
K13-ES-5-Spot 32	78	107392	2.3	9.7121	1.1	4.2685	1.6	0.3007	1.1	0.72	1694.6	16.9	1687.3	12.9	1678.2	20.0	1678.2	20.0	101.0
K13-ES-5-Spot 33	204	73500	2.8	9.5195	1.1	4.3231	1.6	0.2985	1.1	0.71	1683.7	17.0	1697.8	13.3	1715.1	20.9	1715.1	20.9	98.2
K13-ES-5-Spot 34	101	65190	1.5	9.9360	1.3	4.0938	2.0	0.2950	1.5	0.75	1666.5	21.6	1653.1	15.9	1636.0	23.9	1636.0	23.9	101.9
K13-ES-5-Spot 35	193	128736	3.0	9.5744	1.1	4.2703	1.8	0.2965	1.3	0.76	1674.1	19.8	1687.7	14.5	1704.5	21.0	1704.5	21.0	98.2
K13-ES-5-Spot 36	199	68597	1.7	9.9068	0.9	4.2272	1.6	0.3037	1.4	0.84	1709.8	20.7	1679.3	13.5	1641.5	16.6	1641.5	16.6	104.2
K13-ES-5-Spot 37	464	73740	7.4	9.2212	0.9	4.6490	1.7	0.3109	1.5	0.86	1745.2	22.5	1758.1	14.4	1773.5	16.3	1773.5	16.3	98.4
K13-ES-5-Spot 38	417	1502609	1.0	9.5366	0.9	4.4034	1.5	0.3046	1.2	0.80	1713.9	17.6	1713.0	12.1	1711.8	16.1	1711.8	16.1	100.1
K13-ES-5-Spot 39	177	71061	2.1	9.7323	0.9	4.0128	1.2	0.2832	0.9	0.71	1607.7	12.2	1636.8	9.8	1674.4	15.8	1674.4	15.8	96.0
K13-ES-5-Spot 40	174	187487	1.5	9.6931	1.2	4.2783	1.7	0.3008	1.3	0.74	1695.1	18.7	1689.2	14.0	1681.8	21.3	1681.8	21.3	100.8
K13-ES-5-Spot 42	138	79084	1.1	9.8345	0.9	4.0635	1.4	0.2898	1.1	0.78	1640.7	15.4	1647.0	11.2	1655.0	16.1	1655.0	16.1	99.1
K13-ES-5-Spot 43	725	65835	1.5	9.3380	0.9	4.5651	1.8	0.3092	1.5	0.87	1736.6	23.6	1742.9	14.9	1750.5	16.3	1750.5	16.3	99.2
K13-ES-5-Spot 44	316	201337	2.1	9.2827	1.2	4.5313	1.6	0.3051	1.1	0.70	1716.4	17.2	1736.7	13.6	1761.3	21.3	1761.3	21.3	97.5
K13-ES-5-Spot 46	462	122431	1.4	9.5843	1.0	4.1223	1.7	0.2865	1.4	0.81	1624.3	20.0	1658.7	14.0	1702.6	18.3	1702.6	18.3	95.4
K13-ES-5-Spot 47	179	97973	1.3	9.8066	1.1	3.9170	1.9	0.2786	1.6	0.81	1584.3	21.8	1617.2	15.5	1660.3	20.7	1660.3	20.7	95.4
K13-ES-5-Spot 48	261	150630	2.9	9.4522	1.0	4.3079	1.7	0.2953	1.4	0.82	1668.1	20.9	1694.9	14.2	1728.2	18.1	1728.2	18.1	96.5
K13-ES-5-Spot 49	184	1354937	1.4	9.9025	1.1	4.0801	1.7	0.2930	1.3	0.78	1656.7	19.1	1650.3	13.7	1642.3	19.6	1642.3	19.6	100.9
K13-ES-5-Spot 50	533	78644	2.0	9.5034	0.8	4.3442	1.8	0.2994	1.6	0.88	1688.5	23.4	1701.8	14.7	1718.2	15.4	1718.2	15.4	98.3
K13-ES-5-Spot 51	183	114358	1.9	9.5846	0.8	4.2800	1.4	0.2975	1.1	0.80	1679.0	16.1	1689.5	11.2	1702.6	14.8	1702.6	14.8	98.6
K13-ES-5-Spot 52	135	113823	1.2	9.5666	0.8	4.3293	1.6	0.3004	1.3	0.86	1693.2	20.1	1699.0	12.9	1706.0	14.7	1706.0	14.7	99.2
K13-ES-5-Spot 53	782	78051	3.1	9.6856	0.8	4.2380	1.8	0.2977	1.6	0.90	1679.9	23.8	1681.4	14.7	1683.3	14.4	1683.3	14.4	99.8
K13-ES-5-Spot 54	198	62943	5.9	8.9828	0.8	4.9660	1.5	0.3235	1.3	0.86	1807.0	21.0	1813.6	13.1	1821.1	14.4	1821.1	14.4	99.2

K13-ES-5-Spot 55	165	59469	1.9	9.7221	1.0	4.1128	1.5	0.2900	1.2	0.77	1641.5	17.0	1656.8	12.5	1676.3	18.2	1676.3	18.2	97.9
K13-ES-5-Spot 56	159	63824	1.4	9.7538	1.0	4.1853	1.6	0.2961	1.3	0.77	1671.8	18.5	1671.1	13.4	1670.3	19.4	1670.3	19.4	100.1
K13-ES-5-Spot 58	366	283935	7.2	9.2229	0.9	4.5844	1.7	0.3067	1.4	0.84	1724.2	21.4	1746.4	14.0	1773.1	16.6	1773.1	16.6	97.2
K13-ES-5-Spot 59	80	108760	1.4	9.8522	1.2	4.0547	1.7	0.2897	1.2	0.69	1640.2	17.1	1645.2	13.9	1651.7	23.0	1651.7	23.0	99.3
K13-ES-5-Spot 60	723	74357	0.9	9.7700	0.8	4.0919	1.6	0.2899	1.3	0.85	1641.3	19.2	1652.7	12.7	1667.2	14.9	1667.2	14.9	98.4
K13-ES-5-Spot 61	174	169667	4.4	8.9143	1.3	4.9071	2.0	0.3173	1.5	0.76	1776.3	23.9	1803.5	17.1	1835.0	23.9	1835.0	23.9	96.8
K13-ES-5-Spot 62	76	59748	1.7	9.8461	1.1	4.3197	2.0	0.3085	1.7	0.83	1733.2	25.5	1697.1	16.7	1652.9	20.9	1652.9	20.9	104.9
K13-ES-5-Spot 63	416	76258	1.9	9.5359	0.8	4.4375	1.4	0.3069	1.2	0.83	1725.4	18.1	1719.4	12.0	1712.0	14.8	1712.0	14.8	100.8
K13-ES-5-Spot 64	105	101633	1.9	9.8952	1.1	4.0789	1.7	0.2927	1.3	0.75	1655.1	18.3	1650.1	13.5	1643.6	20.2	1643.6	20.2	100.7
K13-ES-5-Spot 65	124	137119	1.4	9.7808	0.9	4.1838	1.5	0.2968	1.3	0.82	1675.4	18.6	1670.9	12.7	1665.2	16.5	1665.2	16.5	100.6
K13-ES-5-Spot 66	435	1038469	2.7	9.5458	0.9	3.5795	1.5	0.2478	1.2	0.80	1427.2	15.2	1545.0	11.9	1710.1	16.7	1710.1	16.7	83.5
K13-ES-5-Spot 67	361	244105	4.8	8.8863	0.8	4.9087	1.8	0.3164	1.6	0.88	1771.9	24.3	1803.7	15.1	1840.7	15.4	1840.7	15.4	96.3
K13-ES-5-Spot 68	104	40714	1.4	9.4848	1.1	4.2560	1.7	0.2928	1.3	0.75	1655.4	18.8	1684.9	14.1	1721.8	20.8	1721.8	20.8	96.1
K13-ES-5-Spot 69	128	91938	1.4	9.6301	1.0	4.4769	1.6	0.3127	1.3	0.79	1753.9	19.8	1726.7	13.6	1693.9	18.7	1693.9	18.7	103.5
K13-ES-5-Spot 70	85	199333	2.2	9.8217	1.2	4.0772	2.0	0.2904	1.5	0.78	1643.7	22.1	1649.8	15.9	1657.5	22.7	1657.5	22.7	99.2
K13-ES-5-Spot 71	87	33494	2.0	9.9370	1.2	3.9497	2.0	0.2847	1.6	0.79	1614.8	22.3	1623.9	16.1	1635.8	22.7	1635.8	22.7	98.7
K13-ES-5-Spot 72	124	43552	2.0	9.7952	0.9	4.1334	1.5	0.2936	1.2	0.81	1659.7	18.0	1660.9	12.3	1662.5	16.3	1662.5	16.3	99.8
K13-ES-5-Spot 73	825	56048	3.6	9.2334	0.8	4.3587	1.8	0.2919	1.7	0.91	1651.0	24.2	1704.5	15.1	1771.0	13.8	1771.0	13.8	93.2
K13-ES-5-Spot 74	229	56031	1.4	9.7081	0.8	4.0842	1.4	0.2876	1.1	0.80	1629.4	15.9	1651.1	11.2	1679.0	15.3	1679.0	15.3	97.0
K13-ES-5-Spot 75	427	446185	1.0	9.6949	0.7	4.2538	1.4	0.2991	1.2	0.85	1686.9	17.6	1684.5	11.5	1681.5	13.5	1681.5	13.5	100.3
K13-ES-5-Spot 76	143	1996964	2.0	9.7317	1.0	4.1376	1.6	0.2920	1.3	0.80	1651.7	18.9	1661.8	13.2	1674.5	17.8	1674.5	17.8	98.6
K13-ES-5-Spot 77	144	109037	1.4	9.7768	1.0	3.9285	1.8	0.2786	1.5	0.85	1584.1	21.8	1619.6	14.8	1665.9	18.0	1665.9	18.0	95.1
K13-ES-5-Spot 78	344	120531	3.2	9.4830	1.1	3.6581	2.4	0.2516	2.2	0.89	1446.7	28.2	1562.3	19.5	1722.2	20.4	1722.2	20.4	84.0
K13-ES-5-Spot 80	193	54920	2.3	9.6518	0.9	4.0734	1.9	0.2851	1.6	0.86	1617.2	23.3	1649.0	15.4	1689.7	17.4	1689.7	17.4	95.7
K13-ES-5-Spot 81	164	74484	1.6	9.5748	1.0	4.2942	1.5	0.2982	1.2	0.78	1682.4	17.7	1692.2	12.6	1704.5	17.6	1704.5	17.6	98.7
K13-ES-5-Spot 82	135	627180	2.6	9.6200	1.2	4.2413	1.8	0.2959	1.3	0.75	1671.0	19.4	1682.1	14.5	1695.8	21.6	1695.8	21.6	98.5
K13-ES-5-Spot 83	289	125218	1.9	9.4278	0.9	4.3868	1.7	0.3000	1.4	0.83	1691.1	20.8	1709.9	14.0	1732.9	17.4	1732.9	17.4	97.6
K13-ES-5-Spot 84	250	133592	3.0	9.5280	0.8	4.3423	1.5	0.3001	1.3	0.84	1691.7	19.0	1701.4	12.5	1713.5	15.2	1713.5	15.2	98.7
K13-ES-5-Spot 86	112	104152	1.5	9.6659	1.0	4.0464	1.5	0.2837	1.2	0.77	1609.8	16.6	1643.6	12.3	1687.0	17.7	1687.0	17.7	95.4
K13-ES-5-Spot 87	152	252799	2.3	9.6037	0.9	4.2667	1.4	0.2972	1.1	0.75	1677.4	15.8	1687.0	11.7	1698.9	17.2	1698.9	17.2	98.7
K13-ES-5-Spot 88	617	221867	1.9	9.5841	0.8	4.2374	1.2	0.2945	0.9	0.76	1664.2	13.3	1681.3	9.8	1702.7	14.1	1702.7	14.1	97.7
K13-ES-5-Spot 89	265	203631	1.8	9.6806	1.0	4.0805	1.6	0.2865	1.2	0.79	1624.0	17.9	1650.4	12.9	1684.2	17.9	1684.2	17.9	96.4
K13-ES-5-Spot 90	81	93204	1.9	9.6271	1.2	4.2666	2.0	0.2979	1.5	0.78	1680.9	22.6	1687.0	16.0	1694.4	22.3	1694.4	22.3	99.2
K13-ES-5-Spot 91	120	65705	2.2	9.7288	1.0	4.0261	1.5	0.2841	1.2	0.75	1611.9	16.5	1639.5	12.4	1675.0	18.5	1675.0	18.5	96.2
K13-ES-5-Spot 92	490	229082	1.1	9.4407	0.8	4.0420	1.5	0.2768	1.2	0.84	1575.0	17.4	1642.7	12.1	1730.4	14.8	1730.4	14.8	91.0
K13-ES-5-Spot 93	414	58337	2.1	9.2222	0.9	4.6325	1.5	0.3098	1.2	0.82	1739.9	18.8	1755.1	12.6	1773.3	15.7	1773.3	15.7	98.1
K13-ES-5-Spot 94	529	61777	1.2	9.8048	0.6	3.6809	1.4	0.2618	1.2	0.89	1498.8	16.4	1567.2	11.0	1660.7	11.7	1660.7	11.7	90.3
K13-ES-5-Spot 95	163	70457	2.2	9.8105	0.9	4.0929	1.6	0.2912	1.4	0.83	1647.6	19.8	1652.9	13.4	1659.6	16.8	1659.6	16.8	99.3
K13-ES-5-Spot 96	304	106775	2.5	9.5283	0.9	4.2393	1.4	0.2930	1.1	0.78	1656.3	15.6	1681.7	11.3	1713.4	15.9	1713.4	15.9	96.7
K13-ES-5-Spot 97	104	161359	1.5	9.8934	1.2	3.9801	1.9	0.2856	1.4	0.76	1619.4	20.3	1630.2	15.1	1644.0	22.5	1644.0	22.5	98.5
K13-ES-5-Spot 98	101	163593	1.7	9.3619	0.8	4.4798	1.6	0.3042	1.4	0.86	1712.0	20.5	1727.2	13.2	1745.8	15.1	1745.8	15.1	98.1
K13-ES-5-Spot 99	118	68060	1.0	9.8571	1.3	4.0150	2.1	0.2870	1.6	0.78	1626.7	22.9	1637.2	16.7	1650.8	24.1	1650.8	24.1	98.5
K13-ES-5-Spot 100	111	76345	1.3	9.8719	1.1	4.0802	1.6	0.2921	1.1	0.70	1652.2	16.1	1650.4	12.9	1648.0	20.9	1648.0	20.9	100.3

K13-ES-5-Spot 101	354	94165	1.1	9.9228	1.1	3.9555	1.6	0.2847	1.2	0.73	1614.8	17.1	1625.1	13.3	1638.5	21.0	1638.5	21.0	98.6
K13-ES-5-Spot 102	130	163681	2.2	9.5113	1.1	4.3486	1.9	0.3000	1.5	0.80	1691.2	22.3	1702.6	15.6	1716.7	21.0	1716.7	21.0	98.5
K13-ES-5-Spot 103	275	54967	1.8	9.8974	1.0	4.0141	1.6	0.2881	1.2	0.76	1632.3	17.1	1637.1	12.7	1643.2	19.0	1643.2	19.0	99.3
K13-ES-5-Spot 105	253	532709	1.4	9.8030	0.9	4.0900	1.5	0.2908	1.2	0.81	1645.5	17.5	1652.3	12.2	1661.0	16.4	1661.0	16.4	99.1
K13-ES-5-Spot 106	229	199393	1.4	9.6638	1.1	4.2070	1.8	0.2949	1.4	0.79	1665.8	21.1	1675.4	14.9	1687.4	20.4	1687.4	20.4	98.7
K13-ES-5-Spot 107	165	103283	2.0	9.5860	0.9	4.3108	1.6	0.2997	1.4	0.84	1689.8	20.3	1695.4	13.5	1702.3	16.5	1702.3	16.5	99.3
K13-ES-5-Spot 108	382	161299	4.0	9.5245	1.0	4.3111	1.7	0.2978	1.4	0.80	1680.4	20.1	1695.5	14.1	1714.2	18.9	1714.2	18.9	98.0
K13-ES-5-Spot 110	239	83528	2.2	9.5103	1.1	4.3219	1.5	0.2981	1.0	0.70	1681.9	15.3	1697.5	12.2	1716.9	19.5	1716.9	19.5	98.0
K13-ES-5-Spot 111	267	183780	3.6	9.5631	1.0	4.2607	1.6	0.2955	1.2	0.78	1669.0	18.1	1685.8	13.0	1706.7	18.1	1706.7	18.1	97.8
K13-ES-5-Spot 112	196	50469	1.6	9.7148	0.9	4.1552	1.5	0.2928	1.1	0.78	1655.4	16.5	1665.2	11.9	1677.7	17.0	1677.7	17.0	98.7
K13-ES-5-Spot 113	447	228290	7.2	8.7963	0.7	5.1172	1.4	0.3265	1.2	0.86	1821.2	19.3	1839.0	11.9	1859.1	12.8	1859.1	12.8	98.0
K13-ES-5-Spot 115	310	184058	1.8	9.7970	0.9	4.0088	1.8	0.2848	1.5	0.86	1615.7	22.1	1636.0	14.7	1662.1	17.3	1662.1	17.3	97.2
K13-ES-5-Spot 116	75	36528	2.4	9.7897	1.2	4.0927	1.6	0.2906	1.1	0.67	1644.5	15.9	1652.9	13.4	1663.5	22.6	1663.5	22.6	98.9
K13-ES-5-Spot 117	134	140019	1.5	9.6866	1.3	4.1395	1.8	0.2908	1.3	0.71	1645.6	19.2	1662.1	15.1	1683.1	23.8	1683.1	23.8	97.8
K13-ES-5-Spot 118	132	197133	1.5	9.6823	1.1	4.3007	2.0	0.3020	1.6	0.82	1701.3	24.3	1693.5	16.3	1683.9	21.0	1683.9	21.0	101.0
K13-ES-5-Spot 119	182	81218	2.2	9.2181	1.0	4.5682	1.6	0.3054	1.3	0.79	1718.1	19.5	1743.5	13.6	1774.1	18.1	1774.1	18.1	96.8
K13-ES-5-Spot 120	170	119255	1.4	9.7613	0.8	4.1552	1.7	0.2942	1.5	0.87	1662.3	21.5	1665.2	13.7	1668.9	15.2	1668.9	15.2	99.6
K13-ES-5-Spot 121	261	155321	2.6	9.7397	1.0	4.1909	1.8	0.2960	1.5	0.84	1671.6	22.4	1672.2	14.9	1673.0	18.4	1673.0	18.4	99.9
K13-ES-5-Spot 122	555	376924	1.8	9.9009	0.8	4.0241	1.6	0.2890	1.4	0.87	1636.4	19.9	1639.1	12.9	1642.6	14.6	1642.6	14.6	99.6
K13-ES-5-Spot 123	272	109379	1.1	9.8344	0.9	3.7320	1.6	0.2662	1.3	0.82	1521.4	18.1	1578.3	13.1	1655.1	17.5	1655.1	17.5	91.9
K13-ES-5-Spot 124	68	73390	1.4	9.9510	1.1	3.9713	1.7	0.2866	1.3	0.77	1624.6	18.8	1628.4	13.8	1633.2	20.3	1633.2	20.3	99.5
K13-ES-5-Spot 125	86	33341	1.2	9.7203	1.2	4.1669	1.6	0.2938	1.1	0.69	1660.3	16.3	1667.5	13.2	1676.7	21.5	1676.7	21.5	99.0
K13-ES-5-Spot 126	187	2246619	1.0	9.6410	0.9	4.1643	1.6	0.2912	1.4	0.82	1647.4	19.6	1667.0	13.5	1691.8	17.4	1691.8	17.4	97.4
K13-ES-5-Spot 127	356	112997	1.1	9.8452	0.9	3.9868	1.6	0.2847	1.3	0.82	1614.8	18.5	1631.5	12.8	1653.0	16.8	1653.0	16.8	97.7
K13-ES-5-Spot 128	244	138660	2.6	9.5570	1.0	4.3358	1.8	0.3005	1.5	0.84	1694.0	22.8	1700.2	15.1	1707.9	18.4	1707.9	18.4	99.2
K13-ES-5-Spot 129	97	200929	1.4	9.8079	1.1	4.0818	2.0	0.2904	1.6	0.83	1643.3	23.9	1650.7	16.1	1660.1	20.2	1660.1	20.2	99.0
K13-ES-5-Spot 130	1005	300082	1.5	9.5128	0.8	3.7919	1.7	0.2616	1.5	0.89	1498.1	20.4	1591.0	13.8	1716.4	14.2	1716.4	14.2	87.3
K13-ES-5-Spot 131	91	42148	1.9	9.7824	0.9	4.0632	1.8	0.2883	1.6	0.88	1632.9	23.2	1646.9	15.0	1664.9	16.3	1664.9	16.3	98.1
K13-ES-5-Spot 132	136	108818	1.1	9.8285	1.0	3.9462	1.8	0.2813	1.5	0.81	1597.9	20.6	1623.2	14.5	1656.2	19.4	1656.2	19.4	96.5
K13-ES-5-Spot 133	194	216039	1.4	9.8542	0.9	4.0377	1.3	0.2886	1.0	0.75	1634.4	14.3	1641.8	10.8	1651.3	16.2	1651.3	16.2	99.0
K13-ES-5-Spot 134	124	231056	0.9	9.7881	0.8	4.0118	1.3	0.2848	1.1	0.81	1615.5	15.5	1636.6	10.9	1663.8	14.7	1663.8	14.7	97.1
K13-ES-5-Spot 135	225	235176	2.1	9.9434	0.9	3.9992	1.6	0.2884	1.3	0.82	1633.6	19.4	1634.0	13.3	1634.6	17.4	1634.6	17.4	99.9
K13-ES-5-Spot 136	308	218153	2.8	8.8969	0.9	4.8867	1.3	0.3153	0.9	0.72	1766.8	14.5	1800.0	11.0	1838.5	16.3	1838.5	16.3	96.1
K13-ES-5-Spot 137	150	87974	1.5	9.5595	0.8	4.2639	1.5	0.2956	1.3	0.86	1669.6	19.2	1686.4	12.5	1707.4	14.4	1707.4	14.4	97.8
K13-ES-5-Spot 138	99	676638	1.9	9.7264	1.1	4.1824	1.5	0.2950	1.1	0.71	1666.6	15.5	1670.6	12.3	1675.5	19.6	1675.5	19.6	99.5
K13-ES-5-Spot 139	264	277706	1.9	9.6032	0.8	4.1055	1.5	0.2859	1.3	0.85	1621.2	18.2	1655.4	12.2	1699.0	14.6	1699.0	14.6	95.4
K13-ES-5-Spot 140	496	244357	3.1	9.4296	0.7	4.4567	1.4	0.3048	1.2	0.86	1715.0	18.4	1723.0	11.8	1732.6	13.1	1732.6	13.1	99.0
K13-ES-5-Spot 141	313	91673	1.3	8.8035	0.8	5.2630	1.4	0.3360	1.1	0.81	1867.6	18.2	1862.9	11.8	1857.6	14.7	1857.6	14.7	100.5
K13-ES-5-Spot 143	187	576931	1.7	9.8329	0.9	3.9905	1.4	0.2846	1.1	0.75	1614.4	15.5	1632.3	11.7	1655.3	17.4	1655.3	17.4	97.5
K13-ES-5-Spot 144	245	208845	0.8	9.9204	0.9	4.0199	1.5	0.2892	1.2	0.79	1637.7	16.8	1638.2	12.0	1638.9	17.0	1638.9	17.0	99.9
K13-ES-5-Spot 145	329	172856	2.8	9.6757	0.9	4.1414	1.5	0.2906	1.2	0.79	1644.6	16.9	1662.5	12.1	1685.1	16.8	1685.1	16.8	97.6
K13-ES-5-Spot 146	309	131267	1.7	9.9148	0.8	4.0066	1.5	0.2881	1.3	0.85	1632.1	18.7	1635.5	12.4	1640.0	14.8	1640.0	14.8	99.5
K13-ES-5-Spot 147	271	197110	1.3	9.9234	1.2	3.9768	1.7	0.2862	1.2	0.71	1622.6	17.5	1629.5	13.8	1638.4	22.2	1638.4	22.2	99.0

K13-ES-5-Spot 148	64	31312	1.7	9.8776	1.3	4.1661	1.8	0.2985	1.3	0.70	1683.7	18.7	1667.4	14.7	1646.9	23.6	1646.9	23.6	102.2
K13-ES-5-Spot 149	300	117916	1.2	9.7662	0.9	4.1130	1.9	0.2913	1.6	0.87	1648.2	23.4	1656.9	15.1	1668.0	16.9	1668.0	16.9	98.8
K13-ES-5-Spot 150	255	124069	2.5	9.4631	0.8	4.4352	1.5	0.3044	1.2	0.84	1713.1	18.4	1718.9	12.0	1726.0	14.4	1726.0	14.4	99.2
K13-ES-5-Spot 151	171	51606	2.9	9.6776	0.8	4.2321	1.3	0.2970	0.9	0.74	1676.7	13.7	1680.3	10.3	1684.8	15.5	1684.8	15.5	99.5
K13-ES-5-Spot 152	143	67706	3.5	9.7060	1.1	4.2759	1.9	0.3010	1.6	0.82	1696.3	23.2	1688.7	15.7	1679.4	20.2	1679.4	20.2	101.0
K13-ES-5-Spot 153	127	104435	1.5	9.6496	1.2	4.2666	1.6	0.2986	1.1	0.69	1684.4	16.4	1686.9	13.2	1690.1	21.4	1690.1	21.4	99.7
K13-ES-5-Spot 155	131	173894	1.7	9.9442	1.0	3.7832	1.7	0.2729	1.3	0.79	1555.3	18.2	1589.2	13.4	1634.5	19.1	1634.5	19.1	95.2
K13-ES-5-Spot 156	281	77589	2.9	9.1988	0.8	4.6873	1.7	0.3127	1.5	0.88	1754.1	23.0	1765.0	14.2	1777.9	14.6	1777.9	14.6	98.7
K13-ES-5-Spot 157	407	83826	2.6	9.5591	0.9	4.2388	1.7	0.2939	1.5	0.87	1660.9	22.1	1681.6	14.3	1707.5	16.0	1707.5	16.0	97.3
K13-ES-5-Spot 158	483	100584	5.6	9.6193	0.9	4.3410	1.5	0.3029	1.3	0.82	1705.4	18.7	1701.2	12.6	1695.9	16.0	1695.9	16.0	100.6
K13-ES-5-Spot 160	88	60076	1.9	9.6558	1.2	4.2737	1.9	0.2993	1.5	0.76	1687.8	21.6	1688.3	15.8	1688.9	23.0	1688.9	23.0	99.9
K13-ES-5-Spot 161	69	27326	1.6	8.9082	2.9	4.5620	3.4	0.2947	1.8	0.52	1665.2	26.0	1742.4	28.1	1836.2	52.0	1836.2	52.0	90.7
K13-ES-5-Spot 163	128	246545	1.2	9.8470	1.0	4.0684	1.5	0.2906	1.2	0.78	1644.3	17.3	1648.0	12.5	1652.7	17.9	1652.7	17.9	99.5
K13-ES-5-Spot 164	95	174856	2.0	9.8501	1.2	4.0248	1.9	0.2875	1.4	0.76	1629.2	20.6	1639.2	15.3	1652.1	22.6	1652.1	22.6	98.6
K13-ES-5-Spot 165	97	62925	2.2	9.6889	1.1	4.2675	1.9	0.2999	1.6	0.84	1690.7	23.9	1687.1	15.8	1682.6	19.5	1682.6	19.5	100.5
K13-ES-5-Spot 166	197	169438	1.9	9.5432	1.1	4.2445	1.7	0.2938	1.3	0.77	1660.4	18.9	1682.7	13.8	1710.5	19.7	1710.5	19.7	97.1
K13-ES-5-Spot 168	645	66635	9.4	9.0390	1.2	4.2699	2.9	0.2799	2.7	0.92	1591.0	37.7	1687.6	24.0	1809.8	20.9	1809.8	20.9	87.9
K13-ES-5-Spot 169	163	107598	1.3	9.7351	0.8	4.1542	1.6	0.2933	1.4	0.85	1658.1	20.0	1665.0	13.1	1673.8	15.4	1673.8	15.4	99.1
K13-ES-5-Spot 170	134	132966	1.9	9.6064	1.0	4.2355	1.8	0.2951	1.5	0.84	1666.9	22.6	1680.9	15.0	1698.4	18.1	1698.4	18.1	98.1
K13-ES-5-Spot 171	217	172341	1.3	9.5844	0.9	3.7416	2.1	0.2601	1.9	0.91	1490.3	25.0	1580.3	16.6	1702.6	16.2	1702.6	16.2	87.5
K13-ES-5-Spot 172	212	1194356	2.0	9.5552	0.7	4.3427	1.4	0.3010	1.2	0.85	1696.0	18.0	1701.5	11.7	1708.2	13.7	1708.2	13.7	99.3
K13-ES-5-Spot 173	67	354504	1.3	9.7123	1.3	4.1803	1.9	0.2945	1.3	0.70	1663.8	19.2	1670.2	15.4	1678.2	24.9	1678.2	24.9	99.1
K13-ES-5-Spot 174	75	50674	1.5	9.7235	1.0	4.1402	1.5	0.2920	1.1	0.75	1651.4	16.7	1662.3	12.5	1676.1	18.5	1676.1	18.5	98.5
K13-ES-5-Spot 175	207	53394	1.5	9.5508	1.0	4.3846	1.7	0.3037	1.4	0.82	1709.7	21.0	1709.4	14.0	1709.1	17.7	1709.1	17.7	100.0
K13-ES-5-Spot 176	483	66657	1.8	9.4688	0.7	4.3903	1.0	0.3015	0.7	0.73	1698.8	10.8	1710.5	8.2	1725.0	12.3	1725.0	12.3	98.5
K13-ES-5-Spot 177	48	25466	2.0	9.7820	1.3	4.1205	1.8	0.2923	1.2	0.69	1653.2	17.9	1658.4	14.6	1665.0	24.0	1665.0	24.0	99.3
K13-ES-5-Spot 178	318	196703	1.6	6.8164	0.7	8.7028	1.5	0.4302	1.3	0.88	2306.8	25.1	2307.4	13.4	2307.8	12.0	2307.8	12.0	100.0
K13-ES-5-Spot 179	112	82050	1.6	9.8772	1.0	4.1175	1.6	0.2950	1.3	0.81	1666.3	19.6	1657.8	13.4	1647.0	17.8	1647.0	17.8	101.2
K13-ES-5-Spot 180	575	100960	3.9	9.4576	0.9	4.2211	1.5	0.2895	1.1	0.78	1639.2	16.5	1678.1	11.9	1727.1	16.5	1727.1	16.5	94.9
K13-ES-5-Spot 181	497	130684	6.6	9.7869	0.8	3.9340	1.7	0.2792	1.5	0.87	1587.5	20.4	1620.7	13.5	1664.0	15.1	1664.0	15.1	95.4
K13-ES-5-Spot 182	113	102353	1.8	9.6013	1.0	4.2045	1.5	0.2928	1.0	0.70	1655.4	14.9	1674.9	11.9	1699.4	19.1	1699.4	19.1	97.4
K13-ES-5-Spot 183	127	55857	2.2	9.5490	1.0	4.2799	1.7	0.2964	1.4	0.80	1673.5	20.4	1689.5	14.2	1709.4	19.0	1709.4	19.0	97.9
K13-ES-5-Spot 185	619	109210	1.4	9.3772	0.9	4.4496	1.4	0.3026	1.1	0.77	1704.3	16.0	1721.6	11.5	1742.8	16.2	1742.8	16.2	97.8
K13-ES-5-Spot 186	187	87269	2.8	9.5984	1.0	4.3382	1.6	0.3020	1.3	0.79	1701.2	19.4	1700.6	13.6	1699.9	18.7	1699.9	18.7	100.1
K13-ES-5-Spot 187	119	59668	3.0	9.4506	0.9	4.5270	1.7	0.3103	1.4	0.82	1742.1	20.8	1735.9	13.8	1728.5	17.3	1728.5	17.3	100.8
K13-ES-5-Spot 188	139	52871	1.4	9.5785	1.3	4.2179	2.1	0.2930	1.6	0.77	1656.6	23.5	1677.5	17.1	1703.8	24.4	1703.8	24.4	97.2
K13-ES-5-Spot 189	354	172861	1.5	9.0834	0.9	4.7077	1.7	0.3101	1.5	0.86	1741.4	22.5	1768.6	14.3	1800.9	15.6	1800.9	15.6	96.7
K13-ES-5-Spot 190	390	153875	2.5	9.4515	0.7	3.8238	1.6	0.2621	1.4	0.89	1500.7	19.2	1597.8	12.9	1728.3	13.2	1728.3	13.2	86.8
K13-ES-5-Spot 192	440	113099	5.1	9.2897	0.7	4.3348	1.5	0.2921	1.3	0.88	1651.8	19.6	1700.0	12.6	1759.9	13.5	1759.9	13.5	93.9
K13-ES-5-Spot 193	560	465230	3.8	9.6183	0.8	4.3414	1.6	0.3029	1.4	0.87	1705.4	20.8	1701.3	13.2	1696.1	14.6	1696.1	14.6	100.5
K13-ES-5-Spot 194	365	130274	1.9	9.7504	1.0	4.1242	1.8	0.2917	1.5	0.84	1649.8	22.3	1659.1	14.9	1670.9	18.0	1670.9	18.0	98.7
K13-ES-5-Spot 195	200	140641	1.6	9.6837	0.8	4.1440	1.2	0.2910	0.9	0.74	1646.8	13.4	1663.0	10.2	1683.6	15.4	1683.6	15.4	97.8
K13-ES-5-Spot 196	537	25206	1.8	8.7302	2.1	4.3884	2.3	0.2779	1.0	0.43	1580.6	13.9	1710.2	18.8	1872.7	37.0	1872.7	37.0	84.4

K13-ES-5-Spot 197	268	61855	1.7	9.2490	0.8	4.5805	1.5	0.3073	1.3	0.86	1727.2	19.1	1745.7	12.3	1768.0	13.9	1768.0	13.9	97.7
K13-ES-5-Spot 198	272	215540	1.5	9.8351	0.8	3.9481	1.4	0.2816	1.1	0.79	1599.5	15.3	1623.6	11.0	1654.9	15.3	1654.9	15.3	96.7
K13-ES-5-Spot 199	552	538232	2.1	7.6855	1.2	6.8562	2.0	0.3822	1.6	0.81	2086.4	29.1	2093.0	17.8	2099.5	20.6	2099.5	20.6	99.4
K13-ES-5-Spot 200	113	78647	0.9	9.8560	1.1	4.0504	1.6	0.2895	1.2	0.75	1639.2	17.7	1644.4	13.3	1651.0	20.1	1651.0	20.1	99.3
K13-ES-5-Spot 201	95	43323	1.4	9.6484	1.5	4.1161	2.1	0.2880	1.4	0.69	1631.7	20.8	1657.5	17.2	1690.4	28.2	1690.4	28.2	96.5
K13-ES-5-Spot 202	239	73439	2.3	9.5282	0.7	4.1467	1.3	0.2866	1.0	0.82	1624.3	15.0	1663.6	10.4	1713.4	13.2	1713.4	13.2	94.8
K13-ES-5-Spot 203	359	899029	1.1	9.8620	0.8	3.4145	1.8	0.2442	1.6	0.89	1408.6	20.9	1507.7	14.5	1649.9	15.3	1649.9	15.3	85.4
K13-ES-5-Spot 205	120	71799	1.1	9.8375	1.0	3.9456	1.6	0.2815	1.3	0.80	1599.0	18.4	1623.1	13.2	1654.5	18.3	1654.5	18.3	96.6
K13-ES-5-Spot 206	305	195294	2.5	9.5064	0.8	4.3387	1.5	0.2991	1.2	0.85	1687.0	18.5	1700.8	12.0	1717.7	13.9	1717.7	13.9	98.2
K13-ES-5-Spot 207	224	203258	2.0	9.5609	1.1	4.1803	1.7	0.2899	1.4	0.78	1640.9	19.7	1670.2	14.3	1707.1	20.3	1707.1	20.3	96.1
K13-ES-5-Spot 208	440	126571	2.6	9.4677	0.8	4.1296	1.6	0.2836	1.4	0.86	1609.3	19.8	1660.2	13.2	1725.2	15.1	1725.2	15.1	93.3
K13-ES-5-Spot 209	150	310186	0.8	9.7561	1.3	3.8034	1.9	0.2691	1.4	0.75	1536.3	19.7	1593.5	15.4	1669.9	23.5	1669.9	23.5	92.0
K13-ES-5-Spot 210	148	80865	2.2	9.6837	1.0	4.1836	1.6	0.2938	1.3	0.80	1660.6	19.0	1670.8	13.3	1683.6	18.1	1683.6	18.1	98.6
K13-ES-5-Spot 211	187	444905	1.1	9.7966	0.7	4.0748	1.2	0.2895	1.0	0.79	1639.1	13.8	1649.3	9.9	1662.2	13.8	1662.2	13.8	98.6
K13-ES-5-Spot 212	152	81244	1.2	9.7107	1.2	4.1536	1.8	0.2925	1.3	0.73	1654.2	19.2	1664.9	14.7	1678.5	22.4	1678.5	22.4	98.6
K13-ES-5-Spot 213	163	541432	2.6	9.7939	1.2	4.1688	1.9	0.2961	1.5	0.78	1672.0	21.7	1667.9	15.6	1662.7	22.2	1662.7	22.2	100.6
K13-ES-5-Spot 214	133	130559	2.3	9.7708	1.0	4.1742	1.8	0.2958	1.5	0.82	1670.5	21.7	1669.0	14.7	1667.1	19.0	1667.1	19.0	100.2
K13-ES-5-Spot 215	117	44604	2.1	9.6753	1.2	4.1728	1.6	0.2928	1.2	0.71	1655.6	17.2	1668.7	13.5	1685.2	21.2	1685.2	21.2	98.2
K13-ES-5-Spot 216	443	63325	4.6	9.5466	0.6	4.3083	1.3	0.2983	1.1	0.89	1682.9	16.8	1695.0	10.6	1709.9	10.9	1709.9	10.9	98.4
K13-ES-5-Spot 217	110	127855	2.5	9.7011	0.9	4.2081	1.5	0.2961	1.2	0.79	1671.8	17.9	1675.6	12.6	1680.3	17.4	1680.3	17.4	99.5
K13-ES-5-Spot 218	504	164081	2.0	9.4911	0.7	4.2991	1.5	0.2959	1.4	0.90	1671.1	20.4	1693.2	12.6	1720.6	12.2	1720.6	12.2	97.1
K13-ES-5-Spot 219	334	60361	3.0	9.4628	0.8	4.2284	1.5	0.2902	1.3	0.86	1642.5	18.7	1679.5	12.3	1726.1	14.1	1726.1	14.1	95.2
K13-ES-5-Spot 220	328	109974	3.0	9.4309	0.9	4.4232	1.9	0.3025	1.6	0.87	1703.9	24.0	1716.7	15.3	1732.3	17.0	1732.3	17.0	98.4
K13-ES-5-Spot 221	570	93869	5.0	9.2155	0.8	4.2682	1.5	0.2853	1.3	0.84	1617.9	18.5	1687.2	12.7	1774.6	15.3	1774.6	15.3	91.2
K13-ES-5-Spot 222	586	66738	2.5	9.5885	0.9	3.4288	1.9	0.2384	1.7	0.89	1378.6	21.6	1511.0	15.3	1701.8	16.3	1701.8	16.3	81.0
K13-ES-5-Spot 223	297	52323	1.9	9.4512	0.8	4.1773	1.5	0.2863	1.3	0.86	1623.2	18.8	1669.6	12.5	1728.4	14.4	1728.4	14.4	93.9
K13-ES-5-Spot 224	40	31661	0.8	9.8415	1.9	4.0797	2.4	0.2912	1.5	0.60	1647.5	21.1	1650.3	19.6	1653.7	35.6	1653.7	35.6	99.6
K13-ES-5-Spot 225	108	67034	0.9	9.8942	1.0	4.0777	1.5	0.2926	1.2	0.77	1654.6	16.9	1649.8	12.3	1643.8	17.8	1643.8	17.8	100.7
K13-ES-5-Spot 226	181	113395	3.7	9.3509	1.0	4.5898	1.6	0.3113	1.2	0.79	1747.0	18.9	1747.4	13.1	1747.9	17.7	1747.9	17.7	99.9
K13-ES-5-Spot 227	136	113039	1.2	9.7351	0.9	4.1180	1.6	0.2908	1.3	0.83	1645.3	18.9	1657.9	12.8	1673.8	16.3	1673.8	16.3	98.3
K13-ES-5-Spot 228	400	88406	1.4	9.5474	0.9	4.1842	1.4	0.2897	1.1	0.79	1640.2	16.0	1670.9	11.5	1709.8	15.8	1709.8	15.8	95.9
K13-ES-5-Spot 229	147	104536	1.6	9.8139	0.9	4.1160	1.2	0.2930	0.8	0.69	1656.3	12.3	1657.5	9.9	1658.9	16.3	1658.9	16.3	99.8
K13-ES-5-Spot 231	306	183252	2.3	9.4708	1.0	4.4913	1.6	0.3085	1.3	0.79	1733.3	19.4	1729.4	13.4	1724.6	18.1	1724.6	18.1	100.5
K13-ES-5-Spot 232	161	50140	2.2	9.8871	1.1	4.0536	1.6	0.2907	1.2	0.74	1644.9	17.8	1645.0	13.4	1645.2	20.4	1645.2	20.4	100.0
K13-ES-5-Spot 234	306	217591	11.4	9.5243	0.8	4.3088	1.4	0.2976	1.2	0.84	1679.6	17.6	1695.1	11.6	1714.2	14.0	1714.2	14.0	98.0
K13-ES-5-Spot 235	458	98978	2.2	9.4066	0.8	4.3522	1.8	0.2969	1.6	0.89	1676.0	23.6	1703.3	14.9	1737.0	15.0	1737.0	15.0	96.5
K13-ES-5-Spot 236	138	107176	2.0	9.5592	1.3	4.2491	1.9	0.2946	1.4	0.74	1664.4	20.3	1683.6	15.4	1707.5	23.3	1707.5	23.3	97.5
K13-ES-5-Spot 238	134	201804	3.2	9.5764	0.8	4.2940	1.4	0.2982	1.1	0.79	1682.6	16.0	1692.2	11.3	1704.2	15.6	1704.2	15.6	98.7
K13-ES-5-Spot 239	563	778283	2.8	9.5230	1.1	4.3367	1.9	0.2995	1.6	0.82	1688.9	23.7	1700.4	16.0	1714.4	20.2	1714.4	20.2	98.5
K13-ES-5-Spot 240	125	924855	2.0	9.7603	1.1	4.2063	2.0	0.2978	1.6	0.82	1680.2	24.1	1675.3	16.4	1669.1	21.2	1669.1	21.2	100.7
K13-ES-5-Spot 241	277	91092	1.9	9.8058	1.0	4.2284	1.9	0.3007	1.6	0.85	1694.9	23.9	1679.6	15.4	1660.5	18.2	1660.5	18.2	102.1
K13-ES-5-Spot 242	271	340906	1.7	9.9480	0.8	3.9900	1.6	0.2879	1.4	0.88	1630.9	20.8	1632.2	13.2	1633.8	14.1	1633.8	14.1	99.8
K13-ES-5-Spot 243	480	121060	2.9	5.5919	1.1	12.3444	1.8	0.5006	1.5	0.79	2616.6	31.2	2631.0	17.2	2642.0	18.5	2642.0	18.5	99.0

K13-ES-5-Spot 244	53	40224	1.5	9.8472	1.2	4.1095	1.8	0.2935	1.3	0.75	1659.0	19.6	1656.2	14.7	1652.7	22.1	1652.7	22.1	100.4
K13-ES-5-Spot 245	296	124826	5.3	9.6338	0.8	4.2779	1.7	0.2989	1.6	0.90	1685.8	23.3	1689.1	14.3	1693.2	13.8	1693.2	13.8	99.6
K13-ES-5-Spot 246	160	67417	1.5	9.6134	1.0	4.3748	1.8	0.3050	1.4	0.80	1716.2	21.2	1707.6	14.5	1697.1	19.3	1697.1	19.3	101.1
K13-ES-5-Spot 247	124	158893	1.8	9.7378	1.1	4.2788	1.7	0.3022	1.3	0.78	1702.2	20.1	1689.3	14.2	1673.3	19.8	1673.3	19.8	101.7
K13-ES-5-Spot 248	169	55136	1.4	9.8727	1.0	4.0218	1.4	0.2880	1.0	0.70	1631.4	13.8	1638.6	11.1	1647.9	17.9	1647.9	17.9	99.0
K13-ES-5-Spot 249	368	191453	1.7	9.9150	0.9	3.9656	1.4	0.2852	1.0	0.74	1617.3	14.5	1627.2	11.1	1639.9	17.1	1639.9	17.1	98.6
K13-ES-5-Spot 251	175	87391	4.2	9.5442	1.2	4.4989	2.1	0.3114	1.6	0.80	1747.7	25.1	1730.8	17.0	1710.4	22.7	1710.4	22.7	102.2
K13-ES-5-Spot 252	187	81280	2.3	9.2845	1.2	4.6775	1.6	0.3150	1.1	0.69	1765.1	17.4	1763.2	13.6	1761.0	21.5	1761.0	21.5	100.2
K13-ES-5-Spot 253	52	26779	1.1	9.8432	1.5	4.0748	2.0	0.2909	1.2	0.63	1646.0	18.1	1649.3	16.1	1653.4	28.5	1653.4	28.5	99.6
K13-ES-5-Spot 254	112	1956688	1.7	9.6651	0.8	4.2389	1.3	0.2971	1.1	0.80	1677.1	15.7	1681.6	11.0	1687.2	14.9	1687.2	14.9	99.4
K13-ES-5-Spot 255	138	166046	1.9	9.5570	1.0	4.4223	1.7	0.3065	1.4	0.82	1723.6	20.8	1716.5	13.9	1707.9	17.7	1707.9	17.7	100.9
K13-ES-5-Spot 256	174	57911	0.7	9.9381	1.0	3.9932	1.9	0.2878	1.6	0.84	1630.6	22.9	1632.8	15.5	1635.6	19.5	1635.6	19.5	99.7
K13-ES-5-Spot 257	140	108704	0.9	9.7242	1.2	4.1613	2.4	0.2935	2.1	0.87	1658.9	30.9	1666.4	19.8	1675.9	21.9	1675.9	21.9	99.0
K13-ES-5-Spot 258	78	178508	2.3	9.7940	1.3	4.1365	2.2	0.2938	1.7	0.80	1660.6	25.3	1661.5	17.7	1662.7	24.1	1662.7	24.1	99.9
K13-ES-5-Spot 259	201	177591	1.5	10.0097	1.1	3.9867	1.9	0.2894	1.5	0.80	1638.7	21.7	1631.5	15.3	1622.3	21.2	1622.3	21.2	101.0
K13-ES-5-Spot 260	156	238560	2.3	9.7848	1.2	4.1046	2.0	0.2913	1.6	0.81	1648.0	23.4	1655.2	16.2	1664.4	21.5	1664.4	21.5	99.0
K13-ES-5-Spot 261	202	159977	1.9	9.6133	1.1	4.1889	1.7	0.2921	1.4	0.79	1651.8	19.8	1671.9	14.1	1697.1	19.6	1697.1	19.6	97.3
K13-ES-5-Spot 262	146	119568	1.5	9.7412	0.9	4.2100	1.5	0.2974	1.2	0.80	1678.6	18.3	1676.0	12.7	1672.7	17.2	1672.7	17.2	100.4
K13-ES-5-Spot 263	443	297573	2.3	8.7356	0.8	5.2104	1.4	0.3301	1.2	0.82	1838.9	18.4	1854.3	11.9	1871.6	14.3	1871.6	14.3	98.3
K13-ES-5-Spot 264	302	110857	6.4	9.5685	0.7	4.2839	1.3	0.2973	1.1	0.83	1677.9	15.7	1690.3	10.6	1705.7	13.2	1705.7	13.2	98.4
K13-ES-5-Spot 265	251	93947	2.5	9.0849	1.0	4.7464	1.6	0.3127	1.2	0.77	1754.2	18.9	1775.5	13.3	1800.6	18.3	1800.6	18.3	97.4
K13-ES-5-Spot 266	84	508759	1.2	9.7660	1.2	4.1214	1.8	0.2919	1.3	0.75	1651.1	19.2	1658.6	14.3	1668.0	21.5	1668.0	21.5	99.0
K13-ES-5-Spot 267	113	114877	1.6	9.7665	1.1	4.0973	1.6	0.2902	1.1	0.70	1642.6	16.4	1653.8	13.2	1667.9	21.3	1667.9	21.3	98.5
K13-ES-5-Spot 268	231	98471	2.1	9.7597	0.9	4.2254	1.4	0.2991	1.0	0.73	1686.8	15.1	1679.0	11.4	1669.2	17.4	1669.2	17.4	101.1
K13-ES-5-Spot 269	340	205450	2.0	9.7052	0.7	4.2263	1.5	0.2975	1.3	0.89	1678.8	19.3	1679.1	12.0	1679.5	12.4	1679.5	12.4	100.0
K13-ES-5-Spot 270	124	154225	2.9	9.3872	1.2	4.6015	1.9	0.3133	1.5	0.78	1756.8	23.0	1749.5	15.9	1740.8	21.7	1740.8	21.7	100.9
K13-ES-5-Spot 271	270	187078	2.7	9.4909	0.7	4.4395	1.4	0.3056	1.2	0.88	1719.0	18.3	1719.7	11.5	1720.7	12.3	1720.7	12.3	99.9
K13-ES-5-Spot 272	64	45794	1.1	9.8693	1.6	4.0482	2.1	0.2898	1.3	0.65	1640.4	19.5	1643.9	16.9	1648.5	29.3	1648.5	29.3	99.5
K13-ES-5-Spot 273	178	433254	3.3	9.1625	1.1	4.7482	2.0	0.3155	1.6	0.84	1767.9	25.3	1775.8	16.4	1785.1	19.3	1785.1	19.3	99.0
K13-ES-5-Spot 274	80	56874	1.0	9.6500	1.2	4.2445	1.8	0.2971	1.3	0.73	1676.7	19.4	1682.7	14.8	1690.1	22.7	1690.1	22.7	99.2
K13-ES-5-Spot 275	842	130223	1.4	9.6329	0.7	3.8336	1.1	0.2678	0.9	0.78	1529.8	12.0	1599.8	9.1	1693.3	13.2	1693.3	13.2	90.3
K13-ES-5-Spot 276	376	239978	1.9	9.8637	0.8	3.9213	1.4	0.2805	1.1	0.82	1594.0	15.8	1618.1	11.0	1649.6	14.5	1649.6	14.5	96.6
K13-ES-5-Spot 277	388	116296	1.8	9.3494	1.0	4.5590	1.7	0.3091	1.4	0.81	1736.5	20.8	1741.8	14.1	1748.2	18.3	1748.2	18.3	99.3
K13-ES-5-Spot 278	121	147013	1.4	9.9322	1.0	4.0967	1.7	0.2951	1.4	0.83	1667.0	20.9	1653.6	14.0	1636.7	17.7	1636.7	17.7	101.8
K13-ES-5-Spot 279	377	366434	1.6	9.9309	0.8	3.9182	1.7	0.2822	1.5	0.87	1602.5	20.7	1617.4	13.5	1636.9	15.0	1636.9	15.0	97.9
K13-ES-5-Spot 280	114	112795	1.7	9.3657	2.0	4.2806	2.2	0.2908	1.0	0.46	1645.4	14.7	1689.6	18.2	1745.0	35.9	1745.0	35.9	94.3
K13-ES-5-Spot 281	195	208479	2.0	9.7514	1.1	4.1186	1.8	0.2913	1.4	0.80	1648.0	20.7	1658.0	14.5	1670.8	19.5	1670.8	19.5	98.6
K13-ES-5-Spot 282	85	43006	1.7	9.5506	1.5	4.2645	1.9	0.2954	1.2	0.65	1668.4	18.2	1686.5	15.7	1709.1	26.7	1709.1	26.7	97.6
K13-ES-5-Spot 284	70	42914	1.5	9.8536	1.4	4.0875	1.9	0.2921	1.4	0.70	1652.1	19.8	1651.8	15.7	1651.5	25.4	1651.5	25.4	100.0
K13-ES-5-Spot 285	225	123190	1.3	9.7903	1.0	3.9593	1.7	0.2811	1.4	0.83	1597.1	20.2	1625.9	13.9	1663.4	17.8	1663.4	17.8	96.0
K13-ES-5-Spot 286	212	100185	2.2	9.6680	0.9	4.2408	1.8	0.2974	1.6	0.88	1678.2	23.5	1682.0	14.8	1686.6	15.7	1686.6	15.7	99.5
K13-ES-5-Spot 287	68	53641	1.4	9.7171	1.4	4.0489	2.0	0.2853	1.4	0.69	1618.2	19.5	1644.1	16.2	1677.3	26.7	1677.3	26.7	96.5
K13-ES-5-Spot 288	638	133490	2.7	8.7517	0.7	4.3219	1.5	0.2743	1.4	0.88	1562.7	18.7	1697.6	12.7	1868.3	13.3	1868.3	13.3	83.6

K13-ES-5-Spot 289	234	161092	2.2	9.0735	0.9	4.8078	1.4	0.3164	1.1	0.76	1772.1	16.6	1786.3	11.9	1802.9	16.8	1802.9	16.8	98.3
K13-ES-5-Spot 291	250	123779	1.3	9.6050	0.9	3.7468	2.0	0.2610	1.8	0.90	1495.0	24.2	1581.4	16.2	1698.7	16.5	1698.7	16.5	88.0
K13-ES-5-Spot 293	147	48649	0.9	9.3856	1.1	3.7941	1.5	0.2583	1.0	0.66	1481.0	13.3	1591.5	12.2	1741.1	20.7	1741.1	20.7	85.1
K13-ES-5-Spot 294	242	76229	1.8	9.4043	1.0	4.6910	1.8	0.3200	1.6	0.85	1789.5	24.4	1765.6	15.4	1737.5	18.0	1737.5	18.0	103.0
K13-ES-5-Spot 295	113	57546	2.0	9.7031	1.2	4.1379	1.7	0.2912	1.1	0.66	1647.5	15.9	1661.8	13.5	1679.9	22.9	1679.9	22.9	98.1
K13-ES-5-Spot 297	340	99614	2.5	9.5094	0.6	4.0271	1.5	0.2777	1.4	0.90	1580.0	19.0	1639.7	12.2	1717.1	11.9	1717.1	11.9	92.0
K13-ES-5-Spot 298	127	159831	1.7	9.7088	1.0	4.1031	1.8	0.2889	1.5	0.82	1636.1	21.1	1654.9	14.5	1678.9	18.5	1678.9	18.5	97.5
K13-ES-5-Spot 299	90	208478	2.0	9.8086	1.1	4.1833	1.8	0.2976	1.4	0.78	1679.4	20.1	1670.8	14.4	1659.9	20.6	1659.9	20.6	101.2
K13-ES-5-Spot 300	108	190775	1.7	9.7261	1.3	4.2488	2.2	0.2997	1.8	0.82	1689.9	26.7	1683.5	18.0	1675.6	23.2	1675.6	23.2	100.9
K13-ES-5-Spot 301	290	69414	3.3	8.6332	1.0	5.3973	1.7	0.3379	1.3	0.81	1876.8	21.8	1884.4	14.3	1892.8	17.7	1892.8	17.7	99.2
K13-ES-5-Spot 302	136	208286	0.9	9.7955	1.2	3.5405	2.7	0.2515	2.4	0.90	1446.4	31.0	1536.3	21.2	1662.4	22.0	1662.4	22.0	87.0
K13-ES-5-Spot 303	214	67177	2.0	9.9110	0.9	3.9890	1.7	0.2867	1.4	0.85	1625.2	20.4	1632.0	13.5	1640.7	16.2	1640.7	16.2	99.1
K13-ES-5-Spot 304	350	61592	0.9	9.7619	0.9	4.0906	1.4	0.2896	1.0	0.76	1639.6	14.8	1652.4	11.0	1668.8	16.3	1668.8	16.3	98.3
K13-ES-5-Spot 305	433	182571	1.6	9.5333	0.9	4.0016	1.3	0.2767	0.9	0.73	1574.6	13.0	1634.5	10.3	1712.5	15.9	1712.5	15.9	92.0
K13-ES-5-Spot 307	351	221414	1.7	9.7020	0.9	4.1067	1.7	0.2890	1.4	0.84	1636.4	20.6	1655.6	14.0	1680.1	17.3	1680.1	17.3	97.4
K13-ES-5-Spot 308	217	123484	1.7	9.7836	0.9	4.0407	1.6	0.2867	1.3	0.83	1625.1	18.5	1642.4	12.6	1664.6	16.0	1664.6	16.0	97.6
K13-ES-5-Spot 309	468	96791	1.4	9.8114	0.9	3.4638	1.6	0.2465	1.3	0.83	1420.3	16.6	1519.0	12.4	1659.4	16.3	1659.4	16.3	85.6
K13-ES-5-Spot 310	198	406049	1.5	9.7360	0.9	4.0137	1.6	0.2834	1.3	0.83	1608.5	19.1	1637.0	13.1	1673.7	16.4	1673.7	16.4	96.1
K13-ES-5-Spot 311	179	156867	1.4	9.8333	1.0	4.1214	1.8	0.2939	1.6	0.85	1661.1	22.9	1658.6	15.0	1655.3	18.0	1655.3	18.0	100.4
K13-ES-5-Spot 312	281	63369	4.4	5.8849	0.7	11.0685	1.4	0.4724	1.3	0.87	2494.2	26.1	2528.9	13.5	2556.9	11.8	2556.9	11.8	97.5
K13-ES-5-Spot 313	102	141542	2.2	9.5975	1.2	4.3311	1.7	0.3015	1.3	0.73	1698.6	19.1	1699.3	14.4	1700.1	22.0	1700.1	22.0	99.9
K13-ES-5-Spot 314	240	122948	1.3	9.5241	0.9	4.2900	1.5	0.2963	1.2	0.79	1673.1	18.0	1691.4	12.7	1714.2	17.4	1714.2	17.4	97.6
K13-ES-5-Spot 315	123	67887	3.4	9.5867	0.9	4.4528	1.5	0.3096	1.2	0.79	1738.7	18.4	1722.2	12.6	1702.2	17.1	1702.2	17.1	102.1

K15-SAIS-Spot 1	1068	42341	1.0	8.7589	0.7	4.1451	1.3	0.2633	1.1	0.82	1506.8	14.4	1663.2	10.7	1866.8	13.4	1866.8	13.4	80.7
K15-SAIS-Spot 2	311	145465	1.1	9.8571	0.7	4.0394	1.6	0.2888	1.4	0.89	1635.4	20.7	1642.2	13.2	1650.8	13.9	1650.8	13.9	99.1
K15-SAIS-Spot 3	250	56196	2.9	9.6298	0.9	4.2851	1.5	0.2993	1.2	0.80	1687.8	17.2	1690.5	12.0	1693.9	16.2	1693.9	16.2	99.6
K15-SAIS-Spot 4	107	29360	1.4	9.0042	1.4	4.5926	2.3	0.2999	1.8	0.79	1690.9	27.4	1747.9	19.5	1816.8	26.1	1816.8	26.1	93.1
K15-SAIS-Spot 5	390	204749	1.4	9.6583	1.0	4.2597	1.7	0.2984	1.3	0.80	1683.3	19.8	1685.6	13.7	1688.5	18.3	1688.5	18.3	99.7
K15-SAIS-Spot 7	301	140268	1.7	9.2322	0.9	4.7196	1.8	0.3160	1.5	0.86	1770.2	23.3	1770.7	14.7	1771.3	16.5	1771.3	16.5	99.9
K15-SAIS-Spot 8	200	79286	0.2	9.7036	1.0	3.5982	1.9	0.2532	1.6	0.85	1455.1	20.9	1549.1	14.9	1679.8	18.0	1679.8	18.0	86.6
K15-SAIS-Spot 9	519	235473	2.2	9.4864	0.6	4.0194	2.2	0.2765	2.1	0.96	1573.9	29.4	1638.1	17.8	1721.5	10.6	1721.5	10.6	91.4
K15-SAIS-Spot 10	260	69995	1.5	9.8800	0.9	4.0429	1.5	0.2897	1.3	0.82	1640.0	18.1	1642.9	12.4	1646.5	16.0	1646.5	16.0	99.6
K15-SAIS-Spot 11	144	76370	1.6	9.9136	1.2	4.0623	1.9	0.2921	1.5	0.77	1651.9	21.6	1646.8	15.6	1640.2	22.5	1640.2	22.5	100.7
K15-SAIS-Spot 12	353	75021	1.3	9.6557	1.0	3.8778	1.9	0.2716	1.7	0.86	1548.7	22.8	1609.1	15.5	1689.0	17.8	1689.0	17.8	91.7
K15-SAIS-Spot 13	65	208062	1.3	9.8709	1.1	4.0336	1.8	0.2888	1.5	0.81	1635.4	21.6	1641.0	15.0	1648.2	19.8	1648.2	19.8	99.2
K15-SAIS-Spot 14	440	6333224	2.3	9.3648	0.7	4.4189	1.5	0.3001	1.3	0.89	1692.0	19.3	1715.9	12.1	1745.2	12.3	1745.2	12.3	97.0
K15-SAIS-Spot 15	62	69487	1.9	9.6516	1.1	4.3122	1.5	0.3019	1.0	0.68	1700.5	14.8	1695.7	12.1	1689.7	19.8	1689.7	19.8	100.6
K15-SAIS-Spot 16	281	187424	1.4	9.8071	0.9	4.0460	1.4	0.2878	1.1	0.78	1630.4	15.9	1643.5	11.5	1660.2	16.5	1660.2	16.5	98.2
K15-SAIS-Spot 17	147	155376	2.0	9.6531	0.9	4.0309	1.8	0.2822	1.6	0.87	1602.5	22.7	1640.5	15.0	1689.5	17.0	1689.5	17.0	94.9
K15-SAIS-Spot 18	112	152113	1.9	9.6420	0.8	4.3754	1.5	0.3060	1.3	0.85	1720.9	19.2	1707.7	12.3	1691.6	14.3	1691.6	14.3	101.7
K15-SAIS-Spot 19	147	95079	1.0	9.7318	1.2	4.1351	1.7	0.2919	1.3	0.73	1650.8	18.5	1661.3	14.2	1674.5	21.7	1674.5	21.7	98.6

K15-SAIS-Spot 20	439	94377	2.3	9.8535	0.9	4.0584	1.3	0.2900	1.0	0.74	1641.7	14.4	1646.0	10.9	1651.5	16.7	1651.5	16.7	99.4
K15-SAIS-Spot 22	131	54232	1.0	9.8958	0.9	4.0010	1.6	0.2872	1.3	0.81	1627.3	18.6	1634.4	13.0	1643.5	17.6	1643.5	17.6	99.0
K15-SAIS-Spot 23	295	193991	1.5	9.8811	0.8	4.0234	1.6	0.2883	1.4	0.87	1633.2	20.3	1638.9	13.2	1646.3	15.0	1646.3	15.0	99.2
K15-SAIS-Spot 24	158	608724	2.3	6.1646	0.9	10.4506	1.7	0.4672	1.4	0.85	2471.5	29.1	2475.5	15.5	2478.9	14.9	2478.9	14.9	99.7
K15-SAIS-Spot 25	573	6819636	1.7	9.8185	0.6	4.0233	1.2	0.2865	1.0	0.84	1624.0	14.2	1638.9	9.6	1658.1	11.9	1658.1	11.9	97.9
K15-SAIS-Spot 26	101	240405	1.7	9.6039	1.0	4.2808	2.0	0.2982	1.8	0.88	1682.2	26.2	1689.7	16.6	1698.9	17.8	1698.9	17.8	99.0
K15-SAIS-Spot 27	214	621376	1.8	9.8835	0.9	4.0309	1.3	0.2889	1.0	0.73	1636.2	14.1	1640.4	10.8	1645.8	16.8	1645.8	16.8	99.4
K15-SAIS-Spot 28	719	97905	2.1	9.3046	0.9	3.8921	2.8	0.2627	2.7	0.95	1503.4	36.0	1612.0	22.8	1757.0	15.6	1757.0	15.6	85.6
K15-SAIS-Spot 29	151	122597	1.4	9.8514	0.9	4.0513	1.7	0.2895	1.4	0.84	1638.9	20.9	1644.6	14.1	1651.9	17.5	1651.9	17.5	99.2
K15-SAIS-Spot 30	108	229058	1.3	9.8910	1.0	4.0548	1.9	0.2909	1.6	0.84	1645.9	23.1	1645.3	15.5	1644.4	19.4	1644.4	19.4	100.1
K15-SAIS-Spot 31	286	56530	1.9	9.6781	1.0	4.2548	1.5	0.2987	1.2	0.75	1684.6	17.1	1684.7	12.6	1684.7	18.7	1684.7	18.7	100.0
K15-SAIS-Spot 32	201	75051	1.3	9.7706	1.0	3.9006	1.7	0.2764	1.4	0.82	1573.3	19.6	1613.8	13.9	1667.1	18.3	1667.1	18.3	94.4
K15-SAIS-Spot 33	160	127035	1.3	9.6284	1.0	4.3201	1.6	0.3017	1.3	0.79	1699.6	19.6	1697.2	13.6	1694.2	18.4	1694.2	18.4	100.3
K15-SAIS-Spot 34	147	77957	1.9	9.8670	1.1	4.0878	1.8	0.2925	1.5	0.81	1654.2	21.7	1651.9	15.0	1648.9	20.1	1648.9	20.1	100.3
K15-SAIS-Spot 35	74	43973	1.3	9.8257	1.3	4.0663	1.9	0.2898	1.4	0.73	1640.4	20.6	1647.6	15.9	1656.7	24.6	1656.7	24.6	99.0
K15-SAIS-Spot 36	450	507149	1.9	9.5018	0.6	4.4566	1.2	0.3071	1.0	0.85	1726.5	15.8	1722.9	10.2	1718.5	11.9	1718.5	11.9	100.5
K15-SAIS-Spot 37	400	218015	1.1	9.8418	0.7	4.0410	1.5	0.2884	1.3	0.88	1633.7	19.3	1642.5	12.4	1653.7	13.6	1653.7	13.6	98.8
K15-SAIS-Spot 38	183	977588	3.9	9.9163	0.7	3.9885	1.5	0.2868	1.3	0.87	1625.8	18.7	1631.9	12.1	1639.7	13.7	1639.7	13.7	99.2
K15-SAIS-Spot 39	140	90231	0.9	9.7399	1.0	4.1738	1.7	0.2948	1.4	0.82	1665.7	20.3	1668.9	13.8	1672.9	17.8	1672.9	17.8	99.6
K15-SAIS-Spot 41	256	674751	1.3	9.8295	1.1	4.0662	1.9	0.2899	1.6	0.83	1640.9	23.1	1647.6	15.6	1656.0	19.6	1656.0	19.6	99.1
K15-SAIS-Spot 42	149	1785191	2.1	9.5510	0.9	4.2063	1.6	0.2914	1.3	0.84	1648.4	19.5	1675.2	13.1	1709.1	15.7	1709.1	15.7	96.4
K15-SAIS-Spot 43	174	79946	0.7	9.6811	0.9	4.1392	1.6	0.2906	1.3	0.82	1644.7	19.3	1662.1	13.3	1684.1	17.1	1684.1	17.1	97.7
K15-SAIS-Spot 44	612	154162	2.0	9.8109	1.1	4.0379	2.1	0.2873	1.8	0.84	1628.1	25.4	1641.9	17.1	1659.5	21.1	1659.5	21.1	98.1
K15-SAIS-Spot 45	94	216482	1.7	9.8483	1.0	4.1740	1.6	0.2981	1.3	0.78	1682.1	18.9	1668.9	13.4	1652.4	19.0	1652.4	19.0	101.8
K15-SAIS-Spot 46	199	89078	3.2	9.7512	0.9	4.1746	1.5	0.2952	1.2	0.81	1667.6	17.3	1669.0	12.0	1670.8	16.0	1670.8	16.0	99.8
K15-SAIS-Spot 48	643	1039424	1.9	5.9260	1.2	10.5863	1.9	0.4550	1.5	0.78	2417.4	30.2	2487.5	17.8	2545.2	20.1	2545.2	20.1	95.0
K15-SAIS-Spot 49	108	185140	1.1	9.7833	1.2	4.0074	1.9	0.2843	1.4	0.77	1613.2	20.3	1635.7	15.0	1664.7	22.0	1664.7	22.0	96.9
K15-SAIS-Spot 50	103	211798	2.0	9.8676	1.0	4.1554	1.7	0.2974	1.4	0.81	1678.4	21.0	1665.3	14.3	1648.8	18.9	1648.8	18.9	101.8
K15-SAIS-Spot 51	335	229370	1.7	9.8132	1.0	4.1096	1.6	0.2925	1.2	0.78	1654.0	18.0	1656.2	13.0	1659.1	18.4	1659.1	18.4	99.7
K15-SAIS-Spot 52	74	72314	0.8	8.9221	1.1	5.1457	1.7	0.3330	1.3	0.75	1852.8	20.9	1843.7	14.7	1833.4	20.7	1833.4	20.7	101.1
K15-SAIS-Spot 53	160	616073	1.7	9.8396	1.0	4.0115	1.8	0.2863	1.5	0.83	1622.9	21.3	1636.5	14.6	1654.1	18.8	1654.1	18.8	98.1
K15-SAIS-Spot 54	114	69784	1.5	9.7132	1.2	4.1447	1.8	0.2920	1.4	0.76	1651.4	20.2	1663.2	14.9	1678.0	22.0	1678.0	22.0	98.4
K15-SAIS-Spot 55	138	117148	1.5	9.9493	1.1	4.1317	1.6	0.2981	1.2	0.74	1682.1	17.3	1660.6	12.9	1633.5	19.7	1633.5	19.7	103.0
K15-SAIS-Spot 56	266	146879	1.9	9.8415	0.8	4.0388	1.8	0.2883	1.6	0.89	1632.9	22.6	1642.0	14.3	1653.7	14.8	1653.7	14.8	98.7
K15-SAIS-Spot 57	230	173836	3.6	9.8756	0.8	3.9770	1.4	0.2849	1.1	0.81	1615.7	16.1	1629.5	11.3	1647.3	15.3	1647.3	15.3	98.1
K15-SAIS-Spot 59	99	152529	1.4	9.8685	0.9	4.0809	1.5	0.2921	1.3	0.82	1651.9	18.3	1650.5	12.5	1648.6	16.2	1648.6	16.2	100.2
K15-SAIS-Spot 60	164	51008	4.3	9.5578	0.9	4.4424	1.7	0.3079	1.4	0.82	1730.6	20.7	1720.3	13.7	1707.7	17.3	1707.7	17.3	101.3
K15-SAIS-Spot 61	516	94317	1.9	9.8004	0.8	4.0333	1.5	0.2867	1.3	0.86	1624.9	18.5	1640.9	12.3	1661.5	14.5	1661.5	14.5	97.8
K15-SAIS-Spot 62	191	179729	1.1	9.8150	1.3	4.0205	2.1	0.2862	1.6	0.79	1622.5	23.6	1638.4	16.9	1658.7	23.7	1658.7	23.7	97.8
K15-SAIS-Spot 63	171	58497	1.5	9.7653	1.1	4.0129	1.9	0.2842	1.6	0.81	1612.6	22.4	1636.8	15.8	1668.1	21.2	1668.1	21.2	96.7
K15-SAIS-Spot 64	180	141865	1.1	9.9095	0.8	4.0287	1.6	0.2895	1.4	0.86	1639.2	20.3	1640.0	13.2	1641.0	15.3	1641.0	15.3	99.9
K15-SAIS-Spot 65	390	104585	1.9	9.8726	1.0	4.0863	1.6	0.2926	1.3	0.80	1654.5	18.8	1651.6	13.1	1647.9	17.7	1647.9	17.7	100.4
K15-SAIS-Spot 66	130	145506	1.6	9.8361	1.3	4.0258	1.7	0.2872	1.2	0.69	1627.5	17.4	1639.4	14.2	1654.7	23.4	1654.7	23.4	98.4

K15-SAIS-Spot 67	156	197970	1.4	9.5648	1.1	4.2447	1.7	0.2945	1.4	0.79	1663.8	20.0	1682.7	14.3	1706.4	19.8	1706.4	19.8	97.5
K15-SAIS-Spot 68	500	244554	2.0	9.3685	0.9	4.4891	1.5	0.3050	1.3	0.82	1716.1	18.8	1729.0	12.7	1744.5	16.1	1744.5	16.1	98.4
K15-SAIS-Spot 69	222	53423	1.3	9.6872	0.8	4.2431	1.4	0.2981	1.1	0.80	1681.9	16.3	1682.4	11.3	1682.9	15.2	1682.9	15.2	99.9
K15-SAIS-Spot 70	321	55341	1.3	9.8307	0.8	4.1441	1.4	0.2955	1.1	0.81	1668.8	16.5	1663.0	11.4	1655.8	15.3	1655.8	15.3	100.8
K15-SAIS-Spot 71	198	61950	1.2	9.7980	1.1	3.9754	1.5	0.2825	1.1	0.71	1603.9	15.6	1629.2	12.5	1661.9	20.0	1661.9	20.0	96.5
K15-SAIS-Spot 73	259	209069	1.4	9.5801	0.9	4.3018	1.5	0.2989	1.2	0.81	1685.8	17.8	1693.7	12.1	1703.5	15.8	1703.5	15.8	99.0
K15-SAIS-Spot 74	152	145651	2.0	9.4607	1.1	4.2818	1.7	0.2938	1.3	0.78	1660.5	19.2	1689.9	13.9	1726.5	19.6	1726.5	19.6	96.2
K15-SAIS-Spot 75	154	230495	2.6	9.5993	1.0	4.4124	1.7	0.3072	1.4	0.80	1726.9	21.0	1714.7	14.3	1699.8	18.9	1699.8	18.9	101.6
K15-SAIS-Spot 76	456	66624	1.6	9.2990	0.9	4.4846	1.4	0.3024	1.1	0.80	1703.4	16.9	1728.1	11.7	1758.1	15.6	1758.1	15.6	96.9
K15-SAIS-Spot 77	204	185568	1.4	9.7867	0.9	4.0887	1.7	0.2902	1.4	0.83	1642.6	20.4	1652.0	13.8	1664.1	17.4	1664.1	17.4	98.7
K15-SAIS-Spot 78	506	1181053	2.1	9.7865	0.9	4.1844	1.9	0.2970	1.7	0.88	1676.4	24.8	1671.0	15.7	1664.1	16.9	1664.1	16.9	100.7
K15-SAIS-Spot 79	991	130896	6.3	9.3737	0.7	3.8348	1.5	0.2607	1.4	0.90	1493.4	18.5	1600.1	12.5	1743.5	12.4	1743.5	12.4	85.7
K15-SAIS-Spot 80	119	36918	1.7	9.6863	1.1	4.1834	2.4	0.2939	2.2	0.89	1661.0	31.6	1670.8	19.8	1683.1	19.9	1683.1	19.9	98.7
K15-SAIS-Spot 81	427	1044455	1.3	9.5326	1.0	4.3818	1.8	0.3029	1.5	0.83	1705.9	22.5	1708.9	15.0	1712.6	18.6	1712.6	18.6	99.6
K15-SAIS-Spot 82	265	210392	1.0	9.7993	0.9	4.2070	1.3	0.2990	1.0	0.76	1686.3	15.1	1675.4	11.1	1661.7	16.4	1661.7	16.4	101.5
K15-SAIS-Spot 83	168	57971	1.0	9.8508	0.8	4.0924	1.4	0.2924	1.1	0.81	1653.4	16.3	1652.8	11.3	1652.0	15.2	1652.0	15.2	100.1
K15-SAIS-Spot 84	361	5360945	8.1	9.1353	0.7	4.9819	1.2	0.3301	1.1	0.85	1838.8	16.9	1816.3	10.5	1790.5	12.1	1790.5	12.1	102.7
K15-SAIS-Spot 85	44	82163	1.3	9.8182	1.4	4.1824	1.9	0.2978	1.4	0.71	1680.5	20.5	1670.6	16.0	1658.1	25.4	1658.1	25.4	101.4
K15-SAIS-Spot 86	120	51415	1.7	9.8207	0.8	3.9597	1.7	0.2820	1.5	0.87	1601.6	20.9	1626.0	13.8	1657.7	15.7	1657.7	15.7	96.6
K15-SAIS-Spot 87	654	96020	2.0	9.6453	0.8	4.1944	1.8	0.2934	1.7	0.90	1658.6	24.4	1672.9	15.2	1691.0	14.6	1691.0	14.6	98.1
K15-SAIS-Spot 88	190	124634	1.5	9.7950	0.7	4.1104	1.1	0.2920	0.9	0.78	1651.5	12.7	1656.4	9.1	1662.5	13.0	1662.5	13.0	99.3
K15-SAIS-Spot 89	140	357079	1.1	9.8191	1.1	4.0690	1.9	0.2898	1.5	0.80	1640.4	22.1	1648.1	15.5	1658.0	21.1	1658.0	21.1	98.9
K15-SAIS-Spot 90	153	63785	1.0	9.6919	0.9	4.2080	1.6	0.2958	1.3	0.80	1670.4	18.5	1675.6	12.9	1682.1	17.4	1682.1	17.4	99.3
K15-SAIS-Spot 92	362	148542	2.2	9.3467	0.9	4.6261	1.8	0.3136	1.5	0.86	1758.4	23.8	1754.0	15.0	1748.7	16.6	1748.7	16.6	100.6
K15-SAIS-Spot 93	157	99295	1.1	9.6198	1.0	4.1843	1.4	0.2919	0.9	0.69	1651.2	13.6	1671.0	11.1	1695.8	18.2	1695.8	18.2	97.4
K15-SAIS-Spot 94	120	121632	1.1	9.9206	0.9	4.0344	1.6	0.2903	1.3	0.80	1642.9	18.3	1641.2	12.8	1638.9	17.3	1638.9	17.3	100.2
K15-SAIS-Spot 95	246	62202	2.3	9.6618	0.8	4.2164	1.3	0.2955	1.0	0.77	1668.8	15.1	1677.2	10.9	1687.8	15.5	1687.8	15.5	98.9
K15-SAIS-Spot 96	167	127317	1.4	9.8448	1.0	4.0881	1.8	0.2919	1.5	0.82	1651.0	21.7	1651.9	14.8	1653.1	19.0	1653.1	19.0	99.9
K15-SAIS-Spot 97	64	66941	1.8	8.6256	3.4	4.7956	3.6	0.3000	1.3	0.37	1691.3	19.9	1784.1	30.5	1894.4	60.8	1894.4	60.8	89.3
K15-SAIS-Spot 98	227	153420	1.3	9.6444	0.8	4.2229	1.3	0.2954	1.1	0.81	1668.4	15.9	1678.5	11.0	1691.1	14.5	1691.1	14.5	98.7
K15-SAIS-Spot 99	96	106764	1.3	9.6498	0.9	4.4083	1.7	0.3085	1.5	0.85	1733.4	22.4	1713.9	14.4	1690.1	17.0	1690.1	17.0	102.6
K15-SAIS-Spot 100	203	142302	1.1	9.7456	0.9	4.1066	1.6	0.2903	1.3	0.82	1642.8	18.5	1655.6	12.8	1671.9	16.7	1671.9	16.7	98.3
K15-SAIS-Spot 101	590	202089	1.8	9.4539	0.7	4.5511	1.2	0.3120	1.0	0.79	1750.8	14.9	1740.4	10.2	1727.8	13.7	1727.8	13.7	101.3
K15-SAIS-Spot 102	145	108957	2.8	8.2299	0.9	5.9947	1.5	0.3578	1.3	0.83	1971.8	21.5	1975.1	13.3	1978.5	15.1	1978.5	15.1	99.7
K15-SAIS-Spot 103	418	52872	1.6	9.9283	1.1	3.9009	1.8	0.2809	1.5	0.82	1595.9	21.4	1613.9	14.9	1637.4	19.6	1637.4	19.6	97.5
K15-SAIS-Spot 104	481	184426	1.3	9.6821	0.7	4.1889	1.4	0.2941	1.2	0.87	1662.2	17.5	1671.9	11.2	1683.9	12.5	1683.9	12.5	98.7
K15-SAIS-Spot 105	454	57625	1.4	9.5276	0.8	4.4172	1.3	0.3052	1.0	0.77	1717.2	14.7	1715.6	10.5	1713.6	14.8	1713.6	14.8	100.2
K15-SAIS-Spot 107	215	86716	1.7	9.8099	0.9	4.0278	1.4	0.2866	1.1	0.77	1624.3	15.6	1639.8	11.5	1659.7	16.8	1659.7	16.8	97.9
K15-SAIS-Spot 108	233	122663	2.5	9.1730	1.1	4.8011	1.6	0.3194	1.2	0.76	1786.9	19.3	1785.1	13.8	1783.0	19.6	1783.0	19.6	100.2
K15-SAIS-Spot 109	246	178242	1.6	9.9041	0.9	4.1157	1.5	0.2956	1.2	0.81	1669.6	18.3	1657.4	12.5	1642.0	16.6	1642.0	16.6	101.7
K15-SAIS-Spot 110	272	364956	1.4	9.7667	0.8	4.2289	1.3	0.2996	1.0	0.77	1689.1	15.0	1679.6	10.8	1667.9	15.4	1667.9	15.4	101.3
K15-SAIS-Spot 111	132	213186	1.2	9.5864	1.0	4.1535	1.4	0.2888	1.0	0.70	1635.4	14.5	1664.9	11.7	1702.2	18.7	1702.2	18.7	96.1
K15-SAIS-Spot 112	464	10550430	1.8	9.8420	0.7	4.1676	1.5	0.2975	1.3	0.90	1678.8	19.8	1667.7	12.2	1653.6	12.1	1653.6	12.1	101.5

K15-SAIS-Spot 113	680	236511	1.7	9.4208	1.0	4.2165	1.6	0.2881	1.3	0.80	1632.0	19.0	1677.2	13.5	1734.3	17.9	1734.3	17.9	94.1
K15-SAIS-Spot 114	243	113797	1.8	9.8925	0.7	4.0860	1.4	0.2932	1.2	0.86	1657.3	17.2	1651.5	11.2	1644.1	12.9	1644.1	12.9	100.8
K15-SAIS-Spot 115	441	177167	2.2	9.6366	0.5	4.3145	1.1	0.3015	1.0	0.87	1699.0	14.3	1696.1	9.1	1692.6	10.1	1692.6	10.1	100.4
K15-SAIS-Spot 116	123	245099	1.9	9.8066	0.9	4.1963	1.6	0.2985	1.3	0.81	1683.7	19.3	1673.3	13.2	1660.3	17.6	1660.3	17.6	101.4
K15-SAIS-Spot 117	142	167725	2.0	9.8713	0.9	4.1354	1.6	0.2961	1.3	0.81	1671.8	19.1	1661.3	13.2	1648.1	17.6	1648.1	17.6	101.4
K15-SAIS-Spot 118	169	193259	1.6	9.7986	0.8	4.1119	1.6	0.2922	1.4	0.86	1652.6	19.8	1656.7	13.0	1661.8	15.2	1661.8	15.2	99.4
K15-SAIS-Spot 119	194	199190	1.8	9.8441	0.8	4.1987	1.6	0.2998	1.4	0.87	1690.2	20.2	1673.8	12.8	1653.2	14.2	1653.2	14.2	102.2
K15-SAIS-Spot 120	895	87950	1.8	9.3128	0.8	4.4389	1.6	0.2998	1.4	0.87	1690.4	20.2	1719.6	12.9	1755.4	14.1	1755.4	14.1	96.3
K15-SAIS-Spot 122	193	51490	0.8	9.9388	0.9	4.0411	1.7	0.2913	1.4	0.86	1648.0	20.9	1642.5	13.7	1635.5	16.2	1635.5	16.2	100.8
K15-SAIS-Spot 124	109	160284	2.1	9.8025	1.3	4.1205	2.1	0.2929	1.7	0.81	1656.2	25.3	1658.4	17.6	1661.1	23.6	1661.1	23.6	99.7
K15-SAIS-Spot 125	1014	147880	2.4	9.7158	1.0	3.7073	2.2	0.2612	2.0	0.90	1496.2	26.7	1572.9	17.9	1677.5	18.4	1677.5	18.4	89.2
K15-SAIS-Spot 126	385	124568	1.5	9.8868	0.8	3.9894	1.4	0.2861	1.1	0.81	1621.8	16.4	1632.0	11.5	1645.2	15.3	1645.2	15.3	98.6
K15-SAIS-Spot 127	198	132242	1.1	9.9323	0.9	3.9840	1.6	0.2870	1.3	0.83	1626.5	19.2	1630.9	13.1	1636.7	16.9	1636.7	16.9	99.4
K15-SAIS-Spot 128	434	135477	1.2	9.9126	0.6	4.0712	1.2	0.2927	1.0	0.84	1654.9	14.3	1648.5	9.5	1640.4	11.9	1640.4	11.9	100.9
K15-SAIS-Spot 130	159	63487	0.7	9.9213	1.2	4.0364	2.2	0.2904	1.9	0.85	1643.7	27.8	1641.6	18.3	1638.7	21.7	1638.7	21.7	100.3
K15-SAIS-Spot 131	179	99753	1.1	9.9849	1.0	4.0073	1.3	0.2902	0.9	0.67	1642.5	12.7	1635.7	10.6	1626.9	18.0	1626.9	18.0	101.0
K15-SAIS-Spot 132	100	127419	1.1	9.9373	1.0	4.1610	1.4	0.2999	1.0	0.71	1690.8	14.9	1666.4	11.6	1635.8	18.6	1635.8	18.6	103.4
K15-SAIS-Spot 133	173	185914	2.1	9.6947	0.8	4.3719	1.3	0.3074	1.1	0.81	1727.9	16.0	1707.0	10.8	1681.5	14.2	1681.5	14.2	102.8
K15-SAIS-Spot 135	327	148998	1.5	9.7087	0.8	4.2489	1.4	0.2992	1.2	0.83	1687.3	17.7	1683.5	11.8	1678.9	14.9	1678.9	14.9	100.5
K15-SAIS-Spot 136	514	197107	1.2	9.7257	0.9	4.1050	1.3	0.2896	0.9	0.72	1639.3	13.1	1655.3	10.3	1675.6	16.3	1675.6	16.3	97.8
K15-SAIS-Spot 137	214	111952	3.4	9.5464	0.9	4.4048	1.4	0.3050	1.1	0.79	1715.9	16.7	1713.2	11.6	1709.9	15.6	1709.9	15.6	100.4
K15-SAIS-Spot 138	214	179466	2.2	9.8658	0.8	4.0802	1.4	0.2920	1.2	0.84	1651.3	17.1	1650.4	11.4	1649.2	14.0	1649.2	14.0	100.1
K15-SAIS-Spot 139	173	5115097	1.8	9.8582	1.0	4.2625	1.8	0.3048	1.5	0.83	1714.9	22.4	1686.1	14.7	1650.6	18.5	1650.6	18.5	103.9
K15-SAIS-Spot 140	95	76592	2.0	9.6004	0.9	4.3366	1.6	0.3020	1.3	0.81	1701.0	18.8	1700.3	12.9	1699.6	16.9	1699.6	16.9	100.1
K15-SAIS-Spot 141	81	92667	1.5	9.6818	1.0	4.2783	1.5	0.3004	1.1	0.73	1693.4	16.7	1689.2	12.6	1684.0	19.2	1684.0	19.2	100.6
K15-SAIS-Spot 142	181	76087	1.3	9.7737	1.0	4.2676	1.6	0.3025	1.2	0.76	1703.7	17.7	1687.1	12.8	1666.5	18.7	1666.5	18.7	102.2
K15-SAIS-Spot 143	188	125072	2.0	9.6287	0.9	4.4213	1.7	0.3088	1.4	0.84	1734.6	21.4	1716.3	13.9	1694.1	16.6	1694.1	16.6	102.4
K15-SAIS-Spot 144	500	109561	2.3	9.6014	0.8	3.5239	1.4	0.2454	1.1	0.79	1414.7	13.8	1532.6	10.9	1699.4	15.5	1699.4	15.5	83.2
K15-SAIS-Spot 145	114	51387	1.2	9.9154	0.9	3.9456	2.4	0.2837	2.2	0.92	1610.2	30.9	1623.1	19.0	1639.9	17.0	1639.9	17.0	98.2
K15-SAIS-Spot 146	228	236975	1.5	9.8138	0.9	4.0451	1.6	0.2879	1.3	0.81	1631.1	18.2	1643.3	12.7	1659.0	16.9	1659.0	16.9	98.3
K15-SAIS-Spot 147	151	169094	1.8	9.9497	0.7	4.1703	1.4	0.3009	1.2	0.87	1695.9	18.2	1668.2	11.4	1633.4	12.7	1633.4	12.7	103.8
K15-SAIS-Spot 148	252	55107	1.7	9.7625	0.8	4.0677	1.3	0.2880	1.1	0.83	1631.6	15.9	1647.8	10.9	1668.6	14.0	1668.6	14.0	97.8
K15-SAIS-Spot 149	522	149681	3.5	9.7066	1.0	4.1820	1.7	0.2944	1.4	0.80	1663.5	19.8	1670.5	13.8	1679.3	18.4	1679.3	18.4	99.1
K15-SAIS-Spot 150	108	79796	1.0	9.8623	0.9	4.0624	1.7	0.2906	1.4	0.83	1644.4	20.2	1646.8	13.7	1649.8	17.4	1649.8	17.4	99.7
K15-SAIS-Spot 151	144	68859	1.1	9.8250	1.0	3.9117	2.0	0.2787	1.7	0.87	1585.0	24.5	1616.1	16.2	1656.8	18.2	1656.8	18.2	95.7
K15-SAIS-Spot 152	833	156808	3.0	9.4544	0.9	3.9224	1.7	0.2690	1.5	0.85	1535.5	20.1	1618.3	14.0	1727.7	16.5	1727.7	16.5	88.9
K15-SAIS-Spot 153	265	53238	1.3	9.6403	1.1	4.1474	1.9	0.2900	1.5	0.80	1641.4	21.4	1663.7	15.2	1691.9	20.6	1691.9	20.6	97.0
K15-SAIS-Spot 155	260	290621	1.5	9.8670	0.9	4.0764	1.6	0.2917	1.4	0.82	1650.1	19.7	1649.6	13.4	1648.9	17.2	1648.9	17.2	100.1
K15-SAIS-Spot 156	146	103647	1.7	9.7936	0.9	4.1433	2.0	0.2943	1.7	0.88	1663.0	25.2	1662.9	16.0	1662.8	17.1	1662.8	17.1	100.0
K15-SAIS-Spot 157	287	140470	1.4	9.7242	0.9	4.0793	1.6	0.2877	1.3	0.81	1630.0	18.2	1650.2	12.7	1675.9	16.8	1675.9	16.8	97.3
K15-SAIS-Spot 158	239	76473	1.4	9.2071	1.5	4.4188	1.8	0.2951	1.0	0.56	1666.8	14.7	1715.9	14.8	1776.3	26.9	1776.3	26.9	93.8
K15-SAIS-Spot 159	118	66565	1.1	9.9527	0.9	3.9753	1.6	0.2870	1.3	0.84	1626.3	19.2	1629.2	13.0	1632.9	16.2	1632.9	16.2	99.6
K15-SAIS-Spot 160	210	69211	1.3	9.7944	1.1	4.0179	1.6	0.2854	1.2	0.75	1618.6	17.1	1637.8	12.9	1662.6	19.5	1662.6	19.5	97.4

K15-SAIS-Spot 162	272	227786	1.8	9.6341	1.0	4.1956	1.7	0.2932	1.3	0.80	1657.3	19.4	1673.2	13.5	1693.1	18.1	1693.1	18.1	97.9
K15-SAIS-Spot 163	152	73860	1.6	9.7755	0.9	4.1088	1.5	0.2913	1.2	0.78	1648.1	17.1	1656.1	12.2	1666.2	17.2	1666.2	17.2	98.9
K15-SAIS-Spot 164	86	40644	1.4	9.8088	1.1	4.1165	1.7	0.2928	1.3	0.77	1655.7	19.5	1657.6	14.2	1659.9	20.7	1659.9	20.7	99.8
K15-SAIS-Spot 166	90	158931	1.6	9.6955	0.9	4.1474	1.4	0.2916	1.0	0.73	1649.7	14.8	1663.7	11.4	1681.4	17.5	1681.4	17.5	98.1
K15-SAIS-Spot 167	212	172604	1.8	9.7160	0.9	4.2470	2.1	0.2993	1.9	0.91	1687.7	28.6	1683.2	17.4	1677.5	16.4	1677.5	16.4	100.6
K15-SAIS-Spot 168	246	55602	1.0	9.9043	1.1	4.0237	1.7	0.2890	1.2	0.73	1636.7	17.8	1639.0	13.7	1641.9	21.2	1641.9	21.2	99.7
K15-SAIS-Spot 169	126	120185	2.5	9.5803	1.1	4.2365	1.9	0.2944	1.5	0.81	1663.3	22.2	1681.1	15.4	1703.4	20.3	1703.4	20.3	97.6
K15-SAIS-Spot 170	133	508373	1.3	9.8493	1.1	4.0996	1.8	0.2929	1.5	0.82	1655.8	22.0	1654.2	15.1	1652.3	19.7	1652.3	19.7	100.2
K15-SAIS-Spot 171	153	706011	2.0	9.7647	0.9	4.1016	1.6	0.2905	1.3	0.83	1643.9	19.2	1654.6	13.0	1668.2	16.6	1668.2	16.6	98.5
K15-SAIS-Spot 172	120	234988	1.5	9.5643	0.8	4.3153	1.8	0.2993	1.6	0.90	1688.0	23.7	1696.3	14.6	1706.5	14.2	1706.5	14.2	98.9
K15-SAIS-Spot 174	152	1770772	1.4	9.7517	1.0	4.2290	1.5	0.2991	1.2	0.78	1686.8	17.9	1679.7	12.7	1670.7	18.0	1670.7	18.0	101.0
K15-SAIS-Spot 175	412	90263	1.6	9.7473	0.6	4.2753	1.1	0.3022	0.9	0.81	1702.4	13.4	1688.6	9.1	1671.5	11.8	1671.5	11.8	101.8
K15-SAIS-Spot 176	131	227386	1.2	9.8735	1.1	4.0677	2.1	0.2913	1.7	0.84	1648.0	25.2	1647.9	16.9	1647.7	21.1	1647.7	21.1	100.0
K15-SAIS-Spot 178	138	212235	3.2	9.7054	0.9	4.2427	1.5	0.2986	1.2	0.82	1684.6	18.0	1682.3	12.2	1679.5	15.9	1679.5	15.9	100.3
K15-SAIS-Spot 179	167	171908	2.1	9.7994	1.0	4.1630	1.7	0.2959	1.3	0.80	1670.8	19.6	1666.8	13.6	1661.7	18.4	1661.7	18.4	100.5
K15-SAIS-Spot 180	192	49069	2.7	8.7945	1.5	4.2595	3.4	0.2717	3.0	0.90	1549.3	41.9	1685.6	27.9	1859.5	26.9	1859.5	26.9	83.3
K15-SAIS-Spot 181	224	583184	1.6	9.9042	1.0	4.1127	1.6	0.2954	1.3	0.77	1668.6	18.7	1656.8	13.4	1641.9	19.3	1641.9	19.3	101.6
K15-SAIS-Spot 182	651	57027	1.6	9.4842	0.9	4.3637	1.5	0.3002	1.2	0.79	1692.1	17.7	1705.5	12.5	1722.0	17.2	1722.0	17.2	98.3
K15-SAIS-Spot 183	79	100909	1.1	9.7008	1.2	4.1673	1.9	0.2932	1.5	0.77	1657.5	21.5	1667.6	15.6	1680.4	22.3	1680.4	22.3	98.6
K15-SAIS-Spot 184	246	120449	1.5	9.4416	0.9	4.4929	1.6	0.3077	1.3	0.84	1729.2	20.2	1729.7	13.2	1730.2	15.7	1730.2	15.7	99.9
K15-SAIS-Spot 185	167	116174	1.1	9.6390	0.7	4.3609	1.2	0.3049	1.0	0.84	1715.4	15.6	1705.0	10.2	1692.2	12.4	1692.2	12.4	101.4
K15-SAIS-Spot 186	488	93259	3.5	6.9193	0.7	6.8708	1.5	0.3448	1.3	0.89	1909.7	22.0	2094.9	13.3	2282.1	11.9	2282.1	11.9	83.7
K15-SAIS-Spot 187	306	104709	1.0	9.9053	0.9	3.9879	1.5	0.2865	1.2	0.80	1624.0	17.4	1631.7	12.3	1641.7	17.1	1641.7	17.1	98.9
K15-SAIS-Spot 188	151	80707	1.3	9.8794	0.9	4.0650	1.6	0.2913	1.3	0.84	1647.9	19.5	1647.3	13.0	1646.6	16.2	1646.6	16.2	100.1
K15-SAIS-Spot 189	291	76051	1.5	9.8683	0.7	4.0866	1.4	0.2925	1.2	0.86	1653.9	17.9	1651.6	11.7	1648.7	13.6	1648.7	13.6	100.3
K15-SAIS-Spot 190	95	144632	1.0	9.7712	0.9	4.1404	1.6	0.2934	1.3	0.83	1658.6	19.1	1662.3	12.8	1667.0	16.0	1667.0	16.0	99.5
K15-SAIS-Spot 191	263	103626	2.3	9.5451	0.8	4.4552	1.5	0.3084	1.2	0.84	1733.0	18.9	1722.7	12.2	1710.2	14.5	1710.2	14.5	101.3
K15-SAIS-Spot 192	228	150468	1.1	9.8370	0.8	4.1906	1.5	0.2990	1.3	0.84	1686.2	18.6	1672.2	12.2	1654.6	14.8	1654.6	14.8	101.9
K15-SAIS-Spot 193	402	55930	1.3	9.7811	1.0	4.0838	1.7	0.2897	1.4	0.83	1640.1	20.5	1651.1	13.9	1665.1	17.7	1665.1	17.7	98.5
K15-SAIS-Spot 194	53	31139	0.2	8.1652	1.9	5.6276	2.4	0.3333	1.4	0.60	1854.2	23.2	1920.3	20.6	1992.5	33.8	1992.5	33.8	93.1
K15-SAIS-Spot 195	225	91265	2.3	9.8199	0.9	4.0657	1.6	0.2896	1.3	0.82	1639.3	18.7	1647.4	12.8	1657.8	16.5	1657.8	16.5	98.9
K15-SAIS-Spot 196	101	33913	1.3	9.7371	1.1	4.0721	1.7	0.2876	1.4	0.79	1629.4	20.0	1648.7	14.3	1673.5	19.7	1673.5	19.7	97.4
K15-SAIS-Spot 197	615	859938	2.9	9.3075	0.9	4.6106	1.7	0.3112	1.4	0.83	1746.8	21.4	1751.2	14.1	1756.4	17.2	1756.4	17.2	99.4
K15-SAIS-Spot 198	276	220162	2.8	9.5567	0.8	4.2141	1.7	0.2921	1.5	0.89	1652.0	22.3	1676.8	14.2	1707.9	14.7	1707.9	14.7	96.7
K15-SAIS-Spot 199	152	111747	1.3	9.6345	0.7	4.2342	1.6	0.2959	1.4	0.89	1670.8	20.6	1680.7	12.9	1693.0	13.2	1693.0	13.2	98.7
K15-SAIS-Spot 200	143	150423	1.0	9.7534	0.7	4.1499	1.5	0.2936	1.3	0.90	1659.3	19.6	1664.2	12.2	1670.4	12.2	1670.4	12.2	99.3
K15-SAIS-Spot 201	159	144975	1.5	9.7901	0.7	4.1211	1.5	0.2926	1.4	0.89	1654.6	19.9	1658.5	12.6	1663.4	13.2	1663.4	13.2	99.5
K15-SAIS-Spot 202	205	75296	1.2	9.8838	1.1	3.9582	1.8	0.2837	1.4	0.78	1610.2	19.7	1625.7	14.4	1645.8	20.8	1645.8	20.8	97.8
K15-SAIS-Spot 203	232	164146	1.3	9.8074	1.4	4.0293	1.9	0.2866	1.4	0.71	1624.5	20.0	1640.1	15.9	1660.2	25.3	1660.2	25.3	97.9
K15-SAIS-Spot 204	56	64475	1.6	9.6497	1.1	4.4237	1.8	0.3096	1.4	0.78	1738.7	21.6	1716.8	15.0	1690.1	20.9	1690.1	20.9	102.9
K15-SAIS-Spot 205	199	156731	0.9	9.8110	0.8	3.9926	1.3	0.2841	1.1	0.81	1612.0	15.4	1632.7	10.9	1659.5	14.8	1659.5	14.8	97.1
K15-SAIS-Spot 206	288	53004	1.7	9.6375	0.9	4.3103	1.5	0.3013	1.2	0.80	1697.6	17.7	1695.3	12.3	1692.4	16.6	1692.4	16.6	100.3
K15-SAIS-Spot 207	170	149740	2.0	9.5538	1.0	4.4718	1.6	0.3099	1.3	0.79	1740.0	19.4	1725.8	13.3	1708.5	18.0	1708.5	18.0	101.8

K15-SAIS-Spot 208	371	297605	0.9	9.9077	1.0	4.0316	1.6	0.2897	1.2	0.79	1640.0	18.0	1640.6	12.8	1641.3	18.0	1641.3	18.0	99.9
K15-SAIS-Spot 209	161	95713	1.0	9.8756	0.9	3.7024	3.3	0.2652	3.1	0.96	1516.3	42.3	1571.9	26.2	1647.3	17.6	1647.3	17.6	92.0
K15-SAIS-Spot 210	228	141554	1.3	9.9379	0.8	3.8924	1.3	0.2805	1.0	0.77	1594.1	14.1	1612.1	10.5	1635.6	15.3	1635.6	15.3	97.5
K15-SAIS-Spot 211	416	53490	1.2	9.7807	0.8	4.1335	1.6	0.2932	1.4	0.86	1657.6	19.8	1660.9	12.9	1665.2	15.2	1665.2	15.2	99.5
K15-SAIS-Spot 212	93	105813	1.4	9.8203	0.9	4.0610	1.6	0.2892	1.4	0.83	1637.7	19.8	1646.5	13.4	1657.7	16.9	1657.7	16.9	98.8
K15-SAIS-Spot 213	271	158795	1.7	9.7974	1.0	4.1760	1.6	0.2967	1.3	0.79	1675.1	18.7	1669.3	13.1	1662.1	18.2	1662.1	18.2	100.8
K15-SAIS-Spot 214	223	169017	1.8	9.3591	0.9	4.6175	1.4	0.3134	1.1	0.77	1757.6	16.7	1752.4	11.9	1746.3	16.8	1746.3	16.8	100.6
K15-SAIS-Spot 216	334	162147	2.0	9.8601	1.0	4.1372	1.7	0.2959	1.3	0.79	1670.7	19.7	1661.7	13.9	1650.2	19.2	1650.2	19.2	101.2
K15-SAIS-Spot 217	133	215437	1.5	9.7607	1.0	4.1283	1.6	0.2922	1.3	0.77	1652.8	18.3	1659.9	13.3	1669.0	19.1	1669.0	19.1	99.0
K15-SAIS-Spot 218	66	83613	1.4	9.8641	1.6	4.0428	1.9	0.2892	1.2	0.60	1637.7	16.7	1642.9	15.8	1649.5	28.8	1649.5	28.8	99.3
K15-SAIS-Spot 220	158	247437	0.9	9.8093	1.0	4.1533	1.6	0.2955	1.2	0.78	1668.9	18.2	1664.9	13.0	1659.8	18.4	1659.8	18.4	100.5
K15-SAIS-Spot 221	185	216918	1.5	9.9313	0.9	4.0242	1.9	0.2899	1.7	0.88	1640.8	24.6	1639.1	15.7	1636.9	17.2	1636.9	17.2	100.2
K15-SAIS-Spot 222	187	50477	1.2	9.6051	1.2	4.3238	1.6	0.3012	1.0	0.66	1697.3	15.2	1697.9	12.8	1698.7	21.5	1698.7	21.5	99.9
K15-SAIS-Spot 223	185	63388	1.6	9.7223	1.1	4.3009	2.0	0.3033	1.6	0.84	1707.5	24.7	1693.5	16.2	1676.3	19.7	1676.3	19.7	101.9
K15-SAIS-Spot 225	184	189009	2.1	9.7186	0.9	4.1024	1.6	0.2892	1.4	0.82	1637.4	19.6	1654.8	13.5	1677.0	17.3	1677.0	17.3	97.6
K15-SAIS-Spot 226	94	150163	1.7	9.7861	1.0	4.0506	1.6	0.2875	1.3	0.80	1629.0	18.4	1644.4	13.1	1664.2	17.9	1664.2	17.9	97.9
K15-SAIS-Spot 227	403	369391	2.2	9.3118	0.8	4.3112	2.0	0.2912	1.9	0.92	1647.3	27.3	1695.5	16.8	1755.6	14.6	1755.6	14.6	93.8
K15-SAIS-Spot 228	57	40472	2.0	9.6942	1.1	4.3263	1.9	0.3042	1.6	0.81	1712.0	23.3	1698.4	15.9	1681.6	21.0	1681.6	21.0	101.8
K15-SAIS-Spot 229	450	1892003	1.8	9.4908	0.9	4.4741	1.6	0.3080	1.3	0.82	1730.7	19.7	1726.2	13.1	1720.7	16.5	1720.7	16.5	100.6
K15-SAIS-Spot 230	233	245807	1.5	9.8588	1.1	4.1236	1.9	0.2949	1.5	0.82	1665.7	22.5	1659.0	15.3	1650.5	20.1	1650.5	20.1	100.9
K15-SAIS-Spot 231	333	65787	2.0	9.8572	0.7	4.1551	1.3	0.2971	1.1	0.85	1676.7	16.3	1665.2	10.6	1650.8	12.8	1650.8	12.8	101.6
K15-SAIS-Spot 232	212	159421	1.8	9.7520	0.8	4.1408	1.5	0.2929	1.3	0.86	1655.9	18.7	1662.4	12.2	1670.6	14.3	1670.6	14.3	99.1
K15-SAIS-Spot 233	153	61620	1.0	9.7038	0.8	4.2514	1.7	0.2992	1.5	0.88	1687.4	22.8	1684.0	14.4	1679.8	15.3	1679.8	15.3	100.5
K15-SAIS-Spot 234	112	155215	1.2	9.7633	1.0	4.1492	1.6	0.2938	1.3	0.78	1660.5	18.6	1664.1	13.4	1668.5	19.1	1668.5	19.1	99.5
K15-SAIS-Spot 235	281	38019	2.1	9.1983	2.3	4.3404	2.8	0.2896	1.6	0.57	1639.3	22.9	1701.1	23.1	1778.0	42.0	1778.0	42.0	92.2
K15-SAIS-Spot 236	98	206327	1.4	9.8531	1.1	4.0422	1.5	0.2889	1.1	0.72	1635.8	15.9	1642.7	12.5	1651.6	19.9	1651.6	19.9	99.0
K15-SAIS-Spot 237	929	76397	4.6	9.4470	0.6	4.2511	1.7	0.2913	1.5	0.92	1647.9	22.3	1684.0	13.6	1729.2	11.6	1729.2	11.6	95.3
K15-SAIS-Spot 239	97	172970	1.4	9.7359	1.2	4.1276	1.7	0.2915	1.2	0.69	1648.8	17.3	1659.8	14.1	1673.7	23.0	1673.7	23.0	98.5
K15-SAIS-Spot 240	195	167666	2.4	9.5721	1.0	4.3191	1.7	0.2998	1.4	0.82	1690.6	20.6	1697.0	14.0	1705.0	17.9	1705.0	17.9	99.2
K15-SAIS-Spot 241	107	212212	1.2	9.8679	0.9	4.1214	1.7	0.2950	1.4	0.84	1666.3	20.4	1658.6	13.5	1648.8	16.7	1648.8	16.7	101.1
K15-SAIS-Spot 242	101	156438	1.4	9.5657	0.9	4.2897	1.6	0.2976	1.4	0.85	1679.4	20.6	1691.4	13.5	1706.2	16.1	1706.2	16.1	98.4
K15-SAIS-Spot 243	170	117316	1.7	9.8563	1.1	4.1783	1.9	0.2987	1.5	0.82	1684.8	22.6	1669.8	15.3	1650.9	19.9	1650.9	19.9	102.0
K15-SAIS-Spot 244	143	111883	1.6	9.7703	1.0	4.0570	1.8	0.2875	1.5	0.84	1628.9	21.6	1645.7	14.6	1667.2	18.2	1667.2	18.2	97.7
K15-SAIS-Spot 245	170	149523	2.0	9.7672	0.9	4.0507	1.5	0.2869	1.2	0.82	1626.2	17.8	1644.4	12.3	1667.8	16.1	1667.8	16.1	97.5
K15-SAIS-Spot 246	96	133085	1.6	9.6956	1.2	4.1418	2.2	0.2912	1.8	0.83	1647.8	26.2	1662.6	17.8	1681.4	22.7	1681.4	22.7	98.0
K15-SAIS-Spot 248	410	60233	4.9	9.3333	0.9	4.2091	1.6	0.2849	1.3	0.84	1616.1	18.9	1675.8	13.0	1751.4	15.9	1751.4	15.9	92.3
K15-SAIS-Spot 249	501	225673	1.0	9.8448	0.9	3.8514	1.6	0.2750	1.3	0.83	1566.1	18.7	1603.6	13.0	1653.1	16.5	1653.1	16.5	94.7
K15-SAIS-Spot 250	243	127021	1.5	9.8992	0.8	4.0180	1.2	0.2885	0.9	0.77	1633.9	13.6	1637.8	9.9	1642.9	14.4	1642.9	14.4	99.5
K15-SAIS-Spot 251	149	233550	2.1	9.8361	0.8	4.1188	1.5	0.2938	1.2	0.84	1660.6	18.2	1658.0	12.2	1654.8	15.2	1654.8	15.2	100.4
K15-SAIS-Spot 252	186	207113	1.3	9.7026	1.0	4.3787	1.6	0.3081	1.2	0.79	1731.5	18.6	1708.3	12.9	1680.0	17.8	1680.0	17.8	103.1
K15-SAIS-Spot 253	259	161928	0.7	9.8416	0.8	4.1244	1.4	0.2944	1.1	0.83	1663.4	16.6	1659.2	11.1	1653.7	13.9	1653.7	13.9	100.6
K15-SAIS-Spot 254	92	116221	1.7	9.9119	1.2	4.0560	2.1	0.2916	1.7	0.83	1649.4	25.0	1645.5	16.9	1640.5	21.5	1640.5	21.5	100.5
K15-SAIS-Spot 255	143	89202	1.9	9.6370	0.9	4.2964	1.7	0.3003	1.4	0.84	1692.8	21.0	1692.7	13.9	1692.5	17.0	1692.5	17.0	100.0

K15-SAIS-Spot 256	103	169718	1.3	9.7253	1.0	4.1422	1.7	0.2922	1.4	0.83	1652.3	20.5	1662.7	13.9	1675.7	17.7	1675.7	17.7	98.6
K15-SAIS-Spot 257	196	296733	1.3	9.7510	1.0	4.1217	1.6	0.2915	1.3	0.80	1649.0	19.0	1658.6	13.3	1670.8	18.0	1670.8	18.0	98.7
K15-SAIS-Spot 258	97	60799	1.5	9.8001	1.2	4.1656	1.5	0.2961	1.0	0.65	1671.8	14.7	1667.3	12.6	1661.5	21.8	1661.5	21.8	100.6
K15-SAIS-Spot 259	700	162782	1.2	9.2821	0.6	4.4153	1.5	0.2972	1.4	0.91	1677.6	20.2	1715.2	12.5	1761.4	11.6	1761.4	11.6	95.2
K15-SAIS-Spot 260	144	104967	2.7	9.9359	0.9	4.0777	1.7	0.2938	1.5	0.85	1660.7	21.7	1649.9	14.2	1636.0	17.0	1636.0	17.0	101.5
K15-SAIS-Spot 261	79	102044	2.7	9.6075	1.0	4.2697	1.7	0.2975	1.4	0.81	1679.0	20.9	1687.5	14.4	1698.2	18.8	1698.2	18.8	98.9
K15-SAIS-Spot 262	167	93827	1.8	9.6088	0.8	4.4291	1.7	0.3087	1.5	0.87	1734.1	22.6	1717.8	14.1	1697.9	15.4	1697.9	15.4	102.1
K15-SAIS-Spot 263	250	35081	1.2	9.3578	1.9	4.2336	2.4	0.2873	1.4	0.61	1628.2	20.6	1680.6	19.4	1746.6	34.4	1746.6	34.4	93.2
K15-SAIS-Spot 264	155	90451	1.5	9.8059	0.9	4.0595	1.5	0.2887	1.3	0.82	1635.1	18.3	1646.2	12.6	1660.4	16.5	1660.4	16.5	98.5
K15-SAIS-Spot 265	246	205426	3.1	9.8613	0.9	4.0580	1.6	0.2902	1.3	0.83	1642.7	19.0	1645.9	12.9	1650.0	16.4	1650.0	16.4	99.6
K15-SAIS-Spot 266	183	77811	0.8	9.7712	0.8	4.1730	1.4	0.2957	1.1	0.80	1670.1	16.3	1668.7	11.4	1667.0	15.7	1667.0	15.7	100.2
K15-SAIS-Spot 267	192	64944	4.7	9.8601	0.9	4.0602	1.7	0.2904	1.5	0.85	1643.3	21.1	1646.3	14.0	1650.2	16.9	1650.2	16.9	99.6
K15-SAIS-Spot 269	244	197634	3.7	9.9824	0.8	4.0499	1.5	0.2932	1.2	0.83	1657.5	18.0	1644.3	12.1	1627.3	15.6	1627.3	15.6	101.9
K15-SAIS-Spot 271	138	237275	1.2	9.8434	0.9	4.1098	2.0	0.2934	1.8	0.89	1658.5	26.5	1656.3	16.6	1653.4	16.8	1653.4	16.8	100.3
K15-SAIS-Spot 272	276	230002	1.3	9.8404	1.4	4.0314	2.0	0.2877	1.5	0.73	1630.1	21.2	1640.5	16.3	1653.9	25.4	1653.9	25.4	98.6
K15-SAIS-Spot 273	137	307388	1.3	9.8780	0.9	4.0233	1.6	0.2882	1.4	0.82	1632.7	19.6	1638.9	13.4	1646.9	17.4	1646.9	17.4	99.1
K15-SAIS-Spot 275	472	174438	2.6	9.5833	0.8	4.4617	1.3	0.3101	1.0	0.77	1741.2	14.8	1723.9	10.5	1702.8	14.9	1702.8	14.9	102.3
K15-SAIS-Spot 276	114	61841	1.6	9.6584	1.0	4.1953	1.6	0.2939	1.2	0.79	1660.9	18.2	1673.1	12.9	1688.5	17.6	1688.5	17.6	98.4
K15-SAIS-Spot 277	230	145710	2.3	9.3633	0.9	4.4628	1.7	0.3031	1.4	0.86	1706.5	21.3	1724.1	13.8	1745.5	15.7	1745.5	15.7	97.8
K15-SAIS-Spot 278	55	34306	1.1	9.8773	1.4	4.0752	2.1	0.2919	1.5	0.74	1651.2	22.1	1649.4	16.7	1647.0	25.7	1647.0	25.7	100.3
K15-SAIS-Spot 280	130	219875	1.3	9.8933	1.0	4.0783	1.6	0.2926	1.2	0.77	1654.7	17.4	1650.0	12.6	1644.0	18.4	1644.0	18.4	100.6
K15-SAIS-Spot 281	251	153937	1.1	9.6832	0.8	4.2604	1.5	0.2992	1.3	0.85	1687.4	18.9	1685.7	12.3	1683.7	14.5	1683.7	14.5	100.2
K15-SAIS-Spot 282	87	47860	1.2	9.6482	1.0	4.1189	1.7	0.2882	1.4	0.82	1632.6	20.1	1658.1	13.9	1690.4	17.8	1690.4	17.8	96.6
K15-SAIS-Spot 283	147	135392	2.5	8.6918	0.9	5.4182	1.7	0.3416	1.4	0.83	1894.2	23.1	1887.7	14.6	1880.7	17.1	1880.7	17.1	100.7
K15-SAIS-Spot 284	148	201731	2.4	9.7168	0.9	4.1799	1.6	0.2946	1.4	0.84	1664.3	20.1	1670.1	13.4	1677.3	16.3	1677.3	16.3	99.2
K15-SAIS-Spot 285	173	71966	1.9	9.8811	1.0	3.9565	1.8	0.2835	1.4	0.81	1609.2	20.4	1625.3	14.3	1646.3	19.2	1646.3	19.2	97.7
K15-SAIS-Spot 286	235	69731	0.7	9.9826	0.9	3.8568	1.3	0.2792	1.0	0.73	1587.5	13.4	1604.7	10.6	1627.3	16.7	1627.3	16.7	97.6
K15-SAIS-Spot 287	75	157377	1.7	9.8307	1.1	4.1619	1.8	0.2967	1.5	0.79	1675.1	21.5	1666.6	15.0	1655.8	20.7	1655.8	20.7	101.2
K15-SAIS-Spot 288	638	113489	4.1	7.9907	0.8	5.2767	1.7	0.3058	1.5	0.89	1720.0	23.3	1865.1	14.7	2030.8	13.6	2030.8	13.6	84.7
K15-SAIS-Spot 289	295	84360	4.1	9.5400	0.9	4.4062	1.8	0.3049	1.5	0.85	1715.4	22.6	1713.5	14.7	1711.2	17.4	1711.2	17.4	100.2
K15-SAIS-Spot 290	125	148667	1.3	9.7105	1.0	4.1354	1.4	0.2912	1.1	0.75	1647.8	15.7	1661.3	11.8	1678.5	17.8	1678.5	17.8	98.2
K15-SAIS-Spot 291	219	1363254	2.1	9.8722	0.9	3.8790	1.3	0.2777	1.0	0.74	1580.0	13.4	1609.3	10.5	1648.0	16.3	1648.0	16.3	95.9
K15-SAIS-Spot 292	250	244212	3.1	9.5657	0.7	4.2943	1.2	0.2979	1.0	0.80	1681.0	14.8	1692.3	10.3	1706.2	13.7	1706.2	13.7	98.5
K15-SAIS-Spot 293	292	204623	0.8	9.8189	0.7	4.1076	1.3	0.2925	1.1	0.86	1654.1	16.1	1655.8	10.5	1658.0	12.2	1658.0	12.2	99.8
K15-SAIS-Spot 294	256	85191	1.6	9.7004	0.9	4.1942	1.4	0.2951	1.1	0.77	1666.9	16.0	1672.9	11.7	1680.4	16.9	1680.4	16.9	99.2
K15-SAIS-Spot 295	330	198098	1.3	9.6246	0.7	4.1549	1.2	0.2900	0.9	0.79	1641.7	13.5	1665.2	9.6	1694.9	13.1	1694.9	13.1	96.9
K15-SAIS-Spot 296	469	478209	3.5	9.6725	0.9	4.3199	1.5	0.3030	1.2	0.79	1706.4	18.3	1697.2	12.7	1685.8	17.3	1685.8	17.3	101.2
K15-SAIS-Spot 297	505	377035	2.2	9.7363	0.7	4.2113	1.4	0.2974	1.2	0.85	1678.3	17.0	1676.2	11.2	1673.6	13.4	1673.6	13.4	100.3
K15-SAIS-Spot 298	376	190216	1.5	9.6811	0.9	3.7849	1.5	0.2658	1.2	0.80	1519.2	16.4	1589.5	12.1	1684.1	16.6	1684.1	16.6	90.2
K15-SAIS-Spot 299	336	58794	1.5	9.6696	0.7	4.1804	1.3	0.2932	1.1	0.83	1657.4	16.2	1670.2	11.0	1686.3	13.8	1686.3	13.8	98.3
K15-SAIS-Spot 300	258	1750884	0.7	9.7721	1.1	3.8449	1.9	0.2725	1.6	0.82	1553.5	21.9	1602.2	15.6	1666.8	20.4	1666.8	20.4	93.2
K15-SAIS-Spot 301	190	210318	1.7	9.6250	1.1	4.2335	1.7	0.2955	1.3	0.76	1669.1	19.0	1680.5	13.8	1694.8	20.0	1694.8	20.0	98.5
K15-SAIS-Spot 302	296	247540	1.2	9.8988	0.7	4.0616	1.2	0.2916	1.0	0.83	1649.5	14.8	1646.6	10.0	1643.0	12.8	1643.0	12.8	100.4

K15-SAIS-Spot 303	389	84845	1.6	9.7484	0.6	4.2080	1.1	0.2975	0.9	0.85	1679.0	13.1	1675.6	8.6	1671.3	10.4	1671.3	10.4	100.5
K15-SAIS-Spot 304	313	390354	1.6	9.8982	1.1	4.0192	1.5	0.2885	1.1	0.73	1634.2	16.2	1638.1	12.5	1643.1	19.6	1643.1	19.6	99.5
K15-SAIS-Spot 305	403	125048	1.9	9.6832	0.7	4.3505	1.5	0.3055	1.3	0.86	1718.7	19.0	1703.0	12.1	1683.7	13.6	1683.7	13.6	102.1
K15-SAIS-Spot 306	71	57456	1.2	9.8971	1.1	4.1676	1.7	0.2991	1.3	0.76	1687.1	19.7	1667.7	14.2	1643.3	20.9	1643.3	20.9	102.7
K15-SAIS-Spot 307	336	104129	2.3	9.8439	0.7	4.0910	1.5	0.2921	1.3	0.86	1651.9	18.4	1652.5	12.0	1653.3	13.9	1653.3	13.9	99.9
K15-SAIS-Spot 308	382	88947	1.5	9.3884	0.7	4.5332	1.2	0.3087	1.0	0.83	1734.2	15.7	1737.1	10.3	1740.6	12.8	1740.6	12.8	99.6
K15-SAIS-Spot 309	295	71107	2.5	9.4395	0.8	4.4884	1.1	0.3073	0.8	0.71	1727.3	12.4	1728.8	9.5	1730.6	14.9	1730.6	14.9	99.8
K15-SAIS-Spot 310	123	65713	2.2	9.8309	1.0	4.1379	1.8	0.2950	1.5	0.83	1666.6	22.4	1661.8	15.1	1655.7	19.3	1655.7	19.3	100.7
K15-SAIS-Spot 311	480	216266	2.4	9.5131	0.6	4.4945	1.2	0.3101	1.0	0.86	1741.2	15.8	1730.0	9.9	1716.4	11.2	1716.4	11.2	101.4
K15-SAIS-Spot 312	251	73578	1.1	9.7734	0.8	3.6445	1.6	0.2583	1.4	0.86	1481.3	18.5	1559.3	13.0	1666.6	15.7	1666.6	15.7	88.9
K15-SAIS-Spot 313	265	104925	1.8	9.8255	0.8	4.0134	1.7	0.2860	1.5	0.87	1621.5	21.5	1636.9	14.0	1656.7	15.7	1656.7	15.7	97.9
K15-SAIS-Spot 314	532	223356	1.2	9.6064	0.9	4.2857	1.5	0.2986	1.2	0.79	1684.3	17.2	1690.6	12.0	1698.4	16.4	1698.4	16.4	99.2
K15-SAIS-Spot 315	145	96004	1.4	9.5925	1.0	4.1062	1.5	0.2857	1.2	0.77	1619.9	17.1	1655.5	12.6	1701.1	18.0	1701.1	18.0	95.2

K12-NCM-QTZ-1	102	99041	2.1	9.5668	0.6	4.2651	1.6	0.2959	1.5	0.93	1671.1	22.0	1686.7	13.3	1706.0	11.2	1706.0	11.2	98.0
K12-NCM-QTZ-3	96	123337	1.3	9.4342	0.8	4.5393	1.2	0.3106	0.9	0.75	1743.6	14.0	1738.2	10.1	1731.7	14.7	1731.7	14.7	100.7
K12-NCM-QTZ-4	174	4923	2.5	9.4982	0.8	4.0792	3.6	0.2810	3.5	0.97	1596.4	50.2	1650.1	29.7	1719.3	15.5	1719.3	15.5	92.9
K12-NCM-QTZ-5	132	162412	2.3	9.4830	0.7	4.4545	1.0	0.3064	0.7	0.73	1722.8	10.7	1722.5	8.0	1722.2	12.0	1722.2	12.0	100.0
K12-NCM-QTZ-6	134	22924	1.1	9.4365	0.9	4.5885	5.0	0.3140	5.0	0.98	1760.5	76.3	1747.2	41.9	1731.2	16.2	1731.2	16.2	101.7
K12-NCM-QTZ-7	89	114253	2.5	9.6023	0.7	4.4000	1.3	0.3064	1.1	0.83	1723.1	17.0	1712.4	11.1	1699.2	13.7	1699.2	13.7	101.4
K12-NCM-QTZ-8	87	8230	1.9	9.4528	0.5	4.4141	14.4	0.3026	14.4	1.00	1704.3	216.0	1715.0	120.0	1728.0	9.3	1728.0	9.3	98.6
K12-NCM-QTZ-9	186	5923	1.5	9.5162	1.0	4.3579	6.4	0.3008	6.3	0.99	1695.1	94.0	1704.4	52.7	1715.8	17.5	1715.8	17.5	98.8
K12-NCM-QTZ-10	122	122348	2.0	9.5991	0.4	4.4287	1.1	0.3083	1.0	0.94	1732.5	15.2	1717.7	8.8	1699.8	6.9	1699.8	6.9	101.9
K12-NCM-QTZ-12	205	36182	1.9	9.5364	0.4	4.5662	1.5	0.3158	1.4	0.97	1769.3	21.7	1743.1	12.1	1711.9	6.7	1711.9	6.7	103.4
K12-NCM-QTZ-13	127	149182	2.4	9.4633	0.6	4.6021	2.4	0.3159	2.3	0.96	1769.5	35.7	1749.6	20.0	1726.0	11.8	1726.0	11.8	102.5
K12-NCM-QTZ-14	88	235930	1.0	9.4973	0.6	4.6278	2.0	0.3188	1.8	0.95	1783.7	28.8	1754.3	16.3	1719.4	11.4	1719.4	11.4	103.7
K12-NCM-QTZ-15	88	78269	1.0	9.4536	0.8	4.5929	1.2	0.3149	0.9	0.76	1764.8	14.1	1748.0	9.9	1727.9	14.2	1727.9	14.2	102.1
K12-NCM-QTZ-16	235	3098	1.1	9.2878	1.6	3.7351	11.6	0.2516	11.5	0.99	1446.7	149.4	1578.9	93.5	1760.3	30.0	1760.3	30.0	82.2
K12-NCM-QTZ-17	146	117289	1.6	9.5127	0.5	4.5504	1.7	0.3139	1.6	0.96	1760.1	25.1	1740.2	14.1	1716.4	8.9	1716.4	8.9	102.5
K12-NCM-QTZ-18	202	356774	1.6	9.4949	0.2	4.5414	1.6	0.3127	1.6	0.99	1754.2	24.6	1738.6	13.4	1719.9	3.4	1719.9	3.4	102.0
K12-NCM-QTZ-19	107	115353	2.3	9.5459	0.6	4.5477	3.1	0.3149	3.1	0.98	1764.5	47.8	1739.7	26.2	1710.0	10.7	1710.0	10.7	103.2
K12-NCM-QTZ-20	167	138582	1.7	9.4649	0.4	4.6599	1.9	0.3199	1.8	0.97	1789.1	28.7	1760.1	15.8	1725.7	8.2	1725.7	8.2	103.7
K12-NCM-QTZ-21	133	57144	1.6	9.5007	0.7	4.5749	1.9	0.3152	1.8	0.93	1766.4	27.4	1744.7	15.9	1718.8	13.3	1718.8	13.3	102.8
K12-NCM-QTZ-23	151	360691	1.5	9.4650	0.5	4.4704	1.0	0.3069	0.9	0.86	1725.3	12.9	1725.5	8.2	1725.7	9.2	1725.7	9.2	100.0
K12-NCM-QTZ-24	55	62032	1.5	9.4052	1.0	4.4774	1.4	0.3054	1.0	0.72	1718.1	15.0	1726.8	11.4	1737.3	17.5	1737.3	17.5	98.9
K12-NCM-QTZ-25	115	44336	1.4	9.4775	1.3	4.6568	4.4	0.3201	4.2	0.96	1790.2	66.4	1759.5	37.0	1723.3	23.3	1723.3	23.3	103.9
K12-NCM-QTZ-26	205	9891	2.0	9.4775	0.6	4.2335	1.7	0.2910	1.6	0.94	1646.5	22.8	1680.5	13.7	1723.3	10.6	1723.3	10.6	95.5
K12-NCM-QTZ-27	448	67291	2.4	9.3970	0.2	4.3846	2.2	0.2988	2.2	0.99	1685.5	32.3	1709.4	18.1	1738.9	4.2	1738.9	4.2	96.9
K12-NCM-QTZ-28	148	126787	2.3	9.5812	0.3	4.3114	1.2	0.2996	1.1	0.96	1689.3	17.0	1695.5	9.8	1703.2	6.3	1703.2	6.3	99.2
K12-NCM-QTZ-29	94	184438	1.4	9.5066	0.8	4.6265	2.3	0.3190	2.2	0.94	1784.8	33.7	1754.1	19.3	1717.6	15.0	1717.6	15.0	103.9
K12-NCM-QTZ-30	138	205751	2.3	9.4250	0.6	4.5267	2.5	0.3094	2.5	0.97	1737.9	37.7	1735.9	21.2	1733.5	11.0	1733.5	11.0	100.3
K12-NCM-QTZ-31	169	21183	2.3	9.5049	0.6	4.4627	2.6	0.3076	2.5	0.97	1729.1	38.2	1724.1	21.5	1717.9	11.2	1717.9	11.2	100.6

K12-NCM-QTZ-32	156	58735	1.6	9.5244	0.5	4.4306	2.4	0.3061	2.3	0.98	1721.3	34.9	1718.1	19.6	1714.2	8.8	1714.2	8.8	100.4
K12-NCM-QTZ-34	107	286203	1.2	9.4467	0.5	4.3970	1.9	0.3013	1.8	0.97	1697.5	27.5	1711.8	15.8	1729.2	9.0	1729.2	9.0	98.2
K12-NCM-QTZ-35	177	137500	1.9	9.5568	0.4	4.3451	1.1	0.3012	1.1	0.95	1697.1	15.7	1702.0	9.2	1707.9	6.5	1707.9	6.5	99.4
K12-NCM-QTZ-36	147	27363	1.8	9.5424	0.8	4.4299	1.4	0.3066	1.1	0.79	1723.9	16.7	1718.0	11.5	1710.7	15.6	1710.7	15.6	100.8
K12-NCM-QTZ-37	164	137584	1.8	9.5785	0.4	4.5611	2.1	0.3169	2.0	0.98	1774.4	31.7	1742.2	17.3	1703.8	7.4	1703.8	7.4	104.1
K12-NCM-QTZ-38	147	85303	1.7	9.5292	0.5	4.5720	1.5	0.3160	1.5	0.95	1770.1	22.5	1744.2	12.7	1713.3	8.7	1713.3	8.7	103.3
K12-NCM-QTZ-39	158	130888	2.0	9.4789	0.6	4.5049	2.9	0.3097	2.9	0.98	1739.2	43.5	1731.9	24.2	1723.0	10.4	1723.0	10.4	100.9
K12-NCM-QTZ-40	87	137765	1.8	9.4824	0.8	4.4393	1.7	0.3053	1.5	0.88	1717.6	22.7	1719.7	14.2	1722.3	15.0	1722.3	15.0	99.7
K12-NCM-QTZ-41	131	46886	1.9	9.4666	1.5	4.6251	3.2	0.3176	2.8	0.87	1777.8	43.3	1753.8	26.6	1725.4	28.4	1725.4	28.4	103.0
K12-NCM-QTZ-42	127	122375	1.4	9.5556	0.8	4.3267	1.8	0.2999	1.7	0.91	1690.6	24.6	1698.5	15.0	1708.2	14.0	1708.2	14.0	99.0
K12-NCM-QTZ-43	103	114474	1.6	9.4309	0.6	4.5248	1.4	0.3095	1.3	0.91	1738.2	19.3	1735.5	11.6	1732.3	10.6	1732.3	10.6	100.3
K12-NCM-QTZ-44	190	6441	1.5	9.5150	0.6	4.1579	2.6	0.2869	2.5	0.98	1626.2	36.4	1665.8	21.3	1716.0	10.5	1716.0	10.5	94.8
K12-NCM-QTZ-45	140	100630	1.6	9.5318	0.8	4.4097	1.7	0.3048	1.5	0.88	1715.3	22.4	1714.2	14.1	1712.8	15.0	1712.8	15.0	100.1
K12-NCM-QTZ-46	197	56415	1.0	9.3593	0.9	4.6138	2.9	0.3132	2.8	0.95	1756.4	43.2	1751.8	24.6	1746.3	16.3	1746.3	16.3	100.6
K12-NCM-QTZ-47	237	71507	1.4	9.5394	0.4	4.4513	1.4	0.3080	1.4	0.95	1730.7	20.7	1721.9	11.9	1711.3	7.9	1711.3	7.9	101.1
K12-NCM-QTZ-48	185	220599	3.6	9.3218	0.5	4.7845	1.4	0.3235	1.3	0.94	1806.7	20.3	1782.2	11.5	1753.6	8.5	1753.6	8.5	103.0
K12-NCM-QTZ-49	171	326351	1.5	9.3937	0.7	4.5195	2.5	0.3079	2.4	0.95	1730.4	36.4	1734.6	20.9	1739.6	13.7	1739.6	13.7	99.5
K12-NCM-QTZ-50	178	22808	1.3	9.3623	0.7	4.2222	4.7	0.2867	4.7	0.99	1625.0	66.9	1678.3	38.6	1745.7	12.0	1745.7	12.0	93.1
K12-NCM-QTZ-51	204	13894	3.3	9.3979	0.3	4.2859	1.5	0.2921	1.5	0.97	1652.1	21.6	1690.7	12.5	1738.7	6.4	1738.7	6.4	95.0
K12-NCM-QTZ-52	119	32476	2.2	9.4080	0.3	4.3283	1.8	0.2953	1.8	0.99	1668.1	26.2	1698.8	14.9	1736.8	5.2	1736.8	5.2	96.0
K12-NCM-QTZ-53	159	4444	2.4	9.3928	1.1	4.4202	2.8	0.3011	2.6	0.91	1696.8	38.4	1716.1	23.3	1739.7	20.9	1739.7	20.9	97.5
K12-NCM-QTZ-55	82	113256	1.3	5.4603	0.3	13.3366	1.8	0.5282	1.7	0.98	2733.7	38.5	2703.8	16.6	2681.5	5.5	2681.5	5.5	101.9
K12-NCM-QTZ-56	183	84318	0.9	9.4578	0.5	4.4411	1.2	0.3046	1.1	0.92	1714.3	15.9	1720.0	9.6	1727.1	8.5	1727.1	8.5	99.3
K12-NCM-QTZ-57	106	215906	1.9	9.5305	0.6	4.3560	1.0	0.3011	0.8	0.80	1696.7	11.6	1704.0	8.1	1713.0	10.9	1713.0	10.9	99.1
K12-NCM-QTZ-58	108	124099	2.0	9.3154	0.6	4.7115	1.3	0.3183	1.2	0.90	1781.5	18.2	1769.3	10.9	1754.9	10.3	1754.9	10.3	101.5
K12-NCM-QTZ-60	237	68468	1.6	9.4876	0.3	4.3836	0.9	0.3016	0.9	0.93	1699.4	12.8	1709.3	7.6	1721.3	6.3	1721.3	6.3	98.7
K12-NCM-QTZ-61	137	10215	1.9	9.5033	0.7	3.9394	8.9	0.2715	8.9	1.00	1548.5	122.3	1621.8	72.2	1718.3	12.1	1718.3	12.1	90.1
K12-NCM-QTZ-62	65	52338	1.9	9.5327	1.0	4.5202	8.3	0.3125	8.2	0.99	1753.1	125.8	1734.7	68.7	1712.6	18.5	1712.6	18.5	102.4
K12-NCM-QTZ-63	264	13331	3.0	9.3384	0.4	4.1529	2.5	0.2813	2.4	0.98	1597.7	34.1	1664.8	20.1	1750.4	8.1	1750.4	8.1	91.3
K12-NCM-QTZ-64	129	2148	1.7	9.3707	3.4	4.4727	4.2	0.3040	2.5	0.59	1711.0	36.9	1725.9	34.5	1744.0	61.4	1744.0	61.4	98.1
K12-NCM-QTZ-66	128	166528	1.5	9.4410	0.4	4.6070	1.2	0.3155	1.1	0.95	1767.5	17.1	1750.5	9.7	1730.3	7.0	1730.3	7.0	102.1
K12-NCM-QTZ-68	458	45495	2.7	9.5542	0.3	4.4918	1.7	0.3113	1.7	0.99	1746.9	25.6	1729.5	14.1	1708.4	5.1	1708.4	5.1	102.2
K12-NCM-QTZ-69	220	5644	1.3	9.4941	0.7	4.3783	4.6	0.3015	4.6	0.99	1698.6	68.4	1708.3	38.3	1720.0	12.1	1720.0	12.1	98.8
K12-NCM-QTZ-70	92	177311	1.4	9.5398	0.9	4.5401	3.7	0.3141	3.6	0.97	1761.0	55.0	1738.4	30.6	1711.2	16.4	1711.2	16.4	102.9
K12-NCM-QTZ-71	136	156061	2.7	9.4233	0.4	4.6469	1.1	0.3176	1.1	0.95	1777.9	16.4	1757.7	9.3	1733.8	6.7	1733.8	6.7	102.5
K12-NCM-QTZ-72	162	155540	1.5	9.5920	0.3	4.4787	2.6	0.3116	2.5	0.99	1748.5	38.8	1727.0	21.2	1701.2	5.2	1701.2	5.2	102.8
K12-NCM-QTZ-73	369	5610	1.2	9.3257	2.2	4.2855	4.4	0.2899	3.9	0.87	1640.8	56.0	1690.6	36.6	1752.9	40.2	1752.9	40.2	93.6
K12-NCM-QTZ-75	106	15221	1.9	9.5148	0.9	3.9102	3.4	0.2698	3.2	0.96	1540.0	44.4	1615.8	27.3	1716.0	17.5	1716.0	17.5	89.7
K12-NCM-QTZ-77	113	27352	1.7	9.5311	0.7	3.9784	5.2	0.2750	5.1	0.99	1566.2	71.5	1629.8	42.2	1712.9	13.4	1712.9	13.4	91.4
K12-NCM-QTZ-78	147	257436	1.9	9.4291	0.5	4.5169	2.1	0.3089	2.0	0.97	1735.3	31.1	1734.1	17.5	1732.6	8.8	1732.6	8.8	100.2
K12-NCM-QTZ-79	214	180533	2.9	9.3753	0.5	4.6486	1.5	0.3161	1.4	0.94	1770.6	21.7	1758.0	12.4	1743.1	9.0	1743.1	9.0	101.6
K12-NCM-QTZ-80	148	83756	2.0	9.5559	0.4	4.4930	3.7	0.3114	3.6	0.99	1747.5	55.6	1729.7	30.4	1708.1	8.1	1708.1	8.1	102.3
K12-NCM-QTZ-81	193	6251	1.5	9.4518	1.1	4.2766	12.2	0.2932	12.2	1.00	1657.3	177.9	1688.9	100.9	1728.2	20.2	1728.2	20.2	95.9

K12-NCM-QTZ-82	68	86680	1.4	9.5238	1.1	4.4366	1.7	0.3064	1.2	0.74	1723.2	18.8	1719.2	13.9	1714.3	20.7	1714.3	20.7	100.5
K12-NCM-QTZ-83	171	38634	1.8	9.5455	0.6	4.4272	1.9	0.3065	1.8	0.95	1723.5	28.0	1717.4	16.0	1710.1	10.6	1710.1	10.6	100.8
K12-NCM-QTZ-84	156	12898	1.8	9.4994	0.6	4.3888	1.6	0.3024	1.5	0.94	1703.0	22.8	1710.2	13.4	1719.0	10.3	1719.0	10.3	99.1
K12-NCM-QTZ-85	136	4987	2.1	9.4644	0.9	3.8966	2.4	0.2675	2.2	0.93	1527.9	30.1	1613.0	19.2	1725.8	15.8	1725.8	15.8	88.5
K12-NCM-QTZ-86	135	4724	1.4	9.3830	1.2	4.1979	3.4	0.2857	3.2	0.94	1619.9	46.5	1673.6	28.3	1741.6	21.5	1741.6	21.5	93.0
K12-NCM-QTZ-88	290	6575	1.2	9.4541	0.6	4.0591	3.5	0.2783	3.5	0.98	1582.9	49.1	1646.1	28.9	1727.8	11.3	1727.8	11.3	91.6
K12-NCM-QTZ-89	172	146892	1.6	9.5863	0.4	4.4454	1.4	0.3091	1.4	0.95	1736.1	20.6	1720.8	11.8	1702.3	7.9	1702.3	7.9	102.0
K12-NCM-QTZ-90	90	180447	2.0	9.5326	0.9	4.4898	1.8	0.3104	1.6	0.87	1742.7	24.0	1729.1	14.9	1712.6	16.1	1712.6	16.1	101.8
K12-NCM-QTZ-91	201	243315	2.2	9.4997	0.5	4.6145	3.1	0.3179	3.1	0.99	1779.6	47.4	1751.9	25.8	1719.0	8.8	1719.0	8.8	103.5
K12-NCM-QTZ-92	221	14749	1.6	9.5091	0.5	4.5227	8.0	0.3119	7.9	1.00	1750.1	121.8	1735.1	66.3	1717.1	9.3	1717.1	9.3	101.9
K12-NCM-QTZ-93	136	26886	2.2	9.4834	0.5	4.3968	1.1	0.3024	1.0	0.88	1703.3	14.4	1711.7	9.1	1722.1	9.7	1722.1	9.7	98.9
K12-NCM-QTZ-94	206	8524	1.3	9.4418	0.5	4.5061	4.4	0.3086	4.4	0.99	1733.7	67.0	1732.1	36.9	1730.2	8.4	1730.2	8.4	100.2
K12-NCM-QTZ-95	117	15171	1.6	9.6083	1.0	3.8071	2.5	0.2653	2.3	0.92	1516.9	31.1	1594.2	20.2	1698.0	18.6	1698.0	18.6	89.3
K12-NCM-QTZ-96	121	3978	2.2	9.4733	2.3	3.8027	3.7	0.2613	2.9	0.79	1496.3	38.8	1593.3	29.7	1724.1	41.8	1724.1	41.8	86.8
K12-NCM-QTZ-97	147	10295	2.1	9.4674	0.7	4.4608	1.8	0.3063	1.7	0.93	1722.4	25.9	1723.7	15.3	1725.2	12.6	1725.2	12.6	99.8
K12-NCM-QTZ-98	164	264277	2.3	9.5925	0.5	4.4153	1.0	0.3072	0.8	0.83	1726.8	12.2	1715.2	8.0	1701.1	9.8	1701.1	9.8	101.5
K12-NCM-QTZ-99	121	38973	1.6	9.5272	0.6	4.3242	1.6	0.2988	1.4	0.93	1685.3	21.4	1698.0	12.9	1713.6	10.8	1713.6	10.8	98.3
K12-NCM-QTZ-100	109	7694	2.2	9.3676	1.2	4.4682	1.8	0.3036	1.4	0.75	1709.0	20.4	1725.1	15.0	1744.7	21.9	1744.7	21.9	98.0
K12-NCM-QTZ-101	205	9365	1.7	9.4752	0.4	4.2593	1.5	0.2927	1.5	0.96	1655.0	21.7	1685.5	12.7	1723.7	7.7	1723.7	7.7	96.0
K12-NCM-QTZ-102	118	240153	2.8	9.5063	0.3	4.6528	2.3	0.3208	2.2	0.99	1793.6	35.1	1758.8	18.9	1717.7	5.4	1717.7	5.4	104.4
K12-NCM-QTZ-103	99	117552	1.5	9.5734	0.8	4.4096	1.9	0.3062	1.8	0.90	1721.8	26.5	1714.1	16.1	1704.7	15.4	1704.7	15.4	101.0
K12-NCM-QTZ-104	141	49734	1.2	9.4485	0.5	4.5922	1.1	0.3147	0.9	0.87	1763.8	14.4	1747.9	8.9	1728.9	9.8	1728.9	9.8	102.0
K12-NCM-QTZ-105	133	157096	3.4	9.4077	0.5	4.6830	2.4	0.3195	2.3	0.98	1787.4	36.3	1764.2	19.9	1736.8	9.1	1736.8	9.1	102.9
K12-NCM-QTZ-106	88	74120	2.3	9.4718	1.1	4.4093	4.0	0.3029	3.8	0.96	1705.7	57.0	1714.1	32.8	1724.4	20.2	1724.4	20.2	98.9
K12-NCM-QTZ-107	95	113738	1.8	9.5406	0.7	4.6071	1.2	0.3188	1.0	0.85	1783.8	16.3	1750.6	10.3	1711.1	12.0	1711.1	12.0	104.3
K12-NCM-QTZ-108	126	93803	2.2	9.5160	0.8	4.6629	2.0	0.3218	1.8	0.91	1798.6	28.4	1760.6	16.6	1715.8	15.0	1715.8	15.0	104.8
K12-NCM-QTZ-109	133	33917	1.8	9.5414	0.7	4.3397	1.4	0.3003	1.2	0.86	1692.8	17.5	1700.9	11.3	1710.9	12.7	1710.9	12.7	98.9
K12-NCM-QTZ-110	123	20326	2.2	9.5765	0.5	4.2521	1.2	0.2953	1.0	0.88	1668.1	15.1	1684.1	9.6	1704.1	10.1	1704.1	10.1	97.9
K12-NCM-QTZ-112	104	6165	2.3	9.4176	1.4	4.3067	4.3	0.2942	4.1	0.95	1662.3	60.3	1694.6	35.7	1734.9	25.0	1734.9	25.0	95.8
K12-NCM-QTZ-113	121	93154	1.9	9.5435	0.2	4.5468	3.0	0.3147	3.0	1.00	1763.8	45.8	1739.6	24.8	1710.5	4.3	1710.5	4.3	103.1
K12-NCM-QTZ-114	165	53967	1.6	9.4961	1.0	4.4145	1.5	0.3040	1.1	0.74	1711.3	16.9	1715.1	12.5	1719.7	18.7	1719.7	18.7	99.5
K12-NCM-QTZ-115	201	8726	1.1	9.5810	0.6	4.0097	3.0	0.2786	2.9	0.98	1584.4	41.3	1636.2	24.5	1703.3	11.9	1703.3	11.9	93.0
K12-NCM-QTZ-117	133	70700	1.5	9.4264	0.9	4.5699	3.3	0.3124	3.2	0.97	1752.7	49.6	1743.8	27.9	1733.2	15.9	1733.2	15.9	101.1
K12-NCM-QTZ-118	142	24561	1.7	9.5595	0.9	4.2268	2.3	0.2931	2.1	0.92	1656.8	30.4	1679.2	18.6	1707.4	16.3	1707.4	16.3	97.0
K12-NCM-QTZ-119	160	209478	1.8	9.4922	0.3	4.5816	1.7	0.3154	1.7	0.98	1767.3	26.1	1745.9	14.3	1720.4	6.0	1720.4	6.0	102.7
K12-NCM-QTZ-120	128	197935	1.8	9.4634	0.5	4.4996	3.1	0.3088	3.1	0.99	1734.9	47.3	1730.9	26.2	1726.0	9.2	1726.0	9.2	100.5

Table A3-6. Lu-Hf isotope results from detrital zircon (ALC)

Sample	(176Yb + 176Lu) / 176Hf (%)	Volts Hf	$^{176}Hf/^{177}Hf$	± (1s)	$^{176}Lu/^{177}Hf$	$^{176}Hf/^{177}Hf$ (T)	E-Hf (0)	E-Hf (0) ± (1s)	E-Hf (T)	Age (Ma)

K12-NCM-QTZ-4	53.0	0.8	0.282189	0.000110	0.004030	0.282057	-21.1	3.9	12.9	1719
K12-NCM-QTZ-5	19.2	1.9	0.282050	0.000048	0.001536	0.282000	-26.0	1.7	10.9	1722
K12-NCM-QTZ-40	14.6	2.3	0.282007	0.000038	0.000973	0.281975	-27.5	1.4	10.0	1722
K12-NCM-QTZ-39	15.6	2.2	0.282056	0.000034	0.001016	0.282023	-25.8	1.2	11.7	1723
K12-NCM-QTZ-31	18.1	1.9	0.282028	0.000036	0.001181	0.281989	-26.8	1.3	10.4	1718
K12-NCM-QTZ-26	18.5	1.7	0.282043	0.000047	0.001232	0.282002	-26.3	1.7	11.0	1723
K12-NCM-QTZ-93	22.6	2.5	0.281990	0.000031	0.001537	0.281940	-28.1	1.1	8.8	1722
K12-NCM-QTZ-91	19.7	2.1	0.282075	0.000040	0.001144	0.282038	-25.1	1.4	12.2	1719
K12-NCM-QTZ-96	24.1	1.9	0.282090	0.000035	0.001387	0.282044	-24.6	1.2	12.5	1724
K12-NCM-QTZ-97	17.0	1.9	0.282104	0.000047	0.000984	0.282071	-24.1	1.7	13.5	1725
K12-NCM-QTZ-41	45.8	1.9	0.281988	0.000057	0.002986	0.281890	-28.2	2.0	7.1	1725
K12-NCM-QTZ-84	12.9	2.0	0.282041	0.000039	0.000806	0.282014	-26.3	1.4	11.3	1719
K12-NCM-QTZ-85	19.5	1.8	0.282081	0.000042	0.001129	0.282044	-24.9	1.5	12.6	1726
K12-NCM-QTZ-14	8.5	2.0	0.281951	0.000033	0.000493	0.281935	-29.5	1.2	8.5	1719
K12-NCM-QTZ-61	18.2	1.8	0.282135	0.000038	0.001174	0.282097	-23.0	1.4	14.2	1718
K12-NCM-QTZ-17	13.1	2.0	0.282041	0.000036	0.000931	0.282011	-26.3	1.3	11.2	1716
K12-NCM-QTZ-20	19.2	1.7	0.282081	0.000034	0.001241	0.282040	-24.9	1.2	12.4	1726
K12-NCM-QTZ-18	14.1	2.2	0.281934	0.000037	0.000906	0.281904	-30.1	1.3	7.5	1720
K12-NCM-QTZ-119	16.9	1.7	0.282117	0.000056	0.001064	0.282082	-23.6	2.0	13.8	1720
K12-NCM-QTZ-23	6.2	2.0	0.281938	0.000033	0.000364	0.281926	-29.9	1.2	8.4	1726
K12-NCM-QTZ-25	16.7	1.8	0.282043	0.000035	0.000962	0.282011	-26.2	1.2	11.3	1723
K12-NCM-QTZ-21	12.2	1.9	0.281961	0.000037	0.000758	0.281936	-29.2	1.3	8.6	1719
K12-NCM-QTZ-55	10.7	2.3	0.281279	0.000031	0.000648	0.281246	-53.3	1.1	6.4	2682
K12-NCM-QTZ-60	19.6	2.1	0.282097	0.000038	0.001437	0.282050	-24.3	1.3	12.7	1721
K12-NCM-QTZ-69	31.1	1.6	0.282015	0.000044	0.001933	0.281952	-27.2	1.5	9.2	1720
K12-NCM-QTZ-101	16.9	1.9	0.282064	0.000044	0.001073	0.282029	-25.5	1.6	12.0	1724
K12-NCM-QTZ-102	16.6	1.2	0.282132	0.000060	0.001226	0.282092	-23.1	2.1	14.1	1718
K12-NCM-QTZ-106	15.3	2.3	0.282097	0.000031	0.000918	0.282067	-24.3	1.1	13.3	1724
K12-NCM-QTZ-119	18.5	2.3	0.282073	0.000040	0.001254	0.282032	-25.2	1.4	12.0	1720
K15 Estadio-3 9	19.0	6.5	0.281902	0.000025	0.001174	0.281865	-31.2	0.9	5.0	1666
K15 Estadio-3 22	21.7	5.6	0.281944	0.000031	0.001469	0.281898	-29.7	1.1	6.2	1666
K15 Estadio-3 38	14.6	6.9	0.281889	0.000016	0.000976	0.281859	-31.7	0.6	4.8	1666

K15 Estadio-3 60	10.6	6.6	0.280726	0.000028	0.000830	0.280674	-72.8	1.0	-0.8	3231
K15 Estadio-3 68	10.0	5.8	0.281043	0.000025	0.000845	0.281003	-61.6	0.9	-7.1	2466
K15 Estadio-3 69	17.2	6.4	0.282010	0.000025	0.001075	0.281977	-27.4	0.9	8.1	1626
K15 Estadio-3 85	30.2	5.0	0.282031	0.000031	0.002116	0.281965	-26.7	1.1	7.8	1630
K15 Estadio-3 106	18.6	5.3	0.281987	0.000034	0.001352	0.281944	-28.2	1.2	8.0	1673
K15 Estadio-3 111	6.8	7.4	0.281900	0.000024	0.000444	0.281886	-31.3	0.8	7.3	1732
K15 Estadio-3 113	22.0	5.5	0.282032	0.000023	0.001473	0.281986	-26.6	0.8	9.4	1672
K15 Estadio-3 117	24.5	5.3	0.281991	0.000031	0.001691	0.281939	-28.1	1.1	6.9	1632
K15 Estadio-3 119	26.8	5.5	0.281940	0.000036	0.001990	0.281873	-29.9	1.3	7.6	1767
K15 Estadio-3 120	22.3	6.1	0.281943	0.000028	0.001557	0.281894	-29.8	1.0	5.8	1655
K15 Estadio-3 121	16.1	4.2	0.281930	0.000027	0.001304	0.281888	-30.2	1.0	6.1	1678
K15 Estadio-3 122	20.6	7.3	0.281950	0.000022	0.001408	0.281905	-29.5	0.8	6.5	1667
K15 Estadio-3 102	19.8	7.9	0.281978	0.000023	0.001410	0.281934	-28.5	0.8	6.7	1630
K15 Estadio-3 112	25.8	5.1	0.281896	0.000019	0.001860	0.281832	-31.5	0.7	7.0	1801
K15-Estadio-3 125	28.8	4.4	0.281986	0.000034	0.001717	0.281928	-28.2	1.2	10.1	1791
K15-Estadio-3 144	16.5	6.8	0.281910	0.000026	0.001264	0.281870	-30.9	0.9	5.2	1666
K15-Estadio-3 156	36.0	5.4	0.282060	0.000024	0.002658	0.281976	-25.6	0.8	8.9	1665
K15-Estadio-3 167	27.0	4.2	0.281954	0.000026	0.002159	0.281880	-29.4	0.9	8.4	1790
K15-Estadio-3 181	14.0	4.7	0.281880	0.000032	0.001027	0.281845	-32.0	1.1	7.0	1781
K15-Estadio-3 190	9.1	5.9	0.281949	0.000025	0.000530	0.281931	-29.6	0.9	10.2	1791
K15-Estadio-3 203	19.1	6.7	0.281687	0.000028	0.001287	0.281640	-38.8	1.0	2.5	1904
K15-Estadio-3 206	19.0	2.4	0.281645	0.000057	0.001260	0.281600	-40.3	2.0	-0.1	1852
K15-Estadio-3 208	37.3	2.7	0.281851	0.000054	0.002419	0.281769	-33.0	1.9	4.3	1783
K15-Estadio-3 238	15.5	4.1	0.281560	0.000048	0.001361	0.281495	-43.3	1.7	11.2	2497
K15-Estadio-3 241	26.1	5.6	0.281949	0.000032	0.001781	0.281889	-29.6	1.1	8.8	1794
K15-Estadio-3 243	35.7	1.3	0.282072	0.000048	0.003037	0.281978	-25.2	1.7	8.2	1629
K15-Estadio-3 245	20.0	2.6	0.282036	0.000032	0.001449	0.281983	-26.5	1.1	14.9	1914
K15-Estadio-3 258	20.8	6.5	0.282049	0.000023	0.001442	0.282000	-26.0	0.8	12.7	1794
K15-Estadio-3 289	28.2	5.2	0.281236	0.000022	0.001843	0.281146	-54.8	0.8	0.0	2553
K15-ES1 8	14.5	5.9	0.281991	0.000028	0.000902	0.281963	-28.1	1.0	7.6	1627
K15-ES1 15	22.3	7.3	0.282008	0.000016	0.001430	0.281961	-27.5	0.6	10.3	1749
K15-ES1 18	28.8	7.3	0.282017	0.000016	0.001708	0.281963	-27.2	0.6	8.5	1665

K15-ES1 40	19.5	4.5	0.281966	0.000024	0.001367	0.281917	-29.0	0.8	11.5	1864
K15-ES1 51	21.7	6.5	0.281976	0.000024	0.001419	0.281927	-28.6	0.9	11.1	1835
K15-ES1 52	12.1	5.5	0.281986	0.000023	0.000792	0.281961	-28.3	0.8	7.6	1628
K15-ES1 53	23.4	7.1	0.282004	0.000021	0.001454	0.281950	-27.6	0.8	14.0	1924
K15-ES1 56	27.4	5.8	0.282049	0.000025	0.001855	0.281991	-26.0	0.9	9.5	1666
K15-ES1 58	16.6	6.2	0.282035	0.000021	0.001009	0.282003	-26.5	0.7	10.7	1700
K15-ES1 66	27.0	7.3	0.282010	0.000020	0.001899	0.281950	-27.4	0.7	8.0	1665
K15-ES1 71	19.5	7.0	0.282003	0.000022	0.001237	0.281963	-27.7	0.8	8.5	1666
K15-ES1 86	12.1	6.6	0.282010	0.000021	0.000749	0.281987	-27.4	0.8	8.1	1610
K15-ES1 89	13.2	7.7	0.281778	0.000020	0.000770	0.281752	-35.6	0.7	3.9	1791
K15-ES1 93	19.5	6.8	0.282022	0.000019	0.001206	0.281984	-27.0	0.7	9.2	1665
K15-ES1 104	18.1	5.8	0.281253	0.000019	0.001083	0.281198	-54.2	0.7	3.2	2609
K15-ES1 110	17.6	6.5	0.281998	0.000020	0.001095	0.281963	-27.8	0.7	8.5	1665
K15-ES1 134	22.2	5.3	0.282026	0.000027	0.001489	0.281981	-26.8	0.9	8.1	1620
K15-SAIS 1	53.8	4.1	0.282010	0.000025	0.003262	0.281895	-27.4	0.9	10.7	1867
K15-SAIS 24	20.7	4.3	0.281650	0.000027	0.001600	0.281574	-40.1	1.0	13.5	2479
K15-SAIS 35	16.4	5.9	0.282001	0.000022	0.001111	0.281966	-27.7	0.8	8.4	1657
K15-SAIS 41	26.2	4.8	0.281979	0.000030	0.001831	0.281922	-28.5	1.1	6.8	1656
K15-SAIS 48	14.6	8.2	0.281606	0.000020	0.000848	0.281564	-41.7	0.7	14.7	2545
K15-SAIS 68	34.2	4.7	0.281942	0.000039	0.002912	0.281845	-29.8	1.4	6.1	1744
K15-SAIS 70	32.8	5.1	0.282009	0.000028	0.002083	0.281944	-27.4	1.0	7.6	1656
K15-SAIS 79	13.7	4.7	0.281988	0.000027	0.000911	0.281958	-28.2	1.0	10.1	1743
K15-SAIS 84	5.9	2.4	0.281780	0.000026	0.000468	0.281764	-35.6	0.9	4.3	1791
K15-SAIS 108	27.1	5.0	0.281773	0.000029	0.002073	0.281703	-35.8	1.0	2.0	1783
K15-SAIS 111	61.3	7.1	0.281958	0.000045	0.004282	0.281820	-29.2	1.6	4.3	1702
K15-SAIS 131	25.1	5.0	0.281985	0.000033	0.001778	0.281931	-28.3	1.2	6.5	1627
K15-SAIS 186	24.4	6.5	0.281729	0.000025	0.001604	0.281659	-37.3	0.9	12.0	2282
K15-SAIS 180	18.5	5.9	0.281995	0.000018	0.001549	0.281941	-27.9	0.6	12.2	1859
K15-SAIS 235	25.1	5.1	0.282015	0.000024	0.001805	0.281954	-27.2	0.8	10.8	1778
K15-SAIS 251	30.4	7.1	0.281956	0.000021	0.002213	0.281886	-29.3	0.7	5.5	1655
K15-SAIS 269	67.1	3.6	0.281960	0.000042	0.004959	0.281807	-29.2	1.5	2.1	1627
K15-SAIS 275	29.7	5.1	0.281934	0.000024	0.002115	0.281865	-30.1	0.9	5.9	1703

K15-SAIS 283	10.7	4.9	0.281659	0.000022	0.000851	0.281628	-39.8	0.8	1.6	1881
K15-SAIS 286	54.4	4.9	0.282020	0.000050	0.003429	0.281914	-27.1	1.8	5.9	1627
K15-SAIS 308	25.6	4.4	0.281869	0.000028	0.001771	0.281810	-32.4	1.0	4.8	1741
K15-SAIS 310	25.5	3.9	0.282027	0.000032	0.002032	0.281963	-26.8	1.1	8.3	1656
K15-SAIS 315	23.8	5.7	0.281989	0.000023	0.001829	0.281930	-28.1	0.8	8.1	1701
K13-ES-5 8	12.1	6.0	0.281865	0.000021	0.000759	0.281841	-32.5	0.8	4.3	1670
K13-ES-5 56	23.5	4.7	0.281851	0.000027	0.001511	0.281803	-33.0	1.0	2.9	1670
K13-ES-5 67	26.3	4.9	0.281759	0.000025	0.001400	0.281711	-36.3	0.9	3.6	1841
K13-ES-5 113	10.3	6.3	0.281741	0.000022	0.000695	0.281717	-36.9	0.8	4.2	1859
K13-ES-5 124	15.2	5.1	0.282011	0.000021	0.000931	0.281982	-27.4	0.7	8.4	1633
K13-ES-5 136	20.6	6.2	0.281899	0.000022	0.001302	0.281854	-31.3	0.8	8.6	1839
K13-ES-5 141	20.4	3.5	0.281669	0.000036	0.001348	0.281622	-39.5	1.3	0.8	1858
K13-ES-5 161	19.7	5.5	0.281924	0.000020	0.001255	0.281881	-30.4	0.7	9.5	1836
K13-ES-5 182	15.0	5.5	0.281882	0.000022	0.001001	0.281850	-31.9	0.8	5.3	1699
K13-ES-5 186	13.9	5.7	0.281952	0.000026	0.000893	0.281924	-29.4	0.9	7.9	1700
K13-ES-5 194	40.3	4.7	0.282006	0.000026	0.002275	0.281934	-27.5	0.9	7.6	1671
K13-ES-5 209	29.2	2.4	0.282068	0.000037	0.002109	0.282001	-25.4	1.3	9.9	1670
K13-ES-5 222	46.1	2.7	0.281984	0.000035	0.002807	0.281894	-28.3	1.2	6.9	1702
K13-ES-5 242	17.5	3.9	0.281944	0.000031	0.001211	0.281907	-29.7	1.1	5.8	1634
K13-ES-5 259	33.0	5.4	0.282003	0.000022	0.002256	0.281934	-27.6	0.8	6.5	1622
K13-ES-5 281	22.8	6.2	0.281992	0.000018	0.001392	0.281947	-28.1	0.7	8.1	1671
K13-ES-5 313	27.5	6.0	0.281828	0.000018	0.001648	0.281775	-33.8	0.6	2.6	1700
K13-ES-5 315	16.2	2.8	0.281845	0.000042	0.001056	0.281811	-33.2	1.5	3.9	1702

CHAPTER 3 Proterozoic zircon U-Pb and Hf isotope record of southern Laurentia document southward lithospheric growth between Nuna and Rodinia assembly

Mark E. Holland[1], Karl E. Karlstrom[1], George E. Gehrels[2], Graham Begg[3], Elena Belousova[4], and William Griffin[4]

[1]Department of Earth and Planetary Sciences, University of New Mexico, Northrop Hall, 221 Yale Boulevard NE, Albuquerque, New Mexico 87131, USA;

[2]Arizona LaserChron Center, Department of Geoscience, University of Arizona, Tucson, Arizona 85721, USA

[3]Minerals Targeting International PL, West Perth, WA 6005, Australia

[4]Australian Research Council Centre of Excellence for Core to Crust Fluid Systems/GEMOC, Macquarie University, Sydney, NSW 2109, Australia

ABSTRACT

A compilation of 3540 paired U-Pb ages and Hf-isotope analyses from 2.0 to 1.0 Ga plutonic, volcanic, and metasedimentary rocks in southwestern Laurentia documents the southward growth of a >1000-km-wide belt of continental lithosphere along a long-lived convergent margin from ~1.8-1.0 Ga. From 1.8-1.6 Ga, εHf(t) values show a trend towards positive values that approach concurrent depleted mantle indicating that addition of predominantly juvenile crust accompanied accretionary orogenesis. From 1.5-1.3 Ga, Hf-isotopes reflect outboard juvenile crust formation and inboard partial melting of previously formed lithosphere in intracratonic plutons. From 1.3-1.0 Ga εHf(t) values trend towards lower εHf(t) through time indicating increased crustal reworking leading up to and during the Grenville orogeny. The southern Laurentian Hf-isotope variation in time and space supports addition of increasingly juvenile 1.8-1.5 Ga crust to the newly

assembled core of Nuna, followed by introversion of Nuna, continental growth along a long-lived accretionary orogenic system extending to Baltica, Australia, and Amazonia, and crustal recycling during the Grenville orogenic system. This suggests that Nuna was assembled by ~ 1.8 Ga and challenges paleomagnetic data that Nuna did not finish its assembly until ~1.5 Ga, indicating the need for better integration of geologic, isotopic, and paleomagnetic studies.

INTRODUCTION

The origin and evolution of continental crust is a fundamental and debated topic in geoscience. In the past decade, numerous studies have interrogated the global zircon record to determine what could be learned about the origin and evolution of continental crust, and how it is archived in the geologic record (Belousova et al., 2010; Dhuime et al., 2012; Cawood et al., 2013; Roberts and Spencer, 2014). Zircon is ideally suited for such studies because it is the most physically and chemically enduring terrestrial material (Valley et al., 2014), it is nearly ubiquitous in crustal rocks, and because silicate melting and crystallization of zircon causes fractionation in isotope systems that track secular variation in crustal and mantle sources (Vervoort and Kemp, 2016). Paired U-Th-Pb and Lu-Hf analyses in zircon have informed estimates of crustal growth through time (Condie et al., 2005; Roberts and Spencer, 2014), and the relationship between crustal growth and the supercontinent cycle (Condie et al., 2009; Gardiner et al., 2016).

U-Th-Pb zircon dating indicates that the global record of zircon crystallization is non-uniform (Voice et al., 2011). This punctuation of global crystallization ages has been interpreted as either a preservation bias imposed by the supercontinent cycle where continental crust is preserved from destructive processes such as subduction erosion at

convergent margins by shielding within a supercontinent (Hawkesworth et al., 2018), or increased global magmatism in response to mantle overturn or plume events (Rino et al., 2004; Condie et al., 2017). Roberts (2012) used secular variation in Hf-isotope composition of the global zircon record to test the preservation bias hypothesis based on Hf-isotope trends documented in Phanerozoic accretionary (circum-Pacific) versus collisional (Alpine-Himalayan) orogenic systems (Collins et al., 2011). Zircon from these different orogenic systems yielded contrasting Hf-isotope trends through time suggesting that collisional orogens are characterized by a wide range of Hf-isotope compositions and a negative εHf(t) excursions indicative of increased crustal recycling, whereas accretionary orogens are characterized by a climbing Hf-isotope signature and positive εHf(t) excursions indicative of increased juvenile crustal additions (Figure 3-1 inset). Peaks in zircon crystallization ages in the global dataset correspond with lower mean Hf-isotope compositions (Roberts, 2012; Gardiner et al., 2016).

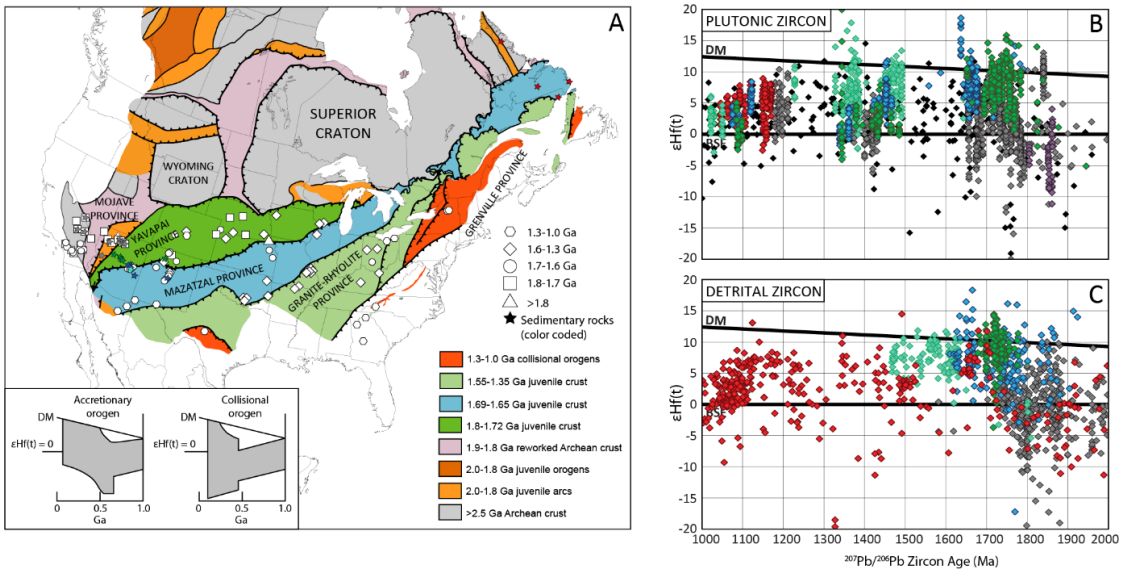

Figure 3-1. A) Tectonic map of Laurentia modified after Whitmeyer and Karlstrom (2007). Locations of all samples compiled in this study are shown; plutonic samples are shown in white and their symbol shape denotes age. The location of metasedimentary samples are plotted as stars, and their depositional age is color coded to match orogenic

provinces with which they are associated. Inset shows predicted trends in time-integrated Hf-isotope data from contrasting orogenic systems modified from Collins et al., 2011. B) Plutonic zircon record of southern Laurentia. Each diamond represents a dated zircon and its Hf-isotope composition, color coded based on location within orogenic provinces of southern Laurentia. C) Detrital zircon record of southern Laurentia from sedimentary and/or metasedimentary rocks associated with each orogenic province in southern Laurentia; diamonds are color coded based on depositional age, as stars in A.

Proterozoic crust of southern Laurentia offers a globally significant field laboratory to test models for crustal growth, and refine the applicability of using Hf-isotope variation in the zircon record to infer the timing of supercontinent assembly and dispersal. Here we address how/if the supercontinent cycle modulates crustal growth and preservation of continental crust. Laurentia is one of the most thoroughly studied continents on earth (Whitmeyer and Karlstrom, 2007), and was likely a central continent in both the Nuna/Columbia (~1.8-1.4 Ga) and Rodinia (~1.0 Ga) supercontinents. In this paper, we compile >3,500 paired U-Pb and Lu-Hf isotope analyses from plutonic and detrital zircon from southern Laurentia. This dataset offers provides an in-situ test for models that link Hf-isotope composition in zircon, crustal formation and preservation, and the supercontinent cycle. Specifically, we test the hypothesis that 1) crustal growth occurred along the southern margin of Laurentia via long-lived accretionary orogenesis from 1.8-1.0 Ga, 2) accretionary orogenesis initiated during final stages of assembly of Nuna and crustal growth occurred mainly during the reconfiguration of Nuna into Rodinia, and 3) the temporal, spatial, and isotopic trends observed in the Laurentian dataset are representative of the global tectonic regime from 2.0-1.0 Ga support modulation of the global zircon record by the prevalence of accretionary versus collision orogenic systems (Roberts, 2012) in both Phanerozoic and Proterozoic orogens.

METHODS

We use the Hf-isotope composition of zircon from basement and cover sequences to elucidate the tectonic history of southern Laurentia. We sampled sedimentary/metasedimentary and igneous rocks that formed during major pulses of crust formation and orogenesis in southwestern Laurentia (Doe et al., 2013; Holland et al., 2015; 2018; Mako et al., 2015). In addition, we compiled U-Th-Pb and Lu-Hf isotope data from igneous and detrital zircon associated with Proterozoic orogenic belts across southern Laurentia. In conjunction with our new data, the compilation covers most major crustal provinces delineated by Whitmeyer and Karlstrom (2007) (Figure 3-1).

Combined analysis of the plutonic and detrital zircon record provides a unique perspective on crust forming processes along convergent margins (Holland et al., 2018). Zircon from plutonic rocks provide temporal, spatial, and isotopic constraints on magmatic contributions to the crust during crustal growth. Additionally, detrital zircon grains constrain the age and isotopic maturity of crust exposed at the surface during orogenesis, provide additional insight into tectonic setting (Cawood et al., 2012), and allow us to identify local versus exotic detritus which can be used for supercontinent reconstruction (Doe et al., 2013; Holland et al., 2018).

Our approach is to compare the detrital zircon U-Pb and Lu-Hf characteristics of sedimentary/metasedimentary and plutonic rocks associated with major crust forming/orogenic pulses in southern Laurentia using the tectonic model of Whitmeyer and Karlstrom (2007) for data visualization. Data from plutonic rocks are shown on εHf vs. time plots according to their location with major crustal provinces (Figure 3-1). The spatial location of detrital zircon samples with respect to crustal province is less critical

because, for example, many sedimentary rocks associated with the Grenville orogeny were deposited far inboard of the main orogeny (Timmons et al., 2005; Mulder et al., 2017) so detrital zircon are plotted on εHf vs. time plots according to their depositional age (Figure 3-1).

RESULTS AND DISCUSSION

The initiation of accretionary orogens along continental margins has been suggested to be a response to global plate kinematics changes triggered by continental collision during supercontinent assembly (Cawood and Buchan, 2007). Abundant geologic evidence indicates that subduction-related accretionary orogenesis began along the southern margin of Laurentia synchronously with, or shortly after, assembly of the Canadian Shield during the Trans-Hudson orogeny (Whitmeyer and Karlstrom, 2007). Southern Laurentia then grew southward behind long-lived convergent margin from approximately 1.8-1.0 Ga (Karlstrom et al., 2001), representing one of the largest additions of juvenile crust in Earth history (Reymer and Shubert, 1989; Condie, 2013).

The Mojave province is distinctive in southwestern Laurentia for its evolved isotope signatures. Holland et al. (2018) documented temporal, spatial, and isotopic variation in the Hf-isotope composition of plutonic zircon in the Mojave province similar to those documented in the Circum-Pacific orogenic system (Kemp et al., 2009; Collins et al., 2011). Holland et al. (2018) attributed the evolved isotopic signature of Mojave province plutonic rocks to mixing of depleted mantle melts with older crustal components during crustal formation. Detrital zircon of the newly defined Vishnu basin indicate that the older crust responsible for the evolved isotopic signature of the Mojave province may

be of Australian and/or Antarctic affinity (Holland et al., 2018), suggesting that those cratons were juxtaposed prior to Vishnu basin deposition at ~1.8 Ga.

Plutonic zircon from the Yavapai province yield higher εHf values than contemporaneous plutonic rocks in the Mojave province (Figure 3-1). The Hf-isotope composition of Yavapai province plutons are nearly equal to the depleted mantle, indicating substantial juvenile crustal addition in the Yavapai province. Metasedimentary rocks in the Yavapai province are dramatically different than those of the Vishnu basin, though both successions were deformed and metamorphosed during the Yavapai orogeny. Metasedimentary rocks in the Yavapai province are characterized by strongly unimodal detrital zircon peaks with juvenile Hf-isotope compositions that are identical to the plutonic rocks of the Yavapai province (Doe, 2014). The similarity in depositional age and detrital zircon age populations indicate that Yavapai province metasedimentary rocks were likely deposited in arc-related basins (Cawood et al., 2012), and the dramatic different between Yavapai province successions and the Vishnu basin suggests that they were separated in time and space before amalgamation in the Yavapai orogeny.

Plutonic zircon of the Mazatzal province are similar to those of the Yavapai province in that they yield εHf values nearly identical to concurrent depleted mantle values (Figure 3-1). Metasedimentary successions in the Mazatzal province are similar to those of the Yavapai province in that their detrital zircon populations are dominated by zircons similar in age and Hf-isotope composition to the basement upon which they are deposited, however they are in some cases much more compositionally mature (Jones et al., 2009). Older Paleoproterozoic and Archean detrital zircon grains are present in these successions, but far less abundant than in those of the Vishnu basin. Jones et al. (2009)

suggested that repeated episodes of slab rollback, basin formation, and inversion could be responsible for generating these enigmatic deposits. A refined model for the origin of the Mazatzal province based on Hf-isotope composition of plutonic, metavolcanic, and detrital zircon suggests that the Mazatzal province formed as a retreating continental margin arc built atop the Yavapai province, and that supracrustal rocks across the Mazatzal province were deposited during cycles of upper-plate extension, rhyolite volcanism, and back arc basin development (Holland et al., in prep.).

Following the North American Tectonic Gap from 1.6-1.5 Ga, a continental arc system developed along the southern margin of Laurentia (Bickford et al., 2015). This arc system accommodated extensive, yet diachronous, juvenile crust formation southeast of the "Nd-line" from 1.5-1.33 Ga in the Granite-Rhyolite province. Farther inboard, voluminous intra-cratonic magmatism accompanied juvenile crust formation across previously accreted crustal provinces. These plutons are characterized by lower εHf(t) values consistent with derivation from the crust that they intrude (Figure 3-1). Previously unrecognized sedimentary rocks associated with intracratonic tectonism in southwestern Laurentia were discovered in New Mexico and Arizona (Jones et al., 2011; Doe et al., 2012). Detrital zircon from these successions include abundant exotic grains that were linked to Australia (Doe et al., 2012; 2013), indicating a long-term association between Australia and Laurentia.

The Grenville orogenic province represents the cessation of Paleo-to-Mesoproterozoic convergent margin tectonism along the Laurentian margin during a protracted collisional orogeny (Hynes and Rivers, 2010). Extensive magmatism from ~1.2-1.0 Ga occurred along the entire Laurentian margin, including the enigmatic and

voluminous anorthosite-mangerite-charnokite-granite (AMCG) suite, and syn-collisional magmatism. Hf-isotope compositions from zircon grains associated with the Grenville orogeny show a marked departure towards more evolved compositions (Figure 3-1), reflecting an increase in crustal reworking and/or protracted mantle enrichment (Chiarenzelli et al., 2010). Sedimentary rocks associated with the Grenville orogeny were distributed across Laurentia (Timmons et al., 2005; Mulder et al., 2017). Recent Hf-isotope analysis of pre, syn, and post-orogenic sedimentary rocks shows excellent agreement with the plutonic record, displaying progressively lower εHf(t) values from ~1.3-1.0 Ga (Spencer et al., 2015) (Figure 3-1).

Implications for the global zircon record and supercontinent cycles

Proterozoic crust of southern Laurentia records the growth of continental crust along a long-lived accretionary orogen, culminating in continental collision during the Grenville orogeny. The Hf-isotope composition of plutonic and detrital zircon from the Mojave, Yavapai, Mazatzal, and Granite-Rhyolite provinces trends towards more juvenile values from ~1.8-1.3 Ga (Figure 3-1). This trend is similar in time and space to the zircon record of the Phanerozoic accretionary Circum-Pacific orogenic system (Collins et al., 2011) (Figure 3-2). Similarly, the Hf-isotope composition of plutonic and detrital zircon associated with the Grenville orogeny shows a departure towards lower εHf(t) values typical of collisional orogens. Together, the entire dataset yields a pattern that resembles an inverted U (Smits et al., 2014).

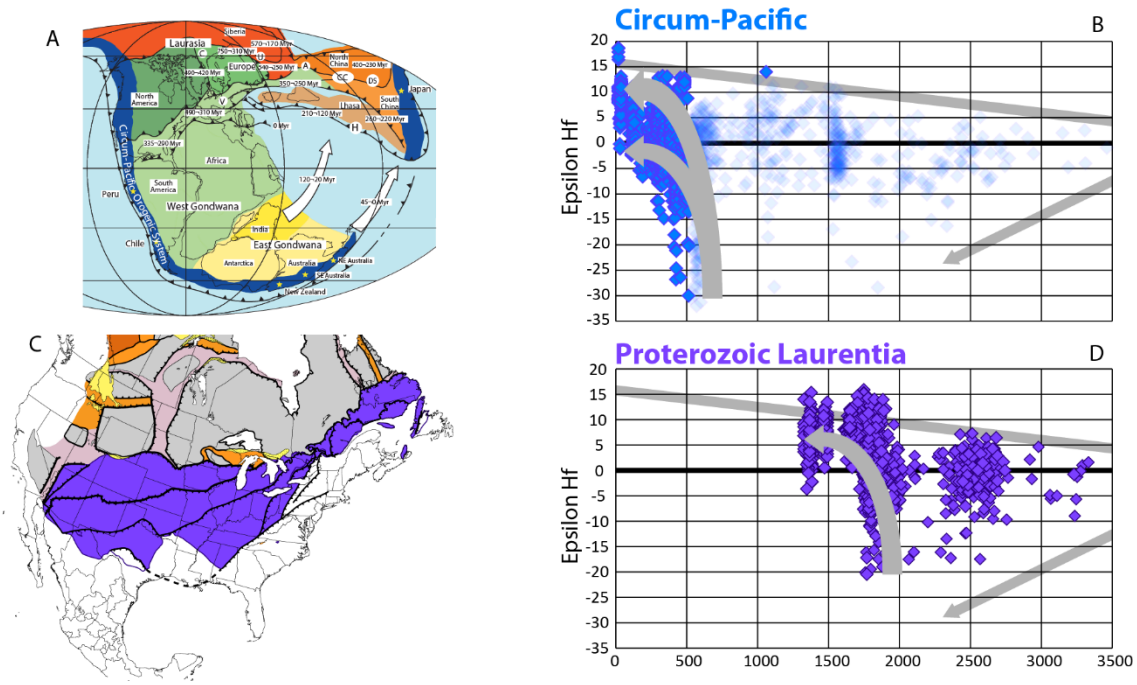

Figure 3-2. Comparison of the Hf-isotope composition of accretionary orogens of southern Laurentia with the Phanerozoic circum-Pacific orogenic system (Collins et al., 2011). A) Paleogeographic map of continental landmasses at ~500 Ma (after Collins et al., 2011. B) Hf-isotope record of the circum-Pacific orogenic system showing a climbing trend in Hf-isotope composition due to progressive subduction related juvenile crust formation along a long-lived accretionary margin. C) Simplified tectonic map of accretionary orogenic belts in southern Laurentia. D) Hf-isotope record of igneous and detrital zircon from southern Laurentia displays the same climbing trend through space and time as the Phanerozoic circum-Pacific orogenic system.

The inverted-U shape of the zircon Hf-isotope record of southern Laurentia is mimicked in the global dataset (Roberts, 2012; Gardiner et al., 2016) (Figure 3-3). This suggests that the tectonic regime described by the Laurentian Proterozoic example of continental amalgamation at 1.8 Ga, followed by crustal growth along an accretionary subduction system dominated the global zircon record. We argue that the well characterized geochronologic, isotopic, and orogenic evolution of southern Laurentia thus serves as a positive test for global crustal growth via accretionary tectonics during the interval between Nuna and Rodinia.

The configuration, timing of assembly, and dispersal of Nuna are actively debated. Here, we highlight similarities between the geologic and isotopic record of Laurentia and other cratons in order to make the case that much of the Nuna supercontinent assembled by ~1.8 Ga and long-lived ocean-facing orogens were active on many cratons that likely linked into a circum-global belt resembling the Phanerozoic circum-Pacific orogen. The same inverted-U trend in Hf-isotope composition through time has been documented in Australia (Smits et al., 2014), and Baltica (Roberts and Slagstad, 2015) (Figure 3-3). The similarities between Australian and Antarctic tectonic histories to that of southern Laurentia have been documented (Betts et al., 2008, 2011, 2016; Aitken et al., 2016; Goodge and Fanning, 2016; Holland et al., 2018), along with the Laurentia-Baltica connection (Karlstrom et al., 2001; Johansson, 2009; Roberts and Slagstad, 2015; Cawood and Pisarevsky, 2017). The Amazonian craton is often considered to be located further along the same convergent margin as Laurntia and Baltica throughout the Paleo-Mesoproterozoic due to similarly aged accretionary orogenic belts culminating in the (Johanson, 2009; Cawood and Pisarevsky, 2017), and the Hf-isotope record of detrital zircon from South America clearly displays the same inverted-U trend (Ibanez-Mejia et al., 2015; Pepper et al., 2016) (Figure 3-3).

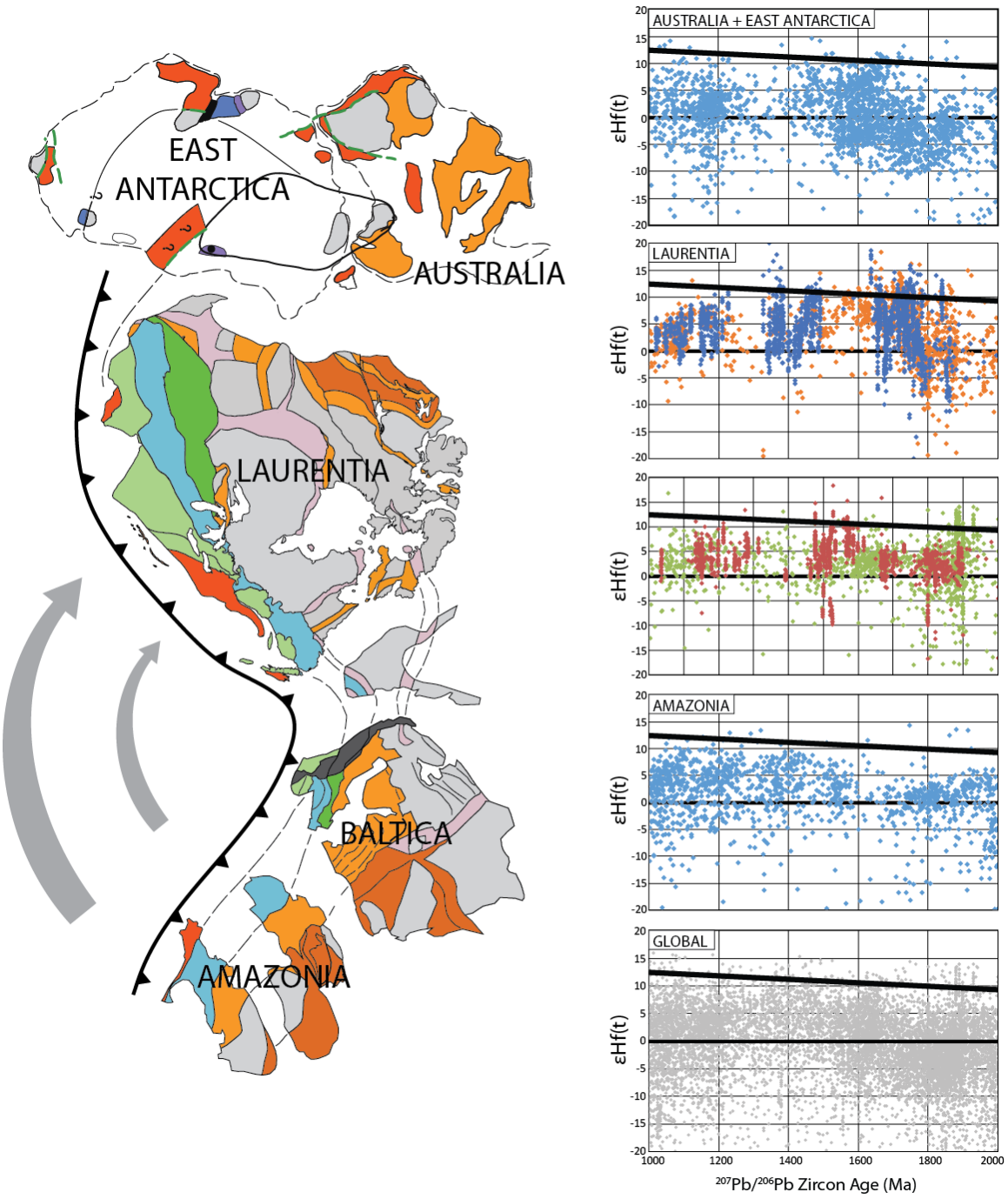

Figure 3-3. Reconstruction of cratons on the margin on Nuna at ~1.8 Ga modified after Whitmeyer and Karlstrom, (2007), Johansson, (2009), and Goodge and Fanning, (2016). The Hf-isotope record of each craton is shown from 2.0-1.0 Ga and compared with the global record of Roberts and Spencer (2014).. Laurentia and Baltica have excellent in-situ plutonic records, and plutonic vs. detrital samples are shown separately for these cratons (this study; Roberts and Slagstad, 2015). Data from Australia and Antarctica, and Amazonia are from the global compilation of Roberts and Spencer, (2014).

Paleomagnetic constraints on the configuration of Nuna are subject to ~100-300 Ma gaps which render the available data "insufficient to rigorously test [Nuna] configurations for any extended interval of the Paleo-Mesoproterozoic range from ~1.8 to 1.3 Ga" (Meert and Santosh, 2017). Despite this caveat, Meert and Santosh (2017) suggest that "maximum packing" of the Nuna supercontinent may have been at 1.5-1.4 Ga rather than 1.8 Ga as proposed here. However, a recent study of global ore deposits integrated with geochronologic, stratigraphic, and paleomagnetic databases supports the assembly of the bulk of the Nuna supercontinent by 1.85-1.80 Ga (Pehrsson et al., 2016). In their reconstruction, Australia, Laurentia, Baltica, and Amazonia are shown assembled on the margin of the supercontinent facing a large ocean basin. Following the interpretation that the Grenville orogeny in Laurentia involved collision with the Amazonian craton (Li et al., 2008), an accretionary orogenic system developed along the margin of the Nuna supercontinent, and was introverted (Murphy and Nance, 2013) to form Rodinia (Johansson, 2009; Spencer et al., 2013; Cawood and Pisarevsky, 2017) (Figure 3-3).

CONCLUSIONS

Southern Laurentia is one of the largest and most well characterized accretionary orogenic belts on Earth (Whitemeyer and Karlstrom, 2007). Comprehensive sampling of plutonic basement and associated metasedimentary rocks from every major crustal province provides an important test for models of the crustal growth related to the supercontinent cycle developed mainly through interrogation of the global zircon record. Our results show that the ~1.8-1.6 Ga phase of accretionary orogenesis in southwestern Laurentia is characterized by a major shift towards juvenile Hf-isotope compositions

consistent with crustal growth in an accretionary orogen (Collins et al., 2011). Following the North American tectonic gap, juvenile crust formation continued southeast of the Nd-line, and intracratonic magmatism recycled previously accreted Paleoproterozoic crust. The final stage of orogenesis from ~1.3-1.0 Ga is characterized by a shift towards more evolved Hf-isotope compositions, culminating in the collisional Grenville orogenic system. The trends in zircon Hf-isotope composition through space and time in southern Laurentia are consistent with models of crustal growth and preservation based on the global zircon record, and supported by similar geologic and isotopic evidence from Australia, Baltica, and Amazonia. Paleomagnetic studies broadly support several aspects of this model, however global compilations suggest that "maximum packing" of Nuna occurred during the Mesoproterozoic, reinforcing the need for further integration of geologic and paleomagnetic studies.

REFERENCES CITED

Aitken, A.R.A., Betts, P.G., Young, D.A., Blankenship, D.D., Roberts, J.L., and Siegert, M.J., 2016, The Australo-Antarctic Columbia to Gondwana transition: Gondwana Research, v. 29, p. 136–152, doi: 10.1016/j.gr.2014.10.019.

Belousova, E.A., Kostitsyn, Y.A., Griffin, W.L., Begg, G.C., O'Reilly, S.Y., and Pearson, N.J., 2010, The growth of the continental crust: Constraints from zircon Hf-isotope data: Lithos, v. 119, p. 457–466, doi: 10.1016/j.lithos.2010.07.024.

Betts, P.G., Armit, R.J., Stewart, J., Aitken, A.R.A., Ailleres, L., Donchak, P., Hutton, L., Withnall, I., and Giles, D., 2016, Australia and Nuna: Geological Society, London, Special Publications, v. 424, p. 47–81, doi: 10.1144/SP424.2.

Betts, P.G., Giles, D., and Aitken, A., 2011, Palaeoproterozoic accretion processes of

Australia and comparisons with Laurentia: International Geology Review, v. 53, p. 1357–1376, doi: 10.1080/00206814.2010.527646.

Betts, P.G., Giles, D., and Schaefer, B.F., 2008, Comparing 1800-1600 Ma accretionary and basin processes in Australia and Laurentia: Possible geographic connections in Columbia: Precambrian Research, v. 166, p. 81–92, doi: 10.1016/j.precamres.2007.03.007.

Bickford, M.E., Van Schmus, W.R., Karlstrom, K.E., Mueller, P.A., and Kamenov, G.D., 2015, Mesoproterozoic-trans-Laurentian magmatism: A synthesis of continent-wide age distributions, new SIMS U-Pb ages, zircon saturation temperatures, and Hf and Nd isotopic compositions: Precambrian Research, v. 265, p. 286–312, doi: 10.1016/j.precamres.2014.11.024.

Cawood, P.A., and Buchan, C., 2007, Linking accretionary orogenesis with supercontinent assembly: Earth-Science Reviews, v. 82, p. 217–256, doi: 10.1016/j.earscirev.2007.03.003.

Cawood, P.A., Hawkesworth, C.J., and Dhuime, B., 2012, Detrital zircon record and tectonic setting: Geology, v. 40, p. 875–878, doi: 10.1130/G32945.1.

Cawood, P.A., Hawkesworth, C.J., and Dhuime, B., 2013, The continental record and the generation of continental crust: Bulletin of the Geological Society of America, v. 125, p. 14–32, doi: 10.1130/B30722.1.

Cawood, P.A., and Pisarevsky, S.A., 2017, Laurentia-Baltica-Amazonia relations during Rodinia assembly: Precambrian Research, v. 292, p. 386–397, doi: 10.1016/j.precamres.2017.01.031.

Chiarenzelli, J., Lupulescu, M., Cousens, B., Thern, E., Coffin, L., and Regan, S., 2010,

Enriched Grenvillian lithospheric mantle as a consequence of long-lived subduction beneath Laurentia: Geology, v. 38, p. 151–154, doi: 10.1130/G30342.1.

Collins, W.J., Belousova, E. a., Kemp, A.I.S., and Murphy, J.B., 2011, Two contrasting Phanerozoic orogenic systems revealed by hafnium isotope data: Nature Geoscience, v. 4, p. 333–337, doi: 10.1038/ngeo1127.

Condie, K.C., Arndt, N., Davaille, A., and Puetz, S.J., 2017, Zircon age peaks: Production or preservation of continental crust? Geosphere, v. 13, p. 227–234, doi: 10.1130/GES01361.1.

Condie, K.C., Belousova, E., Griffin, W.L., and Sircombe, K.N., 2009, Granitoid events in space and time: Constraints from igneous and detrital zircon age spectra: Gondwana Research, v. 15, p. 228–242, doi: 10.1016/j.gr.2008.06.001.

Condie, K.C., Beyer, E., Belousova, E., Griffin, W.L., and O'Reilly, S.Y., 2005, U-Pb isotopic ages and Hf isotopic composition of single zircons: The search for juvenile Precambrian continental crust: Precambrian Research, v. 139, p. 42–100, doi: 10.1016/j.precamres.2005.04.006.

Dhuime, B., Hawkesworth, C.J., Cawood, P.A., and Storey, C.D., 2012, A change in the geodynamics of continental growth 3 billion years ago: Science, v. 335, p. 1334–1337.

Doe, M.F., Jones, J. V., Karlstrom, K.E., Dixon, B., Gehrels, G., and Pecha, M., 2013, Using detrital zircon ages and Hf isotopes to identify 1.48-1.45Ga sedimentary basins and fingerprint sources of exotic 1.6-1.5Ga grains in southwestern Laurentia: Precambrian Research, v. 231, p. 409–421, doi: 10.1016/j.precamres.2013.03.002.

Doe, M.F., Jones, J. V., Karlstrom, K.E., Thrane, K., Frei, D., Gehrels, G., and Pecha,

M., 2012, Basin formation near the end of the 1.60-1.45 Ga tectonic gap in southern Laurentia: Mesoproterozoic Hess Canyon Group of Arizona and implications for ca. 1.5 Ga supercontinent configurations: Lithosphere, v. 4, p. 77–88, doi: 10.1130/L160.1.

Gardiner, N.J., Kirkland, C.L., and Kranendonk, M.J. Van, 2016, The Juvenile Hafnium Isotope Signal as a Record of Supercontinent Cycles: Nature Publishing Group, p. 1–10, doi: 10.1038/srep38503.

Goodge, J.W., and Fanning, C.M., 2016, Mesoarchean and Paleoproterozoic history of the Nimrod Complex, central Transantarctic Mountains, Antarctica: Stratigraphic revisions and relation to the Mawson Continent in East Gondwana: Precambrian Research, v. 285, p. 242–271, doi: 10.1016/j.precamres.2016.09.001.

Hawkesworth, C., Cawood, P., Kemp, T., Storey, C., Hawkesworth, C., Cawood, P., Kemp, T., Storey, C., and Dhuime, B., 2018, A Matter of Preservation: Science, v. 323, p. 49–50.

Holland, M.E., Karlstrom, K.E., Doe, M.F., Gehrels, G.E., Pecha, M., Shufeldt, O.P., Begg, G., Griffin, W.L., and Belousova, E., 2015, An imbricate midcrustal suture zone: The mojave-yavapai province boundary in grand canyon, arizona: Bulletin of the Geological Society of America, v. 127, p. 1391–1410, doi: 10.1130/B31232.1.

Holland, M.E., Karlstrom, K.E., Gehrels, G., Shufeldt, O.P., Begg, G., Gri, W., and Belousova, E., 2018, The Paleoproterozoic Vishnu basin in southwestern Laurentia: Implications for supercontinent reconstructions, crustal growth, and the origin of the Mojave crustal province: Precambrian Research, v. 308, p. 1–17, doi: 10.1016/j.precamres.2018.02.001.

Ibanez-Mejia, M., Pullen, A., Arenstein, J., Gehrels, G.E., Valley, J., Ducea, M.N., Mora, A.R., Pecha, M., and Ruiz, J., 2015, Unraveling crustal growth and reworking processes in complex zircons from orogenic lower-crust: The Proterozoic Putumayo Orogen of Amazonia: Precambrian Research, v. 267, p. 285–310, doi: 10.1016/j.precamres.2015.06.014.

Johansson, Å., 2009, Baltica, Amazonia and the SAMBA connection-1000 million years of neighbourhood during the Proterozoic? Precambrian Research, v. 175, p. 221–234, doi: 10.1016/j.precamres.2009.09.011.

Jones, J. V., Connelly, J.N., Karlstrom, K.E., Williams, M.L., and Doe, M.F., 2009, Age, provenance, and tectonic setting of Paleoproterozoic quartzite successions in the southwestern United States: Bulletin of the Geological Society of America, v. 121, p. 247–264, doi: 10.1130/B26351.1.

Jones III, J. V., Daniel, C.G., Frei, D., and Thrane, K., 2011, Revised regional correlations and tectonic implications of Paleoproterozoic and Mesoproterozoic metsedimentary rocks in northern New Mexico, USA: New findings from detrital zircon studies of the Hondo Group, Vadito Group, and Marquenas Formation: Geosphere, v. 7, p. 974, doi: 10.1130/GES00614.1.

Karlstrom, K.E., Åhäll, K.I., Harlan, S.S., Williams, M.L., McLelland, J., and Geissman, J.W., 2001, Long-lived (1.8-1.0 Ga) convergent orogen in southern Laurentia, its extensions to Australia and Baltica, and implications for refining Rodinia: Precambrian Research, v. 111, p. 5–30, doi: 10.1016/S0301-9268(01)00154-1.

Kemp, A.I.S., Hawkesworth, C.J., Collins, W.J., Gray, C.M., and Blevin, P.L., 2009, Isotopic evidence for rapid continental growth in an extensional accretionary

orogen: The Tasmanides, eastern Australia: Earth and Planetary Science Letters, v. 284, p. 455–466, doi: 10.1016/j.epsl.2009.05.011.

Mako, C.A., Williams, M.L., Karlstrom, K.E., Doe, M.F., Powicki, D., Holland, M.E., Gehrels, G., and Pecha, M., 2015, Polyphase Proterozoic deformation in the Four Peaks area, central Arizona, and relevance for the Mazatzal orogeny: Geosphere, v. 11, p. 1975–1995, doi: 10.1130/GES01196.1.

Meert, J.G., and Santosh, M., 2017, The Columbia supercontinent revisited: Gondwana Research, v. 50, p. 67–83, doi: 10.1016/j.gr.2017.04.011.

Mulder, J.A., Karlstrom, K.E., Fletcher, K., Heizler, M.T., Timmons, J.M., Crossey, L.J., Gehrels, G.E., and Pecha, M., 2017, The syn-orogenic sedimentary record of the Grenville Orogeny in southwest Laurentia: Precambrian Research, v. 294, p. 33–52, doi: 10.1016/j.precamres.2017.03.006.

Murphy, J.B., and Nance, R.D., 2013, Speculations on the mechanisms for the formation and breakup of supercontinents: Geoscience Frontiers, v. 4, p. 185–194, doi: 10.1016/j.gsf.2012.07.005.

Pehrsson, S.J., Eglington, B.M., Evans, D.A.D., Huston, D., and Reddy, S.M., 2016, Metallogeny and its link to orogenic style during the Nuna supercontinent cycle, *in* Li, Z.X., Evans, D.A.D., and Murphy, J.B. eds., Supercontinent Cycles Through Earth History, Geological Society of London, https://doi.org/10.1144/SP424.5.

Pepper, M., Gehrels, G., Pullen, A., Ibanez-Mejia, M., Ward, K.M., and Kapp, P., 2016, Magmatic history and crustal genesis of western South America: Constraints from U-Pb ages and Hf isotopes of detrital zircons in modern rivers: Geosphere, v. 12, p. 1532–1555, doi: 10.1130/GES01315.1.

Rino, S., Komiya, T., Windley, B.F., Katayama, I., Motoki, A., and Hirata, T., 2004, Major episodic increases of continental crustal growth determined from zircon ages of river sands; implications for mantle overturns in the Early Precambrian: Physics of the Earth and Planetary Interiors, v. 146, p. 369–394, doi: 10.1016/j.pepi.2003.09.024.

Roberts, N.M.W., 2012, Increased loss of continental crust during supercontinent amalgamation: Gondwana Research, v. 21, p. 994–1000, doi: 10.1016/j.gr.2011.08.001.

Roberts, N.M.W., and Slagstad, T., 2015, Continental growth and reworking on the edge of the Columbia and Rodinia supercontinents; 1.86-0.9 Ga accretionary orogeny in southwest Fennoscandia: International Geology Review, v. 57, p. 1582–1606, doi: 10.1080/00206814.2014.958579.

Roberts, N.M.W., and Spencer, C.J., 2014, The zircon archive of continent formation through time: Geological Society, London, Special Publications, v. 389, p. 197–225, doi: 10.1144/SP389.14.

Smits, R.G., Collins, W.J., Hand, M., Dutch, R., and Payne, J., 2014, A Proterozoic Wilson cycle identified by Hf isotopes in central Australia: Implications for the assembly of Proterozoic Australia and Rodinia: Geology, v. 42, p. 231–234, doi: 10.1130/G35112.1.

Spencer, C.J., Cawood, P.A., Hawkesworth, C.J., Prave, A.R., Roberts, N.M.W., Horstwood, M.S.A., and Whitehouse, M.J., 2015, Generation and preservation of continental crust in the Grenville Orogeny: Geoscience Frontiers, v. 6, p. 357–372, doi: 10.1016/j.gsf.2014.12.001.

Spencer, C.J., Hawkesworth, C., Cawood, P.A., and Dhuime, B., 2013, Not all supercontinents are created equal: Gondwana-rodinia case study: Geology, v. 41, p. 795–798, doi: 10.1130/G34520.1.

Timmons, J.M., Karlstrom, K.E., Heizler, M.T., Bowring, S.A., Gehrels, G.E., and Crossey, L.J., 2005, Tectonic inferences from the ca. 1255-1100 Ma Unkar Group and Nankoweap Formation, Grand Canyon: Intracratonic deformation and basin formation during protracted Grenville orogenesis: Bulletin of the Geological Society of America, v. 117, p. 1573–1595, doi: 10.1130/B25538.1.

Valley, J.W., Cavosie, A.J., Ushikubo, T., Reinhard, D.A., Lawrence, D.F., Larson, D.J., Clifton, P.H., Kelly, T.F., Wilde, S.A., Moser, D.E., and Spicuzza, M.J., 2014, Hadean age for a post-magma-ocean zircon confirmed by atom-probe tomography: Nature Geoscience, v. 7, p. 219–223, doi: 10.1038/ngeo2075.

Vervoort, J.D., and Kemp, A.I.S., 2016, Clarifying the zircon Hf isotope record of crust-mantle evolution: Chemical Geology, v. 425, p. 65–75, doi: 10.1016/j.chemgeo.2016.01.023.

Voice, P.J., Kowalewski, M., and Eriksson, K. a., 2011, Quantifying the Timing and Rate of Crustal Evolution: Global Compilation of Radiometrically Dated Detrital Zircon Grains: The Journal of Geology, v. 119, p. 109–126, doi: 10.1086/658295.

Whitmeyer, S.J., and Karlstrom, K.E., 2007, Tectonic model for the Proterozoic growth of North America: Geosphere, v. 3, p. 220, doi: 10.1130/GES00055.1.